UNIVERSITY OF LONDON THESIS

Degree PhD Year 2007 Name of Author ELEONERA JOVCEVA

COPYRIGHT

This is a thesis accepted for a Higher Degree of the University of London. It is an unpublished typescript and the copyright is held by the author. All persons consulting the thesis must read and abide by the Copyright Declaration below.

COPYRIGHT DECLARATION

I recognise that the copyright of the above-described thesis rests with the author and that no quotation from it or information derived from it may be published without the prior written consent of the author.

LOAN

Theses may not be lent to individuals, but the University Library may lend a copy to approved libraries within the United Kingdom, for consultation solely on the premises of those libraries. Application should be made to: The Theses Section, University of London Library, Senate House, Malet Street, London WC1E 7HU.

REPRODUCTION

University of London theses may not be reproduced without explicit written permission from the University of London Library. Enquiries should be addressed to the Theses Section of the Library. Regulations concerning reproduction vary according to the date of acceptance of the thesis and are listed below as guidelines.

A. Before 1962. Permission granted only upon the prior written consent of the author. (The University Library will provide addresses where possible).

B. 1962 - 1974. In many cases the author has agreed to permit copying upon completion of a Copyright Declaration.

C. 1975 - 1988. Most theses may be copied upon completion of a Copyright Declaration.

D. 1989 onwards. Most theses may be copied.

This thesis comes within category D.

☐ This copy has been deposited in the Library of UCL

☐ This copy has been deposited in the University of London Library, Senate House, Malet Street, London WC1E 7HU.

FUNCTIONAL PROTEOMIC AND GENOMIC ANALYSIS OF CYTOSKELETAL ORGANISATION IN DROSOPHILA

Eleonora JOVCEVA

DEPARTMENT OF BIOCHEMISTRY AND MOLECULAR BIOLOGY,
UNIVERSITY COLLEGE LONDON
Gower Street, LONDON

THIS THESIS IS SUBMITTED IN PARTIAL FULFILMENT OF THE REQUIREMENTS FOR THE DEGREE OF DOCTOR OF PHILOSOPHY FROM THE UNIVERSITY OF LONDON

ProQuest LLC
789 East Eisenhower Parkway
P.O. Box 1346
Ann Arbor, MI 48106-1346

ABSTRACT

Phosphoinositide 3-kinase (PI3K) plays an important role in cellular signalling by generating phospholipid second messengers at the plasma membrane. A large repertoire of signalling and actin-binding proteins, which consistently regulate the dynamic assembly and spatial organisation of actin filaments, binds phospholipid second messengers, through their pleckstrin homology (PH) domains, and regulates changes in actin cytoskeleton dynamics and organisation in response to external stimuli. Thus, the actin cytoskeleton, which functions in the generation and maintenance of cell morphology and polarity, regulation of endocytosis and intracellular trafficking, contractility, motility and cell division, is considered as an integral part of the cell signal transduction system. PI3K-dependent actin cytoskeleton reorganisation has been the subject of intensive studies, as alteration in the cytoskeleton and thus in cell morphology and migration appear to be common signatures of malignancy where PI3K activation is significantly involved. PI3K-dependent regulation of actin cytoskeleton dynamics is proposed to be achieved by cross-talk with the Rho-family small GTPases, major regulators of actin cytoskeleton organisation. However, the molecular mechanisms behind PI3K-dependent actin reorganisation and their interaction with small GTPases in not yet clearly defined. The aim of this project was to investigate the role of the PI3K signalling in controlling actin cytoskeleton, and to explore possible common targets of PI3K and Rho-family small GTPase signalling pathways, as well as to search for new targets downstream of PI3K. Initially, the role of PI3K in the regulation of the actin cytoskeleton in *Drosophila* cells was defined. Furthermore, a "loss-of-function approach" based on RNA interference for genes involved in PI3K and small GTPase signalling was combined with quantitative differential protein expression analysis and mass spectrometry. The differentially expressed proteins, many of which were cytoskeleton proteins, metabolic and redox enzymes, were linked to signalling pathways and associated with the morphological phenotype of each knockdown. Finally, the research was focused on studying the regulation of phosphorylation of cofilin, an actin depolymerising protein. It has been established that cofilin phosphorylation and activity is not directly regulated by upstream signalling events, but by changes in the levels of filamentous actin itself, with slingshot, the cofilin phosphatase, being a key regulator in sensing the dynamic changes in F-actin levels. Thus, cofilin phosphorylation is a homeostatic sensor of actin polymerisation, which self-limits protrusive response to external stimuli.

ACKNOWLEDGMENTS

Firstly, I sincerely thank my supervisors Professor Michael Waterfield, for giving me the opportunity to carry out the research presented in this thesis, and for keeping me inspired and enthusiastic about cell signalling pathways and proteomics – it was a great pleasure to work with him; and Dr John Timms, for his excellent daily supervision throughout the course of my research, for numerous discussions and for his support during writhing of this thesis. I also want to thank Dr Buzz Baum for introducing me with fly tissue culture, cell cytoskeleton and the world of RNAi, for his supervision and useful discussions from which I learnt a lot, and for the lovely retreats he orgniased for the lab.

To all my present and past colleagues in the Cancer Proteomics lab: Hong-Lin, Musarat, Mariana, Severine, Akunna, Richard, Bertran, Andrew, John, Mark, Carmen, Stephan, Hong-Lei, Sharon; and Morphogenesis group at LICR: Veronica, Tao, Patricia, Yukako and David for their friendship, for allowing me to share my PhD experience with them, for many fun outside the lab, for making London a great place to work and live and for giving me many happy memories.

I would like to thank Professor Danica Roganovic-Zafirova, for her unconditional support, guidance, encouragement and motivation during my study at the higher education.

I am grateful to my mother Bosilka Jovceva for her love, encouragement, and support. I would also like to thank the other family members in Macedonia for their love and understanding.

Finally, and most of all, I would like to thank to my lovely husband Novak Roganovic. I am forever grateful for the unconditional love, trust, support and understanding he continuously has given me thought years. He supported me in every step of the way, he gave me strength, courage and motivation to carry this out thought to the end.

ABBREVIATIONS

Chemicals and reagents

AEBSF	4-(2-aminethyl)benzenesulfonyl fluoride hydrochloride
BSA	bovine serum albumin
NHS-Cy2	3-(4-carboxymethyl)phenylmethyl)-3' -ethyloxacarbocyanine halide N-hydroxy-succinimidyl ester
NHS-Cy3	1-(5-carboxypentyl)-1'-propylindocarbocyaninehalide N-hydroxy-succinimidyl ester
NHS-Cy5	1-(5-carboxypentyl)-1'-methylindodi-carbocyanine halide N-hydroxy-succinimidyl ester
DHB	2, 5-hydroxybenzoic acid
DMSO	dimethyl sulphoxide
DTT	dithiothreitol
EDTA	ethylenediaminetetraacetic acid
FCS	foetal calf serum
HCl	hydrogen chloride
HEPES	N-(2-hydroxyethyl)piperazine-N'-(2-ethanesulfonic acid)
IAM	iodoacetamide
NaCl	sodium chloride
NHS	N-hydroxy succinimidyl
NP-40	nonidet P-40
PBS	phosphate-buffered saline
SDS	sodium dodecyl sulphate
TFA	trifluoroacetic acid
Tris	tris-(hydroxymethyl)aminomethane

Software and instrumentation

BVA	biological variance analysis
DIA	difference in-gel analysis
ESI	electrospray ionisation
MS	mass spectrometry
MS/MS	tandem mass spectrometry
MALDI	matrix-assisted laser desorption/ionisation
PMF	peptide mass fingerprinting
PMT	photomultiplier tube
TOF	time-of-flight

General

2D	two-dimensional

Ab	antibody
DIGE	difference gel electrophoresis
dsRNA	double stranded RNA
FITC	fluorescein isothiocyanate
HMLEC	human mammary luminal epithelial cells
IEF	Isoelectric focusing
kDa	kilo Dalton
MW	molecular weight
m/z	mass-to-charge ratio
pI	isoelectrical point
PAGE	polyacrylamide gel electrophoresis
PCR	polymerase chain reaction
PH	pleckstrin homology domain
PVDF	polyvinylidene fluoride
RISC	RNA-induced silencing complex
RNAi	RNA interference
TRITC	tetramethylrhodamine isothiocyanate
Vhr	volt hour

Proteins, enzymes, growth factors and inhibitors

ADF	Actin depolymerising factor
Arp	actin related protein
CytoD	cytochalasin D
EGF	epidermal growth factor
EGFR	epidermal growth factor receptor
ERK	extracellular signalling regulated kinase
GAP	GTPase activating protein
GEF	GTP exchange factor
IGF	insulin-like growth factor
InR	insulin receptor
Jas	jasplakinolide
LatB	latrunculin B
MAPK	mitogen activated protein kinase
PDGF	platelet-derived growth factor
PI3K	phosphatidylinositol 3-kinase
PIP	phosphatidylinositol phosphate
PIP2	phosphatidylinositol (4,5) bi-phosphate
PIP3	phosphatidylinositol (3,4,5) tri-phosphate
Ras	retrovirus-associated DNA sequence
ROS	reactive oxygen species
RTK	receptor tyrosine kinase
SH2	src homology-2 domain

SSH	slingshot
STAT	signal transducers and activators of transcription
Tsr	twinstar/cofilin
VEGF	vascular endothelial growth factor
WASP	Wiskott–Aldrich syndrome protein

TABLE of CONTENT

LIST of FIGURES

CHAPTER 1:

CHAPTER 3:

CHAPTER 4:

CHAPTER 5:

CHAPTER 7

LIST of TABLES

Chapter 1: Introduction

1.1. Cellular signalling pathways

The ability of cells to respond to stimuli derived from the environment is essential to their survival and normal physiological function. In order to communicate with each other and with their environment, cells express cell surface receptor proteins. Binding of a ligand to its membrane receptor results in changes in their biochemical or physical states that typically initiates a cascade of signalling events within the cell (Pawson, 1995; Rosales et al., 1995). Intracellular signal transduction might involve physical processes (such as diffusion), chemical changes (such as phosphorylation) of signalling intermediates, or both. For most characterised signal transduction pathways, the initial signalling event and the final effectors are known, but intermediate events that transmit the signal are either partially or completely unknown. In order to understand fully intracellular signal transduction and complex signalling networks, it is essential to identify the intermediate signalling molecules and to understand how information flows from one to the next. Even though every signalling network is organised such that cell surface receptor proteins, recognising specific stimuli, transmit information to downstream components of individual signal transduction pathways, which terminate with effectors that elicit a specific cellular response (e.g., proliferation, differentiation, survival, secretion and morphogenesis), individual signalling pathways differ in their complexity. The simplest signalling pathway is the linear signalling cascade, involving a specific receptor and a single effector (Figure 1.1a). Over time, this linear cascade evolved, becoming divergent with multiple steps between arms of the signalling pathways and using mechanisms involving cross-talk between signalling pathways (Figure 1.1b and c).

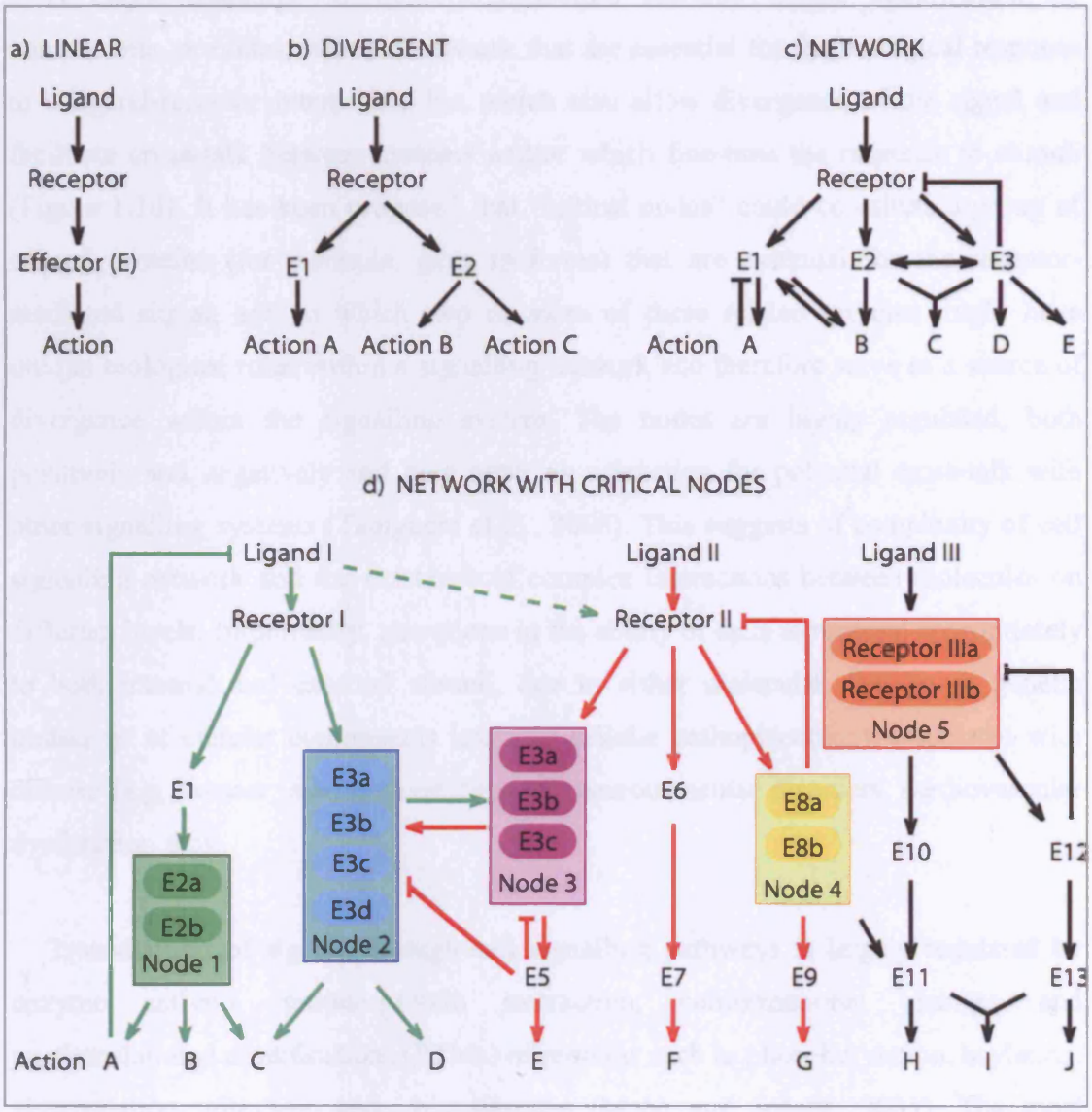

Figure 1.1 Diagram of signalling pathways. The binding of a ligand to its receptor triggers the activation of signalling pathways through effector (E) proteins that transduce signals to several intracellular second-messenger systems, which eventually lead to biological actions. The proposed concepts of signalling pathways have evolved from simple linear cascades (**a**) to complex networks (**b** and **c**), and currently networks with critical nodes that participate in the cross-talk between signalling networks (**d**, represented by the shaded/coloured boxes). In panel **d**, network 1 is represented by the green arrows, network 2 by the red arrows, and network 3 by the black arrows. Plain arrows represent an activation process, dashed arrows represent an activation process with less intensity, and blocked arrows represent an inhibition process. The numbers beside every component of the network (I, II, III for receptors and 1 to 13 for effectors) represent distinct proteins, whereas the small letters indicate different isoforms of the same protein. Adapted from Taniguchi *et al.* 2006.

A major challenge in signal transduction research is the identification of components, or nodes, within a network that are essential for the biological response to a ligand-receptor interaction, but which also allow divergence of the signal and facilitate cross-talk between systems and/or which fine-tune the response to stimuli (Figure 1.1d). It has been proposed that "critical nodes" could constitute a group of related proteins (for example, gene isoforms) that are essential for the receptor-mediated signal, and in which two or more of these related proteins might have unique biological roles within a signalling network and therefore serve as a source of divergence within the signalling system. The nodes are highly regulated, both positively and negatively and they serve as a junction for potential cross-talk with other signalling systems (Taniguchi et al., 2006). This suggests of complexity of cell signalling network and the existence of complex interactions between molecules on different levels. Importantly, alterations in the ability of cells to respond appropriately to both internal and external stimuli, due to either molecular damage or genetic mutations of cellular components leads, to cellular pathophysiology associated with disease (e.g., cancer, autoimmune diseases, neuromuscular disorders, cardiovascular dysfunction etc).

Transduction of signals through cell signalling pathways is largely regulated by enzyme activity, protein-protein interaction, conformational changes and posttranslational modifications (PTMs) of proteins such as phosphorylation, acylation, glycosylation, nitration, and ubiquitination (Mann and Jensen, 2003). The most studied PTM is protein phosphorylation. Phosphorylation is a mechanism that can turn proteins "on" and "off" by altering their activation state (Hunter, 1995). In addition, phosphorylation can change the binding properties of a particular protein or drive its translocation to a different cellular compartment. Protein phosphorylation is mediated by protein kinases and is negatively regulated by phosphatases. Thus, protein kinases and phosphatases play a key role in signal transduction and virtually all the major regulatory processes in normal and disease state cells are controlled directly or indirectly by phosphorylation. In addition to protein kinases, lipid kinases also play a major role in intracellular signal transduction. One of the intensively studied signalling pathways in which lipid kinases are involved is the phosphatidylinositol-3-OH kinases (PI3K) signalling pathway. This chapter focuses

on the classification and structure of this family of lipid kinases, and provides a brief overview of our current knowledge of PI3K signalling, cellular processes it regulates and a special overview of the cross–talk that exist between PI3K and the small Rho GTPases in controlling the actin cytoskeleton.

1.2 Phosphatidylinositol-3-OH kinase signalling pathway

1.2.1 The structure of PI3K family

PI3Ks belong to a large family of PI3K-related kinases or PIKK. Other members of this family include protein kinases: mTOR (mammalian target of rapamycin), ATM (ataxia telangiectasia mutated), ATR (ATM and RAD3 related) and DNA-PK (DNA-dependent protein kinase). All possess the characteristic PI3K-homologous kinase domain and a highly conserved carboxyl-terminal tail (Kuruvilla and Schreiber, 1999). Importantly, all members of the PIKK family have been implicated in human cancer both as oncogenes in the case of class I PI3K, or as tumour suppressor genes in the case of ATM and ATR.

PI3Ks are members of a unique and conserved family of intracellular lipid kinases that phosphorylate the 3'-hydroxyl group of phosphatidylinositol (PtdIns) (Figure 1.2 A) and phosphoinositides. D3-phosphorylated phosphoinositides act as lipid second messengers and activate many intracellular signalling pathways that regulate various cellular functions including cell metabolism, survival, proliferation, polarity, actin reorganisation and vesicle trafficking (Vanhaesebroeck et al., 2001; Engelman et al., 2006). Figure 1.2 B shows pathways that contribute to the biosynthesis of individual phosphorylated derivates of phosphatidylinositol and the enzymes that are involved in these processes.

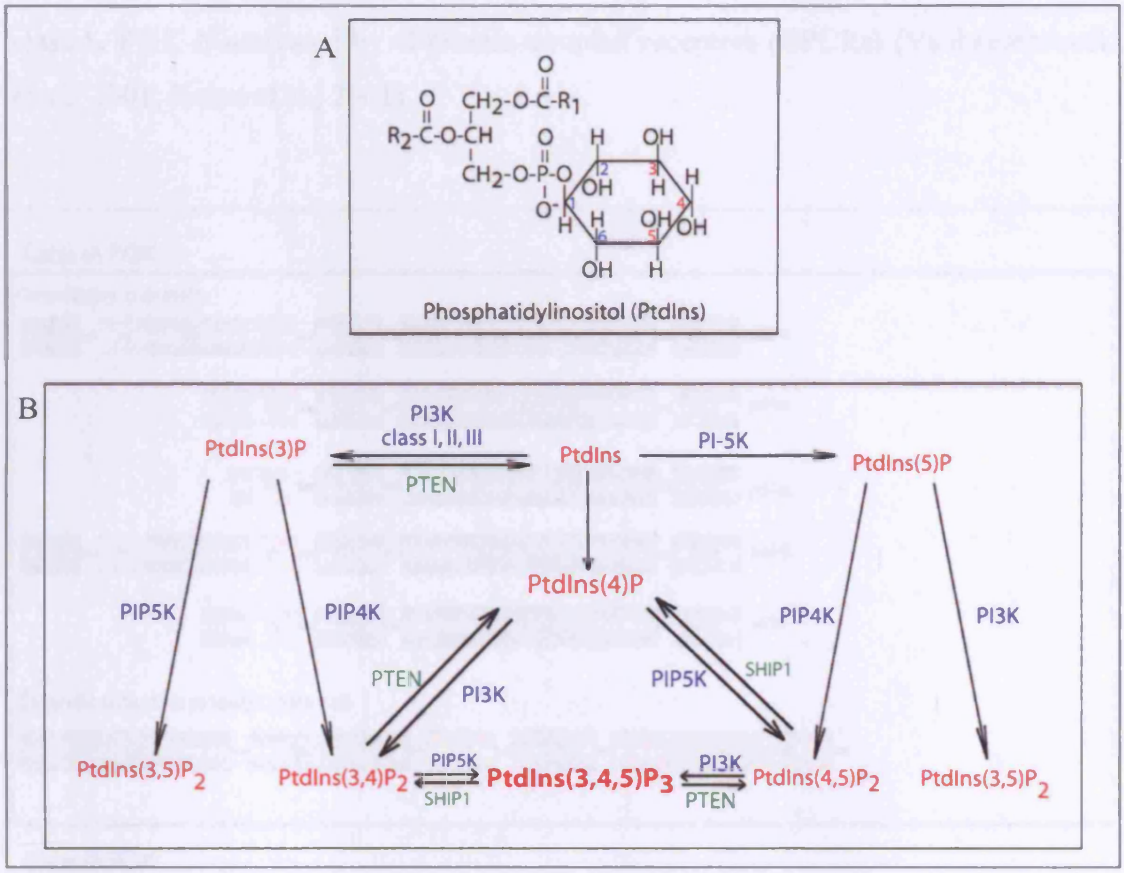

Figure 1.2 Pathways of phosphoinositide phosphorylation and dephosphorylation. A) The molecular structure of phosphatidylinositol. Hydroxyl groups numbered in red can be phosphorylated **B)** Pathways of phosphoinositide phosphorylation and phosphatase-catalysed hydrolysis in mammalian cells. In red are phosphoinositides. Numbers in parentheses indicate the sites of phosphorylation on the inositol ring. Two known phosphoinositide phosphatases (PTEN and SHIP1) are indicated in green, and the kinases are indicated in blue.

The PI3Ks are divided in three classes (I-III) on the basis of their structural characteristics and substrate specificity (Vanhaesebroeck et al., 1997a) (Figure 1.3). Different classes of PI3K, as well as different isoforms within each class have distinct roles in cellular signal transduction.

Class I PI3Ks consists of heterodimeric enzymes composed of a catalytic subunit and an adaptor or regulatory subunit. This class is further divided into two classes, I_A and I_B, based on the receptors to which they couple. Class I_A PI3Ks are activated by growth factor receptors with intrinsic tyrosine kinase activity (RTKs) or non-receptor tyrosine kinases, such as src-family kinases or Janus type kinases (JAKs), whereas the

class I_B PI3K is activated by G-protein-coupled receptors (GPCRs) (Vanhaesebroeck *et al.*, 2001; Katso et al., 2001).

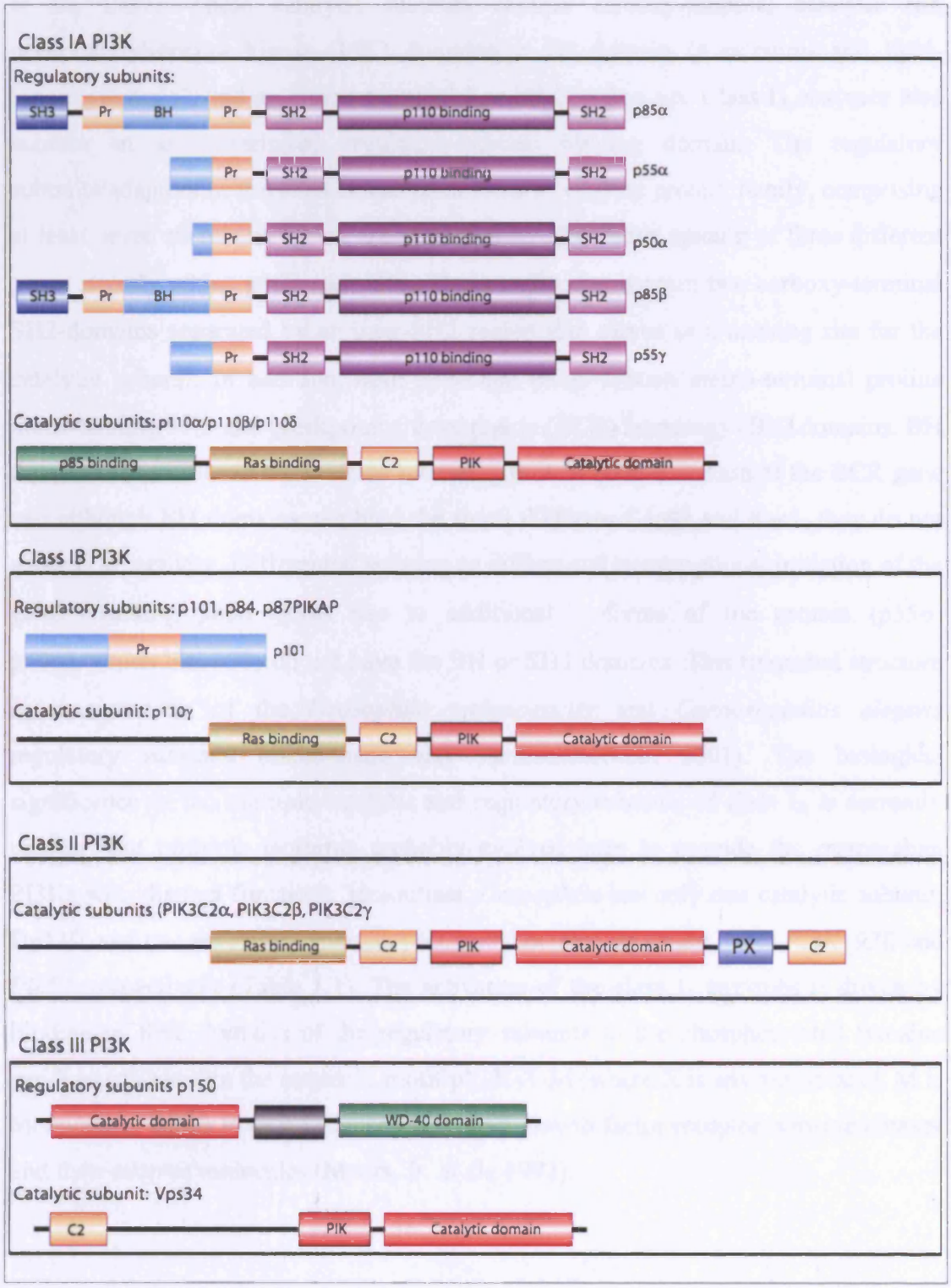

Figure 1.3 Classification of PI3K family members

The class I_A enzymes comprise three different isoforms derived from three separate genes: p110α (*PIK3CA*) and p110β (*PIK3CB*) that are expressed in many tissues, and p110δ (*PIK3CD*), which is expressed predominantly in haematopoietic cells (Chantry et al., 1997). These catalytic subunits contain carboxy-terminal catalytic and phosphatidylinositol kinase (PIK) domains, a C2 domain (a calcium- and lipid-binding domain), and an amino-terminal Ras binding domain. Class I_A enzymes also contain an amino-terminal regulatory-subunit binding domain. The regulatory subunits/adaptors of the class I_A enzymes form a complex protein family, comprising at least seven members, which are generated by alternative spicing of three different genes namely p85α, p85β and p55γ. These molecules contain two carboxy-terminal SH2-domains separated by an inter-SH2 region that serves as a docking site for the catalytic subunit. In addition, both p85α and p85β contain amino-terminal proline motif-binding SH3 and breakpoint cluster region (BCR) homology (BH) domains. BH domains are similar to the GTPase activating protein (GAP) domain of the BCR gene and although BH domains can bind the small GTPases Cdc42 and Rac1, they do not show GAP activity. Differential splicing or differential transcriptional initiation of the gene encoding p85α gives rise to additional isoforms of the protein (p55α, p50α), which like p55γ do not have the BH or SH3 domains. This truncated structure is characteristic of the *Drosophila melanogaster* and *Caenorhabditis elegans* regulatory subunits (Okkenhaug and Vanhaesebroeck, 2001). The biological significance of the multiple catalytic and regulatory subunits of class I_A is currently unclear, but multiple isoforms probably evolved later to provide the mammalian PI3Ks with distinct functions. In contrast, *Drosophila* has only one catalytic subunit, Dp110, and one regulatory subunit, p60, both encoded by single genes *Pi3K_92E* and *Pik57*, respectively (Table 1.1). The activation of the class I_A enzymes is driven by binding of SH2 domains of the regulatory subunits to the phosphorylated tyrosine residues (pY) within the sequence motif pY-X-X-M (where X is any amino-acid, M is methionine) which is found in many activated growth factor receptor tyrosine kinases and their adaptor molecules (Myers, Jr. et al., 1992).

Class	Type	Mammals	*Drosophila melanogaster*
Class IA	Catalytic	*PIK3CA* (p110α) *PIK3CB* (p110β) *PIK3CD* (p110δ)	*Pi3K_92E* (Dp110)
	Regulatory	*PIK3R1* (p85α/p55α/p50α) *PIK3R2* (p85β) PIK3R3 (p55γ)	*Pik57* (p60)
Class IB	Catalytic	*PIK3CG* (p110γ)	None
	Regulatory	*PIK3R5* (101) *p84* *PIK3R6* (p87PIKAP)	
Class II	Catalytic	*PIK3C2α* *PIK3C2β* *PIK3C2γ*	*Pi3K_68D*
Class III	Catalytic	*VPS34*	*Pi3K_59F* (DVps34p)
	Regulatory	*PIK3R4 (p150)*	*Vps15-like*

Table 1.1 Homology between mammalian and *Drosophila* PI3K family members.

Class I_B is represented by a single member, p110γ, present only in mammals and is expressed mainly in leukocytes (Vanhaesebroeck et al., 1997b). The p110γ catalytic subunit binds p101, a regulatory subunit that is unrelated to the regulatory subunits of the class I_A enzymes. Binding of p110γ to p101 renders it significantly more sensitive to activation by the β/γ G protein complex. There is no class I_B PI3K in *D. melanogaster* or *C. elegans*, suggesting that the capacity of GPCRs to directly activate PI3K signalling is a trait that has evolved in mammals. However, under some circumstances p110β may also be activated by GPCRs, so it is possible that in lower organisms class I_A PI3K mediates GPCR signals as well (Kurosu et al., 1997).

The class II PI3K family contains three members: PI3KC2α and PI3KC2β, expressed ubiquitously, and PI3KC2γ expressed primarily in hepatocytes (Vanhaesebroeck et al., 2001). All three isoforms share significant sequence homology with the class I p110 subunits. In addition, class II PI3K has an extended divergent N-terminus and additional PX and C2 domains at the C-terminus (Figure 1.3). These enzymes have no known regulatory subunits. *In vitro,* these enzymes preferentially phosphorylate PtdIns and, to a lesser extent, PtdIns4P. However, PtdIns(4,5)P_2 is a poor substrate for these enzymes (Engelman et al., 2006). Class II PI3Ks bind clathrin and localize to coated pits, indicating that they function in regulating membrane trafficking and receptor internalization (Gaidarov et al., 2001).

Although this class has not been studied extensively, there is an evidence that class II PI3Ks can be activated downstream of growth factor receptors, integrins and chemokine receptors, although their role in signalling is not clear (Katso et al., 2001). A single *Drosophila* homologue *Pi3K_68D* exists (Table 1.1).

The single class III PI3K (VpS34) only phosphorylates PtdIns to generate PtdIns3P (Koyasu, 2003). As it is the only class of PI3K enzyme present in yeast, it is thought to represent a primordial PI3K that gave rise to the other classes. The Vps34p (vacuolar protein-sorting defective) yeast catalytic subunit and its mammalian homologue, both contain carboxy-terminal catalytic and PIK domains, as well as a domain that binds a regulatory subunit. The regulatory subunit, VPS15p/p150 contains an amino-terminal myristylation signal, a serine/threonine kinase domain, a series of leucine-rich repeats, and a carboxy-terminal WD (tryptophan-aspartate repeat) motif. Studies, primarily in yeasts, have revealed that this class of PI3Ks plays an important role in vesicle trafficking, endocytosis and osmoregulation (Wendland et al., 1998). Recently, Vps34 was found to regulate mammalian target of rapamycin (mTOR) activity in response to amino-acid availability, suggesting that this enzyme is also crucial for controlling cell size (Byfield et al., 2005).

1.2.2 Negative regulation of PI3K signalling

Two types of lipid phosphatase negatively regulate lipid production through PI3K activity: PTEN (phosphatase and tensin homolog deleted on chromosome 10)/MMAC1 (mutated in multiple advanced cancers)/TEP-1(TGFβ-regulated and epithelial cell enriched phosphatase) (hereafter referred as to PTEN) and SHIP1/2 (SH2-containing inositol phosphatase). Both phosphatases are responsible for dephosphorylating PtdIns(3,4,5)P_3 (Figure 1.2).

PTEN was originally identified as a tumour suppressor gene that maps to human chromosome 10q23 and was found to be inactivated in breast cancer and glioblastomas during tumour progression (Li et al., 1997; Steck et al., 1997). The

PTEN protein is both a protein and a lipid phosphatase (Cantley and Neel, 1999). PTEN hydrolyses the 3'-phosphate and plays a central role in limiting cellular levels of PtdIns(3,4,5)P_3, thereby opposing PI3K-dependent proliferation and survival responses, and other downstream signalling cascades dependent on PtdIns(3,4,5)P_3 levels. Indeed, cells lacking PTEN function can exhibit a two fold increase in PtdIns(3,4,5)P_3 levels (Stambolic et al., 1998). Early studies showed that overexpression of PTEN reduced insulin-induced PtdIns(3,4,5)P_3 production in human 293 cells without affecting insulin-induced PI3K activation. Further, transfection of a catalytically inactive mutant of PTEN (C124S) causes PtdIns(3,4,5)P_3 accumulation in the absence of insulin stimulation (Maehama and Dixon, 1998). In contrast to PTEN, the SHIP1/2 removes the 5' phosphate from PtdIns(3,4,5)P_3 to generate PtdIns(3,4)P_2. PtdIns(3,4)P_2 can function as a second messenger to recruit pleckstrin homology (PH) domain containing proteins, such as Akt and PDK1. Thus, although both PTEN and SHIP1/2 reduce levels of PtdIns(3,4,5)P_3 in cells, SHIP1/2 activity may alter the spectrum of PtdIns(3,4,5)P_3-dependent signals rather than simply opposing all PI3K-mediated signalling, which appears to be the major function of PTEN (Luo et al., 2003).

1.2.3 PI3K signalling pathway

Much of our current understanding of PI3K-dependent signal transduction is based on studies of the class I PI3Ks. Products of their kinase activity, PtdIns3P, PtdIns(3,4)P_2 (herafter PIP2) and PtdIns(3,4,5)P_3 (hereafter PIP3), act as lipid second messengers, which primarily provide docking sites for recruitment of cellular proteins with unique lipid-binding motifs (such as pleckstrin homology (PH), Src Homology-2 (SH2) or FYVE Ring Finger domains) to membranes. This results in changes activation status of the proteins. For instance, PH domains are found in a wide variety of proteins (dynamin, spectrin, pleckstrin, phospholipase D, Btk, Akt, PDK1 etc.), which, through their interaction with these lipids, undergo changes in their sub-cellular localization, conformation, activation state and interaction with other proteins (Chan et al., 1999). The function of PI3Ks in regulating protein translocation was shown to be conserved throughout eukaryotes (plants, yeast, fruit flies, mammals and

other higher organisms) (Vanhaesebroeck *et al.*, 1997a; Vanhaesebroeck *et al.*, 2001), with the finding that signalling proteins accumulate at sites of PI3K activation by direct binding to PIP3. The most studied downstream targets of PI3K-dependent PIP3 production are the serine/threonine kinases Akt/PKB and PDK1. Association of these two proteins with PIP3 brings them into proximity and facilitates the activation of PDK1 followed by phosphorylation of Akt by PDK1 at Thr308 in its activation loop (Vanhaesebroeck and Alessi, 2000). This subsequently leads to Akt activation. It has been reported that for full activation, Akt should be phosphorylated at Ser473 in the kinase tail, as well. The kinase responsible for this phosphorylation is still controversial, although several kinases are listed as potential candidates including PDK1 (Balendran et al., 1999), possible autophosphorylation (Toker and Newton, 2000), DNA-PK (Feng et al., 2004) or mTor/Rictor (Sarbassov et al., 2005). Active Akt phosphorylates many downstream target proteins, thereby regulating a range of cellular processes including cell proliferation, survival, response to nutritional status, growth, metabolism, cell cycle, motility, and vesicle sorting (Figure 1.4).

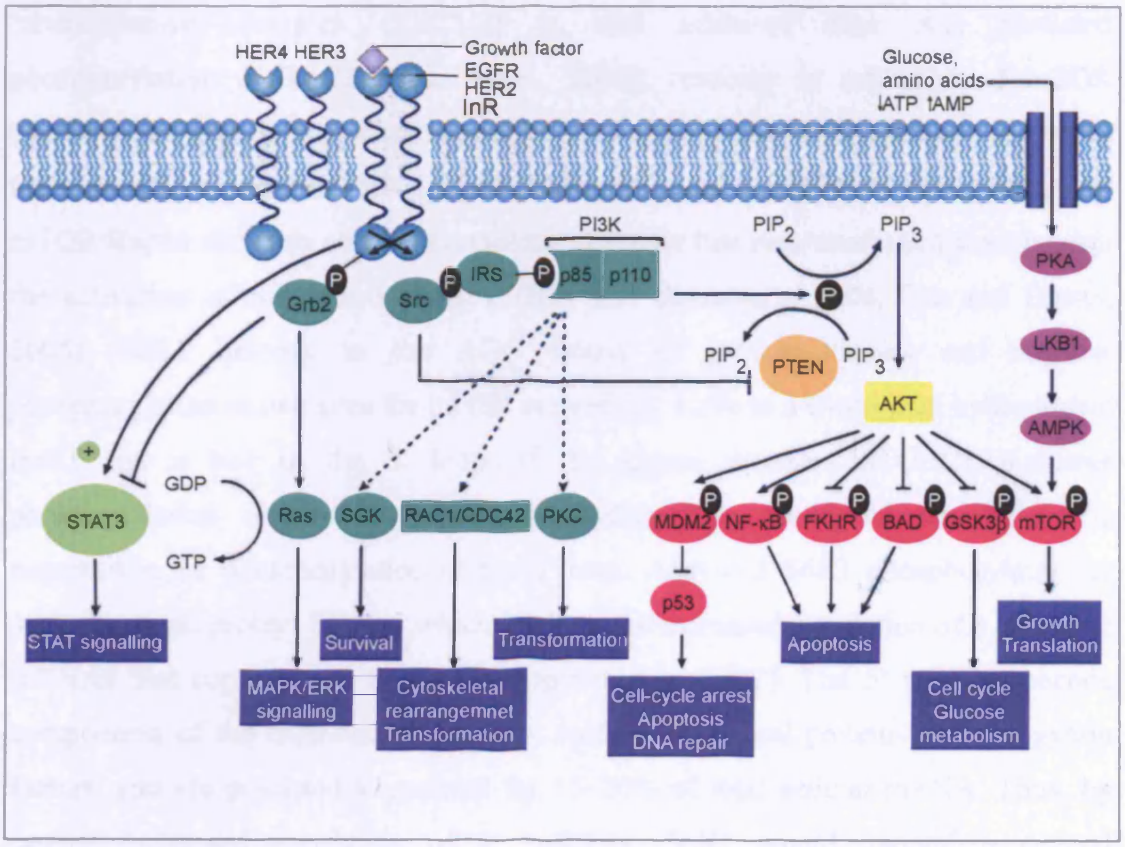

Figure 1.4 Schematic representation of signalling through PI3K pathway.

Many Akt targets become inhibited by the phosphorylation event induced by Akt. Such protein targets include Forkhead-related transcription factors (FKHRs) and the apoptosis-inducing protein Bad. Akt phosphorylation on both proteins creates a binding site for 14-3-3 proteins. The complex of FKHR and 14-3-3 is retained in the cytosol blocking nuclear translocation of FKHR and transcription of genes normally stimulated by FKHR (Brunet et al., 1999). Similarly, Akt phosphorylates BAD, which induces dissociation of BAD from Bcl-2 and Bcl-X_L and formation of a Bad-14-3-3 complex, leading to inhibition of the pro-apoptotic function. Another target negatively regulated by Akt phosphorylation is glycogen synthase kinase (GSK3) which is constitutively active in un-stimulated cells. Phosphorylation of GSK3-α and GSK3-β by Akt turns off the catalytic activity of these enzymes, leading to activation of pathways normally repressed by GSK3, which regulates gene transcription, cell cycle, cell proliferation and survival (Cohen and Frame, 2001; Vivanco and Sawyers, 2002). GSK3 phosphorylates several downstream proteins (glycogen synthase, c-Myc, cyclin D) to keep them inactive or to promote their degradation (Cohen et al., 2001). The tuberosclerosis complex (TSC1/2) is also inhibited after Akt mediated phosphorylation of TSC2 (Inoki et al., 2002), resulting in activation of mTOR (mammalian target of rapamycin). mTOR is a serine/threonine kinase that can exist in two complexes as mTORC1 (mTOR/Raptor) and mTORC2 (mTOR/Rictor). mTOR/Raptor complex serves as a molecular sensor that regulates translation through the activation of S6K1 and 4E-BP1 (Hay and Sonenberg, 2004; Tee and Blenis, 2005). S6K1 belongs to the AGC family of protein kinases and requires phosphorylation at two sites for its full activation; a site in a C-terminal hydrophobic motif and a site in the T loop of the kinase domain. mTORC1 mediates phosphorylation of Thr389 within the hydrophobic motif, whereas PDK1 is responsible for phosphorylation of the T loop. Activated S6K1 phosphorylates the 40S ribosomal protein S6, and which leads to the increased translation of a subset of mRNAs that contain a 5' tract of oligopyrimidine (TOP). The 5' mRNAs encode components of the translation apparatus, such as ribosomal proteins and elongation factors, and are predicted to account for 15–20% of total cellular mRNA. Thus, by causing increased translation of 5' mRNAs, S6K1 would upregulate general translation capacity. However, this model has now lost favour due to the recent findings that translation of 5' mRNAs does not depend on S6K (S6K1 and S6K2)

activity nor on S6 phosphorylation (Pende et al., 2004; Ruvinsky et al., 2005). The mTORC2 complex (mTOR/Rictor) has been reported to phosphorylate Ser473 of Akt (Sarbassov et al., 2004) and also to play a role in actin cytoskeleton organisation (Jacinto et al., 2004; Sarbassov *et al.*, 2005). The direct targets of mTORC2 that mediate signalling to the actin cytoskeleton are unknown, but may involve PKCα and the small GTPases Rho and Rac (Sarbassov et al., 2004).

Even though Akt is considered a crucial downstream target of PI3K and is likely to be responsible for many of the biological consequences of PI3K-dependent PIP3 production, several studies have demonstrated that there are a number of PI3K-dependent, but Akt-independent cellular responses. For example, gain- or loss-of-function mutations in PI3K *versus* Akt gave non-overlapping phenotypes in several model systems, including transgenic and knockout mice, indicating that these genes are not purely epistatic. This Akt-independence seems to be involved in the regulation of the small Rho GTPases: Cdc42 and Rac, and potentially some of their GTP-exchange factors (GEFs), which have been shown to be regulated by PI3K, but not to be downstream of Akt (Welch et al., 1998; Han et al., 1998). Other PH domain-containing proteins that bind to PIP3 include some small GTPases and actin binding proteins. Through such interactions, it has been proposed that PI3K can regulate actin cytoskeleton organisation, and hence cell shape and motility. This will be discussed in more detail in the following sections.

1.2.4 Actin cytoskeleton and its regulation by Rho-GTPases

The cytoskeleton is a complex network of protein filaments that extends through the cytoplasm. It provides mechanical support for eukaryotic cells, allowing them to adopt a variety of shapes and to carry out coordinated and directed movements. As a highly dynamic structure, the cytoskeleton is reorganised continuously as the cell changes shape, divides, and/or responds to the environment. An essential component of the cytoskeleton in eukaryotic cells is actin, which is a structurally globular protein that polymerises in a helical fashion to form an actin filament. Actin filaments work

in a complex network that is highly dynamic and functions with various actin binding proteins to control cell surface movements. The actin cytoskeleton functions in the generation and maintenance of cell morphology and polarity, in endocytosis and intracellular trafficking, in contractility, motility and cell division. Actin filaments lying just beneath the plasma membrane are cross linked into a network by various actin-binding proteins to form the cell cortex. The location and orientation of the cortical actin filaments is controlled by nucleation sites in the plasma membrane, and different regions of the membrane direct the formation of distinct actin-filament–based structures. A large repertoire of actin-binding proteins consistently regulates the dynamic assembly and spatial organisation of actin filaments, thus orchestring the motile behaviour of cells. Among these are proteins that

i) promote the branched nucleation of actin filaments, such as the Arp2/3 complex, or the linear nucleation of actin, such as the formins (Faix and Grosse, 2006);
ii) promote depolymerisation or severing of actin filaments, such as the actin-depolymerising factor (ADF/cofilin) family (Bamburg, 1999),
iii) associate with monomeric G-actin, such as profilin and β-thymosin to allow regulation of new filaments (Pollard et al., 2000),
iv) cap the ends of actin filaments to prevent extension, such as the capping proteins (Wear and Cooper, 2004) and
v) cross-link actin filaments to each other and to different cellular structures (Louvet-Vallee, 2000; Revenu et al., 2004).

Coordination and integration of the activities of this basic set of proteins is essential to control site-dependent actin polymerisation *in vivo* (Pantaloni et al., 2001; Pollard and Borisy, 2003). Furthermore, actin-binding proteins are also targets of various signalling pathways emanating from diverse extracellular stimuli, such as those from receptor tyrosine kinases (RTKs). These links allow rapid rearrangement of the cortical meshwork of actin filaments in response to extracellular signals. In this way, the actin cytoskeleton is considered an integral part of the cell signal transduction system, and its reorganisation is tightly controlled by cell signalling events. Within these signalling pathways, Rho-family GTPases play a key role acting as molecular switches at which signal inputs converge and are then transmitted as a coordinated array of output events regulating various location-specific cytoskeletal

events (Figure 1.6). In addition, the Rho GTPases also regulate many other cellular processes including gene transcription, the cell cycle, vesicle transport and numerous enzymatic activities including PI3Kinase and NADP oxidase in mammalian cells and glucan synthase in yeast (Figure 1.5) (Hall, 1998; Hall, 2005). In this way, central nodes are created that can coordinate many cellular events.

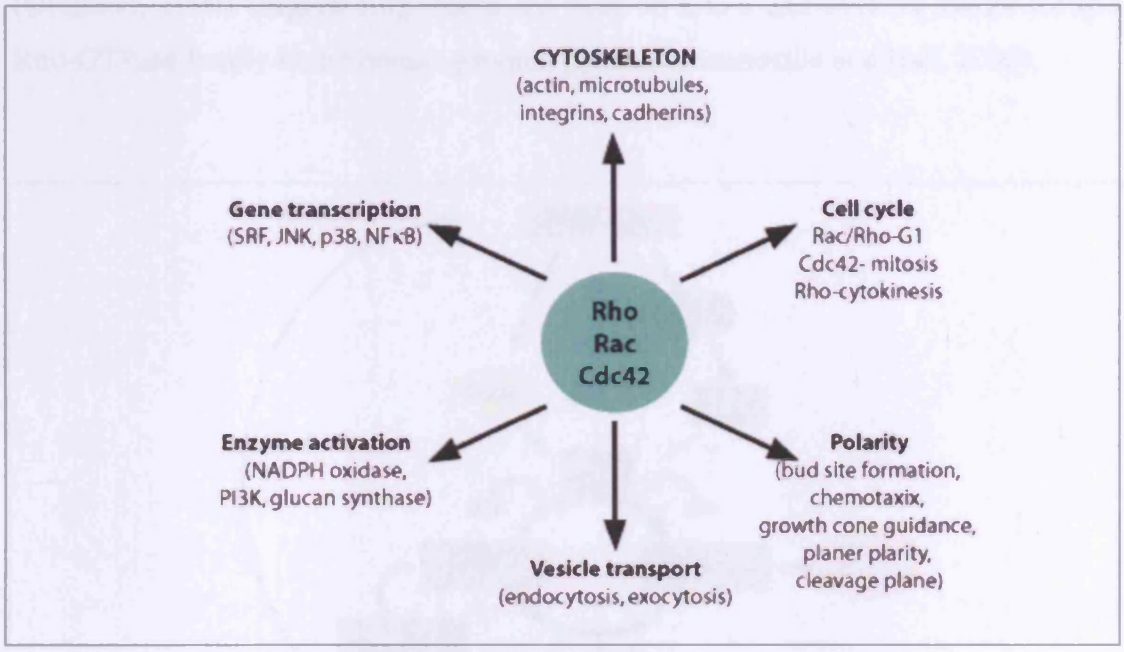

Figure 1.5 Cellular effects of Rho GTPases. (Hall, 2005)

Rho GTPases belong to the Ras superfamily of small GTPases and are highly conserved throughout eukaryotes. To date, 22 genes encoding different members of the Rho family have been identified in the human genome: RhoA, RhoB, RhoC, Rac1, Rac2, Rac3, Cdc42, RhoD, Rnd1, Rnd2, RhoE/Rnd3, RhoG, TC10, TCL, RhoH/TTF; Chp, Wrch-1; Rif, RhoBTB1, RhoBTB2; and Miro-1 and 2 (Jaffe and Hall, 2005). The yeast *S. cerevisiae* has five Rho proteins (Rho 1, 2, 3, 4 and Cdc42), whereas *C. elegans* and *D. melanogaster* are predicted to have 10 and 11, respectively. Rho, Rac, and Cdc42 were first recognized in the early 1990s for their unique ability to induce specific filamentous actin structures in fibroblasts; stress fibres, lamellipodia/membrane ruffles, and filopodia, respectively (Hall, 1998) and since then have been studied in great detail.

Rho GTPases act as molecular switchers by cycling between a guanosine diphosphate (GDP) inactive and a guanosine triphosphate (GTP) active bound state. This cycle is regulated by guanine nucleotide exchange factors (GEFs) (Schmidt and Hall, 2002) and GTPase activating proteins (GAPs) (Bernards, 2003), which stimulate GTP loading and hydrolysis, respectively, and guanine nucleotide dissociation inhibitors (GDIs), whose role appears to be to block spontaneous activation (Olofsson, 1999) (Figure 1.6). There are over 60 GEFs and over 70 GAPs for the Rho-GTPase family in the human genome (Etienne-Manneville and Hall, 2002).

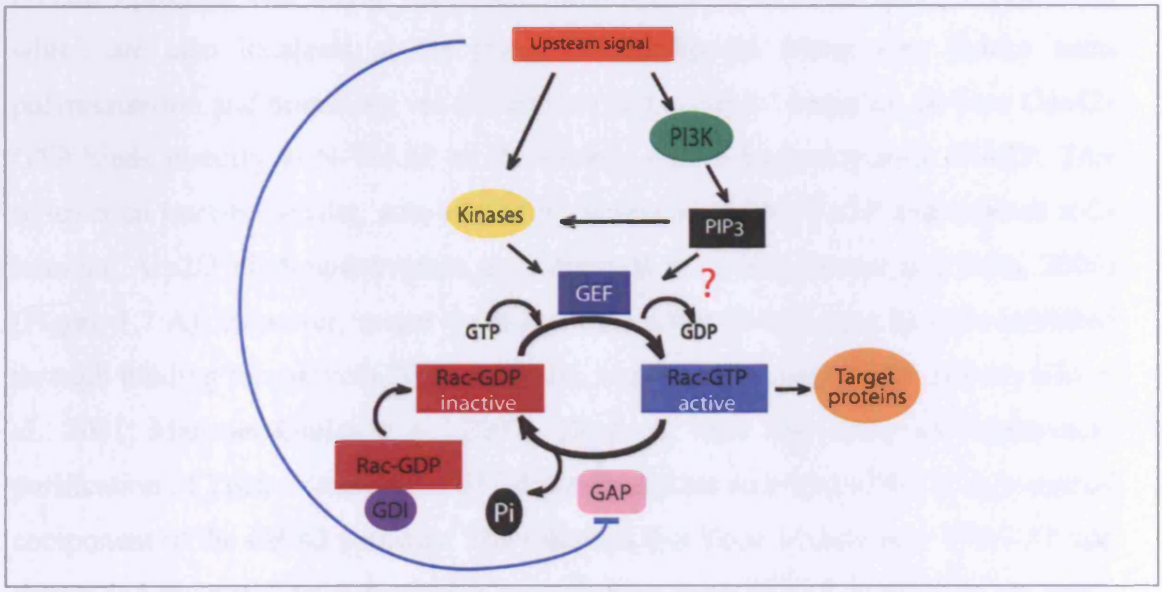

Figure 1.6 The GTPase cycle. Rho GTPases cycle between an inactive GDP bound form and an active GTP-bound form. Their activity is regulated by GEFs, GAPs and GDIs. Active GTPases interact with effector proteins to mediate a response.

When bound to GTP, Rho GTPases interact with a variety of effectors. For Rac, Rho and Cdc42 over 60 targets (serine/threonine kinases, lipid kinases, lipidases, oxidases and scaffold proteins) have so far been identified using yeast two-hybrid and affinity chromatography techniques (Etienne-Manneville et al., 2002). Finally, Rho GTPases can be regulated through direct phosphorylation or ubiquitination (Lang et al., 1996; Wang et al., 2003), but the extent to which these covalent modifications play a role in normal physiology is unclear.

To affect membrane dynamics and actin organisation, Rho GTPases need to act at membranes where they are usually activated by GEFs (Ridley, 2006). The activation of Rac and Cdc42 leads to the assembly of contractile actin:myosin filaments, protrusive actin-rich lamellipodia, and protrusive actin-rich filopodia, respectively (Etienne-Manneville et al., 2002). Lamellipodia are broad sheet-like protrusions containing a network of branching actin filaments and are found at the front of migratory cells. Both Rac and Cdc42 are active at the leading edge of cells and inhibition of each reduces lamellipodial extension (Nobes and Hall, 1995; Kurokawa et al., 2004). Target proteins for Cdc42 and Rac are Wiskot-Aldrich syndrome (WASP) proteins and WASP Verprolin-homologous (WAVE) proteins, respectively, which are also localised at the front of lamellipodia where they induce actin polymerisation and branching via recruitment of the Arp2/3 complex. *In vitro* Cdc42-GTP binds directly to N-WASP or the closely related haematopoietic WASP. This relieves an intra-molecular, auto-inhibitory interaction of N-WASP and exposes a C-terminal Arp2/3 binding/activation site (Ibarra et al., 2005; Stradal and Scita, 2006) (Figure 1.7 A). However, recent work has shown that WASP may be trans-inhibited through binding to a protein, WIP or CR16, which suppressed WASP activity (Ho et al., 2001; Martinez-Quiles et al., 2001). Ho *et al.* have also described biochemical purification of Toca-1 (transducer of Cdc42-dependent actin assembly) as an essential component of the Cdc42 pathway. They showed that Toca-1 binds both N-WASP and Cdc42 and promotes actin nucleation by activating the N-WASP-WIP/CR16 complex, the predominant form of N-WASP in cells. Thus, the cooperative actions of two distinct Cdc42 effectors, the N-WASP-WIP complex and Toca-1, are required for Cdc42-induced actin assembly (Ho et al., 2004). The proposed model is shown in Figure 1.7 B.

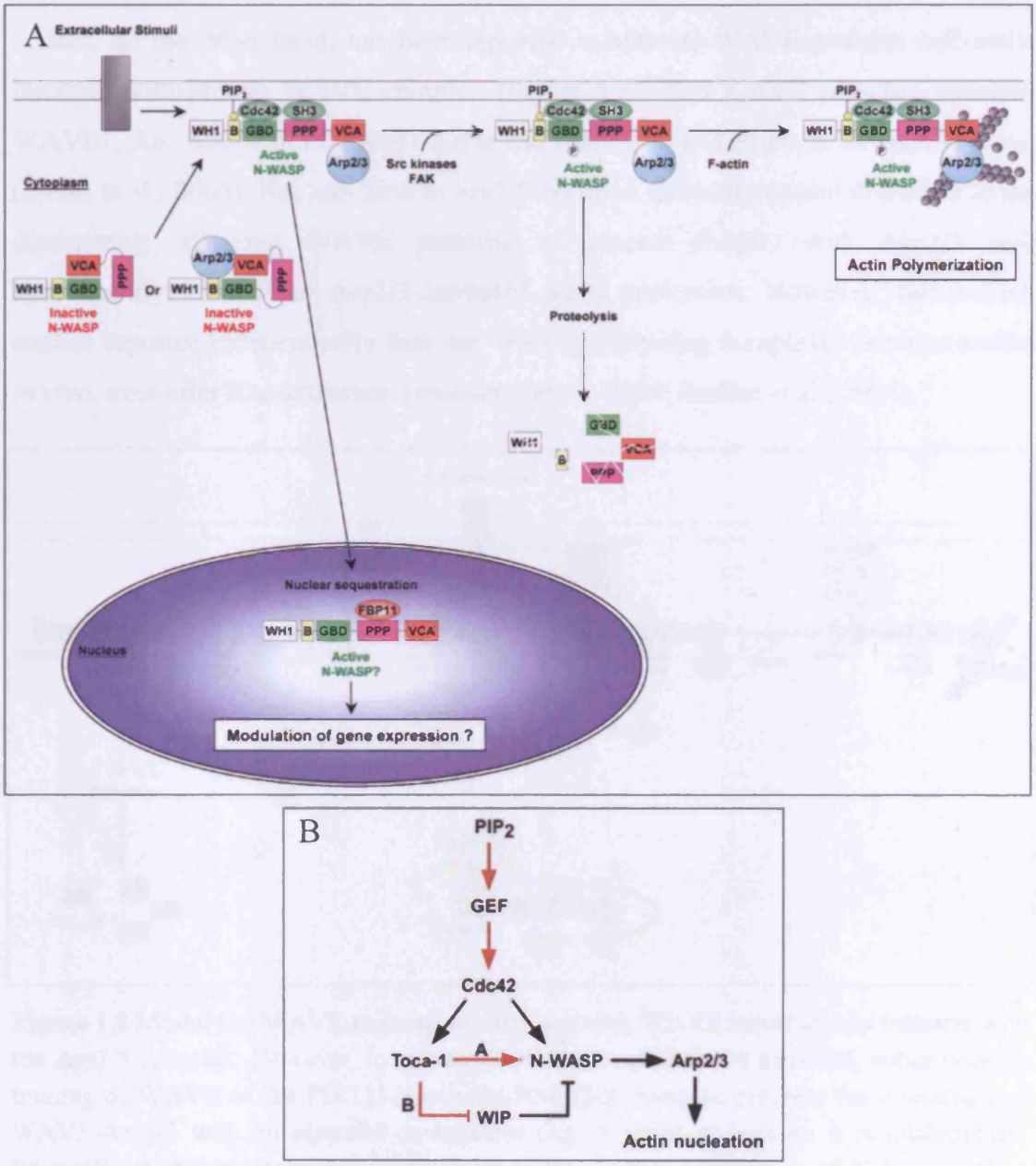

Figure 1.7 Model for N-WASP regulation. A) Under resting conditions, N-WASP is maintained in an inactive state in the cytosol. Auto-inhibition is via interaction of the G-protein binding domain (GBD) and the C-domain of the VCA module. Alternatively, direct interaction with the basic-rich region could inhibit the activity of a pre-bound Arp2/3 complex. In response to extracellular stimuli, N-WASP autoinhibition is relieved by the binding of GTP-bound Cdc42 and PtdIns(4,5)P_2 or SH3 containing proteins. In the open conformation, N-WASP can be imported into the nucleus, where it may be retained by FBP11 and regulate gene expression. Alternatively, active N-WASP can stay in the cytosol. Phosphorylation by tyrosine kinases enhances the ability of N-WASP to activate the Arp2/3 complex in cooperation with F-actin and prevents its nuclear import. In certain models this may induce its degradation through the proteasome pathway. (Bompard and Caron, 2004). **B)** A model of N-WASP regulation by Toca-1 (transducer of Cdc42-dependent actin assembly) (Ho et al., 2004).

Rac, on the other hand, has been reported to activate WAVE proteins indirectly through multi-protein WAVE complex (Figure 1.8). The WAVE complex includes WAVE1, Abi, Sra1/PIR121, Nap1/Kette and HSPC300 and exists in an inactive state (Ibarra et al., 2005). Rac can bind to Sra1/PIR121 in the complex and this leads to its disassembly allowing WAVE proteins to interact directly with Arp2/3 and subsequently to activate Arp2/3-mediated actin nucleation. However, two recent studies reported independently that the WAVE-containing complexes remains stable *in vivo,* even after Rac activation (Innocenti et al., 2004; Steffen et al., 2004).

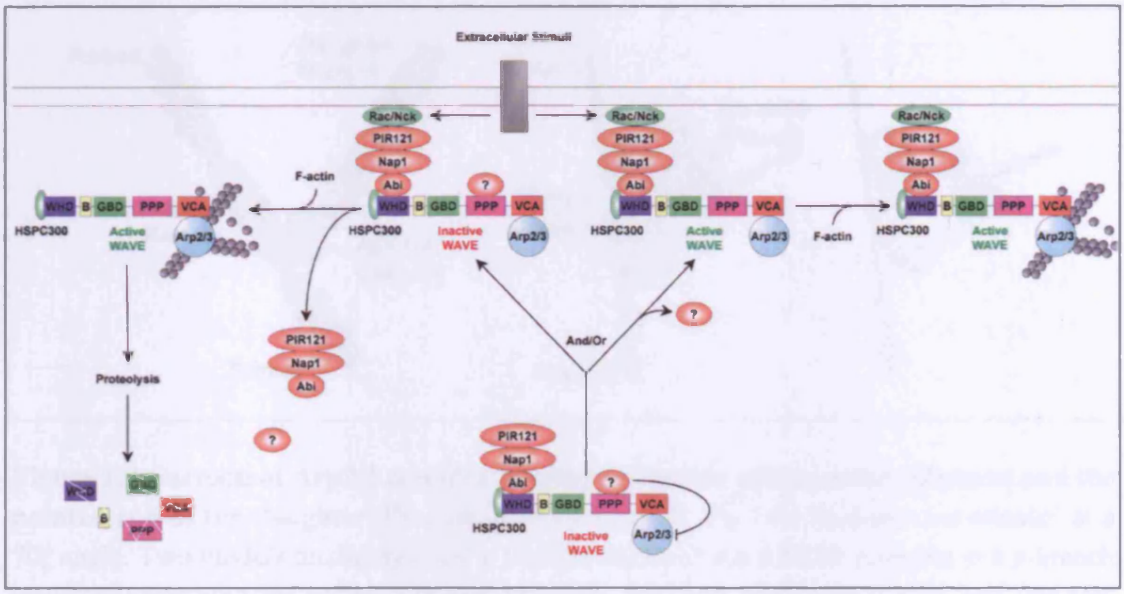

Figure 1.8 Model for WAVE regulation. In this model, WAVE constitutively interacts with the Arp2/3 complex. However, in resting conditions Arp2/3 is not activated, either because binding of WAVE to the PIR121-Nap1-Abi-HSPC300 complex prevents the interaction of WAVE-Arp2/3 with an essential co-activator (e.g. F-actin) or because it is mislocalised. Extracellular stimuli, through the activation of Rac or the mobilization of Nck, recruit the pentameric complex to the plasma membrane. WAVE activation requires its proper localisation plus, in this model, the presence of F-actin and/or the release of the additional protein(s). Alternatively, a complex composed of WAVE, HSPC300, and Arp2/3 is released first, and then activation takes place in the presence of F-actin and the signal is terminated by the degradation of free WAVE proteins. (Bompard et al., 2004)

The Arp2/3 complex is a stable complex of seven proteins, including two actin-related proteins Arp2 and Arp3, and the subunits p40, p34, p20 and p16. Electron microscopy analysis of the branched filament array in lamellipodia has shown that the Arp2/3 complex sits at the branch junctions of filaments in the actin network

(Svitkina and Borisy, 1999). Accordingly, biochemical and microscopic experiments have established that the Arp2/3 complex causes branching of new actin filaments (daughter filaments) at 70° angles from pre-existing filaments (mother filaments) (Amann and Pollard, 2001; Millard et al., 2004). Branching can also occur from the barbed ends of growing filaments (Pantaloni et al., 2001) (Figure 1.9). Notably, Arp2/3 alone displays no activity on actin polymerisation *in vitro* and only its association with "nucleation promoting factors" such as WAVE or WASP leads to initiation of filament branching.

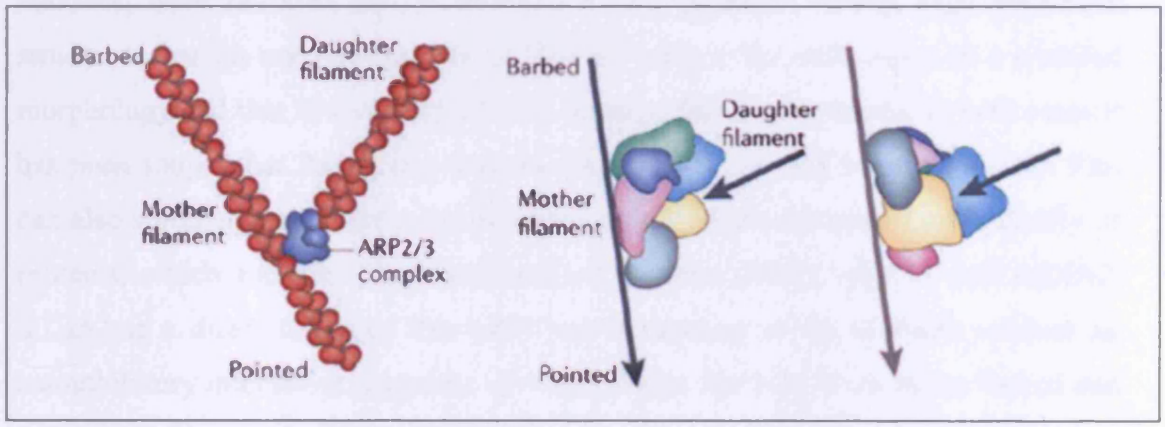

Figure 1.9 Cartoon of Arp2/3 complex binding to the side of the mother filament and the pointed end of the daughter filament in the y-branch. The two filaments are oriented at a 70° angle. Two models on the right show the orientation of the ARP2/3 complex at a y-branch junction. Light blue and yellow subunits represent Arp2 and Arp3 respectively, and associate with the pointed end of the daughter filament. The other subunits mediate contacts with the mother filament. (Goley and Welch, 2006)

Rho proteins, as members of Rho family small GTPases, have an important role in regulating actin organisation, especially in motile cells. Microinjection of constitutively active Rho or extracellular signals, such as lysophosphatidic acid (LPA) and bombesin, which lead to the activation of Rho, induced formation of actin stress fibres and focal adhesions in fibroblasts (Ridley et al., 1992). In addition, Rho proteins have been known to act at the rear of the migratory cells and to be responsible for stress fibre formation and adhesion dynamics (Amano et al., 1997). Active Rho generates contractile forces through ROCK activation. ROCK is a serine/threonine kinase that mediates myosin light chain (MLC) phosphorylation leading to formation of stress fibres and focal adhesions. However, recent studies

have shown that RhoA can also accumulate at membrane protrusions during cell migration in randomly migrating cells and also sporadically in retracting tails, but is present in lower levels in the cell body. In contrast to randomly migratory cells, PDGF stimulation can induce membrane protrusions even though RhoA activity is low, perhaps because PDGF strongly activates Rac, which has previously been shown to antagonise RhoA activity (Pertz et al., 2006). These and other data show that different extracellular cues induce distinct patterns of RhoA signalling during membrane protrusion. Cell migration studies in tumour cells, using three-dimensional matrices, have revealed that some tumour cells generate leading edge protrusive structures that do not require Rho or ROCK, while other cells move in a rounded morphology and that Rho and ROCK are essential for the movement. In both cases it has been shown that Rac is required for migration (Sahai and Marshall, 2003). Rho can also stimulate new actin polymerisation at barbed ends through formin family of proteins, which includes diaphanous-related formins (DRF), mDIA1 and mDIA2. mDIA1 is a direct target of Rho-GTP and its binding to the GTPases relieves an autoinhibitory interaction, exposing an FH2 domain that then binds to the barbed end of an actin filament. mDIA1 also contains an essential FH1 domain, which interacts with the profilin/actin complex and hence delivers it to the filament end. The main characteristic of mDIA is that once it has added an actin monomer to the existing actin filament, it remains bound to the barbed end and is ready to add another actin monomer. This progressive mechanism is known as a "leaky cap" mechanism (Figure 1.10).

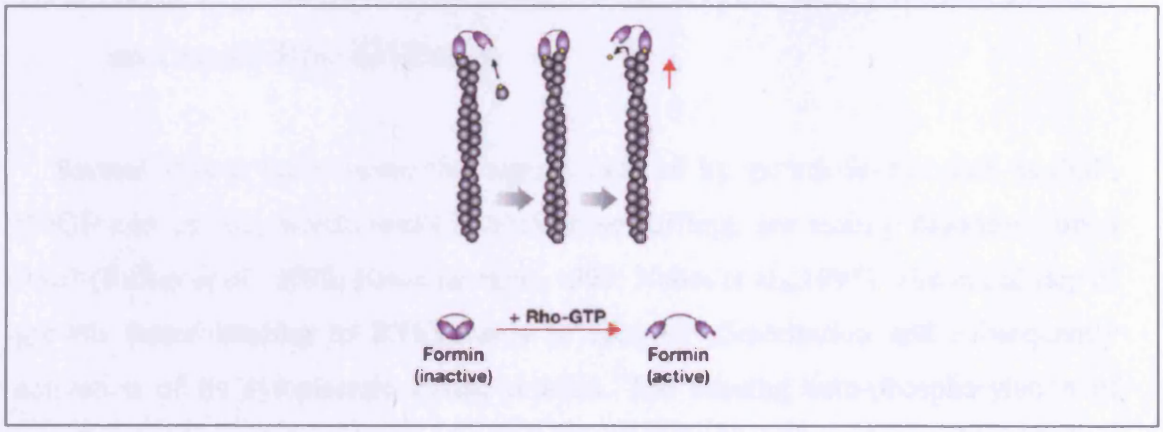

Figure 1.10 Rho-dependent activation of formins. Rho activates formins to promote linear elongation of filaments at barbed ends. (Jaffe et al., 2005)

In addition to the control of site-directed *de novo* actin nucleation, Rac, Cdc42 and Rho have also been shown to mediate a signalling cascade leading to the regulation of actin depolymerising proteins (ADF/Cofilin). ADF/cofilin severs actin filaments leading to an increase in uncapped barbed ends that serves as sites for actin polymerisation and filament elongation (Ghosh et al., 2004) and promotes actin monomer dissociation (depolymerisation) from the pointed ends (Pollard et al., 2003). These two processes are important for progressive membrane protrusions and actin turnover. Cofilin activity is tightly regulated by upstream signalling events and is affected by phosphorylation, phosphoinisitol-lipid binding, changes in intracellular pH and through protein-protein interactions. Phosphorylation at Ser-3 site in cofilin blocks its ability to bind to actin and therefore its severing and depolymerisation activity. Cofilin phosphorylation is promoted by LIMK, which in turn is activated by PAK-family of Rac and Cdc42-dependent kinases (Yang et al., 1998) (Figure 1.11). LIMK–dependent phosphorylation of cofilin can also been induced by Rho acting through its target Rho kinase (ROCK) in an event in the stabilisation the actin:myosin filaments (Ohashi et al., 2000). Slingshot (SSH) is the Ser-3 cofilin phosphatase and can re-activate cofilin (Niwa et al., 2002). Signalling events upstream of SSH are not well defined, although there are reports linking SSH to PI3K (Nishita et al., 2004) and Rho (Tanaka et al., 2005) signalling.

1.2.5 Actin organisation regulated through cross-talk between PI3K and small Rho-GTPases

Several studies have shown that signals induced by growth factors such as EGF, PDGF and insulin, which result in membrane ruffling, are mainly dependent upon Rac1 (Ridley *et al.*, 1992; Hawkins et al., 1995; Nobes et al., 1995). The initial step of growth factor binding to RTKs leads to receptor dimerisation and subsequently activation of its cytoplasmic kinase domain. The ensuing auto-phosphorylation of tyrosine residues of the receptor C-terminal tail and adaptor proteins enables binding of a variety of SH2 and PTB (phosphotyrosine binding) domain-containing effector proteins, thus leading to the generation of signalling platforms composed of

multiprotein complexes. One such complex is a heterodimeric PI3K. Importantly, the activation of PI3K is shown to link insulin-dependent stimulation to Rho family small GTPases activation, primarily Rac and actin cytoskeleton rearrangements (Figure 1.11).

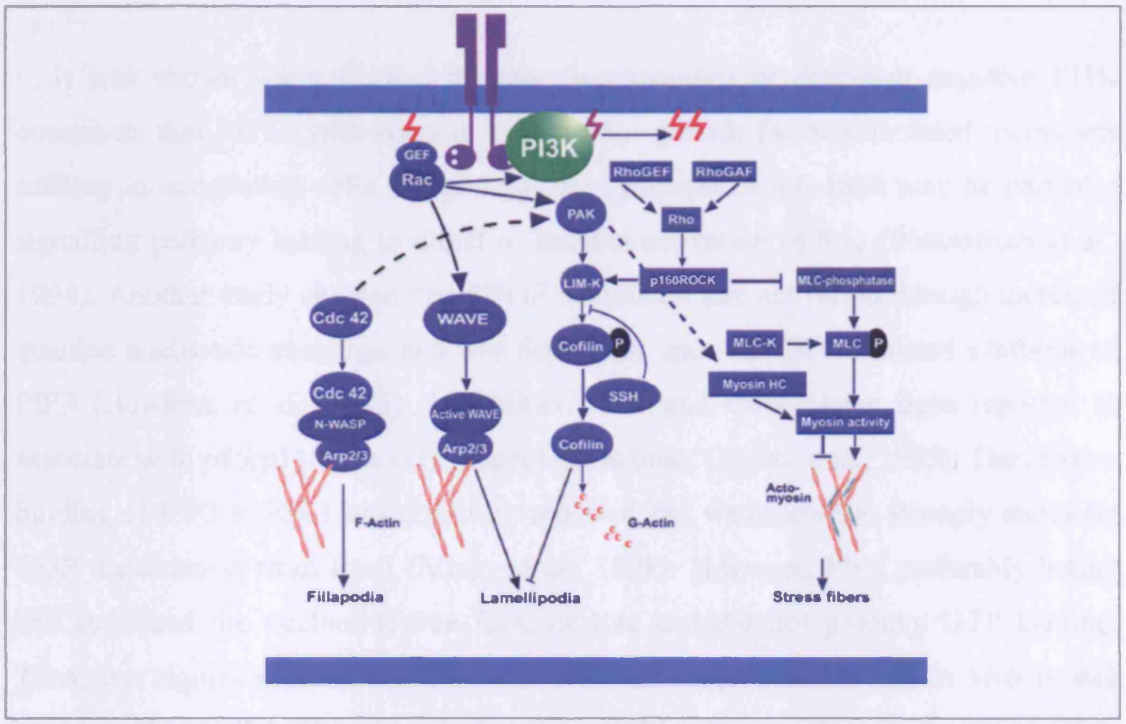

Figure 1.11 Signalling pathways downstream of PI3K affecting actin cytoskeleton organisation.

The actin cytoskeleton facilitates propagation of the morphological, metabolic, and nuclear effects of growth factors such as insulin by regulating proper subcellular distribution of signalling molecules that participate in the insulin signalling pathway (Tsakiridis et al., 1999). Studies on the involvement of the actin cytoskeleton in the initiation and regulation of insulin signals showed in muscle cells in vitro that insulin induces a rapid actin filament reorganization that coincides with plasma membrane ruffling and intense accumulation of pinocytotic vesicles. Initiation of these effects of insulin requires an intact actin cytoskeleton and activation of PI3K. The recruitment of PI3K subunits and glucose transporter proteins to regions of reorganized actin have been observed. In both muscle and adipose cells, actin disassembly inhibits early insulin-induced events such as recruitment of glucose transporters to the cell surface and enhanced glucose transport. Additionally, actin disassembly inhibits more

prolonged effects of insulin, including DNA synthesis and expression of immediate early genes such as c-fos. Intact actin filaments appear to be essential for mediation of early events such as association of Shc with Grb2 in response to insulin, which leads to stimulation of gene expression.

It was shown using PI3K inhibitors (wortmannin) or dominant negative PI3K constructs that PIP3 synthesis was required for growth factor-stimulated membrane ruffling in endothelial cells, suggesting that synthesis of this lipid may be part of a signalling pathway leading to direct or indirect activation of Rac (Wennstrom et al., 1994). Another study showed that PDGF stimulated Rac activation through increased guanine nucleotide exchange and was dependent upon PDGR-stimulated synthesis of PIP3 (Hawkins et al., 1995). In addition, Rac and Cdc42 have been reported to associate with p85/p110 in a GTP-dependent manner (Tolias et al., 1995). The *in vitro* binding of PIP3 to Rac1 has also been reported and was shown to strongly stimulate GDP dissociation from Rac1 (Missy et al., 1998). However, PIP3 preferably bound and stabilised the nucleotide-free form of Rac and did not promote GTP loading. Thus, the significance of this interaction for the regulation of Rac *in vivo* is still unclear. The availability of *in vivo* assays capable of measuring the levels of GTP-loaded Rac has helped to reinforce the functional link between PI3K and Rac activation, providing the biochemical evidence of a PI3K-Rac signalling pathway.

It is also important to note that Rac is not involved in all aspects of PI3K signalling. For example, PI3K does not use Rac to couple the insulin receptor to glucose uptake in adipocytes, but Rac is required for insulin stimulated membrane ruffling (Marcusohn et al., 1995). Cdc42 activity has also been linked to the PI3K signalling. Jimenez *et al.* have shown that PDGF stimulates Cdc42 activity by a pathway that involves N-WASP and the p85 subunit of the PI3K, but is independent of the catalytic activity of PI3K (Jimenez et al., 2000).

The important functional link of PI3Ks to the actin cytoskeleton is the observed role for these enzymes in the regulation of cell migration, towards chemical gradients (Servant et al., 2000; Jin et al., 2000), since PIP3 has been found to mediate the effect of the growth factors on the formation of the peripheral ruffles implicated in cell

migration (Merlot and Firtel, 2003). It has been proposed that a PIP3/PIP2 gradient exists in migratory cells upon growth-factor stimulation, with PIP3 at the leading edge, PIP2 at the rear, and mainly Cdc42 recruited at the leading edge as a major regulator of cell polarity. Also in the moving cells that respond to chemotactic gradients, such as in neutrophils and *D. discoideum*, PIP3 is produced locally and transiently at the leading edge of these cells (Van Haastert and Devreotes, 2004). The potential to trigger Arp2/3–dependent actin assembly at the membrane sites, by the production of PIP2 or PIP3, depends on which membrane receptors are stimulated and which cell system is used (Insall and Weiner, 2001).

The missing molecular links in PI3K signalling to small GTPases appear to be GEFs and GAPs, as it seems that some of them have PH-domains (Di Paolo and De Camilli, 2006). In the past few years, several GEFs (e.g. Vav1, DOCK180, Sos1, TIAM1) have been implicated as PI3K-dependent, linking Rac downstream of the PI3K signalling pathway *in vivo* (Han *et al.*, 1998; Kobayashi et al., 2001; Innocenti et al., 2003). For example, son of sevenless (Sos) is a dual-specificity GEF, with one Ras-specific catalytic domain and another domain for Rac. *In vitro*, PIP3 has been shown to bind to the PH domain of Sos and weakly activate Rac-GEF activity in immunoprecipitates from COS cells (Innocenti et al., 2003). The Sos1 Rac-GEF activity downstream of receptor tyrosine kinase appears to require a complex with Eps8 and Abi1 (Scita et al., 1999; Scita et al., 2001). Localisation of Sos1 to actin structures is mediated by Eps8, while its Rac–GEF activity appears to depend on the interaction of the p85 regulatory subunit of class Ia PI3K with Abi1 (Innocenti et al., 2003). The upstream signal for recruitment of p85 to this complex is unclear, and it may be constitutively associated. Recently, it has been reported that class II phosphoinositide 3-kinase C2β (PI3KC2β) associates with the Eps8/Abi1/Sos1 complex and is recruited to the EGF receptor as a part of a multiprotein signalling complex that also involves Shc and Grb2 (Katso et al., 2006). Increased expression of PI3KC2β in A-431 epidermoid carcinoma cells resulted in stimulated Rac activity and enhanced membrane ruffling, and increased migration speed of the cells. Tiam1 (T-cell lymphoma invasion and metastasis) comprises a DH domain, consensus sequences for phosphorylation by several protein kinases, a PEST domain, a Discs-large homology region and two PH domains, one located on each side of the DH

domain. N-terminal PH domain can interact with PIP3, bringing Tiam1 to the plasma membrane. When cellular PI3K activity is stimulated, GTP-Rac increases in agreement with the idea that PIP3 stimulates the GEF activity of Tiam1 (Fleming et al., 2004). Vav is probably the most studied Rac-GEF. Crespo et *al.* showed that upon stimulation with antigens or mitogens, Vav1 is tyrosine phosphorylated and this is sufficient to activate Vav Rac-GEF activity *in vitro* and *in vivo* (Crespo et al., 1997). PI3K is thought to modulate the activation of Vav1 by influencing its degree of tyrosine phosphorylation, but this was found to be dependent entirely on the system used.

Finally, phosphoinositides may regulate actin polymerisation through direct binding with small Rho-GTPases. PIP2 governs actin polymerisation through its binding to N-WASP and cooperation with Cdc42. It is thought that PIP2 triggers a conformational change in N-WASP that allows its binding to and activation of the Arp2/3 complex (Miki et al., 1996). Binding to PIP2 also appears critical for the function of proteins such as the ezrin/radixin/moesin family that act as adaptors linking the plasma membrane to the actin cytoskeleton. Thus, any changes in the actin cytoskeleton organisation are mirrored by changes in cell membrane dynamics. Several other actin binding proteins also appeared to have PIP2 binding domains, suggesting these are important for maintaining actin organisation and cell shape. PIP3 may also be important for directly controlling actin assembly, as it appears that WAVE can bind preferentially to PIP3 (Oikawa et al., 2004). In addition, given the relative low abundance of agonist stimulated PI3K lipid products in comparison with PIP2 or other PIs, it is generally believed that PI3K phosphoinisitides (i.e. PIP3) play a regulatory rather than a direct mechanistic role in the organisation of the actin cytoskeleton.

In conclusion, cross-talk between small Rho GTPases and PI3K signalling has been intensively studied and it has been firmly established that changes in cell morphology, polarity and motility are dependent upon PI3K activity mediated by Rho family GTPases or through direct binding to phosphoinositides. Numerous downstream targets of small Rho GTPases have also been extensively investigated for their ability to contribute to actin dynamics. Currently there are three major models,

through which small Rho GTPases, particularly Rac, could regulate actin dynamics, all contributing to enhance protrusions at the cell cortex:

- *De novo* nucleation of actin filaments (F-actin) from monomers (G-actin) and filament elongation, resulting in the formation of a branched array of filaments by proteins of the profilin, WASP, WAVE and Arp2/3 complexes.
- Acceleration of actin turnover by proteins such as ADF/cofilin.
- Regulated exposure of existing barbed ends after dissociation of high affinity filament capping proteins, such as gelsolin.

Figure 1.12 is a hypothetical model that integrates all three models for regulation of actin dynamics in response to external stimuli (Pollard et al., 2001).

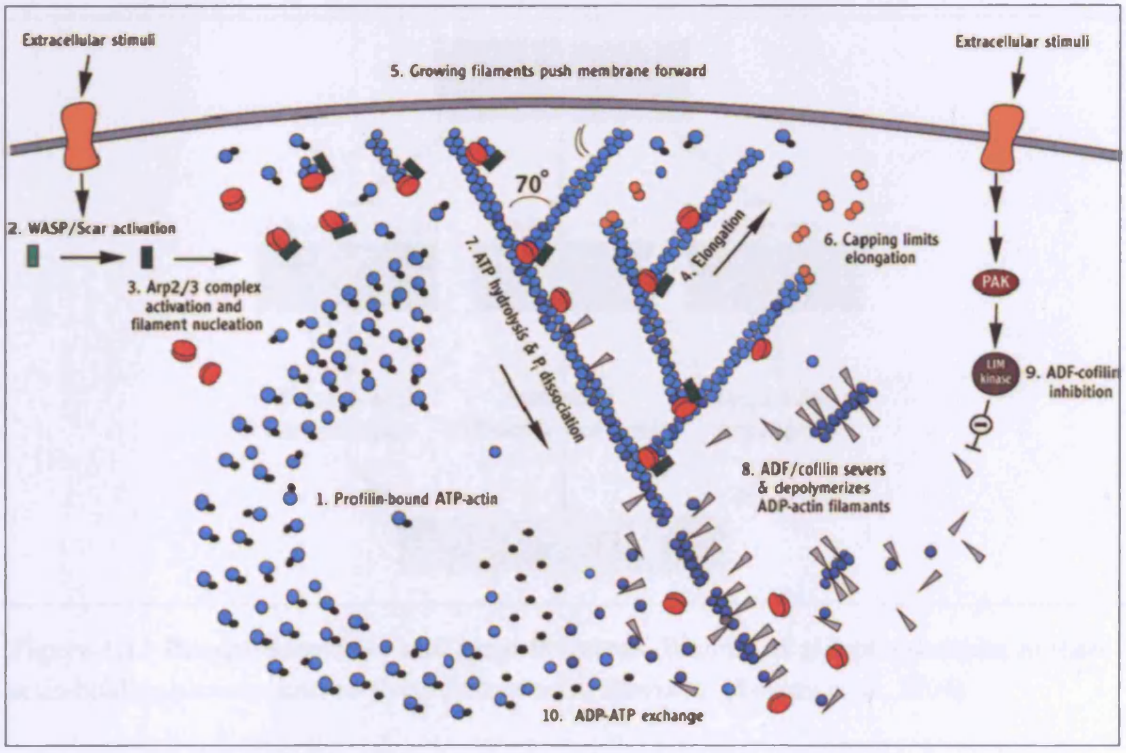

Figure 1.12 Hypothetical cartoon of dendritic nucleation model for actin polymerisation, capping, and network formation at the leading edge of a motile cell (Pollard et al., **2001).** The model proposes that, in the absence of free barbed ends, cytoskeletal components are held in a metastable state, poised for assembly (**step 1**). Activation of WASP family proteins (**step 2**) activates the Arp2/3 complex to create new barbed ends at a constant rate (**step 3**). These filaments grow rapidly (**step 4**) and push the membrane forward (**step 5**). After a short time, growth of barbed ends is terminated by capping (**step 6**). Constitutive ATP hydrolysis within actin filaments and dissociation of phosphate (**step 7**) triggers severing and depolymerisation of older filaments by ADF/cofilins (**step 8**) at a rate that is controlled by some of the same signals that stimulate assembly (**step 4**). Nucleotide exchange catalysed by profilin recycles ADP-actin subunits back to the ATP-actin monomer pool (**step 10**). In a continuously moving cell, assembly and disassembly are balanced.(Pollard et al., 2001)

Arp2/3, cofilin and other actin binding proteins involved in Rac-dependent changes in actin organisation have domains that bind to phosphatidylinositols, mainly PIP2 or PIP3 (Machesky and Insall, 1999; Condeelis et al., 2001; Xian and Janmey, 2002; Pollard *et al.*, 2003), thus providing an additional link between PI3K and Rac in the regulation of actin cytoskeleton organisation. Figure 1.13 is a simplified schematic representation of this cross-talk. The signalling cascades are likely to be more complicated as the various inputs from other signalling pathways activated by RTKs and negative feedback loops in the signalling network could feed into any of the downstream targets, contributing to regulated changes that drive the alterations in actin organisation.

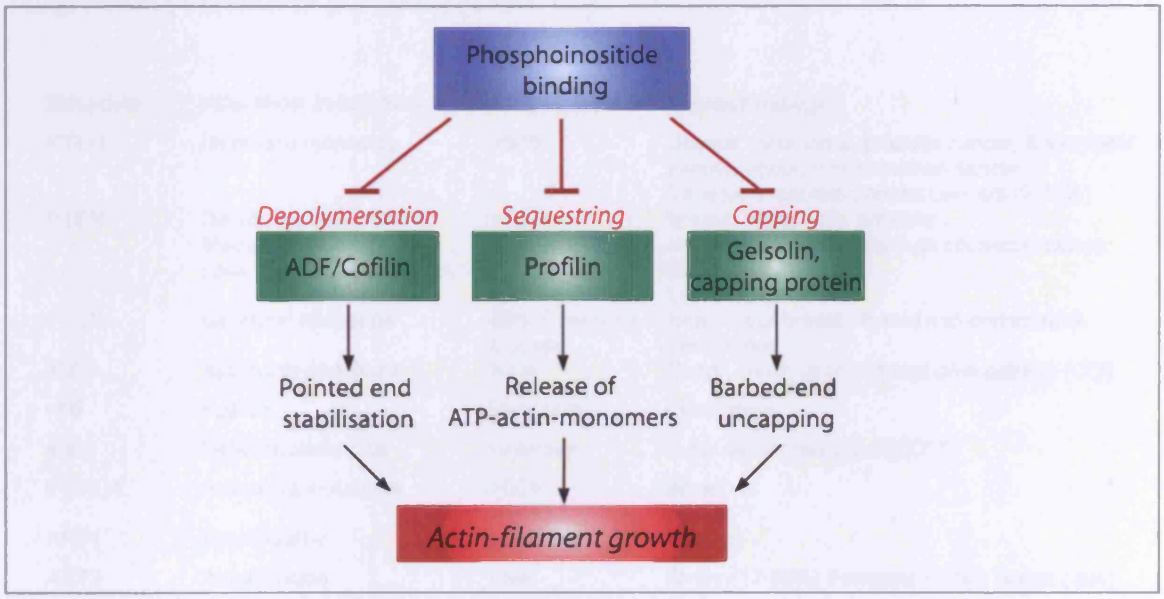

Figure 1.13 Phosphoinositides and actin filaments. Binding of phosphoinositides to these actin-binding proteins favours the growth of actin filaments. (Revenu et al., 2004)

The focus of my study in this thesis is on PI3K signalling-dependent change and the actin cytoskeleton in response to growth factor treatment, as well as in examining cross talk between PI3K and small Rho GTPases and actin-binding proteins, which I have carried out using a combination of proteomic, genomic and cell biology methods.

1.2.6 PI3K signalling and cancer

The PI3K signalling pathway regulates many normal cellular processes including cell proliferation, survival, growth, and motility (i.e. growth regulation is important during development and in adulthood, to ensure that an organism and its organs grow to appropriate and reproducible size). However, the PI3K signalling pathway is also targeted by genomic aberrations including mutations, amplifications and rearrangements more frequently than any other pathway in human cancer, with the exception of the p53 and retinoblastoma (Rb) pathways, which also cross-talk at multiple levels and constitute a signalling network implicated in tumour initiation and progression (Vivanco et al., 2002) (Table 1.2).

Molecule	Alteration in tumours	Frequency	Tumour lineage
PTEN	Mutations (somatic)	>50%	Glioma, melanoma, prostate cancer, Endometria cancer, endometrioid ovarian cancer Variable in sporadic breast cancers (2-30%)
PTEN	Decreased expression Methylation Loss of heterozygosity	>50%	Breast, melanoma, prostate Microsatellite instability-high colorectal cancer Endometrial cancer Leukaemia
PTEN	Germinal mutations	80% Cowden's disease	High risk of breast, thyroid and endometrial carcinomas
p85	Activating mutations	Rare	Ovary, colon, glioma, lymphoma cell line (CO)
p85	Fusion	Very rare	Lymphoma
p85γ	Deletion mutations	Unknown	Lung cancer cell line (HCC15)
PI3KCA	Activating mutations	>50% >20%	Bowel Breast
AKT1	Amplification	Low	Gastric
AKT2	Amplification	Low	Ovary (12-25%) Pancreas (20%), breast (rare)
AKT2	Mutation	Low	Colorectal
AKT3	Overexpression	Low	Hormone-resistant prostate and breast cancer
PDK1	Mutation	Low	Colorectal
$p70^{S6}$ kinase	Amplification	30%	Breast
TSC1/2	Mutation	>50%	Tuberous sclerosis
Forkhead family	Translocations	>50% Low	Alveolar rhabdomyosarcoma Acute leukaemia
TCL1	Rearrangement	Unclear	T-cell leukaemia Chronic lymphocytic leukaemia

Table 1.2 Abnormalities in the PI3K/Akt signalling pathway in cancer. (Hennessy et al., 2005)

The first link between PI3K and tumourgenesis was established in the 1980s, when PI3K was discovered due to its association with the oncoproteins (Sugimoto et al.,

1984). In addition, mutants of polyoma middle T that failed to bind PI3K were compromised in their ability to transform fibroblasts and polyoma middle T-transformed cells had elevated levels of PIP3 (Whitman et al., 1985). In 1997, the p110α catalytic subunit of PI3K was identified as an avian retrovirus-encoded oncogene that could transform chick embryo fibroblasts *in vitro* (Chang et al., 1997).

PI3K generates cell survival signals that allow them to withstand apoptotic stimuli. Many tumour cells display elevated levels of PI3K products as a result of deletion of the phosphatase PTEN, activation of Ras or expression of autocrine growth factor and under these conditions cells are relatively resistant to apoptosis (Downward, 2004a). Several studies have supported the role of PI3K as an oncogene in tumourgenesis. For example, Samuels *et al.* reported that *PIK3CA* gene, which encodes the p110α catalytic subunit, was the only gene with somatic (i.e., tumour-specific) mutations after they have examined 117 exons that encode the predicted kinase domain of the PI3K and PI3K-like genes in 35 colorectal cancers. Subsequent sequence analysis of all coding exons of *PIK3CA* in 199 additional colorectal cancers revealed mutations in a total of 74 tumours (32%). Further analysis from this work also showed that *PIK3CA* mutations generally arise late in tumourgenesis, just before or coincident with invasion (Samuels et al., 2004). These data suggest that *PIK3CA* is likely to function as an oncogene in human cancer, and clustering of mutations within *PIK3CA* could make this gene an excellent marker for early detection of cancers or monitoring cancer progression.

As mention previously, PTEN is a negative regulator of PI3K. It was identified as a tumour suppressor when genetic studies revealed that a locus on chromosome 10q23, in which the PTEN gene was found, was frequently mutated in advanced cancers. PTEN has been found to undergo inactivation in a number of additional neoplasia, most frequently endometrial and prostate carcinomas, melanomas and thyroid tumours (Vivanco et al., 2002). In addition, germinal mutation of PTEN has been linked to conditions with an increased predisposition to cancer (Cowden's disease, Bannayan-Zonan, Riley-Ruvalcaba, and Lhermitte-Duclos syndromes) (Waite and Eng, 2002). Interestingly, inactivation of the PTEN gene by homologous

recombination in mice gave rise to animals with increased predisposition to neoplasia (Stambolic et al., 2000).

Furthermore, Akt, which appears to be the main downstream target of PI3K, is involved in the development of tumours, since its amplification and aberrant upregulation were found to be a significant signature in various human malignancies (ovarian, pancreatic, breast, gastric, head and neck) (Testa and Bellacosa, 2001; Altomare and Testa, 2005). During tumourgenesis, active Akt can turn off cell apoptosis by phosphorylation and inactivation of FOXO family of forkhead transcription factors (AFX, FKHR and FKHRL1) and pro-apoptotic Bcl-2 family member Bad. In addition, Akt promotes cell survival by indirectly activating the pro-survival transcription factor nuclear factor-κB (NF-κB) through phosphorylation and inhibition of I-kB kinase (IKK). Furthermore, Akt blocks apoptosis by inactivating the tumour-suppressor p53, a nuclear transcription factor that affects cellular functions such as transcription, DNA synthesis and repair, cell cycle arrest, senescence and apoptosis. This indirect inactivation of p53 is mediated by Akt-induced phosphorylation of the oncoprotein Mdm2 (murine double minute), which in the phosphorylated state cannot enter into the nucleus and activate p53. The PI3K/Akt signalling pathway also regulates cell proliferation by controlling cell cycle progression and growth. Cell growth is controlled mainly by regulation of protein synthesis, thus the deregulation of proteins synthesis can contribute to the abnormal growth seen in tumour cells. Protein synthesis and cell growth mainly depend on nutrition and growth factors and they are regulated by the target of rapamycin (TOR) and S6K signalling pathways, downstream of PI3K/Akt. PI3K may contribute to other aspects of tumourgenesis in Akt-independent manner as well. As mention previously, PIP3 regulates small GTPase by activating a subset of GTP-GDP exchange factors (Bar-Sagi and Hall, 2000). Since Rac controls the actin cytoskeleton and cell motility and is important for Ras-mediated transformation, PI3K might activate both Rac and Ras-dependent invasion events that contribute to metastasis (Rodriguez-Viciana et al., 1997). Furthermore, the mTOR/Rictor complex, which is downstream of Akt, was found to modulate the phosphorylation of protein kinase C α (PKCα) and alters the actin cytoskeleton (Sarbassov et al., 2004). Akt can also phosphorylate and activate endothelial nitric oxide synthase (eNOS) and the production of nitric oxide (NO), an

important regulator of endothelial cells. Overexpression of eNOS has been associated with tumours, thus the PI3K/Akt pathway may also contribute to tumour angiogenesis. Given the importance of the PI3K signalling pathway in cancer and knowing that PI3K pathway is activated during tumourgenesis, makes PI3K an optimal target for drug development in cancer therapy. More than 20 companies and academic centres have declared active programs in this area (Table 1.3).

Effect on pathway	Target	Example	Company/centre	Status
Direct	PI3K	LY294002	Lilly	Poor pharmacology
		Wortmannin analogues	PROLX	Preclinical
		PX-866	Lilly	Preclinical leads
		SF1124	Semafore	Preclinical leads
		PEG Wortmannin	Echelon	Preclinical
			Wyeth	Preclinical
			Baxter	Preclinical
			ICOS	Preclinical
	p110δ		Piramed	
	p110α		Piramed	
	Pan-inhibitor		Cerylid	
		KN309	Cerylid/Kinacia	
	PDK1		Berlex	All are preclinical
			Lilly	
			ICOS	
			Vertex	
	ILK		QLT	Preclinical
	AKT kinase domain		QLT	
			Abbott	
			Novartis	
			Lilly	
			Vertex	
			Roche	
			Celgene	
			Kinacia/Cerylid	
		PX316	BioImage	Screening
			PROLX	Preclinical
	PH domain	Milefosine	Zentaris	Approved in Europe for breast cancer
			Keryx	In clinical trails for leishmaniasis
			NIH	Preclinical
			Schering	
			Celgene	
	mTOR	Rapamycin	Wyeth	
		CCI779	Wyeth/NCI/CTEP	Approved
		Rad 001	Novartis	Phase II
		AP23573	Ariad	Phase II
		AP23841	Ariad	Phase II
		AP23573	Ariad	Preclinical
	$p70^{S6}$ kinase		Lilly	
	Forkhead family	Calmodulin inhibitors	Harvard	Clinical trails
			BioImage	Preclinical
Indirect	Growth factor receptors	EGFR	Multiple	Preclinical to approved
		HER2		
		Insulin		
		Integrins		
	Intracellular kinases	Src	Multiple	
		Abl		

Table 1.3 List of drugs in development that target the PI3K or related pathways. (Hennessy et al., 2005)

1.3 Background to methodology

1.3.1 RNA interference

RNA interference (RNAi) or post-transcriptional gene silencing is an ancient natural antiviral mechanism that can be used to turn off gene expression in a sequence specific-manner (Downward, 2004b). In the early 1990s, attempts to manipulate gene expression by scientists working in three different fields resulted in unanticipated gene silencing effects. Rather than ignoring such results, these researchers went on to document and further investigate the nature of such silencing, which was named "co-suppression" in plants, "quelling" in fungi and "RNA interference" in nematodes (Hammond et al., 2001). It all started in 1989, with the unexpected outcome of experiments performed by plant scientists at Advanced Genetic Sciences in Oakland, California (Napoli et al., 1990). The goal was to produce petunia plants with improved flower colours. To achieve this goal, they introduced additional copies of a gene encoding a key enzyme for flower pigmentation into petunia plants. Surprisingly, many of the petunia plants carrying additional copies of this gene did not show the expected deep purple or deep red flowers, but carried fully white or partially white flowers. When the scientists had a closer look, they discovered that both types of genes, the endogenous and the newly introduced transgenes had been turned off, and because of this observation, the phenomenon was first named "co-suppression of gene expression". However, the molecular mechanism behind this event remained unknown. Plant virologists made similar observations. At that time, it was known that plants expressing virus-specific proteins showed enhanced tolerance or even resistance against viral infection. They concluded that short viral RNA sequences could attack incoming viruses and stop them from multiplying and spreading throughout the plant. They performed reverse experiments and placing short pieces of plant gene sequences into plant viruses. After the infection of plants with these modified viruses, the expression of the targeted plant gene was suppressed. They named this phenomenon "virus-induced gene silencing" (VIGS). The two phenomenona, co-suppression and virus-induced gene silencing were later named post-transcriptional gene silencing (PTGS). PTGS was later detected in fungi and was

termed "quelling" (Romano and Macino, 1992). The wild type strains of the fungus *Neurospora crassa* were transformed with *albino* (*al-1*, *al-2* and *al-3*) transgenes that are required for carotenoid biosynthesis. It was observed that the transformed strains frequently displayed a white (albino) phenotype, indicating that both endogenous *albino* genes and the introduced *albino* transgenes were inactivated. Later, the phenomenon of quelling was found to be a general silencing phenomenon, and has not being restricted only to the albino genes. In 1998, a *Nature* paper by Craig C. Mello and Andrew Z. Fire reported a potent gene silencing effect after the injection of double stranded RNAs (dsRNAs) into *C. elegans* (Fire et al., 1998). In investigating the regulation of muscle protein production, they observed that neither mRNA nor antisense RNA injections had effects on protein production, but dsRNA successfully silenced the targeted gene. Because of this work, they coined the term RNA interference (RNAi). Eight years after this discovery, which over the years has proven to be an important research tool for studying different biological questions, Craig C. Mello and Andrew Z. Fire were awarded the Nobel Prize for medicine and physiology.

In nature, RNAi is considered an ancient evolutionary mechanism for protecting organisms from viral infections. Many viruses have RNA as a genetic material rather than DNA and go through at least one stage of their life cycle when they make double stranded RNA. When exposed to foreign genetic material (RNA or DNA), many organisms activate a highly specific immune response in order to silence the invading nucleic-acid sequences before these sequences can integrate into the host genome or subvert cellular processes. At the centre of these immune responses is a conserved enzyme machinery that integrates with dsRNAs and complementary mRNA (Mello and Conte, Jr., 2004). The general mechanism of RNAi has two main steps: initiation and effector steps (illustrated in Figure 1.14). In the first initiation step, dsRNAs, taken up by cells from the medium, are recognised by enzymatic machinery that converts the silencing trigger to ~21-25 nucleotide base pair RNAs called short interfering RNAs (siRNAs) (Figure 1.14 A). This ATP-dependent cleavage of dsRNA into siRNA is conducted by RNase III enzymes, known as Dicer enzymes. These enzymes are evolutionarily conserved from *Drosophila*, *Arabidopsis*, *Caenorhabditis* and *Neurospora*. The next effector step is enforced by the RNA Inducing Silencing

Complex (RISC), which uses siRNAs to recognise and cleave target mRNAs (Figure 1.14 B1-B4), which is then followed by degradation by exonucleases (Figure 1.14 B5).

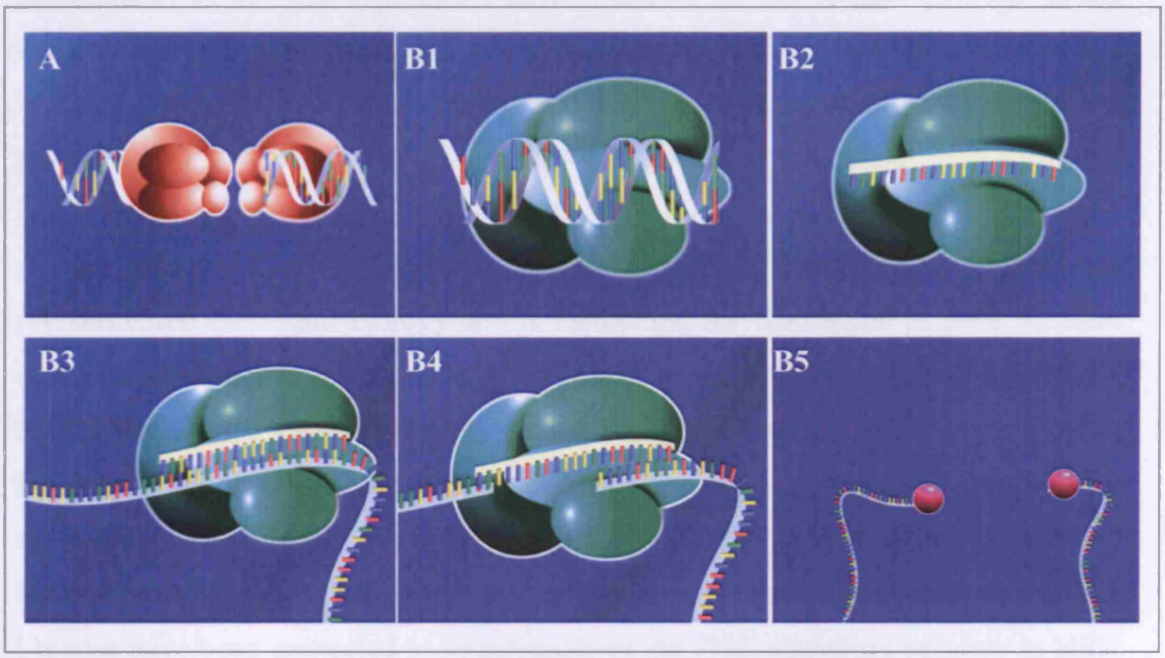

Figure 1.14 Mechanism of RNA interference. **A)** Initiation step: dsRNA is digested into 21-23 nt siRNAs by Dicer; **B**) Effector steps: **B1**) siRNA assembles into RISC; **B2**) Unwinding of siRNA by RISC in an ATP-dependent reaction; **B3**) siRNA guide the RISC to complementary mRNA; **B4**) RISC causes cleavage of mRNA; **B5)** Exonucleases degrade cleaved mRNA resulting in gene silencing.

Interestingly, RNAi does more than help to defend cells against foreign nucleic acids. It also guides endogenous developmental gene regulation, and can even control the modification of cellular DNA and associated chromatin. In some organisms, the RNAi signal is transmitted horizontally among cells, and in certain cases, vertically through the germ line from one generation to the next (Mello et al., 2004). The early useful application of RNAi technology in human cells proved difficult since the introduction of dsRNA into cells induces antiviral responses, which includes interferon production. This leads to altered gene expression and often cell death, limiting the ability of viruses (or alien dsRNA) to replicate and spread through the organism. The theory behind this is that the Dicer machinery had been lost during evolution of mammals and replaced with more sophisticated and complex defence

mechanisms which include the interferon system that is not present in invertebrates (Downward, 2004b). However, nowadays RNAi can be applied in mammalian systems by directly introducing siRNA molecules of less than 30 nucleotide base pairs, which do not induce the interferon response, but can trigger cleavage of the complementary mRNA sequences and silence genes. This is proof that evolution has kept the RNAi as a back-up system even after the development of the interferon system.

The emergence of RNAi as a technique to suppress gene expression has revolutionised molecular biology and is facilitating the elucidation of gene function on a genome-wide scale through large scale screening of phenotypic changes induced by RNAi-mediated gene silencing (Kiger et al., 2003; Dasgupta and Perrimon, 2004; Friedman and Perrimon, 2006). *C. elegans* and *D. melanogaster* are probably the most exploited species used in these types of studies, due to the fact, that *in vitro* RNAi treatments are highly efficient in gene expression knockdown. For example, siRNA libraries have been generated to target genes of the PI3K signalling pathway in HEK 293T cells (Hsieh et al., 2004), searching for genes that affected phosphorylation of Akt. To obtain a global view of RTK/ERK signalling, Friedman *et al.* performed an unbiased, RNAi genome-wide, high-throughput screen in *Drosophila* cells using a novel, quantitative, cellular assay monitoring ERK activation, and this revealed a list of effectors which can be targeted for drug therapy (Friedman et al., 2006). RNAi has also been used in parallel with drug inhibitor treatment in studying signalling pathways (O'Grady et al., 2005). Since the RNAi-mediated gene-silencing machinery is also intact in cancer cells, multiple *in vitro* siRNA studies have been carried out to evaluate the knockdown phenotype of oncogenes. For example, the effect of targeting the Bcr-Abl kinase oncogene in chronic myelogenous leukaemia (CML) cells was tested by Wilda *et al.* (Wilda et al., 2002). Silencing the Bcr-Abl fusion protein by siRNA induced a strong apoptotic response in CML cells, which was comparable with the cell death caused by treatment with Abl kinase inhibitor Gleevec (imatinib mesylate). Despite the proliferation of promising *in vitro* and *in vivo* studies for RNAi-based drugs, some concern has been raised regarding the safety of RNAi, especially the potential for "off-target" effects in which a gene with a coincidentally similar sequence to the targeted gene is also repressed (Bartz and Jackson, 2005). A

computational genomic study estimated that the error rate of off-target interactions is about 10%. One major study of liver disease in mice led to high death rates in the experimental animals, suggested by researchers to be the result of "over-saturation" of the dsRNA pathway (Grimm et al., 2006). Additionally, delivery of siRNA into mammalian cells remains a major hurdle for RNAi therapy. The two approaches to deliver siRNA *in vivo*: i) stably expressed siRNA precursor, such as short-hairpins RNAs, from viral vectors using gene therapy, and ii) delivery of synthetic siRNA by covalently linking the duplex RNA with lipids and/or delivery proteins, are often inefficient. Thus, if siRNAs are to be used as therapeutics further studies and optimisation are required. However, the advantage of RNAi therapy is that unlike resistance to other small molecules, which leads to an expensive and time-consuming search for new therapeutic agents, resistance to RNAi may be overcome by introducing a new siRNAs that targets a different site on the same mRNA. Moreover, siRNAs that target conserved sequences or multiple sequences at once may provide a solution to this problem (Dykxhoorn and Lieberman, 2005).

1.3.2 Proteomics and 2D gel-based protein separation

Proteomics is the large-scale study of proteins, their structure, function and expression, in a cell, organism or biological fluid. All of the proteins in an organism throughout its life cycle are considered to be its proteome. Compared to the genome, which is constant, the proteome is dynamic and changes throughout its biochemical interactions with both the genome and the environment. In an organism, there can be different proteome activities in various parts of the body, in different environmental conditions and at different life stages. Depending on which aspect of proteins is studied, proteomics can be divided into proteomic profiling, functional and structural proteomics based and can involve a broad range of combined technologies (Figure 1.15). Protein expression proteomics or profiling proteomics is the quantitative study of protein expression between samples that differ by some treatment variable. In this approach, protein expression of the entire proteome or of sub-proteomes between samples require the use of protein or peptide separation methods that are linked to

quantitation and protein identification methods (e.g. immunodetection or mass spectrometry-based identification). Information obtained by this approach can lead to discovery of proteins expressed differentially between samples, and the identification of novel proteins in signal transduction or disease-specific proteins. Functional proteomics is the study of the role of proteins, based on the presence of specific functional groups or based on their involvement in protein-ligand interactions and protein complexes. Many proteins need to interact with other molecules in order to perform their role. Therefore, knowing the interactions and the partners of a protein could help to discover and define its role in a cell. Functional proteomics also involves the study of protein post-translational modifications, such as phosphorylation, which could help define the activity, localization, and degradation of proteins and are often the key to understanding the function of proteins. Signalling pathways, which are considered as cascades of specific interacting protein required to activate cellular functions, can often be deciphered by functional proteomics. Structural proteomics attempts to determine the tertiary structure of proteins, the structure of protein complexes and small molecule-protein complexes. X-ray crystallography and prediction of protein structures by computational biology are its main tools. The information obtained from profiling, functional and structural proteomics will help piece together the overall architecture of cells and explain how expression of certain proteins gives a cell its unique characteristics.

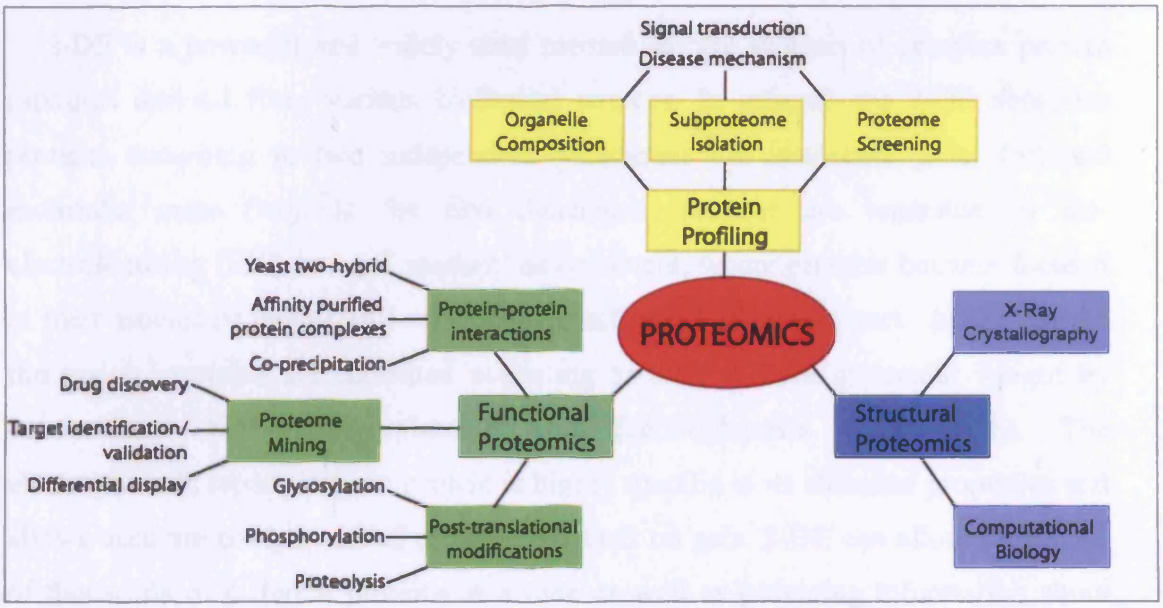

Figure 1.15 Types of proteomics and their application to biology.

Initial protein expression profiling studies began in 1975 with the introduction of two-dimensional gel electrophoresis by O'Farrell, who began mapping proteins from *Escherichia coli* (O'Farrell, 1975). Although many proteins could be separated and visualized, they could not be identified. Despite these limitations, shortly thereafter a large-scale analysis of all human proteins was proposed. The goal of this project, termed "the human protein index", was to use two-dimensional protein electrophoresis (2-DE) and other methods to catalogue all human proteins. However, lack of funding and technical limitations, such as the unavailability of robust tools for high-throughput identification of the proteins displayed by 2-DE, prevented this project from continuing. An important step in the 2-DE strategy was an introduction of protein labelling and detection methods, which were needed to define quantitative and qualitative differences between complex protein samples. The sensitivity of protein stains has always been a factor influencing the amount of information that can be extracted from 2D gels. In addition, the most significant breakthrough in proteomics has been the application of mass spectrometric methods for identification of gel-separated proteins, which has extended analyses beyond the mere display of proteins.

1.3.3 2-Dimensional gel electrophoresis and 2D-DIGE

2-DE is a powerful and widely used method for the analysis of complex protein mixtures derived from various biological sources. In general, the 2-DE separates proteins according to two independent parameters i.e. isoelectric point (pI) and molecular mass (M_r). In the first dimension, proteins are separated by iso-electrofocusing (IEF) in a pH gradient environment, where proteins become focused at their isoelectric points (pI) when they reach a net charge of zero. In the second dimension, proteins are separated according to their relative molecular weight by conventional SDS Polyacrylamide Gel Electrophoresis (SDS-PAGE). The electrophoretic separation of a protein is highly specific to its chemical properties and allows accurate comparison of proteins analysed on gels. 2-DE can allow separation of thousands of different proteins at a time as well as providing information about protein pI, M_r, post-translational modifications (which affect pI and MW) and the

relative amount of each protein, when a suitable protein staining or labelling method is used in combination. Usually each spot on the resolving two-dimensional gel corresponds to a single protein species within the sample, although in certain cases more than one protein can be found to co-migrate on a 2D gel. At present, there are no other techniques that are capable of simultaneously resolving thousands proteins from complex biological samples in one separation procedure. However, there are some drawbacks of 2-DE (i.e. poor resolution of high and low molecular weight proteins and hydrophobic and basic proteins, low gel-to-gel reproducibility in different experimental runs, it is also a labour intensive and expensive technique) that has limited its application in some proteomic studies.

Several reviews have outlined the different methods of choice for detection of gel separated proteins (Patton, 2000; Rabilloud, 2000; Patton and Beechem, 2002). Most strategies for protein detection in 2D gels use post-electrophoretic protein staining and a multitude of different methods have been described which differ in their sensitivity, specificity, linear dynamic range and compatibility with downstream identification mainly by mass spectrometry. Common strategies include:

i) Colloidal Coomassie blue G-250 staining, that has a detection range of 8-50 ng of protein/spot. It is simple to use and compatible with downstream MS (Neuhoff et al., 1988).

ii) Silver staining methods are employed normally with analytical gels due to their high sensitivity (typically 2-4 ng of protein/spot). However, classical silver-staining methods can be complex and are often incompatible with MS because of the aldehyde-based cross-linkers used in the sensitisation steps, and because silver ions can interfere with MS analysis. The non-linearity of the dynamic range in silver staining and the tendency of the dye to stain differently, based on protein amino acid composition, makes silver staining a poor choice for quantitation of protein expression.

iii) Fluorescent stains. There are numbers of these stains including SYPRO Ruby, SYPRO Orange, Deep purple etc. SYPRO Ruby is a transition metal organic complex that binds directly to proteins by electrostatic interactions, providing sensitivity similar to that of classical silver staining (1-2 ng of protein/spot) with a broad linear dynamic range, and is compatible with downstream mass

spectrometry-based protein identification. However, fluorescent dyes are usually expensive and require fluorescence scanners for analysis. Fluorescent stains have also been developed for the detection of specific sub-groups pf proteins, e.g. Pro-Q Diamond and Pro-Q Emerald have been reported for the detection of phosphorylated and glycolysated proteins, respectively. However, these stains have not been widely used. In addition, there are fluorescent stains (e.g. fluorescamine, fluorescein isocyanate, N-(7-di-methylamino-4-methylcoumarinyl) maleimide and dansyl chloride) that bind covalently to proteins. However, this type of labelling was reported to have low sensitivity and poor resolution on 2D gels.

Proteins can also be labelled prior to the electrophoretic separation using:

i) Radioactive labelling - perhaps the most sensitive covalent labelling method is *in vivo* (with $^{32}P/^{34}S/^{131-135}I$ isotopes incorporation) and *in vitro* (^{32}P-ATP kinase assay) radioactive labelling, which provides the widest linear dynamic range of detection. Radioactive labelled proteins are detected in-gel by exposing a film (autoradiography) or using a phosphorimager, which has a wider dynamic range than autoradiography, thus enabling better quantitative analysis. Although this detection method is powerful, it has some limitations. Radioactivity causes DNA damage and increased levels of p53 followed by cell cycle arrest and apoptosis. Moreover, radioactive compounds have a hazardous nature and are expensive.

ii) Fluorescent tags have been used for covalent labelling of proteins prior the separation (e.g. 5-(4,6-dichlorotriazine) aminofluorescein, 2-methoxy-2,4-diphenyl-3(2H)-furanone (MDPF) and dansyl chloride). Most of such dyes possess a charge that affects the electrophoretic properties of proteins and can cause artificial protein modification that can dramatically affect the ability to subsequent identifiy proteins by mass spectrometry. Importantly, advanced fluorescent covalent labelling of proteins was developed with the introduction of monobromobimane (MMBr)- and cyanine (Cy)- based dyes that react with cysteine and lysine residue, respectively.

Fluorescence two-dimensional difference gel electrophoresis (2D-DIGE) is a recently developed 2D gel-based proteomics technique that provides a sensitive, rapid and quantitative analysis of differential protein expression between two or more biological samples. Developed by Unlu *et al.* (Unlu *et al.* 1997), the technique utilizes charge- and mass- matched chemical derivatives of spectrally distinct fluorescent cyanine dyes (Cy3 and Cy5) which are used to covalently label protein lysine residues in different samples prior to mixing and separating the proteins on the same 2D gel. These cyanine fluorophors were modified to create the N-hydroxysuccinimidyl (NHS)-ester derivatives NHS-propyl-Cy3 and NHS-methyl-Cy5. A third cyanine dye, NHS-Cy2, was introduced, and these labels are commercially available from GE Healthcare (Figure 1.16).

Initially, NHS Cy3 and Cy5 dyes were used to label two different protein samples prior to running them on the same 2D gel electrophoresis (Unlu et al., 1997). This allows running two samples under identical electrophoretic conditions in a type of differential display format. Theoretically, to compare proteins derived from two differently-labelled samples, the dyes should be mass and charge matched and the dye modifications should not perturb the electrophoretic mobility of labelled proteins. For this reason, the size of the aliphatic chain (Figure 1.16 A) in the Cy dyes was originally modified to maintain a similar molecular weight between each dye and the dyes possess a positive charge which matches the positively charged amino groups they modify. The advantage of using lysine labelling is that almost all proteins contain at least one lysine residue, so most proteins in a complex sample can be labelled. The dyes are used under conditions of minimal stoichiometrical labelling, and ideally, just a single lysine residue in a protein molecule is labelled with estimated 3-5% of the total pool of the protein labelled. This minimal labelling is to keep proteins soluble, prevent large mass shift between labelled and unlabelled populations of proteins and reduce sample heterogeneity (Chan et al., 2005), while maintaining the sensitivity of detection (~1 ng of a protein per spot) and secure linearity over a wide dynamic range.

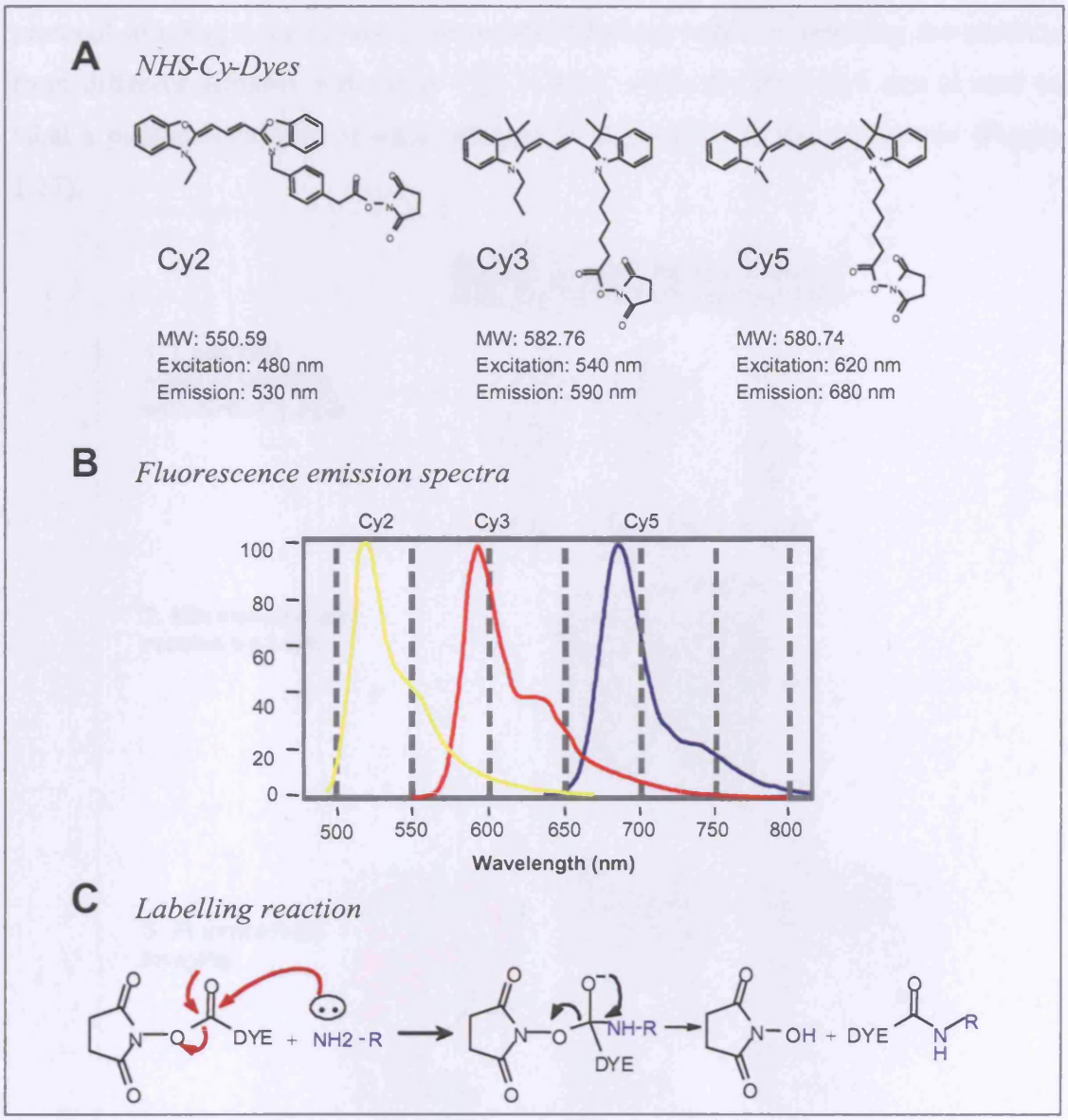

Figure 1.16 Characteristics of the NHS-Cy-dyes. A) Structure of the NHS-Cyanine dyes. Cy2, 3-(4-carboxymethyl)phenylmethyl)-3'-ethyloxacarbocyanine halide *N*-hydroxy-succinimidyl ester; Cy3, 1-(5-carboxypentyl)-1'-propylindocarbocyanine halide *N*-hydroxysuccinimidyl ester; and Cy5, 1-(5-carboxypentyl)-1'-methylindodicarbocyanine halide *N*-hydroxysuccinimidyl. Each dye has a similar molecular weight and single positive charge matching the charge of the modified primary amino group. **B**) Each dye displays distinct emission spectra enabling the individual detection of differentially labelled proteins at the appropriate wavelength without overlap of signals. **C**) The dyes have an *N*-hydroxysuccinimidyl ester reactive group triggering covalent interaction with the primary amine groups of lysine residues or the N-terminus.

The method of using the three Cy dyes was originally evaluated and applied by Tonge *et al.* and Gharbi *et al.* (Tonge et al., 2001; Gharbi et al., 2002). The general

protocol of using three Cy-dyes for protein labelling relies on labelling the proteins from different samples with either Cy3 or Cy5, while the third Cy2 dye is used to label a pooled consisting of equal amount of all samples in the experiment (Figure 1.17).

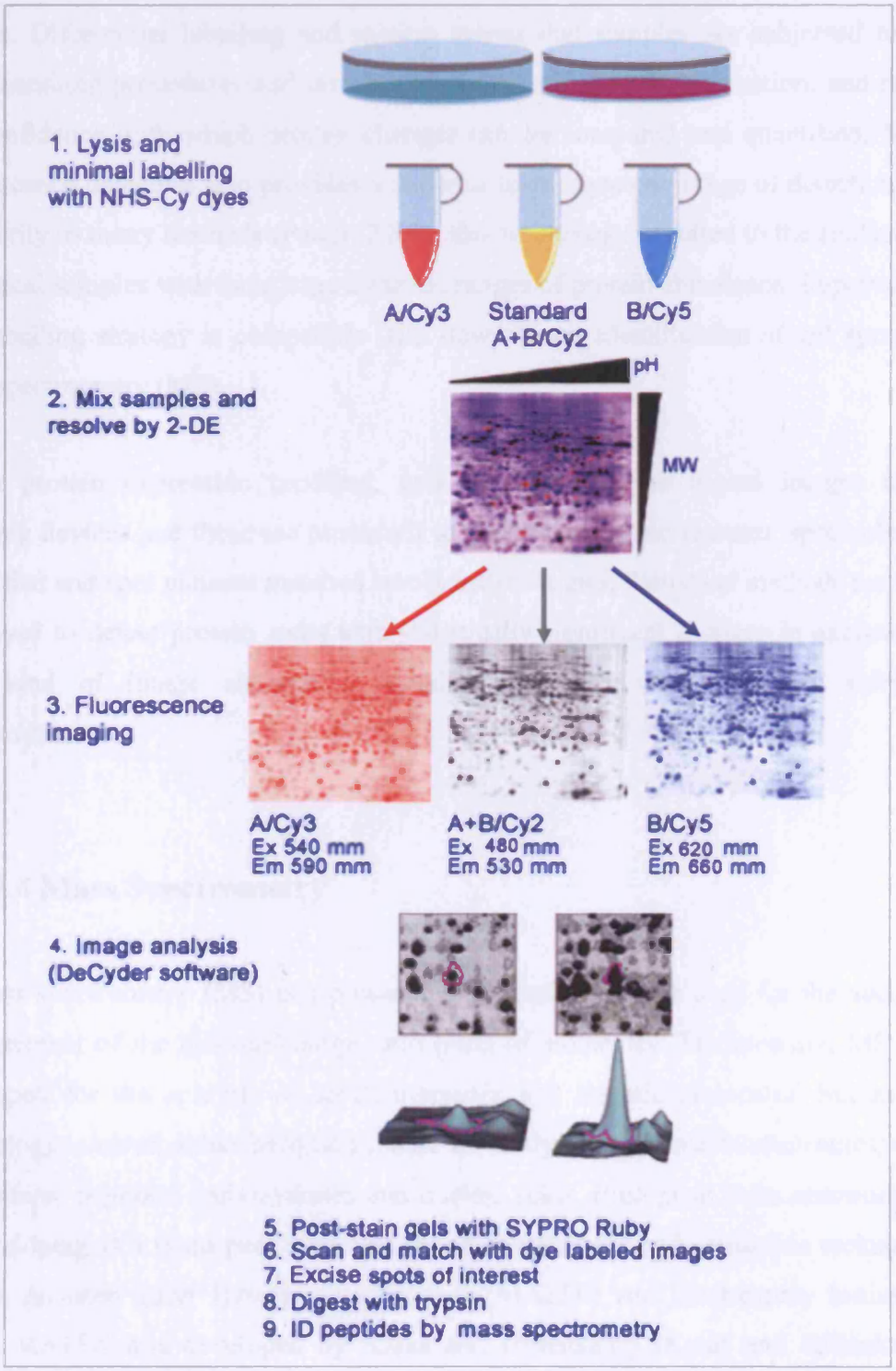

Figure 1.17 Schematic representation of 2D-DIGE protocol for minimal lysine labelling and using an internal standard for normalization.

Samples are then mixed appropriately and run in 2-D gel electrophoresis. The Cy2-labelled pool is run on all gels and acts as an internal standard for every protein spot on each of the gels, thereby improving spot matching across gels and increasing the accuracy of quantitation and statistical confidence of protein expression difference studies. Differential labelling and mixing means that samples are subjected to the same handling procedures and micro-environments during 2D separation, and raises the confidence with which protein changes can be compared and quantified. Since fluorescence detection also provides a superior linear dynamic range of detection and sensitivity to many methods (Patton 2000), this technology is suited to the analysis of biological samples with their large dynamic ranges of protein abundance. Importantly, this labelling strategy is compatible with downstream identification of gel spots by mass spectrometry (MS).

For protein expression profiling, gels are converted to digital images using scanning devices and these are processed to detect the protein features, spot volumes quantified and spot patterns matched across different gels. Statistical methods are then employed to detect protein spots with statistically significant changes in expression. This kind of image analysis is usually performed with dedicated software programmes.

1.3.4 Mass Spectrometry

Mass spectrometry (MS) is a powerful analytical technique used for the accurate measurement of the mass-to-charge ratio (*m/z*) of molecules. Traditionally, MS was developed for the analysis of small inorganic and organic molecules, but as the technology evolved, it has become suitable for analysis of various biomolecules, such as proteins, peptides, carbohydrates and nucleic acids. Biological mass spectrometry is developing at a rapid pace since the introduction of the soft ionisation techniques Matrix Assisted Laser Desorption Ionisation (MALDI) and Electrospray Ionisation (ESI). MALDI was developed by Karas and Hillenkamp (Karas and Hillenkamp, 1988; Hillenkamp et al., 1991) and Tanaka. ESI was developed by Fenn (Fenn et al.,

1989). In recognition of the development of ESI and for the development of soft laser desorption (SLD) Fenn and Tanaka received the Nobel Prize for Chemistry in 2002.

By definition, a mass spectrometer is composed of: i) an ion source; ii) a mass analyser; and iii) an ion detector. The function of the ion source is to convert an analyte into gas phase ions in a vacuum. The ions are then accelerated in an electric field into the analyser, which separates ions according to their *m/z* ratios. The function of the detector is to record the impact of individual ions and measure their intensity. Typical workflow of proteomic analysis involving mass spectrometry-based protein identification is shown on Figure 1.18

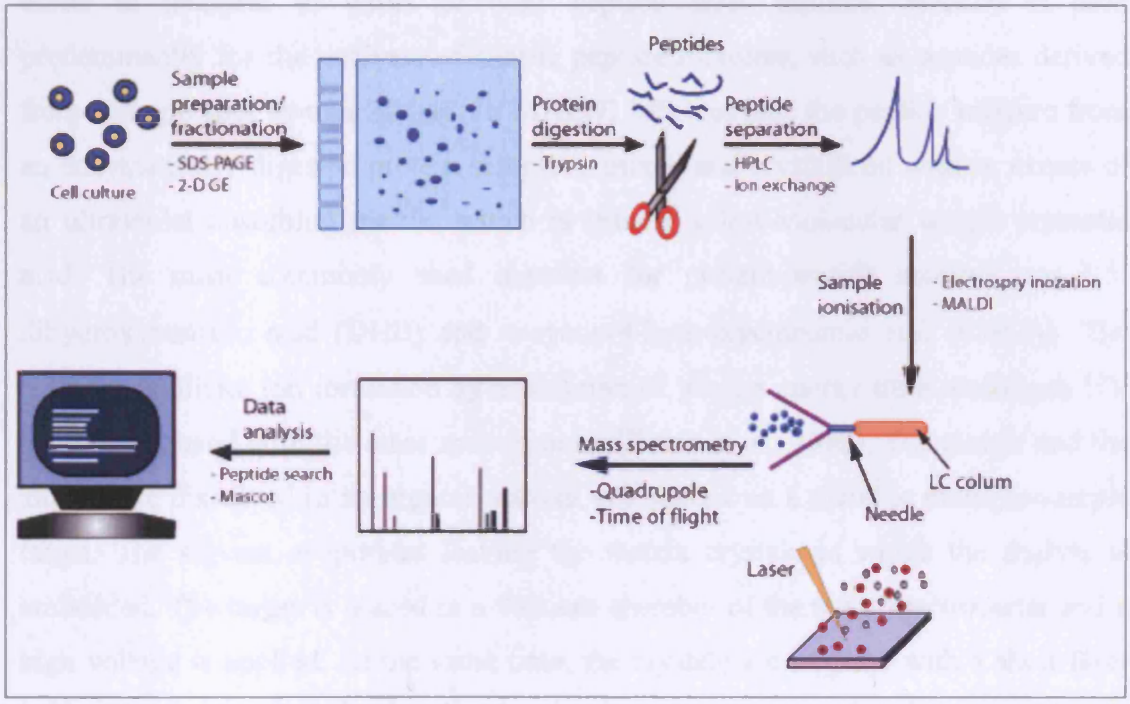

Figure 1.18 Typical workflow of a proteomics/mass spectrometry experiment. A protein sample obtained from different biological sources, (for e.g. cell culture) can be separated into simpler fractions or even single protein spots using 1-D or 2-D gel electrophoresis. Proteins are then in-gel digested using proteases (usually trypsin). The generated peptide mixture can be further separated using peptide separation techniques. Peptides are then ionized by electrospray ionisation (ESI) or matrix-assisted laser desorption ionisation (MALDI) and analysed by mass spectrometry (time-of-flight or quadropole instruments). Finally, peptide-mass data is searched against databases using a search engine (e.g. Mascot). Adapted from (Aebersold and Mann, 2003).

In proteomics, an analyte is usually a collection of peptides derived from a protein sample digested with trypsin or a similar enzyme. Two types of analysis are typically performed:

i) The analysis of intact peptide ions allows the masses of individual peptides to be calculated, and then proteins identified by correlative database searching.

ii) The fragmentation of peptide ions and determination of parent and daughter ion masses. These masses are then used in database searching to derive peptide sequences.

MALDI is an ideal first pass analysis method as it has a relatively high-throughput and generates predominantly singly charged ions $[M^+H]^+$ and the mass spectra are easier to interpret in terms of their peptide mass profiles. MALDI is used predominantly for the analysis of simple peptide mixtures, such as peptides derived from a single spot from a 2D gel. In MALDI MS analysis, the peptide mixture from an enzymatically digested protein sample is mixed and crystallised with an excess of an ultraviolet absorbing matrix, which is usually a low-molecular weight aromatic acid. The most commonly used matrices for protein/peptide analysis are 2,5-dihydroxybenzoic acid (DHB) and α-cyano-4-hydroxycinnamic acid (CHCA). The matrices facilitate ion formation by absorption of photon energy from a nitrogen UV laser beam used with the mass spectrometer (Karas et al., 1988). The matrix and the analyte are dissolved in an organic solvent and placed on a metallic multiple-sample target. The solvent evaporates leaving the matrix crystals in which the analyte is embedded. The target is placed in a vacuum chamber of the mass spectrometer and a high voltage is applied. At the same time, the crystals are targeted with a short laser pulse. The laser energy is absorbed by the crystals and emitted as heat, resulting in rapid sublimation that converts the analyte into gas phase ions. These ions accelerate away from the target through the analyser towards the detector with different speeds depending of their *m/z* ratios. It is reported that protein digests can be analysed by MALDI MS with detection limits in the low femtomole range. In addition, compatibility of protein stains with MALDI MS has been demonstrated for a variety of staining methods including colloidal Coomassie blue, silver staining and SYPRO Ruby, which makes this ionisation applicable for protein analysis from gel pieces.

In contrast to MALDI, ESI ionises analytes from a solution. The analyte is dissolved in an organic solvent mixture and is forced through a narrow capillary held at a high voltage. A fine spray of charged droplets emerges from the capillary and is directed into the vacuum chamber of the mass spectrometer through a small orifice. An electrostatic field is formed between the capillary and the walls of the mass spectrometer, and as the droplets travel, they evaporate resulting in the formation of gas-phase ions that are accelerated through the analyser towards the detector. As ESI produces gas-phase ions from solution, it is readily integrated with upstream protein separation carried out by capillary liquid-chromatography (LC). The sensitivity of ESI MS, like MALDI MS, is in low femtomole range. However, an integrated liquid chromatography ESI MS system (LC-ESI MS) can be used for the analysis of more complex samples, since it provides on-line separation of peptides.

The core of each mass spectrometer is the mass analyser. There are three basic types of analyser: time-of-flight (TOF), quadrupole and ion traps. They differ in design and performance and can stand independently or can be put together in tandem to generate different types of data (e.g. Q-TOF, Q-TRAP). The key parameters of mass analysers are mass accuracy, sensitivity and resolution. The MALDI ion source is usually coupled to a time-of-flight (TOF) analyser for analysis of intact peptide ions (MALDI-TOF MS). TOF analysers exploit the fact that in any mixture of ions carrying the same charge, as in the case of MALDI, heavy ions will take longer to travel down an electric field–free flight tube than lighter ones. Thus, the time of flight of any ion is inversely proportional to the square root of its molecular mass. The final product of this kind of analysis is a list of *m/z* ratios that represents a peptide mass map, also called a peptide mass fingerprint (Mann et al., 1993; Yates, III et al., 1993; Henzel et al., 1993; James et al., 1993). The tryptic peptide masses in the mass spectrum are then matched to calculate theoretical tryptic peptide masses for each protein in the database. ESI sources have been coupled mostly to ion traps and triple quadropole analysers. The quadrupole consists of four parallel metal rods. Each opposing rod pair is connected together and a radio frequency (RF) voltage is applied between each pair. A direct current voltage is then superimposed on the RF voltage. Ions travel down the quadrupole in between the rods. Only ions of a certain *m/z* will reach the detector for a given ratio of voltages, while other ions have unstable

trajectories and will collide with the rods. This allows selection of a particular ion, or scanning by varying the voltages. A triple quadrupole mass spectrometer has a linear series of three quadrupoles. The first (Q1) and third (Q3) quadrupoles act as mass filters, and the middle (Q2) quadrupole is employed as a collision cell. The collision cell is an RF only quadrupole (non-mass filtering) using Ar or He gas to induce collisional dissociation of selected parent ions from Q1. Subsequent fragments (daughter ions) are passed through to Q3 where they may be filtered or scanned fully, generating a collision–induced dissociation (CID) spectrum. Peptide fragmentation caused by collision mainly occurs at the lowest energy amide bonds of peptides. When the charge is retained by the amino terminal fragment, b-ions are formed, while y-ions are formed when the charge is retained by the carboxy-terminal fragment. The mass difference between sequential b- and y- ions thus corresponds to the mass of the amino acids in the sequence. A schematic representation of this peptide sequencing is shown in Figure 1.19.

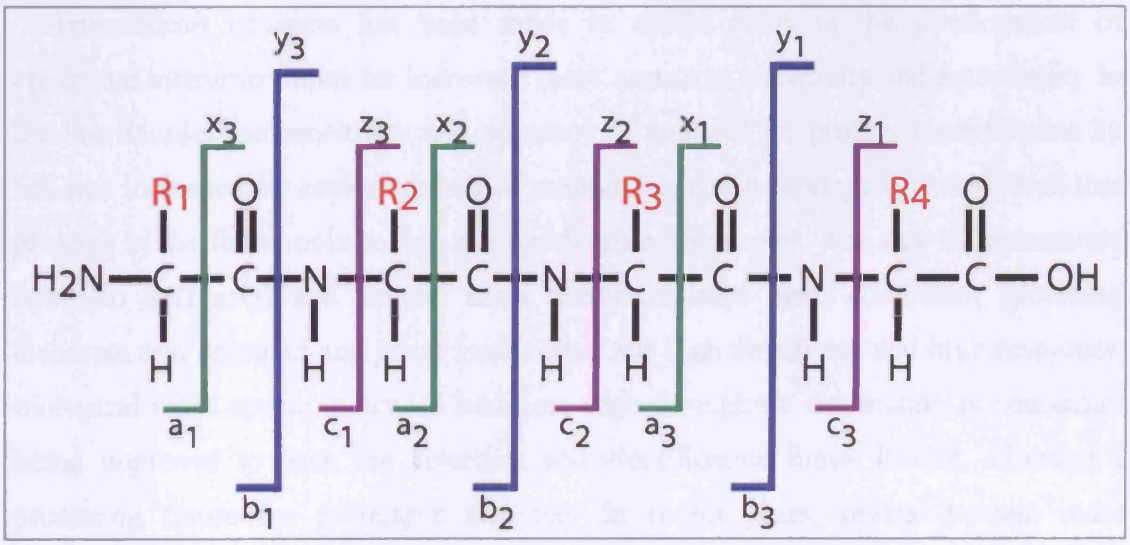

Figure 1.19 Schematic representation of peptide fragment nomenclature. A schematic overview of the possible fragmentation on the peptide backbone and the nomenclature of resulting fragment ions are shown. Different amino acids are distinguished by the side groups displayed in red (R1-R4). When the charge is retained on the C-terminal side of the peptide, fragments are named x, y and z, whiles they are named a, b and c ions when the charge is retained on the N-terminal side. The resulting fragments are dependent on many factors, such as the type of fragmentation method, analyser principle and primary sequence dependency. The mass difference between sequential b- and y- ions thus correspond to the mass of the amino acids in the sequence. Also fragmentations on the side chains are possible. These ions are known as v and w ions (not shown in this figure).

The generated lists of peptide (or fragment ion) masses are searched against the theoretical masses for all proteins stored in a database (SwissProt, NCBI, IPI etc). Several search engines are available (Mascot, Prospector, Spectrum Mill etc.). They allow searching according to the proteolytic enzyme of choice, and can deal with missed cleavages, possible post-translational modifications and known chemical modifications. They generate a list of potential matches ranked according to a scoring system depending on best probability of a match being real at define mass tolerance (e.g. 50-100 ppm). Confidence in the identification process depends on the species of the sequence identified *versus* that studied, the mass and pI of the protein observed on a gel *versus* that predicted, the number of peptides matching the protein sequence of a particular protein, the mass accuracy of detection, the protein sequence coverage, the number of missed cleavages during the proteolysis process and the type of modifications observed, which reflects the process of sample handling.

Tremendous progress has been made in recent years in the development of optimised instrumentation for increased mass accuracy, sensitivity and automation. In the last decade, the sensitivity and accuracy of analysis for protein identification by MS has increased by several orders of magnitude, and nowadays it is estimated that proteins in the femtomolar range can be identified from gels. The size of instruments has also decreased and several mass analysers have been combined, providing elaborate and compact analytical instruments for high sensitivity and high-resolution biological mass spectrometry. In addition, high-throughput automation is constantly being improved to push the detection and identification limits further, allowing a promising future for proteomic analyses. In recent years, several tandem mass spectrometry-based quantitative proteomic techniques have been developed and optimized for wide use in proteomic studies. These technique include i) *in vivo* metabolic stable-isotope labelling and SILAC (stable isotope labelling with amino acids in cell culture), ii) *in vitro* chemical methods of stable isotope incorporation such as ICAT (isotope coded affinity tag) and iTRAQ (isobaric tags for relative and absolute quantification) or iii) adding an internal standard (a peptide with defined *m/z*) in samples prior to MS analysis. However, there are still other major challenges in proteomics, such as improvement of sample preparation protocols for reduction of

sample complexity and increasing delectability of low-abundance proteins and proteomic coverage, which scientists need to tackle on a daily basis studying the proteomes.

1.3 Aims of the study

In the last two decades, research on PI3Ks has shown that they have a critical role in tumourgenesis, although the precise mechanisms are still not fully clear. Indeed, the elucidation of the role of PI3K and its downstream effectors in controlling cellular functions such as growth, proliferation, survival and morphogenesis is important to discover how aberrant PI3K signalling contributes to tumour development and progression. Perhaps the biggest challenge of all is to define the interaction and cross-talk of the PI3K signalling pathway with other signalling pathways (Ras/MAPK, Rho-family GTPases etc.) in order to define how systematic molecular mechanisms are orchestrated in a cell to allow it to function normally, and to respond to external stimuli in an appropriate way. The main aim of my study was to examine the role of PI3K signalling pathway with particular focus on its role in actin cytoskeleton organisation and determination of cell shape.

Thus, the specific aims of my project were:

- To identify new protein targets of PI3K signalling and to understand their function and regulation. My initial aim was to establish a model cell system for studying PI3K–dependent signalling and to monitor acute changes of the cellular complement of proteins and their phosphorylation status following PI3K activation and inhibition. A model of breast luminal epithelial cells, HB4a, was chosen in which to examine PI3K signalling in response to growth factor stimulation. A combination of 2D-DIGE, mass spectrometry and immunoblotting was employed.

- To develop an alternative cell model in which to study PI3K-dependent regulation of the actin cytoskeleton in *Drosophila* haemocytes. Cell lines were selected and

insulin stimulation was used to trigger acute PI3K signalling, and common PI3K inhibitors were used to block PI3K activity. The effects on the actin cytoskeleton were monitored by fluorescence and time-lapse microscopy.

- To understand the biochemical mechanisms that link PI3K to downstream pathways, which regulate changes in the actin cytoskeleton. The real challenge here is to delineate each signalling cascade and to identify nodes where pathways cross-talk. Thus, my objective was to try to understand how molecular mechanisms are governed in a coordinated ways that allow a cell to respond in an appropriate way to external stimuli. Previous studies had reported the existence of cross-talk between PI3K and small GTPase signalling pathways during cell shape changes and movement. My aim in this thesis was to try to understand signalling cross-talk and to try to identify common downstream targets by using genomic and proteomic techniques in parallel. A "loss-of-function" approach based on RNA interference was used with quantitative two-dimensional difference gel electrophoresis (2D-DIGE), to carry out a screen of differential protein expression of knockdown cells. The RNAi-strategy was used for disruption of translation of selected target genes involved in PI3K, Ras and small Rho-GTPase mediated signalling. Mass spectrometry was employed for the identification of the differentially expressed proteins between control and RNAi treatments. Alterations in protein expression were validated by western blotting. A list of proteins linked to the signal pathways was generated and the proteomic profiles were correlated with the observed morphological changes in the actin cytoskeleton in each knockdown.

- Finally, my study was extended to functionally characterise targets of interest identified from the proteomic screen. Cofilin, an actin depolymerising protein, was selected as an interesting target to follow up on its regulation, since its phosphorylation, which determines its activation status, was found to be perturbed by RNAi-induced silencing of PI3K, Rho-family small GTPases and actin modulators.

Chapter 2: MATERIALS AND METHODS

2.1. Cell culture

2.1.1 *Drosophila* cell lines

In this study, four cell lines derived from *Drosophila melanogaster* embryos were used. S2R+, Kc167 and S2 cells are haemocyte cells, while Clone 8 cells originate from the wing disc. Cells were maintained at 24°C in Schneider's *Drosophila* medium (Invitrogen) or Shields and Sang M3 insect medium (Sigma Aldrich) supplemented with 10% (v/v) foetal calf serum (FCS) (Helena Biosciences; heat-inactivated at 60°C for 5 minutes), and antibiotics (50 IU/mL penicillin and 50 μg/mL streptomycin; both from Sigma). Cells were split (1:2 or 1:3) every 3-4 days depending on their confluence. For splitting, S2R+ cells were removed from culture flasks using trypsin-EDTA (Invitrogen). Trypsin treatment was not required for semi-adherent Kc167, S2 and Clone 8 cell lines.

2.1.2. Human mammary luminal epithelial cells (HMLECs)

The immortalised human mammary luminal epithelial cell line HB4a was obtained from Dr. M. O'Hare (Ludwig Institute) and was derived as described (Harris et al. 1999). Cells were maintained in RPMI-1640 medium containing 10% (v/v) FCS, 2 mM L-glutamine, 100 μg/mL streptomycin, 100 IU/ml penicillin (all from Gibco-Invitrogen Corp., UK), 5 μg/mL insulin and 5 μg/mL hydrocortisone (both from

Sigma) in tissue culture dishes at 37°C in a 10% CO_2 humidified incubator. Cells were passaged when they reached 80 to 90% confluence by trypsinisation according to standard procedures. Stocks of human mammary luminal epithelial cells (HMLEC) and fly cells were stored in liquid nitrogen and new batches of low passage number cells were used for experiments. Prolonged passaging of cells was avoided to prevent potential genetic drift. For freezing, trypsinised cells (fly and human cell lines) were pelleted and resuspended in 10% (v/v) DMSO and 90% (v/v) FCS. Cells were slowly taken to –80°C in a propanol container and then transferred to liquid nitrogen for long-term storage. Rapid thawing was carried out in a 37°C water bath and DMSO was removed by centrifugation prior to plating. Cells were allowed to recover for two to three passages prior to sampling.

2.2 Growth factor and inhibitor treatments

Prior to growth factor treatment, fly cell lines S2R+, Kc167 and S2 were grown in serum-free insect medium supplemented with antibiotics for 16 to 24 hours. Cells were then treated for various times with 10 μg/mL bovine insulin (Sigma). Other growth factors used in this study were human epidermal growth factor (EGF) (200 ng/mL) (R&D Systems), murine VEGF (50 ng/mL) and human PDGF-BB (125 ng/mL) (both from PeproTech Inc.). For PI3K inhibitor treatment, fly cells were treated with wortmannin (100 nM) or LY294002 (10, 50 or 100 μM) (both from Calbiochem) diluted in DMSO. DMSO served as a vehicle-alone control. In some experiments, the PI3K inhibitors were added to the cells prior to insulin treatment. Actin-modulating drugs used were latranculin B (1 μg/mL) (Calbiochem), cytochalasin D (2 μg/mL) (Sigma) and jasplakinolide (1 μg/mL) (Invitrogen).

HMLECs were treated for various times with 1 nM EGF (R&D systems), a ligand specific for ErbB family members. Prior to treatment, cells were first serum-starved for 48 hours in 0.1% (v/v) FCS in RPMI-1640 media supplemented with L-glutamine (2 mM), hydrocortisone (5 μg/ml) and antibiotics. Specific PI3K inhibitors (10 μM LY294002, 100 nM wortmannin or 2 μM D000) were also used to study PI3K-dependent changes in the HMLEC proteome and were typically added 30 minutes

prior to treatment with growth factor. Inhibition of the proteasome was achieved by treatment with 1 μM PS341 (gift from Peter Elliot, Millenium Pharmaceuticals, Inc.).

2.3 Sample preparation for 1D and 2D SDS-PAGE

2.3.1 Cell lysis and protein extraction

Cells were washed with ice-cold phosphate-buffered saline (PBS) and lysed in the appropriate lysis buffer. For one dimensional sodium dodecyl sulphate-polyacrylamide gel electrophoresis (1D SDS-PAGE), cells were lysed in NP40 lysis buffer (50 mM HEPES; 150 mM NaCl; 1% NP40; 1 mM EDTA) supplemented with protease inhibitors (17 μg/mL aprotinin; 1 μg/mL pepstatin; 1 μg/mL leupeptin, 100 μg/mL AEBSF) and phosphatase inhibitors (5 μg/mL BpVphen, 5 μM fenvalerate, 1 μM okadaic acid, 2 mM sodium orthovanadate). Lysates were left for 15 minutes on ice, and then centrifuged at 13000 rpm for 10 min at 4°C to clear the insoluble cell debris. Protein concentrations were determined using a Bradford microtitre plate assay. Briefly, 2 μL of total cell lysate was mixed with 200 μL of Coomassie Protein Assay Reagent (Pierce-Perbio). The absorbance was read at 595 nm in a microtitre plate spectrophotometer (Spectra Max Plus, Molecular Devices). Standard curves were determined using bovine serum albumin (BSA) standards diluted in the same lysis buffer at the following concentrations: 0, 0.25, 0.5, 0.75, 1, 2.5, 5 and 10 μg/μL. Standards and samples were assayed in triplicate. The protein concentrations of the samples within an experiment were adjusted to the same concentration by adding lysis buffer and were denaturated in laemmli sample buffer (50 mM Tris pH 6.8, 10% (v/v) glycerol, 2% (w/v) SDS, 0.1% (w/v) bromophenol blue, 2% (v/v) β-mercaptoethanol; final concentrations) and heated at 100°C for 5 min. 1D SDS-PAGE was performed following standard procedures using an appropriate % resolving gel for the proteins to be analysed.

For 2D-DIGE, cells were washed with ice cold PBS and lysed in 2D-DIGE lysis buffer (8 M urea, 2 M thiourea, 4% (w/v) CHAPS, 0.5% (w/v) NP40, 10 mM Tris-

HCl pH 8.3) supplemented with protease and phosphatase inhibitors (as above). The preferred pH of the buffer is 8.3 since the dye labelling is most efficient at pH 8-9. DTT was omitted from the buffer since high concentrations would interfere with dye labelling efficiency. Cell lysates were homogenised by passage (six times) through a 25G needle. Insoluble material was removed by centrifugation (13,000 rpm/10 min/4°C). Protein concentrations were determine by Bradford assay (as above), and aliquots of equal amounts of protein were covalently labelled with NHS-Cyanine dyes as described in the following section.

2.3.2 Protein labelling with NHS-cyanine dyes (DIGE-labelling)

The NHS-cyanine dye Cy2 was purchased from GE Healthcare, whilst NHS-Cy3 and NHS-Cy5 were synthesised "in house" by Dr P. Gaffney (Imperial College London). Stocks were stored at a concentration of 1 mM in dimethyl formamide (DMF) at -20°C. Protein labelling and 2D-DIGE were performed according to Gharbi *et al.* (Gharbi et al., 2002). Prior to protein labelling, the Cy dyes were diluted in DMF and kept on ice, in the dark. Typically, 100 μg of total protein extract was labelled with NHS-Cy3 or NHS-Cy5 at 4 pmol dye/μg protein on ice in the dark for 30 min. Equal amounts of protein extracts from each experimental condition were also pooled together and labelled with NHS-Cy2 to create an internal standard which was run on all gels against the Cy3- and Cy5-labelled samples to aid in spot matching and quantitation. Labelling reactions were quenched with a 20-fold molar excess of free L-lysine to dye on ice in the dark for 10 minutes: for 400 pmol CyDye, 0.8 μL of 10 mM L-lysine solution was added. Equal amounts of proteins labelled with Cy3 and Cy5 were mixed appropriately and the same amount of Cy2-labelled pool was added to each mixture. Samples were reduced by adding 1.3 M dithiothreitol (DTT) to a final concentration of 65 mM for 15 minutes. Ampholine/Pharmalyte carriers (1:1) mix; pH 3 to 10 were added to a final concentration of 2% and bromophenol blue was added to each sample. The final volume of each sample was adjusted to 350 μL or 450 μL with 2D-DIGE lysis buffer plus DTT to allow appropriate re-swelling of 18 cm or 24 cm immobilised pH gradient (IPG) strips, respectively.

2.4 Two- dimensional gel electrophoresis

For isoelectric focusing (IEF), 18 cm or 24 cm, non-linear pH 3-10 IPG strips (GE Healthcare) were rehydrated with Cy-dye labelled samples in a re-swelling tray overnight in the dark at RT, according to the manufacturer's guidelines. The separation of the Cy-dye labelled proteins in the first dimension by IEF was carried out on a Multiphor II apparatus (GE Healthcare) for a total of 80 kVh at 18°C. For protein separation in the second dimension, 1.5 mm 12% SDS-PAGE gels were cast between 18 cm or 24 cm low-fluorescence glass plates. The inner surface of one plate of each set was covered with Bind Silane solution (PlusOne, GE Healthcare) to bond the gels. This allowed easier handling of gels during scanning and protein post-staining, storage and spot excision. Fluorescent reference markers were placed at the edges of these bonded plates to facilitate the generation of coordinates of each protein feature in the pick list. The inner surface of the other plate was treated with Repel Silane (PlusOne, GE Healthcare) to ensure easy separation of plates after running. After IEF, IPG strips were equilibrated in equilibration buffer (6 M urea, 30% (v/v) glycerol, 50 mM Tris-HCl pH 6.8, and 2% (w/v) SDS) in two steps for 15 minutes each with gentle rocking. In the first step, the equilibration buffer was supplemented with 65 mM DTT to reduce disulphide bonds, while in the second step 240 mM iodoacetamide (IAM) was added to the equilibration buffer to alkylate reduced thiol groups. IPG strips were then rinsed with Tris-HCl/SDS electrophoresis buffer and transferred onto the second dimension gels. Strips were overlaid with 0.5% (w/v) low-melting point agarose in Tris-Glycine-SDS electrophoresis buffer (Severn Biotech) with bromphenol blue. Gels were run in Protean II tanks (BioRad) at 10 mA per gel or in an Ettan 12 apparatus (GE Healthcare) at 2 W per gel at 8°C until the dye front had run off completely, thereby avoiding fluorescence signals from bromophenol blue and free dye. All steps were carried out in a dedicated clean room.

2.5 Detection of Cy-dye labelled proteins

Gel images were obtained by scanning the gels between plates on a Typhoon^{TM} 9400 mutliwavelength fluorescence scanner using ImageQuant software (both from

GE Healthcare). Excitation and emission wavelengths of each dye used in this study are shown in Table 2.1. The photomultiplier tube voltage of the Typhoon scanner was adjusted for each channel (Cy2, Cy3 and Cy5) in preliminary low-resolution scans (1000 μm) to give maximum pixel values within 10% for each Cy-dye image, but below the saturation level. These settings were then used for high-resolution (100 μm) scanning. Images were generated as .gel files (same as Tagged Image File Format (TIFF)) and exported to image analysis software for further analysis.

	Excitation (nm)	Emission (nm)
Cy2	480	530
Cy3	540	590
Cy5	620	680
CCB	620	/
SYPRO Ruby	400	632
Pro-Q Diamond	550	580

Table 2.1 Excitation and emission wavelengths used to detect each of Cy-dyes and dyes used in gel post-staining.

2.6 Image analysis

Gel images were analysed using DeCyder™ image analysis software *ver.4.0* (GE Healthcare). Firstly, images were analysed using the Differential In-Gel analysis (DIA) module. DeCyder DIA processes the three images derived from the three wavelengths (Cy2, Cy3 and Cy5) representing profiles of each of three labelling conditions run on a single gel, and performs automatic spot detection, filtering, background subtraction and normalisation. DIA also quantifies spot protein abundance on each image and expresses these values as ratios, indicating changes in expression levels by direct comparison of corresponding spots. This ratio can be used to directly evaluate changes between two labelled protein samples run on a single gel. Alternatively, the ratio can be used for protein spot quantitation against the same spot in the internal standard to allow accurate inter-gel protein spot comparisons. Features resulting from non-protein sources (e.g. dust particles and scratches on glass plates)

were filtered out. Subsequently, the Biological Variance Analysis (BVA) module of DeCyder was used for matching protein spots from different conditions across gels by matching to a user selected master gel image, thus identifying common protein spots across the gels. User intervention was required at this stage to set landmarks on gels for accurate cross-gel matching. Comparison of test spot volumes with the corresponding standard spot volumes gave a standardised abundance for each matched spot and values were averaged across triplicates for each experimental condition and data plotted graphically within BVA. Statistical analysis was performed and spots displaying a ≥ 1.5 average-fold increase or ≤ -1.5 average-fold decrease in abundance with p values < 0.05 from a Student's T-Test were selected for spot picking and MS-based identification.

2.7 Protein post-staining and spot excision

Bonded 2D gels were post-electrophoretically stained using several staining methods to visualise proteins for accurate spot picking and to detect phosphorylated proteins.

2.7.1 Colloidal Coomassie Blue

Gels were post-stained with colloidal Coomassie blue G-250 (CCB) according to a modified protocol by (Neuhoff et al., 1988). Bonded gels were fixed in 35% (v/v) ethanol with 2% (v/v) phosphoric acid for more than three hours on a shaking platform and then washed three times for 30 min each in ddH_2O. Gels were then incubated in 34% (v/v) methanol, 17% (w/v) ammonium sulphate and 3% (v/v) phosphoric acid for one hour prior to the addition of 0.5 g/L Coomassie G-250 (Merck Biosciences) and left to stain for two to three days. De-staining was not required. Post-stained gels were scanned on the Typhoon™ 9400 scanner using the red laser with no emission filter. Post-stained scanned images were imported into the BVA module of DeCyder and matched with the Cy dye images. Using the reference markers fixed onto the glass plates at casting, a pick list of coordinates (.txt file) for

protein features that were differentially expressed was created for automated spot picking. An Ettan automated spot picker (GE Healthcare) was used with a 2 mm picking head, which excised protein features from gels submerged under 1-2 mm of ddH_2O. Spots were collected in 96-well plates, drained and stored at -20°C prior to MS analysis. In some cases protein spots were picked manually by cutting the stained protein spots using a scalpel.

2.7.2 SYPRO Ruby fluorescent staining

In some experiments, bonded gels with separated cyanine Cy-dye labelled proteins were post-stained with SYPRO Ruby fluorescent protein stain (Molecular Probes, USA). Following electrophoresis, gels were fixed for at least 3 hours in fixing solution (30% (v/v) methanol, 7.5% (v/v) acetic acid, in ddH_2O). Lower concentrations of methanol and acetic acid were used in order to avoid shrinkage and cracking of bonded gels. Gels were washed twice in water and then incubated in SYPRO Ruby staining solution for a minimum of 3 hours in the dark. Gels were then washed briefly in water to remove excess dye. Gels were then scanned on the Typhoon™ 9400 scanner (Table 2.1).

2.7.3 Pro-Q Diamond phosphoprotein gel staining

In some experiments gels were stained with Pro-Q diamond to detect phosphoproteins. Bonded gels were fixed in 10% trichloroacetic acid and 35% methanol with gentle agitation overnight at RT. Gels were washed in ddH_2O for 5 x 15 minutes to remove methanol and trichloracetic acid. Gels were stained with Pro-Q Diamond gel stain (Molecular Probes) with gentle agitation in the dark for ~3-4 hours. Gels were then incubated in destaining solution (4% acteonitrile, 50 mM sodium acetate, pH 4.0) in the dark at RT, with four changes of the destaining solution. The final destaining step was done overnight. Gels were scanned on the Typhoon™ 9400 (Table 2.1).

2.8 Protein in-gel digestion

For further analysis by mass spectrometry, gel pieces were washed three times with 50% (v/v) acetonitrile, dried in a SpeedVac for 10 minutes, reduced with 10 mM DTT in 5 mM ammonium bicarbonate pH 8.0 (AmBic) for 45 minutes at 50°C and then alkylated with 50 mM iodoacetamide (IAM) in 5 mM AmBic for one hour in the dark at RT. Gel pieces were then washed three times in 50% (v/v) acetonitrile and vacuum-dried prior to re-swelling with 50 ng of modified trypsin (Promega) in 5 mM AmBic pH 8.0. The gel pieces were then overlaid with 10 µL of 5 mM AmBic and digested for 16 hours at 37°C. Supernatants were collected and tryptic digests were further extracted by washing the gel pieces twice with 5% (v/v) trifluoroacetic acid in 50% acetonitrile. Peptide extracts from each gel piece were pooled, vacuum-dried and resuspended in 5 µL of 0.1% formic acid and stored at -20°C prior to MS analysis.

2.9 Protein identification

Protein identification was carried out using matrix-assisted laser desorption/ ionisation time-of-flight (MALDI-TOF) MS by peptide mass fingerprinting. For this, 0.5 µL of the trypsin digest was mixed with 1 µL of matrix solution (saturated aqueous 2,5-dihydroxybenzoic acid, DHB), and applied to a sample target plate and air dried. MALDI-TOF mass spectra were acquired using an externally calibrated Ultraflex mass spectrometer (Bruker Daltonics) in the reflector, positive ion mode. The mass spectrometer was calibrated using a standard mixture of peptides (calibration mixture 2 from the Sequazyme kit, Applied Biosystems). Internal calibration of each mass spectrum was performed using reference trypsin autolysis peaks: *m/z* 842.51 and *m/z* 2211.10. Prominent peaks in the mass range *m/z* 500-5000 were then used to generate a peptide mass fingerprint, which was searched against NCBI database using the Mascot search engine, version 2.0.02 (Matrix Sciences Ltd.). For the search criteria, carbamidomethylation of cysteines was selected as a fixed modification, while oxidation on methionine, N-acetylation and pyro-glutamate were selected as variable modifications. A positive identification was accepted when a minimum of 6 peptide masses matched a particular protein (mass error of ± 50-100

ppm, allowing 1 missed cleavage), sequence coverage was >25%, MOWSE scores were higher than a threshold value where p=0.05, the predicted protein mass agreed with the gel-based mass and the correct species sequence was identified. When a protein 'hit' fulfilled the specified thresholds of validation for protein identification, unmatched peptides were systematically re-submitted to the database in a search for possible multiple proteins per gel piece and potential sites of post-translational modification (e.g. phosphorylation).

Some identifications were made using nano-HPLC-electrospray ionization collision-induced dissociation tandem MS (nano-LC-MS/MS). This was performed on an Ultimate HPLC (Dionex) with a PepMap C18 75-μm inner diameter column (LC Packings) at a flow rate of 300 nL/min, coupled to a Quadrupole Time-Of-Flight 1 (QTOF1) mass spectrometer (Waters/Micromass, Manchester, UK). Spectra were processed using MassLynx software (Waters) and submitted to Mascot database search routines including +2 and +3 peptide charge, and a mass tolerance of ±100 ppm. Positive identifications were accepted when at least two peptide sequences matched an entry with MOWSE scores above the p=0.05 threshold value.

2.10 Phosphopeptide analysis using titanium dioxide micro-columns and LC-MS/MS

Enrichment of phosphorylated peptides from peptides generated by in-gel digestion of selected protein spots (Cofilin) was performed using titanium dioxide essentially as described (Larsen et al., 2005). Briefly, titanium dioxide (TiO_2) micro-columns with a length of ~3 mm were packed in GELoader tips with a small C8 3M Empore plug. The trypsin digest from the two Cofilin protein spots were diluted into 5% TFA, 80% acetonitrile (with inclusion of phthalic acid) and loaded onto the TiO_2 micro-columns. The columns were washed with 5% TFA, 80% acetonitrile and bound phosphorylated peptides were eluted with 15 μL ammonia solution (10 μL ammonia (25% solution) in 490 μL water). Eluates were acidified and analyzed by MALDI-TOF MS and nano-LC-MS/MS. MALDI-TOF MS was performed on a Voyager STR mass spectrometer (PerSeptive Biosystems, Framingham, MA). All spectra were obtained in the positive

reflector mode and DHB (20 g/L) in 50% acetonitrile, 1% phosphoric acid was used as the matrix. Data analysis was performed using MoverZ software (www.proteometrics.com) and peptide assignment was accomplished using GPMAW software (welcome.to/gpmaw). Nano-LC-MS/MS was performed on a Proxeon Biosystem Easy-nLC nanoflow system (Proxeon Biosystem A/S, Odense, Denmark) coupled to a QTOF Ultima mass spectrometer (Waters/Micromass, Manchester, UK). Peptides were loaded onto a 75 μm inner diameter fused silica pre-column (ReproSil–Pur, Ammerbuch-Entringen, Germany) and eluted with a 1.5% gradient (A buffer: 0.5% acetic acid; B buffer: 0.5% acetic acid in 80% acetonitrile) onto a 50 μm inner diameter fused silica analytical column (ReproSil-Pur) and into the mass spectrometer. The mass spectrometer was operated in data dependent acquisition mode and two of the most intense ions were selected for collision induced dissociation per MS scan. The data were processed using MassLynx software and pkl files were searched using Mascot.

2.11 Double-stranded RNA production and RNAi treatment

RNA interference (RNAi) was performed on fly cells, by transfection with gene specific dsRNAs. Pairs of gene-specific primers were taken from existing primer libraries or designed *de novo* using the E-RNAi primer design tool (http://e-rnai.dkfz.de/). Primer sequences of ~21 bp length (Table 2.2) flanked with T7 sites were chosen for PCR amplification of approximately 600 bp of exonic sequences of the genes to be silenced. PCR reactions were prepared with the forward and reverse primer set, fly genomic DNA, PCR buffer with Mg^{2+}, DNA nucleotides (ATP, TTP, GTP and CTP) and "HotStart" DNA polymerase. The reagents for the PCR were supplied by Qiagen. The initial step for each PCR was a "hotstart" step at 95°C for 15 minutes followed by 30 cycles of denaturation at 94°C for 30 seconds, annealing at 50-60°C for 30 seconds and an extension step at 72°C for 1 minute. PCRs were terminated with a final extension at 72°C for 30 minute. PCR amplification was confirmed by 1% (w/v) agarose gel electrophoresis using GeneRuler 1 kb marker to assess the size of PCR products. DsRNAs were generated from PCR products by *in vitro* transcription using the MEGAscript™ High Yield Transcription Kit (Ambion)

containing RNA nucleotides (ATP, UTP, GTP and CTP), 10x reaction buffer and T7 RNA polymerase. Reactions were conducted at 37°C overnight and dsRNAs were purified using Multiscreen PCR_{96} purification plates (Millipore) attached to a vacuum pump. Purified dsRNAs were re-suspended in TE buffer (10 mM Tris-HCl pH 8.0, 1 mM EDTA) and annealed at 95°C for 15 minutes followed by slow cooling to room temperature (RT). The dsRNA concentration was estimated on 1% (w/v) agarose gels using 500 ng GeneRuler 1 kb ladder. dsRNAs were stored at -20°C prior to use.

FBgn0020510	Abi	Abi	CATGCCAATGTGACTCTGCT	CCATCAAGTATGTGCGCAAG
FBgn0000042	Actin	CG4027	ATTGCGGCTGATAAGGTTTT	GTTGGGAAGGGGAAAGCTAC
FBgn0010379	Akt	CG4006	GCTACTTCGTGCTCCACTCC	TTTTGATCGCGTACAGCTTG
FBgn0033504	CAP	CG18408	TACAACTTCCAGGCCCAGTC	GATCGATCTCCTCTAGGCCC
FBgn0011744	Arp66B	CG7558	CCATACTCCTCGTAGGCAGC	CACTGCTACATCTGTCCCGA
FBgn0010341	Cdc2	CG12530	CCAGTGTAATCCGGCAAACT	TTTTCTTTGTGGGCTCTGGT
FBgn0011771	Hem	Hem 2	TCTATGCACTGCGAAACCTG	GGCTGTTCGAAGAAACTTGC
FBgn0041203	LIMK	CG1848	TCCTTGGGTATCTCGACCAG	CCAAGGCACAAAAACATTCC
FBgn0015279	PI3K92E	CG4141	CGATGTGAAAAAGCTGCAAA	GCAGTGGTGTAACTCCCGAT
FBgn0000308	Profilin	CG9553	TCCGTCCATTAGTCCATTCC	CTTTCTCCACCTCTCGTTGC
FBgn0026379	PTEN	CG5671	CGGTCCTTTGTACGCTTCTC	GAAGACAAGCACTGGTTCCC
FBgn0010333	Rac1	CG2248	TCGAACACGGTGGGTATGTA	AAATTTGAACAGTCCAGCCG
FBgn0014011	Rac2	CG8556	CCAGTGGCTCAACTGGTTTT	CTGCCACAGAAAATCAGCAA
FBgn0003205	Ras85D	CG9375	ATTCGGCTTGTTCATTTTGC	GCACAGTCACCCACACAAAC
FBgn0029157	SSH	CG6238	GGGCAATAGCAAAGGAAACGA	GCATGCCCGAGGTATTCTTGT
FBgn0011726	TSR	CG4254	TGGCTTCTGGTGTAACTGTG	AGTTTCTCCTCGACGGCTTC

Table 2.2 Forward and reverse primers sequences used to generate dsRNAs.

For RNAi experiments, fly cells were typically suspended in Schneider's serum-free medium and plated at $2x10^6$cells/mL in tissue culture dishes (Falcon, BD Biosciences). DsRNA was added directly to the medium to a final concentration of 0.3 μM, followed by gentle agitation. Cells were incubated for 30 minutes at room temperature, followed by addition of Schneider's medium supplemented with 10% FCS. For 2D-DIGE experiments, each RNAi treatment was conducted as biological triplicates. For immunofluorescence staining analysis, RNAi treatment was usually performed in 384-well plates or 8-well chamber slides. Cells were incubated for 4-5 days to allow turnover of target proteins, prior to harvesting or fixing for analysis.

2.12 Immunoblotting

Immunoblotting was used to validate protein expression differences and protein identities. Briefly, cell extracts were separated by 1D or 2D SDS-PAGE and electro-blotted onto polyvinylidene fluoride membrane (Immobilon P, Millipore) in a transfer tank using transfer buffer (195 mM glycine, 25 mM Tris, 20% (v/v) methanol). Membranes were blocked for one hour with 5% (w/v) low fat milk or 5% (w/v) bovine serum albumin (BSA, Sigma) in Tris-buffered saline (50 mM Tris pH 8.0, 150 mM NaCl) with 0.1% (v/v) Tween-20 (TBS-T). Membranes were incubated with primary antibodies in TBS-T for one and a half hour at room temperature or overnight at 4°C. The list of primary antibodies used in this study is shown in Table 2.3. Membranes were washed with TBS-T three times for 10 minutes, and then probed with the appropriate horseradish peroxidase-coupled secondary antibody (GE Healthcare) for about 50 minutes. Membranes were washed three times for 10 minutes in TBS-T and immuno-probed proteins were visualised using enhanced chemiluminescence (PerkinElmer, Life Sciences Inc.). Developed films were scanned on a BioRad GS-800 densitometer generating .tif files. Tiff images from 2D-western blotting were aligned to 2D gel images using Adobe Photoshop. For membrane re-probing, membranes were first stripped (by incubating with 0.2 M glycine pH 2, 2x 30 minutes, and then washed with TBS-T, 3x 10 minutes) and then blocked with 5% BSA.

2.13 Immunofluorescence staining

Randomly growing cells or RNAi-treated cells were re-seeded onto serum-coated cover slips or left in 384-well plates depending on the experiment. For immunostaining, cells were washed with PBS and fixed with 3.7% (v/v) formaldehyde in PBS for 10 min. After washing with PBS, cells were permeabilised with 0.1% (v/v) Triton X-100 in PBS for 5 min, washed again and blocked with 5% (w/v) BSA in PBS for 1 h.

Antibody	Supplier/ Donation	Monoclonal/ Policlonal	Working concn. for WB
4E-BP1anti-phospho (Ser65)	CST	rabbit pAb	1:1000
Actin	Sigma	mouse mAb	1:2000
Akt	CST	rabbit pAb	1:2000
Akt (anti-phospho Ser473)	CST	rabbit pAb	1:1000
Akt (anti-phospho Ser505)	S. Leevers	rabbit pAb	1:1000
Cofilin (anti phospho Ser3)	Eurogentec	rabbit pAb	1:1000
cyclin D1 (DCS6)	PharMingen	mouse mAb	1:500
ERK1/2	Promega	rabbit pAb	1:5000
ERK1/2 (anti phosphoThr198/Tyr200)	Sigma	mouse mAb	1:1000
GSK3 alpha/beta anti-phospho (Ser21/9)	CST	rabbit pAb	1:1000
GSK3 clone 4G-1E (a and b)	UBI	mouse mAb	1:1000
Kip1/p27 (clone 57)	Trans labs	mouse mAb	1:3000
p90 RSK (anti-phosphoT359/S363)	CST	rabbit pAb	1:4000
Phospho-(Ser) PKC substrate	CST	rabbit pAb	1:1000
Phospho-(Ser/Thr) Akt substrate	CST	rabbit mAb	1:1000
Phospho-(Thr) PDK1	CST	rabbit pAb	1:1000
Phospho-tyrosine, clone 4G10	UBI	mouse mAb	1:1000
Phospho-tyrosine, pY99	Santa Cruz	mouse mAb	1:5000
S6 ribosomal protein (anti phospho Ser235)	I. Gout	rabbit pAb	1:1000
S6K (anti phospho Thr398)	CST	rabbit pAb	1:1000
Stat3	CST	rabbit pAb	1:1000
Stat3 (anti-phospho Ser727)	CST	rabbit pAb	1:1000

Table 2.3 List of antibodies used for validation of differentially expressed proteins in immunoblotting analyses including antibodies used for immunofluorescence staining. (CST stands for Cell Signalling Technology)

For pSer505-Akt staining, cells were incubated with primary antibody (1:300 in PBS) overnight at 4°C, followed by incubation with secondary anti-rabbit antibody (1:300) conjugated to Cy5 for 1 h at RT. For pY20 staining, cells were incubated with the primary mouse antibody (1:300 in PBS) overnight at 4°C, followed by incubation with anti-mouse secondary antibody conjugated with FITC (1:300 in PBS). For F-actin, tubulin and DNA staining, cells were incubated for 1 h at RT with rhodamine-phalloidin (Sigma) (1:1000), FITC-conjugated anti-tubulin (1:1000) (Molecular Probes) and 4',6-diamidino-2-phenylindole (DAPI) (1:2000), respectively, all diluted in PBS. Cover slips were sealed, while PBS supplemented with 10% NaN_3 was added to the 384-well plates to keep fixed cells wet and to prevent contamination. Cells were analysed by fluorescence and confocal microscopy. Fluorescent images were acquired using a Nikon 2000E microscope with 20x and 40x objectives and fitted with a cooled CCD camera (Cool Snap; Roper) and using MetaMorph software (Universal Imaging

Inc.). Confocal images were acquired using an LSM 510 camera (Zeiss, Welwyn Garden City, UK) mounted over an Axioplan microscope (Zeiss) using a 40x/1.30 Plan Neofluar oil immersion objective.

2.14 Time- lapse microscopy

For time-lapse microscopy, cells were plated onto optical quality glass-bottomed culture dishes made with optical quality glass to provide high-resolution images (Mat Tek Corporation, USA). Phase-contrast and fluorescence time-lapse movies were taken on a Nikon 2000E microscope with a Hamamatus DCAM digital camera, using Andor iQ 1.4 software, with a 100 x oil-immersion lens at 20 seconds intervals. Actin dynamics were analysed in live RNAi-treated cells by time-lapse fluorescence microscopy using GFP-moesin to visualise F-actin. For this, cells were treated for five days with dsRNAs and then plated onto uncoated glass dishes. Baculovirus harbouring DNA for the expression of the actin-binding region of moesin fused to GFP was then added to the cells and incubated overnight (Kunda et al., 2003). Cells were then imaged on a Nikon 2000E microscope with a Hamamatsu DCAM digital camera, using Andor iQ 1.4 software. Typically, actin re-organisation in the cells was filmed using the FITC channel with a 100x oil-immersion lens at 20 sec intervals for 3 minutes before and for 10 minutes after addition of 10 μg/mL insulin. Membrane dynamics were filmed by phase-contrast microscopy, with a 100x oil-immersion lens. Kymographs of actin and membrane dynamics at the cell edge were generated from time-lapse movie images with MetaMorph software using a one pixel wide line drawn across the cell membrane at random points. Pixel data taken for each line from all images of each movie was combined to generate the kymographs.

Chapter 3: Proteomic analysis of PI3K signalling in human mammary luminal epithelial cells

3.1 Introduction

Many critical events involved in the cellular response to external stimuli are mediated by changes in post-translational protein modifications (PTM) rather than by transcriptional changes. PTMs are processes modifying the primary structure of proteins in a sequence-specific way that includes the reversible addition or removal of functional groups by phosphorylation, acylation, glycosylation, nitration, and ubiquitination (Mann and Jensen, 2003; Seo and Lee, 2004). These modifications induce structural changes in proteins and modulate their activities, subcellular localisation, stability and interactions with other proteins and molecules. The complexity of the proteome is increased significantly by post-translational modification, particularly in eukaryotes where many proteins exist as a heterogeneous mixture of alternatively modified forms. To date, at least 300 different types of PTMs have been identified (Jensen, 2004). One of the most studied PTM is protein phosphorylation, because it is vital for a large number of protein functions that are important to cellular processes such as signal transduction, cell differentiation, development, cell cycle control and metabolism. A primary role of phosphorylation is to act as a switch to turn "on" or "off" a protein activity or a cellular pathway in an acute and reversible manner (Hunter, 1995). Furthermore, it is estimated that up to one third of all proteins in eukaryotic cells are phosphorylated at some point in their life cycle and many possess more than one phosphorylation site and thus exist as a mixture of alternative phospho-forms (Zolnierowicz and Bollen, 2000). Today, it is accepted that almost all processes regulated by protein phosphorylation are reversible and controlled by the combined actions of two different classes of enzymes, namely protein kinases and phosphatases. These kinases and phosphatases constitute about

2% of the human genome (there are about 500 kinase and 100 phosphatase genes in the humane genome) (Venter et al., 2001; Manning et al., 2002; Alonso et al., 2004). The discovery of phosphorylation as a key regulatory mechanism of cell life, and the finding that perturbation in the protein phosphorylation status often leads to disturbance in cell biochemical and signalling pathways leading to abnormal information processing and development of various malfunctions that range from developmental defects to cancer, chronic inflammatory syndromes and diabetes (Yarden and Sliwkowski, 2001; Gray et al., 2003), has made protein phosphorylation an important study subject for many years.

Cell signalling through receptor tyrosine kinases (RTKs) plays a highly conserved role in metazoans, controlling fate determination, differentiation, proliferation, survival, migration and growth (Hunter, 2000). Autophosphorylation events on the tyrosine-kinase receptor following ligand binding and induced conformational change creates docking sites for many downstream adaptor and effector proteins, which then promote further activation of downstream signalling cascades. RTKs activate multiple downstream pathways, and one particularly well studied and evolutionary conserved component of these pathways is the lipid kinase PI3K family of enzymes, which have been implicated in the regulation of many important cellular functions (see Chapter 1). Akt takes a central place in PI3K-dependent signalling and it controls the activity of numerous proteins involved in important cellular processes such as cell survival, proliferation, size control and metabolism. Interestingly, it has been reported that there are a large number of potential Akt substrates (over 5700) identified by database searching (EBI Database-International Protein Index) using the Akt phosphorylation consensus motif (Zhang et al., 2002), so it is likely that many of these substrates remain to be characterised. In addition, Akt is an extremely important signalling node and has been proposed as a therapeutic target for the treatment of inflammatory diseases, diabetes and cancer (Vivanco and Sawyers, 2002; Altomare and Testa, 2005; Cheng et al., 2005). However, although the PI3K/Akt signalling pathway is well studied, there are still gaps in our understanding of the complexity of this pathway, its cross-talk with other signalling pathways and the existence of other downstream targets regulated by the PI3K/Akt cascade.

The work described in this chapter was designed to establish a model cell system for studying PI3K–dependent signalling and to monitor acute changes of the cellular complement of proteins and their phosphorylation status, which follow the PI3K-dependent activation. These aims were targeted using proteomic analysis consisting of 1D and 2D immunoblotting in combination with 2D gel-based proteomics. This was combined with immunoblotting analysis, which employed specific phospho-kinase substrate antibodies, such as a phospho-Akt substrate antibody, to monitor changes in protein expression and phosphorylation of Akt-specific substrates. In addition, the immunoblotting analysis was reinforced by employing 2D-DIGE analysis, which makes use of three charge- and size-matched, but spectrally distinct fluorescent tags (NHS-Cy2, -Cy3 and –Cy5), used for covalent labelling different samples prior mixing and separation on the same 2D gels. This system allows accurate and sensitive quantitation of protein expression across multiple biological samples (Chapter 1). Currently, 2D gel electrophoresis is the only method capable of simultaneously resolving several thousands of proteins (Kawada et al., 2001), including protein variants produced by post-translational processing such as phosphorylation, glycosylation, and sulfation (Guy et al., 1994) in one run. The phosphorylation of a protein often leads to a decrease in its pI and consequently in its coordinates in a 2D gel. Thus, 2D gel electrophoresis has been used to discriminate phosphoproteins from nonphosphorylated proteins and post-electrophoretical gel staining techniques have been used to detect phosphoproteins to distinguish them from total proteome. Furthermore, combining 2D gel electrophoresis with mass spectrometry allows identification of proteins with differential expression or phosphorylation.

To investigate the role of PI3K signalling in response to EGF, a cellular model of breast epithelial cells, the HB4a cell line, was chosen. This immortalised luminal epithelial cell line was derived from reduction mammoplasty tissue of a normal subject (Stamps et al., 1994). These cells are conditionally immortal cells derived by infection of human breast epithelial cells with an amphotropic retrovirus, which transduced a ts mutant of SV40 large T-antigen. This process of immortalisation involves the sequestration and inactivation of the tumour suppressor proteins p53 and pRb by the SV40 large-T antigen. These proteins normally downregulate the cell cycle, but also act as sensors of cell damage to induce cell cycle arrest and apoptosis,

given the appropriate stimuli. HB4a cells display several markers of the luminal epithelial cell type and have a characteristic luminal epithelial cellular morphology in culture. This cell line also responds to EGF stimulation as the cells express the EGF receptor, and are able to activate PI3K signalling pathway in response to various growth factor treatments or stress-inducing treatments, e.g. H_2O_2, as shown from previous work in our laboratory (Timms et al., 2002; White et al., 2004; Chan et al., 2005).

3.2 Examination of PI3K signalling in luminal epithelial cells in response to EGF

For preliminary examination of EGF-dependent PI3K signalling in HB4a cells, an experiment was carried out where HB4a cells were pre-incubated with LY294002, a synthetically produced and widely used PI3K inhibitor (Vlahos et al., 1994), prior to EGF stimulation. For this purpose serum-starved HB4a cells, at 80% confluence, were pre-treated with 10 μM LY294002 for 30 min, followed by treatment with 1 nM EGF over a time course. DMSO served as a vehicle control to the LY294002 treatment. Cells were lysed, protein concentration was measured and equal amounts of proteins from different samples were separated by 1D SDS-PAGE and transferred onto membranes for western blot analysis. The membranes were probed with phosphospecific antibodies, and then reprobed with the respective pan antibodies. The use of the phosphospecific antibodies allowed detection of the fraction of a protein that is phosphorylated, whereas the pan antibodies detected the total amount of the respective kinase and/or its substrate.

PI3K signalling was monitored by measuring the phosphorylation of Akt, GSK-3 and 4E-BP1 over time following stimulation with EGF. Akt, a direct downstream target of PI3K signalling pathway, is activated in response to PIP3 production that drives Akt-membrane recruitment through binding to its pleckstrin homology (PH) domain, followed by phosphorylation of Akt at Thr308 and Ser473 sites. In this experiment, EGF stimulation induced Akt phosphorylation at the Ser473 site in control cells, but EGF-dependent Ser473-Akt phosphorylation was largely blocked by

LY294002 treatment, confirming the findings of many reports that Akt is downstream of PI3K (Figure 3.1). In addition, the phosphorylation of 4E-BP1 was tested. 4E-BP1 is a downstream target of the Akt/mTOR signalling branch, and it binds cap-dependent eukaryotic initiation factor (eIF4E) to inhibit translation (Beretta et al., 1996; Gingras et al., 1998). Hyperphosphorylation of 4E-BP1 disrupts this binding and activates cap-dependent translation. In this experiment, phosphorylation at Ser65 site of 4E-BP1 was tested, which revealed that PI3K inhibition by LY294002 prevented EGF-induced 4E-BP1 phosphorylation. Glycogen synthase kinase 3 (GSK3) can phosphorylate and inactivate glycogen synthase, cyclin D1 and other targets, and is an important element of PI3K/Akt cell survival signalling branch (Cohen and Frame, 2001). Mammals harbour two distinct genes for GSK3 encoding related protein kinases, GSK3-α and β, with similar catalytic properties. The activity of GSK3 can be inhibited by PI3K/Akt–mediated phosphorylation of GSK3-α at Ser21 and GSK3-β at Ser9 (Cross et al., 1995). In this experiment EGF induced the phosphorylation of GSK3-β on Ser9, and while LY294002 blocked basal phosphorylation of GSK3-β on Ser9, it did not noticeably block EGF-induced phosphorylation, although it has been reported that LY294002 prevents PI3K/Akt-mediated phosphorylation on GSK3-β (Cross *et al.*, 1995).

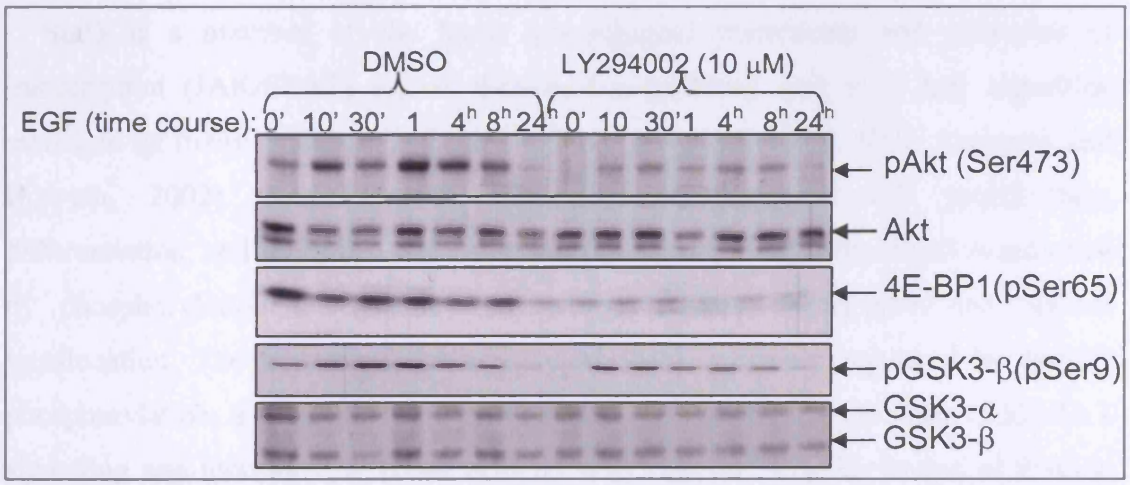

Figure 3.1 Effect of EGF stimulation and LY294002 treatment on PI3K pathway activity in HB4a cells. HB4a cells were maintained in serum free medium for 48 h. Cells were then pre-treated with DMSO or LY294002 (10 μM) for 30 minutes, followed by 1 nM EGF treatment over the indicated time course. Antibodies specific for phosphorylated Akt, GSK3-β and 4E-BP1 were used to test for the EGF-dependent phosphorylation of these downstream PI3K targets. Pan specific antibodies against Akt and GSK3 were also used to monitor loading and changes in the expression levels of the proteins.

In parallel to PI3K signalling, MAPK signalling was also monitored by blotting the same samples with antibodies against phosphorylated ERK1/2 and p90RSK (Figure 3.2). The ERK (MAPK) signalling cascade is activated downstream of many tyrosine kinase receptors in response to ligand binding and regulates many cellular processes (Schaeffer and Weber, 1999). In this study, EGF treatment induced phosphorylation of ERK at the Thr202/Tyr204 sites in the first minutes of the treatment and this phosphorylation was sustained for the following 8 hours, after which it declined to background levels by 24 hours. The EGF-dependent phosphorylation of Erk1/2 was not blocked by LY294002, confirming that the EGFR/Ras/MAPK signalling cascade acts independently of the EGFR/PI3K signalling cascade in HB4a cells. p90RSK (MAPK-activated protein kinase-1), a downstream target of ERK1/2, is a member of the RSK family of widely expressed serine/threonine kinases activated by MAPKs in response to many growth factors. p90RSK regulates a number of cellular functions through phosphorylation and regulation of multiple transcriptional factors (Frodin and Gammeltoft, 1999). In this work, phosphorylation of p90RSK at Thr359 and Ser363 sites, which are necessary for its activation (Dalby et al., 1998), was also found to be EGF-dependent. Controversially, LY294002 partially blocked this phosphorylation of p90RSK, suggesting that PI3K may contribute to p90RSK activation.

Stat3 is a member of the Janus kinase/signal transducers and activators of transcription (JAK/STAT) signal transduction pathway and is a key signalling molecule for many cytokines and growth factor receptors (Heim, 1999; Aaronson and Horvath, 2002). Activation of this pathway stimulates cell proliferation, differentiation, cell migration and apoptosis (Rawlings et al., 2004). Stat3 is activated by phosphorylation at tyrosine 705, which induces dimerisation and nuclear translocation. The transcriptional activity of Stat3 is further regulated by Ser727 phosphorylation, apparently via MAPK and/or mTOR. PI3K-dependent JAK/STAT signalling was monitored in HB4a cells by following the phosphorylation of Stat3 at the Ser727 site (Figure 3.2). Here, EGF treatment resulted in the stimulation of Ser727 phosphorylation, which reached a maximum at 1 hour after the stimulation. In the cells pre-treated with LY294002 there was a diminished response, suggesting a modulatory role for PI3K activity in Stat3 signalling.

Mitogen-dependent changes in the expression of two critical cell cycle regulatory proteins ($p27^{Kip1}$ and cyclin D1) were also monitored to assess the role of PI3K signalling in cell cycle control (Figure 3.2). $p27^{Kip1}$ is a member of the cyclin-dependent kinase inhibitor proteins. These inhibitors form heterotrimeric complexes with cyclins and cyclin dependent kinases (CDKs), inhibiting kinase activity and blocking progression through G1/S phase (Pestell et al., 1999). Levels of $p27^{Kip1}$ are upregulated in quiescent cells and in cells treated with negative regulators of the cell cycle. In this experiment, there were no significant changes in the levels of $p27^{Kip1}$ over time with EGF stimulation in both cells pre-treated with DMSO and LY294002, suggesting that EGF stimulation, as well as PI3K inhibition do not overtly perturb the total level of this protein in these cells.

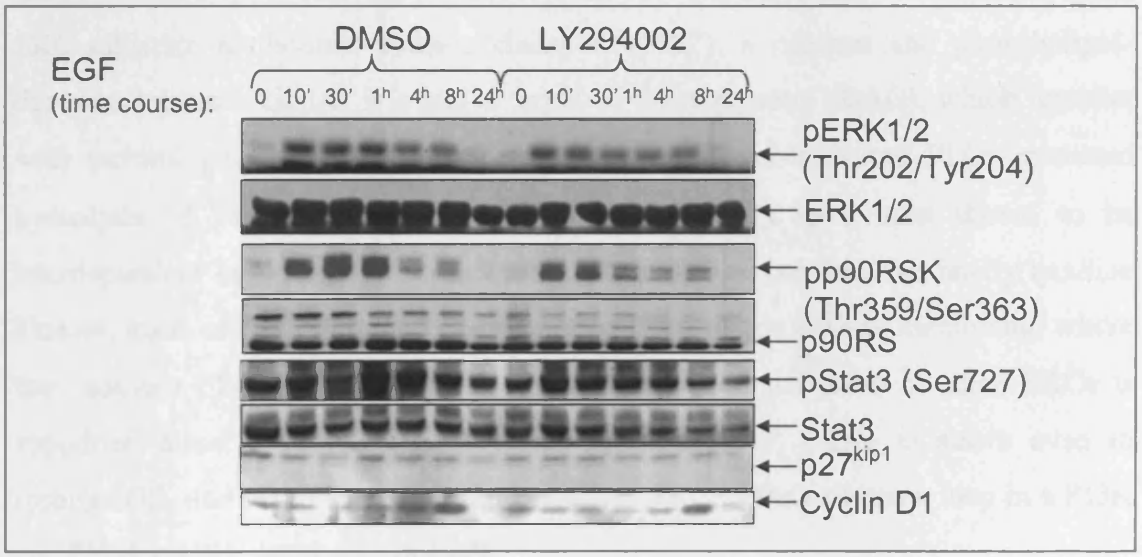

Figure 3.2 Effect of EGF stimulation and LY294002 treatment on MAPK and STAT pathway activation in HB4a cells. HB4a cells were maintained in serum free medium for 48h. Cells were then pre-treated with DMSO or LY294002 (10 μM) for 30 minutes followed by 1 nM EGF treatment over the indicated time course. Antibodies specific for phosphorylated p90RSK, ERK and Stat3 were used to test the EGF-dependent stimulation of these EGFR downstream targets. In addition, pan-antibodies against p90RSK, ERK and Stat3 were also used to reprobe membranes to monitor total expression and loading of the protein samples. Antibodies against cyclin D1 and $p27^{Kip1}$ were also used to test effects on cell cycle proteins.

Cyclin D1 regulates the transition from G1 to S phase of the cell cycle. Its expression is induced by mitogens and it peaks during G1 phase when it binds to and activates cyclin-dependent kinases (Cdks), such as Cdk4 and Cdk6 (Harbour et al.,

1999). In this experiment, cyclin D1 expression was induced maximally at a late time point (8 hours) and was then reduced to background levels after 24 h (Figure 3.2), in accordance with its known ubiquitin-dependent proteosomal degradation (Diehl et al., 1997). There was a minimal effect of the LY294002 treatment on this response, indicating that PI3K signalling does not play a major role in regulating cell cycle progression in these cells.

Having established that HB4a cells can respond to EGF by activating PI3K-dependent signalling, the next goal was to look globally at specific kinase-dependent phosphorylation events. In order to detect PI3K-dependent phosphorylation changes in Akt- or PKC-substrates in response to EGF treatment, protein samples were immunoblotted with anti phospho-(Ser/Thr) Akt substrate and anti phospho-(Ser) PKC-substrate antibodies. Protein kinase C (PKC), a calcium and phospholipid-dependent protein kinase, is a major target of diacylglycerol (DAG), which together with inositol phosphate are direct products of receptor-activated PLCγ–mediated hydrolysis of PIP2. Importantly, the PI3K and PLCγ have been shown to be interdependent because PIP3 binds to the PH domains of certain Tec family tyrosine kinases, such as Btk, Itk and Tec, localising them to the plasma membrane, where they activate PLCγ and DAG production. In addition, activation of some PKCs is supported directly by PI3K-independent PDK1 activity. PDK1 is active even in resting cells, and it can bind and phosphorylate PKC in the activation loop in a PI3K and PH-domain independent manner.

The phospho-(Ser/Thr) Akt substrate antibody used recognises preferentially peptides and proteins containing phospho-(Ser/Thr) preceded by Lys or Arg at positions -5 and -3, in a manner largely independent of other surrounding amino acids in the sequence. The phospho-(Ser) PKC substrate antibody detects endogenous levels of many cellular proteins only when phosphorylated at serine residues surrounded by Lys or Arg at the -2 and +2 positions with a hydrophobic residue at the +1 position. In both western blot analyses, the most obvious difference found was an increase of a signal at around ~30 kDa in response to EGF stimulation, which was blocked (pAkt-substrates) or reduced in (pPKC-substrates) samples pre-treated with LY294002 (Figure 3.3). Other differences were also evident, but were poorly resolved. Thus, the

observed change in phosphorylation of a protein at ~30 kDa was an interesting target for further investigation. In addition, in order to monitor PI3K-dependent tyrosine phosphorylation events, a membrane was probed with the anti-phosphotyrosine (pY) antibody clone 4G10 (Figure 3.3). EGF treatment was found to increase a phosphotyrosine signal in the first few minutes and hours of the stimulation, which weakened in the later time points. A similar phosphorylation pattern was observed in the cells pre-treated with LY294002, showing that "bulk" tyrosine phosphorylation events induced by EGF are not dependent upon PI3K.

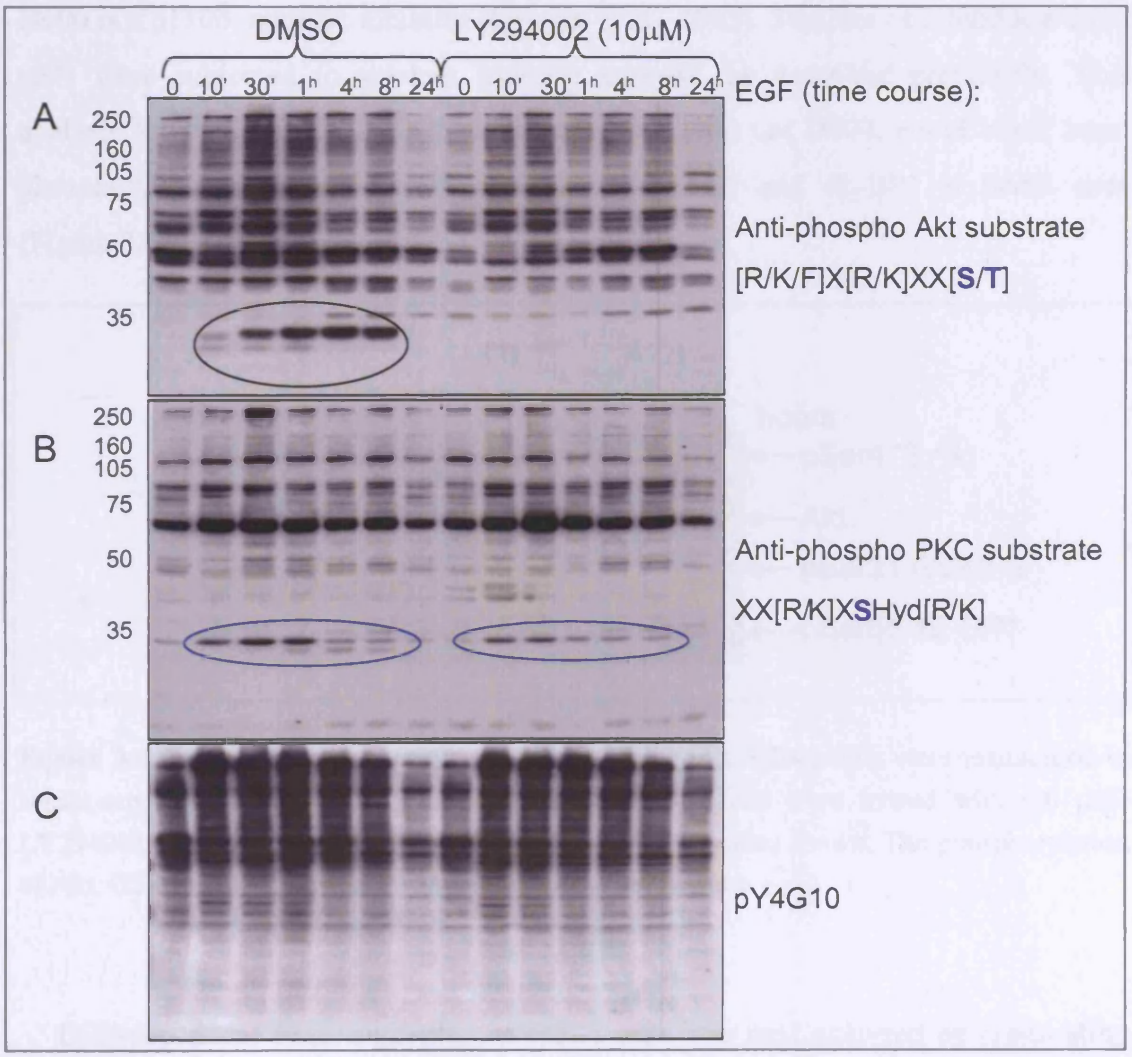

Figure 3.3 PI3K-dependent phosphorylation of Akt- and PKC- substrates and phosphotyrosine in response to EGF stimulation. HB4a cells were maintained in serum free medium for 48h. Cells were then pre-treated with DMSO or LY294002 (10 μM) for 30 minutes followed by 1 nM EGF treatment for the indicated times. Phospho-Akt (**A**) and phospho-PKC (**B**) substrate antibodies that recognise specific phosphorylation of Ser/Thr in the Akt motif and phosphorylation of Ser in the PKC motif, as well as an anti-pY antibody (**C**), were used for immunoblotting.

3.3. Examination of PI3K inhibitor-specific effects in HB4a cells in response to EGF

To examine PI3K inhibitor-specific effects on the basal phosphorylation level of downstream targets of PI3K, randomly growing cells were treated with three different PI3K inhibitors. The inhibitors LY294002, wortmannin and D000 were used. Wortmannin is a fungal metabolite potent at inhibiting PI3K activity (Arcaro and Wymann, 1993), and like LY294002, is widely active across the PI3K family, while D000 is a p110δ–specific inhibitor (Sawyer et al., 2003). Samples of inhibitor-treated cells were subjected to western blotting analysis, as described previously. This analysis showed that LY294002 and wortmannin, but not D000, could block basal phosphorylation of Akt at Ser473, GSK3-α at Ser21 and 4E-BP1 at Ser65 sites (Figure 3.4).

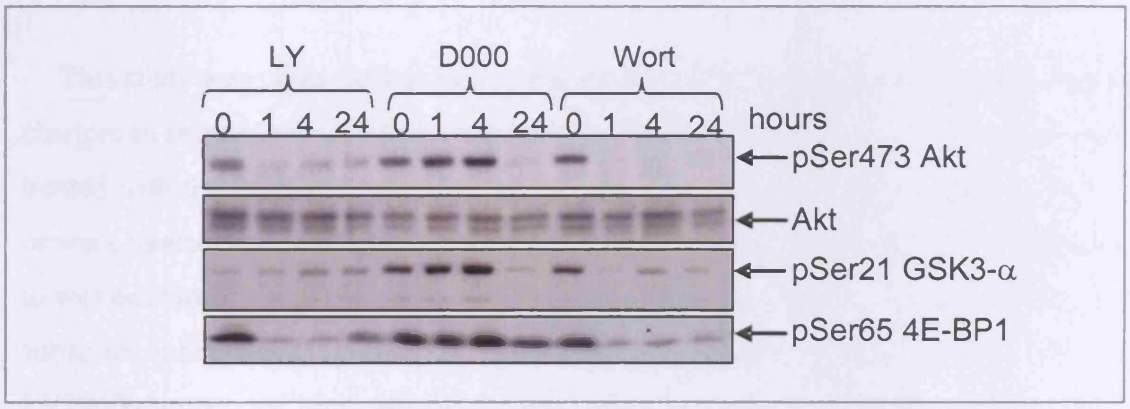

Figure 3.4 PI3K inhibitor-specific effects on PI3K/Akt. HB4a cells were maintained in serum-supplemented medium prior to drug treatment. Cells were treated with (10 μM) LY294002, wortmannin (100nM) or D000 (2μM) for the times shown. The phosphorylation of Akt, GSK3, and 4E-BP1 were analysed by western blotting.

EGF-dependent PI3K signalling in HB4a cells was next analysed by pre-treating randomly growing cells with the three PI3K inhibitors followed by EGF for 1 hour. Samples were immunoblotted with antibodies against specific phosphorylation sites of Akt and GSK3 (Figure 3.5). The analysis revealed that wortmannin and LY294002 blocked EGF-induced phosphorylation of Ser473-Akt and had a slight effect on Ser9-

GSK3-β. D000 failed to block EGF-induced phosphorylation of the two targets analysed.

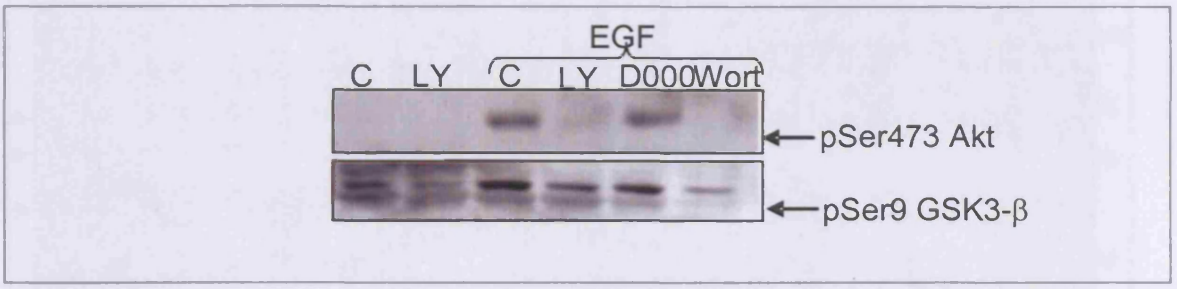

Figure 3.5 Effect of different PI3K inhibitors on EGF-activated PI3K/Akt signalling. Serum-starved HB4a cells were treated with PI3K inhibitors (10 μM LY294002, 100 nM wortmannin or 2 μM D000) for 30 min., prior to 1 nM EGF stimulation for 1 h. Western blot analysis was carried out using anti-phospho Ser473-Akt and Ser9-GSK3-β antibodies. C stands for control pre-treated with DMSO.

This study was taken further by examining global PI3K-dependent phosphorylation changes in response to inhibitor treatment and EGF stimulation. HB4a cells were pre-treated with the PI3K inhibitors for 30 minutes, followed by EGF stimulation for 1 h, or were treated with vehicle (DMSO), LY294002 or EGF alone. Cells were subjected to western blotting analysis using anti-Akt, anti-PDK1 and anti-PKC phospho-specific substrate antibodies (Figure 3.6). This analysis confirmed the previously observed LY294002-mediated blockade of phosphorylation events and an apparent mass shift of a putative Akt and PDK1 substrate of ~30 kDa whose phosphorylation was induced by EGF. The appearance of the lower mass form may represent a dephosphorylation-induced shift in apparent molecular weight, although it would appear that this form is still phosphorylated perhaps on another site or sites. Other altered bands were also apparent in the gels. The same phenomena were observed in wortmannin, but not in D000 pre-treated cells, suggesting that observed phosphorylation events are probably p110α- and p110β-dependent and not dependent on p110δ. This is likely to be true because p110δ expression is low in these cells and displays a more haematopoietic pattern of expression (Sawyer et al., 2003). The inhibitors had little effect on the phosphorylation of putative PKC substrates, although the 30 kDa protein was just detectable.

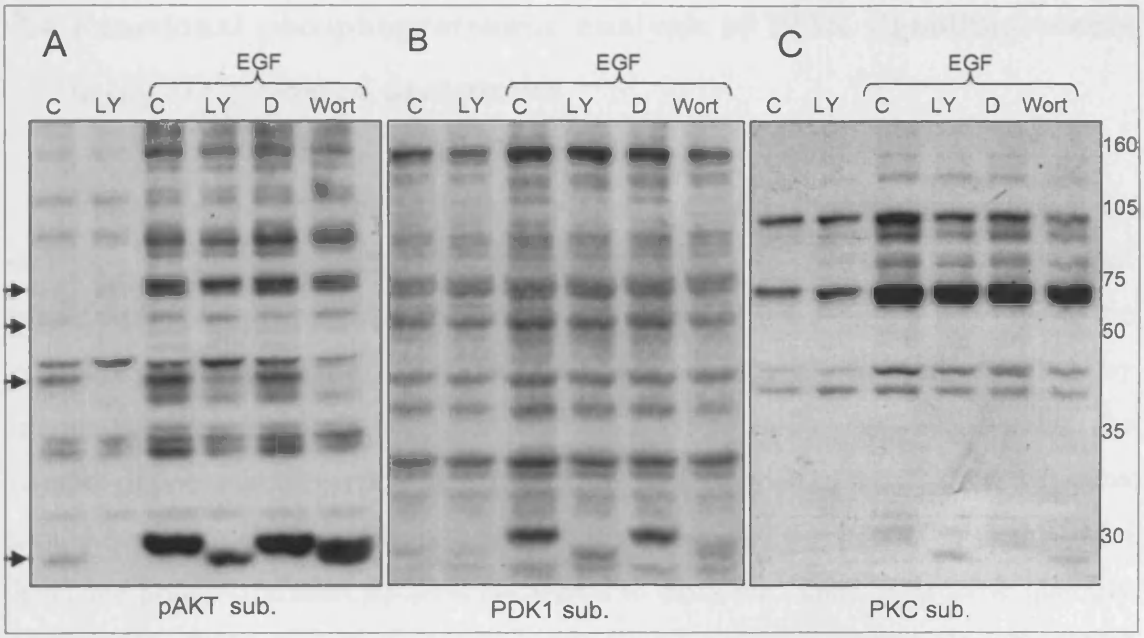

Figure 3.6 Effect of PI3K inhibitors on phosphorylation of Akt-, PDK1- and PKC-substrates in response to EGF stimulation. HB4a cells were maintained in serum free medium for 48h. Cells were then pre-treated with LY294002 (10 μM), wortmannin (100 nM) and D000 (2 μM) for30 minutes, followed by 1 nM EGF treatment for 1h. Anti phospho-Akt (**A**), phospho-PDK1 (**B**) and phospho-PKC (**C**) substrate antibodies recognising specific phosphorylation site motifs for these kinases were used for western blotting. Arrows indicate altered band intensities. (C, D, LY and Wort stand for DMSO treated control, D000-, LY294002-, and wortmannin treated cells, respectively).

Taken together, it can be concluded that LY294002 and wortmannin both block the phosphorylation events induced by EGF stimulation. In contrast, it was expected that D000 would not have an inhibitory effect on the EGF-induced stimulation of downstream targets of PI3K signalling in the mammary luminal epithelial cells, since the p110δ is most likely not expressed in these cells. In my work here, I have found that despite the ability to identify differentially expressed or phosphorylated kinase substrates that depended upon PI3K activity this kind of 1D blotting-based analysis method is limited. Further experimentation using more advanced proteomic techniques such as fluorescence protein labelling in combination with 2D gel electrophoresis and protein identification by mass spectrometry were used to facilitate quantitative protein expression profiling of PI3K-dependent signalling events and help to identify new targets of PI3K activity.

3.4 Functional phosphoproteomic analysis of PI3K signalling events using 2D gel-based proteomics

Immunoblotting analysis can be a very sensitive and highly specific approach for detection of changes in protein levels as well as of altered post-translational modifications. In the previous sections, it was shown that although differences in the phosphorylation dynamics of putative kinase substrates can be detected by immunoblotting, these protein substrates could not be easily identified, because the number of potential theoretical substrates with phosphorylation motifs for a particular kinase is often high. In addition, quantitation of observed differences in total protein level and phosphorylation status is not trivial to carry out. Thus, in order to quantify and identify PI3K-dependent changes in the total proteome and in phosphorylated proteins in response to EGF, a functional proteomics approach combining immunoblotting and 2D-DIGE was carried out.

In a preliminary 2D-DIGE experiment, HB4a cells were pre-treated with LY294002 (LY) or vehicle (DMSO) alone for 30 minutes followed by EGF treatment for 1 hour. Cells were lysed in a urea-CHAPS based 2D-lysis buffer and subjected to 2D-DIGE analysis, as described in the methods in Chapter 2. Briefly, equal amount of protein lysate from the two conditions were labelled with Cy3 and Cy5, respectively. The samples were mixed and run on an 18 cm pH 3-10 non-linear IPG strip in the first dimension, followed by 10% SDS-PAGE in the second dimension (Figure 3.7 A). The gel was scanned at two different excitation/emission wavelength combinations generating two fluorescent images of proteins labelled with Cy3 and Cy5. Images were imported into DeCyder software for image analysis. Paired fluorescent images were automatically matched using the DIA module of the software, as the images are directly superimposable (Figure 3.7 A). Gel images were then normalised and processed to calculate spot abundances and fold ratios of abundance between the two samples. This quantitative analysis showed 15 differentially expressed protein features (>1.5 fold changes in abundance) between EGF and EGF+LY treated samples out of 1986 detected features. Of these, 12 protein spots were upregulated in the EGF-treated sample versus the EGF+LY sample and 3 were downregulated (Figure 3.7 B).

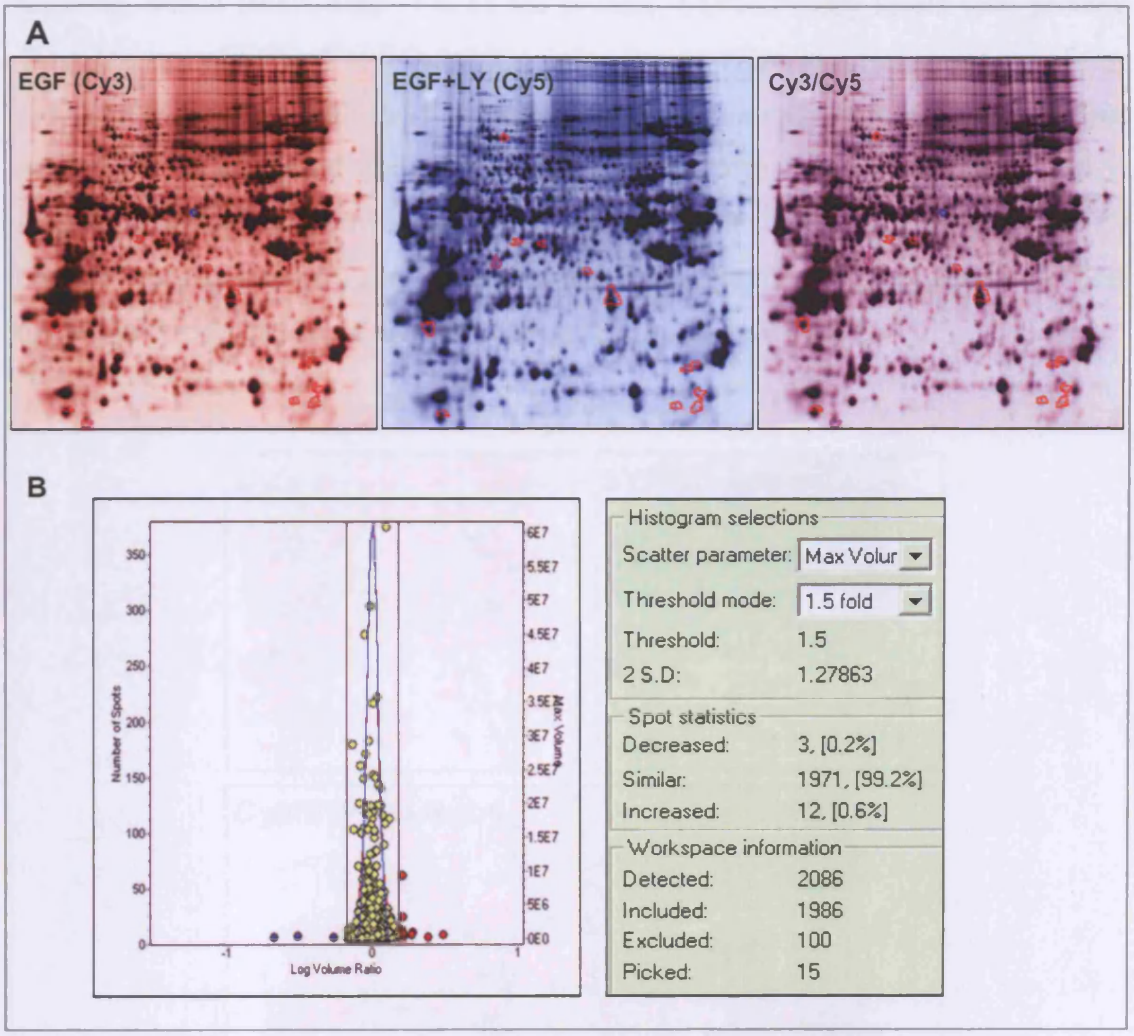

Figure 3.7 Example of DIA module analysis in DeCyder software. HB4a cells were treated with EFG (1 nM) alone for 1 hour and EGF following 30 minutes LY294002 (10 μM) pretreatment. Cell lysates from the two conditions were labelled with Cy3 and Cy5, respectively, mixed and run on the same 2-D electrophoresis gel. Gel images were curated using the DIA module of DeCyder software. **A)** Separate Cy3 and Cy5, as well merged Cy3 and Cy5 gel images, edited in Photoshop for presentation purpose only, are shown. **B)** Scatter plot of spot volume and number versus volume ratio is shown with a threshold ratio set at 1.5 (+/- 2SD) (vertical lines) and spot statistic information.

Following the image analysis, the gel was stained with SYPRO Ruby. SYPRO Ruby detects most proteins including those which are difficult to stain such as glycoproteins, calcium-binding proteins, lipoproteins and fibrillar proteins, without staining nucleic acids (Berggren et al., 2000). It can detect as little as 1-2 ng of protein, similar to the detection limit of silver staining, but having greater sensitivity than Coomassie Brilliant Blue, both of which are used for protein staining of 2D gels (Berggren et al., 2000; Gorg et al., 2000). In contrast to non-saturating Cy-dye

labelling, which labels only ~5% of the protein, SYPRO Ruby labels total protein. Thus, the aim of using SYPRO Ruby staining was to allow accurate matching of Cy-dye labelled proteins with the total protein pool to facilitate automated protein spot picking. The Cy-labelled fluorescent images were matched with the SYPRO Ruby-stained gel image and showed an almost perfect match (Figure 3.8), although a shift between the Cy-labelled and total pool has been previously observed in the low molecular weight region of the 2D-DIGE gels (Gharbi et al., 2002).

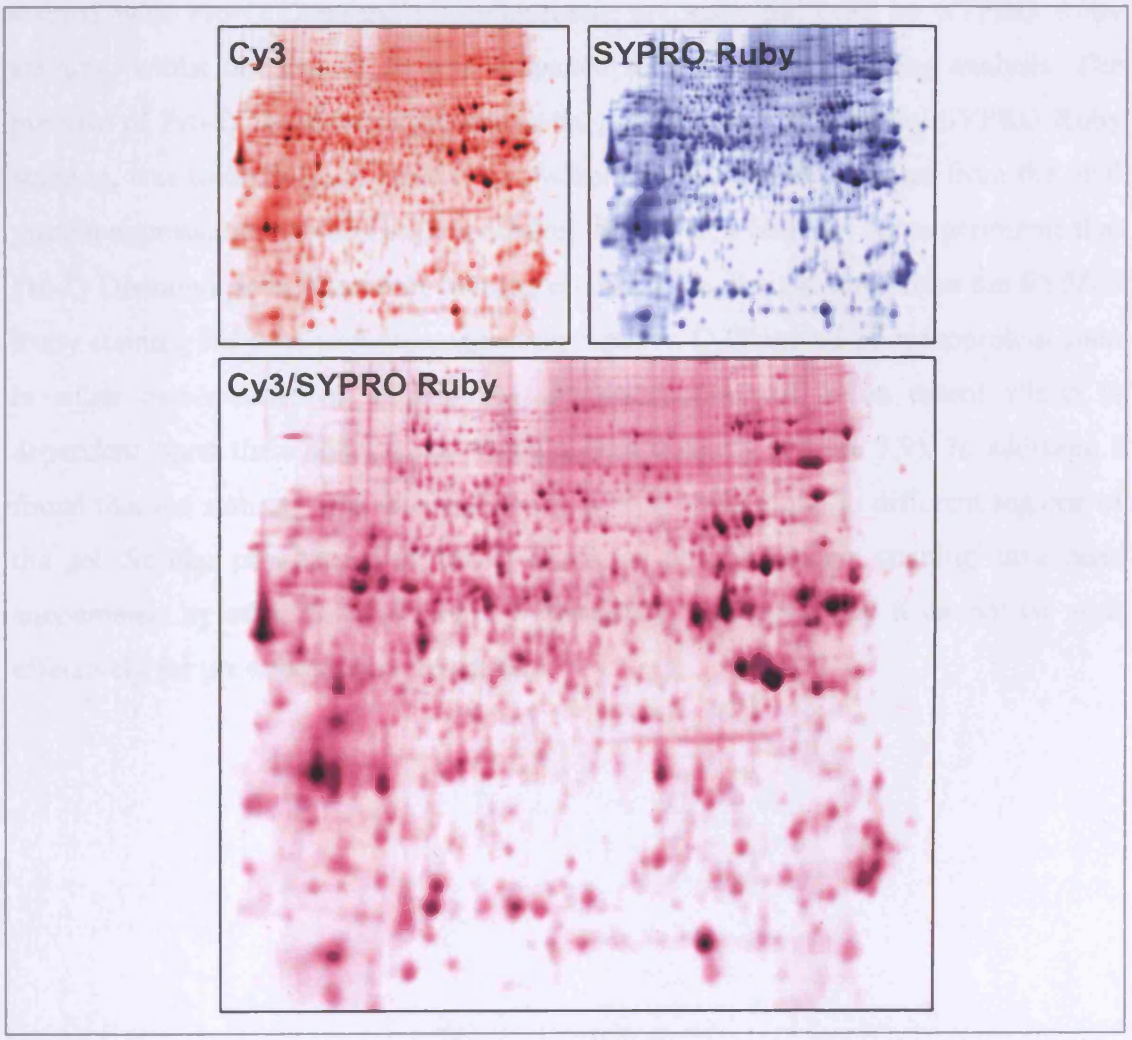

Figure 3.8 Post-staining of 2D-DIGE gel with SYPRO Ruby. Differently treated HB4a cells were lysed and labelled with Cy3 and Cy5and proteins were separate by 2-DE. The same 2D gel was used for post-staining with SYPRO Ruby stain. The Cy3 image (red) was merged with SYPRO Ruby image (blue) to match total protein with the Cy-dye labelled proteins and possibly to detect any shift in the protein migration caused by Cy-dye labelling. Cy3, SYPRO Ruby and the merged image were edited in Photoshop for presentation purposes only.

The specific staining of phosphoproteins was also attempted using the fluorescent Pro-Q Diamond phosphoprotein stain (Schulenberg et al., 2003). Pro-Q Diamond phosphoprotein stain has been reported to detect phosphate groups attached to tyrosine, serine and threonine residues, and it is advertised as an ideal stain for detection of kinase targets in signal transduction pathways and for phosphoproteomic studies, with the signal intensity correlating with the number of protein phosphates. Thus, in parallel to the 2D-DIGE analysis, two pairs of 2D gels were run. In each set, EGF and LY294002+EGF samples were run separately. One gel from each set was stained with Pro-Q Diamond phosphoprotein gel stain followed by SYPRO Ruby staining, whilst the second set was subjected for 2D western blotting analysis. The purpose of Pro-Q Diamond phosphoprotein gel staining, followed by SYPRO Ruby staining, was to distinguish potentially phosphorylated protein features from the total protein expression profile in each condition. However, I found in my experiments that Pro-Q Diamond phosphoprotein staining could not be distinguished from the SYPRO Ruby staining for total protein, suggesting that Pro-Q Diamond phosphoprotein stain is either non-specific or all proteins are phosphorylated to an extent which is dependent upon their abundance, which seems unlikely (Figure 3.9). In addition, I found that the staining was uneven, giving a high background in different regions of the gel. Similar problems with Pro-Q Diamond phosphoprotein staining have been encountered by other members of my laboratory, indicating that it cannot be used effectively for phosphoprotein detection.

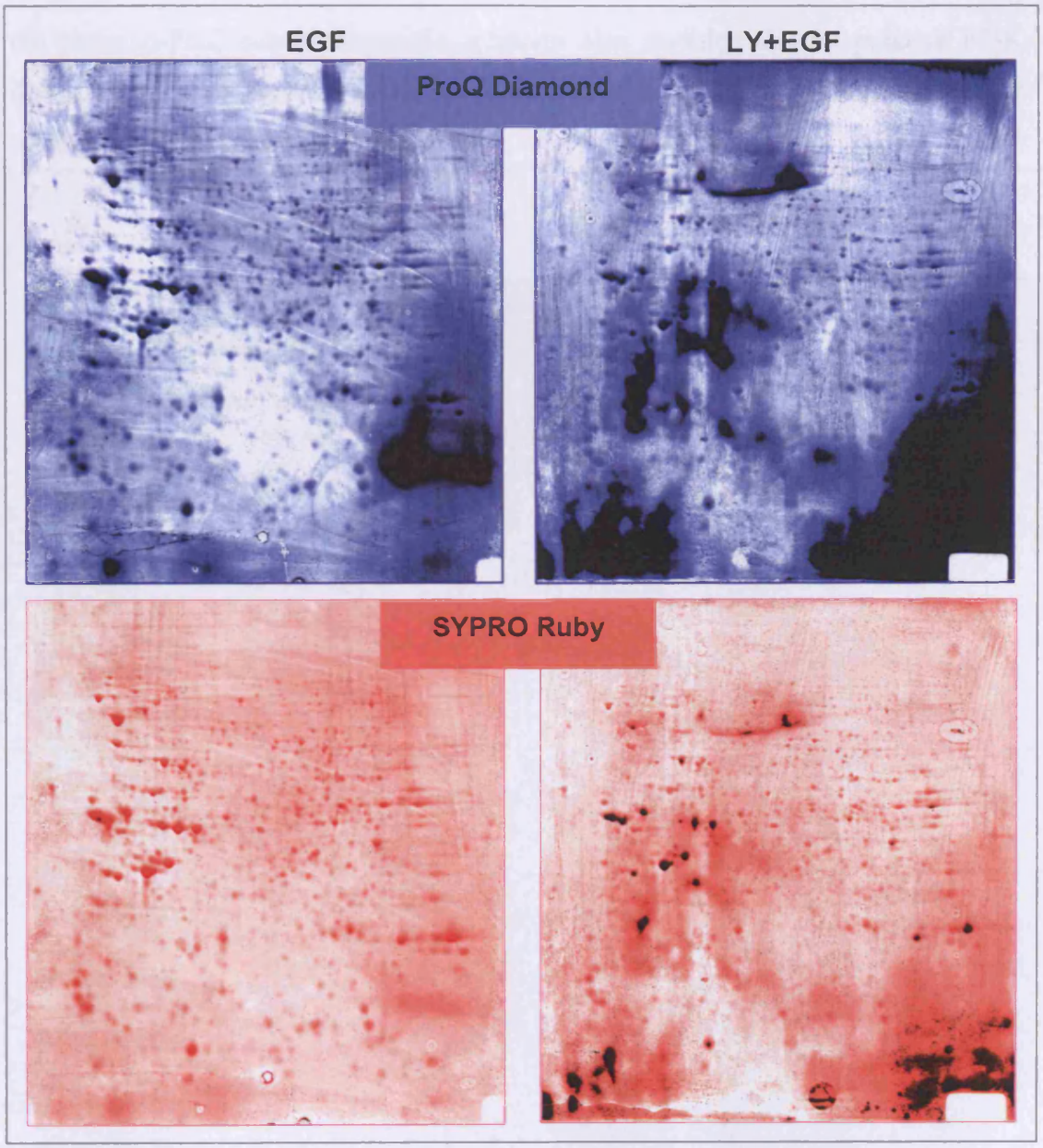

Figure 3.9 Pro Q-Diamond and SYPRO Ruby staining of 2D gels. 2D gels were subjected to phosphoprotein staining with Pro Q-Diamond, scanned and then destained for re-staining for total protein with SYPRO Ruby. Scanning was performed on a Typhoon multi-wavelength fluorescence scanner.

2D immunoblotting analysis of phosphorylated Akt substrates in the two treatments (EGF and LY294002+EGF) once more detected a phosphorylation event at ~30 kDa in EGF treated cells, which was blocked in cells pre-treated with LY294002 (Figure 3.10). There were also several other phosphorylation events, which were absent or altered in LY294002 treated cells, suggesting that phosphorylation of these Akt substrates in response to EGF was blocked by LY294002. Immunoblotting with

the phospho-PKC substrate-specific antibody also revealed several putative PI3K-dependent PKC substrates, some of which appeared to be cross-reactive with the Akt-specific substrate antibody (Figure 3.10).

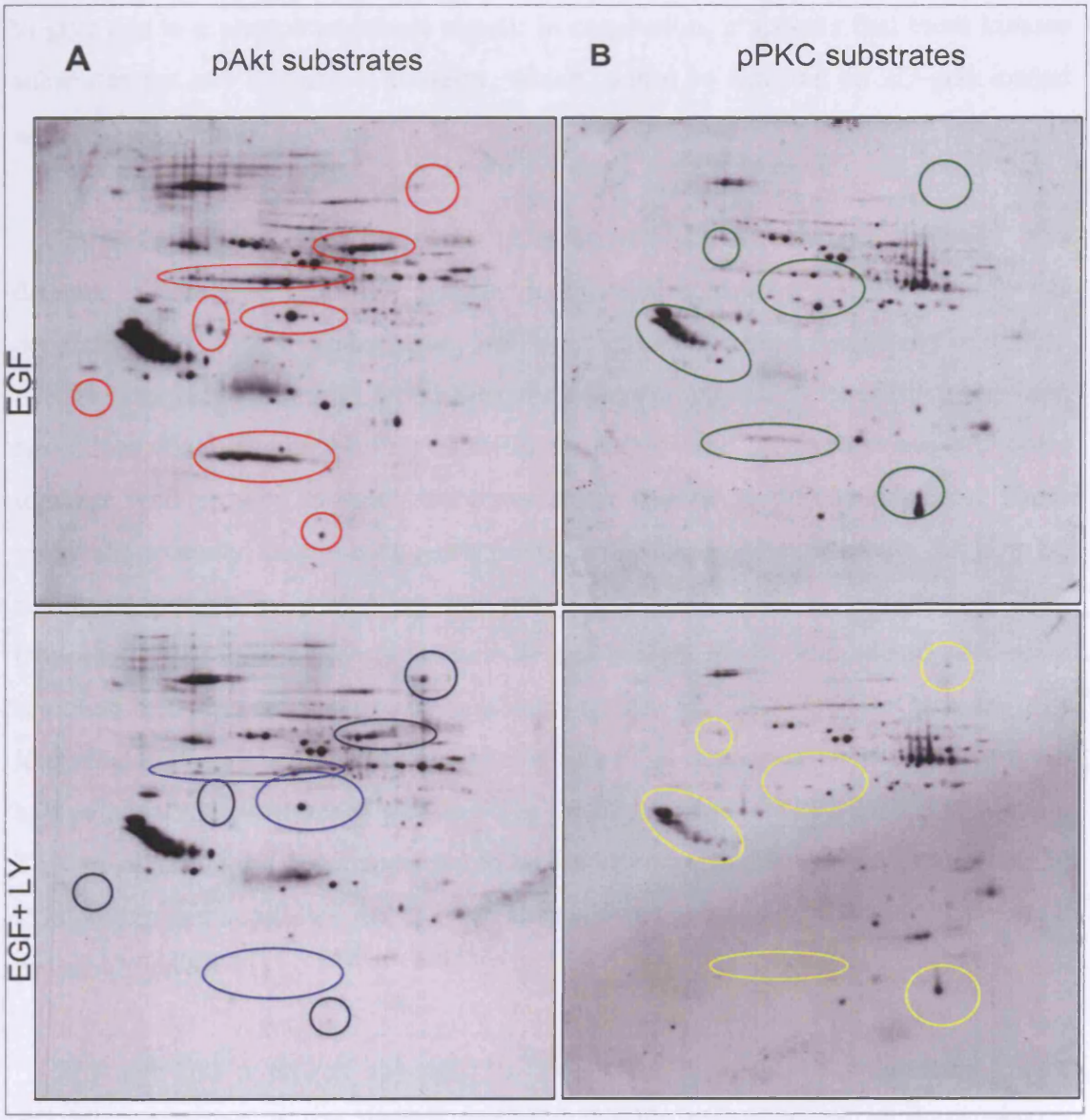

Figure 3.10 Detection of PI3K-dependent phosphorylation of Akt- and PKC- substrates in response to EGF by 2D immunoblotting. Serum starved HB4a cells were pre-treated with LY294002 for 30 min, followed by EGF stimulation for 1 h. Protein lysates were subjected to 2D immunoblotting using antibodies against phosphorylated Akt (**A**) and PKC (**B**) substrates that recognise specific phosphorylated motifs. Circled futures in red represent prominent differential pAkt substrates in EGF treated cells versus the same protein feature (blue circle) in cells pre-treated by LY294002. Circled futures in green represent differential pPKC substrates in EGF treated cells versus the same protein feature (yellow circle) in cells pre-treated by LY294002.

Although NHS-Cy labelling is quite sensitive, the observed differences in phosphosubstrate signals could not be aligned with Cy-dye images from the preliminary DIGE analysis. Moreover, none of the 15 altered protein spots appeared to give rise to a phosphosubstrate signal. In conclusion, it appears that these kinases substrates are low abundance proteins, which cannot be detected on 2D gels loaded with 300 μg of protein lysate.

An earlier study using the same phosphospecific Akt substrate antibody also detected a change in a 30 kDa protein in ES cells in response to EGF, which was dependent upon PDK1 (Zhang *et al.*, 2002). In this study immunoreactivity of PDK1-/- ES cell extracts with wild type ES extracts were compared by combining one- and two-dimensional immunoblotting analysis using Akt- and PKC- substrate antibodies together with protein database searching using epitope specificity matrices. These scientists predicted and subsequently identified phosphorylation in the 30 kDa S6 ribosomal protein in wild type, but not PDK1-/- ES cells in response to EGF treatment. This information was used in the present study, and membranes were reprobed with a phosphospecific antibody against S6. This western blot analysis identified EGF-induced S6 phosphorylation as a PI3K-dependent event and S6 protein as a putative Akt substrate as well as S6 as the highly likely 30 kDa candidate protein. This phosphorylation event appeared to be associated with a large shift in pI of the 30 kDa protein and suggested that the two altered features could be isoforms of the same protein (Figure 3.11).

Although this approach appeared to be a sensitive method for detecting kinase specific substrates, it has limited potential for the identification of these protein substrates. Firstly, I found that it is hard to predict which of the protein substrates change even when using database information, so that targets can be validated using specific antibodies against them. Secondly, it is hard to match 2D immunoblotting images with 2D fluorescence gel images, most likely due to the low abundance of these putative signalling molecules; matching would facilitate detection of the right protein spot from a 2D gel for subsequent picking and identification by mass spectrometry.

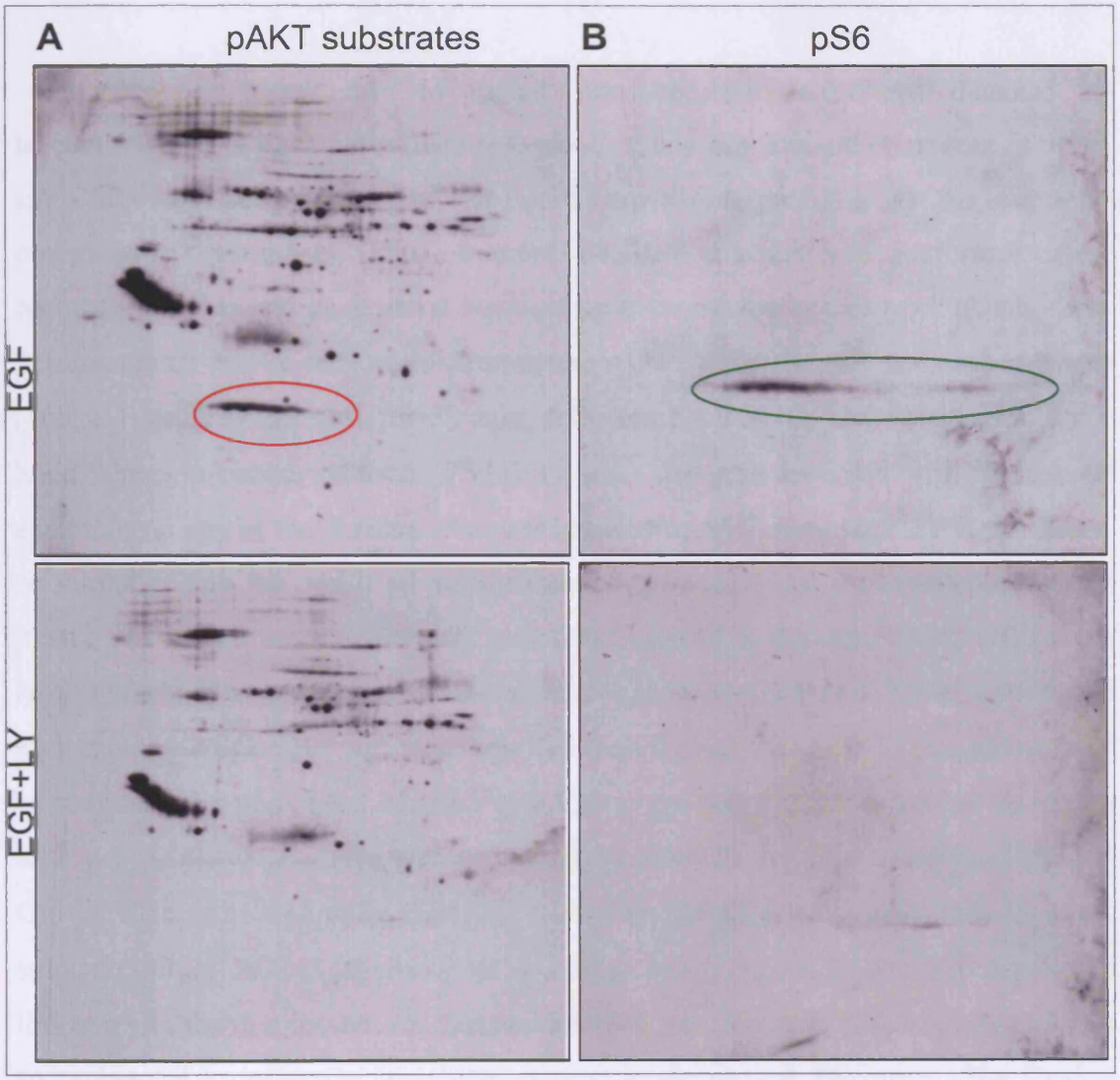

Figure 3.11 Identification of S6 protein as an Akt substrate. Serum starved HB4a cells were pre-treated with LY294002 for 30 min, followed by EGF stimulation for 1 h. Protein lysates were subjected to 2D immunoblotting for phosphorylated Akt-substrates (**A**) and pS6 (Ser235/236) (**B**) using the corresponding antibodies. The red circled feature represents the ~30 kDa Akt-substrate whose phosphorylation was inhibited by the LY294002. The green circled feature represents protein isoforms recognised by a specific anti-phospho-Ser235/236 S6 antibody.

3.5 The effect of PI3K inhibitors on global protein expression examined by 2D-DIGE

Despite not being able to match phosphorylated substrates detected by immunoblotting with Cy-dye labelled spots, it appears that other targets of PI3K signalling can be detected by 2D-DIGE expression profiling as suggested by preliminary experiments. Thus, a more detailed analysis was performed using replicate samples and an internal standard to increase the accuracy of quantitation. Serum-starved HB4a cells were pre-treated with LY294002 (10 μM), wortmannin (100 nM) or D000 (2 nM) for 30 min, followed by EGF (1 nM) stimulation for 1 hour. The proteosome inhibitor PS341 (1 μM) was also included with the aim of examining if any of the detected changes induced by EGF-dependent PI3K activation or inhibition are the result of proteasomal degradation. An un-stimulated control treated just with a vehicle (DMSO) was also included in the experiment. Cells were lysed in NHS-lysis buffer and processed as described in Chapter 2. Equal amounts of each protein sample (100 μg) were labelled with Cy3 or Cy5. Also, equal amounts of all samples were mixed and labelled with Cy2 to provide a standard pool to be run on each gel. Triplicate samples were prepared for each of the six conditions. Cy3 and Cy5 labelled protein samples (100 μg) were then mixed appropriately with an equal amount (100 μg) of Cy2 labelled pool and subjected to IEF on 24 cm, 3-10 non-linear IPG strips in the first dimension. Strips were then transferred to 12% SDS-PAGE gels and subjected to molecular weight separation in the second dimension. The Cy-dye labelling combinations for the six different conditions (control, EGF-treated cells and four different drug treatments: LY294002, wortmannin, D000 or PS134 prior to EGF stimulation) run in triplicate resulted in the running of nine 2D gels. Gels were scanned at the corresponding wavelengths for Cy2, Cy3 and Cy5 detection (Chapter 2) and 27 protein spot maps were generated. Fluorescence images were imported into DeCyder software for image analysis. Experimental design and Cy3 and Cy5 images generated for each gel, as well as, merged Cy3 and Cy5 images, are shown in Figure 3.12.

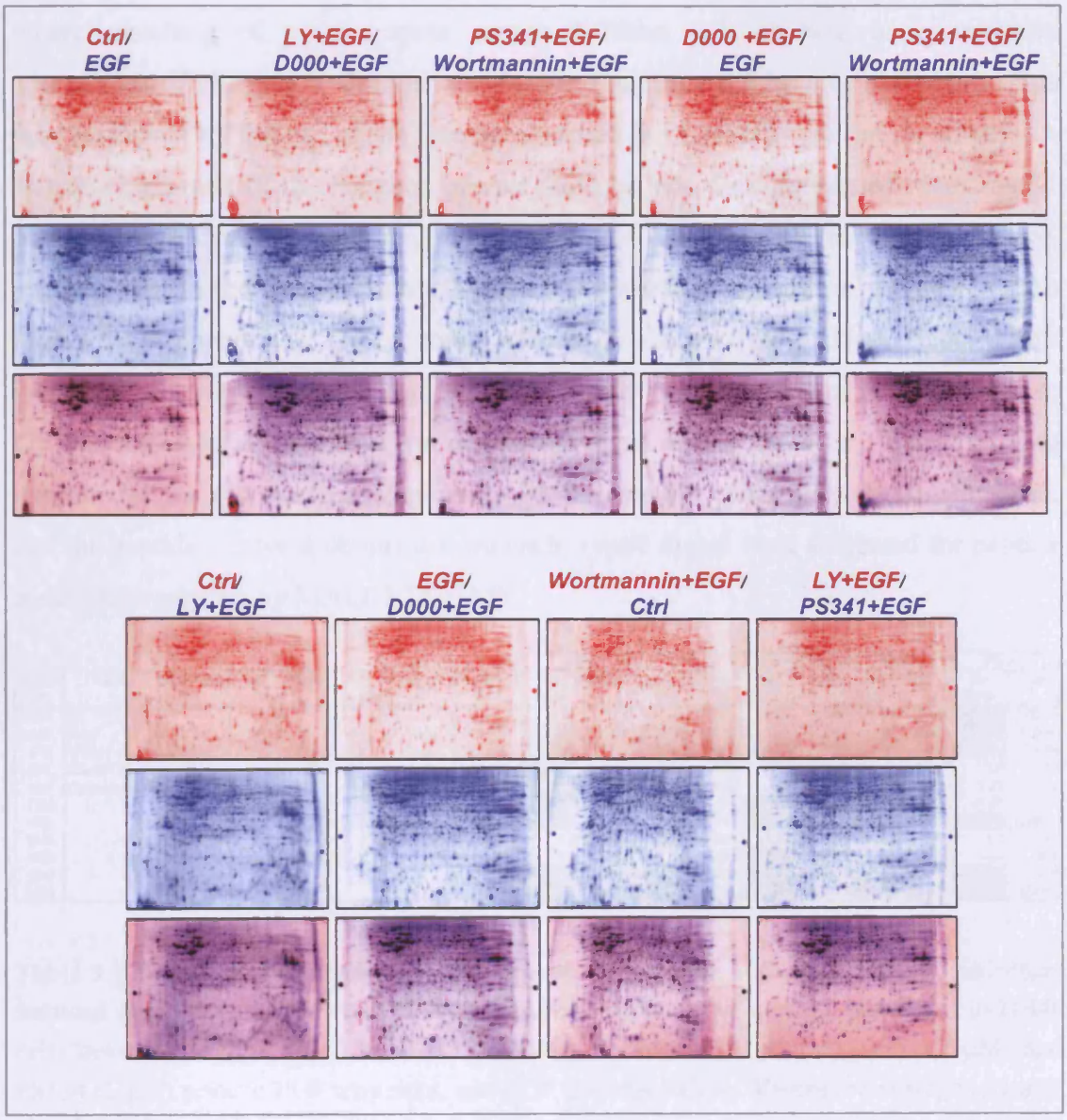

Figure 3.12 Representation of the experimental design in the study of PI3K-dependent changes in response to EGF treatment. HB4a cells were pre-treated with the following inhibitors: LY294002 (10 μM), wortmannin (100 nM), D000 (2 nM) or PS 341 (1 μM), including pre-treatment with DMSO (a vehicle) for 30 min, followed by EGF (1 nM) stimulation for 1 hour. Un-stimulated control and EGF-alone treated cells were also prepared. Cells were lysed in NHS-lysis buffer and processed as described Chapter 2. Equal amount of protein lysates were labelled with Cy3 or Cy5 dyes. A mixture of equal amounts of each sample labelled with Cy2 was also prepared as an internal standard. Triplicate Cy3 and Cy5 labelled samples were then mixed appropriately as shown in the figure, together with an equal amount of the Cy2 labelled pool and run on 9 large format 2D gels. Respective gel images of samples labelled with Cy3 (red) and Cy5 (blue), including merged Cy3 and Cy5 gel images (purple) are shown.

Image analysis was then performed using the BVA module of DeCyder software where matching of protein spots across different gels as well as quantitative comparison of changes in abundance between multiple samples was performed. This was facilitated by the use of the internal standard pool, which was run on all gels. A statistical analysis of the matched protein features was then performed revealing 11 protein features differentially expressed (>1.5 or <-1.5 fold difference in abundance, $p<0.05$, n=3) in the five different treatments compared to the control un-treated cells (Table 3.1, Appendix 1). These protein spots were assigned for picking. Selected gels were post-electrophoretically stained with SYPRO Ruby and images were matched to Cy-dye fluorescence images in order to align spots and to generate a list of picking coordinates for automatic spot picking. Picked protein spots were trypsin digested, and the peptide mixtures obtained from each tryptic digest were subjected for peptide mass fingerprinting by MALDI-TOF MS.

								EGF		LY		Wortmannin		D000		PS341	
Master No.	Name	NCBI Acc No.	Seq. Cov.	Score	No. peptide	Predicted pI	Predicted MW	Av. Ratio	T-test	Av. Ratio	T-test	Av. Ratio	T-test	Av. Ratio	T-test	Av. Ratio	T-test
261								-1.32	0.1	-1.11	0.51	-1.02	0.93	-1.43	0.024	-2.13	0.0015
417	Ezrin	119717	24	86	15	5.94	69470	1.51	0.025	1.59	0.014	1.43	0.015	1.34	0.028	1.8	0.038
478	Moezin	4505357	26	100	12	6.02	67892	1.5	0.015	1.59	0.018	1.32	0.022	1.21	0.063	1.61	0.039
877	Keratin 7	67782365	35	109	16	5.4	51412	1.54	0.0072	1.24	0.38	1.37	0.015	1.41	0.012	1.28	0.29
898	Cytokeratin 8	181573	53	216	31	5.52	53529	1.51	0.022	1.28	0.19	1.4	0.037	1.33	0.059	1.21	0.26
1352								-1.61	0.047	-2.01	0.069	-1.72	0.015	-1.88	0.0022	-1.43	0.11
1485								1.91	0.0018	2.04	0.0035	1.77	0.0035	1.97	0.0017	1.92	0.0023
1918								1.2	0.36	-1.75	0.041	-1.23	0.37	-1.11	0.62	-1.3	0.35
1926								1.4	0.064	1.14	0.79	1.51	0.016	1.16	0.074	1.26	0.5
1957								2.37	0.0004	1.93	0.032	2.32	0.0013	2.28	0.0007	1.93	0.078
1964								-2.00	0.0039	-2.05	0.021	-1.67	0.017	-2.37	0.0018	-2.4	0.0091

Table 3.1 2D-DIGE differential protein expression analysis of EGF and PI3K inhibitor-induced changes in HB4a cells. Protein features displaying differential expression in HB4a cells treated with inhibitors LY294002 (10 μM), wortmannin (100 nM), D000 (2 μM) and PS134 (1 μM) prior to EGF treatment, and EGF treatment alone. Values are average ratios of abundance from different treatments applied *versus* control cells, where each condition was prepared in triplicate. Values for protein isoforms shaded in light and dark grey were significantly up- or down regulated (1.5 fold; $p\leq 0.05$; n=3), respectively. Proteins were identified by MALDI-TOF peptide mass fingerprinting. Protein name, NCBI accession number from database searches, sequence coverage (%), Mowse score and number of matched peptides are given for each of the identified proteins.

Among the differentially expressed protein species, two cytokeratins, cytokeratin 7 and cytokeratin 8 were significantly upregulated following EGF treatment, but only moderately suppressed by the inhibitor treatments (Figure 3.13, Table 3.1). Cytokeratins (CKs) form intermediate filaments and are part of the cytoskeleton. They are epithelial cells and differentiation markers, which are dynamically regulated, and

interact with a range of cellular proteins. In general, CKs are organised in a complex network between the cell membrane and the nuclear surface and are involved in the organisation of the cytoplasm and cellular communication mechanisms. They are also involved in cell movement, cell-cell adhesion and connecting cells to the underlying connective tissue (Coulombe and Wong, 2004).

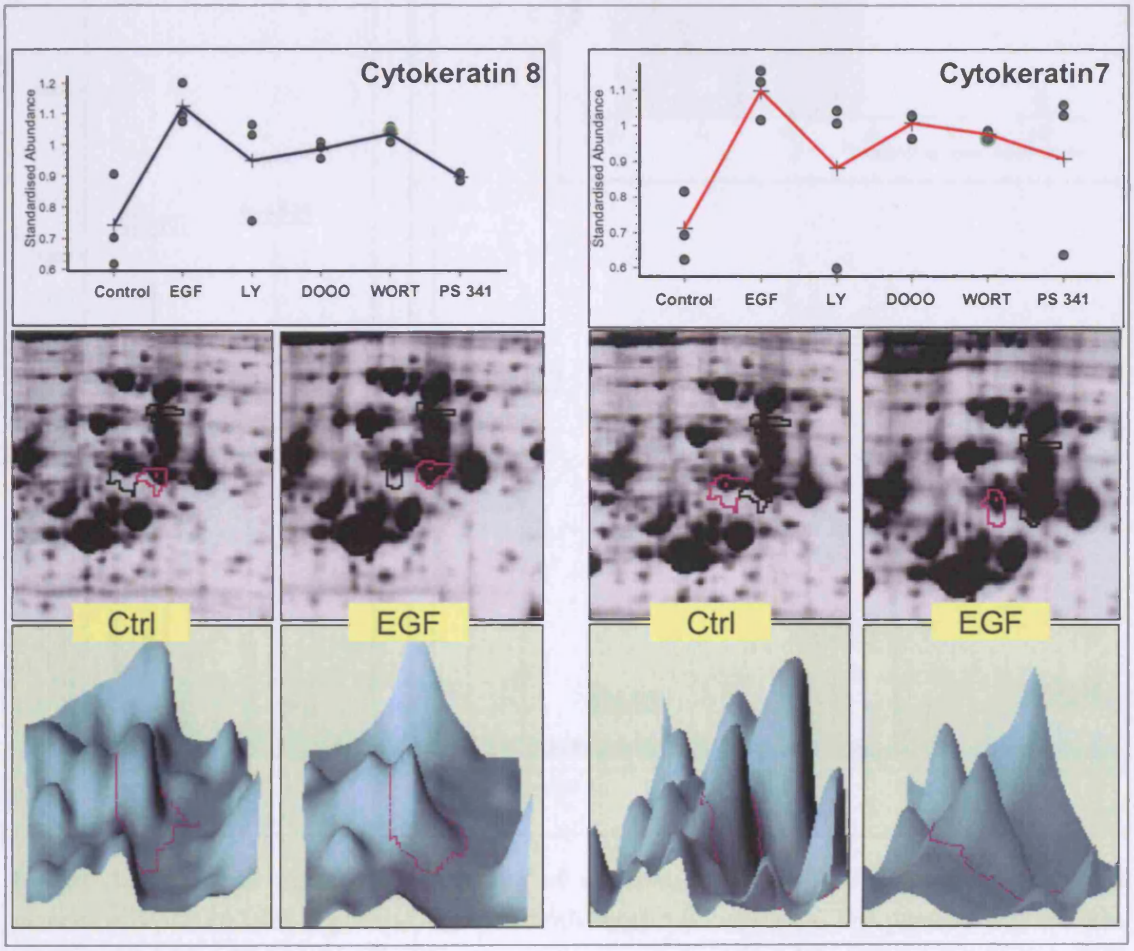

Figure 3.13 Examples of proteins displaying EGF-dependent changes. Cytokeratin 7 and Cytokeratin 8 were induced by EGF. Graphs were derived from DeCyder image analysis where the standardised abundance was the ratio of the volume of a gel feature for each condition replicate *versus* the volume of the corresponding standard gel feature. Triplicate data points are shown for spots from the untreated and treated samples with lines joining the average values. Examples of gel migration and 3D images of these to spots are shown for untreated and EGF-treated samples.

Ezrin and moesin (Figure 3.14) were two actin binding proteins upregulated in the EGF, LY294002+EGF and PS341+EGF treatments (Table 3.1), suggesting that whilst their abundance is affected by EGF signalling, this may not be subject to regulation by PI3K or proteosome degradation. Ezrin and moesin belong to a family of plasma

membrane-localised actin binding proteins. They have been proposed to link the actin cytoskeleton to the plasma membrane and to be involved in signal transduction, growth control, cell-cell adhesion, and microvilli formation (Louvet-Vallee, 2000).

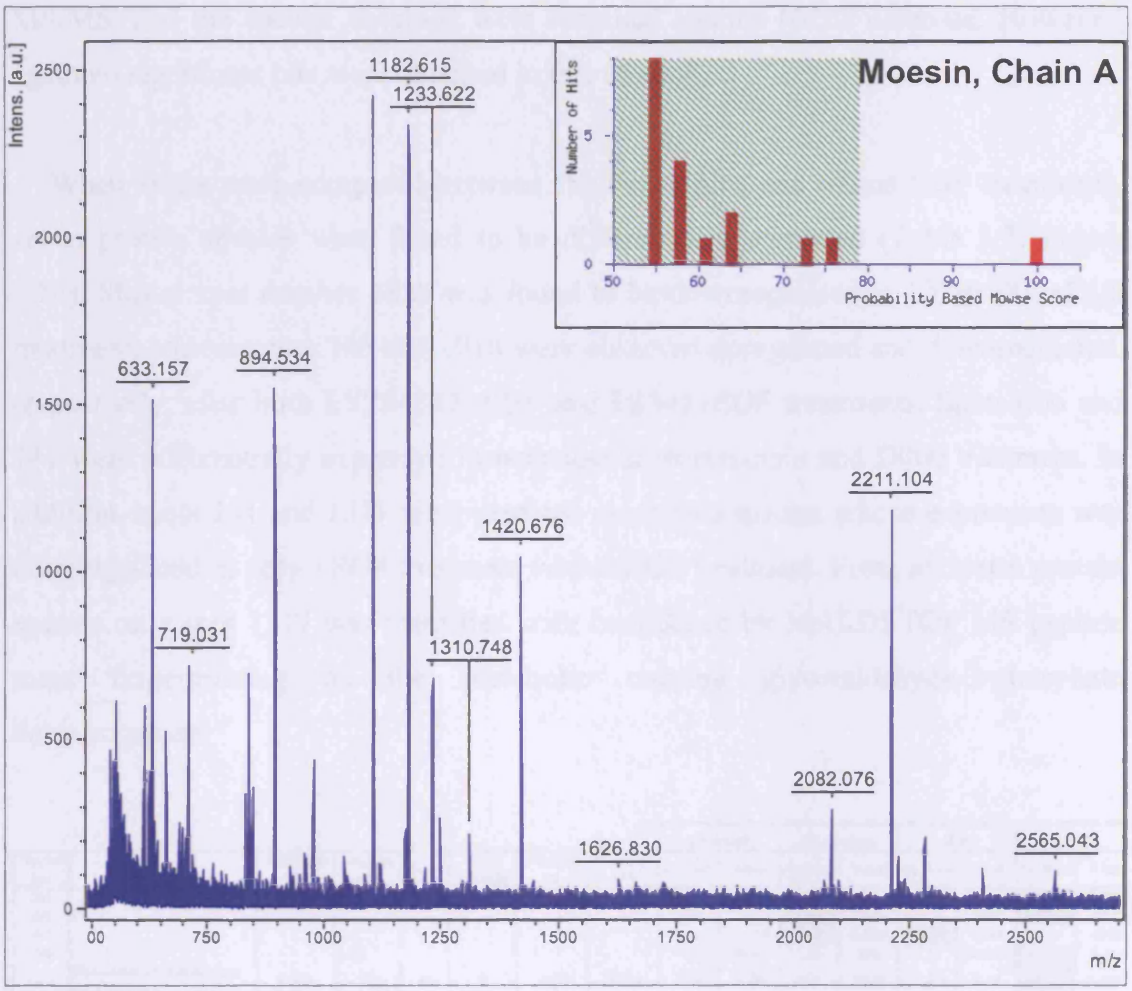

Figure 3.14 Peptide mass fingerprinting of moesin, chain A. A differentially expressed protein was picked from a gel and digested with trypsin (Chapter 2). The peptide mixture was then analysed by MALDI-TOF MS giving the spectrum. The list of peaks was searched against the NCBI database, giving a significant hit for moezin, chain A.

Protein species with master spot numbers 1485, 1957 and 1964 had the same pattern of regulation across the five treatments compared to the control cells, suggesting that these changes are only EGF-dependent, and independent of the drug treatments applied. Master spots 1918 and 1926 were only differentially regulated in LY294002+EGF treated cells (-1.75) and wortmannin+EGF treated cells (1.5 fold), respectively, compared to the control sample, suggesting that basal effects of these inhibitors might occur. One protein species (master spot 261) was differentially

expressed only in cells subjected to proteasome inhibition. Unfortunately, MALDI-TOF MS analysis and database searching did not return any significant "hits" for these proteins. Thus, the peptide mixtures were additionally analysed by LC-ESI MS/MS, and the spectra obtained were searched against NCBI database. However, again no significant hits were obtained in this attempt.

When ratios were compared between inhibitors plus and minus EGF treatments, seven protein species were found to be differentially regulated (Table 3.2, Figure 3.15). Master spot number 1823 was found to be downregulated in LY294002+EGF treatment, whereas spot 745 and 1918 were observed upregulated and downregulated, respectively, after both LY294002+EGF and PS341+EGF treatments. Spots 606 and 741 were differentially expressed in response to wortmannin and D000 treatment. In addition, spots 261 and 1317 were detected as protein species whose expression was downregulated in only +EGF treatment *versus* EGF treatment. From all seven protein species only spot 1317 was identified with confidence by MALDI-TOF MS peptide mass fingerprinting as the metabolic enzyme glyceraldehyde-3-phosphate dehydrogenase.

								LY294002		Wortmannin		D000		PS 341	
Master No.	Name	NCBI Acc No.	Seq.Cov. (%)	Score	No. Peptides	Predicted pI	Predicted MW	Av. Ratio	T-test	Av. Ratio	T-test	Av. Ratio	T-test	Av. Ratio	T-test
261								1.19	0.3	1.29	0.1	1.3	0.0009	-1.77	0.0045
606								1.34	0.1	1.93	0.0066	-1.3	0.019	2.13	0.045
741								-1.35	0.074	-1.53	0.0037	-1.71	0.028	1.14	0.42
745								1.6	0.16	1.15	0.22	1.12	0.092	1.85	0.011
1317	Glyceraldehyde-3-phosphate dehydrogenase	31654	32	64	9	8.58	36070	-1.2	0.36	-1.1	0.098	-1.23	0.15	-1.57	0.0009
1823								-1.79	0.046	-1.21	0.4	-1.32	0.26	-1.48	0.048
1918								-2.09	0.017	-1.48	0.14	-1.09	0.43	-1.56	0.18

Table 3.2 2D-DIGE differential protein expression analysis of EGF-treated HB4a cells *versus* cells pre-treated with inhibitors. Protein features displaying differential expression in HB4a cells treated with inhibitors LY294002 (10 μM), wortmannin (100 nM), D000 (2 μM) or PS134 (1 μM), compared to their counterparts in EGF treatment. Values are average ratios of abundance from inhibitor pre-treated cells *versus* EGF-only treated cells, where each condition was prepared as a triplicate. Values for protein isoforms shaded in light and dark grey were significantly up- or down regulated (1.5 fold; $p \leq 0.05$; n=3), respectively. Proteins were identified by MALDI-TOF peptide mass fingerprinting. Protein name, NCBI accession number, sequence coverage (%), Mowse score and number of matched peptides are given for each of the identified proteins.

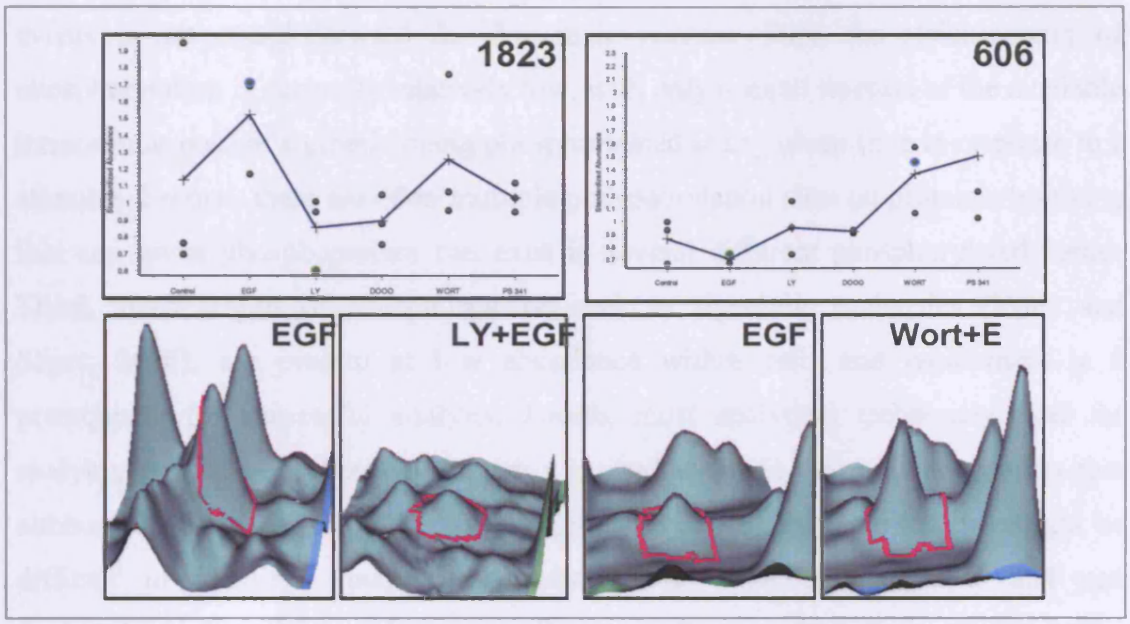

Figure 3.15 Examples of proteins displaying PI3K-dependent changes in response to EGF stimulation. Protein spots 606 and 1823 displayed PI3K-dependent differential expression. The peptide mixtures of the trypsin digestion from each of these protein spots were analysed by MALDI-TOF MS and the list of peptide masses generated were searched using Mascot. Graphs were derived from DeCyder image analysis where the standardised abundance is the ratio of the volume of a gel feature from PI3K inhibitor with EGF-treated test samples *versus* the volume of the corresponding gel feature in the EGF-treated sample. Data points are shown for triplicate measurements with lines joining the average values. 3D images of spots are shown for EGF treated and PI3K inhibitors (LY294002, wortmannin) plus EGF treated samples.

In summary, the work carried out in this section showed that only a few abundant protein species could be detected, which displayed altered expression following EGF and/or inhibitor treatments. In addition, only a third of differentially expressed proteins could be identified using MALDI-TOF MS and LC-MS/MS.

3.6 Conclusions

Since the discovery of phosphorylation as a key regulatory mechanism in almost all cellular processes, the analysis of the phosphoproteome has been an attractive area of study. However, despite a growing knowledge of many phosphorylation consensus sequences, this posttranslational modification cannot usually be predicted accurately from translation of the gene sequence alone. In addition, analysis of phosphorylation

events is not straightforward for five main reasons. First, the stoichiometry of phosphorylation is generally relatively low, with only a small fraction of the available intracellular pool of a protein being phosphorylated at any given time in response to a stimulus. Second, there are often multiple phosphorylation sites on proteins, implying that any given phosphoprotein can exist in several different phosphorylated forms. Third, many targets of phosphorylation such as signalling molecules (Yoon and Seger, 2006), are present at low abundance within cells and enrichment is a prerequisite for successful analysis. Fourth, most analytical techniques used for studying protein phosphorylation have a limited dynamic range, which means that although major phosphorylation sites might be located easily, minor sites might be difficult to identify. Finally, phosphatases are often highly active and can dephosphorylate residues unless precautions are taken to inhibit their activity during preparation and purification steps of cell lysates.

The aim of my work in this chapter was to establish a model cell system for studying PI3K–dependent signalling and to monitor changes in global protein expression and phosphorylation events, which happened in response to activation of PI3K signalling. The aim was tackled using proteomic analysis consisting of 1D and 2D immunoblotting in combination with 2D gel-based proteomics. Immunoblotting analysis employing kinase-specific substrate antibodies, such as Akt, PKC and PDK1 substrate antibodies, were used to monitor changes in protein expression and phosphorylation of kinase-specific substrates. In parallel, I employed 2D-DIGE analysis for the accurate and sensitive quantitation of protein expression across multiple biological samples and combined with mass spectrometry to allow me to identify differentially expressed proteins. An additional aim of mine was to try to correlate 2D immunoblotting data with the data obtained from 2D-DIGE analysis. Post-electrophoretic gel staining for the detection of phosphoproteins was also applied to try to distinguish phosphoproteins from the total proteome.

In an initial experiment to assess PI3K activation in a cell model of breast luminal epithelial cells (HB4a cells), PI3K inhibitors (LY294002, wortmannin and D000) were combined with EGF treatment to show whether the PI3K signalling pathway is responsive to EGF treatment. In the first instance, selected antibodies that recognise

phosphorylation of target proteins of PI3K/Akt and Ras/ MAPK signalling were used and showed that both pathways were activated upon EGFR stimulation by EGF. In addition, this immunoblotting analysis revealed that PI3K inhibitors could block successfully Akt phosphorylation on Ser473, suggesting that the kinase responsible for this phosphorylation is PIP3-dependent as it was inhibited by both LY294002 and wortmannin treatments. In contrast, the p110δ specific inhibitor, D000, did not have an inhibitory effect on this and other PI3K-dependent phosphorylation events, showing that p110δ is not expressed in these cells, as suggested previously. Although it is well established that Akt phosphorylation on Ser473 is PI3K-dependent, there is controversy about the kinase that phosphorylates this site. Proposed kinases responsible for this phosphorylation event are PDK1 (Balendran et al., 1999), DNA-PK (Feng et al., 2004) and most recently the mTOR/Rictor complex (Sarbassov et al., 2005), or perhaps it could be mediated by auto-phosphorylation event (Toker and Newton, 2000). One approach to identify the kinase responsible for phosphorylation of Ser473 in Akt could be to apply a specific RNA interference screen to silence the expression of all kinases and to use anti-phospho Ser473 Akt antibody for detection in a high-throughput manner. In addition to the later work, the application of new generation, highly specific PI3K and protein kinase inhibitors could be applied.

PI3K-dependent signalling induced by EGF was further assessed in this cell model by monitoring the phosphorylation of downstream targets of Akt. EGF-induced phosphorylation on 4E-BP1 was blocked by PI3K inhibitor treatment, showing how PI3K/Akt signalling functions normally to prevent 4E-BP1 from blocking translation through binding of cap-dependent eukaryotic factor eIF4E. It was also observed that the phosphorylation of GSK3-α, and to lesser extent GSK3-β, appeared to be PI3K-dependent. This was surprising since in most studies GSK3-β is described as a direct downstream target of Akt and its phosphorylation and inactivation are prevented by LY294002 treatment. However, GSK3-β can be also be phosphorylated by the MAPK signalling cascade (Shaw and Cohen, 1999). As I observed here that MAPK signalling was activated by EGF in HB4a cells, and that LY294002 had no effect on EGF-induced phosphorylation of ERK or p90RSK, this could suggest that GSK3-β phosphorylation is more dependent upon MAPK signalling in HB4a cells. Further work is required to establish the details of GSK3-β regulation in HB4a cells, indeed

the possibility of cross-talk between the PI3K and MAPK signalling branches cannot be excluded, and this will also require more detailed analysis to resolve it. Monitoring the expression and phosphorylation of cell cycle regulatory proteins, such as $p27^{Kip}$ and cyclin D1 showed that the expression of these proteins was not perturbed after blocking the PI3K signalling suggesting that PI3K does not play a major role in regulating cell cycle progression in these cells. Furthermore, the phosphorylation of Stat3 at Ser727 was not perturbed by inhibition of PI3K indicating that Stat-dependent transcription in HB4a cells is not dependent on the PI3K signalling cascade.

1D and 2D immunoblotting using substrate-specific antibodies that recognise the phosphorylation consensus motifs of Akt, PDK1 and PKC revealed several putative protein targets of these kinases, which were EGF-dependent and PI3K-dependent. In particular, the ~30 kDa phosphorylation event induced by EGF stimulation, but blocked by LY294002 was validated as the phosphorylation of ribosomal protein S6 on Ser235/236. S6 is a downstream target of S6K whose activation and phosphorylation is stimulated downstream of PI3K/Akt and the mTor/Raptor complex following RTK activation (Miron et al., 2003; Lizcano et al., 2003). Whilst the identity of this protein was predicted from a previous study (Zhang et al., 2002) and validated here by using immunoblotting, the same EGF- and/or PI3K-dependent phosphorylation event could not be matched to any of the changes observed in the 2D-DIGE analysis. The work from the 2D-DIGE experiments showed that only a few abundant protein species had altered expression after the treatments applied. For example, the expression of ezrin and moesin, as well as cytokeratin 7 and 8, appeared to be differentially regulated in response to EGF treatment. Ezrin and moesin belong to a group of closely related membrane-cytoskeleton linkers (ERM proteins) that regulate cell adhesion and cortical morphogenesis. They have been proposed to link the actin cytoskeleton to the plasma membrane and to be involved in signal transduction, growth control, cell-cell adhesion, and microvilli formation (Louvet-Vallee, 2000). ERM proteins can be phosphorylated on different sites and this may regulate their activities. The observed differential expression of ezrin and moesin in response to EGF treatment could be due to their post-translation modification, such as phosphorylation, as EGF-induced phosphorylation on ezrin and moesin has been observed in other cell types (Krieg and Hunter, 1992). This however needs to be

further validated in HB4a cells. Cytokeratin 7 and 8 belong to the epithelial keratins or cytokeratins (CKs) that are part of an intermediate system of fibrous filaments contributing to the cytoskeleton (Lazarides, 1980). The CK family members are expressed in different epithelial cells and constitute useful markers of epithelial sub-type and differentiation. The EGF-induced upregulation of cytokeratin 7 and 8 expression could also be linked to PTM of these proteins in response to EGF and be dependent upon PI3K activity. This interesting observation requires further analysis. The major disadvantage of the 2D-DIGE approach was that only a third of the differentially expressed proteins could be identified with confidence using MALDI-TOF MS and LC-MS/MS. Although some of these changes may represent altered phosphorylation, rather than altered protein expression, post-staining with Pro-Q Diamond phospho-stain failed to show any phospho-specific staining. The reason for this observation remains unclear and further optimisation of the protocol may be required.

Finally, the comparison of immunoblotting and 2D-DIGE showed no correlation of the differences observed in the two methods, most likely because of the low abundance of downstream targets of Akt, PDK1 and PKC, which cannot be detected by the staining or labelling methods used in 2D gel electrophoresis. Thus, it can be concluded that this approach for functional cell signalling studies of protein phosphorylation on a global scale is rather limited. Firstly, although 2D gel electrophoresis and protein staining/labelling can provide valuable information, it suffers from several limitations, such as an inability to detect low-copy number proteins, as well as very small or large proteins and hydrophobic proteins such as membrane proteins due to their aggregation during IEF. Phosphoprotein gel staining was shown to be non-specific approach and so limited the analysis. In addition, although western blotting allows the detection of very low abundance phosphoproteins, I found that this method is not very suitable for quantitative analysis due to the variability of the amount of proteins transferred to the membrane and low-linear dynamic range of enhanced chemiluminescence (ECL) detection. In addition, the selectivity and affinity characteristics of the antibodies are of major importance since "false positive" interactions may be detected, thus reducing the applicability of this approach.

In recent years, several other methods have been proposed as highly specific and selective for large scale quantitative and qualitative analysis of the phosphoproteome. Ptacek *et al.* reported the use of proteome chip technology where synthetic peptides served as kinase substrates to allow extraction of consensus motifs (Ptacek et al., 2005), which were then be incorporated into *in silico* prediction programs for generation of phosphorylation maps. However, this approach also appeared to have limitations, as kinases are often less specific *in vitro* than they are *in vivo*. Thus, in the last few years mass spectrometry has proven to be powerful technology for proteomics and a method of choice for unbiased (i.e hypothesis-free) analysis of *in vivo* phosphorylation. Olsen *et al.* reported a general mass spectrometry technology for identification and quantitation of phosphorylation sites as a function of stimulus, time and subcellular location (Olsen et al., 2006). They combined "double-triple labelling" using SILAC (Stable isotope labelling with amino acids in cell culture; (Ong et al., 2002)) for quantitation, strong-cation exchange chromatorgraphy (SCX) and titanium dioxide (TiO_2) chromatography for phosphopeptide enrichment (Larsen et al., 2005), and high accuracy multistage MS, to examine EGF-stimulated phosphorylation events in HeLa cells. They detected 6600 phosphorylation sites on 2244 proteins and determined their temporal dynamics after stimulation with EGF and recorded these dynamic changes in the Phosida (phosphorylation site) database. In another study, an isotopically labelled internal standard (IS) was employed to provide a quantitative measure of kinase activation status in absolute units. Cutillas P.R. *et al.* used MS for the quantification of PI3K-dependent protein kinase activity toward a substrate (Akt) that is highly selective for this pathway. They applied the analytical strategy of using IS to the PI3K/Akt pathway and show that it is possible to quantify signal transduction pathway activation with great precision, with high sensitivity and in a specific manner (Cutillas et al., 2006). This kind of approaches for studying dynamics of signalling networks, although complex, have been proposed to provide a missing link for cellular regulation and dynamics in signal transduction, and they could be employed in a future research project as a platform to study PI3K-dependent phosphorylation events in HB4a cells.

Chapter 4: Characterisation of insulin- and PI3K-dependent actin cytoskeleton organisation

4.1 Introduction

The actin cytoskeleton forms a complex dynamic network of filaments that maintain cell shape, enable certain cell movements and play important roles in both intracellular transport (for e.g. the movement of vesicles and organelles) and cellular division. To perform all these biological functions, the organisation of the actin cytoskeleton must be tightly regulated both temporally and spatially. Many proteins associated with the actin cytoskeleton are thus likely targets of signalling pathways that control actin assembly and reorganisation. A large number of actin-binding proteins regulate cytoskeleton organisation by controlling filament formation and contraction and also cross-linking of the actin network (Pollard and Cooper, 1986; Stossel, 1993; Welch et al., 1994; Schafer and Cooper, 1995). The activities of these proteins are often modulated by signalling molecules such as kinases and phosphorylated phosphoinositides (Janmey, 1994) as a part of complex signalling pathways.

In this chapter, the possible role of growth factor/PI3K mediated actin cytoskeleton organisation in fly haemocyte cell lines will be investigated. Most of the current knowledge about PI3K signalling-dependent actin reorganisation comes from studies of initiation of motility induced by growth factors (PDGF, EGF, IGF and insulin) in migratory cells (see Introduction). In 1994, Kotani *et al.* showed that insulin and IGF-1 can both induce membrane ruffling in a PI3K-dependent manner (Kotani et al., 1994). They showed that by microinjecting phosphorylated peptides, containing Y-M-X-M motifs or a mutant p85 regulatory subunit, which lacks a binding site for the

catalytic p110 subunit of PI3K, into the cytoplasm of human epidermoid carcinoma KB cells, the association of insulin receptor substrate-1 (IRS-1) with PI3K was blocked. Importantly, this inhibited insulin- or IGF-1-induced, but not EGF-induced, membrane ruffling in KB cells. In addition, wortmannin inhibited insulin- or IGF-1-induced membrane ruffling. It has been also reported that a mutation in the PDGF receptor can eliminate binding to and activation of PI3K, which then leads to a failure of porcine aortic endothelial cells to ruffle and chemotax in response to PDGF (Kundra et al., 1994; Wennstrom et al., 1994a; Wennstrom et al., 1994b). Furthermore, constitutively active PI3K mutants or the addition of exogenous PIP3 can initiate cell motility and membrane ruffling, and the use of PI3K inhibitors LY294002 and wortmannin in many studies has shown how PI3K activity is required in actin reorganisation (Arcaro and Wymann, 1993; Wymann and Arcaro, 1994).

However, in addition, with these findings, PI3K-independent growth factor mediated actin reorganisation and motility has also been reported. For example, Kovacsovics *et al.* showed that although thrombin receptor-activating peptide (TRAP) can activate PI3K signalling, neither wortmannin nor LY294002 altered the kinetics of actin assembly or the exposure of nucleation sites in TRAP-stimulated platelet cells. In contrast, PI3K inhibitors showed a specific inhibitory pattern of cell aggregation (Kovacsovics et al., 1995). Higaki *et al.* reported that in vascular smooth muscle cells, PDGF-induced chemotaxis is independent of PI3K activity, while PDGF-induced amino acid uptake, glucose incorporation, and cytoskeletal reorganisation are dependent on PI3K. They showed that wortmannin blocked PI3K activity induced by PDGF, but did not inhibit PDGF-induced chemotaxis in smooth muscle cells and Swiss 3T3 cells. They also reported that Chinese hamster ovary/Delta p85 cells overexpressing a dominant negative p85 subunit of PI3K showed a chemotactic response comparable to that of parental cells while showing a remarkable decrease in PI3K activity (Higaki et al., 1996). In addition, wortmannin and LY294002 inhibited PDGF-induced amino acid uptake and actin-stress fibre reorganization in Swiss 3T3 cells. In addition, although growth factor-mediated PI3K-dependent actin reorganisation has been proposed to occur through cross-talk between PI3K and the Rho-family small GTPases, a master regulator of the actin cytoskeleton (see Introduction), the molecular mechanisms involved are poorly understood.

The main aim of the research presented in this chapter was to establish a role for PI3K signalling in modulating actin cytoskeletal reorganisation in fly haemocyte cell lines, and to establish a model cell system that could be further used to delineate the signalling pathways downstream of PI3K that feed into the actin cytoskeleton, thereby to define possible common targets in both PI3K and small Rho GTPase signalling cascades. For these purposes, a series of experiments were conducted to assess the activation of PI3K signalling and actin cytoskeleton reorganisation induced by growth factor (insulin) treatment in the presence or absence of commonly used PI3K inhibitors in fly cells. One of the reasons for choosing fly haemocyte cells for this study is that very little is known about growth factor- and PI3K-mediated actin reorganisation in fly haemocytes in this system. Also, decades of study have revealed that *D. melanogaster,* which bears little resemblance to humans, nevertheless shares much of our genetic heritage and possess strikingly similar versions of the genes that promote normal human development and, when altered, contribute to disease. Moreover, numerous studies have demonstrated homology in the signalling and biochemical pathways between flies and humans. Fly cells also have a simpler genome, for example expressing only one gene for each class of PI3K. Finally, available molecular biology tools such as RNAi interference for knockdown of the expression of targeted genes are more easily employed in fly cells, facilitating specific and high-throughput functional analyses.

4.2 Insulin-dependent PI3K signalling

In order to test if PI3K signalling is linked to actin cytoskeleton remodelling in cultured *Drosophila* haemocyte cell lines, the first goal was to select an appropriate cell line and growth factor stimulus that can activate PI3K signalling. Three different *Drosophila* cell lines including S2R+, Kc167 and S2 were used. These cell lines have distinct cell shape, size and adhesion properties. The properties and culturing conditions for these haemocyte fly cell lines are presented in Table 4.1.

Although these cell lines are apparently derived from embryonic haemocytes (insect blood cells), S2 and Kc167 cells are small and round (10 μm diameter)

(Schneider, 1972), whereas S2R+ (S2 receptor plus) cells (Yanagawa et al., 1998) are large (averaging 50 μm), flat and strongly adherent to glass, plastic and extracellular matrix. Staining the three cell lines for filamentous actin with rhodamine-phalloidin showed prominent differences in their actin organisation (Figure 4.1). S2R+ cells display large wide lamellipodia and thick cortical actin, whereas in S2 and Kc167 cells the actin is accumulated in the rounded cell body, and in a thinner cortical ring, with the S2 cells displaying more heterogenouse staining. All three cell lines were used to test the growth factor-mediated activation of PI3K signalling and further to test PI3K-dependent actin cytoskeleton reorganisation. However, S2R+ cells were mostly used in further studies due to their morphological properties, and knowing that there are a large number of distinct actin-related phenotypes that can be readily distinguished when gene silencing strategy, such as RNAi, is employed to these cells (Kiger et al., 2003).

Cell line name:	Kc167	S2	S2R+
Origin:	DM dissociated embryos, 8-12h	DM dissociated embryos, near hatching	DM dissociated embryos, near hatching
Characteristics:	Hemocyte-like gene expression, phagocytic, uniformly round, clamp in sheets, ecdysone, responsive into adherent, bipolar spindle-shaped cells	Hemocyte-like gene expression, phagocytic, semi-adherent in colonies, round, ganular cytoplasm	Hemocyte like gene expression, phagocytic, flat cells; Fz+ and Wg-responsive
Growth media:	Schnieder's	Schnieder's	Schnieder's and M3
Doubling time (~23°C):	Approx 24hrs	Approx 24hrs	3-4 days
Recommended splitting frequency:	2-3 days	2-3 days	2-3 days
Recommended splitting dilution:	Split 1:4	Split 1:4	Split 1:2
RNAi treatable:	+++	+++	+++
Transfectable:	++	++	+++
Motility:	-	-	-
Adherence:	Semi-adherent	Semi-adherent	Adherent

Table 4.1 *Drosophila* haemocyte cell line characteristics

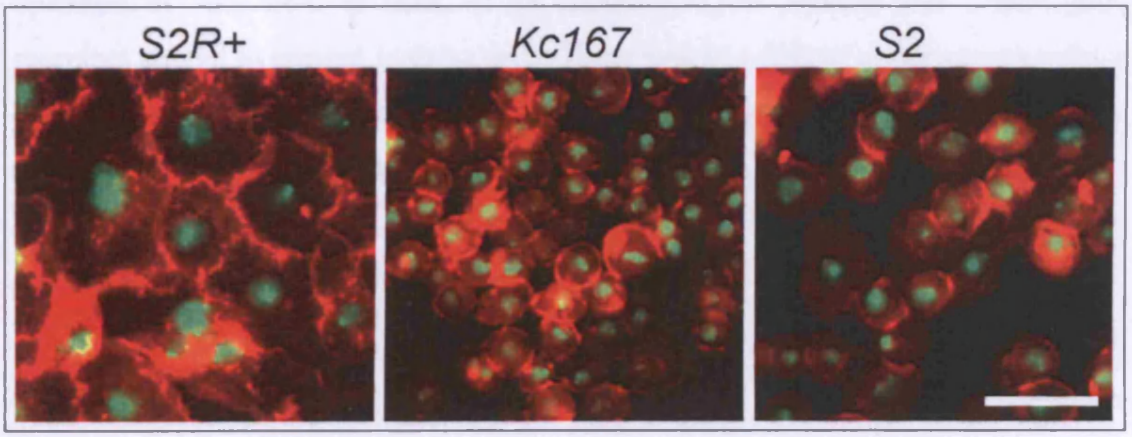

Figure 4.1 F-actin staining of *Drosophila* haemocyte cell lines. Cells were fixed and stained for F-actin and nuclei with rhodamine phalloidin (red) and DAPI (green), respectively. Images were acquired on a fluorescence microscope using a 40x objective. Scale bar = 50 μm.

Initially, to identify a suitable growth factor that can activate PI3K signalling, serum-starved S2R+ cells were stimulated with different purified or recombinant growth factors (10% foetal calf serum, bovine insulin, human EGF, mouse VEGF and human PDGF). These were chosen since they have been reported to activate PI3K signalling and to promote actin remodelling in different cell systems. Conditioned medium from cells grown for two days in serum-supplemented Schneider's medium was also used to test whether there were any cell secreted (autocrine) factors that could promote activation of PI3K. The activation of PI3K signalling was assessed by immunoblotting for phosphorylation of Ser505 of *Drosophila* Akt, a homologous site to Ser473 in the C-terminal hydrophobic kinase tail of mammalian Akt, which is required for its activation (see Introduction). The immunoblotting revealed increased phosphorylation of Akt and indicated that activation of PI3K took place in response to bovine insulin alone (Figure 4.2). Insulin also stimulated the phosphorylation of Thr398 of *Drosophila* S6K, a homologous site to Thr389 of mammalian S6K, which is critical for release of the auto-inhibitory state of S6K, and allows phosphorylation of Thr229 at the catalytic domain of S6K and kinase activation (Pullen et al., 1998). The phosphorylation of *Drosophila* S6K at Thr398 and its activation is known to occur downstream of PI3K/Akt in response to insulin (Lizcano et al., 2003). A moderate increase in the phosphorylation of *Drosophila* ERK was also detected only under insulin treatment, suggesting activation of MAPK signalling. It was notable that the other growth factors (EGF, VEGF and PDGF) and FCS treatment did not promote phosphorylation of Akt or ERK, suggesting that these growth factors of non-fly origin cannot activate the respective *Drosophila* membrane tyrosine kinase receptors upstream of Akt, S6K or ERK in fly haemocytes, or possibly that homologous receptors are not expressed in these cells. There was no effect of conditioned medium on the phosphorylation of Akt, S6K and ERK suggesting that there are no factors secreted from the cells that have potency to activate PI3K or MAPK signalling.

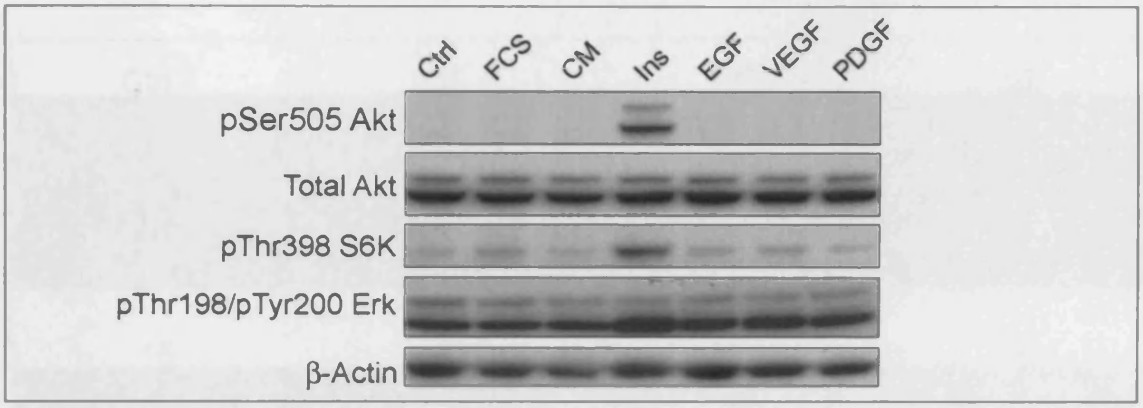

Figure 4.2 Investigation of mitogen-activated signalling in S2R+ cells treated with different growth factors. S2R+ cells were maintained in serum-free Schneider's medium overnight (Ctrl), followed by stimulation with 10% foetal calf serum (FCS), condition medium (CM), bovine insulin (10 μg/mL), human EGF (200 ng/mL), human PDGF (125 ng/mL) or mouse VEGF (50 ng/mL) for 30 min. After treatment, cells were washed with ice cold PBS and lysed in NP40 lysis buffer. Using immunoblotting, equal amounts of protein lysates were probed for pSer505-Akt, pThr398-S6K and pThr198/pTyr200-Erk. Membranes were stripped with 0.2 M glycine (pH 2) and re-probed for total Akt and β-actin as loading controls.

Insulin binds to the insulin receptor (InR), which possesses tyrosine kinase activity. This triggers auto-phosphorylation of the receptor on multiple tyrosine sites and downstream substrates with subsequent recruitment and activation of downstream targets such as PI3K. After establishing bovine insulin as an activator of signalling events in fly haemocytes, the induction of tyrosine phosphorylation by insulin was examined in S2R+ cells by immunostaining of fixed cells with anti-phosphotyrosine antibody (anti-pY20 Ab) (Figure 4.3). This staining revealed a signal that was heterogeneously dispersed throughout the cells before insulin treatment. Following insulin stimulation, the phosphotyrosine signal became rapidly localised to the membrane and is likely to correspond to the phosphorylation and activation of the InR and its immediate downstream targets. The staining was sustained at the membrane for around 30 minutes. After one hour of insulin stimulation, membrane staining had decreased dramatically with punctuate staining around the nucleus, suggesting that the signal of tyrosine phosphorylated proteins was internalised.

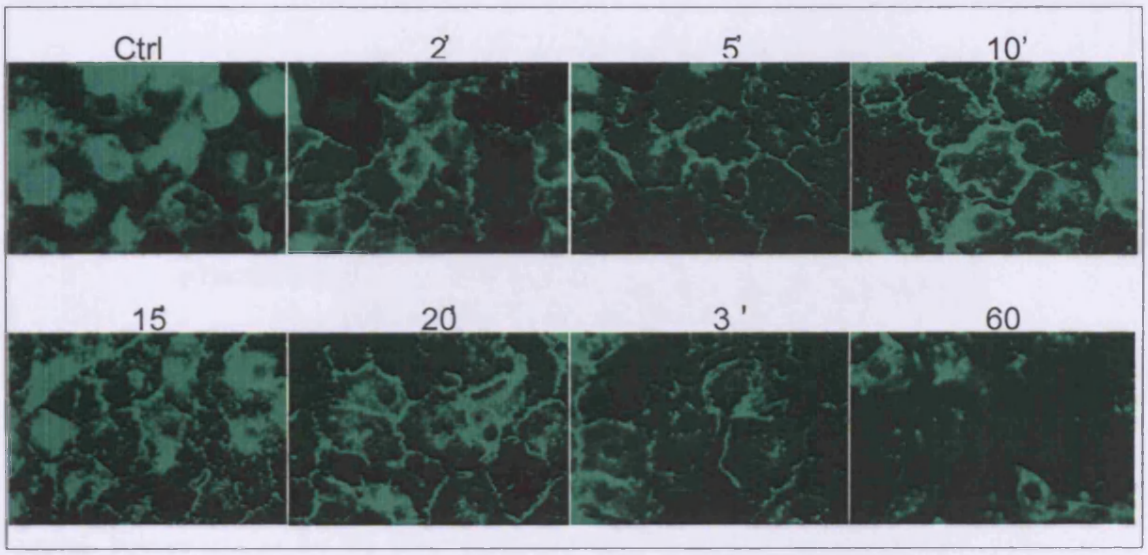

Figure 4.3 Distribution of cellular phosphotyrosine in S2R+ cells following insulin treatment. Cells were plated into a 384-well plate and maintained in Schneider's medium supplemented with 10% FCS, overnight. 10 μg/mL insulin was used to stimulate cells for different times. Cells were then fixed, permeabilised and blocked with 5% BSA in PBS for 1h, followed by overnight incubation with mouse anti-pY20 antibody. Cells were then incubated with a secondary anti-mouse antibody conjugated with FITC (1:300). Images were acquired on a Nikon 2000E fluorescent microscope using a 40x objective.

To investigate in more detail the kinetics of insulin-induced PI3K activation in S2R+ cells, a time course of insulin stimulation was performed and Ser505 phosphorylation of Akt was examined by immunoblotting. Insulin induced a rapid (within 2 minutes) phosphorylation of Akt that was sustained for the following 10 to 15 minutes, before gradually declining (Figure 4.4). Phosphorylation of the downstream kinase S6K on Thr389 was also examined and displayed a delayed response compared to Akt. S6K phosphorylation increased gradually and remained elevated for up to two hours. This data confirmed that insulin is able to activate PI3K/Akt signalling and its downstream target S6K in S2R+ cells, although the kinetics of their activation is different.

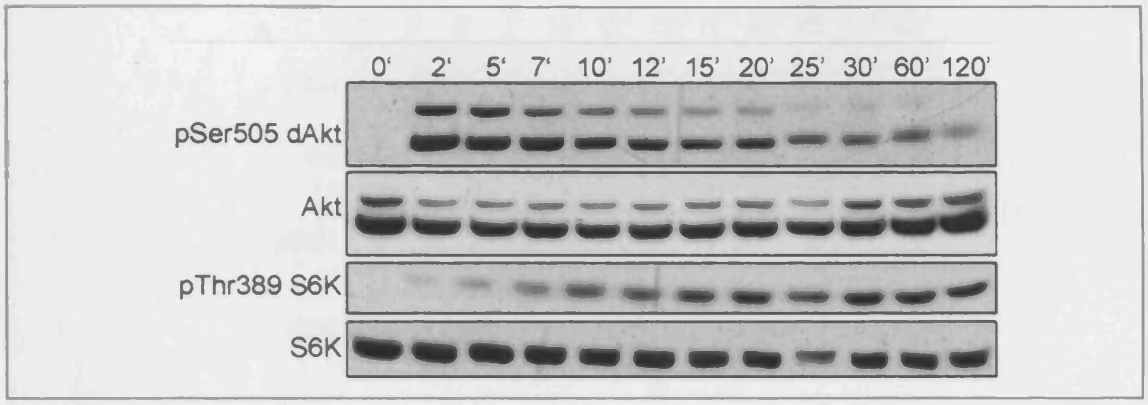

Figure 4.4 Time course of Akt and S6K phosphorylation in *Drosophila* S2R+ cells. S2R+ cells were maintained in serum-free medium overnight, followed by stimulation with 10 μg/mL bovine insulin for the time points indicated. Cell lysates were immunoblotted with antibodies that recognise pSer505-Akt and pThr389-S6K. Membranes were then stripped and reprobed for total Akt and S6K.

Insulin-induced signalling was also examined in S2 cells. One set of S2 cells were maintained in serum-supplemented medium and another set were maintained in serum-free medium overnight, prior to insulin stimulation. Cell lysates from each time point were then subjected to immunoblotting for pAkt, pS6K and total Akt and S6K (Figure 4.5 A and B). In both cases, the phosphorylation of Akt was not detectable prior to insulin treatment. As seen previously in S2R+ cells, addition of insulin induced the rapid intense phosphorylation of Ser505-Akt in S2 cells. In both cases, phosphorylation of Akt was sustained at the later time points of stimulation when compared to insulin treatment in S2R+ cells, although the response appeared to be biphasic in the serum-starved cells. In both conditions there was a detectable phosphorylation of Thr389-S6K before insulin treatment, with the cells that were maintained in serum-free medium displaying a more delayed response to insulin stimulation. This may suggest that factors present in bovine serum, although not able to activate PI3K signalling on there own, can augment the insulin-induced activation.

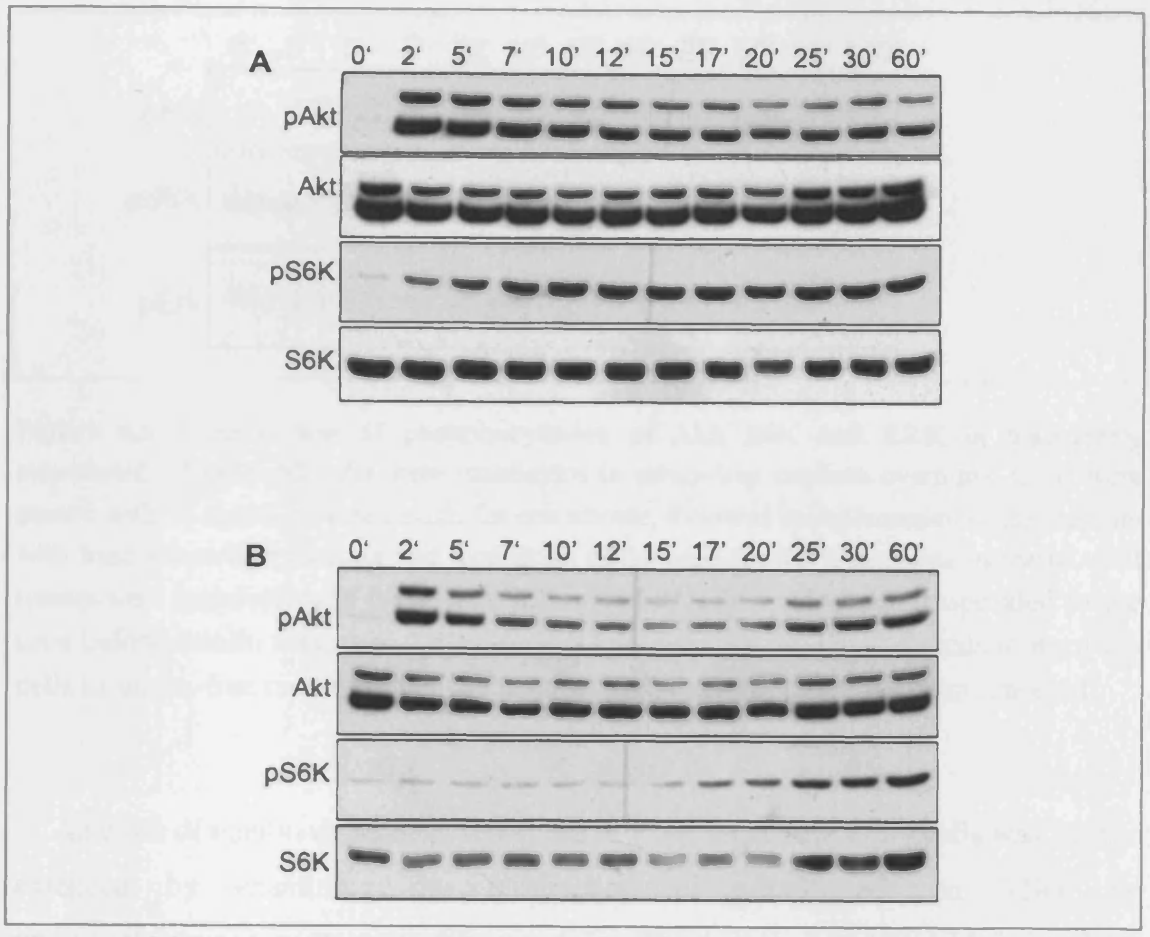

Figure 4.5 Kinetics of Akt and S6K phosphorylation in S2 cells stimulated with insulin. **A)** S2 cells were maintained in serum-supplemented Schneider's medium overnight, prior to treatment with 10 μg/mL insulin over a time course. **B)** S2 cells were maintained in serum-free Schneider's medium for ~16 h prior to treatment with 10 μg/mL insulin over a time course. In both cases, cells were lysed in NP40 lysis buffer and lysates were analysed for pSer505-Akt and pThr389-S6K by immunoblotting. Membranes were reprobed for total Akt and S6K.

To exclude the constant triggering of *Drosophila* InR/PI3K signalling by insulin, which was present in the medium during the treatment, an experiment was performed where serum-starved S2 cells were treated with insulin for only one minute. The medium was then replaced with serum-free medium for the rest of the time course. In this experiment, the result from the immunblotting suggested that S6K and ERK were phosphorylated before the insulin treatment and prior to phosphorylation of Akt (Figure 4.6). This suggests that pThr398-S6K might not be directly dependent on Akt activation, and could be related to ERK signalling or be directly regulated through InR/PI3K/PDK1 cascade as previously reported (Radimerski et al., 2002). A transient decrease of Akt phosphorylation was also observed as previously shown.

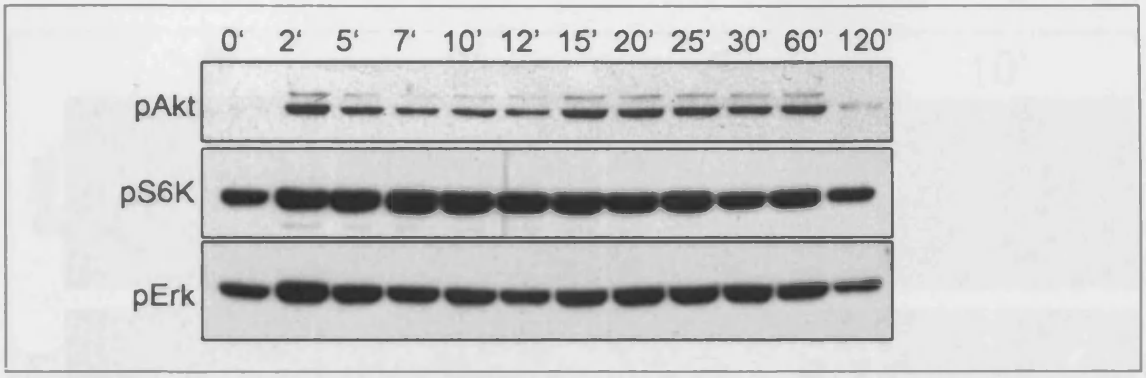

Figure 4.6 Time course of phosphorylation of Akt, S6K and ERK in transiently stimulated S2 cells. S2 cells were maintained in serum-free medium overnight. Cells were treated with 10 μg/mL bovine insulin for one minute, followed by replacement of the medium with fresh serum-free medium and incubation of the cells for the time points indicated. Cell lysates were immunoblotted for pAkt, pS6K and pERK. Zero minute corresponded to the time before insulin treatment. Other time points indicate the time of incubation of the cells in serum-free medium after the insulin-containing medium had been replaced.

Analysis of insulin-dependent activation of PI3K signalling in fly cells was further extended by examining the localisation of pSer505-Akt in S2R+ by immunofluorescence staining (Figure 4.7). There was no detectable signal of pSer505-Akt in serum-starved cells prior to insulin addition. Adding insulin promoted membrane and cytoplasmic localisation of pSer505-Akt, with the most intense membrane staining detected after 10 minutes of treatment. This process most likely represents recruitment of Akt to sites on the membrane where PIP3 is generated and it follows observed insulin-induced phosphotyrosine staining of the membrane (Figure 4.3). Interestingly, the signal of pSer505-Akt was also detectable in nuclei over the entire time course with insulin, but peaked at 10 minutes. Cells were stained in parallel for DAPI, to serve as a staining control and to detect nuclei.

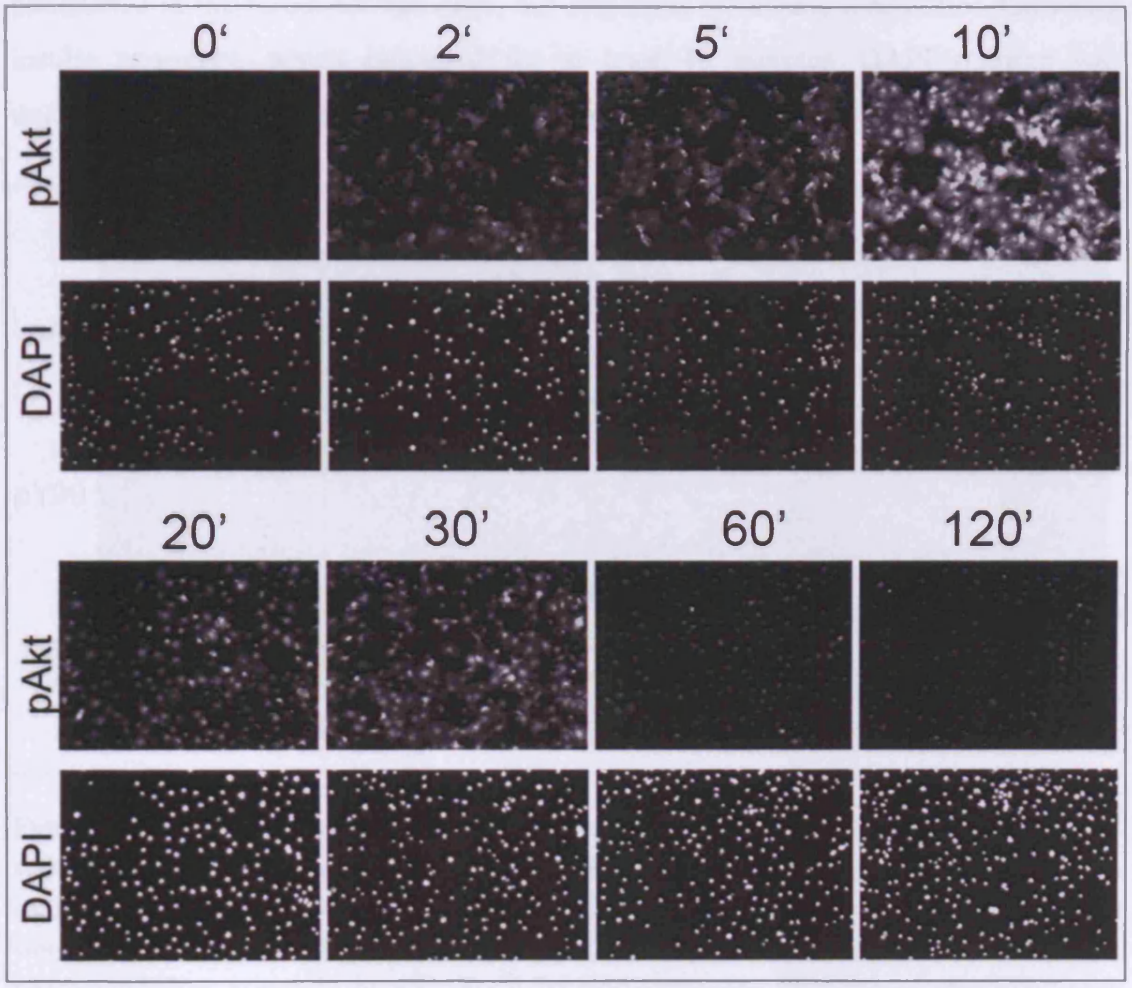

Figure 4.7 Immunostaining of pSer505-Akt in S2R+ cells stimulated with insulin. S2R+ cells were plated into a 384-well plate and maintained in serum-free Schneider's medium overnight. Schneider's medium supplemented with 10 μg/mL insulin was then added to the cells for the time points indicated. Cells were then fixed, permeabilised and blocked prior to incubation with anti pSer505-Akt antibody overnight at 4°C. For immunofluorescence detection of pSer505-Akt, a secondary anti-rabbit antibody conjugated to FITC was used. Cells were also stained with DAPI to detect nuclei. Images were acquired on a Nikon 2000E fluorescent microscope using a 20x objective.

Localisation of pSer505-Akt following insulin stimulation was also examined in the less-adherent rounded Kc167 cells. Serum-starved cells treated with insulin were subjected to immunofluorescence analysis using anti-pSer505-Akt and pY99 antibodies. As with the S2R+ cells, the same phenomenon of membrane localisation of pSer505-Akt in response to insulin stimulation was observed (Figure 4.8). Membrane localisation of pSer505-Akt was detected after two minutes of insulin stimulation and remained for up to 40 minutes. Phosphotyrosine staining was more

punctuated in the serum-starved cells, but displayed membrane localisation following insulin treatment, which remained for at least 40 minutes. DAPI staining was unaffected and served as a staining control for nuclei.

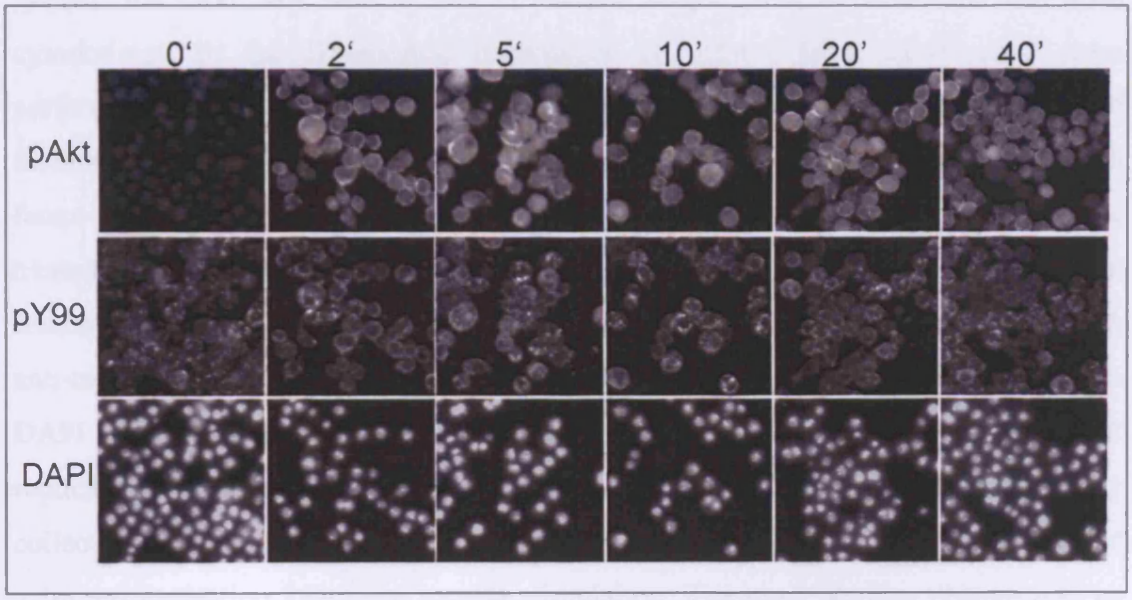

Figure 4.8 Insulin-dependent Akt activation and tyrosine phosphorylation in Kc167 cells. Kc167 cells were plated into a 384-well plate and maintained in serum-free Schneider's medium overnight. Cells were stimulated with 10 μg/mL insulin over a time course. Cells were then fixed, permeabilised and blocked prior to incubation with anti pSer505-Akt and anti pY99 antibodies overnight at 4°C. For immunofluorescence detection of pSer505-Akt, a secondary anti-rabbit antibody conjugated to Cy5 was used, and for detection of pY99 a secondary anti-mouse antibody conjugated to FITC was used. Cells were also stained with DAPI to detect nuclei. Images were acquired on a Nikon 2000E fluorescent microscope using a 40x objective.

Taken together, these data show that insulin can promote membrane associated tyrosine phosphorylation in different *Drosophila* haemocyte cell lines and a parallel membrane associated activation of PI3K/Akt signalling with a delayed activation of the downstream target S6K.

4.3 Insulin-dependent actin reorganisation

Following on from the finding, that insulin activates PI3K signalling in this system, the next step was to test if insulin would have an effect on the actin cytoskeleton in the *Drosophila* haemocyte cell lines. Most experiments were performed with S2R+ cells as they display morphological properties that could facilitate the examination of changes in the actin cytoskeleton induced by growth factor-mediated PI3K activation. For this purpose, serum-starved S2R+ cells were treated with bovine insulin over a time course and cells were fixed and stained for filamentous actin (F-actin) using rhodamine-phalloidin. Cells were also stained with anti-tubulin antibody, to assess any changes in the microtubule network, and with DAPI to stain nuclei. Images were acquired automatically and captured from eight replicates, with four different fields for each replicate. Thus, a total of 32 images were collected for each time point and each staining condition. This experiment revealed actin reorganisation following insulin stimulation. The most obvious change was an increase in F-actin staining at the cell cortex at the early time points (2-30 minutes) of the stimulation. By 60 minutes the cortical actin staining was lost and appeared as intense punctuated staining within the cell (Figure 4.9). Tubulin staining was relatively unaffected by insulin treatment up to 30 minutes, although at later time points there were some indications of reorganisation of microtubule network revealed by more condensed staining patterns.

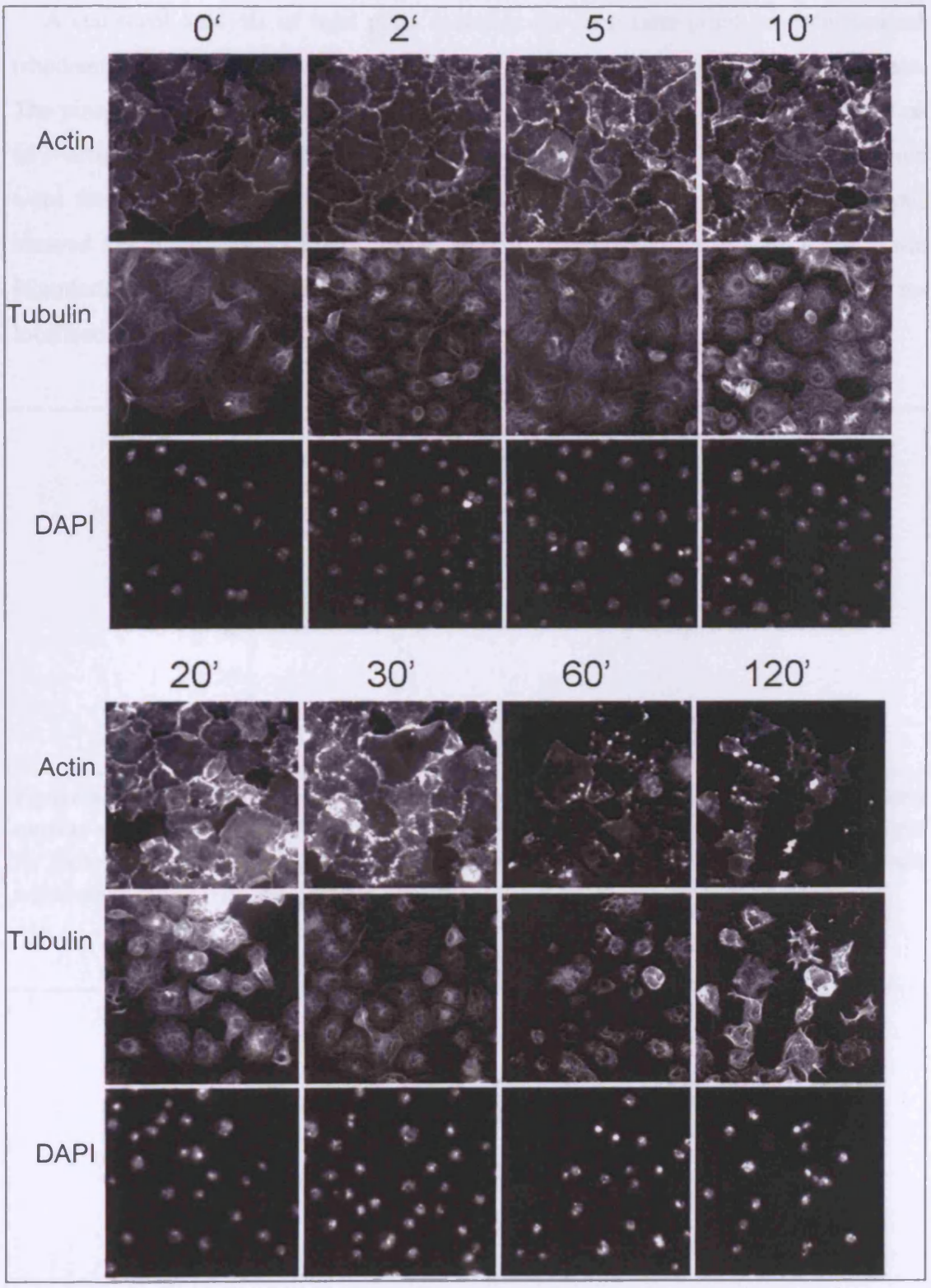

Figure 4.9 Insulin-dependent actin cytoskeleton reorganisation in S2R+ cells. S2R+ cells were plated into a 384-well plate in serum-free Schneider's medium overnight. Cells were then treated with 10 μg/mL bovine insulin over a time course. Cells were then fixed, permeabilised and stained with rhodamine-phalloidin (1:1000), FITC-conjugated anti-tubulin antibody (1:300) and DAPI (1:2000) for 1 h. Images were collected automatically on a Nikon 2000E fluorescence microscope, using a 20x objective.

A statistical analysis of total pixel intensity for each time point on each channel (rhodamine-phalloidin, FITC and DAPI) was carried out using MetaMorph software. The pixel intensities at each time point (Figure 4.10) were used to calculate the ratios of F-actin/tubulin (TRITC/FITC) and F-actin/nuclear staining (TRITC/DAPI), which were then plotted against time of insulin stimulation (Figure 4.11). This analysis showed that there was no significant change in the level of total F-actin with insulin stimulation, suggesting that insulin only promotes F-actin reorganisation and re-localisation, rather than altering the F-actin expression level.

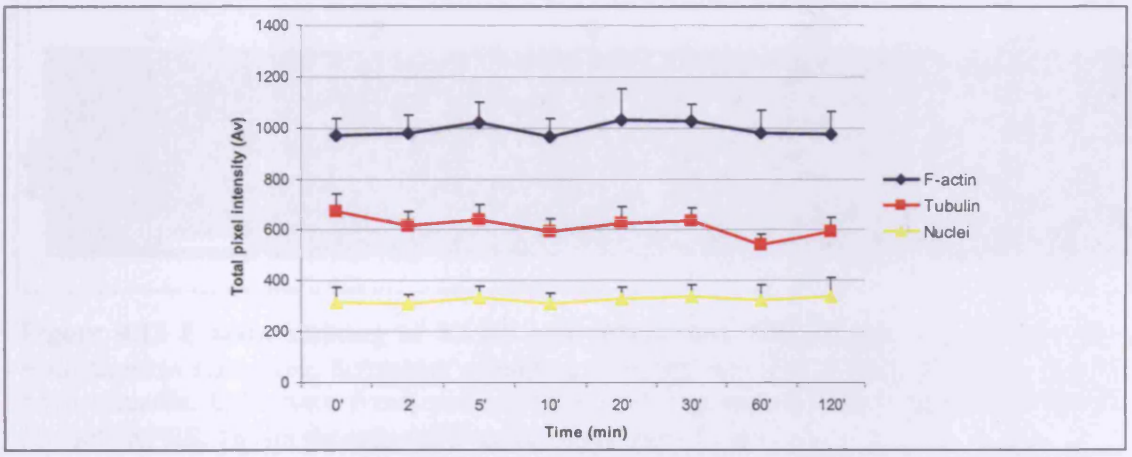

Figure 4.10 Graphical representation of the total pixel intensity for actin, tubulin and nuclear staining in S2R+ cells stimulated with insulin. Total pixel intensities of 32 images for each time point and each staining condition were calculated using MetaMorph software and average values with standard deviation (SD) bars for each time point were plotted.

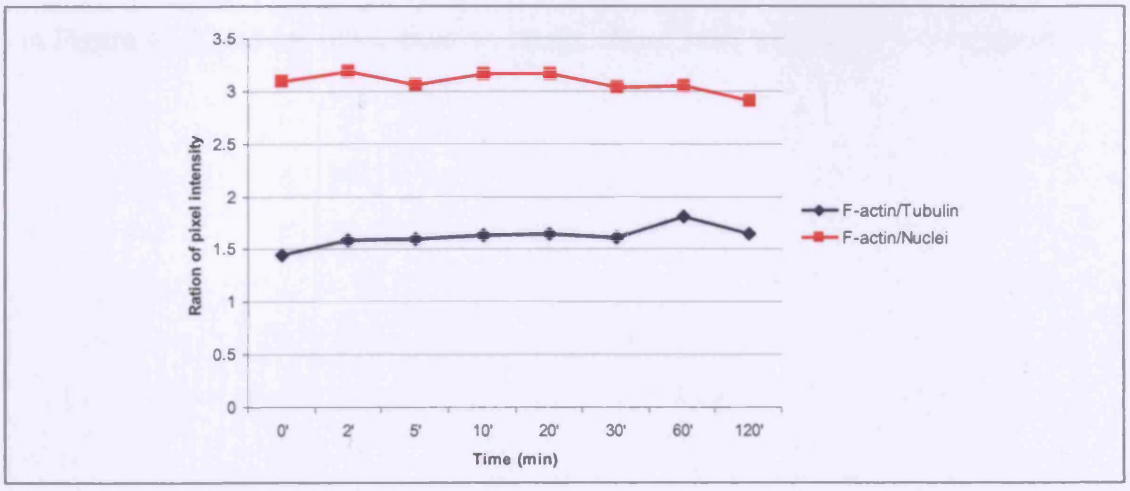

Figure 4.11 Graphical representation of the ratio of F-actin/tubulin and F-actin/nuclear staining intensities in S2R+ cells stimulated with insulin.

In addition to the S2R+ cells, Kc167 cells were also used as a second cell model to test the effect of insulin on actin cytoskeleton reorganisation. Kc167 cells, in general, have a different morphology than S2R+ cells, being more rounded with no cortical lamella. Kc167 were starved overnight and then stimulated with insulin over a time course, followed by fixing and staining for F-actin (Figure 4.12). This experiment showed that even in rounded cells insulin promoted actin reorganisation, characterised by a transient increase in F-actin staining at the cell cortex, similar to that observed in S2R+ cells.

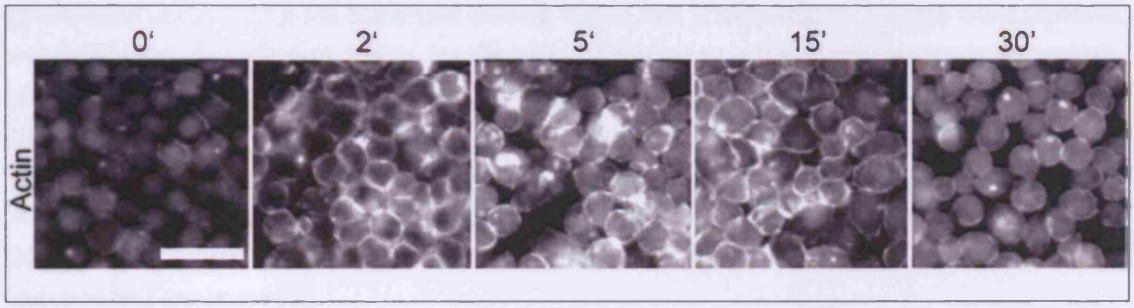

Figure 4.12 F-actin staining of Kc167 cells stimulated with insulin. Kc167 cells were maintained in serum-free Schneider's medium overnight and then stimulated with 10 μg/mL bovine insulin. Cells were fixed, permeabilised and then stained with rhodamine phalloidin (1:1000 in PBS, 1h) for detection of F-actin. Scale bar = 50 μm.

To study time-dependent membrane dynamics related to insulin-mediated cortical actin reorganisation, S2R+ cells were also filmed by time-lapse microscopy before and after insulin stimulation. Snap-shots of the movie and a kymograph are presented in Figure 4.13, and are representative images from three independent experiments.

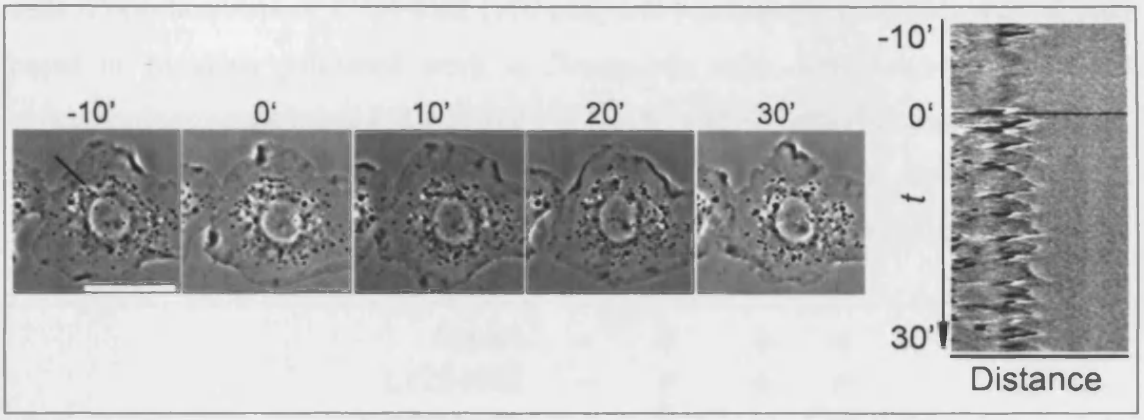

Figure 4.13 Insulin induces intense membrane ruffling in S2R+ cells. S2R+ cells were plated onto uncovered glass-bottomed culture dishes and phase-contrast images were captured every 20 seconds before and after insulin stimulation using a time-lapse microscopy system, with a 100x oil-immersion objective. Cell images are shown from the movie at the indicated time points with zero minute representing the time point of insulin addition. On the right is a kymograph showing the pixel intensities across a section of the cell membrane over the time course (indicated in black line in the first image). The kymograph was generated in MetaMorph software. The scale bar = 50 μm. (The figure is a representative from four independent experiments).

This time-lapse approach revealed that quiescent S2R+ cells display a low level of membrane ruffling characterised by dynamic protrusions and retraction of the cell edge which was increased in response to insulin treatment. This intense membrane ruffling is likely to be driven by insulin-dependent reorganisation of cortical actin.

4.4 PI3K-dependent actin reorganisation

Data from the previous sections showed that insulin activates PI3K signalling in *Drosophila* cell lines and results in actin cytoskeleton reorganisation in cells with different morphologies. In order to test if this insulin-induced actin cytoskeleton reorganisation is PI3K-dependent, several experiments were performed using the commercially available and widely used PI3K inhibitors LY294002 and wortmannin.

Firstly, the PI3K inhibitors were tested to see if they could block insulin-dependent activation of PI3K. This was monitored by immunoblotting for pSer505-Akt in S2R+

cells. Concentrations of LY294002 (100 μM) and wortmannin (100 nM) were chosen based on previous published work in *Drosophila* cells, which showed that these concentrations could block PI3K activity in Kc167 and S2 cells (Lizcano *et al.*, 2003). Both LY294002 and wortmannin were able to block the insulin-dependent phosphorylation of Akt at Ser505 confirming previous observations (Figure 4.14).

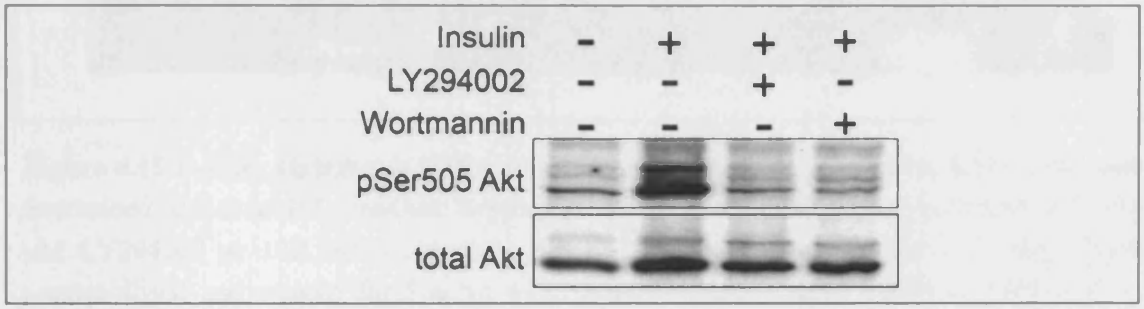

Figure 4.14 PI3K inhibitors block insulin-dependent phosphorylation of Akt. S2R+ cells were plated at 80% confluence in Schneider's medium supplemented with 10% FCS. After ~16 hours, cells were pre-treated with 100 μM LY294002 or 100 nM wortmannin for 20 min, followed by 20 minutes treatment with 10 μg/mL bovine insulin. Cells were lysed in NP40 lysis buffer, and lysates were subjected to immunoblotting for pSer505-Akt, followed by stripping blots and re-probing for total Akt.

To test whether actin cytoskeleton organisation is dependent upon PI3K in *Drosophila* haemocytes, S2R+ and Kc167 cells were treated with LY294002 and wortmannin, before fixing and staining for F-actin with rhodamine-phalloidin (Figure 4.15). It was evident that PI3K inhibition disrupted the normal actin structure of S2R+ cells as shown by a loss of cortical F-actin staining and with retraction of the cell edges leaving a few processes attached to the substrate. This was more evident in LY294002 *versus* wortmannin treated cells.

Figure 4.15 F-actin staining of S2R+ cells treated with PI3K inhibitors. S2R+ cells were maintained in Schneider's medium supplemented with 10% FCS before treatment with 100 μM LY294002 or 100 nM wortmannin for 20 min. Cells were washed with PBS, fixed, permeabilised and stained for F-actin with rhodamine-phalloidin (1:1000 in PBS) for 1h. Pictures were captured on a fluorescence microscope, using a 40x objective. Arrows indicate the spiked structures left at the cell edges following inhibitor-induced retraction. Scale bar = 50 μm.

In Kc167 cells, the well-defined cortical actin ring was also disrupted in response to PI3K inhibition. Cells also displayed spiked structures at the cell edge in response to LY294002 (Figure 4.16), but not in response to wortmannin.

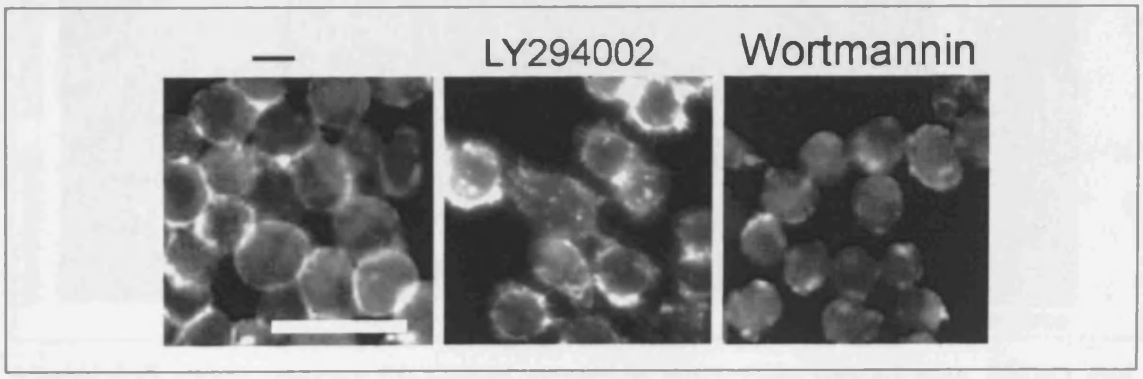

Figure 4.16 F-actin staining of Kc167 cells treated with PI3K inhibitors. Kc167 cells were maintained in Schneider's medium supplemented with 10% FCS before treatment with LY294002 (100 μM) or wortmannin (100 nM) for 20 min. Cells were fixed and permeabilised prior to F-actin staining with rhodamine-phalloidin. Pictures were captured on a fluorescence microscope using a 40 x objective. Scale bar = 50 μm.

To test if insulin-dependent membrane ruffling was regulated by PI3K signalling, S2R+ cells were treated with PI3K inhibitors or DMSO vehicle prior to insulin stimulation and filmed using phase-contrast time-lapse microscopy (Figure 4.17). From the movies themselves and snap-shots taken at various time points, it was obvious that both inhibitors could block membrane ruffling in the cells. Generated kymographs confirmed that these inhibitors blocked virtually all dynamic protrusion of the membranes suggesting a role for PIP3 in the regulation of actin dynamics in cells at steady state. In addition, both induced a retraction of the cell edge, leaving processes attached to the substrate. The insulin–induced increased in membrane ruffling was also blocked by both inhibitors. There were, however, differences in the kinetics of the effects produced by the two inhibitors. Whereas both caused immediate inhibition of membrane ruffling; the cellular retraction, loss of cortical lamella and formation of spiked structures was delayed in LY294002-treated cells *versus* wortmannin-treated cells and did not occur until after insulin treatment.

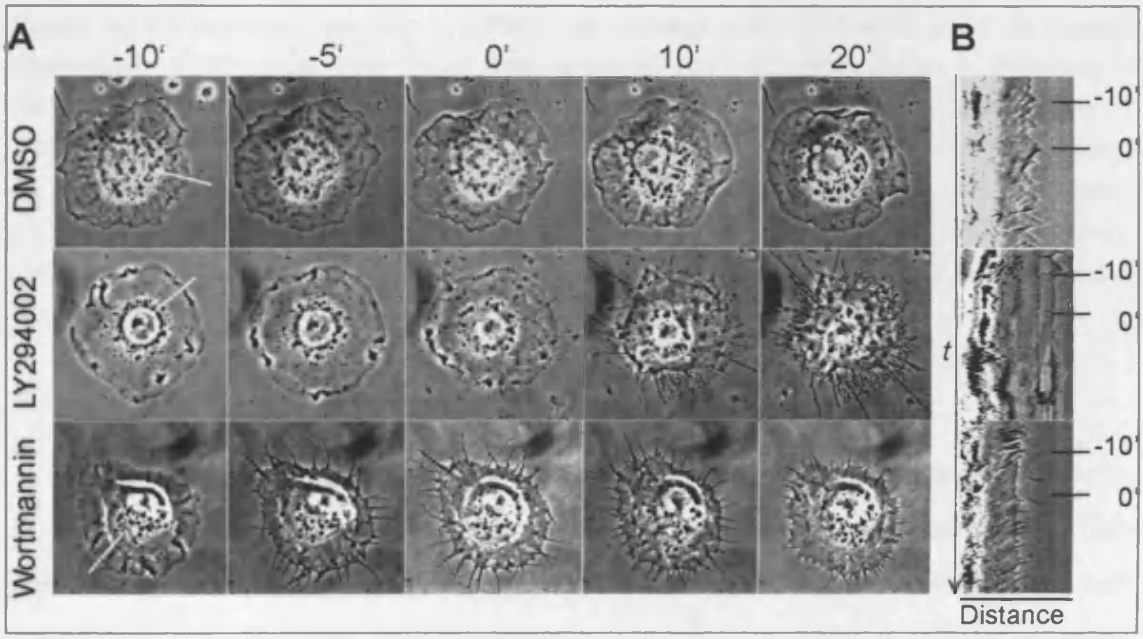

Figure 4.17 Phase-contrast time-lapse movies of S2R+ cells treated with DMSO and PI3K inhibitors, LY294002 and wortmannin prior to insulin stimulation. S2R+ cells were plated onto uncoated glass-bottomed dishes in Schneider's medium supplemented with 10% FCS, overnight. Images for a movie were then captured every 10 seconds using a phase contrast time-lapse microscope with a 100x oil-immersion lens. Cells were filmed for 5 minutes prior to treatment with DMSO, LY294002 (100 μM) or wortmannin (100 nM) (labelled on the figure as -10'), followed by insulin (10 μg/mL) addition after a further 10 minutes (labelled as 0'). On the right are kymographs showing the pixel intensities across a section of the cells (indicated by white lines in left-hand image). Kymographs were generated in MethaMorph software, and are representative from three independent experiments.

Lower concentrations of LY294002 (10 and 50 μM) were also tested and showed that these concentrations of LY294002 could also block basal ruffling and cause cellular contraction. However, at these concentrations insulin-induced membrane spreading and ruffling was not prevented (Figure 4.18).

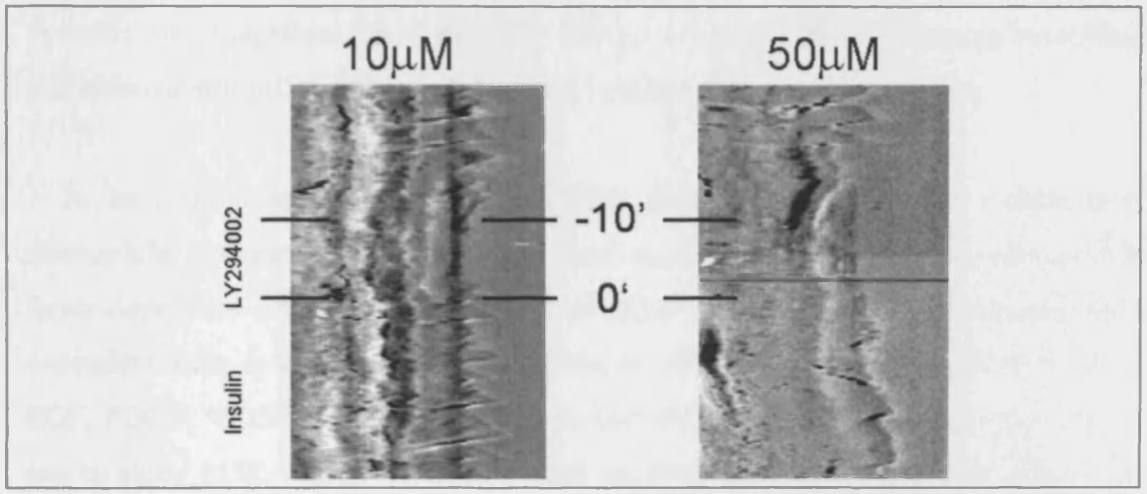

Figure 4.18 Time-lapse movies of S2R+ cells treated with LY294002 prior to insulin stimulation. S2R+ cells were plated onto uncoated-glass bottomed dishes in Schneider's medium supplemented with 10% FCS, overnight. Images were captured every 10 seconds on a phase contrast time-lapse microscope using a 100x oil-immersion lens. Cells were filmed for 15 min. prior to treatment with 10 μM LY294002 or 50 μM LY294002 and 10 minutes after this treatment insulin (10 μg/mL) was added for an additional 20 min. Kymographs were created in Metamorph software by drawing lines perpendicular to the cell membrane and pixel intensities along these lines combined across the time course.

Taken together, these data show that PI3K activity is required for actin cytoskeleton remodelling in response to insulin in fly haemocyte cell lines. This remodelling was characterised by increased filamentous actin staining and cell spreading at the cell cortex and an increase in the rate of membrane ruffling, although no directional cell movement was observed.

4.5 Conclusions

The actin cytoskeleton participates in many cellular processes, including the maintenance of cell shape, coordinated cell movement and intracellular trafficking. To coordinate such a vast array of cellular functions, the actin cytoskeleton must be dynamic and adaptable, i.e. it must be able to adapt to rapidly changing conditions and external stimuli, such as exposure to mitogenic factors and hormones.

In an attempt to define a role for PI3K in regulating the actin cytoskeleton, *Drosophila* haemocyte cell lines were used as a model system to explore growth factor-dependent activation and kinetics of PI3K signalling and growth factor/PI3K-dependent actin cytoskeleton reorganisation *in vitro*. Several growth factors (insulin, EGF, PDGF, VEGF and calf serum) were tested in order to establish the best one to use to study PI3K-dependent actin cytoskeletal reorganisation. Western blotting for pSer505-Akt, an established downstream target of active PI3K, showed that EGF, PDGF, VEGF and calf serum did not promote the phosphorylation of Akt in S2R+ cells, suggesting that *Drosophila* EGFR and PVR, the fly homologues of mammalian VEGFR and PDGFR (Duchek et al., 2001; Cho et al., 2002), do not bind and respond to these non-fly growth factors. In addition, incubation of cells in conditioned medium did not result in Akt phosphorylation, suggesting that there were no autocrine growth factors secreted from cells, which were then able to activate tyrosine kinase receptor signalling and subsequently PI3K activation. Only insulin treatment was able to induce phosphorylation Akt at Ser505 site, suggesting that bovine and fly insulin are similar enough to trigger the *Drosophila* receptor, and confirming previous findings that the main activator of PI3K signalling in *Drosophila* haemocytes occurs through activation of the insulin receptor (InR).

InR is a tyrosine kinase that requires ligand binding for its activation and to promote autophosphorylation on tyrosines, which triggers activation of downstream signalling pathways that regulate glucose uptake, mitogenesis, growth etc. Activated InR is known to be internalised and then subjected to degradation or recycling that brings the receptors back to the plasma membrane (Di Guglielmo et al., 1998). In the study here, the activation of the receptor was indirectly followed by phosphotyrosine

immunostaining in both S2R+ and Kc167 cell lines. It was observed that prior to insulin stimulation the phosphotyrosine signal was distributed heterogeneously inside cells. In the early minutes of insulin stimulation this phosphotyrosine signal was dramatically increased at the cell membrane, suggesting phosphorylation and activation of the InR and its substrates were taken place. The phosphotyrosine signal was found to be sustained on the membrane for around 30 minutes, after which the staining became perinuclear, suggesting that translocation of the receptor to intracellular compartments has happening, and that it could be degraded or recycled, possibly through endosomes, to the cell surface as previously reported in other cell lines (Fehlmann et al., 1982; Carpentier et al., 1985).

PI3K is known to be a downstream target of activated receptor tyrosine kinase and is recruited into a signalling complex through interaction of the two SH2 domains of the regulatory subunit (p85) via the sequence motif pY-X-X-M (where X is any amino acid), which exist in receptor tyrosine kinases (i.e. InR) or their adaptor molecules (i.e. insulin receptor substrate, IRS). This reaction brings PI3K to the inner side of the plasma membrane where it can interact with its substrates, the phosphoinositides, leading to their phosphorylation on position 3' of the inositol ring and the production of lipid second messengers such as PIP3. This is followed by recruitment of PH-domain containing molecules (such as Akt) to the membrane, which is a crucial step for their phosphorylation and activation (Chan et al., 1999). The kinetics of PI3K activation in S2R+ and Kc167 cell was examined by following the phosphorylation of Akt and its cellular localisation. It was observed that the phosphorylated Akt signal was very low in either serum-starved or serum-supplemented randomly growing cells, but was rapidly induced upon insulin stimulation and became localised to the plasma membrane, presumably due to the generation of PIP3 by PI3K. My data reported here thus supports the previous findings in other cell systems.

The pAkt signal was also found to be increased in the nucleus in response to insulin, suggesting that nuclear translocation of phosphorylated Akt has taken place (Webster, 2004). This may be required for the phosphorylation of some Akt targets (e.g. forkhead transcription factors (FOXO), the transcriptional regulator Bcl-6 and

the cell cycle regulators $p27^{Kip1}$ and $p21^{Cip1/WAF1}$, which are nuclear. Recent reports showed that the role of pAkt in the nucleus could be to phosphorylate and inactivate its targets by promoting their translocation out of the nucleus and their accumulation in the cytoplasm (Webster, 2004). For example, when FOXO3a is phosphorylated by Akt in the nucleus, it is expelled from the nucleus and sequestered in an inactive complex with 14-3-3, thus preventing transcription of pro-apoptotic genes such as Bim- and $p27^{Kip1}$, and that promotes cell survival (Webster, 2004; Trotman et al., 2006). In addition, Zhou *et al.* showed that a dominant negative Akt mutant (DN-Akt) inhibits cell growth due to nuclear localisation of $p21^{Cip1/WAF1}$ (Zhou et al., 2001). They demonstrated that Akt normally associates with $p21^{Cip1/WAF1}$ and phosphorylates a consensus threonine residue (Thr145) in its nuclear-localisation signal, leading to the cytoplasmic localisation of $p21^{Cip1/WAF1}$ and preventing it from inhibiting cell cycle progression and promoting cell proliferation. The analysis of PI3K/Akt activation in response to insulin stimulation in S2R+ cells showed that phosphorylation of Ser505-Akt peaked at the very early time points of the insulin stimulation and then gradually declined. Interestingly, a biphasic regulation of pAkt (a transient decrease followed by sustained increase) was induced by insulin in S2 cells, and was shown to be more prominent in serum-starved cells (Figure 4.5). This appears to be a novel observation in fly haemocyte cells, although a biphasic phosphorylation of Akt has been reported previously in other cell types (Nagano et al., 2001). However, it is unclear whether this represents a real cellular response that is relevant to signalling output, or a consequence of different extraction due to the re-localisation of pAkt following growth factor triggering.

The activation of pS6K was also examined since it is known to be a downstream target of PI3K signalling through PDK1 (Williams et al., 2000), Akt (Lizcano et al., 2003) and the mTOR/Raptor complex (Sarbassov et al., 2005). An antibody that recognises phosphorylated Thr389 (which is located in a hydrophobic sequence outside the catalytic domain) was chosen because phosphorylation of this site is known to lead to activation of S6K and phosphorylation of ribosomal protein S6 with concomitant up-regulation of translational capacity of cells including increased ribosome biosynthesis (Pearson et al., 1995). In the study here, only insulin induced the phosphorylation at this site of S6K, and this phosphorylation followed Akt and

MAPK activation. The regulation of pS6K by PI3K/Akt and/or Ras/MAPK signalling is still unclear, but several studies have suggested possible cross-talk between these two signalling pathways. It was shown that PI3K can be activated through direct association with active GTP-bound Ras (Rodriguez-Viciana et al., 1997), perhaps through the Ras-binding domain of the catalytic subunit p110. Ras can activate PI3K *in vitro*, but its relevance for normal PI3K function *in vivo* has not been defined. Humans express two forms of S6K. Although it has been shown that S6K1 can be phosphorylated *in vitro* by Ras/MAPK signalling (Mukhopadhyay et al., 1992), it appears that S6K1 residues are distinctly recognised from the Ras/MAPK-dependent phosphorylation motifs (Ballou et al., 1991). On the other hand, S6K2, which is also regulated by PI3K and mTOR (Lee-Fruman et al., 1999), can be activated *in vivo* by MAPK (Wang et al., 2001). Both human S6K1 and S6K2 are more similar to each other than to the single S6K gene present in *Drosophila*. However, DS6K, like S6K2, contains a C-terminal proline-rich domain which may be involved in SH3 domain-mediated protein-protein interaction important in S6K signalling (Ballou et al., 1991). Here, I showed that DS6K can be activated by insulin, though the kinetics of activation compared with Akt (and ERK) activation varied depending on the conditions in which the cells were maintained. S6K activation was delayed in the absence of serum, suggesting serum factors may prime the activation in response to insulin. As both ERK and Akt were activated by insulin, the relative contribution of MAPK and PI3K signalling to S6K activity is unknown, and further studies will be required to address this signalling event.

After I established the process of insulin-dependent activation of PI3K signalling in the *Drosophila* haemocyte cell models, I then examined the effect of the InR/PI3K signalling cascade on the actin cytoskeleton. One of the early events in the insulin response is the reorganisation of actin filaments and two types of insulin-dependent morphological changes in actin filaments have been described, depending on the cell type studied: an increase in actin stress fibre formation, dynamic polymerisation and depolymerisation of actin below the plasma membrane, more commonly referred to as 'membrane ruffling' (Goshima et al., 1984b; Ridley and Hall, 1992a). It is well established that insulin rapidly induces actin remodelling in a variety of cell types including HeLa cells (Goshima et al., 1984a), Rat-1 fibroblasts and CHO cells

overexpressing the insulin receptor (Knight et al., 1995; Clodi et al., 1998) and Swiss 3T3 fibroblasts (Ridley *et al.*, 1992a; Ridley et al., 1992b). However, no such reports exist for fly haemocytes, widely used in studying the role of the insulin/PI3K signalling, particularly in regulating proliferation, cell size, survival and metabolism (Leevers et al., 1996; Weinkove et al., 1999; Franke et al., 2003). Only recently, a study on fly migratory haemocytes *in vivo* showed that PI3K is an essential mediator for cell polarisation and directed cell migration (Wood et al., 2006). This study showed although haemocyte cells can sense a chemotactic gradient from PDGF/VEGF ligands Pvf2 and Pvf3, these directed migrations occur independently of PI3K signalling. Confocal analysis of embryos expressing a dominant-negative kinase dead form of the *D. melanogaster* PI3K catalytic subunit (Dp110D954A), specifically in haemocytes, showed normal haemocyte distribution at all stages of development, and these cells appeared morphologically indistinguishable from their wild-type counterparts exhibiting dynamic lamellipodia and filapodia formation. However, PI3K was required for haemocytes to polarise and chemotax toward a laser-ablated wound site and in the mutant-expressing embryos, wounds remained largely undetected by the haemocytes. In addition, implantation of DMSO- or LY294002-presoaked beads into the embryos showed that DMSO beads became surrounded by haemocytes, whereas no cells chemotaxed toward the beads soaked in the PI3K inhibitor.

Herein, I showed that PI3K signalling can contribute to actin organisation in fly haemocytes *in vitro* and that this occurs both basally and in response to growth factor (insulin) stimulation. I used a time course of insulin stimulation and statistical analysis of filamentous actin staining to reveal that whilst the total level of F-actin staining did not change dramatically with the treatment, there was a rapid increase in F-actin staining at the cell cortex that remained for 30 minutes. This was followed by a dramatic reorganisation of cytoskeletal structures, both of F-actin and microtubules, observed as a loss of cortical actin lamellipodia and microtubule condensation. Since F-actin reorganisation followed the kinetics of insulin-dependent Akt activation, this suggested to me that cytoskeletal reorganisation might be PI3K-dependent in this cell model. To test this, I used LY294002 and wortmannin to examine the effects of PI3K inhibition on actin reorganisation in response to insulin. Treatment with both

inhibitors resulted in disruption of cortical actin and efficiently blocked basal- and insulin-induced membrane ruffling. This was accompanied by apparent retraction of the cell edges resulting in loss of cortical lamellipodia and in generation of spiked structures that were relatively devoid of F-actin. There were, however, differences in the kinetics of the cell retraction caused by LY294002 and wortmannin. The observed difference in inhibitor efficiency could have been due to the different solubility of the drugs, the time taken for the drugs to enter cells and reach their targets, the half-life of the inhibitors and their target specificity. Moreover, for LY294002 at least, there was a dose-dependent response for blockade of insulin-dependent membrane ruffling; high concentration of LY294002 (100 μM) blocked both basal and insulin-dependent membrane ruffling, whereas only basal ruffling was blocked when cells were pre-treated with lower doses of LY294002 (10 or 50 μM). Although wortmannin and LY294002 have served as powerful tools for implicating PI3Ks in a wide range of physiological processes, and much of our understanding of PI3K action in cells derives from the use of these two reagents, they are broadly active against the whole PI3K family showing little specificity among members. In addition, they also appear to target other kinases such as GSK-3, CK II, and non-kinases (Gharbi et al., 2007). Consequently, little is known about the specific signalling functions of individual PI3Ks and further work could include the use of class specific PI3K inhibitors. Indeed, Knight *et al.* used a set of new generation PI3K class-specific inhibitors to define the PI3K isoforms required for insulin signalling (Knight et al., 2006). They identified p110α as the critical lipid kinase required for insulin signalling in adipocytes and myotubes, whereas p110β and p110δ played a secondary role in insulin signalling in these cells. They also showed that compounds targeting p110α blocked the acute effects of insulin treatment *in vivo*, whereas a p110β inhibitor had no effect. These results illustrate the use of a systematic target validation approach employing a panel of inhibitors that span a protein family. However, these inhibitors have not been tested in fly cells or their specificity towards *Drosophila* PI3K determined. This area could be the subject of future work. Another approach for examining the role of specific molecules in signalling is to employ RNAi-mediated gene silencing. I used this approach in the next chapter to further explore the role of PI3K and other signalling molecules in regulating the actin cytoskeleton.

The physiological role of insulin-triggered cytoskeletal re-arrangements is not completely clear. Although it may be involved in stimulating glucose up-take by promoting GLUT-4 (glucose transporter) insertion at membrane ruffles in some cell types (Khayat et al., 2000), it is also possible that the actin reorganisation itself is permissive for other actions of insulin such as signalling, DNA synthesis and gene expression. In addition, PI3K-induced changes in the actin cytoskeleton can be related to some physiological roles of PI3K signalling in fly haemocyte cells such as phagocytosis. Fly haemocytes have been reported to be phagocytic (Ramet et al., 2002). Phagocytosis is an essential component of the innate immune response that involves extensive cytoskeletal rearrangement and membrane remodelling (Aderem and Underhill, 1999). PI3K activity is known to be required for effective phagocytosis (Araki et al., 1996; Gillooly et al., 2001; Allen et al., 2005). For instance, Allen *et al.* showed that ulcerogenic (type I) strains of *Helicobacter pylori* (Hp) strongly activated class I_A PI3K in macrophages, a process which can coincident with phagocytosis, and caused endogenous p85 and active Akt accumulation in forming phagosomes. In addition, they observed that wortmannin and LY294002 inhibited phagocytosis in a dose-dependent manner, and blockade of engulfment correlated directly with loss of PIP3 in the membrane adjacent to the attached bacteria. In this study, it was also shown that PIP3 regulated actin polymerization at sites of Hp uptake. Further examinations would be required to show if PI3K-mediated actin cytoskeleton organisation and membrane ruffling are required for phagocytosis in fly haemocytes *in vitro*.

In conclusion, the work I presented in this chapter of my thesis has shown that PI3K signalling in fly haemocyte cells *in vitro* can be triggered by insulin and the kinetics of activation of downstream targets depends on the existing growth conditions. Also, dual regulation of p70S6K by PI3K/Akt and Ras/MAPK as a mechanism was implicated, and these pathways are an area for further research. In addition, I established that activation of the insulin receptor signalling pathway can cause dynamic actin reorganisation, which is blocked by PI3K inhibitors and is therefore PI3K-dependent. So most importantly, I developed a cell model system for further examination of the mechanisms involved in PI3K-dependent actin regulation using RNAi and proteomics, the focus of the following chapter.

Chapter 5: Functional proteomic analysis of PI3K signalling and actin regulation in *Drosophila* cells

5.1 Introduction

Work from the previous chapter, showed that PI3K signalling is involved in insulin-stimulated actin cytoskeleton remodelling and that this signal specifically initiates new cortical actin polymerisation in *Drosophila* haemocyte cell lines. The aim of the work I present in this chapter was to identify possible downstream targets of this PI3K activity and to study their molecular function. To study this I used a combination of technologies, RNAi-dependent gene silencing, 2D-DIGE global protein expression profiling and cellular phenotype analysis by fluorescence microscopy.

Initially, a 2D-DIGE analysis experiment was performed using *Drosophila* cell lines with different morphologies to establish culturing conditions, such as generating sufficient amounts of protein, needed for protein expression profiling. In addition, this experiment was also designed to examine the feasibility of matching protein changes with cellular phenotype, particular cellular morphology among cells with different morphologies.

The main aim was then to perform proteomic analysis of S2R+ cells following RNAi knockdown of specific genes involved in the PI3K signalling and actin cytoskeletal regulation (Kiger *et al.*, 2003). The RNAi strategy was applied with the aim of overcoming some of the limitations of PI3K drug treatment, such as hidden target specificity (Brunn et al., 1996; Bain et al., 2003), but also to extend the

functional analysis of putative downstream targets of PI3K. RNAi is a sequence-specific, post-transcriptional, gene silencing process mediated by short interfering RNA (siRNA) molecules (see Chapter 1). In this study, RNAi was applied to silence the expression of genes that are involved in PI3K signalling and cytoskeleton regulation, and it was carried out in a model *Drosophila* cell line. Several factors make RNAi in *Drosophila* cell lines an excellent approach for functional genomic studies. Firstly, the complete genome sequence of *Drosophila melanogaster* has been mapped (Adams et al., 2000), and the well-annotated *Drosophila* genomic sequences have simplified the design of gene-specific double-stranded RNAs (dsRNAs) for knockdown of expression of specific genes. Secondly, RNAi is extremely efficient in *Drosophila* cells, facilitating partial to complete knockdown in 98-100% of cells. Thirdly, RNAi in fly cells is a very simple technique, as it requires simple addition of the dsRNA to the culture medium without the need for expensive transfection reagents. Finally, *Drosophila* has been a favoured tool for genetic studies for over 100 years and is an excellent model in which to identify genes involved in cellular and developmental processes. It is furthermore remarkable that the *Drosophila* genome encodes homologues of over 60% of human disease genes and also lacks much of the genetic redundancy observed in vertebrates (Rubin et al., 2000).

Quantitative proteomic analysis of selective RNAi knockdowns was carried out using 2D-DIGE to define protein profiles for each RNAi treatment. Mass spectrometry was used to identify differentially expressed proteins. In this way novel downstream targets of PI3K and regulators of actin could be identified. Overlapping sets of protein expression changes among the different RNAi treatments were then subject to further analysis, which will aim to carry out pathway mapping. Immunoblotting analyses were used to confirm the results of the 2D-DIGE and MS analyses. Finally, immunofluorescence microscopy was performed to study morphological changes and actin reorganisation in cells subjected to the different RNAi treatments, and to try to link these changes with the observed changes in the proteome.

5.2 Evaluation of 2D-DIGE for comparative analysis of protein expression profiles in *Drosophila* cell lines displaying distinct morphological phenotypes

Initially, a pilot experiment was performed aimed at establishing culturing conditions for the *Drosophila* cells needed to generate sufficient amounts of protein for 2D-DIGE expression profiling. Four different fly cell lines (S2R+, Kc167, S2 and Clone 8) were used and their protein expression profiles were generated by 2D-DIGE, followed by comparative protein abundance analysis. S2R+, S2 and Kc167 cells have been reported to display haemocyte cellular properties (Schneider, 1972). As described previously, S2R+ cells are phagocytic, adherent and flat cells. S2 cells grow in semi-adherent colonies and display a rounded morphology with a granular cytoplasm. Kc167 cells are also phagocytic and uniformly round. Clone 8 cells were derived from the wing disc, they are semi-adherent, elongated and can grow in multiple layers (Peel et al., 1990). Thus, this experiment was designed to examine the feasibility of matching protein changes with cellular phenotype, particular cellular morphology.

The four cell lines were plated at ~1.5x 10^6 cells/mL in 6-well culture dishes, and maintained in the appropriate fly medium supplemented with 10% FCS until they reached confluence. To test for method reproducibility, cells were grown as triplicate cultures, which were analysed separately (biological replicates). Cells were lysed and an equal amount of total protein lysate (100 μg) from each sample was labelled with Cy3 or Cy5 dyes. In parallel, a pool was prepared by mixing an equal amount of protein from each sample and was labelled with Cy2 (Figure 5.1). Protein lysates labelled with Cy3 and Cy5 from different cell lines were mixed appropriately on different gels to avoid biases (Figure 5.1). Cy2-labelled pool was run on each gel to serve as an internal standard to facilitate spot matching, as it is comprised of all proteins from the four different samples used in the analysis, data normalisation across gels in one run and quantitation across the gels (Figure 5.1). The six gels were scanned at three different wavelengths (Chapter 2, Table 2.2) to generate 18 protein spot maps.

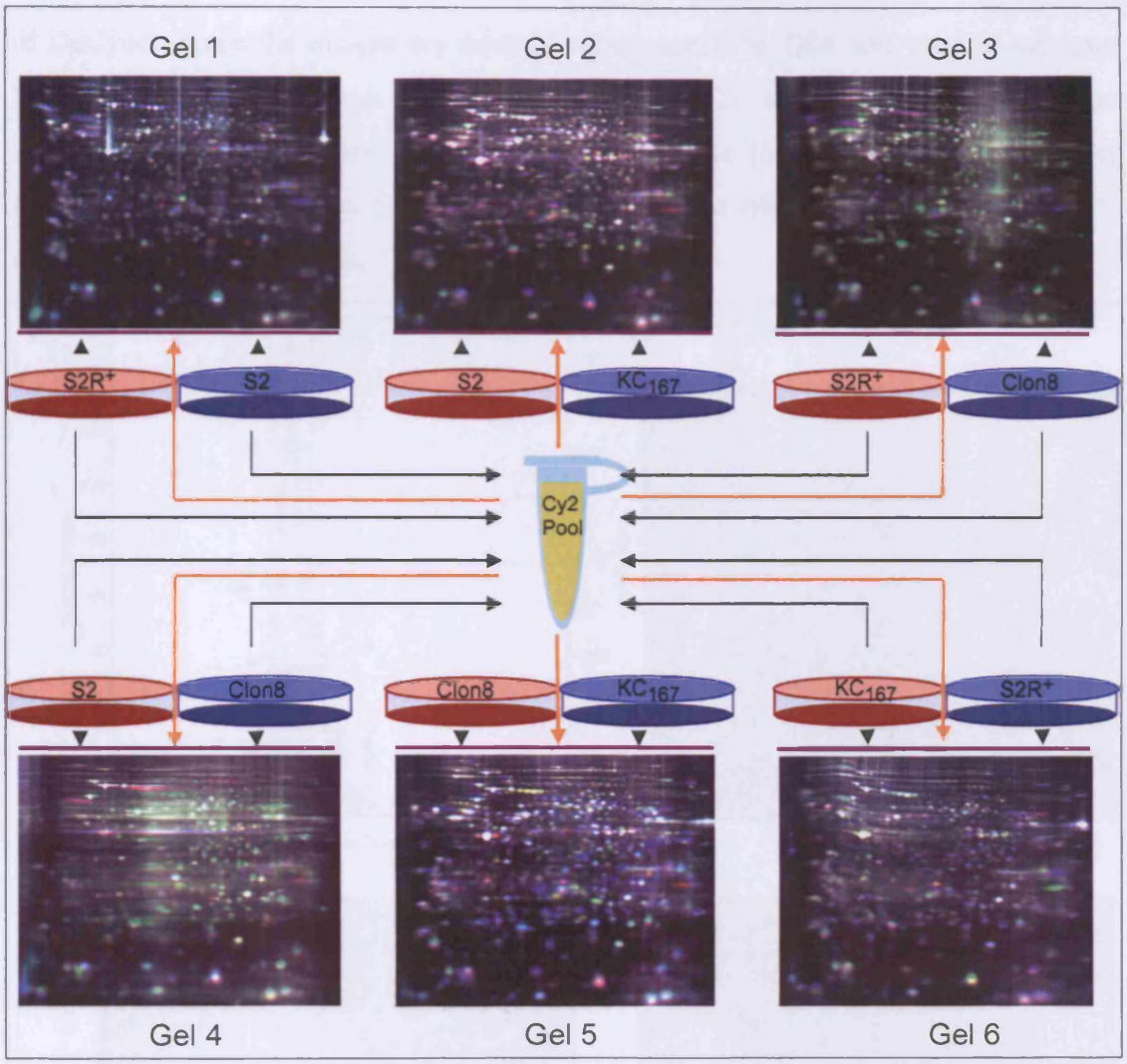

Figure 5.1 Experimental design of NHS-Cy dye labelling to compare protein expression profiles of four different *Drosophila* cell lines by 2D-DIGE. S2R+, S2, Kc167 and Clone 8 cells were grown in triplicate cultures until fully confluent and then lysed in NHS-lysis buffer. Equal amounts of protein lysate (100 μg) were labelled with 400 pmol of Cy3 (red plates) or Cy5 (blue plates). A Cy2-labelled internal standard (yellow) was prepared by mixing equal amounts of each protein lysate. Cy3 and Cy5 labelled samples were then mixed appropriately, including the Cy2 internal standard in each mixture. Mixed samples were then run on six individual 2-D gels and fluorescent images captured. The figure shows the labelling strategy and superimposed images generated for the six gels (from Image Quant software). Changes in expression of specific proteins are shown as green (up in Cy3 channel), red (up in Cy5 channel) and blue (up in Cy2 channel).

Quantitative comparison of protein expression and differential analysis was carried out using DeCyder software. Triple images obtained from the same 2D gels were automatically curated and matched using the differential in-gel analysis (DIA) module

of DeCyder, since the images are directly superimposable. DIA was used to estimate the protein spot number on each gel (Figure 5.2). The matched images were then imported into the biological variance analysis module (BVA), where protein spots from a selected master gel (Figure 5.3) were matched with the corresponding spots across the other gel images.

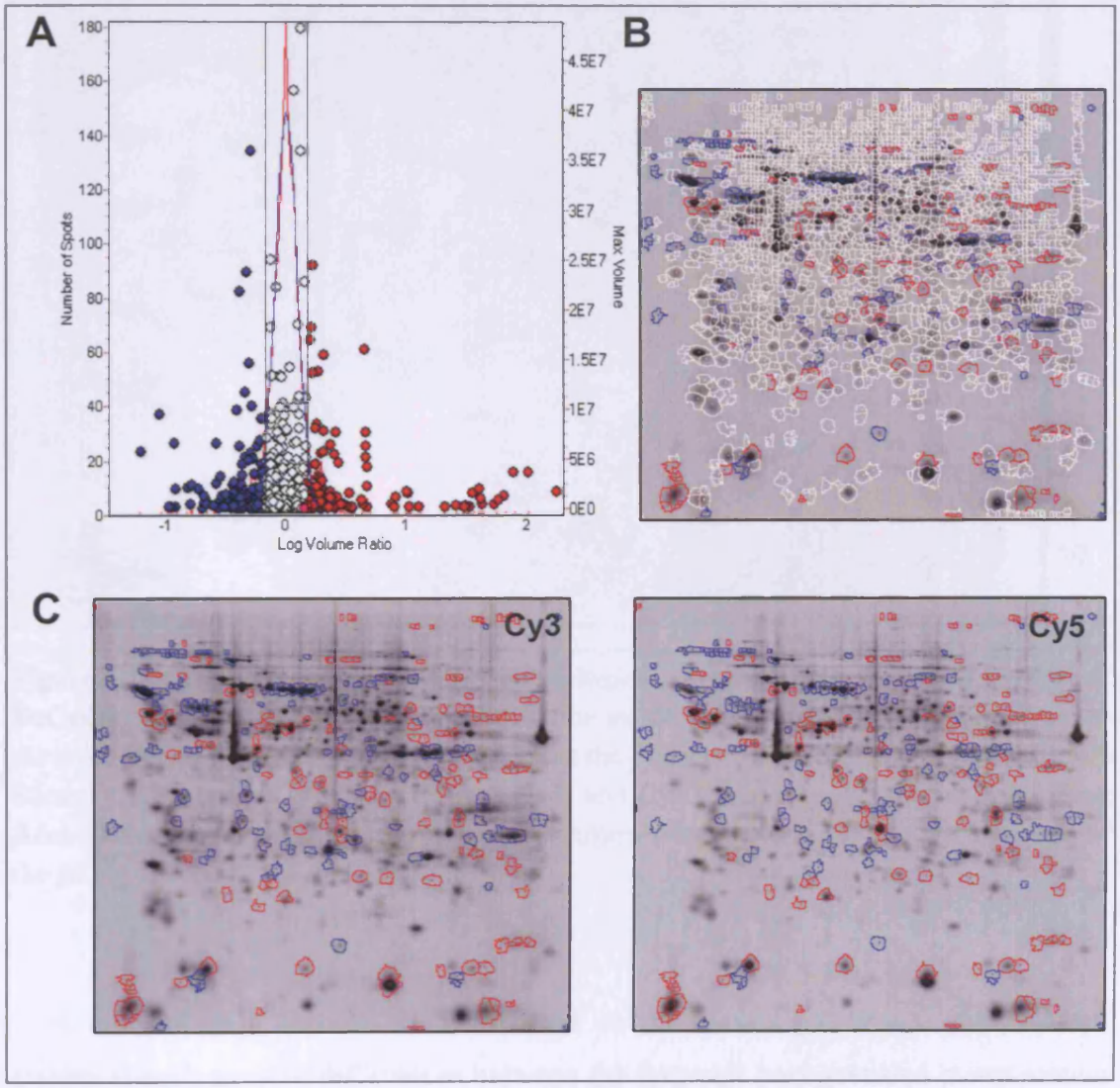

Figure 5.2 Differential image analysis using DeCyder software. A) A scatter plot of spot volumes and number versus volume ratio is shown with the threshold ratio set at +/- 1.5 (+/- 2 SD) (vertical lines). White spots represent matched protein features displaying no changes in abundance between two protein samples run on the same 2-D gel. Red spots represent features from one sample with an increased volume ratio compared to their counterparts from the other sample, while blue spots represent features with decreased volume ratios. **B)** Representative 2D-DIGE image extracted from DIA showing protein features with similar (white), increased (red), and decreased (blue) volume ratios between two samples run on the same gel. **C)** Cy3 and Cy5 separated gel images. Protein features displaying a fold-change in abundance $\geq$1.5 fold or $\leq$ -1.5 are circled red (increased) and blue (decreased), respectively.

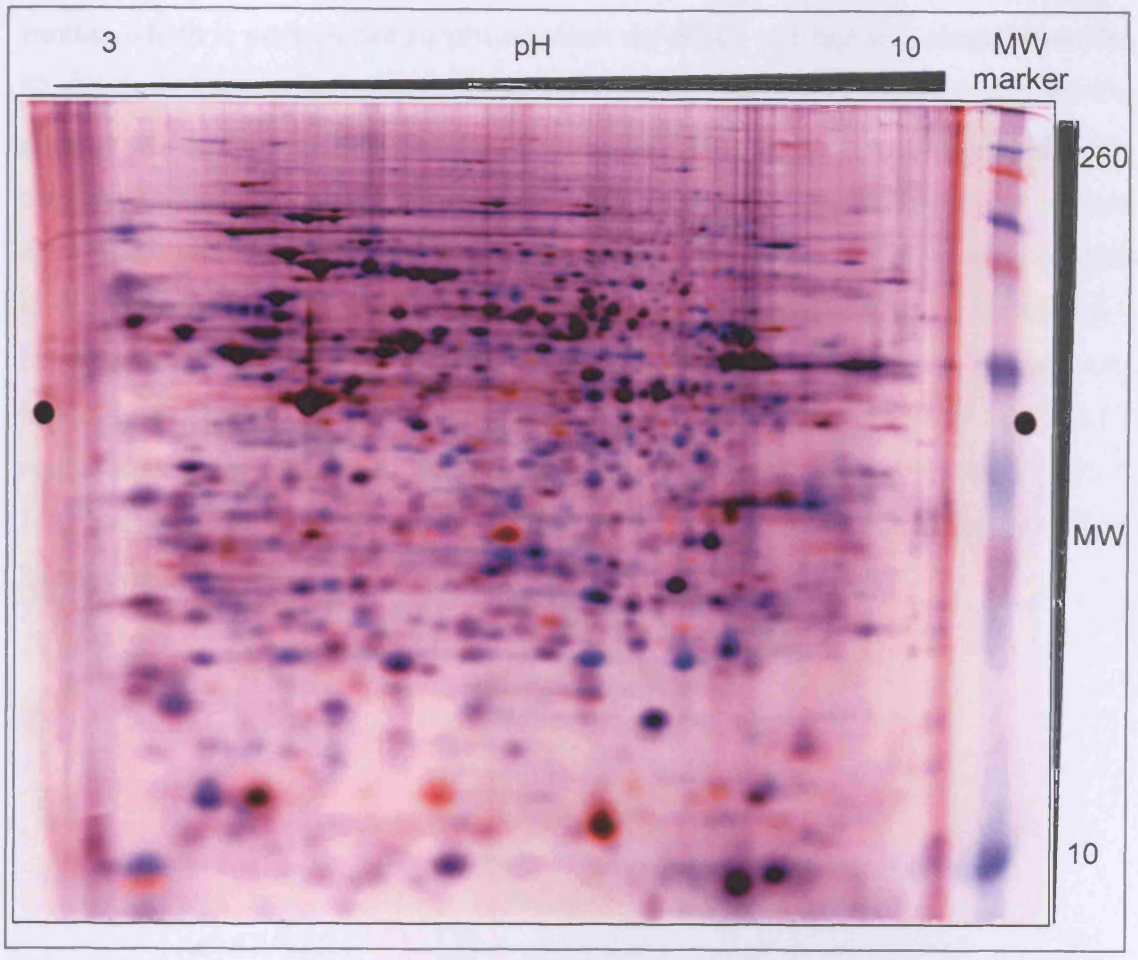

Figure 5.3 Master gel image used in the biological variance analysis (BVA) module of DeCyder. Best resolved gel 1 was selected as the master gel for BVA analysis as it displayed the most protein features. This figure represents the overlaid fluorescent images derived from S2 and Kc167 lysates labelled with Cy3 (red) and Cy5 (blue) respectively, prepared using Adobe Photoshop. Protein molecular weight markers were resolved on the right hand side of the gel.

A total of 1930 features were detected on the master gel. Image analysis and statistical evaluation of differences between the four cell lines revealed many protein features that displayed differential expression ($\geq$ 1.5 or a $\leq$ -1.5 average-fold change in abundance; $p<0.05$, $n=3$). This showed that the cell lines are very different in terms of their expressed proteomes. The number of common proteins differentially expressed between each of the three haemocyte cell lines is presented as a Venn diagram (Figure 5.4). A total of 54, 87 and 90 protein isoforms, of which 17, 17 and 13 unique protein spots, were found differentially expressed when the ratios of the protein abundances were compared between S2R+ and S2, Kc167 and S2, and S2R+ and Kc167 cells, respectively. Thus it would appear that the S2R+ and S2 cells are

similar, which is perhaps not surprising since the S2R+ cell line was cloned from the S2 cell line. The overlap between the comparisons on the Venn diagram represents the number of common protein species whose abundances were changing significantly between the corresponding comparisons. For instance, 9 common protein species were differentially expressed in S2R+ and Kc167 cells, respectively, when compared to the their counterparts in S2 cells; 49 common protein species were differentially expressed in S2 and S2R+ cells, respectively, when compared to the their counterparts in Kc167 cells; 16 protein species were differentially expressed in S2 and Kc167 cells, respectively, when compared to the their counterparts in S2R+ cells. 12 out of 1930 protein features displayed significant differences in abundance among all three haemocyte cell lines.

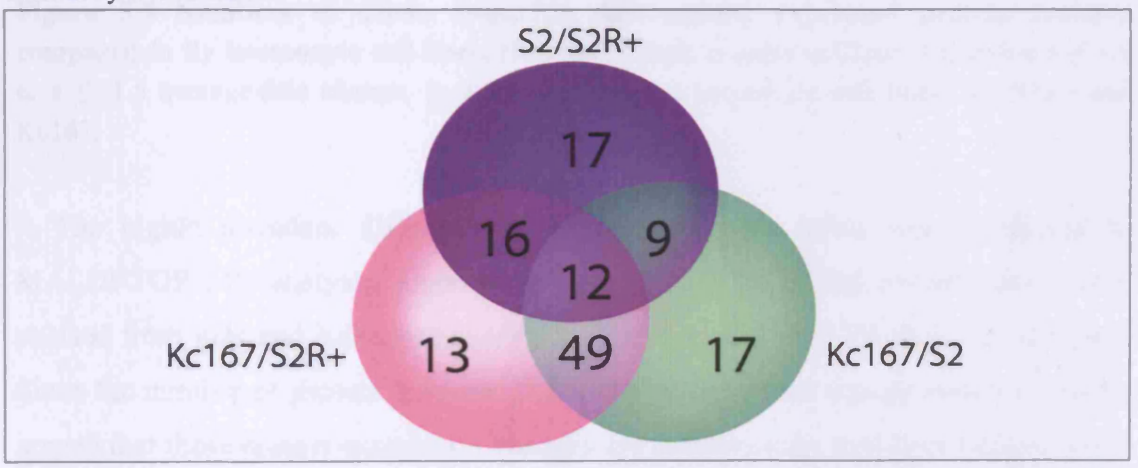

Figure 5.4 Venn diagram showing the number of differences expressed and overlapping protein spots between three haemocyte cell lines. The ratio in abundance of each protein feature was calculated between each haemocyte cell line that displayed a ≥1.5 or a ≤ -1.5 average-fold changes in abundance ($p<0.05$). The overlap of the three comparisons in the ratios of protein abundances (Kc167/S2R+, S2/S2R+ and Kc167/S2) represents the common protein features differentially expressed in all three comparisons. The overlap between each two comparisons represents only protein species differentially expressed in one cell line compared to the other two cell lines.

Clone 8 cells were found to display an even greater number of differentially expressed proteins when compared with each haemocyte cell line (Figure 5.5). 59 protein features were significantly differentially expressed in Clone 8 cells compared to all haemocyte cell lines. In addition, there were 14, 18 and 53 protein features differentially expressed in Clone 8 cells compared to S2, Kc167 and S2R+ cells, respectively. The other overlaps in the sections represent the number of common

protein species differentially expressed in Clone 8 when compared to the two corresponding haemocyte cell lines.

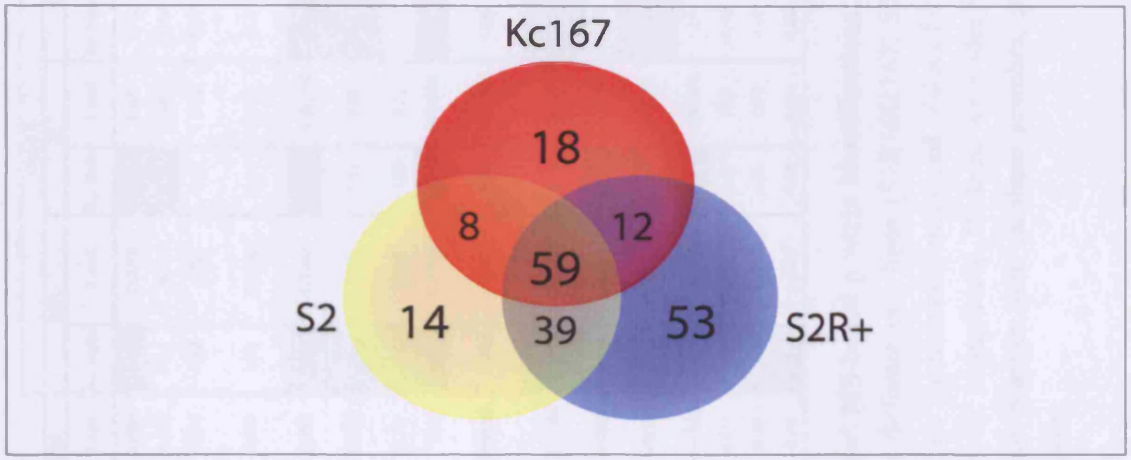

Figure 5.5 Numbers of Clone 8-specific differentially expressed protein features compared to fly haemocyte cell lines. Number of protein spots in Clone 8 showing a $\geq$ 1.5 or a $\leq$ -1.5 average-fold change, ($p<0.05$, n=3) *versus* haemocyte cell lines: S2, S2R+ and Kc167.

The highly abundant differentially expressed protein spots were subjected to MALDI-TOF MS analysis. Gels were stained with CCB and protein spots were excised from gels and subjected to trypsin digestion and MALDI-TOF MS analysis. Since the number of protein features differentially expressed was so high it could be argued that these protein expression changes are unlikely only to reflect differences in the morphologies of the cells alone. Indeed the identification for some of the abundant proteins showed these to be mainly enzymes involved in redox homeostasis (slow superoxidase dismutase, cytosolic thioredoxin peroxidase variant 2, glutathione-S transferase E2) and co-factors involved in protein transcription and translation (EF1beta, eIF-5A, CG5224, 40S ribosomal protein S12, bicaudal-transcription factor) (Table 5.1). Two actin-binding proteins: cofilin and annexin B9a, were also differentially expressed between cell lines. Two isoforms of cofilin were identified, and both were found to be significantly downregulated in S2R+ flat adherent cell line, when compared to cell lines with rounded morphologies (S2 and Kc167). In addition to this, in Clone 8 cells acidic and basic isoforms of cofilin were significantly downregulated and upregulated, respectively, when compared to their counterparts in the haemocyte cell lines S2R+ and S2 cells. Both cofilin isoforms were significantly downregulated in Clone 8 cells when compared to their counterparts in Kc167 cells (Table 5.1, Appendix 2).

								S2R+/Kc167		S2/S2R+		Kc167/S2		Clone 8					
														S2R+		S2		Kc167	
Spot No.	Name	NCBI No.	pI (pred)	MW (pred)	Seq. Cov (%)	Score p=0.05	No. Peptides	Av. Ratio	T-test	Av. Ratio	T-test	Av. Ratio	T-test	Av. Ratio	T-test	Av. Ratio	T-test	Av. Ratio	T-test
1610	AnnexinB9a	10121901	4.77	36302	24	165/59	17	1.77	0.00092	1.04	0.78	1.7	0.0064	-1.59	0.0089	-1.53	0.027	1.12	0.27
1632	CG31196, 14-3-3ε	23171618	4.74	29326	65	169/59	18	-1.07	0.34	1.34	0.028	1.25	0.081	-1.11	0.11	-1.51	0.00075	-1.19	0.052
1768	CG1519, Proteasome α7 subunit	7303843	5.46	27772	65	162/59	17	1.35	0.00005	-1.08	0.45	1.51	0.018	-1.02	0.92	-1.1	0.53	1.32	0.038
1782	EF-1-beta and EF-1-delta stimulate the exchange of GDP bound to EF-1-alpha to GTP	3757564	4.4	24289	54	104/59	12	-1.63	0.00028	-1.37	0.00067	-1.19	0.021	1.32	0.00042	-1.01	0.89	-1.2	0.015
1811	CG5224, translational initiation	21428462	5.57	25363	38	74/59	7	1.16	0.067	-1.13	0.22	1.31	0.055	-2.86	0.00005	-3.22	0.00028	-2.45	0.00028
1824	CG1404,ran, GTPase activity, GTP binding, protein binding	28317119	7.66	24921	72	205/59	18	1.24	0.074	-1.47	0.025	1.83	0.0043	1.64	0.11	1.11	0.59	2.04	0.045
1832	CG17523, Glutathione S transferase E2	19922528	5.39	25440	33	80/59	9	1.27	0.035	-1.21	0.46	1.55	0.19	-1.53	0.042	-1.86	0.12	-1.2	0.24
1841	Cytosolic thioredoxin peroxidase variant 2	12744791	5.52	21952	44	101/59	10	1.79	0.092	1.36	0.29	1.32	0.38	-4.12	0.00083	-3.03	0.00012	-2.3	0.013
1857	similar to CG3644, bicaudal, regulation of transcription from RNA polymerase II promoter	21627285	6.85	17727	48	76/59	6	1.33	0.005	-1.44	0.00037	1.92	0.00038	-1.02	0.49	-1.47	0.00075	1.36	0.09
1874	CG4254, Cofilin, actin severing and depolymerisation	7291724	6.74	17428	82	96/75	18	-2.85	0.00003	2.48	0.00016	-7.07	0.00001	-2.07	0.00021	-1.2	0.079	-5.9	0.00001
1875	eIF-5A, translational initiation	21626716	4.98	17922	49	64/57	8	-7.07	0.00001	1.41	0.0028	-2.36	0.0003	-1.15	0.055	1.62	0.0018	-1.46	0.0069
1882	CG4254, Cofilin, actin severing and depolymerisation	7291724	6.74	17428	68	78/59	19	-3.28	0.00002	1.36	0.0005	-4.45	0.00001	2.11	0.00005	2.86	0.00001	-1.56	0.0012
1885	Slow superoxide dismutase	4572573	5.68	15200	52	86/59	7	-2.03	0.00003	1.2	0.014	-2.03	0.00003	2.08	0.00005	2.5	0.00005	1.24	0.00001
1892	40S ribosomal protein S12	902622	7.1	16970	62	138/59	10	-1.03	0.56	-1.28	0.012	1.24	0.011	1.14	0.056	-1.47	0.29	-1.18	0.018
1894	Cyclophilin 1	33589296	8.43	18067	86	175/59	16	1.81	0.0086	1.62	0.0076	1.08	0.37	-1.76	0.00099	-1.09	0.29	-1.01	0.75
1902	RH27794p	21064703	7.82	17216	60	61/57	13	1.26	0.019	1.3	0.02	-1.03	0.69	-1.62	0.0027	-1.24	0.064	-1.29	0.032

Table 5.1 2D-DIGE protein expression analysis of *Drosophila* cell lines with different morphologies and MS-based protein identifications. Protein features displaying differential expression are shown. Values are average ratios of abundance between different cell lines (S2R+/Kc167, S2R+/S2, Kc167/S2, Clone 8/S2R+, Clone 8/S2 and Clone 8/Kc167). T-test *p* values are given as a measure of confidence for each ratio measured. Values for protein isoforms shaded in light and dark grey were significantly up- and down-regulated (>1.5 fold; $p \leq 0.05$; n=3), respectively. Proteins were identified by MALDI-TOF peptide mass fingerprinting. Protein name and/or Drosophila annotation ID, NCBI accession number from database searches, sequence coverage (%), database search score and number of matched peptides are given for each of the identified proteins.

As this analysis represents only a snap shot of the protein expression that could occur in each cell line, it is hard to link the differentially expressed or cell line-specific proteins to certain biological functions and cell properties with greater assurance. There were no obvious patterns or links to indicate altered morphology or other cellular processes. For these reasons further protein identification by mass spectrometry of the differentially expressed proteins was not carried out. Most importantly, this experiment provided a baseline of the growth conditions and Cy-dye labelling conditions for further analysis of fly proteins by 2D-DIGE.

5. 3 Functional genomic and proteomic analysis of PI3K signalling and actin regulation in S2R+ cells

One of the main aims of this work was to carry out a functional proteomic and genomic analysis of RNAi-treated S2R+ cells as a method to identify PI3K-dependent protein targets that act as morphology modifiers. Taking into account that PI3K signalling induces actin reorganisation in S2R+ cells and that this PI3K-dependent modification of the actin cytoskeleton could be achieved through interaction of selected genes with small GTPases of the Rho-family (see Chapter 1), selected genes of the PI3K and small GTPase signalling pathways were targeted for knockdown of their protein expression using RNAi strategy. Protein expression in these knockdowns was quantified and compared using the 2D-DIGE platform, in combination with mass spectrometry, for protein identification. An additional goal was to correlate protein expression changes resulting from perturbation of these signalling pathways with phenotypic changes (cell morphology, actin cytoskeleton organisation and cell size) resulting from RNAi knockdown. The identification of common targets was carried out as it could assist in mapping the signalling pathways involved, and possibly reveal nodes of signalling cross-talk. This study was performed on S2R+ cells, because of their morphological properties and their potential to reorganise actin cytoskeleton in response to acute activation of PI3K signalling, and also a large number of distinct actin-related phenotypes can be distinguish when RNAi strategy is used, as reported by Kiger *et al.* 2003.

5.3.1 2D-DIGE experimental design

2D-DIGE analysis was used to compare protein expression profiles of total cell lysates from control untreated S2R+ cells and knockdowns treated with interfering dsRNAs for selected genes involved in PI3K and Rho-family small GTPase signalling. Two separate experiments were performed, due to the fact that there is a limitation in the number of 2D gels that can be run in a single experiment. In the first experiment Rac1 plus Rac2, Cdc42 and Arp3 were targeted for RNAi-mediated silencing (Table 5.2 A). These genes are known to be involved in actin polymerisation and formation of lamellipodia (Kunda et al., 2003). In the second experiment, p110 (the catalytic subunit of PI3K), PTEN, Akt, Ras, Abi plus Hem, cofilin and GFP were targeted (Table 5.2 B). GFP would serve as a control to examine possible "off-target" effects of the RNAi treatment itself. Cofilin was actually chosen for the second experiment since it was identified as a differentially expressed protein in the first experiment, and it is known to regulate actin cytoskeleton organisation. Abi and Hem were selected based on their involvement in regulation of actin polymerisation (Bogdan and Klambt, 2003).

To assess reproducibility in both experiments, each RNAi condition was analysed as biological triplicates, meaning that cells were plated and treated with the corresponding dsRNAs in three separate cultures, which were grown and prepared independently. Cells were treated with dsRNAs and maintained in 10% serum-supplemented medium for five days to allow knockdown of expression before harvesting. Equal amounts of proteins from each RNAi condition were then labelled with Cy3 or Cy5. A standard pool was also prepared by mixing equal amount of proteins from each condition and labelled with Cy2. Labelled protein samples and standard pool were mixed appropriately (Table 5.2 A and B), and run on 24 cm, pH 3-10, non linear IPG strips in the first dimension, followed by separation of the proteins by 12% SDS-PAGE in the second dimension.

A

Gel No / Cy dye	Gel 01	Gel 02	Gel 03	Gel 04	Gel 05	Gel 06
Cy3	Ctrl	Ctrl	Arp3	Rac1+Rac2	Cdc42	Cdc42
Cy5	Rac1+Rac2	Arp3	Rac1+Rac2	Cdc42	Ctrl	Arp3
Cy2	Pool	Pool	Pool	Pool	Pool	Pool

B

Gel No / Cy dye	Gel 01	Gel 02	Gel 03	Gel 04	Gel 05	Gel 06
Cy3	Ctrl	Ctrl	p110	p110	Abi+Hem	Abi+Hem
Cy5	Ras	PTEN	PTEN	Cofilin	Cofilin	p110
Cy2	Pool	Pool	Pool	Pool	Pool	Pool

Gel No / Cy dye	Gel 07	Gel 08	Gel 09	Gel 10	Gel 11	Gel 12
Cy3	Ras	Ras	PTEN	Cofilin	Akt	GFP
Cy5	Abi+Hem	Akt	Akt	GFP	GFP	Ctrl
Cy2	Pool	Pool	Pool	Pool	Pool	Pool

Table 5.2 Experimental design for 2D-DIGE analysis of RNAi-treated cells A) 2D-DIGE protein expression comparison of RNAi treatments Rac1 plus Rac2, Cdc42 and Arp3 with untreated cells. The table shows labelling of triplicates from each condition with Cy3 or Cy5, including the Cy2 labelled pool run on each gel. **B)** 2D-DIGE protein expression comparison of RNAi treatments p110, PTEN, Akt1, Ras85, Abi plus Hem, Cofilin and GFP with untreated cells. The table shows the combination of Cy3 and Cy5 labelled sample triplicates run on each gel, including the Cy2 labelled pool.

In the first 2D-DIGE experiment three different RNAi treatments (Arp3, Rac1 plus Rac2 and Cdc42 RNAi knockdowns) prepared as triplicates were compared with untreated controls on 6 gels, thus generating 18 fluorescent spot maps (Table 5.2 A). In the second 2D-DIGE experiment, a combination of eight different conditions (seven RNAi conditions (p110, Akt, Ras85D, PTEN, Cofilin, Abi plus Hem and GFP) plus an untreated control, were prepared as triplicates and run on 12 gels, generating 36 fluorescent images (Table 5.2 B). Examples of one gel set of three images derived from each fluorescence channel for Cy2, Cy3 and Cy5 are shown in Figure 5.6. Image analysis was carried out using DeCyder software. Briefly, triple fluorescent images from the same 2D gel were automatically curated and matched in the DIA module. Then, matching and comparison of protein features across different gels was

performed using internal landmarks comprising abundant protein features present in all gel images using the BVA module.

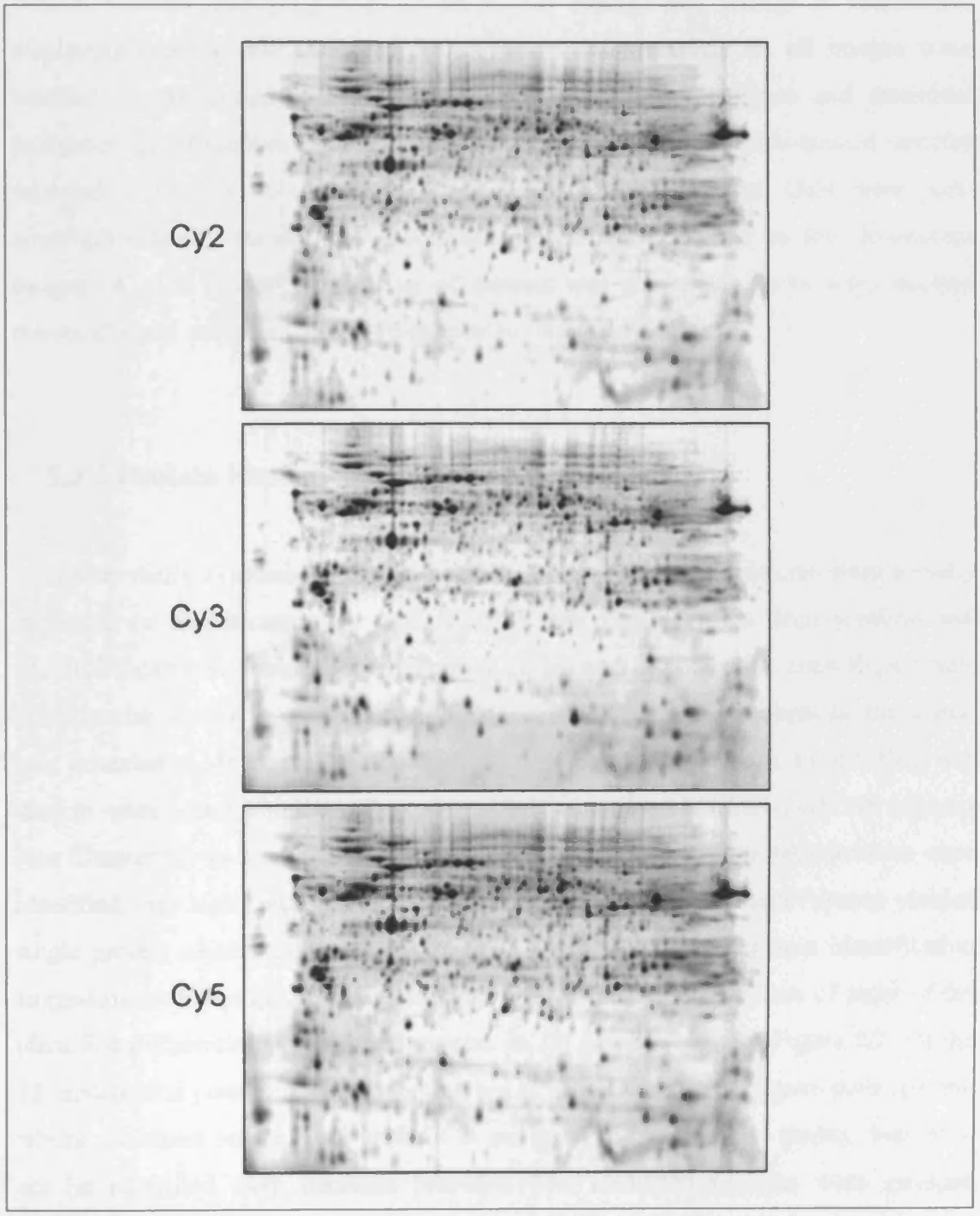

Figure 5.6 Representative Cy2, Cy3, Cy5 fluorescence gel images obtained from a single 2D gel in the 2D-DIGE experiment. Equal amounts of Cy3 and Cy5 labelled protein samples, derived from p110 and cofilin RNAi-knockdown cells were mixed with an equal amount of Cy2-labelled internal standard pool. Proteins were separated by 2D gel electrophoresis, and the gel was scanned at the appropriate excitation/emission wavelengths to generate the set of three images shown.

Subsequently, statistical analysis was performed where the average abundances of protein features for each condition were compared with those of the untreated control. Protein features displaying a $\geq$ 1.5 or $\leq$ -1.5 average-fold change in abundance, displaying reproducible changes ($p<0.05$, n=3) and matching on all images were selected for MS-based identification. The two individual analyses and statistical evaluation of differences between untreated control sample and RNAi-treated samples revealed a total of 40 differentially expressed protein features. Gels were post-electrophoretically stained with CCB and gel images matched to the fluorescent images. A pick list of 39 proteins of interest was generated. Spots were excised robotically and subjected to MS-based protein identification.

5.3.2 Protein identification by mass spectrometry

Differentially expressed proteins from the two 2D-DIGE experiments were initially subjected to identification by MALDI-TOF MS peptide mass fingerprinting and MASCOT database searching (see Chapter 2). In cases were peptide mass fingerprints could not be matched to available predicted *Drosophila* protein sequences, the search was extended to all species available in the databases. Furthermore, LC-MS/MS was used in cases where a protein ID could not be obtained by MALDI-TOF MS analysis (see Chapter 2). In total, 27 of the 40 differentially expressed protein features were identified with high confidence (Table 5.3, Appendix 3). All protein features yielded single protein identifications, and two spots yielded the same protein identification suggesting isoforms of the same gene product. The 2D gel migration of most of the identified differentially expressed proteins in 2D gels is shown in Figure 5.7. Of the 13 unidentified protein features, some were of low abundance and gave poor spectra, whiles the others stained well with CCB and gave spectra of good quality, but could not be identified from database searches. The identified proteins were grouped according to their known biological functions (Figure 5.8).

Spot No.	Name	NCBI No.	pI (gel)	Mw (gel)	pI (pred)	MW (pred)	Seq Cov	Score p=0.05	No. Peptides	Arp3 Av. Ratio	Arp3 T-test	Cdc42 Av. Ratio	Cdc42 T-test	Rac1/2 Av. Ratio	Rac1/2 T-test	PTEN Av. Ratio	PTEN T-test	Ras Av. Ratio	Ras T-test	p110 Av. Ratio	p110 T-test	Akt Av. Ratio	Akt T-test	Cofilin Av. Ratio	Cofilin T-test	Abi/Hem Av. Ratio	Abi/Hem T-test	GFP Av. Ratio	GFP T-test	Function
717	Ubiquitin	158787	3.61	71552	6.56	8540	32	50/33*	2							-1.07	0.56	-1.01	0.95	1....	0.043	-1....	0.0038	1.1	0.52	1.71	0.048	-1....	0.089	Protein modifier, proteasome degradation, other functions
802	CG5438 (HSP88)	7301098	5.65	70571	5.63	70043	4	110/33*	2							1.28	0.0078	1.09	0.18	1	0.94	1.01	0.8	-1.01	0.82	1.54	0.00077	-1.08	0.28	ATP binding, protein folding, stress response
1871	CG9986 (Annexin B11)	7413849	6.08	30045	6.13	32501	55	65/60	25							-2.05	0.07	-1....	0.04	-1.79	0.05	-2....	0.082	-1.74	0.035	-1.61	0.098	-1.80	0.11	calcium-dependent phospholipid and actin binding
1780	CG10424-PA	7293823	7.39	27057	7.07	32532	33	72/59	7							1.57	0.0012	1.16	0.26	1.15	0.35	1.15	0.43	1.25	0.17	1.5	0.06	1.05	0.85	Unknown
1788	CG10180 (Ecdysone-inducible gene L3)	7295348	7.18	27197	8.6	35800	27	328/33*	9							1.75	0.0066	1.06	0.45	1.11	0.16	1.18	0.081	1.21	0.1	1.04	0.53	1.04	0.53	L-lactate dehydrogenase activity, glycolysis
1902	CG8692-PC (Cysteine proteinase-1)	21627209	4.3	25304	6.73	41974	14	129/33*	5							-1.53	0.014	1.21	0.073	1.01	0.9	1.07	0.48	-1.06	0.53	-1.24	0.062	1.01	0.91	Cathepsin L activity, regulation of transcription, nucleic acid binding
1914	CG3083-PA (Peroxiredoxin 6005)	24581278	5.34	25155	5.19	25058	54	78/60	11							1.23	0.0015	1.04	0.21	1.26	0.12	1.23	0.58	1.09	0.66	2.02	0.022	1.11	0.18	Peroxidase activity, cell redox homeostasis, stress response
1929	CG6203-PB (Fragile X-related)	23170873	4.06	24944	6.05	59899	27	65/59	13							-1.64	0.034	-1.11	0.54	-1.32	0.14	-1.31	0.24	-1.51	0.04	-1.66	0.023	1.36	0.58	RNA and protein binding, negative regulation of protein biosynthesis
1930	CG12405 (1-cys peroxiredoxin 2540)	12044383	6	25000	5.97	24926	37	327/33*	7							-1.61	0.0031	-1.07	0.37	-1.07	0.17	1.03	0.6	1.06	0.34	-1.43	0.00086	-1.21	0.032	Peroxidase activity, cell redox homeostasis, stress response
1493	CG7176-PG (Isocitrate dehydrogenase)	28574947	4.18	38505	4.18	38505	56	64/60	29							-1.28	0.37	-1.59	0.091	-1.38	0.12	-1.41	0.23	-1.75	0.052	-1.6	0.049	-1.42	0.22	tricarboxylic acid cycle, oxidoreductase activity
1984	CG17534-PA (GST E9)	7302612	7.98	24386	7.69	25094	9	86/32*	2							1.62	0.015	1.25	0.063	1.04	0.98	1.07	0.67	1.01	0.91	1.19	0.23	1.08	0.012	glutathione transferase activity, defense response
2011	CG12242-PA (GST D5)	45446464	7.17	24102	6.84	24755	26	69/58	9							2.29	0.0061	-1.13	0.38	-1.03	0.85	1.49	0.56	-1.29	0.15	1.29	0.19	-1.26	0.3	Glutathione transferase activity, detoxification, redox homeostasis
2237	CG4254 (Cofilin)	7291724	5.89	19709	6.74	17428	62	80/76	16							-1.57	0.005	-1.02	0.71	1.14	0.063	-1.12	0.063	-4.95	0.00013	-1.6	0.00084	1.02	0.71	Actin filament depolymerization, actin filament organization
2293	CG4254 (Cofilin)	7291724	6.74	17400	6.74	17428	62	90/59	18							-1.07	0.53	1.06	0.72	-1.02	0.9	1.07	0.44	-2.57	0.00078	-1.05	0.63	-1.06	0.67	Actin filament depolymerization, actin organization
685	Albumin (bovine)	162648	5.78	71309	5.82	71244	48	118/76	30							-1.1	0.47	1.15	0.31	1.77	0.039	-1.42	0.031	1.21	0.16	1.74	0.06	1.55	0.016	Contaminant
710	Albumin (bovine)	162648	5.73	71456	5.82	71244	63	107/76	43							-1.2	0.17	1.06	0.64	1.69	0.045	-1....	0.015	1.14	0.3	1.57	0.089	1.49	0.019	Contaminant
693	Unidentified		5.8	71371												-1.36	0.041	-1.09	0.58	1.63	0.16	-1....	0.012	1.06	0.59	1.43	0.15	1.35	0.071	
711	Unidentified		5.67	71456												-1.16	0.47	1.11	0.51	1.62	0.074	-1.35	0.16	1.27	0.19	1.63	0.063	1.61	0.037	
1293	Unidentified		5.74	50691												-1....	0.032	-1.22	0.38	-1.21	0.41	-1.33	0.2	-1.33	0.2	-1.31	0.22	-1.43	0.12	
2052	Unidentified		5.66	23589												-2....	0.05	-1.47	0.21	-2.81	0.073	-1....	0.24	-2.09	0.019	-1.78	0.041	-...	0.088	
328	CG5706	21355211	5.9	63295	5.73	66477	46	210/59	19	1.88	0.0086	1.2	0.23	1.48	0.048															Phenylalanine-tRNA ligase activity
382	CG4199-PA	7290254	5.13	63086	5.51	61481	5	83/48*	2	5.04	0.0041	-1.27	0.39	2.32	0.045															Oxidoreductase activity, reactive oxygen species metabolism
383	CG12101-PB (HSP60)	7292599	5.13	63086	5.38	60885	5	134/31*		2.8	0.09	1.42	0.44	1.79	0.11															Protein folding, stress response
415	CG1424 (Misato)	17737379	3.83	81895	4.93	65256	14	83/58	6	2.79	0.0039	-1.03	0.81	1.65	0.14															Putative component of cytoskelton
781	CG7558 (Arp3)	17737543	5.4	54884	5.87	47459	50	160/58	16	1....	0.07	1.18	0.023	1.01	0.91															Actin filament branching
1184	Capsid polyprotein [Drosophila C virus]	2388674	6.35	44234	5.81	100435	6	111/44*	3	3.5	0.0024	2.14	0.014	3.69	0.00088															Viral capsid protein
1586	CG4254 (Cofilin)	17136986	5.7	17500	6.74	17428	81	107/58	17	1.8	0.0018	2.19	0.00012	1.73	0.00036															
370	Albumin (bovine)	30794280	5.59	62883	5.82	71274	42	218/75	21	3.03	0.0064	1.02	0.99	1.86	0.074															Contaminant
422	Clade A (α-1antiproteinase, antitrypsin) Bos taurus	27806941	3.93	61604	6.05	46417	10	174/54*	3	2.86	0.0048	1.02	0.99	1.9	0.087															Contaminant
436	Clade A (α-1antiproteinase, antitrypsin) Bos taurus	27806941	4.06	61375	6.05	46417	26	103/75	10	2.42	0.0071	1.06	0.77	1.56	0.13															Contaminant
405	Clade A (α-1antiproteinase, antitrypsin) Bos taurus	27806941	3.89	62081	6.05	46417	3	72/54	1	2.92	0.012	-1.22	0.48	1.55	0.28															Contaminant
411	Unidentified		3.82	62152						3.13	0.0048	-1.17	0.55	1.4	0.38															
412	Unidentified		3.75	62015						3.08	0.00058	1.07	0.96	1.81	0.12															
462	Unidentified		8.24	62745						1.79	0.027	1.36	0.26	1.4	0.15															
487	Unidentified		3.93	60598						2.42	0.0055	-1.22	0.11	1.87	0.16															
1182	Unidentified		6.18	44280						1.5	0.035	1.42	0.055	1.36	0.19															
1188	Unidentified		3.8	43914						-1.54	0.0077	-1.23	0.085	-1.25	0.087															
1212	Unidentified		6.08	43000						2.41	0.0021	1.56	0.013	2.48	0.00062															
1231	Unidentified		8.2	27896						1.96	0.00041	1.3	0.082	2.12	0.00033															
1709	Unidentified		3.1	6138						1.87	0.0074	1.5	0.058	1.76	0.0033															

Table 5.3 2D-DIGE differential protein expression analysis of RNAi-treated cells and MS-based protein identifications. Protein features displaying differential expression in S2R+ cells treated with dsRNA for the knockdown of expression of *Drosophila* Arp3, Cdc42, Rac1 plus Rac2, PTEN, Ras, PI3K, Ras, Akt, cofilin, Abi plus Hem and GFP are shown. The table includes data combined from two separate experiments. Values are average ratios of abundance from dsRNA treated cells versus untreated control cells from three separate cultures. T-test *p* values are given as a measure of confidence for each ratio measured. Values for protein isoforms shaded in light and dark grey were significantly up- and down-regulated (>1.5 fold; $p \leq 0.05$; n=3), respectively. Proteins were identified by MALDI-TOF peptide mass fingerprinting and LC-MS/MS peptide sequencing (latter method denoted by * in 'Score' column). Protein name and/or *Drosophila* annotation ID, NCBI accession number from database searches, sequence coverage (%), database search score (denominator is threshold score at p=0.05), number of matched peptides and molecular function are given for each of the identified proteins.

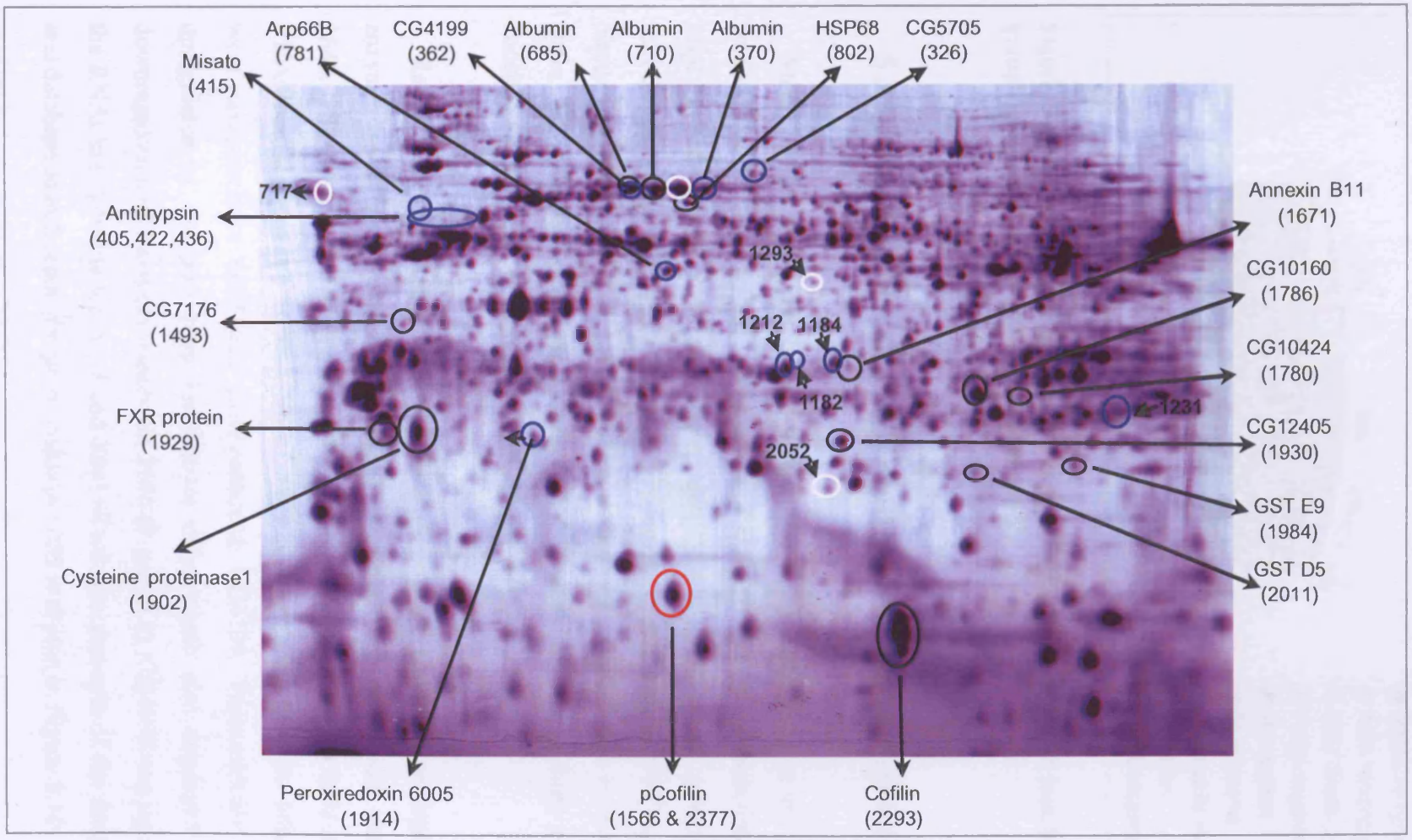

Figure 5.7 A representative gel displaying the position of differentially expressed proteins in the two experiments. Blue circle = proteins identified in the first experiment. Black circle proteins = identified in the second experiment. White circle = unidentified proteins from the first experiment. Red circle = a common protein differentially expressed in the two experiments.

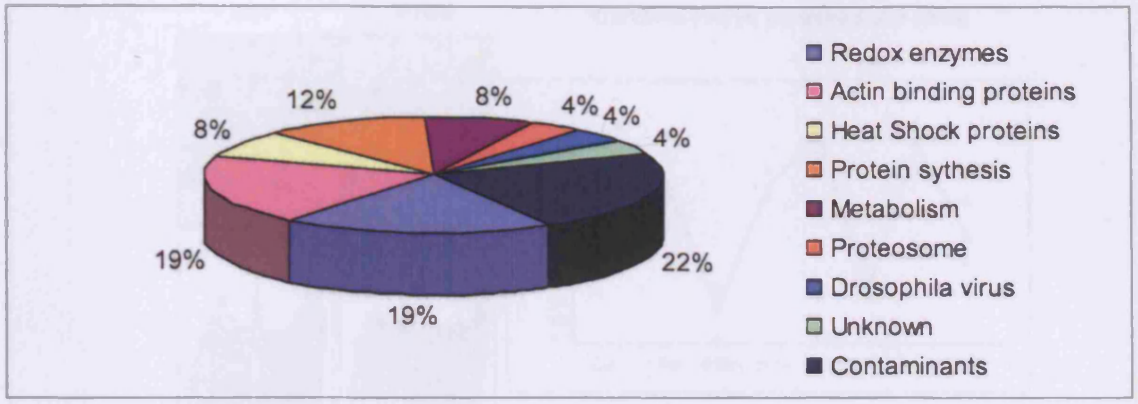

Figure 5.8 Percentage of differentially expressed proteins in RNAi knock-down cells grouped according to their biological functions.

5.3.3 Differentially expressed proteins identified by 2D-DIGE/MS

Metabolic enzymes. Two of the differentially expressed proteins are predicted to be involved in carbohydrate metabolism. CG10160 (Ecdysone-inducible gene L3, ImpL3), with L-lactate dehydrogenase activity, was found to be upregulated (1.75 fold difference) in cells subjected to RNAi-mediated silencing of PTEN, whilst iso-citrate dehydrogenase, a mitochondrial enzyme which participates in the citric acid cycle, was found to be downregulated by 1.75 and 1.6 fold in cells subjected to knockdown of cofilin and Abi plus Hem, respectively.

Redox enzymes. Five of the identified proteins are classified or predicted to be enzymes involved in redox regulation. Three of these enzymes (1-cys peroxiredoxin 2540, GST D5 and GST E9) were differentially expressed only in cells subjected to RNAi treatment for the knockdown of PTEN (Figure 5.9). The two other enzymes were peroxiredoxin 6005 and oxidoreductase CG4199. Peroxiredoxin 6005 was upregulated in Abi plus Hem knockdown cells, which also displayed moderated downregulation of 1-cys peroxiredoxin 2540 (Figure 5.9). CG4199 was upregulated in the RNAi knockdowns for Arp3 and Rac1+Rac2. An example of the mass spectrum and database search report for peroxiredoxin 6005 is shown in Figure 5.10.

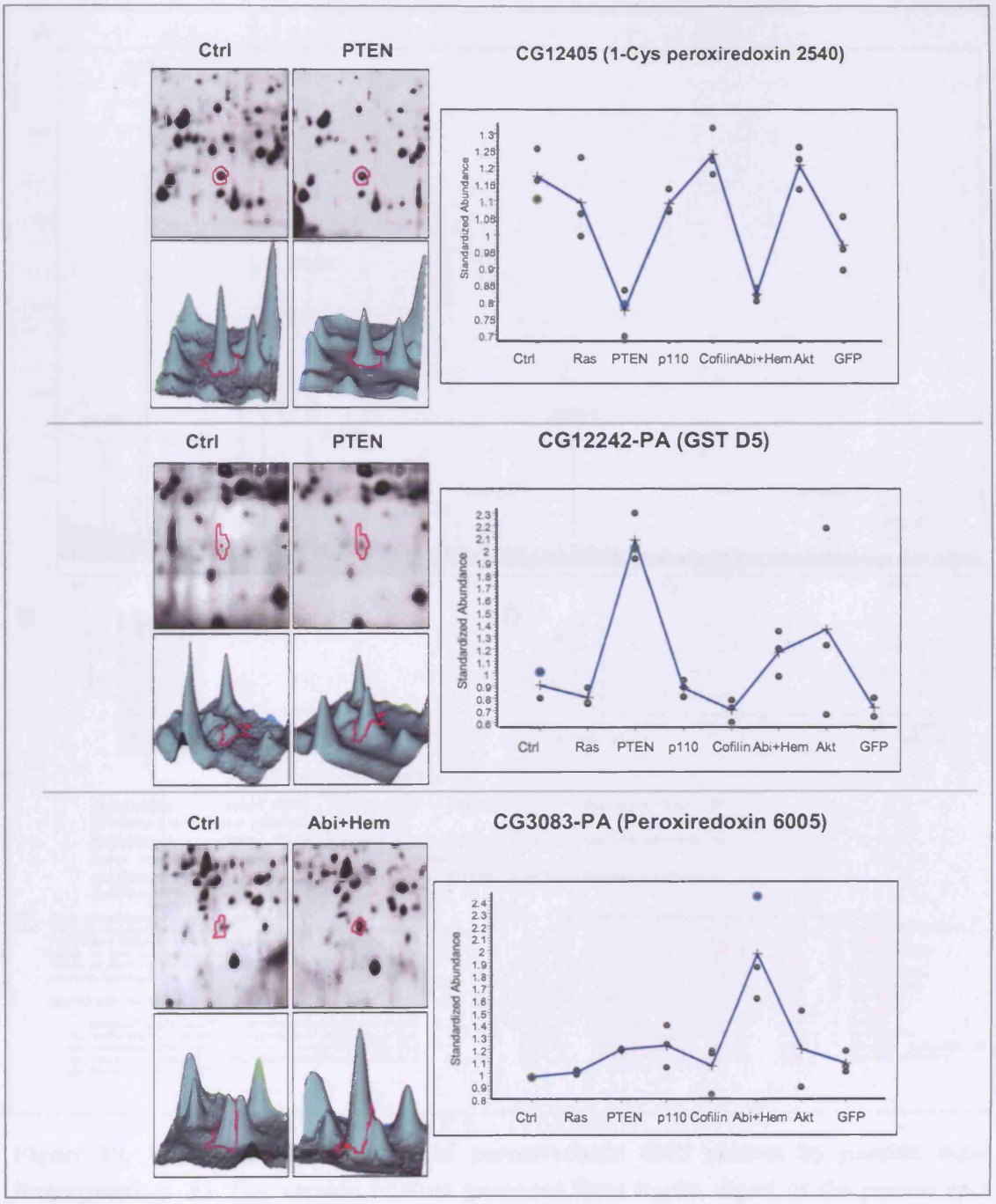

Figure 5.9 Examples of redox enzymes displaying RNAi-induced changes in protein expression. Proteins 1-cys-peroxiredoxin 2540, GST D5 and peroxiredoxin 6005 display differential expression in cells subjected to PTEN and Abi plus Hem RNAi-induced gene silencing. Proteins were identified from gels by MALDI-TOF MS. Examples of gel position and 3D-images of protein spots, as well as graphs showing relative abundance were derived from DeCyder image analysis. Graphs show the standardised protein abundance (ratio of the volume of a test gel feature versus the volume of the corresponding standard gel feature) for each RNAi condition. Triplicate data points are shown for spots from the untreated and treated samples with lines joining the average values.

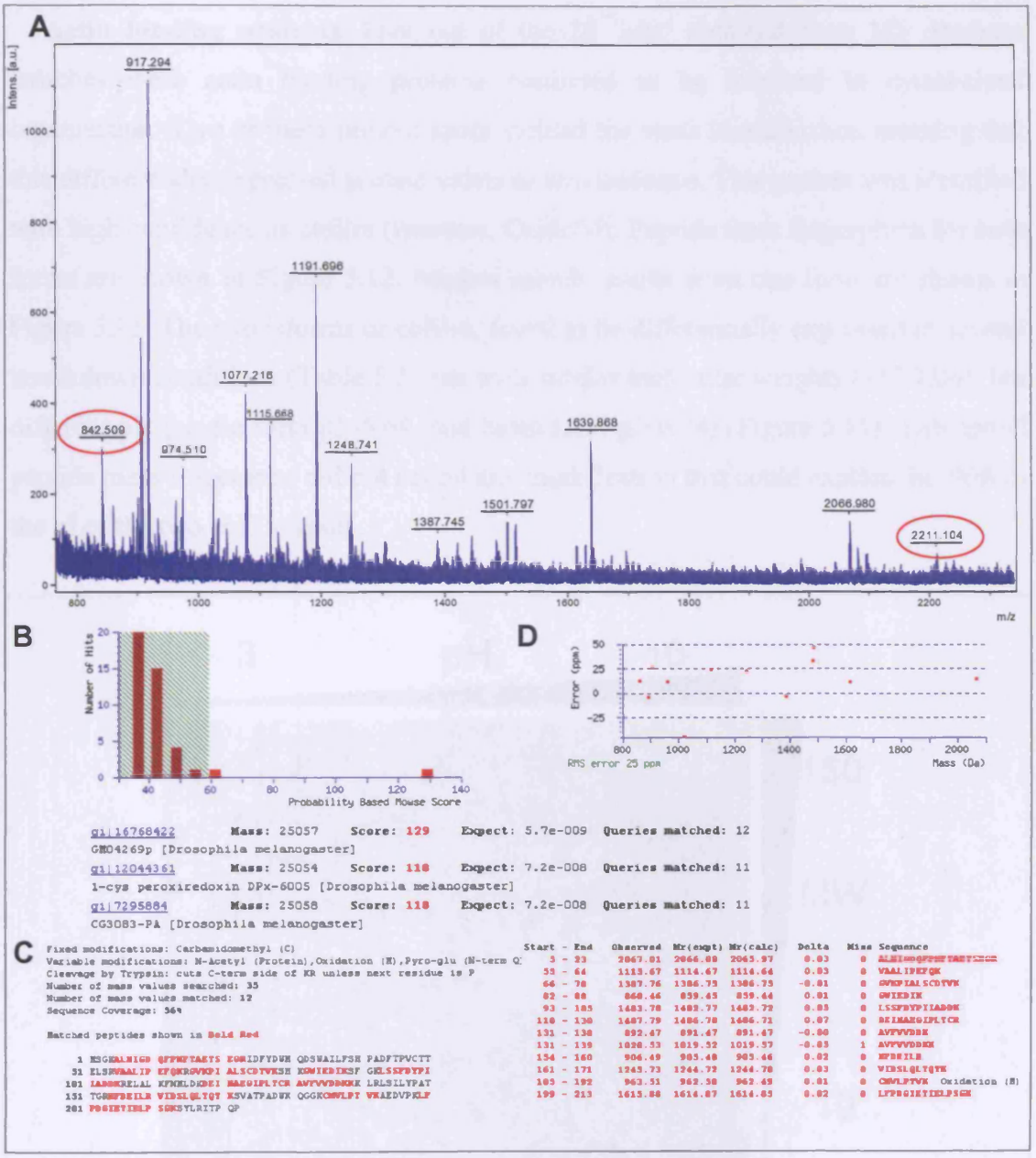

Figure 10. MS-based identification of peroxiredoxin 6005 protein by peptide mass fingerprinting. A) The peptide mixture generated from tryptic digest of the protein spot number 1914 was analysed by matrix-assisted laser-desorption/ionisation time-of-flight MS (MALDI-TOF MS) to generate the mass spectrum shown. Circled masses show the two trypsin peaks (*m/z* 842.509 and 2211.104) used for internal calibration. **B)** The list of peptide masses from the processed spectrum was searched against the NCBI theoretical peptide fragment database using Mascot and gave three 'hits' for peroxiredoxin with probability-based scores higher than the threshold value (59 in this case) where p=0.05 meaning the 'hit' is highly significant. **C)** Protein sequence coverage of the matched peptides for the top 'hit' represents 56% of the sequence of peroxiredoxin 6005. Sequences and masses of the matched peptides are shown at the bottom of the figure. **D)** Error distribution displays the mass error of each peptide in ppm compared to its counterpart in the database.

Actin binding proteins. Five out of the 26 'hits' obtained from MS database searches were actin binding proteins predicted to be involved in cytoskeletal organisation. Two of these protein spots yielded the same identification meaning that this differentially expressed protein exists as two isoforms. This protein was identified with high confidence as cofilin (twinstar, CG4254). Peptide mass fingerprints for both forms are shown in Figure 5.12. Mascot search results from one form are shown in Figure 5.13. The two isforms of cofilin, found to be differentially expressed in several knockdown conditions (Table 5.3) ran with similar molecular weights (~17 kDa), but different pIs (acidic form pI=5.69, and basic form pI=6.74) (Figure 5.11). This initial peptide mass fingerprint did not reveal any modification that could explain the shift in the pI of the two cofilin spots.

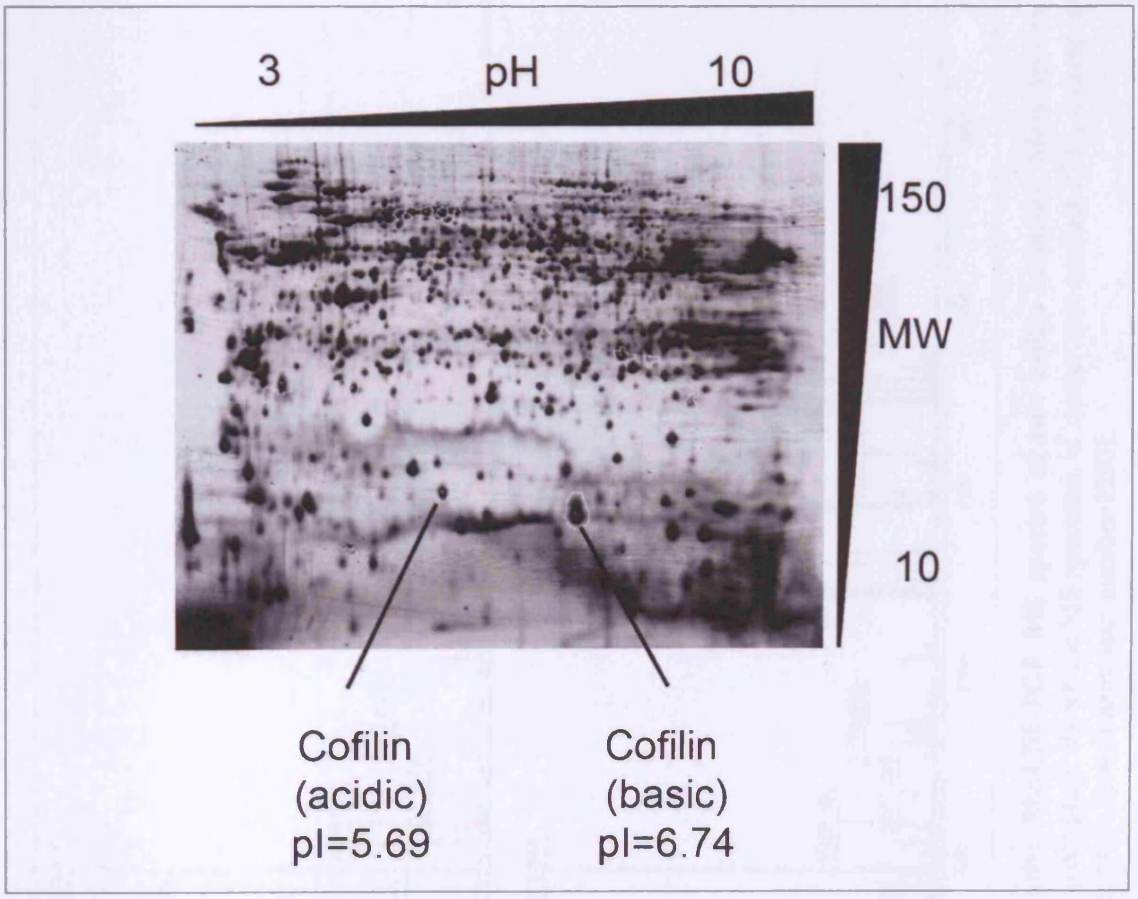

Figure 5.11 Representative 2D-DIGE gel image displaying the position of the acidic and basic cofilin isoforms identified by MS.

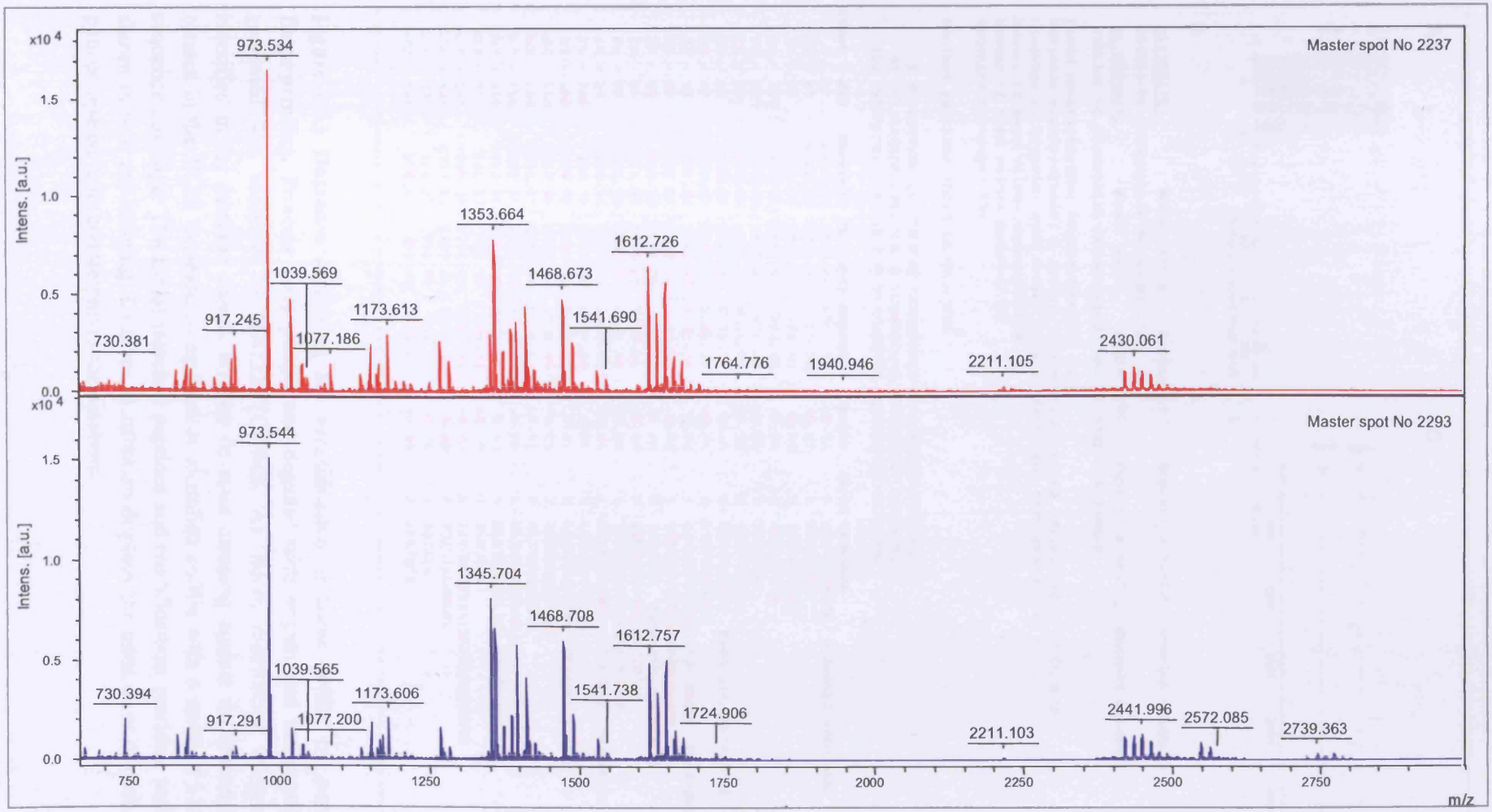

Figure 5.12 Representative MALDI-TOF MS spectra of two cofilin isoforms. Mass spectra were acquired on an Ultraflex MALDI-TOF mass spectrometer. The upper (red) panel shows the MS spectrum of master spot number 2237, corresponding to the acidic isoform, and the lower (blue) panel shows the spectrum of the basic spot (master spot number 2293).

A

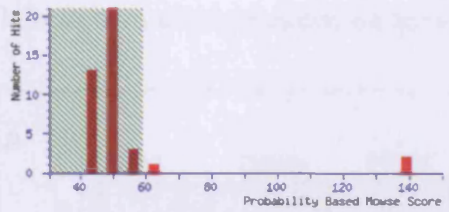

C

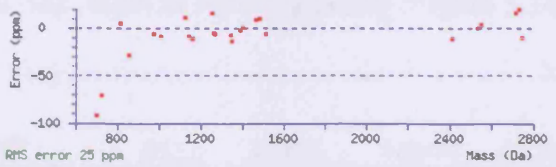

B

gi|7291724 **Mass:** 17428 **Score:** 139 **Expect:** 5.7e-010 **Queries matched:** 25
CG4254-PA [Drosophila melanogaster]
gi|38048613 **Mass:** 15143 **Score:** 102 **Expect:** 2.9e-006 **Queries matched:** 21
similar to Drosophila melanogaster tsr [Drosophila yakuba]

Fixed modifications: Carbamidomethyl (C)
Variable modifications: N-Acetyl (Protein),Oxidation (M),Pyro-glu (N-term Q)
Cleavage by Trypsin: cuts C-term side of KR unless next residue is P
Number of mass values searched: **113**
Number of mass values matched: **25**
Sequence Coverage: **95%**

Matched peptides shown in **Bold Red**

```
    1 MASGVTVSDV CKTTYEEIKK DKKMRYVIFY IRDEKQIDVE TVADRNAEYD
   51 QFLEDIQKCG PGECRYGLFD FEYMMQCQGT SESSKKQKLF LMSWCPDTAK
  101 VKKKMLYSSS FDALKKSLVG VQKYIQATDL SEASREAVEE KLRATDRQ
```

Start - End	Observed	Mr(expt)	Mr(calc)	Delta	Miss	Sequence
2 - 12	1164.54	1163.54	1163.55	-0.01	0	ASGVTVSDVCK N-Acetyl (Protein)
13 - 20	1011.53	1010.52	1010.53	-0.01	1	TTYEEIKK
13 - 22	1254.68	1253.67	1253.65	0.02	2	TTYEEIKKDK
24 - 32	1266.70	1265.69	1265.70	-0.01	1	MRYVIFYIR
26 - 32	973.54	972.54	972.54	-0.01	0	YVIFYIR
26 - 35	1345.70	1344.70	1344.71	-0.01	1	YVIFYIRDEK
36 - 45	1128.57	1127.56	1127.55	0.01	0	QIDVETVADR Pyro-glu (N-term Q)
36 - 45	1145.57	1144.56	1144.57	-0.01	0	QIDVETVADR
36 - 58	2722.33	2721.32	2721.28	0.04	1	QIDVETVADRNAEYDQFLEDIQK Pyro-glu (N-term Q)
36 - 58	2739.36	2738.36	2738.30	0.05	1	QIDVETVADRNAEYDQFLEDIQK
59 - 65	818.30	817.29	817.28	0.00	0	CGPGECR Pyro-glu (N-term Q)
66 - 85	2413.98	2412.97	2413.00	-0.03	0	YGLFDFEYMMQCQGTSESSK
66 - 86	2542.10	2541.09	2541.09	-0.00	1	YGLFDFEYMMQCQGTSESSKK
66 - 86	2558.11	2557.10	2557.09	0.01	1	YGLFDFEYMMQCQGTSESSKK Oxidation (M)
89 - 100	1468.71	1467.70	1467.69	0.01	0	LFLMSWCPDTAK
89 - 100	1484.70	1483.70	1483.68	0.01	0	LFLMSWCPDTAK Oxidation (M)
104 - 116	1517.79	1516.79	1516.80	-0.01	2	KMLYSSSFDALKK
105 - 115	1261.61	1260.60	1260.61	-0.01	0	MLYSSSFDALK
105 - 116	1389.70	1388.70	1388.70	-0.00	1	MLYSSSFDALKK
105 - 116	1405.70	1404.70	1404.70	0.00	1	MLYSSSFDALKK Oxidation (M)
117 - 123	730.39	729.39	729.44	-0.05	0	SLVGVQK
117 - 141	2750.39	2749.39	2749.41	-0.03	2	SLVGVQKYIQATDLSEASREAVEEK
124 - 135	1353.65	1352.64	1352.66	-0.02	0	YIQATDLSEASR
136 - 141	704.28	703.27	703.34	-0.06	0	EAVEEK
142 - 148	859.45	858.44	858.47	-0.02	2	LRATDRQ

Figure 5.13 Database searching for identification of basic cofilin by peptide mass fingerprinting. Proteins were picked and digested with trypsin and the peptide mixture generated was analysed by MALDI-TOF-MS. **A**). Score distribution of protein 'hits' identified in the database search. **B**) Peptide mass mapping against the theoretical peptide masses in the NCBI database using Mascot identified cofilin with a score of 139 and 95% sequence coverage. The list of matched peptides and modifications (variable and fixed) are shown in bold red lettering. **C**) Error distribution displays the mass error of each peptide in ppm compared to its counterpart in the database.

Perhaps the most interesting observation from the analysis was that the acidic cofilin spot displayed an opposite expression profile in the p110 and PTEN knockdown cells, as expected for a bona fide target of PI3K signalling (Figure 5.14)

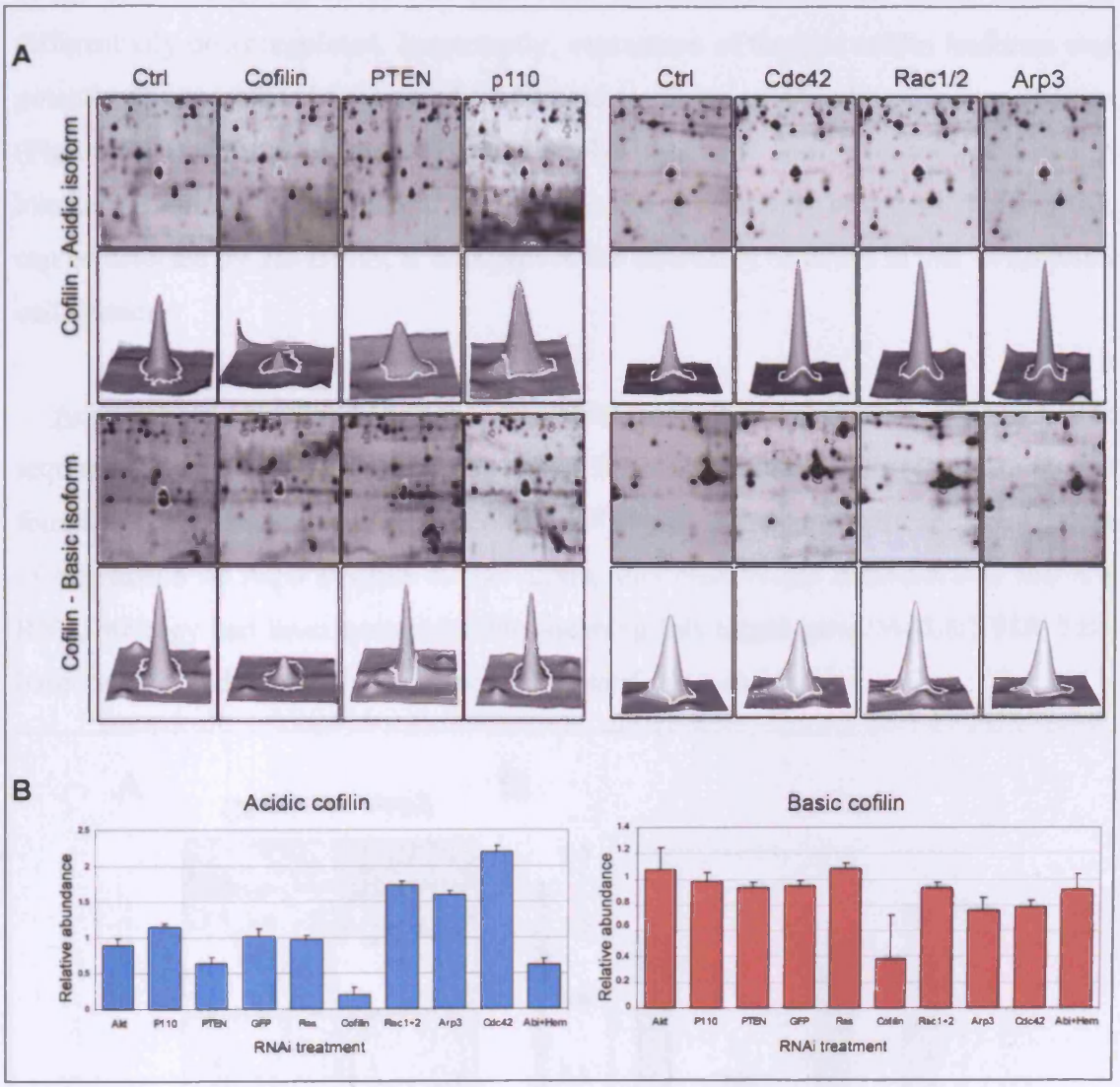

Figure 5.14 The acidic form of cofilin is regulated by both PI3K/PTEN and actin modulators. A) Representative 2D-DIGE gel images and 3-D fluorescence profiles of the acidic and basic cofilin protein isoforms in untreated S2R+ (Ctrl), cofilin, PTEN and p110 knockdown samples, including gel images and 3-D fluorescence profiles of the acidic and basic cofilin protein isoforms in untreated control and cells subjected to RNAi treatments. **B)** Relative abundances of the acidic and basic isoforms of cofilin in respective RNAi-treated cells. Values represent the average of three measurements from biological replicates. Error bars represent the standard deviation.

The acidic cofilin spot was downregulated in PTEN (-1.57 fold) and moderately upregulated in p110 (1.14 fold). Additionally, knockdown of Arp3, Cdc42 and Rac1 plus Rac2 resulted in an up-regulation of the acidic cofilin spot (Figure 5.14), whereas in the double knockdown of Abi plus Hem the expression of the acidic cofilin as differentially downregulated. Importantly, expression of the two cofilin isoforms was potently downregulated in the cells subjected to silencing of cofilin gene expression (Figure 5.14). This confirmed that the dsRNA treatment, over five days, resulted in loss of protein expression and is applicable even to relatively abundant proteins that can be detected by 2D-DIGE. It thus proves the efficiency of RNAi in this *Drosophila* cell system.

Actin related protein 66B (Arp3, CG7558), a component of the Arp2/3 complex required for *de novo* actin nucleation and actin polymerisation (Chapter 1), was also found to be significantly downregulated (-2.83 fold) in cells targeted for knockdown of expression of Arp3 (Figure 5.15). Again, this observation demonstrated that the RNAi strategy had been successful for silencing this target gene. MALDI-TOF MS-based identification of Arp3 is shown in Figure 5.16 A and B.

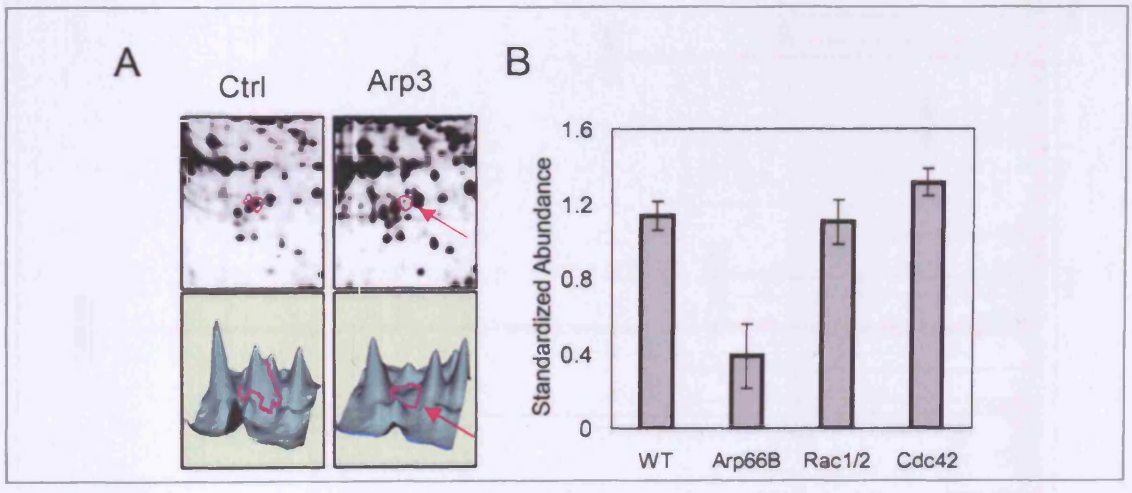

Figure 5.15 Loss of Arp3 protein in cells subjected to RNAi-mediated knockdown of Arp3. A) Migration of Arp3 protein in 2-D gels and its 3-D profile obtained from DeCyder and displaying loss of the Arp3 protein in *arp3* RNAi-treated cells. The pick arrow indicates on the missing protein spot in Arp3 RNAi-mediated knockdown sample. **B)** Histogram showing average standardised abundance of Arp3 expression in untreated (Ctrl), Arp3, Rac1 plus Rac2 and Cdc42 RNAi-treated cells. Error bars show standard error of the mean from triplicate measurements.

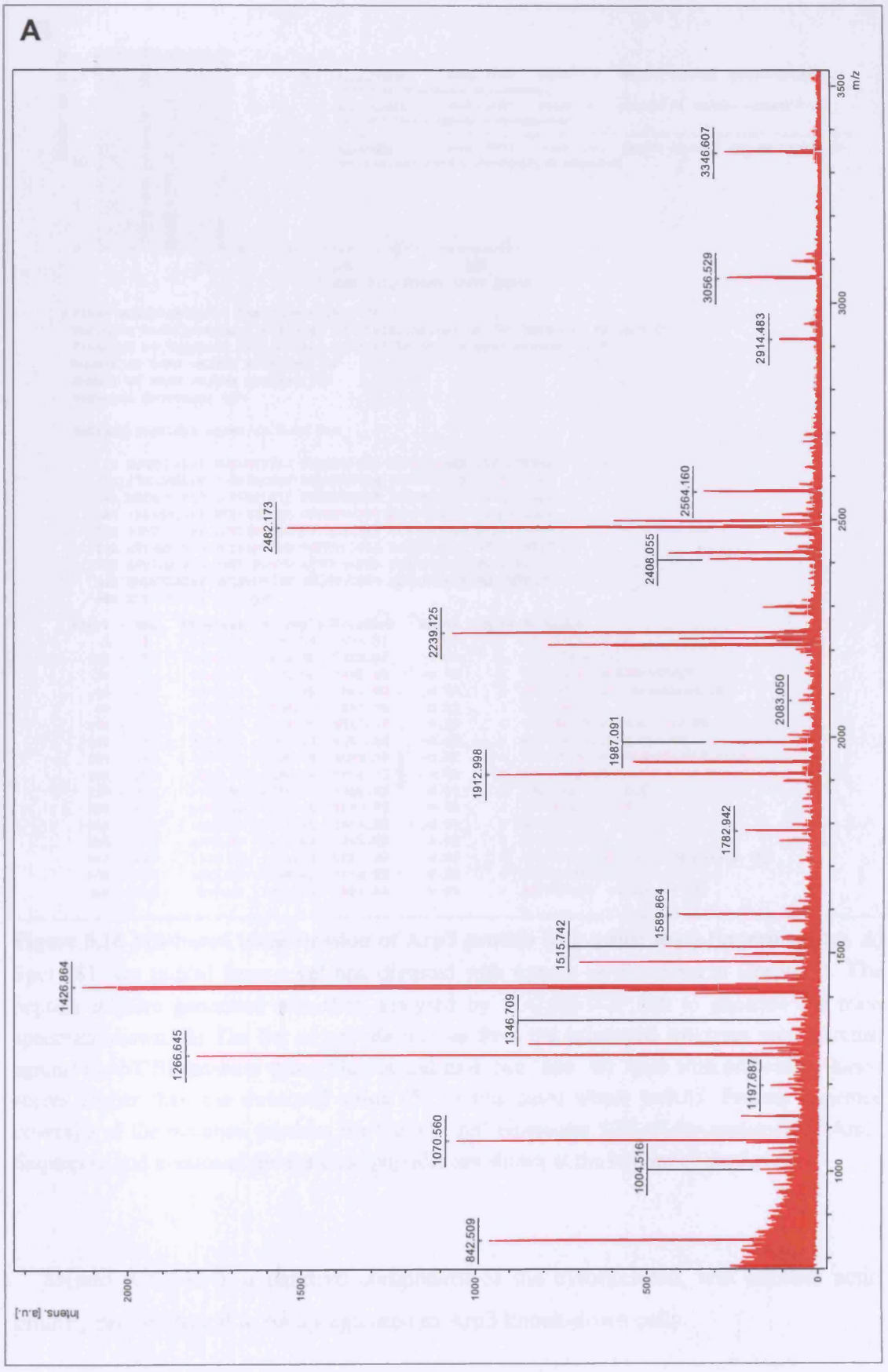
A
Intens. [a.u.]
2000
1500
1000
500
0
m/z
3500
3000
2500
2000
1500
1000
842.509
1004.516
1070.560
1197.687
1266.645
1346.709
1426.864
1515.742
1589.864
1782.942
1912.998
1987.091
2083.050
2239.125
2408.055
2482.173
2564.160
2914.483
3056.529
3346.607

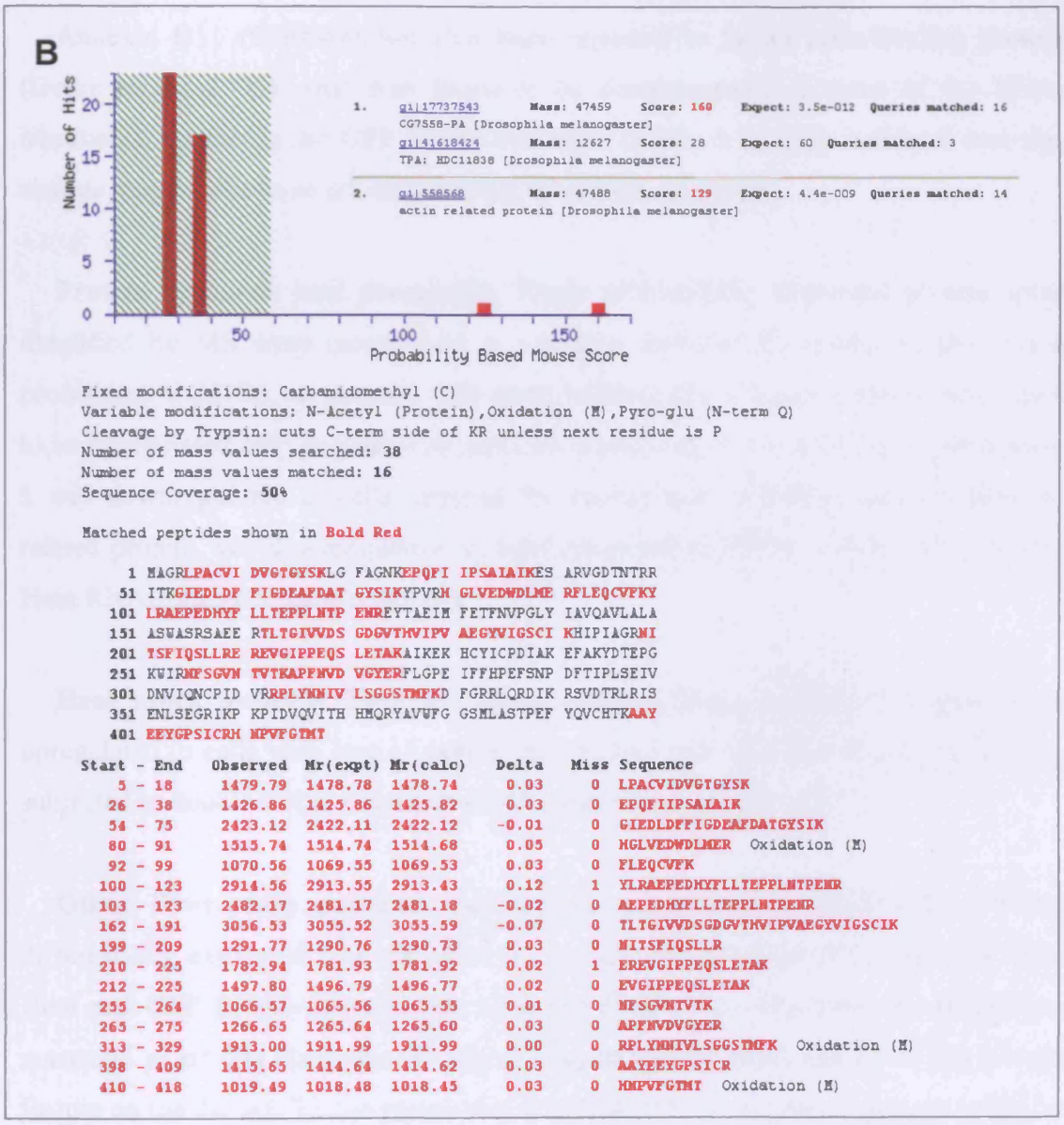

Figure 5.16 MS-based identification of Arp3 protein by peptide mass fingerprinting. A) Spot 781 was picked from a gel and digested with trypsin as described in Chapter 2. The peptide mixture generated was then analysed by MALDI-TOF MS to generate the mass spectrum shown. **B)** The list of peptide masses from the processed spectrum was searched against the NCBI database using Mascot and gave two 'hits' for Arp3 with probability-based scores higher than the threshold value (59 in this case) where p=0.05. Protein sequence coverage of the matched peptides for the top 'hit' represents 50% of the sequence of Arp3. Sequences and masses of the matched peptides are shown at the bottom of the figure.

Misato (CG1424), a putative component of the cytoskeleton, was another actin binding protein found to be upregulated in Arp3 knock-down cells.

Annexin B11 (CG9968) has also been reported to be an actin-binding protein (Gerke et al., 2005) that was found to be downregulated in most of the RNAi treatments, including the GFP RNAi treatment (Table 5.3). This indicated that this change may be due to an off-target effect of dsRNA treatment.

Protein synthesis and processing. Three differentially expressed protein spots identified by MS were categorised as enzymes involved in protein synthesis and processing. CG5706, an enzyme with phenylalanine tRNA ligase activity, was found to be upregulated only in cells with reduced expression of Arp3. Cysteine proteinase-1 was downregulated in cells targeted for knockdown of PTEN, whilst fragile X-related protein was downregulated in cells subjected to PTEN, cofilin and Abi plus Hem RNAi-mediated gene silencing.

Heat shock proteins. Two heat shock proteins (Hsp), Hsp60 and Hsp68, were upregulated in cells with loss of expression of Arp3 and Rac1 plus Rac2, and in cells subjected to double RNAi treatment of Abi plus Hem, respectively.

Other Drosophila proteins. Among the other proteins identified as being differentially expressed was ubiquitin in the cells subjected to p110, Akt, Abi plus Hem and GFP RNAi-induced gene silencing (Table 5.3). However, the theoretical mass and pI of this ubiquitin did not correspond to the mass and pI of the protein feature on the 2D gel. This suggests that this differentially expressed protein might be ubiquitinated. However, other sequence information was not available to enable its identification. CG10424-PA was also identified. This protein has no known or predicted function and was significantly upregulated in the PTEN knockdown cells. Finally, upregulation of the capsid polypeptide derived from *Drosophila* C virus was observed in cells subjected to RNAi treatments for knockdown of Arp3, Cdc42 and Rac1 plus Rac2 expression.

Contaminant proteins. Six protein species were identified as contaminants derived from the bovine serum used in the growth medium. There were different isoforms of albumin and antitrypsin found to be significantly differentially expressed in the samples treated for silencing of expression of p110, Akt1, Arp3 and Rac1 plus

Rac2 (Table 5.3). Since each condition was prepared as biological triplicates, and cells were washed thoroughly and analysed separately, the differential presence of these serum-derived proteins suggests that cells subjected to these RNAi treatments may have altered adhesive properties resulting in retention of these abundant "sticky" serum proteins.

5.3.4 Characterisation of cofilin phosphorylation

The presence of two cofilin isoforms, which had different electrophoretic migration properties, and the observed differential expression of the acidic isoform in p110, PTEN, Arp3, Rac1 plus Rac2, Cdc42 and Abi plus Hem RNAi knockdown cells, suggested that cofilin may be post-translationally modified. Based on previous 2D studies (Hensbergen et al., 2005) and the fact that cofilin can be phosphorylated (Agnew et al., 1995), it was reasoned that the acidic isoform might be a phosphorylated form. To test whether phosphorylation was indeed present, a titanium dioxide (TiO_2) enrichment strategy for phosphopeptides was employed (Larsen et al., 2005) prior to repeat MS analysis. This method was carried out in collaboration with Dr M Larsen, Odense University, Denmark. Briefly, tryptic digests from the two cofilin gel features were loaded onto TiO_2-coated beads packed into gel loading tips. These "microcolumns" were then washed and bound phosphorylated peptides were eluted in ammonia solution. Eluates were acidified and then analysed by MALDI-TOF MS. This approach clearly identified a peptide with mass corresponding to a phosphorylated form of the N-terminal tryptic peptide (Ac-ASGVTVSDVCK+P) (Figure 5.17). Moreover, comparison of spectra from the acidic and basic isofroms, showed that 80 Da sift between peaks corresponding to the phosphorylated and unphosphorylated forms of this peptides, including that the phosphorylation was specific for the acidic isoform (Figure 1.17)

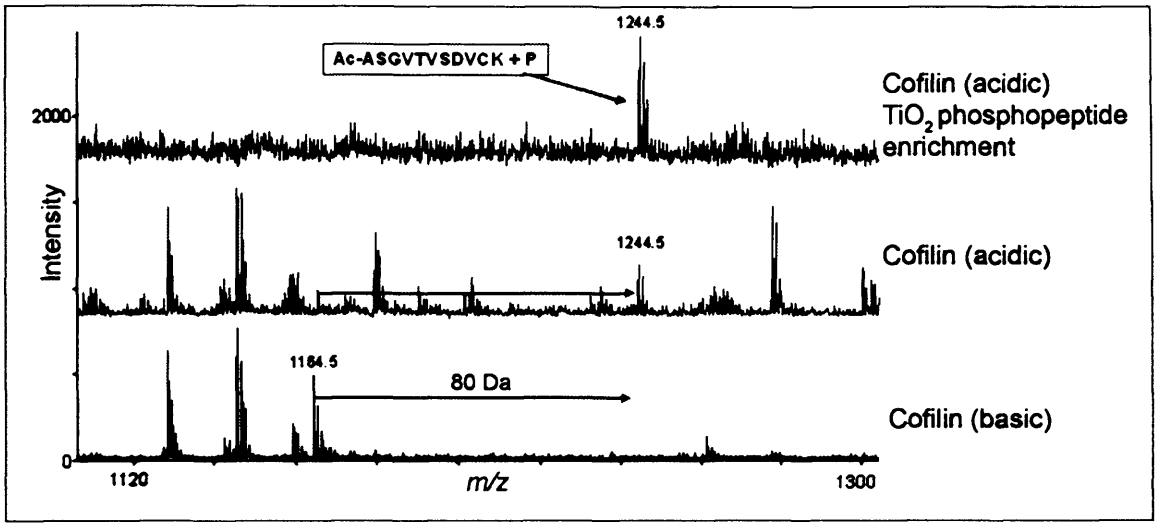

Figure 5.17 Proteomic analysis of cofilin phosphorylation. Enlarged regions of MALDI-TOF MS spectra showing the TiO_2-enriched N-terminal phosphopeptide of *Drosophila* cofilin, and non-enriched tryptic digests from gel pieces containing the acidic and basic Cofilin isoforms. The 80 Da mass difference between the phosphorylated and un-phosphorylated peptides is indicated (Data for the figure were obtained from Dr M Larsen).

Furthermore, LC-MS/MS-based sequencing of the TiO_2-enriched phosphopeptide pool confirmed that this peptide was phosphorylated at Ser3 (Figure 5.18). Significantly, this modification is known to inactivate cofilin, preventing it from binding to and severing actin filaments (Agnew et al., 1995; Bamburg, 1999).

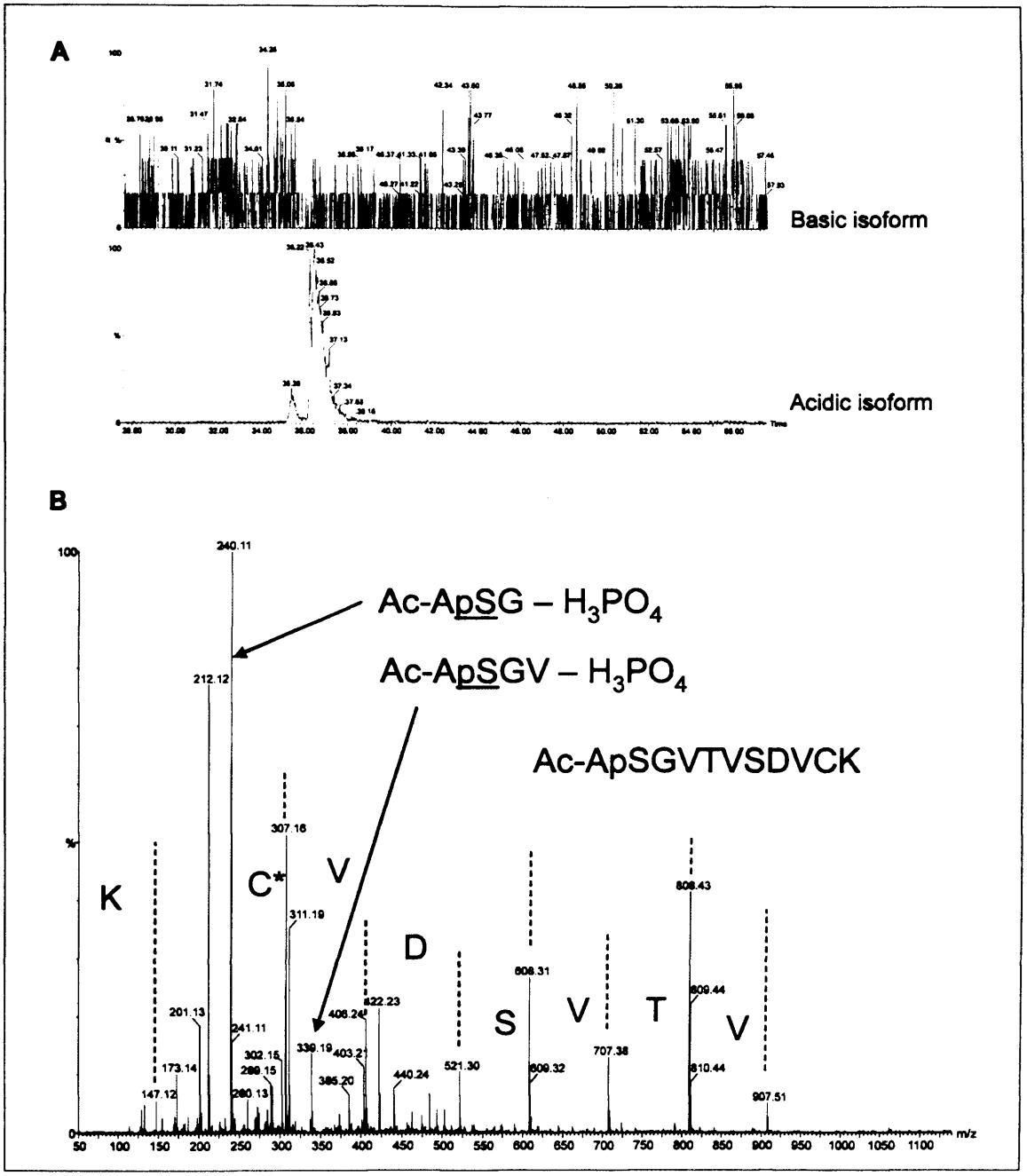

Figure 5.18 Analysis of enriched cofilin phosphopeptides by LC-MS/MS. Titanium dioxide-enriched phosphopeptides from the acidic and basic cofilin spots on the 2D gel were analyzed by LC-MS/MS. **A)** Single ion chromatograms of the doubly charged N-terminal phosphorylated peptide Ac-ApSGVTVSDVCK (*m/z* 622.8). Upper panel shows the single ion chromatogram obtained from the basic cofilin spot and the lower panel shows the single ion chromatogram obtained from the acidic cofilin spot. The ion is only detected in the lower ion chromatogram. **B)** Tandem mass spectrum of the phosphorylated peptide Ac-ApSGVTVSDVCK (* indicates carbamidomethylation of cysteines). The y-ion series is illustrated together with a few b-ion fragments that localise the phosphorylation site to the N-terminal serine residue. (Data for the figure were obtained from Dr M Larsen)

In addition, the MS/MS analysis suggested that cofilin might also be phosphorylated on Thr6 (Figure 5.19) or Ser8, at lower stoichiometry - a finding that needs further validation.

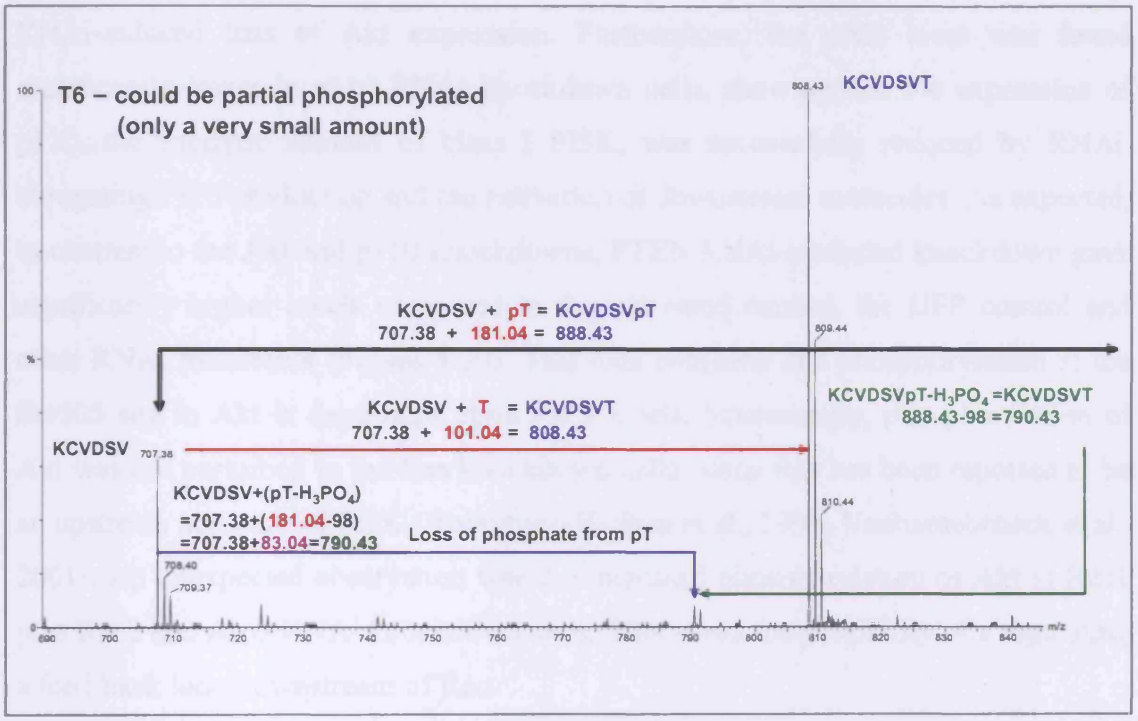

Figure 5.19 Analysis of TiO_2-enriched cofilin phosphopeptides by LC-MS/MS reveals partial phosphorylation on Thr6 in the Ac-ApSGVTVSDVCK peptide. (Data for the figure is obtained from Dr M Larsen). It has been proposed that the y-ion KCVDSVT (*m/z* 808.43) could be partially phosphorylated at threonine. Although KCVDSVpT with *m/z* 888.43 was not seen in the spectra, possible due to the low stoichiometry (black arrow), the peak *m/z* 790.43 could indicate a loss of a phosphate of 98 Da from KCVDSVpT (*m/z* 888.43).

5.3.5 Validation of differences in protein expression observed by 2D-DIGE

The main approach to validate the efficiency of RNAi-induced loss of protein expression relied on the specific detection of proteins by immunoblotting. However, it is important that using 2D-DIGE and MS reduced expression of both Arp3 and cofilin was detected in all the respective RNAi knockdowns. Since the systematic generation of new antibodies is time-consuming and costly, only proteins for which antibodies

were available were further analysed and validated using immunoblotting. Firstly, phosphorylation of Akt at Ser505 and Akt levels in all samples subjected for RNAi were analysed by western blotting, since *Drosophila* specific anti-pSer505-Akt and anti-Akt antibodies were available (Figure 5.22). This immunoblotting revealed the RNAi-induced loss of Akt expression. Furthermore, the pAkt level was found significantly lower in p110 RNAi knockdown cells, showing that the expression of p110, the catalytic subunit of class I PI3K, was successfully reduced by RNAi, abrogating PIP3 production and the activation of downstream molecules. As expected, in contrast to the Akt and p110 knockdowns, PTEN RNAi-mediated knockdown gave significantly higher levels compared to the untreated control, the GFP control and other RNAi treatments (Figure 5.20). This data confirms that phosphorylation at the Ser505 site in Akt is dependent upon PIP3 levels. Interestingly, phosphorylation of Akt was not perturbed in the Ras knockdown cells, since Ras has been reported to be an upstream activator of PI3K (Rodriguez-Viciana et al., 1997; Vanhaesebroeck et al., 2001). An unexpected observation was the increased phosphorylation of Akt in Rac1 plus Rac2 and Arp3 RNAi knockdown cells. This raises the possibility of a regulating a feed-back loop downstream of Rac.

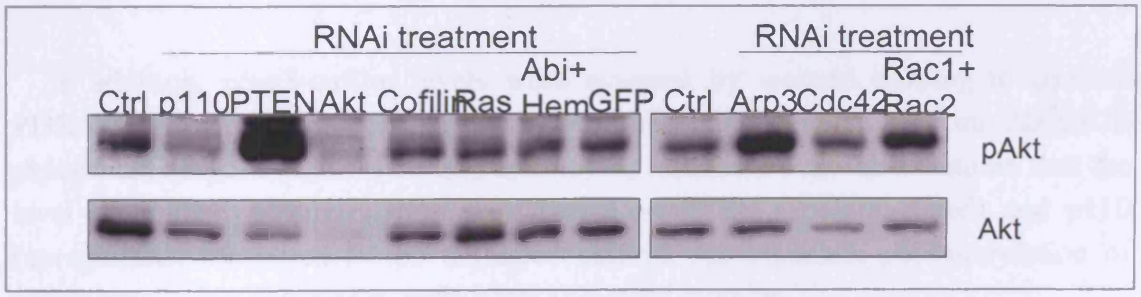

Figure 5.20 Validation of pAkt and Akt levels in the protein lysates derived from RNAi knockdowns. Protein lysates from the respective knockdowns were subjected to 1D SDS-PAGE and western blotting for pSer505-Akt and total Akt. The upper blot showed that the level of pAkt was downregulated in the Akt and p110 knockdowns, and upregulated in the PTEN, Arp3 and Rac1 plus Rac2 knockdowns. The lower blot shows the level of Akt itself, revealing complete loss of Akt in the Akt knockdown sample.

Since it was apparent that cofilin phosphorylation was responsive to changes in both PI3K and Rho-family small GTPase signalling pathway components, *Drosophila* pSer3-cofilin antibody was raised against the *Drosophila* protein, for further study of the signalling events involved. This *Drosophila*-specific antibody was also made

since the available human anti-pSer3-cofilin antibody did not recognise *Drosophila* protein. Once available, the anti-pSer3-cofilin antibody was used to confirm the phosphorylation of Ser3 in the differentially expressed acidic cofilin spot. 2D-immunoblotting revealed that the antibody recognised only the acidic form of cofilin (Figure 5.21). Unfortunately, the lack of an anti-cofilin antibody precluded the validation of the non-phosphorylated cofilin isoform or comparison of the levels of the two cofilin isoforms by immunoblotting.

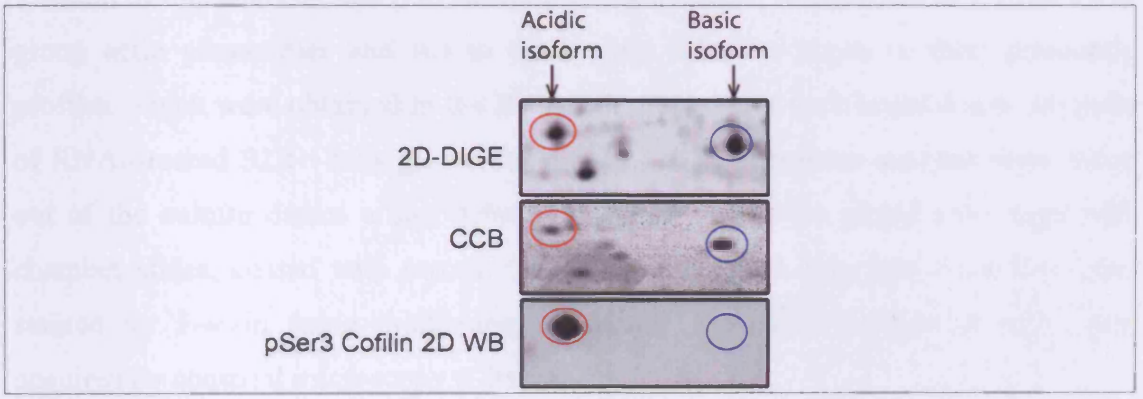

Figure 5.21 Validation of Ser3 phosphorylation of cofilin by 2D immunoblotting. Enlarged and aligned regions of 2D-DIGE, CCB and anti-pSer3-cofilin 2D immunoblot images.

In addition, pSer3-cofilin levels were assessed by western blotting to confirm PI3K-dependent cofilin phosphorylation using the same samples from the 2D-DIGE experiment (Figure 5.24). The immunoblotting confirmed the observations that the level of cofilin phosphorylation was altered in PTEN (downregulated) and p110 (upregulated) compared to the untreated control. As expected, phosphorylation of cofilin was barely detected in cofilin RNAi-treated samples.

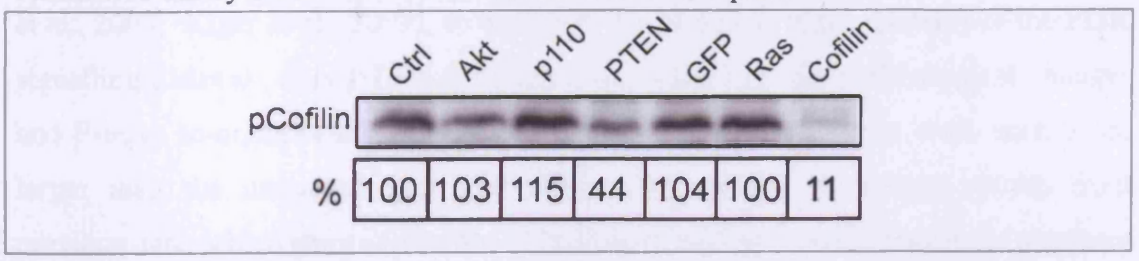

Figure 5.22 Immunoblotting analysis of pSer3-cofilin levels in control untreated and RNAi-treated S2R+ cells confirming PI3K/PTEN modulation of cofilin phosphorylation and cofilin knockdown. Protein lysates from the respective knockdowns were subjected for 1D SDS-PAGE and western blotting for pSer3-cofilin. Relative abundance is shown below the blot as a % of the control, and is the average calculated from densitometry measurements of blots from three independent experiments.

5.3.6 Investigation of morphological changes and actin cytoskeleton organisation in S2R+ cells subjected to specific RNAi-mediated gene silencing

In parallel with the functional proteomic analysis, cell shape and actin organisation were examined in the RNAi knockdowns using fluorescence confocal microscopy. The aim of this analysis was i) to define the shape of each knockdown cell, ii) to try to group actin phenotypes and iii) to try to link the phenotypes to their proteomic profiles, which were obtained in the 2D-DIGE analysis for each knockdown. Aliquots of RNAi-treated S2R+ cells grown for the 2D-DIGE proteomic analysis were taken out of the culture dishes a day before harvesting, and were plated onto eight-well chamber slides, coated with serum. Cells were incubated overnight, then fixed and stained for F-actin using rhodamine-conjugated phalloidin. Images of cells were acquired by confocal microscopy (Chapter 2).

Actin staining of cells revealed the RNA-mediated reduction of expression of Rac1 plus Rac2, Cdc42, Arp3 and double knockdown of Abi plus Hem generated similar cell shapes characterised by the "starfish" morphology and actin phenotypes with reduced levels of cortical F-actin, thus compromising the ability to form lamellipodia (Figure 5.23). The same phenotypes for these knockdowns were previously observed in other functional genomics studies when S2R+ cells were used (Kiger et al., 2003; Kunda et al., 2003). In Kc167 and S2 cells, these genes were also found to regulate cortical F-actin organisation in a similar fashion to experiments using S2R+ (Rogers et al., 2003; Kiger *et al.*, 2003). In the RNAi knockdowns of components of the PI3K signalling pathway, only PTEN-deficient cells showed strong morphological changes and F-actin re-organisation (Figure 5.25). PTEN knockdown cells were seen to be larger than the untreated and GFP RNAi-treated cells, supporting results from previous data, which showed that the PI3K/Akt signalling cascade positively regulates cell size (Leevers et al., 1996; Kozma and Thomas, 2002). In addition, these cells had large lamellipodia (data shown in next chapter) and structures resembling stress fibres, but also showed weak adhesion as they were easily washed off the slides. This latter observation suggests that PTEN-deficient cells may exhibit defects in cell adhesion, as previously reported (Tamura et al., 1998). In addition, p110- and Akt-

gene silenced cells had moderate F-actin reorganisation and defects in cell shape. The cells did not display a decrease in size as would be expected, given the PTEN phenotype, and were viable with no signs of apoptosis. A small cell phenotype was observed in the Ras knockdown cells, where actin was also found to be strongly perturbed. Cell subjected to knockdown of cofilin (twinstar) also showed perturbed F-actin organisation, with an increase in F-actin staining, which has been previously reported (Kiger et al., 2003). Cofilin knockdown cells were found also to be bi- and poly- nuclear (shown in the next chapter), suggesting that cofilin/twinstar protein is important in cell division (Kiger et al., 2003). Finally, the negative control for RNAi treatment (GFP knockdown cells) showed no alteration in morphology or actin cytoskeleton organisation, suggesting that RNAi-mediated silencing itself does not affect actin cytoskeleton organisation.

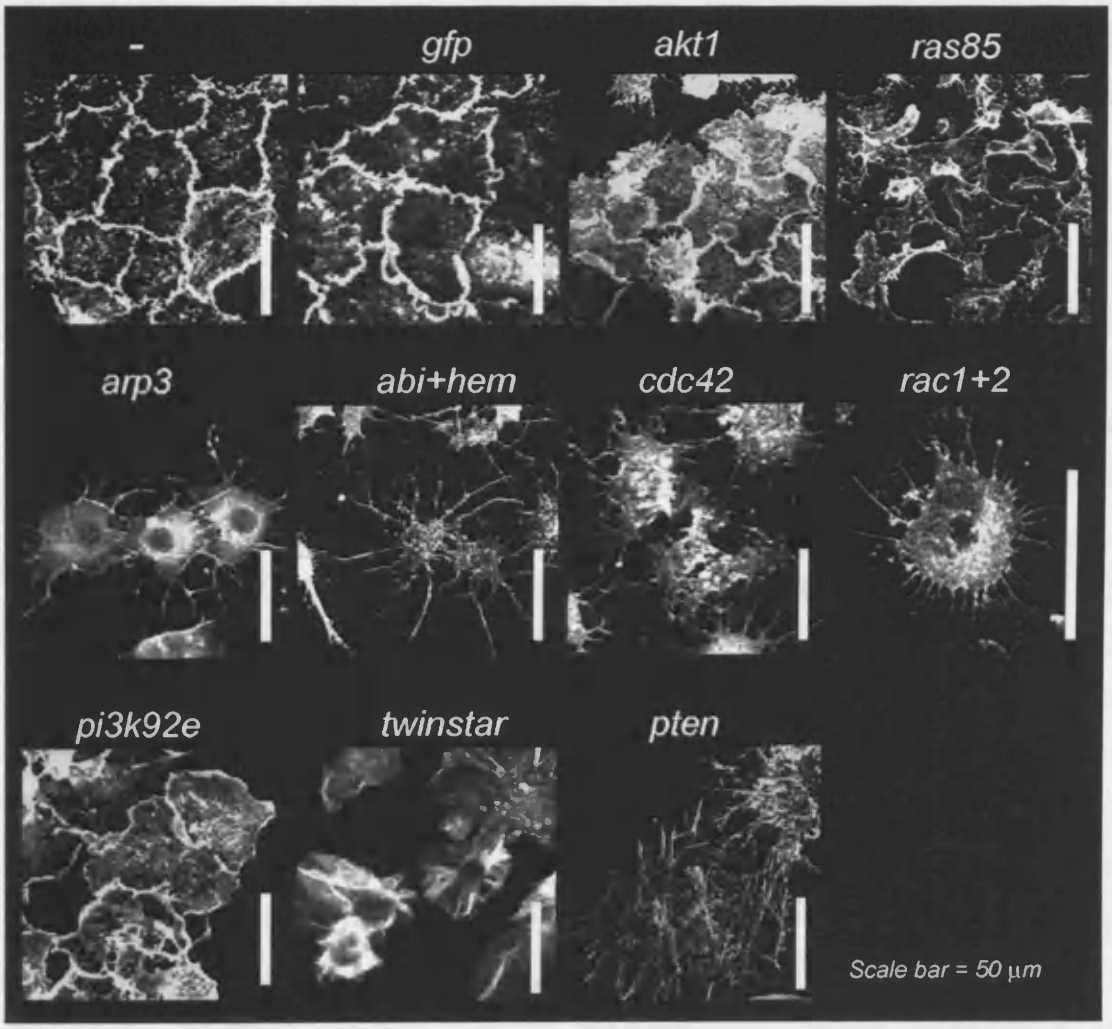

Figure 5.23 F-actin organisation and cell morphology in cells subjected to RNAi-mediated knockdown of expression. S2R+ cells subjected to RNAi treatments were stained for F-actin with rhodamine-phalloidin and images of the cells were captured by confocal microscopy. Scale bars of 50 μm are shown on each image.

5.4 Conclusions

5.4.1 Summary of differentially expressed proteins

A combination of RNAi-specific gene silencing and 2D-DIGE analysis revealed effects on a group of differentially expressed proteins, which are implicated in both PI3K and Rho-family of small GTPase regulated processes, particularly in regulation of actin cytoskeleton organisation and redox homeostasis. From a total of 40 protein isoforms displaying differential expression only 26 were successfully identified with high confidence by MS. Although some of the unidentified protein features were reasonably abundant (could be detected by CCB staining) and gave good quality spectra, 13 protein spots (~33 %) could not be identified from the database searching. Most probably the available databases for fly protein sequences are not fully complete or modifications present in these fly proteins make it difficult to assign protein identities with certainty. It should also be added that searches were repeated on a recently updated version of the NCBI database and using additional modifications without success.

Among the differentially expressed proteins identified, two were metabolic enzymes involved in glycolysis and the citric acid cycle. L-lactate dehydrogenase (LDH) was upregulated only in cells subjected to PTEN knockdown. LDH is an oxidoreductase that catalyses the final step in anaerobic glycolysis; the reduction of pyruvate by NADH to form lactate. It is well established that in the absence of PTEN, PI3K initiates the increased production of PIP3, which leads to constitutive activation of Akt and its downstream targets. The PI3K/Akt signalling pathway can induce increased glucose uptake and glycolysis in cells (Elstrom et al., 2004), which may play a role in Akt-induced cell survival and growth (Rathmell et al., 2003). However, the role of glycolysis under conditions of elevated PI3K/Akt signalling has been controversial, and different models have been proposed where Akt can promote aerobic (Elstrom *et al.*, 2004) or anaerobic glycolysis (Ramanathan et al., 2005). In the absence of PTEN the level of LDH was increased, suggesting that PI3K/Akt activation may drive anaerobic glycolysis in S2R+ cells, although the opposite change was not observed in either the PI3K or Akt knockdowns. The second metabolic

enzyme identified was iso-citrate dehydrogenase (IDH), a mitochondrial enzyme, which participates in the citric acid cycle, and was downregulated in cells treated with dsRNA for silencing of Ras, cofilin and Abi plus Hem. IDH catalyzes the third step of the cycle; the oxidative decarboxylation of iso-citrate, producing alpha-ketoglutarate and CO_2 while converting NAD^+ to NADH. Ras has been previously linked to the regulation of carbohydrate metabolism (Chiaradonna et al., 2006) and the Krebs cycle (Biaglow et al., 1997). In addition, alpha-ketoglutarate, the product of this reaction, is one of the most important nitrogen transporters and an intermediate in metabolic pathways and the urea cycle (Tretter and Adam-Vizi, 2000). Downregulation of a component of the Krebs cycle in the Ras knockdown could suggest that the rate of aerobic glycolysis may be lower, with cells gaining energy though alternative metabolic processes. It is worth mentioning here, that Ras knockdown cells were significantly smaller in size than the control RNAi-untreated cells, suggesting that the alteration in the Krebs cycle and subsequently in the urea cycle, which is important for normal protein metabolism, could be reflected in the cellular phenotype. The finding of reduced iso-citrate dehydrogenase expression, in cofilin and Abi plus Hem RNAi knockdown cells, is more difficult to explain, but could imply that disturbance in actin organisation and the stress that the cells probably go through might alter metabolic energy production pathways.

Five proteins, with known roles in regulating redox metabolism and oxidative stress, were found to be differentially expressed. Cellular oxidative stress arises from significant increase in the concentration of reactive oxygen species (ROS) and reactive nitrogen species (RNS), and/or a decrease in the levels of detoxification or antioxidants (Schrader and Fahimi, 2006). There are many natural sources of oxidative stress that can produce ROS, for example exposure to environmental oxidants, toxins like heavy metals, ionising or UV irradiation, heat shock and inflammation. Major ROS are hydrogen peroxide (H_2O_2), free radical species (containing unpaired electrons), such as the superoxide anion $O_2^{\cdot-}$ and the highly reactive hydroxyl radical ($^{\cdot}OH$). High levels of ROS exert their toxic effects through oxidation of biomolecules such as DNA, proteins and lipids, thus leading to DNA damage and deregulation of redox sensitive metabolic and signalling pathways and to pathogenic conditions. Among ROS, only H_2O_2 has been implicated in the cell

signalling. The enzymatic machinery that minimises potential macromolecular damage influenced by ROS includes peroxiredoxins, superoxide dismutase, catalase, glutathione peroxidise and glutathione transferase. In this study, two *Drosophila* glutathione S-transferases (GST), two peroxiredoxins (Prx) and a predicted oxidoreducatase were found to be differentially expressed in cells with reduced expression of PTEN and the actin cytoskeleton regulators Arp3, Rac1 plus Rac2 and Abi plus Hem.

The peroxiredoxins (Prx) are a major class of cellular reductants, which exhibit thiol-dependent peroxidase activity and are found in a variety of prokaryotes and all eukaryotes (Radyuk et al., 2001). The main function of these proteins is protection from oxidative stress and damage (Wood et al., 2003). Five peroxiredoxin genes have been identified in *D. melanogaster* on the basis of a genome-wide search (Radyuk *et al.*, 2001). They are divided into two subgroups based on the presence of either one (1-Cys Prx) or two (2-Cys Prx) conserved cysteine residues. DPrx-2540 and DPrx-6005 belong to the 1-Cys subgroup, while DPrx-4156, DPrx-4783 and DPrx-5037 to the 2-Cys subgroup. Each of the five genes displays unique developmental expression profile and subcellular localisation, suggesting that these genes have diversified to perform distinct physiological functions. The two Cys-1 Prxs, DPrx-2540 and DPrx-6005, are cytosolic and possess distinctive temporal patterns of expression. DPrx-2540 is expressed at very high levels during embryogenesis and hardly at all thereafter. On the other hand, DPrx-6005 is expressed at all stages of the fly life cycle, with greater abundance in embryos and adult animals. DPrx-2540 was found to be downregulated in cells with reduced expression of PTEN and also moderately in Abi plus Hem knockdown cells. Thus, positive silencing of PTEN expression appears to cause cells to exhibit changes in the expression of their redox machinery. Despite this, DPrx-6005 was found to be upregulated in the double knockdown cells of Abi plus Hem, suggesting that disruption of the Wave/Scar complex could also alter the redox status of the cells. In addition, reducing the expression of Rac1 plus Rac2 or Arp3 resulted in upregulation of CG4199-PA, a predicted disulphide oxidoreductase possibly involved in reactive oxygen species metabolism. Although Rac has been previously linked to the generation of ROS through recruitment of NADPH oxidase (Werner, 2004) there are no reports that the molecules regulating the actin

cytoskeleton downstream of Rac, such as Arp3, Abi, Hem could alter redox homeostasis. It has been proposed that Rac-induced activation of $O_2^{\cdot-}$ production through recruitment of NADH oxidase is permissive for RTK signalling through reversible oxidation and inhibition of protein tyrosine phosphatases Similarly, transient PIP3 production following RTK activation may be augmented by an ROS-dependent inhibition of PTEN (Leslie et al., 2003; Kwon et al., 2004).

GSTs are a family of enzymes that protect cellular molecules from irreversible damage caused by ROS, by catalysing the conjugation of a reduced form of glutathione (GSH), generally making the final products more water soluble and excretable (Enayati et al., 2005). The biological consequences of failure to express GST proteins may result in rapid accumulation of aberrant protein modifications which could lead to the development of pathogenic conditions (McEligot et al., 2005). There are at least two ubiquitously distributed, distantly related groups of GSTs, classified according to their localisation within the cell: microsomal and cytosolic (Enayati et al., 2005; Frova, 2006). A third class, Kappa class GSTs, are localised in mammalian mitochondria and peroxisomes, and are structurally distant from microsomal and cytosolic GSTs. In *Drosophila* there is a single microsomal GST gene, but two main classes (I and II) of cytosolic GSTs. Class II GST orthologues are found in a diverse range of species from nematode to mammals, and are relatively conserved suggesting that they play fundamental roles in conserved physiological processes. In contrast, the class I GSTs are unique to insects and comprise the Delta and Epsilon GSTs, which have evolved independently in various insect species, suggesting that these enzymes play important roles in the adaptation of these species to their environments. Two type of class I cytosolic GSTs, GST D5 and GST E9, were found to be upregulated only in cells with reduced expression of PTEN, suggesting that increased levels of PIP3 can induce changes in redox homeostasis, requiring increased expression of these GSTs for cellular protection. This interpretation assumes that these GST are inducible under high levels of ROS (Kanai et al., 2006; Sharma et al., 2006), although it is difficult to explain why DPrx-2005 expression would be decreased under such conditions. The effects of the studied knockdowns on redox homeostasis requires further examination, although this was beyond the scope of this study.

Two heat shock proteins, Hsp60 and Hsp68, were found to be differentially expressed. Heat shock proteins play different roles in differentiation and development and in adaptation to cellular stress. They are cytoplasmic or ER proteins that bind to nascent or unfolded polypeptides and ensure correct folding and/or transport of proteins. The Hsp60 family are essential proteins that can be divided into two groups based on their sequence homology (Lund et al., 2003). Notably, the group II Hsp60 proteins appear to play a major role in the folding of actin and tubulin, as well as, other substrates (Frankel and Mooseker, 1996). Here, Hsp60 was found to be upregulated in the cells with loss of expression of the actin regulatory proteins Arp3 and Rac1 plus Rac2, whilst Hsp68, of which little is known, was also upregulated in the Abi plus Hem knockdown cells. It is known that the expression levels of Hsps are induced in response to cellular stress. Thus, it would appear that perturbation of the actin cytoskeleton in cells with loss of Abi plus Hem, Rac1 plus Rac2, or Arp3, which display similar morphological phenotypes (Figure 5.23) experience the same form of cellular stress, possibly resulting in the induction of these heat shock proteins. This notion is further supported by the fact that the expression of redox regulated proteins was also perturbed in these cells (see above), although the molecular determinants of this stress response are as yet unclear.

Fragile X mental retardation-related protein (FMR1P) is an RNA-binding protein that acts as a negative translational regulator and is a signature for individuals with fragile X mental retardation, a developmental neurological disorder in humans (O'Donnell and Warren, 2002). The *Drosophila* form of FMR1P was found to be differentially expressed in cells subjected to RNAi-induced knockdown of PTEN, Abi plus Hem and cofilin. FMR1P is present in many cell types and is particularly abundant in the cytoplasm of neurons and in distal dendrites (Caudy et al., 2002). FMRP contains two protein K (KH) homology domains and an RGG box, motifs that are known to be autonomously capable of binding RNA and it has been suggested that FMR1P plays a role in the regulation of local protein synthesis at the postsynaptic site, essential for normal dendritic spine maturation. Thus, abnormal dendritic spines have been observed in both fragile X patients and FMR1P knockdown mice. *Drosophila* contains a single, functionally conserved member of the *fmr* family (Zhang et al., 2001), compared to the three related genes present in mammals, and has

been found to associate with the RNAi-silencing machinery (Caudy et al., 2002). To elucidate the function of FMR1P, Schenck et *al.* initiated a search for interacting proteins by screening an embryonal mouse library using a yeast two-hybrid system (Schenck et al., 2001). They isolated two cytoplasmic proteins that interact with the FMR protein, CYFIP1 (p140Sra-1, specifically Rac1-associated protein) and CYFIP2 (PIR121 or pop), which are 88% identical in their amino acid sequence. The *Drosophila* genome, on the other hand, contains a single ortholog of CYFIP1/2. Both, CYFIP1 and 2, and fly CYFIP have been shown to be specific targets for Rac1, binding only to the GTP-bound form (Billuart and Chelly, 2003). Furthermore, CYFIP2 is a part of the inactive Scar/WAVE complex. Active Scar/WAVE is known to mediate Rac-dependent cytoskeleton remodelling by direct interaction with the Arp2/3 complex, which when activated promotes actin nucleation (Bompard and Caron, 2004). A model of competition between CYFIP/WAVE and CYFIP/FMR1P has been proposed, where Rac1 activation would result in a positive regulation of FMR1P function in regulating the translation of specific mRNAs (Figure 5.24), such as that of the Futsch protein, a *Drosophila* homologue of the microtubule-associated protein 1b (MAP1B) (Zhang et al., 2001). In this model CYFIP binds to activated Rac-GTP, and then FMR1P and WAVE are released and activated so they can regulate the tubulin and actin cytoskeleton, through the control of specific mRNA translation of proteins such MAP1B and through the Arp2/3 complex, respectively (Billuart et al., 2003). Although this model suggests that FMR1P is inactive when bound to CYFIP, it does not provide further information about the importance of the complex for FMR1P stability. For instance, Hem and Abi are both components of the inactive Scar complex. It has been reported that Abi protects the Scar complex from proteosome degradation (Kunda et al., 2003). In the case of reduced levels of Abi, it is possible that CYFIP is degraded. Thus, the reduced level of FMR1P in Abi plus Hem knockdown cells suggests that maybe the FMR1P/CYFIP complex is important for stabilising FMR1P in the same manner as for the SCAR complex proteins. However to prove such a model further experiments are needed.

Lower levels of FMR1P were also detected in PTEN RNAi-treated cells. This suggests that increased PIP3 levels, which could keep Rac activated, would sequester CYFIP2, releasing FMR1P from the complex, leading to FMR1P degradation. The

level of FMR1P was also reduced in cofilin RNAi-knockdown cells. There are no reports linking cofilin function with FMR1P; however, this seems an interesting observation and possibly suggests feedback from the actin cytoskeleton. However, it is important to note that the three knockdown conditions displaying decreased levels of FMR1P, all differed in cell shape and actin organisation.

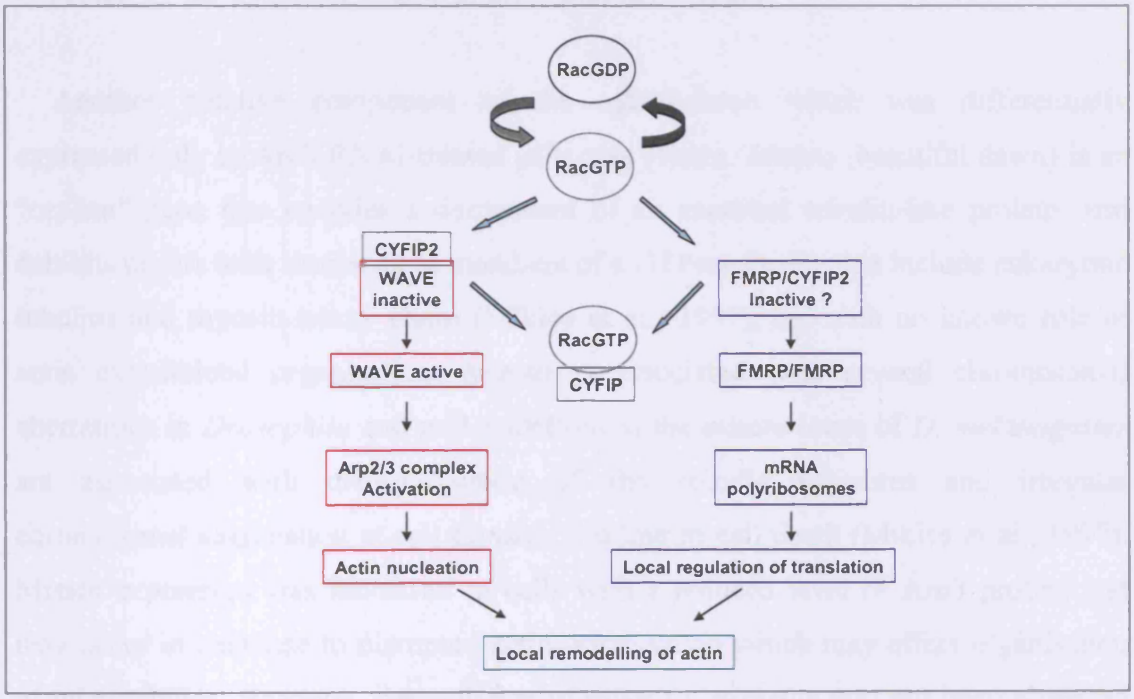

Figure 5.24 Rac-dependent regulation of protein translation by FMR1P and FMR1P indirect control of actin cytoskeleton organisation by FMR1P. Adapted from Billuart *et al.*, 2003.

Four abundant actin binding proteins (Arp3, misato, annexin B11 and cofilin), were differentially expressed under the RNAi conditions applied in this study. Arp3 (CG7558) was found to be downregulated in cells subjected to Arp3 RNAi-induced silencing, showing that the protein knockdown strategy had been successful. Arp3 is a part of the Arp2/3 complex, consisting of seven subunits, two of which are related to actin (Arp2 and Arp3) and five of which are unique. Arp2/3 is a nucleator of new actin filaments at the leading edges of cells and its activity is regulated by proteins of the WASP and WAVE family, which are in turn controlled by signals from receptor tyrosine kinases and the small GTPases Cdc42 and Rac. The active Arp2/3 complex promotes *de novo* actin nucleation and polymerisation supporting cortical actin

formation in adherent cells. Thus, disrupting the Arp2/3 complex in S2R+ resulted in cells with reduced F-actin staining and loss of cortical actin lamellipodia gives rise to a starfish-like phenotype, similar to its upstream regulators Rac, Cdc42 and Abi plus Hem. Despite this, changes in expression of Arp3 did not appear in the other knockdown treatments, suggesting that expression of this protein itself is not regulated by the upstream targets in the signalling cascade.

Another putative component of the cytoskeleton which was differentially expressed only in Arp3 RNAi-treated cells was misato. *Misato* (beautiful dawn) is an "orphan" gene that encodes a descendant of an ancestral tubulin-like protein, and exhibits motifs with similarity to members of a GTPase family that include eukaryotic tubulins and myosin heavy chain (Miklos et al., 1997), but with no known role in actin cytoskeletal organisation. Misato is associated with several chromosomal aberrations in *Drosophila* and null mutations at the *misato* locus of *D. melanogaster* are associated with disorganisation of the spindle apparatus and irregular chromosomal segregation at cell division, leading to cell death (Miklos et al., 1997). Misato expression was increased in cells with a reduced level of Arp3 protein and may occur in response to disrupted actin organisation which may effect organisation of microtubules. However, deregulation of misato expression was not been observed in other knockdowns (e.g. Rac1 plus Rac2, Cdc42, cofilin, Abi plus Hem) that affect the actin cytoskeleton.

Annexin B11, an actin and lipid binding protein, was found to be differentially downregulated in the control for RNAi treatment (GFP RNAi) and in most of the RNAi experiments, suggesting that this change is an off-target effect of the RNAi mechanism. *Drosophila* annexin B11 is a member of the annexin family, which are calcium-dependent phospholipid-binding proteins (Gerke et al., 2005). They are abundant in the eukaryotic kingdom. Annexins are characterised by the unique architecture of their Ca^{2+} binding sites, which enables them to peripherally dock onto negatively charged membrane surfaces (to acidic phospholipids) in their Ca^{2+} bound conformation. These properties link annexins to many membrane-related events, such as the regulated organisation of membrane domains and/or membrane–cytoskeleton linkages, certain exocytic and endocytic transport steps and the regulation of ion

fluxes across membranes. Most of the studies on annexins show that they often function as modulators of these processes, rather than as essential effectors. Importantly, annexins can participate as actin-binding proteins and serve directly as an F-actin interaction platform, especially in regions enriched with PIP2 or highly dynamic actin (Gerke et al., 2005). It has been reported that annexins are involved in endocytosis (Rescher and Gerke, 2004), so the finding of differentially expressed annexin B11 even in the RNAi negative control suggests that it could be involved in dsRNAs uptake, which in fly cells is mediated by endocytosis. Recently, the pathway for dsRNA uptake was identified in *D. melanogaster* S2 cells (Saleh et al., 2006), with dsRNA entering the RNAi pathway through an active and specific pathway that involves clathrin-mediated endocytosis and vesicle-mediated intracellular trafficking that depends upon lipid and cytoskeleton guidance. Considering the biochemical and physiological properties of annexins, the findings reported here could suggest the involvement of annexin B11 in dsRNA uptake. However, this needs to be examined further. Three other proteins were also differentially expressed in GFP RNAi-treated cells, but they could not be identified.

Cofilin (twinstar, CG4254) is another cytoskeletal regulatory protein, which was found to be differential expressed in Rac1 plus Rac2, Cdc42, Abi plus Hem, Arp3, PTEN, p110 and cofilin RNAi-knockdown cells. Cofilin is an actin binding protein potent in severing and depolymerising F-actin, and thus supports the actin recycling (Bamburg, 1999). Here, two isoforms of cofilin were identified. Using a TiO_2 phosphopeptide-enrichment strategy (Larsen et al., 2005) the acidic cofilin isoform was found to be phosphorylated at Ser3. This post-translational modification of cofilin has been identified in systems and is known to inhibit the actin binding ability of cofilin (Agnew et al., 1995). In addition, LC-MS/MS analysis of the enriched phosphopeptides from the acidic cofilin isoform revealed that cofilin could be partially phosphorylated on Thr6 and Ser8, although this finding needs further examination. The basic cofilin isoform was not phosphorylated and represents the active form of cofilin in cells. The two isoforms were downregulated in cofilin knockdown cells, confirming the success of the RNAi strategy. pCofilin was differentially upregulated in cells subjected to the RNAi-mediated knockdown of expression of p110, double Rac1 plus Rac2, Arp3, Cdc42, and downregulated in

PTEN, Abi plus Hem and cofilin RNAi-treated cells. The observation of opposing expression of pCofilin levels in p110 and PTEN RNAi-treated cells compared to the control cells, suggests that regulation of cofilin phosphorylation and activity occurs downstream of PI3K. However, pCofilin did not appear to be differentially expressed in Ras and Akt RNAi-treated cells, suggesting that PI3K probably regulates cofilin activity through interaction with another signal transduction pathway, possibly through regulation of Rho GTPases. Indeed pCofilin levels were increased Rac1 plus Rac2 and Cdc42 RNAi treatments. Surprisingly, pCofilin was also found to be upregulated in Arp3 knockdown cells. Since the Apr2/3 complex is directly linked to actin and regulates polymerisation and branching of the actin network, this suggests a possible negative feed-back mechanism in the regulation of cofilin severing activity on F-actin. Conversely, the double knockdown of Abi and Hem cells were found to express a lower level of phosphorylated cofilin. Both proteins regulate the stability of the WAVE protein in WAVE complex and thus are implicated in actin polymerisation through the Arp2/3 complex (Kunda et al., 2003). It would be expected that knockdown of Abi and Hem should give the same phenotype as Arp3 knockdown cells, which was the case in terms of their similar cell morphologies, but not in terms of cofilin phosphorylation. This difference is difficult to explain at this stage of the analysis and would require further examination. However, the finding of pCofilin as a common target for two major signalling pathways was a potentially exciting discovery. Thus, cofilin regulation by PI3K signalling and Rho-family of small GTPases was the subject of further study and it is presented in the following chapter.

Finally, albumin and antitrypsin were identified as differentially expressed proteins in the proteome of p110, Akt and Ras knockdown cells. Albumin and antitrypsin proteins were derived from the foetal calf serum used in the medium and were thus characterised as contaminates. However, the expression changes were statistically significant suggesting possible changes in adhesive properties of the RNAi targeted cells.

5.4.2 Morphological changes observed and common protein expression patterns among the RNAi-treated cells

RNAi-induced loss-of-gene function analysis used for selected Rho GTPases and components of the WAVE/Scar and Arp2/3 complexes produced results that confirmed the importance of these genes in determining cellular morphology and actin organisation and supports previous observations in S2R+ cells (Kiger *et al.*, 2003; Kunda *et al.*, 2003). Loss of these proteins has shown to result in common "starfish-like" phenotypes, which place these proteins in the same signalling cascade that regulates F-actin remodelling and cortical lamellipodia formation (Kunda *et al.*, 2003). These phenotypes were characterised by deregulation of some common proteins involved in cellular stress responses (Hsp60 and Hsp68, peroxiredoxin) which could suggest that the loss of actin structure induces cell stress and causes the observed upregulation in the expression of these proteins. Cofilin RNAi cells were distinguished by their high levels of F-actin staining, presumably due to the loss of cofilin's ability to depolymerise F-actin. Cofilin knockdown cells showed similarities in their proteome profile with PTEN and Abi plus Hem knockdown cells, but differed in cell morphology. Furthermore PTEN knockdown cells were larger and showed signs of stress fibres structures. The cells also appeared to have an adhesion defect because they were only weakly attached to the culture dishes. In addition, the PTEN knockdown cells displayed a unique proteomic phenotype with a potential increase in anaerobic glycolysis, suggesting that there is misbalance in their redox homeostasis. This observation was further supported by the cells increased expression of GST proteins and decreased expression of a peroxiredoxin. Interestingly, cofilin, Abi plus Hem and PTEN knockdown cells, although displaying different morphologies, had some common differentially expressed proteins, which including downregulation of the same metabolic enzymes and downregulation of cofilin phosphorylation.

PI3K knockdown resulted in only a moderate degree of actin reorganisation phenotype compared to that of the PI3K inhibitors on the actin cytoskeleton reported in the previous chapter. This would suggest that the acute inhibition of the PI3K signalling has a more rapid and prominent effect on the actin cytoskeleton, while in the RNAi-mediated knockdown the perturbation of PIP3 levels may be less intensive,

with any remaining PI3K permitting formation of normal cortical F-actin structures as well as allowing time for adaptive response that maintain the cell shape. Adaptive responses could be a general reason to explain differences between acute (inhibitor and insulin) responses and chronic responses (RNAi). However, it has to be mentioned that PI3K inhibitors may also produce off-target effects, as both LY294002 and wortmannin may not be absolutely specific for *Drosophila* PI3K and could possibly inhibit other kinases. Thus, it was important to test/compare both strategies. Akt knockdown cells also remained relatively unaffected in terms of their actin organisation despite the fact that Akt was shown to be almost completely depleted in the knockdown. This could mean that signalling downstream of Akt may not feed into cytoskeleton regulation despite some recent reports where it does (Vandermoere et al., 2007). This result was also in contrast to the loss of Akt phenotype that was observed in the genome wide screen by Kiger *et al.* where cells were seen as flat, but displayed retracted F-actin (Kiger et al., 2003). These contradictory results required that the Akt knockdown be repeated several times, including targeting the same region of the mRNA sequence as was in Kiger study. However, this revealed the same phenotype, without obvious changes in the actin cytoskeleton. Furthermore, Ras knockdown cells displayed different morphology from PI3K and Akt knockdown cells, even though it has been reported that Ras can act upstream of PI3K. Ras knockdown cells were significantly smaller than the control cells, and appeared to have perturbed actin cytoskeleton organisation. However, their proteomic profile with changes only in metabolic enzyme did not reflect the morphological phenotype of the respective knockdown observed.

In summary, the work I carried out and described in this chapter has revealed the power of 2D-DIGE for quantitative analysis of differential protein expression in the fly proteome. Preliminary work on different cell lines helped to establish the application of 2D-DIGE method for the proteomic analysis of fly cell proteomes. Further analysis was not performed since the differences observed were too numerous and unlikely to reflect differences in cell morphology alone. Combining an RNAi approach for gene silencing with 2D-DIGE analysis proved a valuable strategy for defining the biochemical profiles of cells where crucial signalling molecules and actin modulators where absent due to RNAi-mediated gene silencing. Furthermore, some

common protein targets, presumably acting downstream of the silenced genes were detected. One such protein was cofilin, whose phosphorylation, and hence activation, appeared to be regulated by both PI3K and the Rho-family of small GTPases, suggesting that PI3K and Rac signalling are positively regulated in the same signalling cascade for cofilin regulation. Thus, it can be proposed that in combination with RNAi, 2D-DIGE can be used for monitoring cell signalling events and the regulation of protein expression, although only for reasonably abundant proteins. Importantly, this study opened up the question of the possible negative regulation of cofilin activity by actin itself, as it appeared that perturbations of the Arp2/3 complex can also alter cofilin activity. Cofilin regulation was the subject of further experimentation and is presented in the following chapter.

Chapter 6: Regulation of cofilin phosphorylation and activity

6.1 Cofilin - an actin severing and depolymerising protein

Actin is the most abundant protein in eukaryotic cells and its ability to assemble reversibly into long and flexible polymeric filaments and to form a three-dimensional meshwork provides the foundation upon which many essential cellular processes (e.g. cell division, motility, and determination of shape) rely. Performing these functions demands strict regulation of the spatial and temporal organisation of the actin cytoskeleton. This is facilitated on many levels by a myriad of accessory actin-binding proteins such as sequestering proteins (thymosin β4 and profilin), capping proteins (CapZ), proteins that stimulate polymerisation from the pool of actin monomers in a process known as nucleation (Arp2/3 complex and formins) and proteins that break or "sever" actin filaments and drive depolymerisation (actin depolymerising factor (ADF)/cofilin). In addition, numerous signalling pathways feed into this system, relaying extracellular stimuli to induce changes in the actin cytoskeleton. The primary structure of actin is highly conserved among eukaryotes. Monomeric G-actin is a 43 kDa globular protein with four subunits. ATP, together with Mg^{2+} binds to G-actin and can be hydrolysed to ADP+Pi. Actin polymerisation occurs in an organised manner, involving head-to-tail interactions, producing filament polarity where each filament has a pointed (-) end and a barbed (+) end. During filament growth, incorporation of actin monomers occurs from both ends, however this addition of actin monomers loaded with ATP is asymmetric, such that the barbed end elongates five- to ten-fold faster than the pointed end.

Cofilin is a member of a group of small actin-binding proteins (15-22 kDa), collectively called the ADF/cofilin family that includes destrin, depactin, actophorin, and actin depolymerising factor (ADF), and promotes actin depolymerisation (Bamburg, 1999). The first member of this family, ADF, was identified in extracts of embryonic chick brain (Bamburg et al., 1980), whereas cofilin was purified from porcine brain four years later (Maekawa et al., 1984). Cofilin was characterised primarily as an F-actin binding protein (1:1 ratio with actin subunits) and hence was named for its ability to form cofilamentous structures with actin (Nishida et al., 1984).

The cofilin structure is characterised by the presence of two actin-binding sites; a G/F-site at the N-terminus and an F-site at the C-terminus, thus cofilin can interact with both actin monomers and actin-ADP filaments. The G/F site is responsible for both G- and F-binding and is sufficient for cofilin depolymerising activity. The F-binding site is required in addition to the G/F site for F-actin binding and severing activity. Studies on cofilin have shown that cofilin binds G-actin-ADP with greater affinity than G-actin-ATP at physiological ionic strength. Cofilin also binds F-actin-ADP with greater affinity than it binds to F-actin-ATP or F-actin-ADP+Pi (Carlier et al., 1997). Upon binding to actin filaments, cofilin increases filament twist (McGough et al., 1997) and promotes the turnover of the filaments by increasing the dissociation rate of the monomers at the pointed (-) end of actin filaments without capping the actin filament ends (Carlier et al., 1997), thereby increasing the number of free barbed ends where polymerisation and depolymerisation can occur. The mechanism of cofilin in enhancing actin filament turnover appears to be pH-dependent, as cofilin exhibits stronger depolymerising activity at pHs above 7.5 than at lower pHs. This pH dependence is due to an increase in the critical concentration for actin-cofilin complex formation at higher pHs.

Phosphorylation of cofilin at a conserved serine-3 residue at the N-terminus inhibits its actin binding activity (Agnew et al., 1995). Several studies have used recombinant mutants of cofilin containing an Asp or Glu substitution at Ser3 (or equivalent) to mimic the negative charge of the phosphorylation form. These proteins had a decreased affinity for actin of 10-20 fold when assayed *in vitro* (Agnew et al.,

1995; Smertenko et al., 1998; Ressad et al., 1998). Four different kinases that appear to act downstream of the Rho-family GTPases can phosphorylate cofilin: LIMK1, LIMK2, TESK1 and TESK2 (Yang et al., 1998; Arber et al., 1998; Dan et al., 2001; Rosok et al., 1999; Toshima et al., 2001; Sumi et al., 1999). However, LIMK is the key factor in the cofilin phosphorylation across different eukaryota. LIMK is activated by phosphorylation of Thr508/505 (LIMK1/2) within a kinase loop, through divergent Rho GTPase pathways: Rac/Cdc42 acting through p21-activated kinase 1 (PAK1) and PAK4 (Edwards et al., 1999; Dan et al., 2001), Cdc42 acting through MRCK (myotonic-dystrophy-related Cdc42 binding kinase) (Sumi et al., 2001) and RhoA through ROCK (Rho associated coiled-coil-containing kinase) (Ohashi et al., 2000). Thus, members of the Rho-family GTPases, which regulate the organisation of actin into lamellipodia, filapodia and stress fibres in animal cells, show a common mechanism in the ability to regulate actin dynamics through phosphorylation of cofilin. Functionally, LIMK promotes F-actin stability through cofilin phosphorylation and inactivation, as LIMK overexpression in cells promotes F-actin accumulation (Arber et al., 1998; Yang et al., 1998). Two selective cofilin phosphatases have also been identified; chronophin (CIN) (Gohla et al., 2005) and slingshot (SSH) (Niwa et al., 2002). SSH was identified from genetic studies in flies (Niwa et al., 2002), and is widely expressed in various organisms. SSH can dephosphorylate cofilin at Ser3, thereby suppressing the assembly of actin filaments induced by LIMK-dependent phosphorylation and inactivation of cofilin (Figure 6.1). In addition, it has been reported that endogenous LIMK1 and SSH-1L interact *in vitro* and co-localize *in vivo*, and this interaction results in SSH-1L–induced dephosphorylation and downregulation of LIMK1 activity (Soosairajah et al., 2005). Also the phosphatase activity of purified SSH-1L appears to be F-actin dependent and is negatively regulated via PAK4-mediated phosphorylation at Ser937 and Ser978 sites (Yamamoto et al., 2006; Soosairajah et al., 2005). 14-3-3 zeta protein can also bind to phosphorylated SSH, thus decreasing the amount of SSH that binds to F-actin and its activity to dephosphorylate and activate cofilin (Nagata-Ohashi et al., 2004).

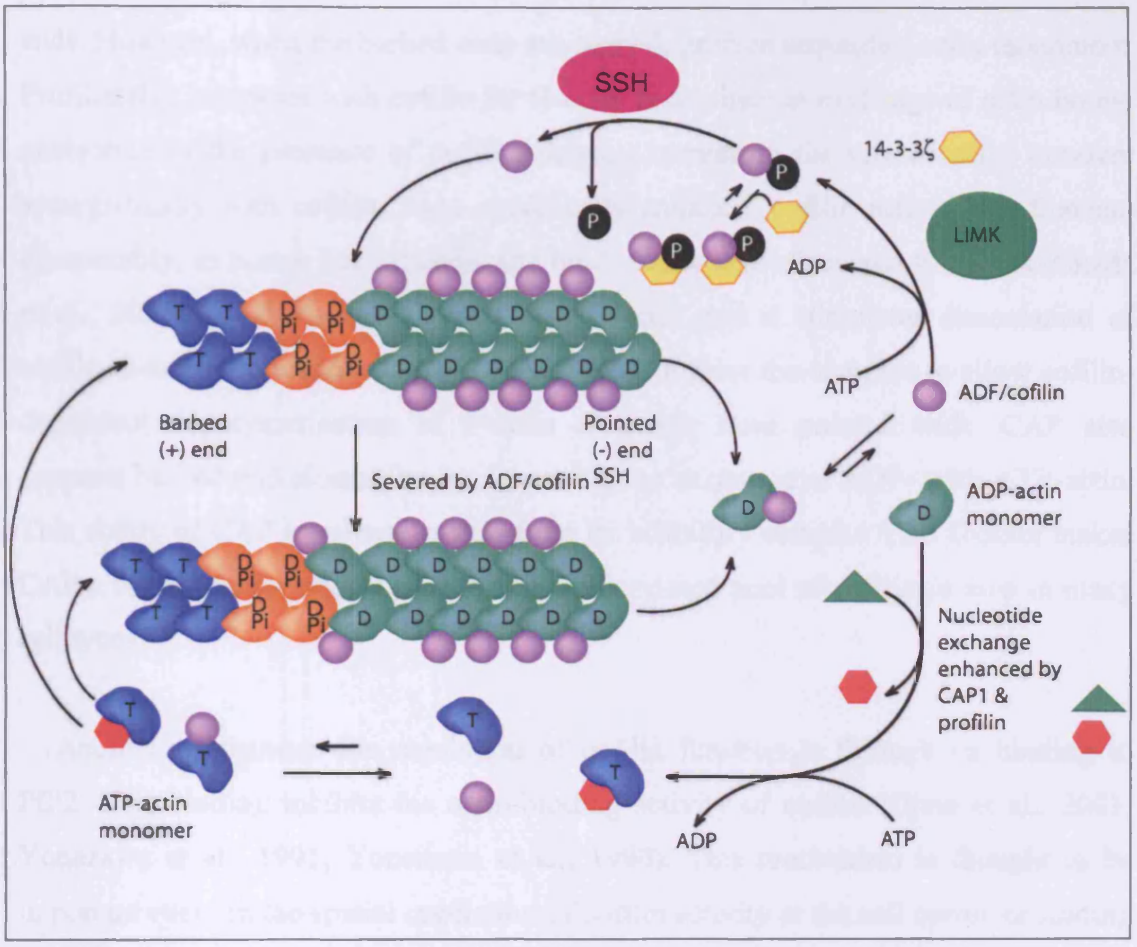

Figure 6.1. The activity of ADF/cofilin is regulated by a balance of phosphorylation and dephosphorylation. Through filament severing and increasing the off-rate from the pointed (-) ends of actin filaments, ADF/cofilin enhances filament turnover. If the pool of assembly-competent actin is high where ADF/cofilin is active, net assembly can occur on the new barbed (+) ends. However, if the actin monomer pool is low, net depolymerization will occur. Mammalian ADF and cofilin are inhibited in their activity towards actin binding and dynamics by kinases LIMK that phosphorylate the proteins on the conserved Ser-3 residue. Dephosphorylation by phosphatases such as slingshot, SSH, activates them.

In addition to this, other actin binding proteins including tropomyosin, profilin, actin-interacting protein (Aip1) and cyclase associated protein (CAP) can interfere with cofilin-dependent actin filament dissociation (reviewed in (Ono, 2003). In general, tropomyosin competes with cofilin for F-actin binding and inhibits depolymerisation. However, in different cell models the spatial organisation between cofilin and tropomyosin differs suggesting that both could regulate different types of actin reorganisation. Profilin, on the other hand, binds G-actin enhancing the exchange of actin-bound ADP with ATP, and promotes filament growth from barbed

ends. However, when the barbed ends are capped, profilin sequesters actin monomers. Profilin also competes with cofilin for G-actin and enhances exchange of actin-bound nucleotide in the presence of cofilin, thereby increasing the rate of actin turnover synergistically with cofilin. Aip1 specifically enhances cofilin activity for filament disassembly, as it caps barbed ends, and binds to the side of severed filaments (Okada et al., 2006). CAP binds and sequesters G-actin and it stimulates dissociation of cofilin-G-actin heterodimers, thus releasing cofilin from the complex to allow cofilin-dependent depolymerisation of F-actin filaments from pointed ends. CAP also supports barbed end elongation by enhancing the exchange of ADP- with ATP-actin. This ability of CAP to release cofilin from its inhibitory complex with G-actin makes CAP a candidate for regulating the dephosphorylated pool of cofilin *in vivo* in many cell types.

Another mechanism for regulation of cofilin function is through its binding to PIP2. This binding inhibits the actin-binding activity of cofilin (Ojala et al., 2001; Yonezawa et al., 1991; Yonezawa et al., 1990). This mechanism is thought to be important event in the spatial regulation of cofilin activity at the cell cortex or leading edge of migratory cells. PIP2 can undergo hydrolysis mediated by PLCγ1 leading to activation of cofilin and other actin binding proteins and thus actin remodelling. (Yonezawa et al., 1991; Yonezawa et al., 1990). PIP2 can also be phosphorylated by PI3K, and this could lead to the release of cofilin from the inhibitory complex with PIP2 and its activation. In some studies of growth factor-mediated stimulation of cells, dephosphorylation of cofilin has been observed in the early time points of the stimulation. For example, in resting cells cofilin was found to be mostly phosphorylated, and stimulation with EGF, which activates PLCγ induced dephosphorylation and activation of cofilin, which matched with early transient barbed end formation during a biphasic actin polymerisation process (Mouneimne et al., 2004). In addition, Nishita *et al.* have reported that in cultured cells, insulin-induced activation of PI3K signalling stimulated cofilin dephosphorylation and its localisation to membrane protrusions through PI3K-dependent regulation of SSH activity (Nishita et al., 2004). However, the acute regulation of cofilin phosphorylation seems to vary by cell type, since in some cells stimulation induces changes in the net phospho-cofilin levels, while in other cells a significant increase in

phospho-cofilin turnover is observed (Arai and Atomi, 2003), indicating the complexity of the regulatory mechanism. Thus, currently it is not clear whether a lack of kinase activity is sufficient to cause a decrease in cofilin phosphorylation that can results in cofilin activation, or whether phosphatase activity is also necessary. Differences between cell types can complicate the analysis because the level of G-actin or F-actin *in vivo* at the start of an experiment might also dictate the outcome.

The ability of eukaryotic cells to control and coordinate cortical actin filament-based protrusive activity suggests the existence of cellular machinery that monitors and regulates actin filament levels. In the previous chapter, I adopted an unbiased approach, using 2D-DIGE to search for protein isoforms that are sensitive to RNAi-induced changes in actin cytoskeleton regulators and mediators of lamellipodia formation such as Rac, Cdc42, Arp3 and Abi with Hem. Cofilin phosphorylation at Ser3 was identified as a common response to the loss of expression of these proteins. In addition, pSer3-cofilin levels were also altered in opposing directions by changes in the level of PIP3, induced following PI3K and PTEN RNAi treatments. This data suggested that the level of cofilin phosphorylation is responsive to changes in actin organisation and is probably regulated by actin signalling events downstream of PIP3. Thus, the main aim of my work in this chapter was to examine the signalling mechanism behind the control of cofilin phosphorylation and its regulation of actin cytoskeleton in fly haemocytes.

6.2 The kinetics of cofilin phosphorylation and actin remodelling following an acute stimulation

Since I had observed opposite changes in the expression of cofilin phosphorylation in cells that lacked PI3K and PTEN when grown at steady state, my next aim was to examine the dynamics of cofilin phosphorylation in cells that undergo acute changes in actin cytoskeleton organisation, induced by activation of PI3K signalling. In Chapter 4, I identified insulin as a potent stimulus that activates PI3K signalling and dynamic actin remodelling (Figure 4.2, 4.9 and 4.13). Thus, an immunoblotting strategy was employed to test if cofilin phosphorylation is responsive to the acute

activation of PI3K signalling and to asses the dynamics of insulin-induced changes in cofilin phosphorylation. Firstly, serum-starved S2R+ cells were stimulated with insulin and cofilin phosphorylation was examined over a time course. Cofilin was phosphorylated transiently on Ser3 in response to insulin, gradually peaking at 30 minutes, after which it started to decline (Figure 6.2).

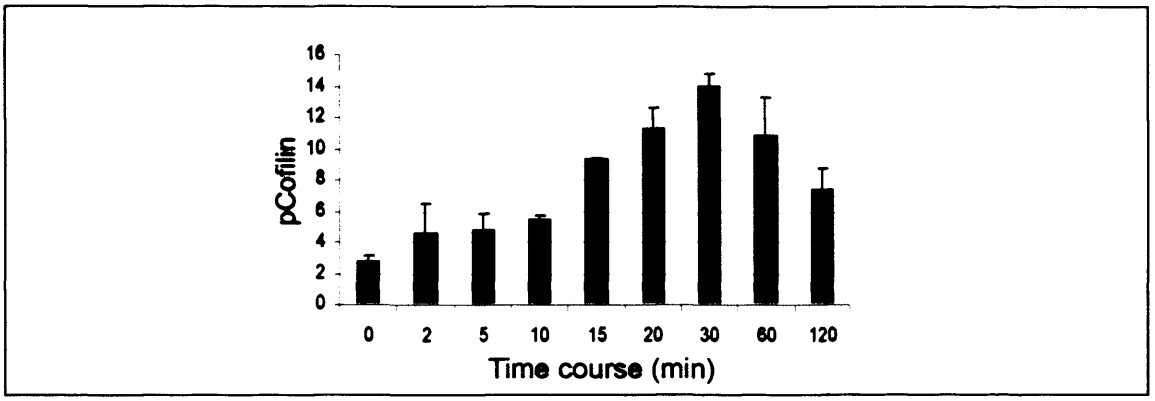

Figure 6.2 Time course of insulin-induced phosphorylation of cofilin. S2R+ cells were grown in serum-free medium overnight and stimulated with 10 μg/mL insulin for the indicated times. Protein lysates were subjected to western blotting with anti-phospho-Ser3 cofilin antibody. Blots were analysed by densitometry. Values represent the mean phospho-cofilin signal from two experiments after normalising with respect to β-actin levels.

Having observed that insulin can induce phosphorylation of cofilin, as well as the robust activation of the PI3K signalling, the next aim was to determine if this phosphorylation event was indeed PI3K-dependent. For this purpose, the PI3K inhibitor LY294002 was used to block insulin-dependent activation of PI3K. Pre-incubation of S2R+ cells with LY294002 significantly reduced the ability of insulin to induce cofilin phosphorylation, suggesting that this cofilin phosphorylation is dependent upon PI3K activity (Figure 6.3).

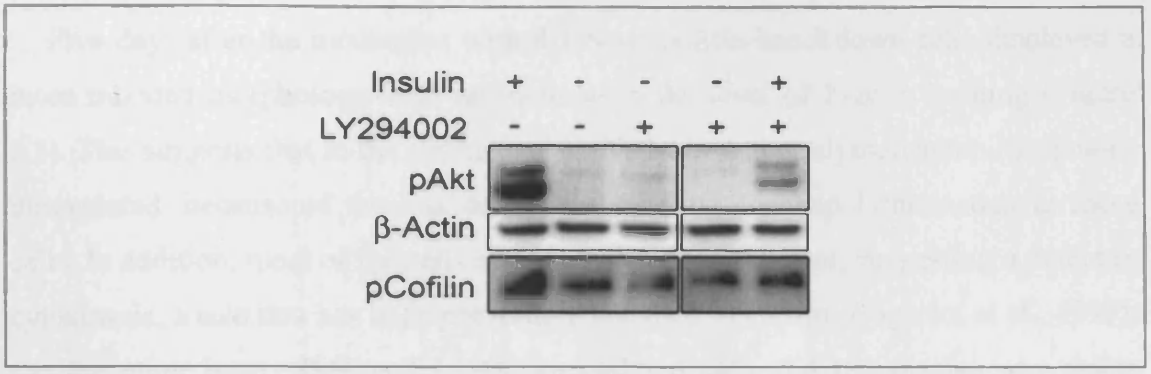

Figure 6.3 LY294002 blocks insulin-induced phosphorylation of cofilin. S2R+ cells were pre-treated for 20 minutes with LY294002 (100 μM) or DMSO vehicle prior to insulin treatment (10 μg/mL), or with neither 20 minutes. Lysates were prepared and subjected to western blotting analysis for pSer505-Akt, β-actin and pSer3-cofilin.

Since PIP3 production is required in S2R+ cells for the maintenance of an actin-rich cortex, the normal ruffling behaviour of resting cells, for insulin-induced actin polymerisation and for cofilin phosphorylation, my next task was to perform functional analysis of cofilin phosphorylation during acute actin signalling. LIMK and slingshot (SSH) have been previously identified in *Drosophila* and other systems as the major cofilin kinase and phosphatase, respectively. Thus, RNAi-induced knockdown of expression of both LIMK and SSH was first carried out and the levels of Ser3-cofilin phosphorylation were assessed in these cells. In addition, these cells and cofilin RNAi treated cells were stained with rhodamine phalloidin to examine the cytoskeleton organisation. It was observed that silencing of LIMK and SSH genes resulted in a decrease and increase in the basal phosphorylation of cofilin, respectively, confirming their known role in regulating cofilin phosphorylation (Figure 6.4). As expected, cells treated with dsRNA against cofilin displayed virtually no cofilin expression.

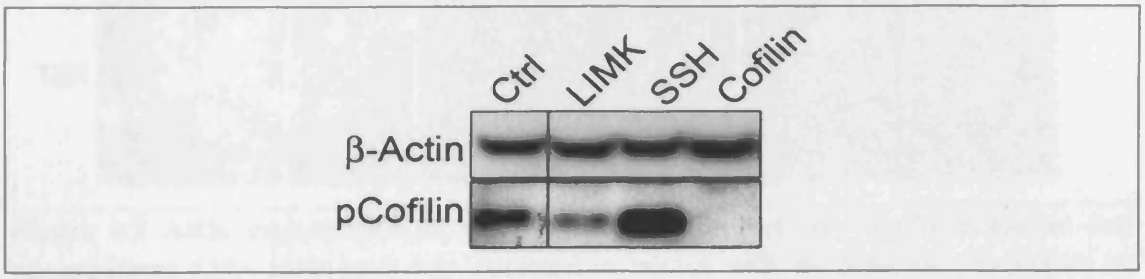

Figure 6.4 LIMK and slingshot are major regulators of cofilin phosphorylation. S2R+ cells were left untreated (Ctrl) or treated with dsRNAs for knockdown of expression of LIMK, SSH and cofilin for five days. Cells were lysed and pSer3-cofilin and β-actin levels were assessed by immunoblotting.

Five days after the incubation with dsRNAs, cofilin knockdown cells displayed a more rounded morphology with an increase in the level of F-actin staining (Figure 6.5). This suggests that in the absence of cofilin, new actin polymerisation continuous unregulated, because of the loss of F-actin severing and depolymerisation in these cells. In addition, most of the cells appeared to be multinuclear, suggesting a defect in cytokinesis, a role that has been previously assigned to cofilin (Nagaoka et al., 1995). On the other hand, SSH and LIMK knockdown cells did not display any major disturbance in F-actin organisation or gave any major distinguishable phenotype (Figure 6.5). They also did not display signs of altered cytokinesis as most of the cells were mononuclear.

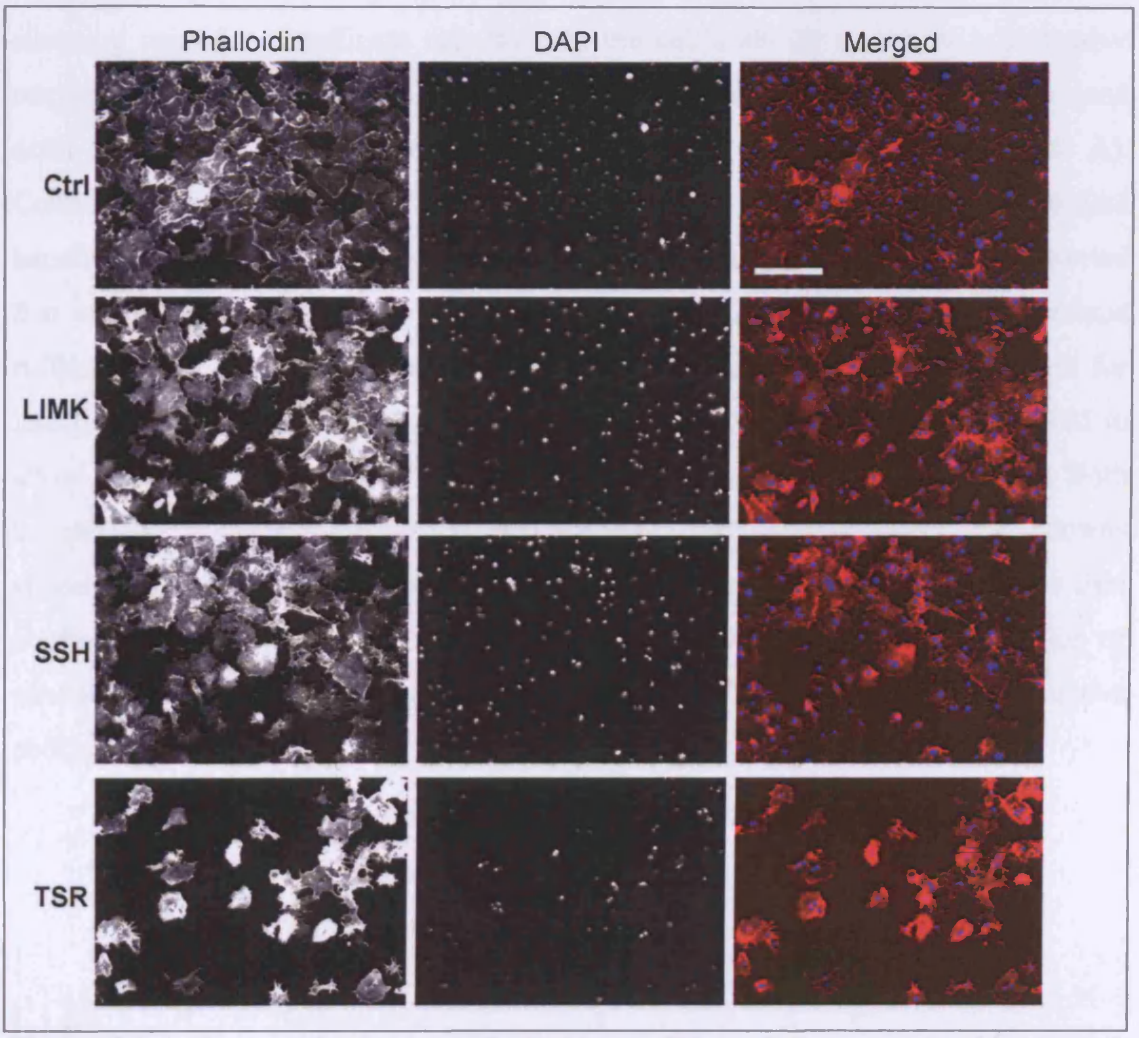

Figure 6.5 Actin organisation in cells lacking cofilin and its respective kinase and phosphatase. S2R+ cells were left untreated or treated with dsRNAs for knockdown of expression of LIMK, SSH and cofilin (TSR) for five days. On day five, cells were fixed and stained for filamentous actin with rhodamine phalloidin (1:1000) and nuclei with DAPI (1:5000). Images were acquired by a fluorescence microscopy at 20x magnification. Scale bar = 100 μm.

Next, to study of actin dynamics and membrane ruffling over time stimulation with insulin LIMK, SSH and cofilin RNAi-knockdown S2R+ cells were stained for actin before and after insulin stimulation and filmed by fluorescence time-lapse microscopy (Figure 6.6 A and B). For the microscpy, cells were infected with baculovirus harbouring a GFP-moesin actin-binding domain fusion protein. This experiment confirmed the previously observed cortical actin reorganisation of cortical actin and increased membrane ruffling in response to insulin stimulation (Figure 6.6 B). Cofilin knockdown cells were unable to reorganise actin or to ruffle in response to insulin, suggesting a role for cofilin in insulin-induced actin polymerisation and reorganisation, as previously described (Ghosh et al., 2004). In addition to this, SSH silencing caused a significant reduction in the cell's ability to mount a protrusive response to insulin stimulation (Figure 6.6 B). However, the overall morphology and actin distribution of SSH knockdown cells were maintained (Figure 6.6 A). Controversially, cells expressing reduced levels of LIMK had a well-defined cortical lamella and ruffled intensively before and after insulin stimulation. This suggested that active unphosphorylated cofilin is required for insulin-dependent membrane ruffling, rather than simply for depolymerisation. Genes known to be required for lamellipodia formation (Rac1 plus Rac2 and Arp3) were also silenced by RNAi to allow examination of their role in insulin-induced actin reorganisation. Both knockdowns displayed a common "starfish-like" phenotype, and both knockdowns appeared unable to mount a morphological response to insulin treatment. These data confirmed that the Rac-Arp2/3 signalling cascade is required for the generation of new F-actin-based protrusions downstream of acute PI3K signalling, as are active cofilin and SSH.

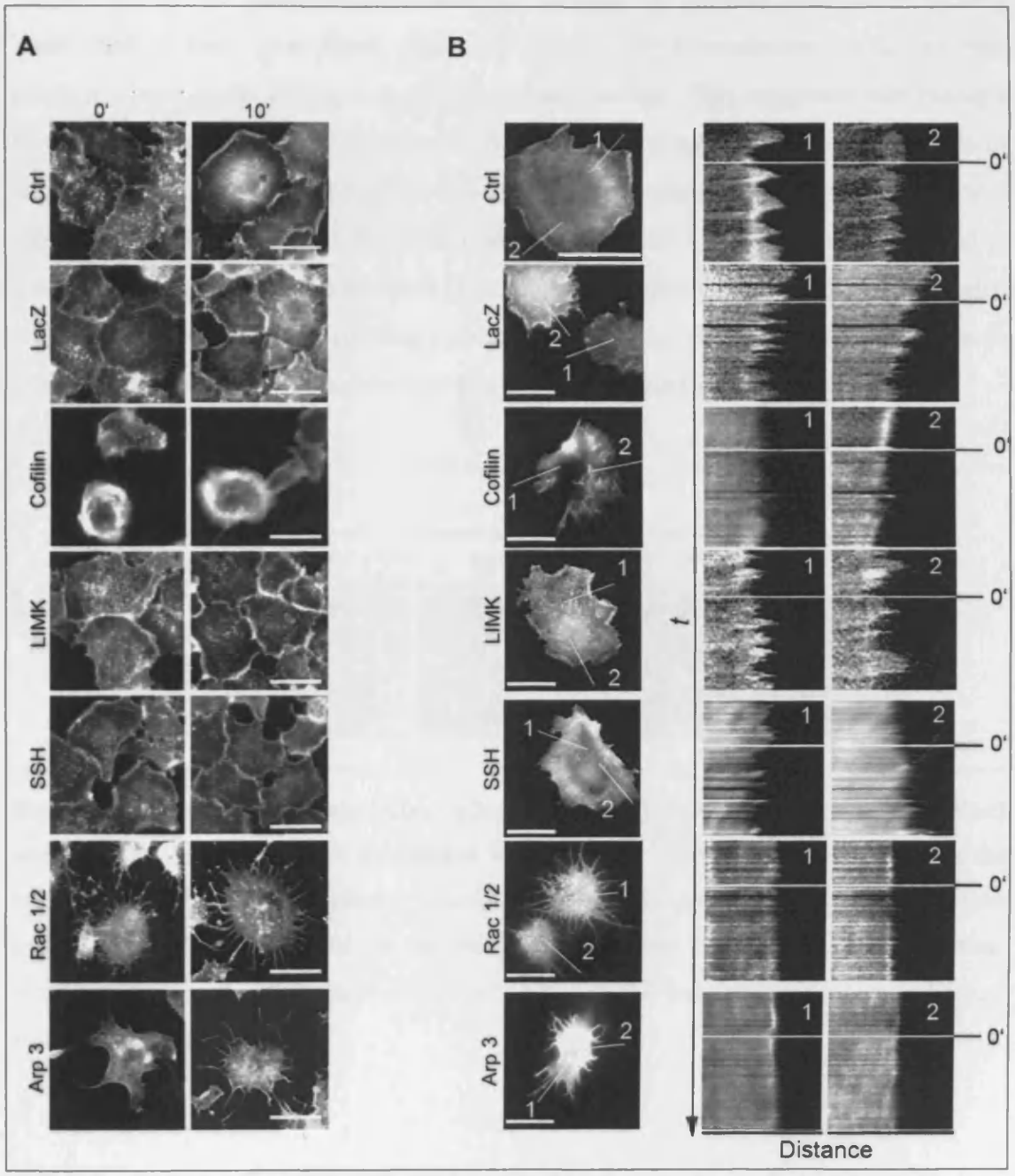

Figure 6.6 Functional analysis of cofilin during acute actin-signalling. A) Actin staining of RNAi-treated cells stimulated with insulin. S2R+ cells were incubated with dsRNAs for LacZ, cofilin, LIMK, SSH, Rac1+2 and Arp3 for five days. On day five, cells were treated with insulin (10 μg/mL) for 10 minutes. Cells were then fixed and stained for F-actin with rhodamine-palloidin. Scale bars = 50 μm. **B)** Visualisation of actin dynamics in dsRNA-treated cells using moesin-GFP. Snapshots of time–lapse movies just prior to insulin addition are shown on the left. Scale bars = 50 μm. The two lines used to generate the kymographs (right hand side) are indicated on the cell images. Actin reorganisation was filmed for 3 minutes before and for 10 minutes after the addition of insulin (10 μg/mL), with the white line on each kymograph representing the point of insulin addition (0'). Images are representative of two independent experiments.

The proteomic analysis presented in Chapter 5 showed that cells lacking lamellipodia (Rac1 plus Rac2, Cdc42 or Arp3 RNAi knockdown cells) express relatively high levels of inactive phosphorylated cofilin. This suggested that changes in cofilin phosphorylation might result directly from changes in the cellular levels of actin filaments and not as a response to upstream signalling events. In support of this idea, cells lacking Rac1 and Rac2 maintained high levels of cofilin phosphorylated at Ser3 independent of insulin addition (Figure 6.7). Similarly, SSH RNAi treated cells, which showed an impaired ruffling response, also did not display dynamic changes in cofilin phosphorylation in response to insulin/PI3K signalling (Figure 6.7).

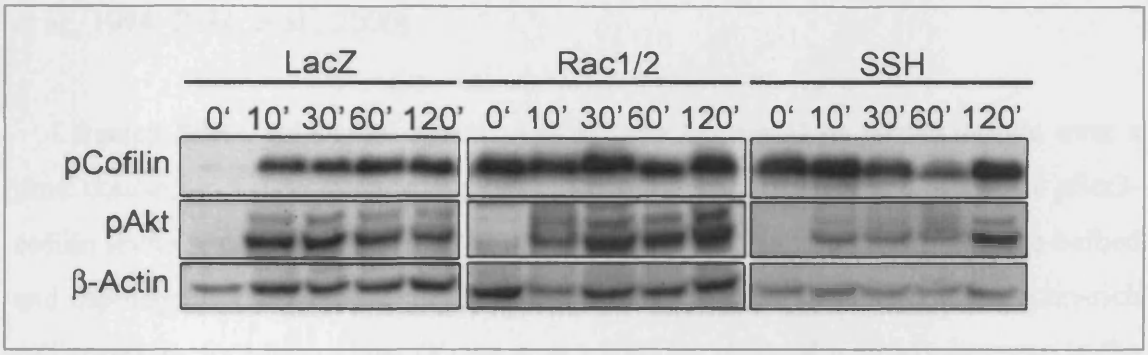

Figure 6.7 Immunoblotting analysis of pSer3-cofilin and pSer505-Akt in Rac1 plus Rac2 and SSH RNAi-treated cells stimulated with insulin. S2R+ cells were cultured in the presence of dsRNAs for knockdown of LacZ, Rac1 plus Rac2 and SSH for five days and then treated with 10 μg/mL insulin for the indicated times prior to lysis and immunoblotting. Samples were analysed for pSer3-cofilin, pSer505-Akt and β-actin. β-actin immunoblotting served as a loading control.

6.3 Regulation of cofilin phosphorylation by actin-targeting agents

To explore in more detail if changes in F-actin organisation are sufficient to directly alter Ser3-cofilin phosphorylation and activity, I used actin-targeting agents to induce acute changes in the relative levels of cellular F- and G-actin. Two different groups of actin-targeting agents were used, those that inhibit filament assembly or destabilise filaments (latrunculin B and cytochalasin D), and those that stabilise actin filaments (jasplakinolide). Latrunculin cytotoxins are potent inhibitors of actin filament formation, which are isolated from the Red Sea sponge *Negombata*

magnifica (Spector et al., 1983). The effect of latrunculin B on actin is strictly limited to actin monomer sequestering, which is due to the conformational changes caused in actin monomers after latruncluin B binding that prevents formation of stable interactions between monomers (Morton et al., 2000). Cytochalasin D is a cell permeable mycotoxin, which is isolated from *Zygosporium mansonii*. Cytochalasin D disrupts actin filaments and inhibits actin polymerisation by binding with high affinity to growing (barbed) ends of actin filaments, and preventing addition of monomers to these sites (Casella et al., 1981). Jasplakinolide is an actin filament stabiliser that is synthesised by the marine sponge *Jaspis johnsonis*. It is a potent inducer of actin polymerisation and decreases the amount of sequestered actin in the cytoplasm (Bubb et al., 1994; Bubb et al., 2000).

I treated S2R+ cells with latrunculin B, cytochalasin D or jasplakinolide over a time course, and then protein lysates were subjected to immunoblotting of pSer3-cofilin levels. Both the G-actin sequestering compound, latrunculin B, and the barbed end capping toxin, cytochalasin D (both previously found to eliminate the actin-rich cell cortex in fly haemocytes (Kiger et al., 2003)), induced a steady increase in the levels of cofilin phosphorylation over a period of 30-60 minutes (Figure 6.8). Conversely, in resting cells, where actin polymerisation is induced by jasplakinolide treatment, basal phosphorylation of cofilin at the Ser3 site was rapidly eliminated, within the first few minutes of the jasplakinolide treatment (Figure 6.8). Notably, total actin levels were unaffected by any of the treatments. These data further supported the idea of there being a direct correlation between the levels of actin filaments present in the cells and the level of phosphorylated cofilin.

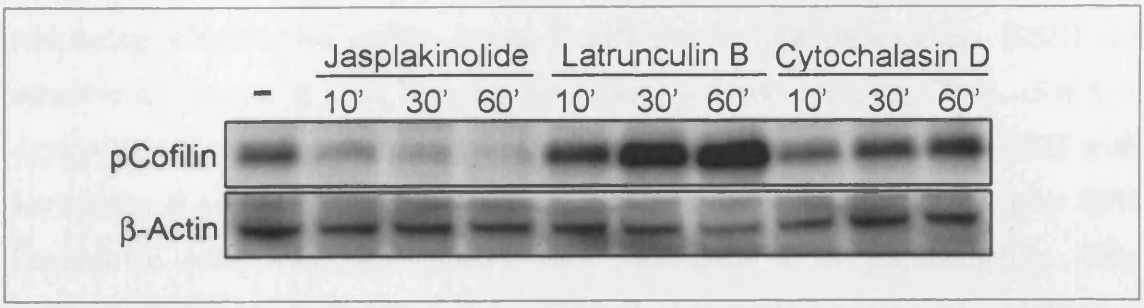

Figure 6.8 The effects of actin-targeting agents on cofilin phosphorylation. Resting S2R+ cells were treated with latrunculin B (1 μg/mL), cytochalasin D (2 μg/mL) or jasplakinolide (1 μg/mL) for the times indicated. Protein lysates were subjected for immunoblotting to pSer3-cofilin and β-actin.

However, to examine if cofilin phosphorylation is a process regulated downstream of PI3K signalling itself or it is regulated only by changes in the actin cytoskeleton in response to upstream signalling events, the actin drugs were tested in S2R+ cells subjected to insulin stimulation. This experiment showed that in latrunculin B pre-treated cells pSer3-cofilin levels stayed high in both insulin-treated and untreated cells. Importantly, the jasplakinolide treatment completely blocked pSer3-cofilin accumulation in response to insulin. Thus, dynamic changes in the cofilin phosphorylation downstream of PI3K signalling are likely to be entirely regulated through changes in cortical actin filaments present in the cells, even in the case of PI3K-mediated actin dynamics.

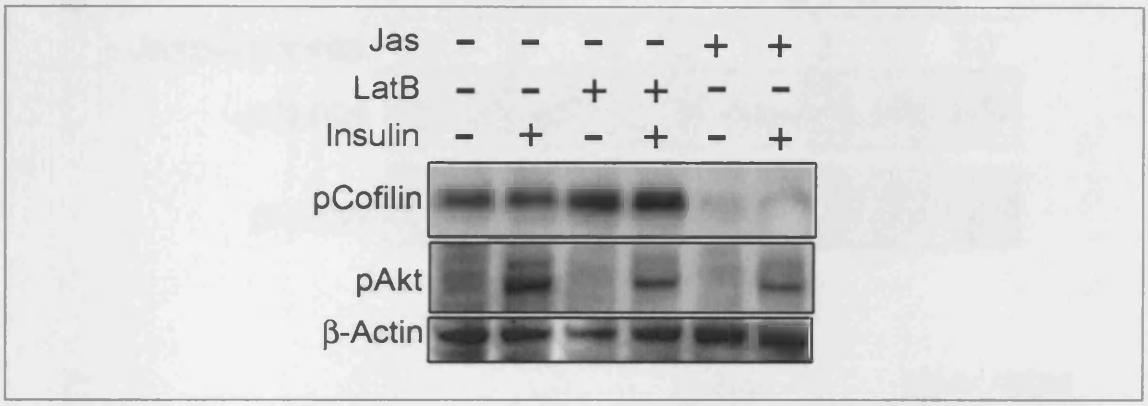

Figure 6.9 Cofilin phosphorylation is not directly regulated by insulin signalling, but is dependent upon insulin-induced actin reorganisation. S2R+ cells were pre-treated with latrunculin B (1 μg/mL) or jasplakinolide (1 μg/mL) followed by 20 minutes of insulin treatment (10 μg/mL) or vehicle alone. Protein lysates were subjected to immunoblotting for pSer3-cofilin, pSer505-Akt and β-actin.

In support of the hypothesis that there is an actin-dependent feedback control mechanism involving cofilin phosphorylation, I performed experiments aimed at addressing whether the cofilin kinase (LIMK) or cofilin phosphatase (SSH) are sensitive to changes in actin homeostasis during protrusive activity. Thus, after five days of RNAi treatment, I treated RNAi knockdown cells for LIMK and SSH with latrunculin B and jasplakinolide, respectively. In addition, double LIMK plus SSH knockdown cells were also treated with latranculin B or jasplakinolide. This experiment showed that cells lacking SSH blocked jasplakinolide-induced loss of cofilin phosphorylation (Figure 6.10 A). This loss of jasplakinolide response appeared not to be due to raised levels of pSer3 cofilin in SSH RNAi cells, as SSH appeared to

block the jasplakinolide-induced decrease in pSer3-cofilin levels in cells also lacking LIMK (Figure 6.10 B).

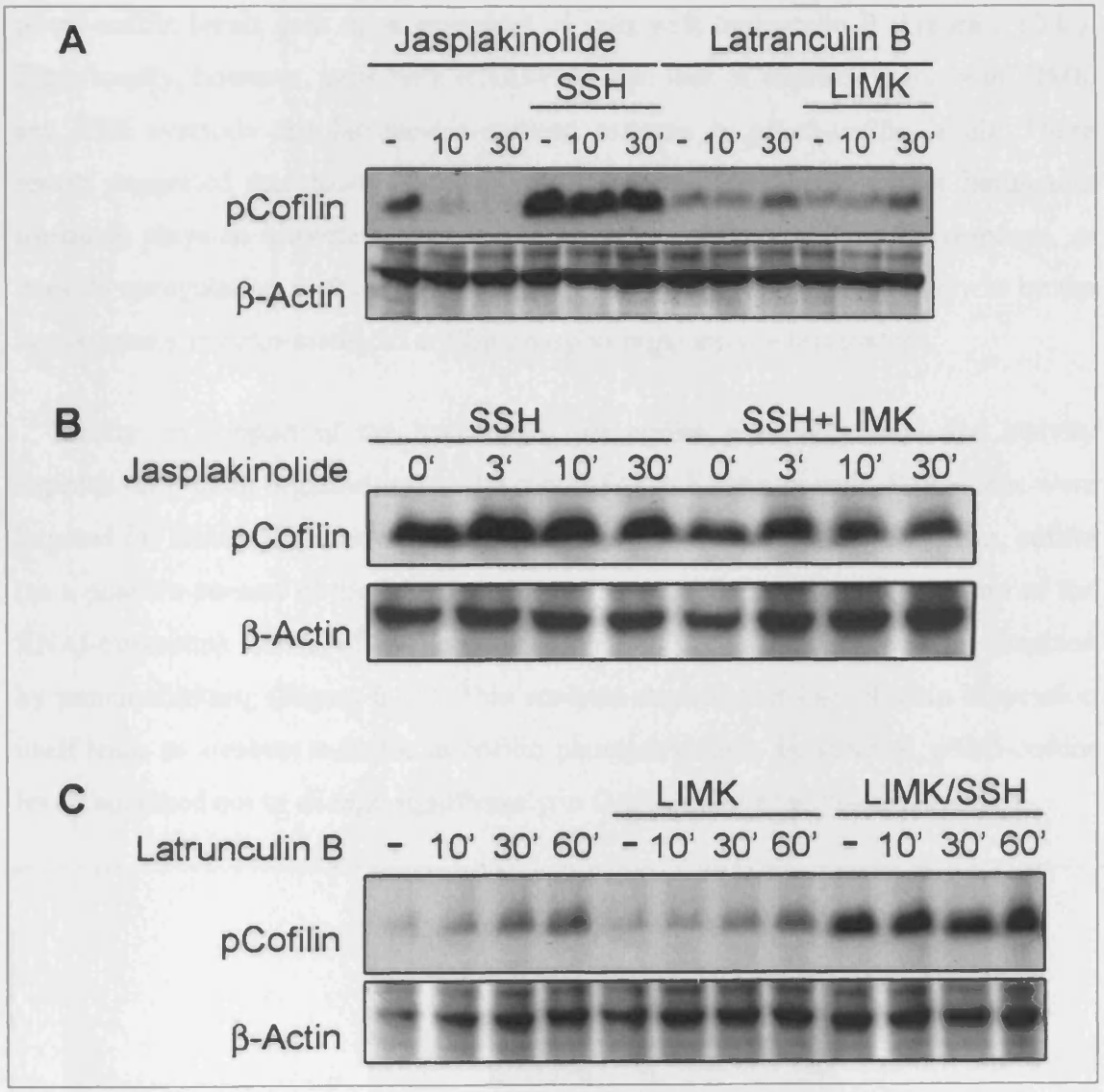

Figure 6.10 Slingshot is the major regulator of actin-dependent cofilin phosphorylation. **(A)** SSH RNAi blocks jasplakinolide-induced loss of cofilin phosphorylation. Control S2R+ cells and cells treated with dsRNA for knockdown of expression of SSH were treated with jasplakinolide (1 μg/mL) for the times indicated and pSer3-cofilin and β-actin levels assessed in the lysates by immunoblotting. **(B)** LIMK RNAi does not reverse SSH RNAi blockade of jasplakinolide-induced loss of cofilin phosphorylation. SSH and SSH plus LIMK RNAi cells were treated with jasplakinolide (1 μg/mL) for the indicated times and pSer3-cofilin and β-actin levels were assessed in lysates by immunoblotting. **(C)** The effect of LIMK and SSH on latrunculin B-induced cofilin-phosphorylation. Control, LIMK and LIMK plus SSH RNAi-treated cells were treated with latrunculin B (1 μg/mL) for the indicated times and pSer3-cofilin and β-actin levels in lysates were determined by immunoblotting.

By contrast, although RNAi-induced silencing of LIMK significantly reduced the overall levels of pSer3-cofilin, it was unable to suppress completely the changes in pSer3-cofilin levels seen upon treatment of cells with latrunculin B (Figure 6.10 C). Significantly, however, cells with RNAi-mediated loss of expression for both LIMK and SSH overrode this latrunculin-induced increase in pSer3-cofilin levels. These results suggested that downregulation of SSH phosphatase activity after latrunculin treatment plays an important role in the regulation of the pSer3-cofilin response, as does its upregulation in the presence of jasplakinolide. Thus, SSH is likely to be the key regulator in actin-mediated cofilin phospho-regulation in this system.

Finally, in support of the hypothesis that cofilin phosphorylation and activity depends on F-actin organisation or the ratio of G to F actin in cells, S2R+ cells were targeted for RNAi-mediated knockdown of expression of actin, CAP, profilin, cofilin (as a positive control of the RNAi-treatment) and LacZ (as a negative control of the RNAi-treatment). Levels of cofilin phosphorylation in each knockdown were assessed by immunoblotting (Figure 6.11). This analysis showed that loss of actin expression itself leads to a robust increase in cofilin phosphorylation. In addition, pSer3-cofilin levels appeared not to change significantly in CAP and profilin knockdown cells.

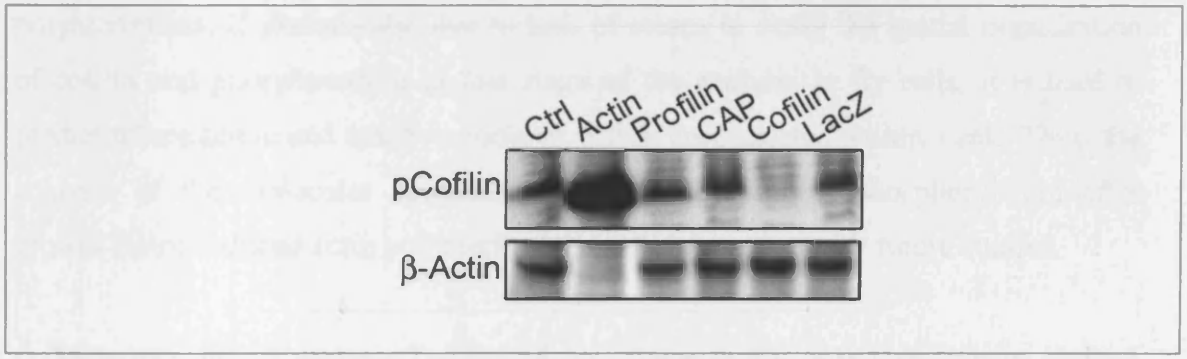

Figure 6.11 Cofilin phosphorylation in cells with loss of actin, CAP and profilin expression. pSer3 cofilin and β-actin levels were determined by immunoblotting in lysates of control (untreated) cells and cells treated with dsRNA targeting actin, profiling, CAP, cofilin and LacZ.

6.5 Conclusions

The work reported in this chapter was carried out to examine the signalling mechanisms by which cofilin phosphorylation is regulated. The results showed that cofilin phosphorylation is regulated directly by changes in actin cytoskeleton that are driven by the signalling events upstream of actin and other actin binding proteins. Cortical actin polymerisation that drives membrane ruffling requires active cofilin, which can sever actin filaments, to provide new growing sites on F-actin, and can depolymerise F-actin to restore the G-actin pool, thereby facilitating actin recycling during dynamic changes in actin reorganisation. With this in mind, and knowing that insulin-induced cortical actin polymerisation and membrane ruffling were PI3K-dependent events, cofilin phosphorylation was examined under conditions of acute PI3K stimulation. I observed that cofilin phosphorylation is transiently induced upon insulin stimulation and this event was found to be PI3K-dependent. This was a surprising result, as the processes of actin polymerisation and cofilin phosphorylation were separated in time. Since actin polymerisation and PI3K activity peaked in the early minutes of the stimulation, whilst cofilin phosphorylation peaked later at 30 minutes, it would be expected that cofilin is unphosphorylated and active during actin polymerisation. Unfortunately, due to lack of means to study the spatial organisation of cofilin and phosphocofilin at this stage of the analysis in fly cells, it is hard to predict where active and inactive pools of cofilin are localised within a cell. Thus, the analysis of the molecular mechanism that governs cofilin phosphorylation after growth factor-induced actin polymerisation could be a subject for future studies.

Moreover, in my analysis I observed that active cofilin was required for cortical actin polymerisation and membrane protrusions, since LIMK knockdown cells, where expression of inactive phosphorylated cofilin was found to be suppressed, displayed high basal cortical actin polymerisation that was further increased in response to insulin treatment. On the other hand, SSH silenced cells, where levels of inactive phosphorylated cofilin were significantly higher, had limited ability to mount a protrusive response to insulin stimulation, even though gross cellular morphology and actin organisation were preserved. Cofilin knockdown cells, although they had high levels filamentous actin, were not able to mount protrusive response to insulin

stimulation, due to the possibility that no free G-actin is available for insulin-induced actin polymerisation. Furthermore, Rac1 plus Rac2 knockdown cells, which displayed high cofilin phosphorylation, were also unable to mount a morphological response to insulin treatment. All these results suggested to me that cofilin activity depends on upstream events controlled by small GTPases that drive actin polymerisation. A big surprise came from analysis of Arp3 RNAi-silenced cells, which like the Rac1 plus Rac2 knockdown cells, displayed a "starfish-like" phenotype with high levels of phosphorylated cofilin, and did not ruffle in response to insulin. Current knowledge about actin cytoskeleton signalling suggests that Arp2/3 complex and cofilin are functionally distinct towards regulating actin cytoskeleton dynamics. However, no reports exist about direct feed-back regulation mechanism between these proteins. In addition, both SSH and Rac1 plus Rac2 knockdown cells did not change the level of phosphorylated cofilin with insulin, suggesting that SSH is sensitive to filamentous actin dynamics and changes in F-actin induced by upstream signalling event. Thus, the data here suggested that cofilin phosphorylation/ dephosphorylation is dependent directly upon the changes in the F-actin dynamics. This hypothesis is in contrast to that based on several other studies where cofilin phosphorylation was reported to be regulated as a direct result of activation of LIMK or inactivation of SSH induced by Rho-family GTPase activity (Yang et al., 1998; Agnew et al., 1995; Soosairajah et al., 2005).

To address the role of actin-dependent changes in mediating cofilin phosphorylation, I examined the effects of actin toxins on the cofilin phosphorylation in resting S2R+ cells. As previously reported in several studies and detected in my own experiments reported here, cofilin phosphorylation was induced upon treatment with G-actin sequestering or F-actin depolymerisation. On the other hand, cofilin was dephosphorylated upon jasplakinolide-induced polymerisation of F-actin. However, I did observe that insulin did not increase cofilin phosphorylation in cells pre-treated with jasplakinolide, furthermore proving that cofilin phosphorylation is not directly regulated by the upstream signalling events that derived from activated PI3K signalling, but is directly regulated by F-actin reorganisation. Thus, I propose SSH, which can bind actin filaments (Tanaka et al., 2005), to be the key regulator of this dynamic cofilin phospho-regulation and the sensor of changes in filamentous actin

levels in S2R+ cells. This conclusion came from examining the contribution of the kinase and the phosphatase in affecting the change in cofilin phosphorylation induced upon altering the levels of filamentous actin. LIMK and SSH dsRNA were applied to reduce the rate of both forward and backward reactions. This analysis revealed that SSH knockdown was able to block the jasplakinolide-induced decrease in pSer3-cofilin levels in cells, and this effect was also observed in the cells lacking both SSH and LIMK. On the other hand, although RNAi-induced silencing of LIMK reduced the overall levels of pSer3-cofilin, it was unable to fully suppress changes in pSer3-cofilin levels seen upon treatment of cells with latrunculin B. Furthermore, addition of SSH dsRNA to LIMK RNAi cells blocked this latrunculin B-induced increase in pSer3-cofilin levels. This result suggests that the downregulation of SSH phosphatase activity after latrunculin treatment plays an important role in the regulation of the pSer3-cofilin response, as does its upregulation in the presence of jasplakinolide.

Finally, RNAi-induced silencing of actin also induced a robust increase in cofilin phosphorylation. This confirms the link between actin filaments and pSer3-cofilin, and suggests that free cofilin could serve as a substrate for constantly active LIMK in cells. Importantly, it also demonstrates that G-actin is not required for a change in F/G actin levels to be translated into change in the extent of cofilin phosphorylation. In addition, CAP and profilin knockdown cells showed no change in the cofilin phosphorylation. Recently it has been reported that both profilin and CAP work synergistically to drive nucleotide exchange (Bertling et al., 2007). Thus, I propose that both CAP and profilin induce exchange of G-actin-ADP into G-actin-ATP to release cofilin from the inhibitory complex with ADP-actin monomers, thus promoting actin turnover in fly haemocytes. In the absence of profilin and CAP, nucleoide exchange on G-actin is possibly limited, further blocking dissociation of cofilin from G-actin-ADP complex and limiting cofilin phosphorylation by LIMK, as well limiting the actin polymerisation. Under these conditions, both the kinase and the phosphatase are limited in their action, as LIMK can phosphorylate only free cofilin, and SSH activity is also decreased due to blocked actin polymerisation. However, to define the exact role of CAP and profilin in the cofilin phosphorylation more work is required and that could be a goal for further examination.

In summary, the work in this chapter suggests that although both LIMK and SSH contribute to the regulation of cofilin phosphorylation, in S2R+ cells, SSH can be assigned as a major regulator in the cofilin phosphorylation as changes in the filamentous actin found to be responsible for dynamic changes in cofilin phosphorylation are mediated through actin-dependent SSH activity.

Chapter 7: DISCUSSION AND FUTURE DIRECTIONS

Soon after completion of the first maps of the human genome by the Human Genome Project and the private company Celera in June 2001, the scientific community found itself in the 'post-genomic era' - where proteomics had taken a prominent position. Proteomics involves not only the systematic separation and cataloguing of all proteins produced in an organism, but also the study of how proteins are regulated, change structure and interact with other proteins and molecules, how they regulate biological pathways and cell processes and perhaps most importantly how protein changes can give rise to disease. Studying proteomes in detail is a challenging task, as the proteome differs from cell to cell in an organism and constantly changes as a consequence of responses to internal regulation and the environment. Since it was proposed that proteomic studies are key to understanding disease, and also in linked drug target discovery, it came as no surprise that many academic institutions, and biotechnology, computer and software companies around the world rushed to pour knowledge, expertise, resources and capital into this new research field. While this was happening, the process and technology of RNA interference were discovered. RNAi is a powerful genomic technology that allows analysis of gene function by post-transcriptional silencing of specific target genes and looking at how cellular function is perturbed.

For the studies described in my thesis, I have used a combination of technologies which includes a proteomic strategy based on 2D-DIGE and MS, and RNAi-mediated gene silencing, to identify targets of PI3K and Rho-GTPases signalling. I then further combined this RNAi strategy with biochemical and cell biology analysis to follow up on the role of the identified targets in the regulation of actin cytoskeleton dynamics. PI3K signalling is involved in the regulation of several important cellular processes

including cell survival, proliferation, growth and metabolism (Vanhaesebroeck et al., 2001). Deregulation of this pathway can lead to alterations in this very important signalling pathway that have been implicated in the origin and progression of diseases such as cancer, auto-immune disorders and diabetes. The complexity of changes in the activity of the PI3K signalling pathway arises as a result of interactions with other signalling pathways such as those involving the Rho family small GTPases, Ras/MAPK and JAK/STAT, which are involved in a complex signalling network that allows a cell to respond appropriately to different stimuli. Identifying the components of these signalling networks and understanding the control mechanisms and cross-talk that occurs between interacting signalling pathways, is a major challenge in cell signal transduction study. In my research program I was interested in exploring cross-talk between the PI3K and small GTPases signalling pathways and how it regulates the actin cytoskeleton and alters cell biology that is dependent on this system.

Initially, I used 2D gel-based proteomic and immunoblotting techniques in a functional proteomic analysis to detect and identify putative targets of the PI3K signalling pathway. Application of PI3K inhibitors and the use of kinase specific substrate antibodies, which recognized phosphorylation motifs for Akt, PDK1 and PKC showed that phosphorylation of several kinase substrates depends upon EGF-induced activation of PI3K signalling in mammary luminal epithelial cells HB4a. However, it was difficult to predict which proteins were changing from this analysis. The combination of 2D-DIGE and 2D immunoblotting, aimed at determining the substrates whose phosphorylation was changing upon PI3K–specific activation, also appeared not to be ideal strategy for functional protein analysis since observed changes in protein expression in 2D-DIGE analysis could not be matched to kinase-specific substrate detection by the immunoblotting technique often related to lack of reagents. However, some revealing targets, such as intermediate cytoskeleton filaments (cytokeratin 7 and cytokeratin 8), and membrane-cytoskeleton linkers (moesin and ezrin) were found in my work, to be differentially expressed upon EGF stimulation in HB4a cells, which implies a reliance on alterations in the cytoskeletal organisation and cell-to-cell contact in these cells to effect physiological changes .

Since this human cell model was not ideal for many functional studies to study PI3K-dependent actin cytoskeleton reorganisation, a fly cell model, which had many other advantages, was developed instead. In Chapter 4, I showed that insulin was able to activate PI3K signalling in haemocytes, a process where I used PI3K inhibitors to define growth factor induced changes in cell shape and dynamics of the cytoskeleton of *Drosophila* haemocytes. I also monitored the insulin-mediated alterations in the actin cytoskeleton using time lapse microscopy, immunostaining and immunoblotting techniques. These experiments showed that insulin activates the PI3K signalling pathway, and subsequently mediates actin reorganisation producing increased membrane ruffling and protrusive activity at the cell edges. The PI3K inhibitors, LY294002 and wortmannin, were used to show that these effects on the actin cytoskeleton were dependent upon PI3K activity. It is important to mention that this Chemical Genetic approach, as some workers call it, has its limitations; because these inhibitors used may also target other kinases. As I proposed earlier, the study of PI3K-dependent actin reorganisation could well be extended by using more specific small molecule inhibitors that have been developed in recent years or by employing specific RNAi-mediated gene targeting. Most importantly, work that I developed has established a model cell system in which to study PI3K dependent signalling events and was the first dissection of PI3K-actin signalling in *Drosophila* haemocytes. My study also follows closely a recent report by Wood *et al.* of a role for PI3K in cell motility during fly development (Wood et al., 2006)

Using this *Drosophila* cell system, my next goal was to examine the biochemical mechanisms that allow PI3K to regulate changes in the actin cytoskeleton, and to test if this process is mediated by cross-talk with small GTPases, as has been suggested to be take place in other cell models. In this work I applied genomic and proteomic techniques in parallel. I used an RNAi "loss-of-function" approach in combination with quantitative 2D-DIGE to carry out differential protein expression analysis of RNAi- targeted cells. dsRNAs were used for disruption of the translation of selective target genes involved in PI3K signalling, Rho family small GTPase-mediated signalling and actin-binding proteins. The proteomic technique appeared to be ideal for monitoring changes in cytoskeletal proteins that have high cellular copy numbers. Through fluorometric scanning of gels, run with mixtures of control and treated

samples, and cell lysates differentially tagged with dye fluorphores, differential protein expression profiles were quantified. I used mass spectrometry for the identification of certain proteins differentially expressed between control and RNAi treatments, and the identity of these proteins, as well as changes in their expression was validated by immunoblotting, where antibodies were available. During the work I identified a number of proteins and tried to link their effects in these experiments to their putative role in signal pathways. Among these proteins most were abundant cytoskeletal proteins, metabolic and redox enzymes. In parallel, I examined changes in the cell morphology (actin cytoskeleton) using fluorescence microscopy. My data showed that the combination of 2D-DIGE and mass spectrometry can be a powerful platform for protein expression profiling, and I was even able to detect changes in the phosphorylation of one targeted protein. In addition, the changes in the proteome I found were reflected in changes in the cellular phenotype of the knockdowns. For example, in PTEN knockdown cells which appeared to have an increased cell size, and alterations in the filamentous actin, which are presumably related to defects in adhesion, profiling of the proteome showed that some proteins that are involved in the regulation of redox homeostasis, protein synthesis and actin cytoskeleton organisation were differentially expressed. Also I found that cells where there was a loss of expression of the actin depolymerising protein cofilin, appeared to have high levels of filamentous actin, while cells lacking a protein that drives actin nucleation and branch polymerisation had "the star-fish" actin phenotype. There were however several limitations to this proteomic approach, such as that imposed by the extent of protein separation, the low protein identification rate caused by several practical problems including sensitivity, the difficulty in matching differential protein expression between gel runs, all of which limited the depth of the analysis. During the course of this study, several other methods have been developed which use protein labelling and mass spectrometry for large scale quantitative and qualitative analysis of proteomes. Strategies such as iCAT (cysteine based labels) or iTRAQ (amino group labels) tagging of sample proteins or peptides *in vitro*; or SILAC - labelling of proteins with light and heavy amino acids (containing deuterium instead of H, ^{13}C instead of ^{12}C, or ^{15}N instead of ^{14}N) *in vivo*, could be used as a step forward in continuing the type of proteomic profiling of RNAi-silenced cells that has been carried out here. For example, the power of RNAi technique to choose genes for studying, could easily

allow the experiments to be extended to profiling and quantifying the proteomes of cells that lack the GEFs or GAPs, or even transcription/translation factors, the design would be varied depending on which aspect of cell signalling is to be addressed. In addition, new work which followed the dynamics of cell signalling events in time, after an acute stimulation (with insulin, for example) would increase the power of the analysis and could lead to identification of additional targets. These labelling strategies combined with sample purification and MS protein identification have proven to be more powerful, sensitive and specific ways to identify differences in protein expression profiles, and PTMs, when two or more conditions are compared (Mann, 2006). The availability on new highly sensitive mass spectrometers with modern LC front ends would also change dramatically the utility of the approach.

In the last part of this thesis, I focused my work on an exploration of the nature of the regulation of cellular cofilin activity which is known to be determined in part by its phosphorylation on Ser3. Significantly, phosphorylation of cofilin on this evolutionarily highly conserved residue prevents the binding of cofilin to actin filaments, completely inhibiting its ability to promote filament disassembly (Bamburg, 1999). Cofilin was selected as an interesting target for further functional analysis as it appeared to be a signalling node regulated by both PI3K and Rho-family small GTPases. Cofilin phosphorylation was identified as being differentially modulated in opposite ways in PI3K- and PTEN-silenced cells, but was unaffected by RNAi-induced silencing of Ras and Akt, suggesting that PI3K regulates cofilin phosphorylation through a signalling cascade independent of Akt. In addition, phospho-cofilin was also expressed more highly in cells where the expression of genes that promote actin nucleation/polymerisation and lamellipodia formation (Cdc42, Rac1 and Rac2) had been silenced. These results came as a surprise to me since previous studies have suggested that Rac activates LIMK to induce cofilin phosphorylation and inhibition. (Yang et al., 1998; Arber et al., 1998). Moreover, cofilin phosphorylation has been seen to be upregulated in Arp3 knockdown cells, where lamellipodia and the underlying cortical actin network are also lost (Biyasheva et al., 2004; Kunda et al., 2003), suggesting that cofilin phosphorylation is probably regulated by the dynamic changes in the actin cytoskeleton in response to signalling

downstream of PIP3 generation (Firtel and Chung, 2000), rather than through a direct signalling pathway. In this model, LIMK would found to be constitutively active.

In addition, it has been reported that even though levels of pSer3-cofilin can respond to PI3K signalling as suggested by the analysis in steady state and observed in other systems (Mouneimne et al., 2004; Nishita et al., 2004), there was evidence in my work that indicated that the observed changes in cofilin phosphorylation status were unlikely to mediate PI3K-induced actin remodelling. First, I found that active dephosphorylated cofilin was required for mounting protrusive dynamics of the actin cytoskeleton. Second, I showed that the morphogenetic response to insulin was unaffected by the loss of LIMK, the kinase responsible for cofilin phosphorylation in this and other systems (Arber et al., 1998; Yang et al., 1998), suggesting that an increase in cofilin phosphorylation is not required for cytoskeletal remodelling during the initial protrusive response. Third, I found that PI3K signalling, cortical actin accumulation and membrane ruffling all occurred within the first few seconds or minutes of insulin addition, whilst an increase in cofilin phosphorylation was delayed. Fourthly, in SSH and Rac RNAi cells, which are unable to generate protrusions, I found that pSer3-cofilin levels remained at a constant and elevated level following insulin stimulation, as would be predicted by such a model. Lastly, it is clear from the literature that the relationship between PI3K-signalling and cofilin phosphorylation varies widely across the different systems in which it has been analysed (Mouneimne et al., 2004; Nishita et al., 2004; Song et al., 2006). Taken together these data suggested an alternative model in which changes in cofilin phosphorylation occur as a result of the downstream effect of PI3K-induced changes in actin filament formation, and favouring a molecular mechanism in which the cofilin phosphatase, SSH, is the key regulator of cofilin phosphorylation which responds to changes in filamentous actin. To examine this hypothesis, where I directly perturbed actin cytoskeleton dynamics and the ratio of G- and F-actin by using actin toxins on cells, I found that cofilin phosphorylation changed in response to changes in the F/G actin ratio induced by these toxins. For example, in cells treated with latrunculin B or cytochalasin D, which induce rapid loss of filamentous actin (Kiger et al., 2003), I found that pSer3-cofilin levels were increased. Conversely in cells treated with the jasplakinolide, which induces ectopic actin filament formation, I saw a relatively rapid and complete

loss of the pSer3-cofilin signal. Moreover, I was able to show that jasplakinolide also could block the ability of insulin to induce cofilin phosphorylation in these cells. Taken together these data indicated to me that actin remodelling is required for dynamic changes in the level of Ser3-cofilin phosphorylation, and that acute changes in F-actin levels are sufficient to alter the cofilin phosphorylation status. Since the increase in cofilin phosphorylation is observed in cells with a paucity of cortical actin filaments, this would limit the rate of filament severing and depolymerisation. Conversely, cofilin is activated in cells with excess actin filaments, thereby maintaining the monomeric actin pool. This suggests to me that dynamic changes in cofilin phosphorylation are required for maintenance of actin filament homeostasis such that actin protrusive activity would be self-limiting. It also suggests there is a sensor that can measure changes in actin filament levels. Four recent studies have sought to implicate cofilin phosphatase SSH as mediating this role, by showing that SSH is activated through binding to actin filaments (Nagata-Ohashi et al., 2004; Soosairajah et al., 2005; Tanaka et al., 2005; Yamamoto et al., 2006).In support of this, my data shows that SSH is likely to be the key regulator of pSer3-cofilin levels in S2R+ cells, since it was required for dynamic changes in pSer3-cofilin levels in response to insulin, and because the kinetics of loss of cofilin phosphorylation following jasplakinolide treatment were more rapid than the effects of latrunculin B. Furthermore, I found that SSH RNAi suppressed both jasplakinolide and latrunculin induced changes in pSer3-cofilin, whereas on its own LIMK RNAi did not produce this effect. Also it is important that RNAi-mediated silencing of actin increased the level of cofilin phosphorylation, meaning that it is unlikely that G-actin levels play a significant role in driving the change in pSer3-cofilin levels that takes place following perturbation of the F/G actin ratio. Finally, limiting the potential for nucleotide exchange on actin monomers by RNAi-mediated silencing of profilin and CAP probably blocks both LIMK and SSH activities, as a limited pool of actin-ATP would be available for polymerisation required for SSH activity and no free cofilin would be available for phosphorylation by LIMK. Thus, in conclusion it appears to me that the binding of SSH to actin filaments acts as a sensor of relative F actin levels.

To reconcile the role of cofilin in the formation of actin-dependent protrusions in S2R+ cells with the observed changes in pSer3-cofilin I found following an acute

PI3K response, I suggested the following scenario (Figure 7.1): Following insulin addition, PI3K is activated within the first few minutes, causing the conversion of PIP2 to PIP3 within the inner leaflet of the plasma membrane. This activates Rac, possibly through the association of an unidentified PH domain-containing Rac-GEF with PIP3, leading to the nucleation of Arp2/3-dependent actin filaments at the cell cortex with subsequent filament elongation and protrusion formation. In these cells, active non-phosphorylated cofilin, at the cell front edge, depolymerises existing ADP-actin filaments to replenish the actin monomer pool and to generate uncapped barbed actin filament ends for new elongation. Thus, the balance between G-actin and F-actin is quickly moved towards F-actin, and cofilin released from G-actin is quickly phosphorylated by constitutively active LIMK. Thus, at the early stages, before significant levels of new actin filaments have been formed, low level SSH activity will act, in opposition to the effects of LIMK, to maintain a limited pool of active cofilin that is sufficient to remodel the existing actin filament network. Later, as new actin filaments accumulate and the PI3K signal declines at ~30 minutes, SSH activity will come to dominate, through its association with actin filaments and, perhaps, through its inhibition of LIMK (Soosairajah et al., 2005). This effect will reduce cofilin phosphorylation and help to restore the F-actin/G-actin equilibrium. I would like to suggest that this dynamic regulation helps to generate the cell's robust but self-limiting actin filament response to acute actin-signalling. In the context of a graded extracellular signal in the developing embryo (Wood et al., 2006), a similar system could act over spatially distinct regions of the cell to facilitate chemotaxis by coordinating the polymerisation of actin filaments at the cell front, with their disassembly at the cell rear. Thus, the next goal will be to examine the proposed model for cofilin regulation *in vivo*.

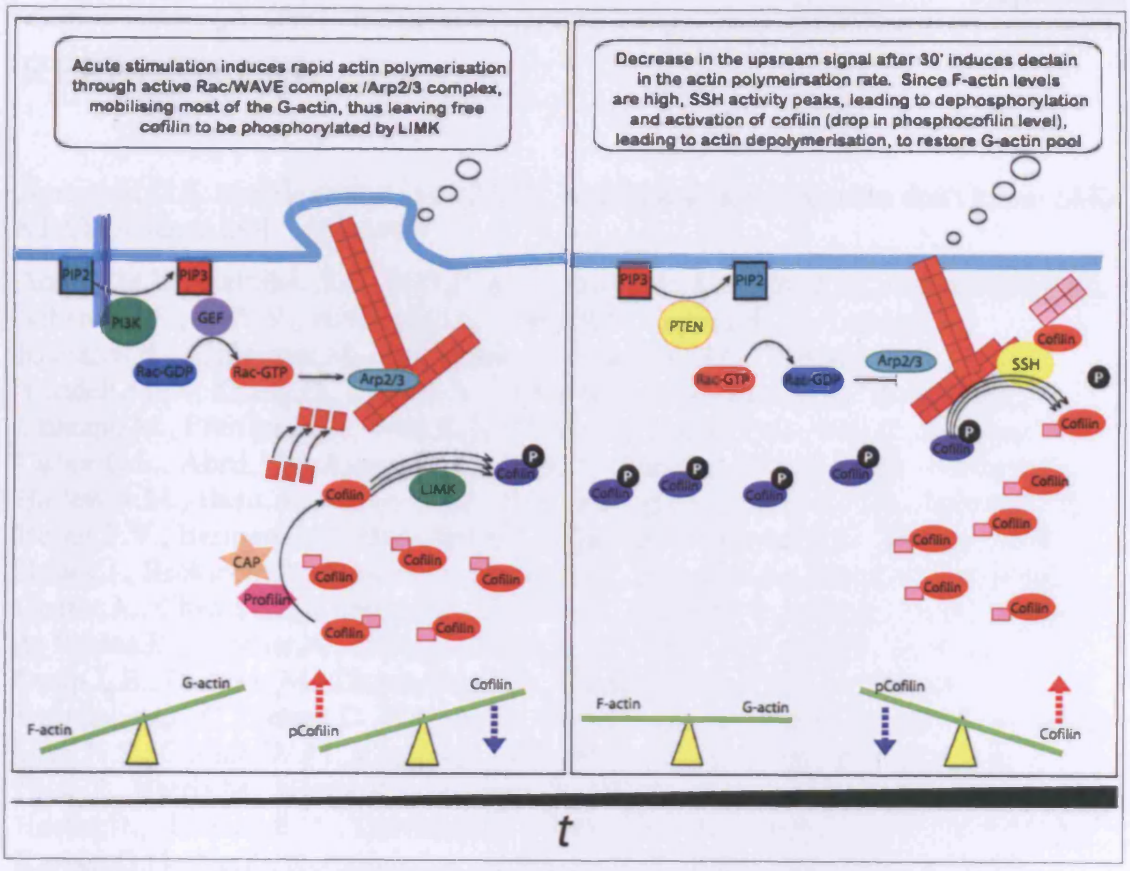

Figure 7.1 Dynamic changes in cofilin phosphorylation upon acute stimulation are dictated by F-actin-dependent changes in SSH activity.

Finally, I would like to conclude that the research work I have presented here shows that using a combination of techniques, genomic and proteomic, for studying cell signalling pathways, is a powerful approach to help address specific biological questions in Cell Biology. As the proteomic profile can be reflected by the cell phenotype, the combination of genomic and proteomic analysis provides more detailed information about the molecular mechanisms involved in cellular processes. Moreover, as in any proteomic profiling study where large databases are often generated, the real challenge arises when the data needs to be integrated in a meaningful way that could represent functional and biochemical properties of proteins involved in specific cell signalling pathways or networks.

REFERENCES:

Aaronson,D.S. and Horvath,C.M. (2002). A road map for those who don't know JAK-STAT. Science 296, 1653-1655.

Adams,M.D., Celniker,S.E., Holt,R.A., Evans,C.A., Gocayne,J.D., Amanatides,P.G., Scherer,S.E., Li,P.W., Hoskins,R.A., Galle,R.F., George,R.A., Lewis,S.E., Richards,S., Ashburner,M., Henderson,S.N., Sutton,G.G., Wortman,J.R., Yandell,M.D., Zhang,Q., Chen,L.X., Brandon,R.C., Rogers,Y.H., Blazej,R.G., Champe,M., Pfeiffer,B.D., Wan,K.H., Doyle,C., Baxter,E.G., Helt,G., Nelson,C.R., Gabor,G.L., Abril,J.F., Agbayani,A., An,H.J., Andrews-Pfannkoch,C., Baldwin,D., Ballew,R.M., Basu,A., Baxendale,J., Bayraktaroglu,L., Beasley,E.M., Beeson,K.Y., Benos,P.V., Berman,B.P., Bhandari,D., Bolshakov,S., Borkova,D., Botchan,M.R., Bouck,J., Brokstein,P., Brottier,P., Burtis,K.C., Busam,D.A., Butler,H., Cadieu,E., Center,A., Chandra,I., Cherry,J.M., Cawley,S., Dahlke,C., Davenport,L.B., Davies,P., de Pablos,B., Delcher,A., Deng,Z., Mays,A.D., Dew,I., Dietz,S.M., Dodson,K., Doup,L.E., Downes,M., Dugan-Rocha,S., Dunkov,B.C., Dunn,P., Durbin,K.J., Evangelista,C.C., Ferraz,C., Ferriera,S., Fleischmann,W., Fosler,C., Gabrielian,A.E., Garg,N.S., Gelbart,W.M., Glasser,K., Glodek,A., Gong,F., Gorrell,J.H., Gu,Z., Guan,P., Harris,M., Harris,N.L., Harvey,D., Heiman,T.J., Hernandez,J.R., Houck,J., Hostin,D., Houston,K.A., Howland,T.J., Wei,M.H., Ibegwam,C., Jalali,M., Kalush,F., Karpen,G.H., Ke,Z., Kennison,J.A., Ketchum,K.A., Kimmel,B.E., Kodira,C.D., Kraft,C., Kravitz,S., Kulp,D., Lai,Z., Lasko,P., Lei,Y., Levitsky,A.A., Li,J., Li,Z., Liang,Y., Lin,X., Liu,X., Mattei,B., McIntosh,T.C., McLeod,M.P., McPherson,D., Merkulov,G., Milshina,N.V., Mobarry,C., Morris,J., Moshrefi,A., Mount,S.M., Moy,M., Murphy,B., Murphy,L., Muzny,D.M., Nelson,D.L., Nelson,D.R., Nelson,K.A., Nixon,K., Nusskern,D.R., Pacleb,J.M., Palazzolo,M., Pittman,G.S., Pan,S., Pollard,J., Puri,V., Reese,M.G., Reinert,K., Remington,K., Saunders,R.D., Scheeler,F., Shen,H., Shue,B.C., Siden-Kiamos,I., Simpson,M., Skupski,M.P., Smith,T., Spier,E., Spradling,A.C., Stapleton,M., Strong,R., Sun,E., Svirskas,R., Tector,C., Turner,R., Venter,E., Wang,A.H., Wang,X., Wang,Z.Y., Wassarman,D.A., Weinstock,G.M., Weissenbach,J., Williams,S.M., WoodageT, Worley,K.C., Wu,D., Yang,S., Yao,Q.A., Ye,J., Yeh,R.F., Zaveri,J.S., Zhan,M., Zhang,G., Zhao,Q., Zheng,L., Zheng,X.H., Zhong,F.N., Zhong,W., Zhou,X., Zhu,S., Zhu,X., Smith,H.O., Gibbs,R.A., Myers,E.W., Rubin,G.M., and Venter,J.C. (2000). The genome sequence of Drosophila melanogaster. Science 287, 2185-2195.

Aderem,A. and Underhill,D.M. (1999). Mechanisms of phagocytosis in macrophages. Annu. Rev. Immunol. 17, 593-623.

Aebersold,R. and Mann,M. (2003). Mass spectrometry-based proteomics. Nature 422, 198-207.

Agnew,B.J., Minamide,L.S., and Bamburg,J.R. (1995). Reactivation of phosphorylated actin depolymerizing factor and identification of the regulatory site. J. Biol. Chem. 270, 17582-17587.

Allen,L.A., Allgood,J.A., Han,X., and Wittine,L.M. (2005). Phosphoinositide3-kinase regulates actin polymerization during delayed phagocytosis of Helicobacter pylori. J. Leukoc. Biol. 78, 220-230.

Alonso,A., Sasin,J., Bottini,N., Friedberg,I., Friedberg,I., Osterman,A., Godzik,A., Hunter,T., Dixon,J., and Mustelin,T. (2004). Protein tyrosine phosphatases in the human genome. Cell 117, 699-711.

Altomare,D.A. and Testa,J.R. (2005). Perturbations of the AKT signaling pathway in human cancer. Oncogene 24, 7455-7464.

Amann,K.J. and Pollard,T.D. (2001). The Arp2/3 complex nucleates actin filament branches from the sides of pre-existing filaments. Nat. Cell Biol. 3, 306-310.

Amano,M., Chihara,K., Kimura,K., Fukata,Y., Nakamura,N., Matsuura,Y., and Kaibuchi,K. (1997). Formation of actin stress fibers and focal adhesions enhanced by Rho-kinase. Science 275, 1308-1311.

Arai,H. and Atomi,Y. (2003). Suppression of cofilin phosphorylation in insulin-stimulated ruffling membrane formation in KB cells. Cell Struct. Funct. 28, 41-48.

Araki,N., Johnson,M.T., and Swanson,J.A. (1996). A role for phosphoinositide 3-kinase in the completion of macropinocytosis and phagocytosis by macrophages. J. Cell Biol. 135, 1249-1260.

Arber,S., Barbayannis,F.A., Hanser,H., Schneider,C., Stanyon,C.A., Bernard,O., and Caroni,P. (1998). Regulation of actin dynamics through phosphorylation of cofilin by LIM-kinase. Nature 393, 805-809.

Arcaro,A. and Wymann,M.P. (1993a). Wortmannin is a potent phosphatidylinositol 3-kinase inhibitor: the role of phosphatidylinositol 3,4,5-trisphosphate in neutrophil responses. Biochem. J. 296 (Pt 2), 297-301.

Arcaro,A. and Wymann,M.P. (1993b). Wortmannin is a potent phosphatidylinositol 3-kinase inhibitor: the role of phosphatidylinositol 3,4,5-trisphosphate in neutrophil responses. Biochem. J. 296 (Pt 2), 297-301.

Bain,J., McLauchlan,H., Elliott,M., and Cohen,P. (2003). The specificities of protein kinase inhibitors: an update. Biochem. J. 371, 199-204.

Balendran,A., Casamayor,A., Deak,M., Paterson,A., Gaffney,P., Currie,R., Downes,C.P., and Alessi,D.R. (1999). PDK1 acquires PDK2 activity in the presence of a synthetic peptide derived from the carboxyl terminus of PRK2. Curr. Biol. 9, 393-404.

Ballou,L.M., Luther,H., and Thomas,G. (1991). MAP2 kinase and 70K S6 kinase lie on distinct signalling pathways. Nature 349, 348-350.

Bamburg,J.R. (1999). Proteins of the ADF/cofilin family: essential regulators of actin dynamics. Annu. Rev. Cell Dev. Biol. 15, 185-230.

Bamburg,J.R., Harris,H.E., and Weeds,A.G. (1980). Partial purification and characterization of an actin depolymerizing factor from brain. FEBS Lett. 121, 178-182.

Bar-Sagi,D. and Hall,A. (2000). Ras and Rho GTPases: a family reunion. Cell 103, 227-238.

Bartz,S. and Jackson,A.L. (2005). How will RNAi facilitate drug development? Sci. STKE. 2005, e39.

Beretta,L., Gingras,A.C., Svitkin,Y.V., Hall,M.N., and Sonenberg,N. (1996). Rapamycin blocks the phosphorylation of 4E-BP1 and inhibits cap-dependent initiation of translation. EMBO J. 15, 658-664.

Berggren,K., Chernokalskaya,E., Steinberg,T.H., Kemper,C., Lopez,M.F., Diwu,Z., Haugland,R.P., and Patton,W.F. (2000). Background-free, high sensitivity staining of proteins in one- and two-dimensional sodium dodecyl sulfate-polyacrylamide gels using a luminescent ruthenium complex. Electrophoresis 21, 2509-2521.

Bernards,A. (2003). GAPs galore! A survey of putative Ras superfamily GTPase activating proteins in man and Drosophila. Biochim. Biophys. Acta 1603, 47-82.

Bertling,E., Quintero-Monzon,O., Mattila,P.K., Goode,B.L., and Lappalainen,P. (2007). Mechanism and biological role of profilin-Srv2/CAP interaction. J. Cell Sci. 120, 1225-1234.

Biaglow,J.E., Cerniglia,G., Tuttle,S., Bakanauskas,V., Stevens,C., and McKenna,G. (1997). Effect of oncogene transformation of rat embryo cells on cellular oxygen consumption and glycolysis. Biochem. Biophys. Res. Commun. 235, 739-742.

Billuart,P. and Chelly,J. (2003). From fragile X mental retardation protein to Rac1 GTPase: new insights from Fly CYFIP. Neuron 38, 843-845.

Bogdan,S. and Klambt,C. (2003). Kette regulates actin dynamics and genetically interacts with Wave and Wasp. Development 130, 4427-4437.

Bompard,G. and Caron,E. (2004). Regulation of WASP/WAVE proteins: making a long story short. J. Cell Biol. 166, 957-962.

Brunet,A., Bonni,A., Zigmond,M.J., Lin,M.Z., Juo,P., Hu,L.S., Anderson,M.J., Arden,K.C., Blenis,J., and Greenberg,M.E. (1999). Akt promotes cell survival by phosphorylating and inhibiting a Forkhead transcription factor. Cell 96, 857-868.

Brunn,G.J., Williams,J., Sabers,C., Wiederrecht,G., Lawrence,J.C., Jr., and Abraham,R.T. (1996). Direct inhibition of the signaling functions of the mammalian target of rapamycin by the phosphoinositide 3-kinase inhibitors, wortmannin and LY294002. EMBO J. 15, 5256-5267.

Bubb,M.R., Senderowicz,A.M., Sausville,E.A., Duncan,K.L., and Korn,E.D. (1994). Jasplakinolide, a cytotoxic natural product, induces actin polymerization and competitively inhibits the binding of phalloidin to F-actin. J. Biol. Chem. 269, 14869-14871.

Bubb,M.R., Spector,I., Beyer,B.B., and Fosen,K.M. (2000). Effects of jasplakinolide on the kinetics of actin polymerization. An explanation for certain in vivo observations. J. Biol. Chem. 275, 5163-5170.

Byfield,M.P., Murray,J.T., and Backer,J.M. (2005). hVps34 is a nutrient-regulated lipid kinase required for activation of p70 S6 kinase. J. Biol. Chem. 280, 33076-33082.

Cantley,L.C. and Neel,B.G. (1999). New insights into tumor suppression: PTEN suppresses tumor formation by restraining the phosphoinositide 3-kinase/AKT pathway. Proc. Natl. Acad. Sci. U. S. A 96, 4240-4245.

Carlier,M.F., Laurent,V., Santolini,J., Melki,R., Didry,D., Xia,G.X., Hong,Y., Chua,N.H., and Pantaloni,D. (1997). Actin depolymerizing factor (ADF/cofilin)

enhances the rate of filament turnover: implication in actin-based motility. J. Cell Biol. 136, 1307-1322.

Carpentier,J.L., Fehlmann,M., Van Obberghen,E., Gorden,P., and Orci,L. (1985). Insulin receptor internalization and recycling: mechanism and significance. Biochimie 67, 1143-1145.

Casella,J.F., Flanagan,M.D., and Lin,S. (1981). Cytochalasin D inhibits actin polymerization and induces depolymerization of actin filaments formed during platelet shape change. Nature 293, 302-305.

Caudy,A.A., Myers,M., Hannon,G.J., and Hammond,S.M. (2002). Fragile X-related protein and VIG associate with the RNA interference machinery. Genes Dev. 16, 2491-2496.

Chan,H.L., Gharbi,S., Gaffney,P.R., Cramer,R., Waterfield,M.D., and Timms,J.F. (2005). Proteomic analysis of redox- and ErbB2-dependent changes in mammary luminal epithelial cells using cysteine- and lysine-labelling two-dimensional difference gel electrophoresis. Proteomics. 5, 2908-2926.

Chan,T.O., Rittenhouse,S.E., and Tsichlis,P.N. (1999). AKT/PKB and other D3 phosphoinositide-regulated kinases: kinase activation by phosphoinositide-dependent phosphorylation. Annu. Rev. Biochem. 68, 965-1014.

Chang,H.W., Aoki,M., Fruman,D., Auger,K.R., Bellacosa,A., Tsichlis,P.N., Cantley,L.C., Roberts,T.M., and Vogt,P.K. (1997). Transformation of chicken cells by the gene encoding the catalytic subunit of PI 3-kinase. Science 276, 1848-1850.

Chantry,D., Vojtek,A., Kashishian,A., Holtzman,D.A., Wood,C., Gray,P.W., Cooper,J.A., and Hoekstra,M.F. (1997). p110delta, a novel phosphatidylinositol 3-kinase catalytic subunit that associates with p85 and is expressed predominantly in leukocytes. J. Biol. Chem. 272, 19236-19241.

Cheng,J.Q., Lindsley,C.W., Cheng,G.Z., Yang,H., and Nicosia,S.V. (2005). The Akt/PKB pathway: molecular target for cancer drug discovery. Oncogene 24, 7482-7492.

Chiaradonna,F., Gaglio,D., Vanoni,M., and Alberghina,L. (2006). Expression of transforming K-Ras oncogene affects mitochondrial function and morphology in mouse fibroblasts. Biochim. Biophys. Acta 1757, 1338-1356.

Cho,N.K., Keyes,L., Johnson,E., Heller,J., Ryner,L., Karim,F., and Krasnow,M.A. (2002). Developmental control of blood cell migration by the Drosophila VEGF pathway. Cell 108, 865-876.

Clodi,M., Vollenweider,P., Klarlund,J., Nakashima,N., Martin,S., Czech,M.P., and Olefsky,J.M. (1998). Effects of general receptor for phosphoinositides 1 on insulin and insulin-like growth factor I-induced cytoskeletal rearrangement, glucose transporter-4 translocation, and deoxyribonucleic acid synthesis. Endocrinology 139, 4984-4990.

Cohen,P. and Frame,S. (2001). The renaissance of GSK3. Nat. Rev. Mol. Cell Biol. 2, 769-776.

Condeelis,J.S., Wyckoff,J.B., Bailly,M., Pestell,R., Lawrence,D., Backer,J., and Segall,J.E. (2001). Lamellipodia in invasion. Semin. Cancer Biol. 11, 119-128.

Coulombe,P.A. and Wong,P. (2004). Cytoplasmic intermediate filaments revealed as dynamic and multipurpose scaffolds. Nat. Cell Biol. 6, 699-706.

Crespo,P., Schuebel,K.E., Ostrom,A.A., Gutkind,J.S., and Bustelo,X.R. (1997). Phosphotyrosine-dependent activation of Rac-1 GDP/GTP exchange by the vav proto-oncogene product. Nature 385, 169-172.

Cross,D.A., Alessi,D.R., Cohen,P., Andjelkovich,M., and Hemmings,B.A. (1995). Inhibition of glycogen synthase kinase-3 by insulin mediated by protein kinase B. Nature 378, 785-789.

Cutillas,P.R., Khwaja,A., Graupera,M., Pearce,W., Gharbi,S., Waterfield,M., and Vanhaesebroeck,B. (2006). Ultrasensitive and absolute quantification of the phosphoinositide 3-kinase/Akt signal transduction pathway by mass spectrometry. Proc. Natl. Acad. Sci. U. S. A 103, 8959-8964.

Dalby,K.N., Morrice,N., Caudwell,F.B., Avruch,J., and Cohen,P. (1998). Identification of regulatory phosphorylation sites in mitogen-activated protein kinase (MAPK)-activated protein kinase-1a/p90rsk that are inducible by MAPK. J. Biol. Chem. 273, 1496-1505.

Dan,C., Kelly,A., Bernard,O., and Minden,A. (2001). Cytoskeletal changes regulated by the PAK4 serine/threonine kinase are mediated by LIM kinase 1 and cofilin. J. Biol. Chem. 276, 32115-32121.

Dasgupta,R. and Perrimon,N. (2004). Using RNAi to catch Drosophila genes in a web of interactions: insights into cancer research. Oncogene 23, 8359-8365.

Di Guglielmo,G.M., Drake,P.G., Baass,P.C., Authier,F., Posner,B.I., and Bergeron,J.J. (1998). Insulin receptor internalization and signalling. Mol. Cell Biochem. 182, 59-63.

Di Paolo,G. and De Camilli,P. (2006). Phosphoinositides in cell regulation and membrane dynamics. Nature 443, 651-657.

Diehl,J.A., Zindy,F., and Sherr,C.J. (1997). Inhibition of cyclin D1 phosphorylation on threonine-286 prevents its rapid degradation via the ubiquitin-proteasome pathway. Genes Dev. 11, 957-972.

Downward,J. (2004a). PI 3-kinase, Akt and cell survival. Semin. Cell Dev. Biol. 15, 177-182.

Downward,J. (2004b). RNA interference. BMJ 328, 1245-1248.

Duchek,P., Somogyi,K., Jekely,G., Beccari,S., and Rorth,P. (2001). Guidance of cell migration by the Drosophila PDGF/VEGF receptor. Cell 107, 17-26.

Dykxhoorn,D.M. and Lieberman,J. (2005). The silent revolution: RNA interference as basic biology, research tool, and therapeutic. Annu. Rev. Med. 56, 401-423.

Edwards,D.C., Sanders,L.C., Bokoch,G.M., and Gill,G.N. (1999). Activation of LIM-kinase by Pak1 couples Rac/Cdc42 GTPase signalling to actin cytoskeletal dynamics. Nat. Cell Biol. 1, 253-259.

Elstrom,R.L., Bauer,D.E., Buzzai,M., Karnauskas,R., Harris,M.H., Plas,D.R., Zhuang,H., Cinalli,R.M., Alavi,A., Rudin,C.M., and Thompson,C.B. (2004). Akt stimulates aerobic glycolysis in cancer cells. Cancer Res. 64, 3892-3899.

Enayati,A.A., Ranson,H., and Hemingway,J. (2005). Insect glutathione transferases and insecticide resistance. Insect Mol. Biol. 14, 3-8.

Engelman,J.A., Luo,J., and Cantley,L.C. (2006). The evolution of phosphatidylinositol 3-kinases as regulators of growth and metabolism. Nat. Rev. Genet. 7, 606-619.

Etienne-Manneville,S. and Hall,A. (2002). Rho GTPases in cell biology. Nature 420, 629-635.

Faix,J. and Grosse,R. (2006). Staying in shape with formins. Dev. Cell 10, 693-706.

Fehlmann,M., Carpentier,J.L., Van Obberghen,E., Freychet,P., Thamm,P., Saunders,D., Brandenburg,D., and Orci,L. (1982). Internalized insulin receptors are recycled to the cell surface in rat hepatocytes. Proc. Natl. Acad. Sci. U. S. A 79, 5921-5925.

Feng,J., Park,J., Cron,P., Hess,D., and Hemmings,B.A. (2004). Identification of a PKB/Akt hydrophobic motif Ser-473 kinase as DNA-dependent protein kinase. J. Biol. Chem. 279, 41189-41196.

Fenn,J.B., Mann,M., Meng,C.K., Wong,S.F., and Whitehouse,C.M. (1989). Electrospray ionization for mass spectrometry of large biomolecules. Science 246, 64-71.

Fire,A., Xu,S., Montgomery,M.K., Kostas,S.A., Driver,S.E., and Mello,C.C. (1998). Potent and specific genetic interference by double-stranded RNA in Caenorhabditis elegans. Nature 391, 806-811.

Franke,T.F., Hornik,C.P., Segev,L., Shostak,G.A., and Sugimoto,C. (2003). PI3K/Akt and apoptosis: size matters. Oncogene 22, 8983-8998.

Frankel,S. and Mooseker,M.S. (1996). The actin-related proteins. Curr. Opin. Cell Biol. 8, 30-37.

Fleming,I.N., Batty,I.H., Prescott,A.R., Gray,A., Kular,G.S., Stewart,H., and Downes,C.P. (2004). Inositol phospholipids regulate the guanine-nucleotide-exchange factor Tiam1 by facilitating its binding to the plasma membrane and regulating GDP/GTP exchange on Rac1. Biochem. J., 382, 857-865.

Friedman,A. and Perrimon,N. (2006). A functional RNAi screen for regulators of receptor tyrosine kinase and ERK signalling. Nature 444, 230-234.

Frodin,M. and Gammeltoft,S. (1999). Role and regulation of 90 kDa ribosomal S6 kinase (RSK) in signal transduction. Mol. Cell Endocrinol. 151, 65-77.

Frova,C. (2006). Glutathione transferases in the genomics era: new insights and perspectives. Biomol. Eng 23, 149-169.

Gaidarov,I., Smith,M.E., Domin,J., and Keen,J.H. (2001). The class II phosphoinositide 3-kinase C2alpha is activated by clathrin and regulates clathrin-mediated membrane trafficking. Mol. Cell 7, 443-449.

Gerke,V., Creutz,C.E., and Moss,S.E. (2005). Annexins: linking Ca2+ signalling to membrane dynamics. Nat. Rev. Mol. Cell Biol. 6, 449-461.

Gharbi,S., Gaffney,P., Yang,A., Zvelebil,M.J., Cramer,R., Waterfield,M.D., and Timms,J.F. (2002). Evaluation of two-dimensional differential gel electrophoresis for

proteomic expression analysis of a model breast cancer cell system. Mol. Cell Proteomics. 1, 91-98.

Gharbi,S.I., Zvelebil,M.J., Shuttleworth,S.J., Hancox,T., Saghir,N., Timms,J.F., and Waterfield,M.D. (2007). Exploring the specificity of the PI3K family inhibitor LY294002. Biochem. J.

Ghosh,M., Song,X., Mouneimne,G., Sidani,M., Lawrence,D.S., and Condeelis,J.S. (2004). Cofilin promotes actin polymerization and defines the direction of cell motility. Science 304, 743-746.

Gillooly,D.J., Simonsen,A., and Stenmark,H. (2001). Phosphoinositides and phagocytosis. J. Cell Biol. 155, 15-17.

Gingras,A.C., Kennedy,S.G., O'Leary,M.A., Sonenberg,N., and Hay,N. (1998). 4E-BP1, a repressor of mRNA translation, is phosphorylated and inactivated by the Akt(PKB) signaling pathway. Genes Dev. 12, 502-513.

Gohla,A., Birkenfeld,J., and Bokoch,G.M. (2005). Chronophin, a novel HAD-type serine protein phosphatase, regulates cofilin-dependent actin dynamics. Nat. Cell Biol. 7, 21-29.

Goley,E.D. and Welch,M.D. (2006). The ARP2/3 complex: an actin nucleator comes of age. Nat. Rev. Mol. Cell Biol. 7, 713-726.

Gorg,A., Obermaier,C., Boguth,G., Harder,A., Scheibe,B., Wildgruber,R., and Weiss,W. (2000). The current state of two-dimensional electrophoresis with immobilized pH gradients. Electrophoresis 21, 1037-1053.

Goshima,K., Masuda,A., and Owaribe,K. (1984b). Insulin-induced formation of ruffling membranes of KB cells and its correlation with enhancement of amino acid transport. J. Cell Biol. 98, 801-809.

Goshima,K., Masuda,A., and Owaribe,K. (1984a). Insulin-induced formation of ruffling membranes of KB cells and its correlation with enhancement of amino acid transport. J. Cell Biol. 98, 801-809.

Gray,S.G., Stenfeldt,M., I, and De Meyts,P. (2003). The insulin-like growth factors and insulin-signalling systems: an appealing target for breast cancer therapy? Horm. Metab Res. 35, 857-871.

Grimm,D., Streetz,K.L., Jopling,C.L., Storm,T.A., Pandey,K., Davis,C.R., Marion,P., Salazar,F., and Kay,M.A. (2006). Fatality in mice due to oversaturation of cellular microRNA/short hairpin RNA pathways. Nature 441, 537-541.

Guy,G.R., Philip,R., and Tan,Y.H. (1994). Analysis of cellular phosphoproteins by two-dimensional gel electrophoresis: applications for cell signaling in normal and cancer cells. Electrophoresis 15, 417-440.

Hall,A. (1998). Rho GTPases and the actin cytoskeleton. Science 279, 509-514.

Hall,A. (2005). Rho GTPases and the control of cell behaviour. Biochem. Soc. Trans. 33, 891-895.

Hammond,S.M., Caudy,A.A., and Hannon,G.J. (2001). Post-transcriptional gene silencing by double-stranded RNA. Nat. Rev. Genet. 2, 110-119.

Han,J., Luby-Phelps,K., Das,B., Shu,X., Xia,Y., Mosteller,R.D., Krishna,U.M., Falck,J.R., White,M.A., and Broek,D. (1998). Role of substrates and products of PI 3-kinase in regulating activation of Rac-related guanosine triphosphatases by Vav. Science 279, 558-560.

Harbour,J.W., Luo,R.X., Dei,S.A., Postigo,A.A., and Dean,D.C. (1999). Cdk phosphorylation triggers sequential intramolecular interactions that progressively block Rb functions as cells move through G1. Cell 98, 859-869.

Hawkins,P.T., Eguinoa,A., Qiu,R.G., Stokoe,D., Cooke,F.T., Walters,R., Wennstrom,S., Claesson-Welsh,L., Evans,T., Symons,M., and . (1995). PDGF stimulates an increase in GTP-Rac via activation of phosphoinositide 3-kinase. Curr. Biol. 5, 393-403.

Hay,N. and Sonenberg,N. (2004). Upstream and downstream of mTOR. Genes Dev. 18, 1926-1945.

Heim,M.H. (1999). The Jak-STAT pathway: cytokine signalling from the receptor to the nucleus. J. Recept. Signal. Transduct. Res. 19, 75-120.

Hennessy,B.T., Smith,D.L., Ram,P.T., Lu,Y., and Mills,G.B. (2005). Exploiting the PI3K/AKT pathway for cancer drug discovery. Nat. Rev. Drug Discov. 4, 988-1004.

Hensbergen,P., Alewijnse,A., Kempenaar,J., van der Schors,R.C., Balog,C.A., Deelder,A., Beumer,G., Ponec,M., and Tensen,C.P. (2005). Proteomic profiling identifies an UV-induced activation of cofilin-1 and destrin in human epidermis. J. Invest Dermatol. 124, 818-824.

Henzel,W.J., Billeci,T.M., Stults,J.T., Wong,S.C., Grimley,C., and Watanabe,C. (1993). Identifying proteins from two-dimensional gels by molecular mass searching of peptide fragments in protein sequence databases. Proc. Natl. Acad. Sci. U. S. A 90, 5011-5015.

Higaki,M., Sakaue,H., Ogawa,W., Kasuga,M., and Shimokado,K. (1996). Phosphatidylinositol 3-kinase-independent signal transduction pathway for platelet-derived growth factor-induced chemotaxis. J. Biol. Chem. 271, 29342-29346.

Hillenkamp,F., Karas,M., Beavis,R.C., and Chait,B.T. (1991). Matrix-assisted laser desorption/ionization mass spectrometry of biopolymers. Anal. Chem. 63, 1193A-1203A.

Ho,H.Y., Rohatgi,R., Lebensohn,A.M., Le,M., Li,J., Gygi,S.P., and Kirschner,M.W. (2004). Toca-1 mediates Cdc42-dependent actin nucleation by activating the N-WASP-WIP complex. Cell 118, 203-216.

Ho,H.Y., Rohatgi,R., Ma,L., and Kirschner,M.W. (2001). CR16 forms a complex with N-WASP in brain and is a novel member of a conserved proline-rich actin-binding protein family. Proc. Natl. Acad. Sci. U. S. A 98, 11306-11311.

Hsieh,A.C., Bo,R., Manola,J., Vazquez,F., Bare,O., Khvorova,A., Scaringe,S., and Sellers,W.R. (2004). A library of siRNA duplexes targeting the phosphoinositide 3-kinase pathway: determinants of gene silencing for use in cell-based screens. Nucleic Acids Res. 32, 893-901.

Hunter,T. (1995). Protein kinases and phosphatases: the yin and yang of protein phosphorylation and signaling. Cell 80, 225-236.

Hunter,T. (2000). Signaling--2000 and beyond. Cell 100, 113-127.

Ibarra,N., Pollitt,A., and Insall,R.H. (2005). Regulation of actin assembly by SCAR/WAVE proteins. Biochem. Soc. Trans. 33, 1243-1246.

Innocenti,M., Frittoli,E., Ponzanelli,I., Falck,J.R., Brachmann,S.M., Di Fiore,P.P., and Scita,G. (2003). Phosphoinositide 3-kinase activates Rac by entering in a complex with Eps8, Abi1, and Sos-1. J. Cell Biol. 160, 17-23.

Innocenti,M., Zucconi,A., Disanza,A., Frittoli,E., Areces,L.B., Steffen,A., Stradal,T.E., Di Fiore,P.P., Carlier,M.F., and Scita,G. (2004). Abi1 is essential for the formation and activation of a WAVE2 signalling complex. Nat. Cell Biol. 6, 319-327.

Inoki,K., Li,Y., Zhu,T., Wu,J., and Guan,K.L. (2002). TSC2 is phosphorylated and inhibited by Akt and suppresses mTOR signalling. Nat. Cell Biol. 4, 648-657.

Insall,R.H. and Weiner,O.D. (2001). PIP3, PIP2, and cell movement--similar messages, different meanings? Dev. Cell 1, 743-747.

Jacinto,E., Loewith,R., Schmidt,A., Lin,S., Ruegg,M.A., Hall,A., and Hall,M.N. (2004). Mammalian TOR complex 2 controls the actin cytoskeleton and is rapamycin insensitive. Nat. Cell Biol. 6, 1122-1128.

Jaffe,A.B. and Hall,A. (2005). Rho GTPases: biochemistry and biology. Annu. Rev. Cell Dev. Biol. 21, 247-269.

James,P., Quadroni,M., Carafoli,E., and Gonnet,G. (1993). Protein identification by mass profile fingerprinting. Biochem. Biophys. Res. Commun. 195, 58-64.

Janmey,P.A. (1994). Phosphoinositides and calcium as regulators of cellular actin assembly and disassembly. Annu. Rev. Physiol 56, 169-191.

Jensen,O.N. (2004). Modification-specific proteomics: characterization of post-translational modifications by mass spectrometry. Curr. Opin. Chem. Biol. 8, 33-41.

Jimenez,C., Portela,R.A., Mellado,M., Rodriguez-Frade,J.M., Collard,J., Serrano,A., Martinez,A., Avila,J., and Carrera,A.C. (2000). Role of the PI3K regulatory subunit in the control of actin organization and cell migration. J. Cell Biol. 151, 249-262.

Jin,T., Zhang,N., Long,Y., Parent,C.A., and Devreotes,P.N. (2000). Localization of the G protein betagamma complex in living cells during chemotaxis. Science 287, 1034-1036.

Kanai,T., Takahashi,K., and Inoue,H. (2006). Three distinct-type glutathione S-transferases from Escherichia coli important for defense against oxidative stress. J. Biochem. (Tokyo) 140, 703-711.

Karas,M. and Hillenkamp,F. (1988). Laser desorption ionization of proteins with molecular masses exceeding 10,000 daltons. Anal. Chem. 60, 2299-2301.

Katso,R., Okkenhaug,K., Ahmadi,K., White,S., Timms,J., and Waterfield,M.D. (2001). Cellular function of phosphoinositide 3-kinases: implications for development, homeostasis, and cancer. Annu. Rev. Cell Dev. Biol. 17, 615-675.

Katso,R.M., Pardo,O.E., Palamidessi,A., Franz,C.M., Marinov,M., De Laurentiis,A., Downward,J., Scita,G., Ridley,A.J., Waterfield,M.D., and Arcaro,A. (2006). Phosphoinositide 3-Kinase C2beta regulates cytoskeletal organization and cell migration via Rac-dependent mechanisms. Mol. Biol. Cell 17, 3729-3744.

Kawada,N., Kristensen,D.B., Asahina,K., Nakatani,K., Minamiyama,Y., Seki,S., and Yoshizato,K. (2001). Characterization of a stellate cell activation-associated protein (STAP) with peroxidase activity found in rat hepatic stellate cells. J. Biol. Chem. 276, 25318-25323.

Khayat,Z.A., Tong,P., Yaworsky,K., Bloch,R.J., and Klip,A. (2000). Insulin-induced actin filament remodeling colocalizes actin with phosphatidylinositol 3-kinase and GLUT4 in L6 myotubes. J. Cell Sci. 113 Pt 2, 279-290.

Kiger,A., Baum,B., Jones,S., Jones,M., Coulson,A., Echeverri,C., and Perrimon,N. (2003). A functional genomic analysis of cell morphology using RNA interference. J. Biol. 2, 27.

Knight,J.B., Yamauchi,K., and Pessin,J.E. (1995). Divergent insulin and platelet-derived growth factor regulation of focal adhesion kinase (pp125FAK) tyrosine phosphorylation, and rearrangement of actin stress fibers. J. Biol. Chem. 270, 10199-10203.

Knight,Z.A., Gonzalez,B., Feldman,M.E., Zunder,E.R., Goldenberg,D.D., Williams,O., Loewith,R., Stokoe,D., Balla,A., Toth,B., Balla,T., Weiss,W.A., Williams,R.L., and Shokat,K.M. (2006). A pharmacological map of the PI3-K family defines a role for p110alpha in insulin signaling. Cell 125, 733-747.

Kobayashi,S., Shirai,T., Kiyokawa,E., Mochizuki,N., Matsuda,M., and Fukui,Y. (2001). Membrane recruitment of DOCK180 by binding to PtdIns(3,4,5)P3. Biochem. J. 354, 73-78.

Kotani,K., Yonezawa,K., Hara,K., Ueda,H., Kitamura,Y., Sakaue,H., Ando,A., Chavanieu,A., Calas,B., Grigorescu,F., and . (1994). Involvement of phosphoinositide 3-kinase in insulin- or IGF-1-induced membrane ruffling. EMBO J. 13, 2313-2321.

Kovacsovics,T.J., Bachelot,C., Toker,A., Vlahos,C.J., Duckworth,B., Cantley,L.C., and Hartwig,J.H. (1995). Phosphoinositide 3-kinase inhibition spares actin assembly in activating platelets but reverses platelet aggregation. J. Biol. Chem. 270, 11358-11366.

Koyasu,S. (2003). The role of PI3K in immune cells. Nat. Immunol. 4, 313-319.

Kozma,S.C. and Thomas,G. (2002). Regulation of cell size in growth, development and human disease: PI3K, PKB and S6K. Bioessays 24, 65-71.

Krieg,J. and Hunter,T. (1992). Identification of the two major epidermal growth factor-induced tyrosine phosphorylation sites in the microvillar core protein ezrin. J. Biol. Chem. 267, 19258-19265.

Kunda,P., Craig,G., Dominguez,V., and Baum,B. (2003). Abi, Sra1, and Kette control the stability and localization of SCAR/WAVE to regulate the formation of actin-based protrusions. Curr. Biol. 13, 1867-1875.

Kundra,V., Escobedo,J.A., Kazlauskas,A., Kim,H.K., Rhee,S.G., Williams,L.T., and Zetter,B.R. (1994). Regulation of chemotaxis by the platelet-derived growth factor receptor-beta. Nature 367, 474-476.

Kurokawa,K., Itoh,R.E., Yoshizaki,H., Nakamura,Y.O., and Matsuda,M. (2004). Coactivation of Rac1 and Cdc42 at lamellipodia and membrane ruffles induced by epidermal growth factor. Mol. Biol. Cell 15, 1003-1010.

Kurosu,H., Maehama,T., Okada,T., Yamamoto,T., Hoshino,S., Fukui,Y., Ui,M., Hazeki,O., and Katada,T. (1997). Heterodimeric phosphoinositide 3-kinase consisting of p85 and p110beta is synergistically activated by the betagamma subunits of G proteins and phosphotyrosyl peptide. J. Biol. Chem. 272, 24252-24256.

Kuruvilla,F.G. and Schreiber,S.L. (1999). The PIK-related kinases intercept conventional signaling pathways. Chem. Biol. 6, R129-R136.

Kwon,J., Lee,S.R., Yang,K.S., Ahn,Y., Kim,Y.J., Stadtman,E.R., and Rhee,S.G. (2004). Reversible oxidation and inactivation of the tumor suppressor PTEN in cells stimulated with peptide growth factors. Proc. Natl. Acad. Sci. U. S. A 101, 16419-16424.

Lang,P., Gesbert,F., Delespine-Carmagnat,M., Stancou,R., Pouchelet,M., and Bertoglio,J. (1996). Protein kinase A phosphorylation of RhoA mediates the morphological and functional effects of cyclic AMP in cytotoxic lymphocytes. EMBO J. 15, 510-519.

Larsen,M.R., Thingholm,T.E., Jensen,O.N., Roepstorff,P., and Jorgensen,T.J. (2005). Highly selective enrichment of phosphorylated peptides from peptide mixtures using titanium dioxide microcolumns. Mol. Cell Proteomics. 4, 873-886.

Lazarides,E. (1980). Intermediate filaments as mechanical integrators of cellular space. Nature 283, 249-256.

Lee-Fruman,K.K., Kuo,C.J., Lippincott,J., Terada,N., and Blenis,J. (1999). Characterization of S6K2, a novel kinase homologous to S6K1. Oncogene 18, 5108-5114.

Leevers,S.J., Weinkove,D., MacDougall,L.K., Hafen,E., and Waterfield,M.D. (1996a). The Drosophila phosphoinositide 3-kinase Dp110 promotes cell growth. EMBO J. 15, 6584-6594.

Leevers,S.J., Weinkove,D., MacDougall,L.K., Hafen,E., and Waterfield,M.D. (1996b). The Drosophila phosphoinositide 3-kinase Dp110 promotes cell growth. EMBO J. 15, 6584-6594.

Leslie,N.R., Bennett,D., Lindsay,Y.E., Stewart,H., Gray,A., and Downes,C.P. (2003). Redox regulation of PI 3-kinase signalling via inactivation of PTEN. EMBO J. 22, 5501-5510.

Li,J., Yen,C., Liaw,D., Podsypanina,K., Bose,S., Wang,S.I., Puc,J., Miliaresis,C., Rodgers,L., McCombie,R., Bigner,S.H., Giovanella,B.C., Ittmann,M., Tycko,B., Hibshoosh,H., Wigler,M.H., and Parsons,R. (1997). PTEN, a putative protein tyrosine phosphatase gene mutated in human brain, breast, and prostate cancer. Science 275, 1943-1947.

Lizcano,J.M., Alrubaie,S., Kieloch,A., Deak,M., Leevers,S.J., and Alessi,D.R. (2003). Insulin-induced Drosophila S6 kinase activation requires phosphoinositide 3-kinase and protein kinase B. Biochem. J. 374, 297-306.

Louvet-Vallee,S. (2000). ERM proteins: from cellular architecture to cell signaling. Biol. Cell 92, 305-316.

Lund,P.A., Large,A.T., and Kapatai,G. (2003). The chaperonins: perspectives from the Archaea. Biochem. Soc. Trans. 31, 681-685.

Luo,J., Manning,B.D., and Cantley,L.C. (2003). Targeting the PI3K-Akt pathway in human cancer: rationale and promise. Cancer Cell 4, 257-262.

Machesky,L.M. and Insall,R.H. (1999). Signaling to actin dynamics. J. Cell Biol. 146, 267-272.

Maehama,T. and Dixon,J.E. (1998). The tumor suppressor, PTEN/MMAC1, dephosphorylates the lipid second messenger, phosphatidylinositol 3,4,5-trisphosphate. J. Biol. Chem. 273, 13375-13378.

Maekawa,S., Nishida,E., Ohta,Y., and Sakai,H. (1984). Isolation of low molecular weight actin-binding proteins from porcine brain. J. Biochem. (Tokyo) 95, 377-385.

Mann,M. (2006). Functional and quantitative proteomics using SILAC. Nat. Rev. Mol. Cell Biol. 7, 952-958.

Mann,M., Hojrup,P., and Roepstorff,P. (1993). Use of mass spectrometric molecular weight information to identify proteins in sequence databases. Biol. Mass Spectrom. 22, 338-345.

Mann,M. and Jensen,O.N. (2003). Proteomic analysis of post-translational modifications. Nat. Biotechnol. 21, 255-261.

Manning,G., Whyte,D.B., Martinez,R., Hunter,T., and Sudarsanam,S. (2002). The protein kinase complement of the human genome. Science 298, 1912-1934.

Marcusohn,J., Isakoff,S.J., Rose,E., Symons,M., and Skolnik,E.Y. (1995). The GTP-binding protein Rac does not couple PI 3-kinase to insulin-stimulated glucose transport in adipocytes. Curr. Biol. 5, 1296-1302.

Martinez-Quiles,N., Rohatgi,R., Anton,I.M., Medina,M., Saville,S.P., Miki,H., Yamaguchi,H., Takenawa,T., Hartwig,J.H., Geha,R.S., and Ramesh,N. (2001). WIP regulates N-WASP-mediated actin polymerization and filopodium formation. Nat. Cell Biol. 3, 484-491.

McEligot,A.J., Yang,S., and Meyskens,F.L., Jr. (2005). Redox regulation by intrinsic species and extrinsic nutrients in normal and cancer cells. Annu. Rev. Nutr. 25, 261-295.

McGough,A., Pope,B., Chiu,W., and Weeds,A. (1997). Cofilin changes the twist of F-actin: implications for actin filament dynamics and cellular function. J. Cell Biol. 138, 771-781.

Mello,C.C. and Conte,D., Jr. (2004). Revealing the world of RNA interference. Nature 431, 338-342.

Merlot,S. and Firtel,R.A. (2003). Leading the way: Directional sensing through phosphatidylinositol 3-kinase and other signaling pathways. J. Cell Sci. 116, 3471-3478.

Miki,H., Miura,K., and Takenawa,T. (1996). N-WASP, a novel actin-depolymerizing protein, regulates the cortical cytoskeletal rearrangement in a PIP2-dependent manner downstream of tyrosine kinases. EMBO J. 15, 5326-5335.

Miklos,G.L., Yamamoto,M., Burns,R.G., and Maleszka,R. (1997). An essential cell division gene of Drosophila, absent from Saccharomyces, encodes an unusual protein

with tubulin-like and myosin-like peptide motifs. Proc. Natl. Acad. Sci. U. S. A 94, 5189-5194.

Millard,T.H., Sharp,S.J., and Machesky,L.M. (2004). Signalling to actin assembly via the WASP (Wiskott-Aldrich syndrome protein)-family proteins and the Arp2/3 complex. Biochem. J. 380, 1-17.

Miron,M., Lasko,P., and Sonenberg,N. (2003). Signaling from Akt to FRAP/TOR targets both 4E-BP and S6K in Drosophila melanogaster. Mol. Cell Biol. 23, 9117-9126.

Missy,K., Van,P., V, Raynal,P., Viala,C., Mauco,G., Plantavid,M., Chap,H., and Payrastre,B. (1998). Lipid products of phosphoinositide 3-kinase interact with Rac1 GTPase and stimulate GDP dissociation. J. Biol. Chem. 273, 30279-30286.

Morton,W.M., Ayscough,K.R., and McLaughlin,P.J. (2000). Latrunculin alters the actin-monomer subunit interface to prevent polymerization. Nat. Cell Biol. 2, 376-378.

Mouneimne,G., Soon,L., DesMarais,V., Sidani,M., Song,X., Yip,S.C., Ghosh,M., Eddy,R., Backer,J.M., and Condeelis,J. (2004). Phospholipase C and cofilin are required for carcinoma cell directionality in response to EGF stimulation. J. Cell Biol. 166, 697-708.

Mukhopadhyay,N.K., Price,D.J., Kyriakis,J.M., Pelech,S., Sanghera,J., and Avruch,J. (1992). An array of insulin-activated, proline-directed serine/threonine protein kinases phosphorylate the p70 S6 kinase. J. Biol. Chem. 267, 3325-3335.

Myers,M.G., Jr., Backer,J.M., Sun,X.J., Shoelson,S., Hu,P., Schlessinger,J., Yoakim,M., Schaffhausen,B., and White,M.F. (1992). IRS-1 activates phosphatidylinositol 3'-kinase by associating with src homology 2 domains of p85. Proc. Natl. Acad. Sci. U. S. A 89, 10350-10354.

Nagano,S., Takeda,M., Ma,L., and Soliven,B. (2001). Cytokine-induced cell death in immortalized Schwann cells: roles of nitric oxide and cyclic AMP. J. Neurochem. 77, 1486-1495.

Nagaoka,R., Abe,H., Kusano,K., and Obinata,T. (1995). Concentration of cofilin, a small actin-binding protein, at the cleavage furrow during cytokinesis. Cell Motil. Cytoskeleton 30, 1-7.

Nagata-Ohashi,K., Ohta,Y., Goto,K., Chiba,S., Mori,R., Nishita,M., Ohashi,K., Kousaka,K., Iwamatsu,A., Niwa,R., Uemura,T., and Mizuno,K. (2004). A pathway of neuregulin-induced activation of cofilin-phosphatase Slingshot and cofilin in lamellipodia. J. Cell Biol. 165, 465-471.

Napoli,C., Lemieux,C., and Jorgensen,R. (1990). Introduction of a Chimeric Chalcone Synthase Gene into Petunia Results in Reversible Co-Suppression of Homologous Genes in trans. Plant Cell 2, 279-289.

Neuhoff,V., Arold,N., Taube,D., and Ehrhardt,W. (1988). Improved staining of proteins in polyacrylamide gels including isoelectric focusing gels with clear background at nanogram sensitivity using Coomassie Brilliant Blue G-250 and R-250. Electrophoresis 9, 255-262.

Nishida,E., Maekawa,S., and Sakai,H. (1984). Cofilin, a protein in porcine brain that binds to actin filaments and inhibits their interactions with myosin and tropomyosin. Biochemistry 23, 5307-5313.

Nishita,M., Wang,Y., Tomizawa,C., Suzuki,A., Niwa,R., Uemura,T., and Mizuno,K. (2004). Phosphoinositide 3-kinase-mediated activation of cofilin phosphatase Slingshot and its role for insulin-induced membrane protrusion. J. Biol. Chem. 279, 7193-7198.

Niwa,R., Nagata-Ohashi,K., Takeichi,M., Mizuno,K., and Uemura,T. (2002). Control of actin reorganization by Slingshot, a family of phosphatases that dephosphorylate ADF/cofilin. Cell 108, 233-246.

Nobes,C.D. and Hall,A. (1995). Rho, rac, and cdc42 GTPases regulate the assembly of multimolecular focal complexes associated with actin stress fibers, lamellipodia, and filopodia. Cell 81, 53-62.

Nobes,C.D., Hawkins,P., Stephens,L., and Hall,A. (1995). Activation of the small GTP-binding proteins rho and rac by growth factor receptors. J. Cell Sci. 108 (Pt 1), 225-233.

O'Donnell,W.T. and Warren,S.T. (2002). A decade of molecular studies of fragile X syndrome. Annu. Rev. Neurosci. 25, 315-338.

O'Farrell,P.H. (1975). High resolution two-dimensional electrophoresis of proteins. J. Biol. Chem. 250, 4007-4021.

O'Grady,M., Raha,D., Hanson,B.J., Bunting,M., and Hanson,G.T. (2005). Combining RNA interference and kinase inhibitors against cell signalling components involved in cancer. BMC. Cancer 5, 125.

Ohashi,K., Nagata,K., Maekawa,M., Ishizaki,T., Narumiya,S., and Mizuno,K. (2000). Rho-associated kinase ROCK activates LIM-kinase 1 by phosphorylation at threonine 508 within the activation loop. J. Biol. Chem. 275, 3577-3582.

Oikawa,T., Yamaguchi,H., Itoh,T., Kato,M., Ijuin,T., Yamazaki,D., Suetsugu,S., and Takenawa,T. (2004). PtdIns(3,4,5)P3 binding is necessary for WAVE2-induced formation of lamellipodia. Nat. Cell Biol. 6, 420-426.

Ojala,P.J., Paavilainen,V., and Lappalainen,P. (2001). Identification of yeast cofilin residues specific for actin monomer and PIP2 binding. Biochemistry 40, 15562-15569.

Okada,K., Ravi,H., Smith,E.M., and Goode,B.L. (2006). Aip1 and cofilin promote rapid turnover of yeast actin patches and cables: a coordinated mechanism for severing and capping filaments. Mol. Biol. Cell 17, 2855-2868.

Okkenhaug,K. and Vanhaesebroeck,B. (2001). New responsibilities for the PI3K regulatory subunit p85 alpha. Sci. STKE. 2001, E1.

Olofsson,B. (1999). Rho guanine dissociation inhibitors: pivotal molecules in cellular signalling. Cell Signal. 11, 545-554.

Olsen,J.V., Blagoev,B., Gnad,F., Macek,B., Kumar,C., Mortensen,P., and Mann,M. (2006). Global, in vivo, and site-specific phosphorylation dynamics in signaling networks. Cell 127, 635-648.

Ong,S.E., Blagoev,B., Kratchmarova,I., Kristensen,D.B., Steen,H., Pandey,A., and Mann,M. (2002). Stable isotope labeling by amino acids in cell culture, SILAC, as a simple and accurate approach to expression proteomics. Mol. Cell Proteomics. 1, 376-386.

Ono,S. (2003). Regulation of actin filament dynamics by actin depolymerizing factor/cofilin and actin-interacting protein 1: new blades for twisted filaments. Biochemistry 42, 13363-13370.

Pantaloni,D., Le Clainche,C., and Carlier,M.F. (2001). Mechanism of actin-based motility. Science 292, 1502-1506.

Pawson,T. (1995). Protein modules and signalling networks. Nature 373, 573-580.

Pearson,R.B., Dennis,P.B., Han,J.W., Williamson,N.A., Kozma,S.C., Wettenhall,R.E., and Thomas,G. (1995). The principal target of rapamycin-induced p70s6k inactivation is a novel phosphorylation site within a conserved hydrophobic domain. EMBO J. 14, 5279-5287.

Peel,D.J., Johnson,S.A., and Milner,M.J. (1990). The ultrastructure of imaginal disc cells in primary cultures and during cell aggregation in continuous cell lines. Tissue Cell 22, 749-758.

Pende,M., Um,S.H., Mieulet,V., Sticker,M., Goss,V.L., Mestan,J., Mueller,M., Fumagalli,S., Kozma,S.C., and Thomas,G. (2004). S6K1(-/-)/S6K2(-/-) mice exhibit perinatal lethality and rapamycin-sensitive 5'-terminal oligopyrimidine mRNA translation and reveal a mitogen-activated protein kinase-dependent S6 kinase pathway. Mol. Cell Biol. 24, 3112-3124.

Pertz,O., Hodgson,L., Klemke,R.L., and Hahn,K.M. (2006). Spatiotemporal dynamics of RhoA activity in migrating cells. Nature 440, 1069-1072.

Pestell,R.G., Albanese,C., Reutens,A.T., Segall,J.E., Lee,R.J., and Arnold,A. (1999). The cyclins and cyclin-dependent kinase inhibitors in hormonal regulation of proliferation and differentiation. Endocr. Rev. 20, 501-534.

Pollard,T.D., Blanchoin,L., and Mullins,R.D. (2000). Molecular mechanisms controlling actin filament dynamics in nonmuscle cells. Annu. Rev. Biophys. Biomol. Struct. 29, 545-576.

Pollard,T.D., Blanchoin,L., and Mullins,R.D. (2001). Actin dynamics. J. Cell Sci. 114, 3-4.

Pollard,T.D. and Borisy,G.G. (2003). Cellular motility driven by assembly and disassembly of actin filaments. Cell 112, 453-465.

Pollard,T.D. and Cooper,J.A. (1986). Actin and actin-binding proteins. A critical evaluation of mechanisms and functions. Annu. Rev. Biochem. 55, 987-1035.

Ptacek,J., Devgan,G., Michaud,G., Zhu,H., Zhu,X., Fasolo,J., Guo,H., Jona,G., Breitkreutz,A., Sopko,R., McCartney,R.R., Schmidt,M.C., Rachidi,N., Lee,S.J., Mah,A.S., Meng,L., Stark,M.J., Stern,D.F., De Virgilio,C., Tyers,M., Andrews,B., Gerstein,M., Schweitzer,B., Predki,P.F., and Snyder,M. (2005). Global analysis of protein phosphorylation in yeast. Nature 438, 679-684.

Pullen,N., Dennis,P.B., Andjelkovic,M., Dufner,A., Kozma,S.C., Hemmings,B.A., and Thomas,G. (1998). Phosphorylation and activation of p70s6k by PDK1. Science 279, 707-710.

Radimerski,T., Montagne,J., Rintelen,F., Stocker,H., van der,K.J., Downes,C.P., Hafen,E., and Thomas,G. (2002). dS6K-regulated cell growth is dPKB/dPI(3)K-independent, but requires dPDK1. Nat. Cell Biol. 4, 251-255.

Radyuk,S.N., Klichko,V.I., Spinola,B., Sohal,R.S., and Orr,W.C. (2001). The peroxiredoxin gene family in Drosophila melanogaster. Free Radic. Biol. Med. 31, 1090-1100.

Ramanathan,A., Wang,C., and Schreiber,S.L. (2005). Perturbational profiling of a cell-line model of tumorigenesis by using metabolic measurements. Proc. Natl. Acad. Sci. U. S. A 102, 5992-5997.

Ramet,M., Manfruelli,P., Pearson,A., Mathey-Prevot,B., and Ezekowitz,R.A. (2002). Functional genomic analysis of phagocytosis and identification of a Drosophila receptor for E. coli. Nature 416, 644-648.

Rathmell,J.C., Fox,C.J., Plas,D.R., Hammerman,P.S., Cinalli,R.M., and Thompson,C.B. (2003). Akt-directed glucose metabolism can prevent Bax conformation change and promote growth factor-independent survival. Mol. Cell Biol. 23, 7315-7328.

Rawlings,J.S., Rosler,K.M., and Harrison,D.A. (2004). The JAK/STAT signaling pathway. J. Cell Sci. 117, 1281-1283.

Rescher,U. and Gerke,V. (2004). Annexins--unique membrane binding proteins with diverse functions. J. Cell Sci. 117, 2631-2639.

Ressad,F., Didry,D., Xia,G.X., Hong,Y., Chua,N.H., Pantaloni,D., and Carlier,M.F. (1998). Kinetic analysis of the interaction of actin-depolymerizing factor (ADF)/cofilin with G- and F-actins. Comparison of plant and human ADFs and effect of phosphorylation. J. Biol. Chem. 273, 20894-20902.

Revenu,C., Athman,R., Robine,S., and Louvard,D. (2004). The co-workers of actin filaments: from cell structures to signals. Nat. Rev. Mol. Cell Biol. 5, 635-646.

Ridley,A.J. (2006). Rho GTPases and actin dynamics in membrane protrusions and vesicle trafficking. Trends Cell Biol. 16, 522-529.

Ridley,A.J. and Hall,A. (1992). The small GTP-binding protein rho regulates the assembly of focal adhesions and actin stress fibers in response to growth factors. Cell 70, 389-399.

Ridley,A.J., Paterson,H.F., Johnston,C.L., Diekmann,D., and Hall,A. (1992). The small GTP-binding protein rac regulates growth factor-induced membrane ruffling. Cell 70, 401-410.

Rodriguez-Viciana,P., Warne,P.H., Khwaja,A., Marte,B.M., Pappin,D., Das,P., Waterfield,M.D., Ridley,A., and Downward,J. (1997). Role of phosphoinositide 3-OH kinase in cell transformation and control of the actin cytoskeleton by Ras. Cell 89, 457-467.

Rogers,S.L., Wiedemann,U., Stuurman,N., and Vale,R.D. (2003). Molecular requirements for actin-based lamella formation in Drosophila S2 cells. J. Cell Biol. 162, 1079-1088.

Romano,N. and Macino,G. (1992). Quelling: transient inactivation of gene expression in Neurospora crassa by transformation with homologous sequences. Mol. Microbiol. 6, 3343-3353.

Rosales,C., O'Brien,V., Kornberg,L., and Juliano,R. (1995). Signal transduction by cell adhesion receptors. Biochim. Biophys. Acta 1242, 77-98.

Rosok,O., Pedeutour,F., Ree,A.H., and Aasheim,H.C. (1999). Identification and characterization of TESK2, a novel member of the LIMK/TESK family of protein kinases, predominantly expressed in testis. Genomics 61, 44-54.

Rubin,G.M., Yandell,M.D., Wortman,J.R., Gabor Miklos,G.L., Nelson,C.R., Hariharan,I.K., Fortini,M.E., Li,P.W., Apweiler,R., Fleischmann,W., Cherry,J.M., Henikoff,S., Skupski,M.P., Misra,S., Ashburner,M., Birney,E., Boguski,M.S., Brody,T., Brokstein,P., Celniker,S.E., Chervitz,S.A., Coates,D., Cravchik,A., Gabrielian,A., Galle,R.F., Gelbart,W.M., George,R.A., Goldstein,L.S., Gong,F., Guan,P., Harris,N.L., Hay,B.A., Hoskins,R.A., Li,J., Li,Z., Hynes,R.O., Jones,S.J., Kuehl,P.M., Lemaitre,B., Littleton,J.T., Morrison,D.K., Mungall,C., O'Farrell,P.H., Pickeral,O.K., Shue,C., Vosshall,L.B., Zhang,J., Zhao,Q., Zheng,X.H., and Lewis,S. (2000). Comparative genomics of the eukaryotes. Science 287, 2204-2215.

Ruvinsky,I., Sharon,N., Lerer,T., Cohen,H., Stolovich-Rain,M., Nir,T., Dor,Y., Zisman,P., and Meyuhas,O. (2005). Ribosomal protein S6 phosphorylation is a determinant of cell size and glucose homeostasis. Genes Dev. 19, 2199-2211.

Sahai,E. and Marshall,C.J. (2003). Differing modes of tumour cell invasion have distinct requirements for Rho/ROCK signalling and extracellular proteolysis. Nat. Cell Biol. 5, 711-719.

Saleh,M.C., van Rij,R.P., Hekele,A., Gillis,A., Foley,E., O'Farrell,P.H., and Andino,R. (2006). The endocytic pathway mediates cell entry of dsRNA to induce RNAi silencing. Nat. Cell Biol. 8, 793-802.

Samuels,Y., Wang,Z., Bardelli,A., Silliman,N., Ptak,J., Szabo,S., Yan,H., Gazdar,A., Powell,S.M., Riggins,G.J., Willson,J.K., Markowitz,S., Kinzler,K.W., Vogelstein,B., and Velculescu,V.E. (2004). High frequency of mutations of the PIK3CA gene in human cancers. Science 304, 554.

Sarbassov,D.D., Ali,S.M., Kim,D.H., Guertin,D.A., Latek,R.R., Erdjument-Bromage,H., Tempst,P., and Sabatini,D.M. (2004). Rictor, a novel binding partner of mTOR, defines a rapamycin-insensitive and raptor-independent pathway that regulates the cytoskeleton. Curr. Biol. 14, 1296-1302.

Sarbassov,D.D., Guertin,D.A., Ali,S.M., and Sabatini,D.M. (2005). Phosphorylation and regulation of Akt/PKB by the rictor-mTOR complex. Science 307, 1098-1101.

Sawyer,C., Sturge,J., Bennett,D.C., O'Hare,M.J., Allen,W.E., Bain,J., Jones,G.E., and Vanhaesebroeck,B. (2003). Regulation of breast cancer cell chemotaxis by the phosphoinositide 3-kinase p110delta. Cancer Res. 63, 1667-1675.

Schaeffer,H.J. and Weber,M.J. (1999). Mitogen-activated protein kinases: specific messages from ubiquitous messengers. Mol. Cell Biol. 19, 2435-2444.

Schafer,D.A. and Cooper,J.A. (1995). Control of actin assembly at filament ends. Annu. Rev. Cell Dev. Biol. 11, 497-518.

Schenck,A., Bardoni,B., Moro,A., Bagni,C., and Mandel,J.L. (2001). A highly conserved protein family interacting with the fragile X mental retardation protein (FMRP) and displaying selective interactions with FMRP-related proteins FXR1P and FXR2P. Proc. Natl. Acad. Sci. U. S. A 98, 8844-8849.

Schmidt,A. and Hall,A. (2002). Guanine nucleotide exchange factors for Rho GTPases: turning on the switch. Genes Dev. 16, 1587-1609.

Schneider,I. (1972). Cell lines derived from late embryonic stages of Drosophila melanogaster. J. Embryol. Exp. Morphol. 27, 353-365.

Schrader,M. and Fahimi,H.D. (2006). Peroxisomes and oxidative stress. Biochim. Biophys. Acta 1763, 1755-1766.

Schulenberg,B., Aggeler,R., Beechem,J.M., Capaldi,R.A., and Patton,W.F. (2003). Analysis of steady-state protein phosphorylation in mitochondria using a novel fluorescent phosphosensor dye. J. Biol. Chem. 278, 27251-27255.

Scita,G., Nordstrom,J., Carbone,R., Tenca,P., Giardina,G., Gutkind,S., Bjarnegard,M., Betsholtz,C., and Di Fiore,P.P. (1999). EPS8 and E3B1 transduce signals from Ras to Rac. Nature 401, 290-293.

Scita,G., Tenca,P., Areces,L.B., Tocchetti,A., Frittoli,E., Giardina,G., Ponzanelli,I., Sini,P., Innocenti,M., and Di Fiore,P.P. (2001). An effector region in Eps8 is responsible for the activation of the Rac-specific GEF activity of Sos-1 and for the proper localization of the Rac-based actin-polymerizing machine. J. Cell Biol. 154, 1031-1044.

Seo,J. and Lee,K.J. (2004). Post-translational modifications and their biological functions: proteomic analysis and systematic approaches. J. Biochem. Mol. Biol. 37, 35-44.

Servant,G., Weiner,O.D., Herzmark,P., Balla,T., Sedat,J.W., and Bourne,H.R. (2000). Polarization of chemoattractant receptor signaling during neutrophil chemotaxis. Science 287, 1037-1040.

Sharma,A., Patrick,B., Li,J., Sharma,R., Jeyabal,P.V., Reddy,P.M., Awasthi,S., and Awasthi,Y.C. (2006). Glutathione S-transferases as antioxidant enzymes: small cell lung cancer (H69) cells transfected with hGSTA1 resist doxorubicin-induced apoptosis. Arch. Biochem. Biophys. 452, 165-173.

Shaw,M. and Cohen,P. (1999). Role of protein kinase B and the MAP kinase cascade in mediating the EGF-dependent inhibition of glycogen synthase kinase 3 in Swiss 3T3 cells. FEBS Lett. 461, 120-124.

Smertenko,A.P., Jiang,C.J., Simmons,N.J., Weeds,A.G., Davies,D.R., and Hussey,P.J. (1998). Ser6 in the maize actin-depolymerizing factor, ZmADF3, is phosphorylated by a calcium-stimulated protein kinase and is essential for the control of functional activity. Plant J. 14, 187-193.

Soosairajah,J., Maiti,S., Wiggan,O., Sarmiere,P., Moussi,N., Sarcevic,B., Sampath,R., Bamburg,J.R., and Bernard,O. (2005). Interplay between components of a novel LIM kinase-slingshot phosphatase complex regulates cofilin. EMBO J. 24, 473-486.

Spector,I., Shochet,N.R., Kashman,Y., and Groweiss,A. (1983). Latrunculins: novel marine toxins that disrupt microfilament organization in cultured cells. Science 219, 493-495.

Stambolic,V., Suzuki,A., de la Pompa,J.L., Brothers,G.M., Mirtsos,C., Sasaki,T., Ruland,J., Penninger,J.M., Siderovski,D.P., and Mak,T.W. (1998). Negative regulation of PKB/Akt-dependent cell survival by the tumor suppressor PTEN. Cell 95, 29-39.

Stambolic,V., Tsao,M.S., Macpherson,D., Suzuki,A., Chapman,W.B., and Mak,T.W. (2000). High incidence of breast and endometrial neoplasia resembling human Cowden syndrome in pten+/- mice. Cancer Res. 60, 3605-3611.

Stamps,A.C., Davies,S.C., Burman,J., and O'Hare,M.J. (1994). Analysis of proviral integration in human mammary epithelial cell lines immortalized by retroviral infection with a temperature-sensitive SV40 T-antigen construct. Int. J. Cancer 57, 865-874.

Steck,P.A., Pershouse,M.A., Jasser,S.A., Yung,W.K., Lin,H., Ligon,A.H., Langford,L.A., Baumgard,M.L., Hattier,T., Davis,T., Frye,C., Hu,R., Swedlund,B., Teng,D.H., and Tavtigian,S.V. (1997). Identification of a candidate tumour suppressor gene, MMAC1, at chromosome 10q23.3 that is mutated in multiple advanced cancers. Nat. Genet. 15, 356-362.

Steffen,A., Rottner,K., Ehinger,J., Innocenti,M., Scita,G., Wehland,J., and Stradal,T.E. (2004). Sra-1 and Nap1 link Rac to actin assembly driving lamellipodia formation. EMBO J. 23, 749-759.

Stossel,T.P. (1993). On the crawling of animal cells. Science 260, 1086-1094.

Stradal,T.E. and Scita,G. (2006). Protein complexes regulating Arp2/3-mediated actin assembly. Curr. Opin. Cell Biol. 18, 4-10.

Sugimoto,Y., Whitman,M., Cantley,L.C., and Erikson,R.L. (1984). Evidence that the Rous sarcoma virus transforming gene product phosphorylates phosphatidylinositol and diacylglycerol. Proc. Natl. Acad. Sci. U. S. A 81, 2117-2121.

Sumi,T., Matsumoto,K., Shibuya,A., and Nakamura,T. (2001). Activation of LIM kinases by myotonic dystrophy kinase-related Cdc42-binding kinase alpha. J. Biol. Chem. 276, 23092-23096.

Sumi,T., Matsumoto,K., Takai,Y., and Nakamura,T. (1999). Cofilin phosphorylation and actin cytoskeletal dynamics regulated by rho- and Cdc42-activated LIM-kinase 2. J. Cell Biol. 147, 1519-1532.

Svitkina,T.M. and Borisy,G.G. (1999). Arp2/3 complex and actin depolymerizing factor/cofilin in dendritic organization and treadmilling of actin filament array in lamellipodia. J. Cell Biol. 145, 1009-1026.

Tamura,M., Gu,J., Matsumoto,K., Aota,S., Parsons,R., and Yamada,K.M. (1998). Inhibition of cell migration, spreading, and focal adhesions by tumor suppressor PTEN. Science 280, 1614-1617.

Tanaka,K., Okubo,Y., and Abe,H. (2005). Involvement of slingshot in the Rho-mediated dephosphorylation of ADF/cofilin during Xenopus cleavage. Zoolog. Sci. 22, 971-984.

Taniguchi,C.M., Emanuelli,B., and Kahn,C.R. (2006). Critical nodes in signalling pathways: insights into insulin action. Nat. Rev. Mol. Cell Biol. 7, 85-96.

Tee,A.R. and Blenis,J. (2005). mTOR, translational control and human disease. Semin. Cell Dev. Biol. 16, 29-37.

Testa,J.R. and Bellacosa,A. (2001). AKT plays a central role in tumorigenesis. Proc. Natl. Acad. Sci. U. S. A 98, 10983-10985.

Timms,J.F., White,S.L., O'Hare,M.J., and Waterfield,M.D. (2002). Effects of ErbB-2 overexpression on mitogenic signalling and cell cycle progression in human breast luminal epithelial cells. Oncogene 21, 6573-6586.

Toker,A. and Newton,A.C. (2000). Akt/protein kinase B is regulated by autophosphorylation at the hypothetical PDK-2 site. J. Biol. Chem. 275, 8271-8274.

Tolias,K.F., Cantley,L.C., and Carpenter,C.L. (1995). Rho family GTPases bind to phosphoinositide kinases. J. Biol. Chem. 270, 17656-17659.

Tonge,R., Shaw,J., Middleton,B., Rowlinson,R., Rayner,S., Young,J., Pognan,F., Hawkins,E., Currie,I., and Davison,M. (2001). Validation and development of fluorescence two-dimensional differential gel electrophoresis proteomics technology. Proteomics. 1, 377-396.

Toshima,J., Toshima,J.Y., Amano,T., Yang,N., Narumiya,S., and Mizuno,K. (2001). Cofilin phosphorylation by protein kinase testicular protein kinase 1 and its role in integrin-mediated actin reorganization and focal adhesion formation. Mol. Biol. Cell 12, 1131-1145.

Tretter,L. and Adam-Vizi,V. (2000). Inhibition of Krebs cycle enzymes by hydrogen peroxide: A key role of [alpha]-ketoglutarate dehydrogenase in limiting NADH production under oxidative stress. J. Neurosci. 20, 8972-8979.

Trotman,L.C., Alimonti,A., Scaglioni,P.P., Koutcher,J.A., Cordon-Cardo,C., and Pandolfi,P.P. (2006). Identification of a tumour suppressor network opposing nuclear Akt function. Nature 441, 523-527.

Tsakiridis,T., Tong,P., Matthews,B., Tsiani,E., Bilan,P.J., Klip,A., and Downey,G.P. (1999). Role of the actin cytoskeleton in insulin action. Microsc. Res. Tech., 47, 79-92.

Unlu,M., Morgan,M.E., and Minden,J.S. (1997). Difference gel electrophoresis: a single gel method for detecting changes in protein extracts. Electrophoresis 18, 2071-2077.

Van Haastert,P.J. and Devreotes,P.N. (2004). Chemotaxis: signalling the way forward. Nat. Rev. Mol. Cell Biol. 5, 626-634.

Vandermoere,F., Yazidi-Belkoura,I.E., Demont,Y., Slomianny,C., Antol,J., Lemoine,J., and Hondermarck,H. (2007). Proteomics exploration reveals that actin is a signaling target of the kinase Akt. Mol. Cell Proteomics. 6, 114-124.

Vanhaesebroeck,B. and Alessi,D.R. (2000). The PI3K-PDK1 connection: more than just a road to PKB. Biochem. J. 346 Pt 3, 561-576.

Vanhaesebroeck,B., Leevers,S.J., Ahmadi,K., Timms,J., Katso,R., Driscoll,P.C., Woscholski,R., Parker,P.J., and Waterfield,M.D. (2001). Synthesis and function of 3-phosphorylated inositol lipids. Annu. Rev. Biochem. 70, 535-602.

Vanhaesebroeck,B., Leevers,S.J., Panayotou,G., and Waterfield,M.D. (1997a). Phosphoinositide 3-kinases: a conserved family of signal transducers. Trends Biochem. Sci. 22, 267-272.

Vanhaesebroeck,B., Welham,M.J., Kotani,K., Stein,R., Warne,P.H., Zvelebil,M.J., Higashi,K., Volinia,S., Downward,J., and Waterfield,M.D. (1997b). P110delta, a novel phosphoinositide 3-kinase in leukocytes. Proc. Natl. Acad. Sci. U. S. A 94, 4330-4335.

Venter,J.C., Adams,M.D., Myers,E.W., Li,P.W., Mural,R.J., Sutton,G.G., Smith,H.O., Yandell,M., Evans,C.A., Holt,R.A., Gocayne,J.D., Amanatides,P., Ballew,R.M., Huson,D.H., Wortman,J.R., Zhang,Q., Kodira,C.D., Zheng,X.H., Chen,L., Skupski,M., Subramanian,G., Thomas,P.D., Zhang,J., Gabor Miklos,G.L., Nelson,C., Broder,S., Clark,A.G., Nadeau,J., McKusick,V.A., Zinder,N., Levine,A.J., Roberts,R.J., Simon,M., Slayman,C., Hunkapiller,M., Bolanos,R., Delcher,A., Dew,I., Fasulo,D., Flanigan,M., Florea,L., Halpern,A., Hannenhalli,S., Kravitz,S., Levy,S., Mobarry,C., Reinert,K., Remington,K., Abu-Threideh,J., Beasley,E., Biddick,K., Bonazzi,V., Brandon,R., Cargill,M., Chandramouliswaran,I., Charlab,R., Chaturvedi,K., Deng,Z., Di,F., V, Dunn,P., Eilbeck,K., Evangelista,C., Gabrielian,A.E., Gan,W., Ge,W., Gong,F., Gu,Z., Guan,P., Heiman,T.J., Higgins,M.E., Ji,R.R., Ke,Z., Ketchum,K.A., Lai,Z., Lei,Y., Li,Z., Li,J., Liang,Y., Lin,X., Lu,F., Merkulov,G.V., Milshina,N., Moore,H.M., Naik,A.K., Narayan,V.A., Neelam,B., Nusskern,D., Rusch,D.B., Salzberg,S., Shao,W., Shue,B., Sun,J., Wang,Z., Wang,A., Wang,X., Wang,J., Wei,M., Wides,R., Xiao,C., Yan,C., Yao,A., Ye,J., Zhan,M., Zhang,W., Zhang,H., Zhao,Q., Zheng,L., Zhong,F., Zhong,W., Zhu,S., Zhao,S., Gilbert,D., Baumhueter,S., Spier,G., Carter,C., Cravchik,A., Woodage,T., Ali,F., An,H., Awe,A., Baldwin,D., Baden,H., Barnstead,M., Barrow,I., Beeson,K., Busam,D., Carver,A., Center,A., Cheng,M.L., Curry,L., Danaher,S., Davenport,L., Desilets,R., Dietz,S., Dodson,K., Doup,L., Ferriera,S., Garg,N., Gluecksmann,A., Hart,B., Haynes,J., Haynes,C., Heiner,C., Hladun,S., Hostin,D., Houck,J., Howland,T., Ibegwam,C., Johnson,J., Kalush,F., Kline,L., Koduru,S., Love,A., Mann,F., May,D., McCawley,S., McIntosh,T., McMullen,I., Moy,M., Moy,L., Murphy,B., Nelson,K., Pfannkoch,C., Pratts,E., Puri,V., Qureshi,H., Reardon,M., Rodriguez,R., Rogers,Y.H., Romblad,D., Ruhfel,B., Scott,R., Sitter,C., Smallwood,M., Stewart,E., Strong,R., Suh,E., Thomas,R., Tint,N.N., Tse,S., Vech,C., Wang,G., Wetter,J., Williams,S., Williams,M., Windsor,S., Winn-Deen,E., Wolfe,K., Zaveri,J., Zaveri,K., Abril,J.F., Guigo,R., Campbell,M.J., Sjolander,K.V., Karlak,B., Kejariwal,A., Mi,H., Lazareva,B., Hatton,T., Narechania,A., Diemer,K., Muruganujan,A., Guo,N., Sato,S., Bafna,V., Istrail,S., Lippert,R., Schwartz,R., Walenz,B., Yooseph,S., Allen,D., Basu,A., Baxendale,J., Blick,L., Caminha,M., Carnes-Stine,J., Caulk,P., Chiang,Y.H., Coyne,M., Dahlke,C., Mays,A., Dombroski,M., Donnelly,M., Ely,D., Esparham,S., Fosler,C., Gire,H., Glanowski,S., Glasser,K., Glodek,A., Gorokhov,M., Graham,K., Gropman,B., Harris,M., Heil,J., Henderson,S., Hoover,J., Jennings,D., Jordan,C., Jordan,J., Kasha,J., Kagan,L., Kraft,C., Levitsky,A., Lewis,M., Liu,X., Lopez,J., Ma,D., Majoros,W., McDaniel,J.,

Murphy,S., Newman,M., Nguyen,T., Nguyen,N., and Nodell,M. (2001). The sequence of the human genome. Science 291, 1304-1351.

Vivanco,I. and Sawyers,C.L. (2002). The phosphatidylinositol 3-Kinase AKT pathway in human cancer. Nat. Rev. Cancer 2, 489-501.

Vlahos,C.J., Matter,W.F., Hui,K.Y., and Brown,R.F. (1994). A specific inhibitor of phosphatidylinositol 3-kinase, 2-(4-morpholinyl)-8-phenyl-4H-1-benzopyran-4-one (LY294002). J. Biol. Chem. 269, 5241-5248.

Waite,K.A. and Eng,C. (2002). Protean PTEN: form and function. Am. J. Hum. Genet. 70, 829-844.

Wang,H.R., Zhang,Y., Ozdamar,B., Ogunjimi,A.A., Alexandrova,E., Thomsen,G.H., and Wrana,J.L. (2003). Regulation of cell polarity and protrusion formation by targeting RhoA for degradation. Science 302, 1775-1779.

Wang,L., Gout,I., and Proud,C.G. (2001). Cross-talk between the ERK and p70 S6 kinase (S6K) signaling pathways. MEK-dependent activation of S6K2 in cardiomyocytes. J. Biol. Chem. 276, 32670-32677.

Wear,M.A. and Cooper,J.A. (2004). Capping protein: new insights into mechanism and regulation. Trends Biochem. Sci. 29, 418-428.

Webster,K.A. (2004). Aktion in the nucleus. Circ. Res. 94, 856-859.

Weinkove,D., Neufeld,T.P., Twardzik,T., Waterfield,M.D., and Leevers,S.J. (1999). Regulation of imaginal disc cell size, cell number and organ size by Drosophila class I(A) phosphoinositide 3-kinase and its adaptor. Curr. Biol. 9, 1019-1029.

Welch,H., Eguinoa,A., Stephens,L.R., and Hawkins,P.T. (1998). Protein kinase B and rac are activated in parallel within a phosphatidylinositide 3OH-kinase-controlled signaling pathway. J. Biol. Chem. 273, 11248-11256.

Welch,M.D., Holtzman,D.A., and Drubin,D.G. (1994). The yeast actin cytoskeleton. Curr. Opin. Cell Biol. 6, 110-119.

Wendland,B., Emr,S.D., and Riezman,H. (1998). Protein traffic in the yeast endocytic and vacuolar protein sorting pathways. Curr. Opin. Cell Biol. 10, 513-522.

Wennstrom,S., Hawkins,P., Cooke,F., Hara,K., Yonezawa,K., Kasuga,M., Jackson,T., Claesson-Welsh,L., and Stephens,L. (1994a). Activation of phosphoinositide 3-kinase is required for PDGF-stimulated membrane ruffling. Curr. Biol. 4, 385-393.

Wennstrom,S., Siegbahn,A., Yokote,K., Arvidsson,A.K., Heldin,C.H., Mori,S., and Claesson-Welsh,L. (1994b). Membrane ruffling and chemotaxis transduced by the PDGF beta-receptor require the binding site for phosphatidylinositol 3' kinase. Oncogene 9, 651-660.

Werner,E. (2004). GTPases and reactive oxygen species: switches for killing and signaling. J. Cell Sci. 117, 143-153.

White,S.L., Gharbi,S., Bertani,M.F., Chan,H.L., Waterfield,M.D., and Timms,J.F. (2004). Cellular responses to ErbB-2 overexpression in human mammary luminal epithelial cells: comparison of mRNA and protein expression. Br. J. Cancer 90, 173-181.

Whitman,M., Kaplan,D.R., Schaffhausen,B., Cantley,L., and Roberts,T.M. (1985). Association of phosphatidylinositol kinase activity with polyoma middle-T competent for transformation. Nature 315, 239-242.

Wilda,M., Fuchs,U., Wossmann,W., and Borkhardt,A. (2002). Killing of leukemic cells with a BCR/ABL fusion gene by RNA interference (RNAi). Oncogene 21, 5716-5724.

Williams,M.R., Arthur,J.S., Balendran,A., van der,K.J., Poli,V., Cohen,P., and Alessi,D.R. (2000). The role of 3-phosphoinositide-dependent protein kinase 1 in activating AGC kinases defined in embryonic stem cells. Curr. Biol. 10, 439-448.

Wood,W., Faria,C., and Jacinto,A. (2006). Distinct mechanisms regulate hemocyte chemotaxis during development and wound healing in Drosophila melanogaster. J. Cell Biol. 173, 405-416.

Wood,Z.A., Schroder,E., Robin,H.J., and Poole,L.B. (2003). Structure, mechanism and regulation of peroxiredoxins. Trends Biochem. Sci. 28, 32-40.

Wymann,M. and Arcaro,A. (1994). Platelet-derived growth factor-induced phosphatidylinositol 3-kinase activation mediates actin rearrangements in fibroblasts. Biochem. J. 298 Pt 3, 517-520.

Xian,W. and Janmey,P.A. (2002). Dissecting the gelsolin-polyphosphoinositide interaction and engineering of a polyphosphoinositide-sensitive gelsolin C-terminal half protein. J. Mol. Biol. 322, 755-771.

Yamamoto,M., Nagata-Ohashi,K., Ohta,Y., Ohashi,K., and Mizuno,K. (2006). Identification of multiple actin-binding sites in cofilin-phosphatase Slingshot-1L. FEBS Lett. 580, 1789-1794.

Yanagawa,S., Lee,J.S., and Ishimoto,A. (1998). Identification and characterization of a novel line of Drosophila Schneider S2 cells that respond to wingless signaling. J. Biol. Chem. 273, 32353-32359.

Yang,N., Higuchi,O., Ohashi,K., Nagata,K., Wada,A., Kangawa,K., Nishida,E., and Mizuno,K. (1998). Cofilin phosphorylation by LIM-kinase 1 and its role in Rac-mediated actin reorganization. Nature 393, 809-812.

Yarden,Y. and Sliwkowski,M.X. (2001). Untangling the ErbB signalling network. Nat. Rev. Mol. Cell Biol. 2, 127-137.

Yates,J.R., III, Speicher,S., Griffin,P.R., and Hunkapiller,T. (1993). Peptide mass maps: a highly informative approach to protein identification. Anal. Biochem. 214, 397-408.

Yonezawa,N., Homma,Y., Yahara,I., Sakai,H., and Nishida,E. (1991). A short sequence responsible for both phosphoinositide binding and actin binding activities of cofilin. J. Biol. Chem. 266, 17218-17221.

Yonezawa,N., Nishida,E., Iida,K., Yahara,I., and Sakai,H. (1990). Inhibition of the interactions of cofilin, destrin, and deoxyribonuclease I with actin by phosphoinositides. J. Biol. Chem. 265, 8382-8386.

Yoon,S. and Seger,R. (2006). The extracellular signal-regulated kinase: multiple substrates regulate diverse cellular functions. Growth Factors 24, 21-44.

Zhang,H., Zha,X., Tan,Y., Hornbeck,P.V., Mastrangelo,A.J., Alessi,D.R., Polakiewicz,R.D., and Comb,M.J. (2002). Phosphoprotein analysis using antibodies broadly reactive against phosphorylated motifs. J. Biol. Chem. 277, 39379-39387.

Zhang,Y.Q., Bailey,A.M., Matthies,H.J., Renden,R.B., Smith,M.A., Speese,S.D., Rubin,G.M., and Broadie,K. (2001). Drosophila fragile X-related gene regulates the MAP1B homolog Futsch to control synaptic structure and function. Cell 107, 591-603.

Zhou,B.P., Liao,Y., Xia,W., Spohn,B., Lee,M.H., and Hung,M.C. (2001). Cytoplasmic localization of p21Cip1/WAF1 by Akt-induced phosphorylation in HER-2/neu-overexpressing cells. Nat. Cell Biol. 3, 245-252.

APPENDIX 1

MOWSE Score, matched peptides and sequence coverage of identified proteins (Table 3.1 and 3.2)

Spot No. 877 Keratin 7

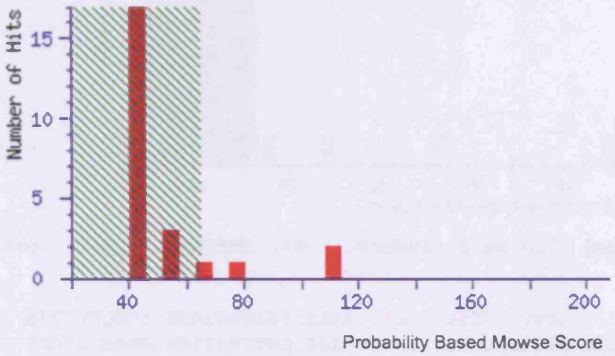

gi|67782365 Mass: 51411 Score: 109 Expect: 2.4e-006 Queries matched: 16
keratin 7 [Homo sapiens]

```
  1 MSIHFSSPVF TSRSAAFSGR GAQVRLSSAR PGGLGSSSLY GLGASRPRVA
 51 VRSAYGGPVG AGIREVTINQ SLLAPLRLDA DPSLQRVRQE ESEQIKTLNN
101 KFASFIDKVR FLEQQNKLLE TKWTLLQEQK SAKSSRLPDI FEAQIAGLRG
151 QLEALQVDGG RLEAELRSMQ DVVEDFKNKY EDEINHRTAA ENEFVVLKKD
201 VDAAYMSKVE LEAKVDALND EINFLRTLNE TELTELQSQI SDTSVVLSMD
251 NSRSLDLDGI IAEVKAQYEE MARCSRAEAE AWYQTKFETL QAQAGKHGDD
301 LRNTRNEISE MNRAIQRLQA EIDNIKNQRA KLEAAIAEAE ERGELALKDA
351 RAKQEELEAA LQRGKQDMAR QLREYQELMS VKLALDIEIA TYRKLLEGEE
401 SRLAGDGVGA VNISVMNSTG GSSSGGGIGL TLGGTMGSNA LSFSSSAGPG
451 LLKAYSIRTA SASRRSARD
```

Start - End	Observed	Mr(expt)	Mr(calc)	Delta	Miss	Sequence
2 - 13	1406.76	1405.76	1405.70	0.06	0	M.SIHFSSPVFTSR.S N-Acetyl (Protein)
53 - 64	1104.62	1103.61	1103.57	0.04	0	R.SAYGGPVGAGIR.E
65 - 77	1453.93	1452.92	1452.83	0.09	0	R.EVTINQSLLAPLR.L
102 - 108	827.41	826.40	826.42	-0.02	0	K.FASFIDK.V
137 - 149	1442.88	1441.87	1441.79	0.08	0	R.LPDIFEAQIAGLR.G
168 - 177	1197.57	1196.57	1196.54	0.03	0	R.SMQDVVEDFK.N
188 - 198	1220.77	1219.76	1219.64	0.11	0	R.TAAENEFVVLK.K
199 - 208	1143.63	1142.62	1142.53	0.09	1	K.KDVDAAYMSK.V Oxidation (M)
215 - 226	1418.81	1417.80	1417.72	0.08	0	K.VDALNDEINFLR.T
254 - 265	1272.72	1271.71	1271.70	0.01	0	R.SLDLDGIIAEVK.A
254 - 273	2239.22	2238.21	2238.11	0.10	1	R.SLDLDGIIAEVKAQYEEMAK.C Oxidation (M)
330 - 342	1400.80	1399.80	1399.73	0.07	1	R.AKLEAAIAEAEER.G
352 - 363	1385.79	1384.78	1384.73	0.05	1	R.AKQEELEAALQR.G
354 - 363	1169.59	1168.58	1168.57	0.01	0	K.QEELEAALQR.G Pyro-glu (N-term Q)
374 - 382	1126.56	1125.55	1125.54	0.01	0	R.EYQELMSVK.L
383 - 393	1277.76	1276.75	1276.70	0.05	0	K.LALDIEIATYR.K

Spot No.898 Cytokeratin 8

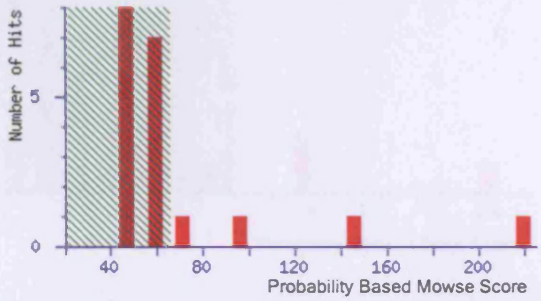

gi|181573 **Mass:** 53529 **Score:** 216 **Expect:** 4.8e-017 **Queries matched:** 31

cytokeratin 8

```
  1 MSIRVTQKSY KVSTSGPRAF SSRSYTSGPG SRISSSSFSR VGSSNFRGGL
 51 GGGYGGASGM GGITAVTVNQ SLLSPLVLEV DPNIQAVRTQ EKEQIKTLNN
101 KFASFIDKVR FLEQQNKMLE TKWSLLQQQK TARSNMDNMF ESYINNLRRQ
151 LETLGQEKLK LEAELGNMQG LVEDFKNKYE DEINKRTEME NEFVLIKKDV
201 DEAYMNKVEL ESRLEGLTDE INFLRQLYEE EIRELQSQIS DTSVVLSMDN
251 SRSLDMDSII AEVKAQYEDI ANRSRAEAES MYQIKYEELQ SLAGKHGDDL
301 RRTKTEISEM NRNISRLQAE IEGLKGQRAS LEAAIADAEQ RGELAIKDAN
351 AKLSELEAAL QRAKQDMARQ LREYQELMNV KLALDIEIAT YRKLLEGEES
401 RLESGMQNMS IHTKTTGGYA GGLSSAYGGS QAGLSYSLGS SFGSGAGSSS
451 FSRTSSSRAV VVKKIETRDG KLVSESSDVL PK
```

Start - End	Observed	Mr(expt)	Mr(calc)	Delta	Miss	Sequence
24 - 32	911.44	910.43	910.41	0.02	0	R.SYTSGPGSR.I
33 - 40	870.47	869.46	869.42	0.04	0	R.ISSSSFSR.V
41 - 47	766.41	765.40	765.38	0.02	0	R.VGSSNFR.G
102 - 108	827.44	826.44	826.42	0.01	0	K.FASFIDK.V
111 - 117	906.47	905.46	905.46	0.00	0	R.FLEQQNK.M
111 - 122	1508.85	1507.84	1507.77	0.07	1	R.FLEQQNKMLETK.W
123 - 133	1358.72	1357.71	1357.75	-0.04	1	K.WSLLQQQKTAR.S
134 - 148	1847.80	1846.79	1846.80	-0.01	0	R.SNMDNMFESYINNLR.R
134 - 148	1879.75	1878.75	1878.79	-0.04	0	R.SNMDNMFESYINNLR.R 2 Oxidation (M)
134 - 149	2019.97	2018.96	2018.89	0.07	1	R.SNMDNMFESYINNLRR.Q Oxidation (M)
159 - 176	2033.96	2032.95	2033.05	-0.10	1	K.LKLEAELGNMQGLVEDFK.N
161 - 176	1792.83	1791.82	1791.87	-0.05	0	K.LEAELGNMQGLVEDFK.N
179 - 186	1066.56	1065.55	1065.51	0.04	1	K.YEDEINKR.T
187 - 197	1352.66	1351.65	1351.67	-0.02	0	R.TEMENEFVLIK.K
187 - 198	1480.77	1479.76	1479.76	-0.01	1	R.TEMENEFVLIKK.D
199 - 207	1084.46	1083.45	1083.45	-0.01	0	K.DVDEAYMNK.V
214 - 225	1419.75	1418.74	1418.74	0.00	0	R.LEGLTDEINFLR.Q
226 - 233	1062.53	1061.52	1061.50	0.01	0	R.QLYEEEIR.E Pyro-glu (N-term Q)
226 - 233	1079.53	1078.52	1078.53	-0.00	0	R.QLYEEEIR.E
234 - 252	2109.01	2108.00	2108.01	-0.01	0	R.ELQSQISDTSVVLSMDNSR.S
234 - 252	2124.97	2123.96	2124.00	-0.04	0	R.ELQSQISDTSVVLSMDNSR.S Oxidation (M)
253 - 264	1320.64	1319.63	1319.66	-0.03	0	R.SLDMDSIIAEVK.A
276 - 285	1169.57	1168.56	1168.54	0.02	0	R.AEAESMYQIK.Y
286 - 295	1137.55	1136.54	1136.57	-0.03	0	K.YEELQSLAGK.H
305 - 312	979.47	978.46	978.44	0.02	0	K.TEISEMNR.N
329 - 341	1344.68	1343.67	1343.67	0.00	0	R.ASLEAAIADAEQR.G
353 - 362	1129.63	1128.62	1128.61	0.01	0	K.LSELEAALQR.A
365 - 372	1000.49	999.48	999.49	-0.01	1	K.QDMARQLR.E Pyro-glu (N-term Q)
373 - 381	1153.55	1152.54	1152.55	-0.01	0	R.EYQELMNVK.L
382 - 392	1277.72	1276.72	1276.70	0.01	0	K.LALDIEIATYR.K
472 - 482	1173.61	1172.60	1172.63	-0.03	0	K.LVSESSDVLPK.-

Spot No. 417 Moesin, Chain A

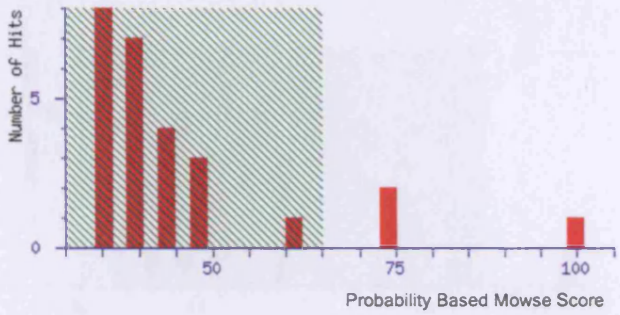

gi|50513540 **Mass:** 35010 **Score:** 100 **Expect:** 2e-005 **Queries matched:** 12

Chain A, Moesin Ferm Domain Bound To Ebp50 C-Terminal Peptide

```
   1 MPKTISVRVT TMDAELEFAI QPNTTGKQLF DQVVKTIGLR EVWFFGLQYQ
  51 DTKGFSTWLK LNKKVTAQDV RRESPLLFKF RAKFYPEDVS EELIQDITQR
 101 LFFLQVKEGI LNDDIYCPPE TAVLLASYAV QSKYGDFNKE VHKSGYLAGD
 151 KLLPQRVLEQ HKLNKDQWEE RIQVWHEEHR GMLREDAVLE YLKIAQDLEM
 201 YGVNYFSIKN KKGSELWLGV DALGLNIYEQ NDRLTPKIGF PWSEIRNISF
 251 NDKKFVIKPI DKKAPDFVFY APRLRINKRI LALCMGNHEL YMRRRKP
```

Start - End	Observed	Mr(expt)	Mr(calc)	Delta	Miss	Sequence
2 - 8	842.51	841.50	841.50	-0.00	1	M.PKTISVR.V N-Acetyl (Protein)
9 - 27	2082.08	2081.07	2081.00	0.07	0	R.VTTMDAELEFAIQPNTTGK.Q Oxidation (M)
28 - 35	976.51	975.50	975.54	-0.04	0	K.QLFDQVVK.T
54 - 60	838.43	837.42	837.44	-0.02	0	K.GFSTWLK.L
72 - 79	961.54	960.53	960.56	-0.03	1	R.KESPLLFK.F
101 - 107	894.53	893.53	893.54	-0.01	0	R.LFFLQVK.E
166 - 171	862.35	861.35	861.36	-0.01	0	K.DQWEER.I
172 - 180	1233.62	1232.61	1232.61	0.01	0	R.IQVWHEEHR.G
238 - 246	1104.61	1103.60	1103.58	0.03	0	K.IGFPWSEIR.N
255 - 262	959.60	958.59	958.59	0.00	0	K.FVIKPIDK.K
263 - 273	1310.75	1309.74	1309.68	0.06	1	K.KAPDFVFYAPR.L
264 - 273	1182.62	1181.61	1181.59	0.02	0	K.APDFVFYAPR.L

Spot No. 1317 Glyceraldehyde-3-phosphate dehydrogenase

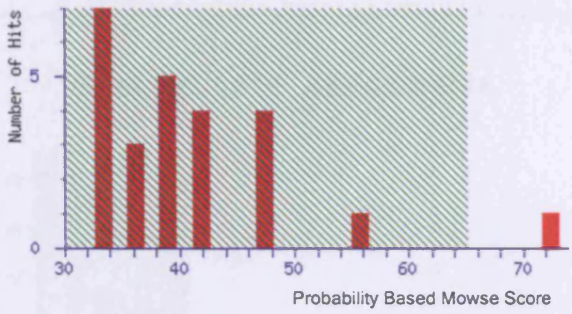

gi|7669492 **Mass:** 36204 **Score:** 74 **Expect:** 0.0084 **Queries matched:** 9
glyceraldehyde-3-phosphate dehydrogenase [Homo sapiens]

```
     1 MGKVKVGVNG FGRIGRLVTR AAFNSGKVDI VAINDPFIDL NYMVYMFQYD
    51 STHGKFHGTV KAENGKLVIN GNPITIFQER DPSKIKWGDA GAEYVVESTG
   101 VFTTMEKAGA HLQGGAKRVI ISAPSADAPM FVMGVNHEKY DNSLKIISNA
   151 SCTTNCLAPL AKVIHDNFGI VEGLMTTVHA ITATQKTVDG PSGKLWRDGR
   201 GALQNIIPAS TGAAKAVGKV IPELNGKLTG MAFRVPTANV SVVDLTCRLE
   251 KPAKYDDIKK VVKQASEGPL KGILGYTEHQ VVSSDFNSDT HSSTFDAGAG
   301 IALNDHFVKL ISWYDNEFGY SNRVVDLMAH MASKE
```

Start - End	Observed	Mr(expt)	Mr(calc)	Delta	Miss	Sequence
6 - 13	805.39	804.38	804.42	-0.04	0	K.VGVNGFGR.I
67 - 80	1613.94	1612.93	1612.89	0.04	0	K.LVINGNPITIFQER.D
119 - 139	2245.12	2244.11	2244.09	0.02	0	R.VIISAPSADAPMFVMGVNHEK.Y
140 - 145	739.33	738.33	738.35	-0.03	0	K.YDNSLK.I
163 - 186	2611.23	2610.22	2610.35	-0.12	0	K.VIHDNFGIVEGLMTTVHAITATQK.'
228 - 234	811.41	810.40	810.41	-0.00	0	K.LTGMAFR.V Oxidation (M)
255 - 260	781.38	780.38	780.40	-0.03	1	K.YDDIKK.V
264 - 271	829.38	828.38	828.43	-0.06	0	K.QASEGPLK.G
310 - 323	1763.82	1762.81	1762.80	0.02	0	K.LISWYDNEFGYSNR.V

APPENDIX 2

MOWSE Score, matched peptides and sequence coverage of identified proteins (Table 5.1)

Spot No. 1610 Annexin B9a

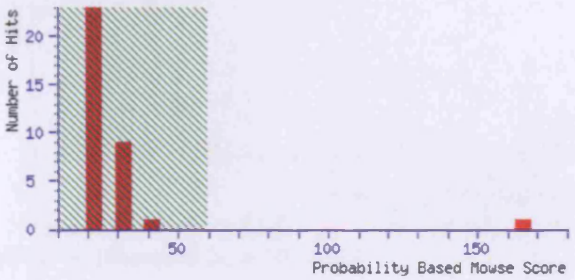

1. gi|10121901 **Mass:** 36302 **Score:** 165 **Expect:** 1.3e-012 **Queries matched:** 17
annexin B9a [Drosophila melanogaster]

```
  1 MSSAEYYPFK CTPTVYPADP FDPVEDAAIL RKAMKGFGTD EKAIIEILAR
 51 RGIVQRLEIA EAFKTSYGKD LISDLKSELG GKFEDVILAL MTPLPQFYAQ
101 ELHDAISGLG TDEEAIIEIL CTLSNYGIKT IAQFYEQSFG KSLESDLKGD
151 TSGHFKRLCV SLVQGNRDEN QGVDEAAAIA DAQALHDAGE GQWGTDESTF
201 NSILITRSYQ QLRQIFLEYE NLSGNDIEKA IKREFSGSVE KGFLAIVKCC
251 KSKIDYFSER LHDSMAGLGT KDKTLIRIIV SRSEIDLGDI KEAFQNKYGK
301 SLESWIKEDA ETDIGYVLVT LTAW
```

Start - End	Observed	Mr(expt)	Mr(calc)	Delta	Miss	Sequence
2 - 10	1133.50	1132.50	1132.51	-0.01	0	SSAEYYPFK N-Acetyl (Protein)
11 - 31	2347.18	2346.17	2346.12	0.05	0	CTPTVYPADPFDPVEDAAILR
36 - 42	753.37	752.37	752.33	0.03	0	GFGTDEK
43 - 50	898.57	897.57	897.56	0.00	0	AIIEILAR
57 - 64	920.50	919.49	919.50	-0.01	0	LEIAEAFK
70 - 76	803.47	802.46	802.44	0.02	0	DLISDLK
130 - 141	1418.65	1417.65	1417.69	-0.04	0	TIAQFYEQSFGK
142 - 148	791.34	790.34	790.41	-0.07	0	SLESDLK
158 - 167	1145.59	1144.59	1144.60	-0.02	0	LCVSLVQGNR
208 - 213	794.44	793.43	793.41	0.02	0	SYQQLR
214 - 229	1894.88	1893.87	1893.90	-0.03	0	QIFLEYENLSGNDIEK Pyro-glu (N-term Q)
214 - 229	1911.90	1910.90	1910.93	-0.03	0	QIFLEYENLSGNDIEK
234 - 241	882.41	881.41	881.41	-0.01	0	EFSGSVEK
242 - 248	747.48	746.47	746.47	0.00	0	GFLAIVK
252 - 260	1144.56	1143.56	1143.56	-0.00	1	SKIDYFSER
254 - 260	929.43	928.43	928.43	-0.00	0	IDYFSER
301 - 307	862.48	861.47	861.46	0.01	0	SLESWIK

Spot No. 1632 CG31196, 14-3-3ε

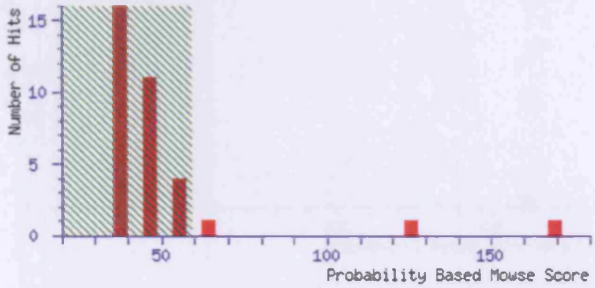

1. gi|23171618 **Mass:** 29326 **Score:** 169 **Expect:** 5.4e-013 **Queries matched:** 18
CG31196-PC, isoform C [Drosophila melanogaster]

```
  1 MTERENNVYK AKLAEQAERY DEMVEAMKKV ASMDVELTVE ERNLLSVAYK
 51 NVIGARRASW RIITSIEQKE ENKGAEEKLE MIKTYRGQVE KELRDICSDI
101 LNVLEKHLIP CATSGESKVF YYKMKGDYHR YLAEFATGSD RKDAAENSLI
151 AYKAASDIAM NDLPPTHPIR LGLALNFSVF YYEILNSPDR ACRLAKAAFD
201 DAIAELDTLS EESYKDSTLI MQLLRDNLTL WTSDMQAEGD GEPKEQIQDV
251 EDQDVS
```

Start - End	Observed	Mr(expt)	Mr(calc)	Delta	Miss	Sequence
1 - 10	1299.61	1298.60	1298.59	0.01	1	MTERENNVYK Oxidation (M)
1 - 12	1524.71	1523.70	1523.74	-0.04	2	MTERENNVYKAK N-Acetyl (Protein)
2 - 10	1194.56	1193.56	1193.57	-0.01	1	TERENNVYK N-Acetyl (Protein)
13 - 19	816.42	815.41	815.41	0.00	0	LAEQAER
13 - 29	2072.93	2071.92	2071.96	-0.04	2	LAEQAERYDEMVEAMKK 2 Oxidation (M)
30 - 42	1477.74	1476.73	1476.71	0.02	0	VASMDVELTVEER
43 - 50	907.52	906.51	906.52	-0.01	0	NLLSVAYK
51 - 56	629.35	628.34	628.37	-0.02	0	NVIGAR
62 - 69	931.51	930.51	930.54	-0.03	0	IITSIEQK
62 - 73	1431.75	1430.74	1430.76	-0.02	1	IITSIEQKEENK
62 - 78	1946.00	1944.99	1945.00	-0.01	2	IITSIEQKEENKGAEEK
124 - 141	2116.91	2115.91	2115.98	-0.07	2	MKGDYHRYLAEFATGSDR
131 - 153	2533.18	2532.17	2532.25	-0.08	2	YLAEFATGSDRKDAAENSLIAYK
142 - 153	1322.65	1321.64	1321.69	-0.05	1	KDAAENSLIAYK
154 - 170	1818.88	1817.87	1817.91	-0.04	0	AASDIAMNDLPPTHPIR
197 - 215	2087.97	2086.96	2086.96	0.00	0	AAFDDAIAELDTLSEESYK
216 - 225	1189.64	1188.63	1188.65	-0.02	0	DSTLIMQLLR
226 - 244	2122.94	2121.94	2121.92	0.02	0	DNLTLWTSDMQAEGDGEPK Oxidation (M)

Spot No. 1768 Proteosome α7 subunit

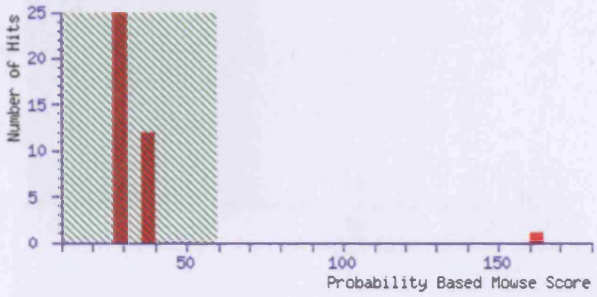

1. gi|7303843 **Mass:** 27772 **Score:** 162 **Expect:** 2.7e-012 **Queries matched:** 17
CG1519-PA, isoform A [Drosophila melanogaster]

```
      1 MSTIGTGYDL SASQFSPDGR VFQIDYASKA VEKSGTVIGI RGKDAVVLAV
     51 EKIITSKLYE PDAGGRIFTI EKNIGMAVAG LVADGNFVAD IARQEAANYR
    101 QQFEQAIPLK HLCHRVAGYV HAYTLYSAVR PFGLSIILAS WDEVEGPQLY
    151 KIEPSGSSFG YFACASGKAK QLAKTEMEKL KMDMRTDELV ESAGEIIYKV
    201 HDELKDKDFR FEMGLVGRVT GGLHLINPSE LTEKARKAGD AANKDEDSDN
    251 ETH
```

Start - End	Observed	Mr(expt)	Mr(calc)	Delta	Miss	Sequence
2 - 20	2000.93	1999.92	1999.91	0.01	0	STIGTGYDLSASQFSPDGR N-Acetyl (Protein)
21 - 29	1070.53	1069.52	1069.54	-0.02	0	VFQIDYASK
34 - 41	802.47	801.47	801.47	-0.00	0	SGTVIGIR
42 - 52	1128.62	1127.61	1127.65	-0.04	1	GKDAVVLAVEK
58 - 66	977.47	976.46	976.46	-0.00	0	LYEPDAGGR
67 - 72	750.44	749.43	749.43	-0.00	0	IFTIEK
73 - 93	2074.04	2073.04	2073.07	-0.03	0	NIGMAVAGLVADGNFVADIAR
73 - 93	2090.02	2089.02	2089.06	-0.05	0	NIGMAVAGLVADGNFVADIAR Oxidation (M)
94 - 100	834.41	833.40	833.37	0.03	0	QEAANYR Pyro-glu (N-term Q)
94 - 100	851.41	850.41	850.39	0.01	0	QEAANYR
101 - 110	1184.61	1183.60	1183.62	-0.02	0	QQFEQAIPLK Pyro-glu (N-term Q)
152 - 168	1764.78	1763.77	1763.78	-0.01	0	IEPSGSSFGYFACASGK
186 - 199	1566.77	1565.76	1565.78	-0.02	0	TDELVESAGEIIYK
200 - 210	1401.70	1400.69	1400.70	-0.02	2	VHDELKDKDFR
211 - 218	908.47	907.47	907.46	0.01	0	FEMGLVGR
211 - 218	924.45	923.44	923.45	-0.01	0	FEMGLVGR Oxidation (M)
219 - 234	1707.91	1706.91	1706.92	-0.01	0	VTGGLHLINPSELTEK

Spot No. 1782 EG:EG0003.7

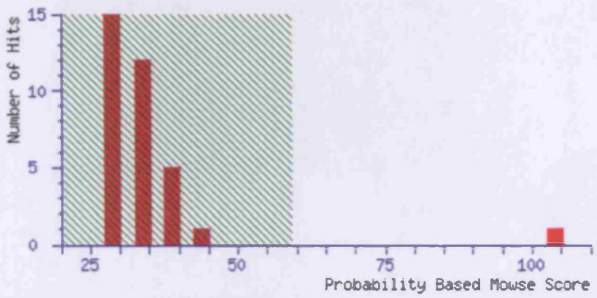

1. gi|3757564 **Mass:** 24289 **Score:** 104 **Expect:** 1.7e-006 **Queries matched:** 12
EG:EG0003.7 [Drosophila melanogaster]

```
  1 MAFGDVTTPQ GLKELNAFLA DNSYISGYTP SKADLSVFDA LGKAPSADNV
 51 NVARVYRHIA SFEAAERAAV SGTPLPQLAG GKPTVAAAAK PAADDDDDVD
101 LFGSDDEEDE EAERIKQERV AAYAAKKSKK PALIAKSSVL LDVKPWDDET
151 DMKEMENNVR TIEMDGLLWG ASKLVPVGYG INKLQIMCVI EDDKVSIDLL
201 QEKIEEFEDF VQSVDIAAFN KI
```

Start - End	Observed	Mr(expt)	Mr(calc)	Delta	Miss	Sequence
2 - 13	1233.63	1232.63	1232.64	-0.01	0	AFGDVTTPQGLK
2 - 13	1275.64	1274.63	1274.65	-0.02	0	AFGDVTTPQGLK N-Acetyl (Protein)
14 - 32	2090.01	2089.00	2089.00	0.00	0	ELNAFLADNSYISGYTPSK
33 - 43	1135.57	1134.57	1134.59	-0.03	0	ADLSVFDALGK
33 - 54	2230.22	2229.21	2229.14	0.07	1	ADLSVFDALGKAPSADNVNVAR
58 - 67	1130.55	1129.54	1129.55	-0.01	0	HIASFEAAER
130 - 136	740.50	739.49	739.50	-0.00	0	KPALIAK
161 - 173	1436.69	1435.68	1435.70	-0.02	0	TIEMDGLLWGASK Oxidation (M)
174 - 183	1059.60	1058.59	1058.61	-0.02	0	LVPVGYGINK
195 - 203	1044.55	1043.54	1043.59	-0.05	0	VSIDLLQEK
204 - 221	2101.16	2100.15	2100.01	0.15	0	IEEFEDFVQSVDIAAFNK
204 - 222	2214.11	2213.10	2213.09	0.01	1	IEEFEDFVQSVDIAAFNKI

Spot No. 1811 CG5224

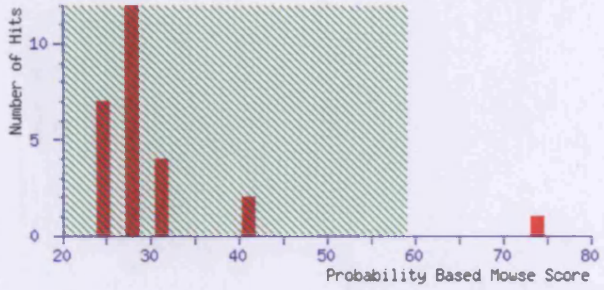

1. gi|21428462 **Mass:** 25363 **Score:** 74 **Expect:** 0.0018 **Queries matched:** 7
LD18692p [Drosophila melanogaster]

```
   1 MSAKPILYYA PRSPPCRAVL LTAAALGLEL DLRLVNVKAG EHKSAEFLKL
  51 NAQHTIPVLD DNGTIVSDSH IICSYLADKY APEGDDSLYP KDPEKRRLVD
 101 ARLYYDCGHL FPRIRFIVEP VIYFGAGEVP SDRVAYLQKA YDGLEHCLAE
 151 GDYLVGDKLT IADLSCIASV STAEAFAPIE PDQFPRLVQW VKRIQALPYY
 201 QKNNQEGLDM LVGLVKGLLA ERQQK
```

Start - End	Observed	Mr(expt)	Mr(calc)	Delta	Miss	Sequence
2 - 12	1320.68	1319.68	1319.72	-0.05	0	SAKPILYYAPR N-Acetyl (Protein)
18 - 33	1638.91	1637.90	1637.97	-0.07	0	AVLLTAAALGLELDLR
103 - 113	1440.60	1439.59	1439.67	-0.08	0	LYYDCGHLFPR
140 - 158	2124.81	2123.81	2123.95	-0.14	0	AYDGLEHCLAEGDYLVGDK
187 - 192	772.46	771.45	771.46	-0.01	0	LVQWVK
194 - 202	1123.54	1122.53	1122.61	-0.07	0	IQALPYYQK
203 - 216	1545.66	1544.65	1544.79	-0.13	0	NNQEGLDMLVGLVK Oxidation (M)

Spot No. 1824 GTP-binding nuclear protein

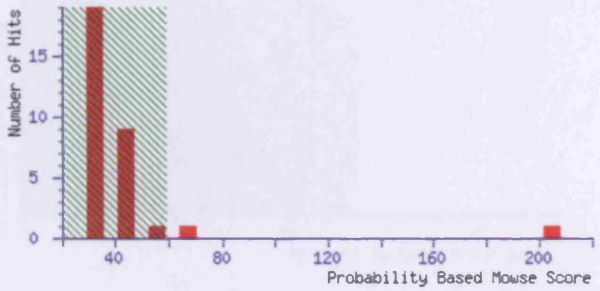

1. gi|28317119 **Mass:** 24921 **Score:** 205 **Expect:** 1.3e-016 **Queries matched:** 18
LD40852p [Drosophila melanogaster]

```
      1 MAQEGQDIPT FKCVLVGDGG TGKTTFVKRH MTGEFEKKYV ATLGVEVHPL
     51 IFHTNRGAIR FNVWDTAGQE KFGGLRDGYY IQGQCAVIMF DVTSRVTYKN
    101 VPNWHRDLVR VCENIPIVLC GNKVDIKDRK VKAKSIVFHR KKNLQYYDIS
    151 AKSNYNFEKP FLWLARKLVG DPNLEFVAMP ALLPPEVKMD KDWQAQIERD
    201 LQEAQATALP DEDEEL
```

Start - End	Observed	Mr(expt)	Mr(calc)	Delta	Miss	Sequence
2 - 12	1275.61	1274.61	1274.61	-0.01	0	AQEGQDIPTFK N-Acetyl (Protein)
30 - 37	978.42	977.41	977.43	-0.02	0	HMTGEFEK
30 - 37	994.41	993.40	993.42	-0.02	0	HMTGEFEK Oxidation (M)
30 - 38	1122.50	1121.50	1121.52	-0.02	1	HMTGEFEKK Oxidation (M)
39 - 56	2066.06	2065.05	2065.11	-0.06	0	YVATLGVEVHPLIFHTNR
61 - 71	1294.60	1293.59	1293.60	-0.00	0	FNVWDTAGQEK
77 - 95	2239.08	2238.07	2238.01	0.07	0	DGYYIQGQCAVIMFDVTSR Oxidation (M)
100 - 106	922.47	921.46	921.46	0.01	0	NVPNWHR
111 - 123	1515.76	1514.76	1514.76	-0.00	0	VCENIPIVLCGNK
111 - 127	1970.99	1969.98	1970.03	-0.05	1	VCENIPIVLCGNKVDIK
111 - 129	2242.02	2241.01	2241.16	-0.15	2	VCENIPIVLCGNKVDIKDR
135 - 140	758.42	757.41	757.42	-0.01	0	SIVFHR
143 - 152	1214.59	1213.58	1213.60	-0.02	0	NLQYYDISAK
153 - 166	1784.95	1783.94	1783.90	0.03	0	SNYNFEKPFLWLAR
167 - 188	2393.19	2392.18	2392.31	-0.13	1	KLVGDPNLEFVAMPALLPPEVK Oxidation (M)
168 - 188	2265.11	2264.11	2264.21	-0.11	0	LVGDPNLEFVAMPALLPPEVK Oxidation (M)
189 - 199	1419.67	1418.66	1418.66	0.00	1	MDKDWQAQIER
189 - 199	1435.67	1434.66	1434.66	0.00	1	MDKDWQAQIER Oxidation (M)

Spot No. 1832 Glutathione S-transferase E2

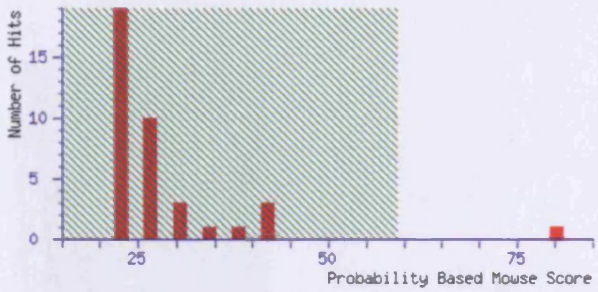

1. gi|19922528 **Mass:** 25440 **Score:** 80 **Expect:** 0.0004 **Queries matched:** 9
CG17523-PA [Drosophila melanogaster]

```
  1 MSDKLVLYGM DISPPVRACK LTLRALNLDY EYKEMDLLAG DHFKDAFLKK
 51 NPQHTVPLLE DNGALIWDSH AIVCYLVDKY ANSDELYPRD LVLRAQVDQR
101 LFFDASILFM SLRNVSIPYF LRQVSLVPKE KVDNIKDAYG HLENFLGDNP
151 YLTGSQLTIA DLCCGATASS LAAVLDLDEL KYPKVAAWFE RLSKLPHYEE
201 DNLRGLKKYI NLLKPVLNLE Q
```

Start - End	Observed	Mr(expt)	Mr(calc)	Delta	Miss	Sequence	
5 - 17	1459.85	1458.84	1458.79	0.05	0	LVLYGMDISPPVR	
5 - 17	1475.81	1474.80	1474.79	0.01	0	LVLYGMDISPPVR	Oxidation (M)
25 - 33	1128.56	1127.56	1127.55	0.01	0	ALNLDYEYK	
90 - 94	615.41	614.41	614.38	0.03	0	DLVLR	
114 - 122	1108.62	1107.61	1107.61	0.00	0	NVSIPYFLR	
123 - 129	770.48	769.47	769.47	0.00	0	QVSLVPK	
185 - 191	878.44	877.43	877.44	-0.01	0	VAAWFER	
195 - 204	1285.63	1284.62	1284.61	0.01	0	LPHYEEDNLR	
209 - 221	1556.89	1555.88	1555.90	-0.01	0	YINLLKPVLNLEQ	

Spot No. 1841 Cytosolic thioredoxin peroxidase variant 2

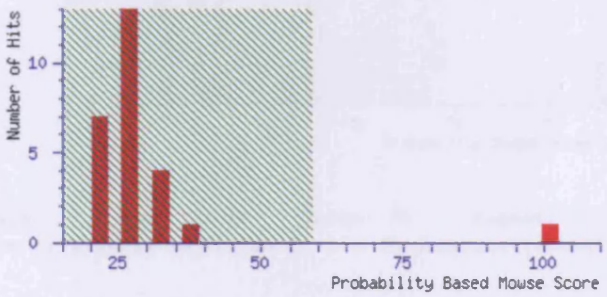

1. gi|12744791 **Mass:** 21952 **Score:** 101 **Expect:** 3.4e-006 **Queries matched:** 10
cytosolic thioredoxin peroxidase variant 2 [Drosophila melanogaster]

```
  1 MPQLQKPAPA FAGTAVVNGV FKDIKLSDYK GKYLVLFFYP LDFTFVCPTE
 51 IIAFSESAAE FRKINCEVIG CSTDSQFTHL AWINTPRKQG GLGSMDIPLL
101 ADKSMKVARD YGVLDEETGI PFRGLFIIDD KQNLRQITVN DLPVGRSVEE
151 TLRLVQAFQY TDKYGEVCPA NWKPGQKTMV ADPTKSKEYF ETTS
```

Start - End	Observed	Mr(expt)	Mr(calc)	Delta	Miss	Sequence
88 - 103	1658.78	1657.77	1657.87	-0.10	1	KQGGLGSMDIPLLADK Oxidation (M)
89 - 103	1530.67	1529.66	1529.78	-0.11	0	QGGLGSMDIPLLADK Oxidation (M)
110 - 123	1610.77	1609.76	1609.76	-0.00	0	DYGVLDEETGIPFR
124 - 131	920.46	919.45	919.50	-0.05	0	GLFIIDDK
124 - 135	1431.77	1430.76	1430.79	-0.02	1	GLFIIDDKQNLR
136 - 146	1194.62	1193.61	1193.64	-0.03	0	QITVNDLPVGR Pyro-glu (N-term Q)
136 - 146	1211.60	1210.60	1210.67	-0.07	0	QITVNDLPVGR
154 - 163	1212.62	1211.61	1211.62	-0.00	0	LVQAFQYTDK
164 - 177	1633.71	1632.70	1632.77	-0.07	0	YGEVCPANWKPGQK
186 - 194	1091.42	1090.41	1090.48	-0.07	1	SKEYFETTS

Spot No. 1857 Similar to CG3644

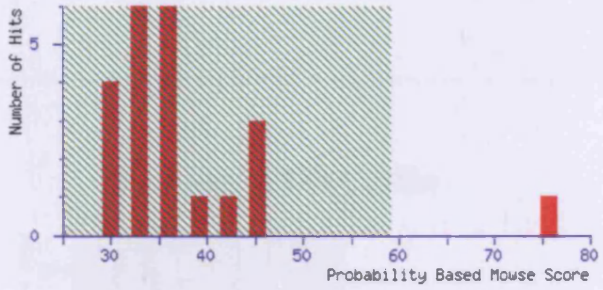

1. gi|38048339 **Mass:** 16392 **Score:** 76 **Expect:** 0.0011 **Queries matched:** 6
similar to Drosophila melanogaster bic [Drosophila yakuba]

```
  1 MNPEKLKKLQ AQVRIGGKGT PRRKKKIVHS TPATDDKKLQ SSLKKLSVNT
 51 IPGIEEVNII KNDGTVIHFN NPKAQASLPT NTFAITGHGE NKTITEMVPG
101 ILTQLGPQDI NQLKKLATEI ANKTGAGGAA GSSAADAGDD DVPDLVENFE
151 EVAIA
```

Start - End	Observed	Mr(expt)	Mr(calc)	Delta	Miss	Sequence	
27 - 38	1311.72	1310.71	1310.68	0.03	1	IVHSTPATDDKK	
45 - 61	1867.05	1866.05	1866.08	-0.04	1	KLSVNTIPGIEEVNIIK	
46 - 61	1738.98	1737.98	1737.99	-0.01	0	LSVNTIPGIEEVNIIK	
62 - 73	1355.64	1354.63	1354.66	-0.03	0	NDGTVIHFNNPK	
74 - 92	1956.96	1955.95	1955.97	-0.02	0	AQASLPTNTFAITGHGENK	
93 - 114	2425.33	2424.32	2424.29	0.03	0	TITEMVPGILTQLGPQDINQLK	Oxidation (M)

Spot No. 1875 eIF-5A, translational initiation

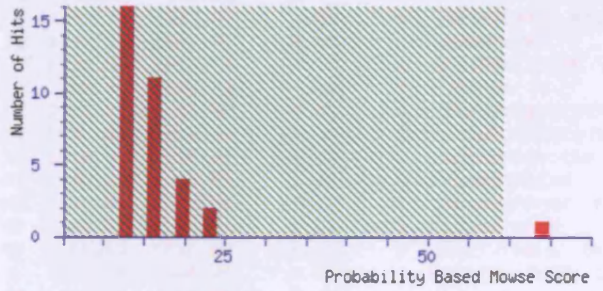

1. gi|21626716 **Mass:** 17922 **Score:** 64 **Expect:** 0.017 **Queries matched:** 8
CG3186-PB, isoform B [Drosophila melanogaster]

```
  1 MAELDDQFET TDSGASTTYP MQCSALRKNG FVMLKSRPCK IVEMSTSKTG
 51 KHGHAKVHMV GIDIFSNKKY EDICPSTHNM DVPNVKREDL QLIAISDDSF
101 LTLMTESGDL REDLKVPEGE LGEQLRLDFD SGKDLLCTVL KACGEECVIA
151 IKTNTALDK
```

Start - End	Observed	Mr(expt)	Mr(calc)	Delta	Miss	Sequence	
29 - 35	824.43	823.42	823.43	-0.01	0	NGFVMLK	Oxidation (M)
41 - 48	910.38	909.37	909.45	-0.08	0	IVEMSTSK	Oxidation (M)
57 - 68	1375.68	1374.67	1374.70	-0.03	0	VHMVGIDIFSNK	Oxidation (M)
69 - 86	2162.79	2161.78	2161.98	-0.19	1	KYEDICPSTHNMDVPNVK	Oxidation (M)
112 - 126	1711.89	1710.89	1710.88	0.01	1	EDLKVPEGELGEQLR	
116 - 126	1226.61	1225.60	1225.63	-0.03	0	VPEGELGEQLR	
127 - 133	781.33	780.32	780.37	-0.04	0	LDFDSGK	
142 - 152	1249.51	1248.50	1248.58	-0.08	0	ACGEECVIAIK	

Spot No. 1874 Cofilin

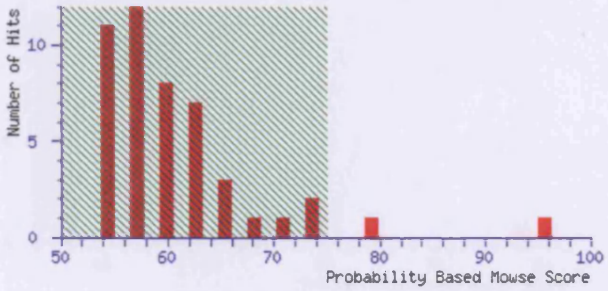

1. gi|17136986 **Mass:** 17428 **Score:** 96 **Expect:** 0.00049 **Queries matched:** 18
CG4254-PA [Drosophila melanogaster]

```
  1 MASGVTVSDV CKTTYEEIKK DKKHRYVIFY IRDEKQIDVE TVADRNAEYD
 51 QFLEDIQKCG PGECRYGLFD FEYMHQCQGT SESSKKQKLF LMSWCPDTAK
101 VKKKMLYSSS FDALKKSLVG VQKYIQATDL SEASREAVEE KLRATDRQ
```

Start - End	Observed	Mr(expt)	Mr(calc)	Delta	Miss	Sequence
2 - 12	1122.59	1121.58	1121.54	0.04	0	ASGVTVSDVCK
2 - 19	1987.02	1986.02	1985.96	0.05	1	ASGVTVSDVCKTTYEEIK
13 - 20	1011.53	1010.53	1010.53	-0.00	1	TTYEEIKK
26 - 32	973.55	972.54	972.54	-0.00	0	YVIFYIR
36 - 45	1128.56	1127.56	1127.55	0.01	0	QIDVETVADR Pyro-glu (N-term Q)
36 - 45	1145.58	1144.57	1144.57	-0.00	0	QIDVETVADR
46 - 58	1612.75	1611.74	1611.74	-0.00	0	NAEYDQFLEDIQK
59 - 65	835.33	834.33	834.31	0.02	0	CGPGECR
66 - 85	2413.93	2412.93	2413.00	-0.07	0	YGLFDFEYMHQCQGTSESSK
66 - 85	2429.98	2428.97	2428.99	-0.02	0	YGLFDFEYMHQCQGTSESSK Oxidation (M)
87 - 100	1707.79	1706.79	1706.82	-0.03	1	QKLFLMSWCPDTAK Pyro-glu (N-term Q)
89 - 100	1468.69	1467.68	1467.69	-0.01	0	LFLMSWCPDTAK
89 - 100	1484.68	1483.67	1483.68	-0.01	0	LFLMSWCPDTAK Oxidation (M)
105 - 115	1261.62	1260.61	1260.61	0.01	0	MLYSSSFDALK
105 - 115	1277.68	1276.67	1276.60	0.07	0	MLYSSSFDALK Oxidation (M)
105 - 116	1405.71	1404.70	1404.70	0.00	1	MLYSSSFDALKK Oxidation (M)
117 - 123	730.42	729.42	729.44	-0.02	0	SLVGVQK
124 - 135	1353.67	1352.66	1352.66	0.01	0	YIQATDLSEASR

Spot No. 1882 Cofilin

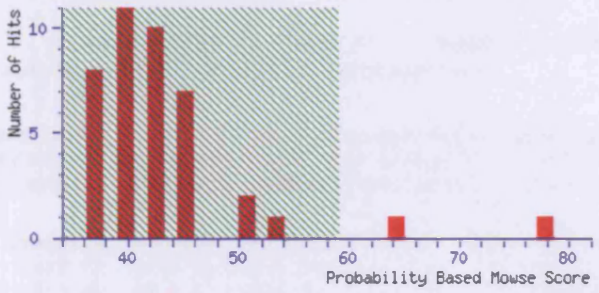

1. gi|7291724 **Mass:** 17428 **Score:** 78 **Expect:** 0.00076 **Queries matched:** 19
CG4254-PA [Drosophila melanogaster]

```
   1 MASGVTVSDV CKTTYEEIKK DKKHRYVIFY IRDEKQIDVE TVADRNAEYD
  51 QFLEDIQKCG PGECRYGLFD FEYMHQCQGT SESSKKQKLF LMSWCPDTAK
 101 VKKKMLYSSS FDALKKSLVG VQKYIQATDL SEASREAVEE KLRATDRQ
```

Start - End	Observed	Mr(expt)	Mr(calc)	Delta	Miss	Sequence	
2 - 12	1164.57	1163.56	1163.55	0.02	0	ASGVTVSDVCK	N-Acetyl (Protein)
13 - 19	883.46	882.45	882.43	0.02	0	TTYEEIK	
13 - 20	1011.52	1010.52	1010.53	-0.01	1	TTYEEIKK	
26 - 32	973.56	972.55	972.54	0.01	0	YVIFYIR	
26 - 35	1345.73	1344.72	1344.71	0.01	1	YVIFYIRDEK	
26 - 45	2472.07	2471.06	2471.27	-0.21	2	YVIFYIRDEKQIDVETVADR	
36 - 45	1128.57	1127.57	1127.55	0.02	0	QIDVETVADR	Pyro-glu (N-term Q)
36 - 45	1145.58	1144.57	1144.57	-0.00	0	QIDVETVADR	
46 - 58	1612.69	1611.69	1611.74	-0.06	0	NAEYDQFLEDIQK	
59 - 65	818.29	817.29	817.28	0.00	0	CGPGECR	Pyro-glu (N-term Q)
59 - 65	835.32	834.31	834.31	-0.00	0	CGPGECR	
89 - 100	1468.68	1467.68	1467.69	-0.01	0	LFLMSWCPDTAK	
89 - 100	1484.66	1483.65	1483.68	-0.03	0	LFLMSWCPDTAK	Oxidation (M)
105 - 115	1261.61	1260.60	1260.61	-0.00	0	MLYSSSFDALK	
105 - 115	1277.59	1276.58	1276.60	-0.02	0	MLYSSSFDALK	Oxidation (M)
105 - 116	1389.68	1388.67	1388.70	-0.03	1	MLYSSSFDALKK	
105 - 116	1405.68	1404.68	1404.70	-0.02	1	MLYSSSFDALKK	Oxidation (M)
124 - 135	1353.65	1352.64	1352.66	-0.02	0	YIQATDLSEASR	
142 - 147	731.37	730.36	730.41	-0.05	1	LRATDR	

Spot No. 1885 Slow superoxide dismutase

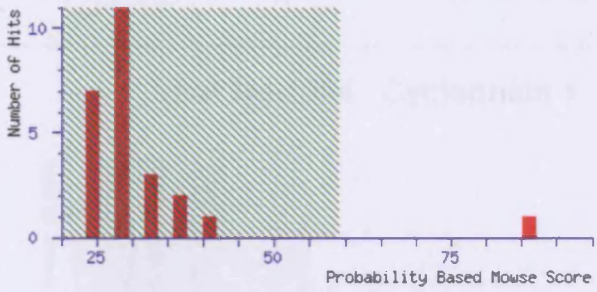

1. gi|4572573 **Mass:** 15200 **Score:** 86 **Expect:** 0.00011 **Queries matched:** 7
slow superoxide dismutase [Drosophila melanogaster]

```
  1 VINGDAKGTV FFEQESSGTP VKVSGEVCGL AKGLHGFHVH EFGDNTNGCM
 51 SSGPHFNPYG KEHGAPVDEN RHLGDLGNIE ATGDCPTKVK ITDSKITLFG
101 ADSIIGRTVV VHADADDLGQ GGHELSKSTG NAGARIGCGV IGIAKV
```

Start - End	Observed	Mr(expt)	Mr(calc)	Delta	Miss	Sequence
8 - 22	1612.75	1611.74	1611.78	-0.04	0	GTVFFEQESSGTPVK
23 - 32	1019.50	1018.49	1018.51	-0.02	0	VSGEVCGLAK
62 - 71	1123.52	1122.51	1122.51	0.00	0	EHGAPVDENR
72 - 88	1797.82	1796.81	1796.84	-0.03	0	HLGDLGNIEATGDCPTK
96 - 107	1262.70	1261.69	1261.70	-0.01	0	ITLFGADSIIGR
108 - 127	2047.95	2046.94	2047.00	-0.05	0	TVVVHADADDLGQGGHELSK
136 - 145	987.53	986.52	986.56	-0.04	0	IGCGVIGIAK

Spot No. 1892 40S ribosomal protein S12

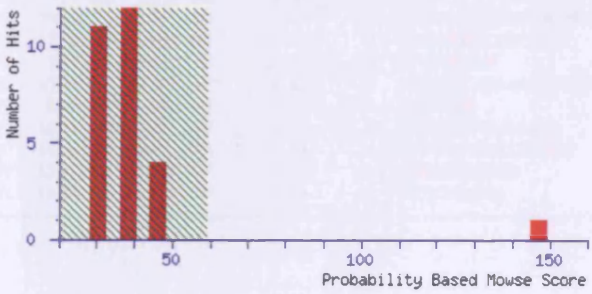

1. gi|38048233 **Mass:** 15501 **Score:** 147 **Expect:** 8.5e-011 **Queries matched:** 10
similar to Drosophila melanogaster RpS12 [Drosophila yakuba]
gi|902622 **Mass:** 16970 **Score:** 138 **Expect:** 6.7e-010 **Queries matched:** 10
40S ribosomal protein S12 [Drosophila melanogaster]

```
  1 LSKVQCILNR RTMADVDVDV PSAAPVLDGA MDINTALQEV LKKSLIADGL
 51 VHGIHQACKA LDKRQAVLCI LAESFDEPNY KKLVTALCNE HQIPLIRVDS
101 HKKLGEWSGL CKIDKEGKPR KVCGCSVVVI KDFGEETPAL DVVKDHLRQN
151 S
```

Start - End	Observed	Mr(expt)	Mr(calc)	Delta	Miss	Sequence	
44 - 59	1718.87	1717.86	1717.89	-0.03	0	SLIADGLVHGIHQACK	
65 - 81	1996.92	1995.91	1995.96	-0.05	0	QAVLCILAESFDEPNYK	
65 - 82	2107.94	2106.94	2107.03	-0.09	1	QAVLCILAESFDEPNYKK	Pyro-glu (N-term Q)
65 - 82	2125.03	2124.02	2124.06	-0.03	1	QAVLCILAESFDEPNYKK	
83 - 97	1776.97	1775.96	1775.97	-0.01	0	LVTALCNEHQIPLIR	
103 - 112	1177.61	1176.60	1176.60	0.00	1	KLGEWSGLCK	
113 - 120	942.54	941.54	941.53	0.01	1	IDKEGKPR	
121 - 131	1248.69	1247.68	1247.67	0.01	1	KVCGCSVVVIK	
132 - 144	1419.67	1418.66	1418.69	-0.03	0	DFGEETPALDVVK	
132 - 148	1940.99	1939.98	1939.96	0.02	1	DFGEETPALDVVKDHLR	

Spot No.1894 Cyclophilin 1

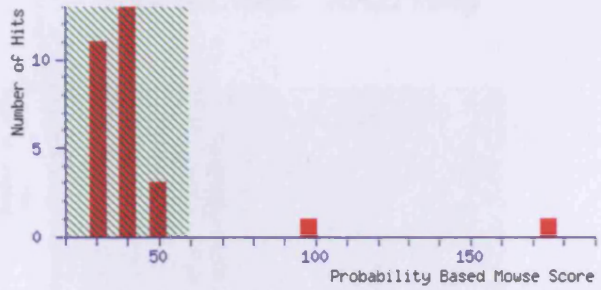

1. gi|33589296 **Mass:** 18067 **Score:** 175 **Expect:** 1.3e-013 **Queries matched:** 16
SD01793p [Drosophila melanogaster]

```
  1 MSTLPRVFFD MTADNEPLGR IVMELRSDVV PKTAENFRAL CTGEKGFGYK
 51 GSIFHRVIPN FMCQGGDFTN HNGTGGKSIY GNKFPDENFE LKHTGSGILS
101 MANAGANTNG SQFFICTVKT AWLDNKHVVF GEVVEGLDVV KKIESYGSQS
151 GKTSKKIIVA NSGSL
```

Start - End	Observed	Mr(expt)	Mr(calc)	Delta	Miss	Sequence
2 - 6	615.38	614.37	614.34	0.04	0	STLPR N-Acetyl (Protein)
7 - 20	1611.81	1610.80	1610.74	0.06	0	VFFDMTADNEPLGR
7 - 20	1627.75	1626.74	1626.73	0.01	0	VFFDMTADNEPLGR Oxidation (M)
21 - 26	760.42	759.41	759.43	-0.02	0	IVMELR
21 - 26	776.42	775.41	775.43	-0.01	0	IVMELR Oxidation (M)
21 - 32	1401.67	1400.66	1400.77	-0.11	1	IVMELRSDVVPK Oxidation (M)
33 - 38	737.31	736.30	736.35	-0.05	0	TAENFR
57 - 77	2251.03	2250.02	2249.99	0.02	0	VIPNFMCQGGDFTNHNGTGGK
78 - 92	1800.87	1799.86	1799.87	-0.02	1	SIYGNKFPDENFELK
84 - 92	1138.51	1137.50	1137.53	-0.03	0	FPDENFELK
93 - 119	2799.33	2798.32	2798.31	0.01	0	HTGSGILSMANAGANTNGSQFFICTVK Oxidation (M)
120 - 126	847.38	846.37	846.42	-0.05	0	TAWLDNK
127 - 141	1625.87	1624.86	1624.88	-0.02	0	HVVFGEVVEGLDVVK
127 - 142	1753.97	1752.97	1752.98	-0.01	1	HVVFGEVVEGLDVVKK
142 - 152	1183.67	1182.66	1182.59	0.07	1	KIESYGSQSGK
156 - 165	1001.61	1000.60	1000.59	0.01	1	KIIVANSGSL

Spot No.1902 RH27794p

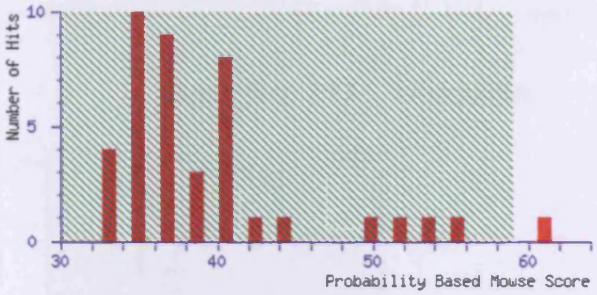

1. gi|21064703 **Mass:** 17216 **Score:** 61 **Expect:** 0.034 **Queries matched:** 13
RH27794p [Drosophila melanogaster]

```
  1 MAANKERTFI MVKPDGVQRG LVGKIIERFE QKGFKLVALK FTWASKELLE
 51 KHYADLSARP FFPGLVNYMN SGPVVPMVWE GLNVVKTGRQ MLGATNPADS
101 LPGTIRGDFC IQVGRNIIHG SDAVESAEKE IALWFNEKEL VTWTPAAKDW
151 IYE
```

Start - End	Observed	Mr(expt)	Mr(calc)	Delta	Miss	Sequence	
8 - 19	1390.77	1389.77	1389.74	0.02	0	TFIMVKPDGVQR	
8 - 19	1406.77	1405.76	1405.74	0.02	0	TFIMVKPDGVQR	Oxidation (M)
25 - 35	1394.89	1393.88	1393.77	0.11	2	IIERFEQKGFK	
29 - 35	883.46	882.46	882.46	-0.00	1	FEQKGFK	
41 - 46	739.37	738.37	738.37	-0.00	0	FTWASK	
47 - 51	631.32	630.31	630.36	-0.04	0	ELLEK	
90 - 106	1724.98	1723.97	1723.86	0.12	0	QMLGATNPADSLPGTIR	Pyro-glu (N-term Q)
90 - 106	1740.93	1739.92	1739.85	0.07	0	QMLGATNPADSLPGTIR	Oxidation (M); Pyro-glu (N-term Q)
90 - 106	1757.92	1756.92	1756.88	0.04	0	QMLGATNPADSLPGTIR	Oxidation (M)
107 - 115	1051.50	1050.50	1050.49	0.01	0	GDFCIQVGR	
116 - 129	1469.73	1468.73	1468.72	0.01	0	NIIHGSDAVESAEK	
130 - 138	1149.60	1148.60	1148.59	0.01	0	EIALWFNEK	

APPENDIX 3

MOWSE Score, matched peptides and sequence coverage of identified proteins (Table 5.3)

Spot No. 717 Ubiquitin

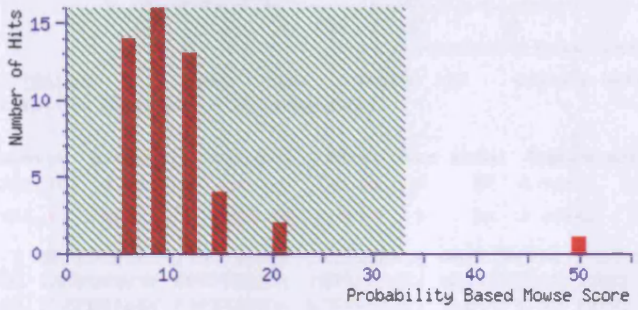

1. gi|158767 **Mass:** 8540 **Score:** 50 **Queries matched:** 2
ubiquitin

	Query	Observed	Mr(expt)	Mr(calc)	Delta	Miss	Score	Expect	Rank	Peptide
☑	16	534.31	1066.61	1066.61	-0.00	0	17	2.1	1	ESTLHLVLR
☑	47	894.46	1786.90	1786.92	-0.02	0	33	0.042	1	TITLEVEPSDTIENVK

1 MQIFVKTLTG KTITLEVEPS DTIENVKAKI QDKEGXPPDQ QRLIFAGKXL
51 EDGRTLSDYN IQKESTLHLV LRLRGG

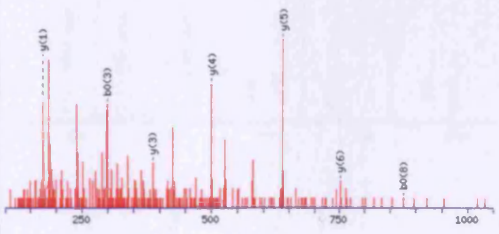

#	b	b++	b0	b0++	Seq.	y	y++	y*	y+++	y0	y0++	#
1	130.05	65.53	112.04	56.52	E							9
2	217.08	109.04	199.07	100.04	S	938.58	469.79	921.55	461.28	920.57	460.79	8
3	318.13	159.57	300.12	150.56	T	851.55	426.28	834.52	417.76	833.54	417.27	7
4	431.21	216.11	413.20	207.11	L	750.50	375.75	733.47	367.24			6
5	568.27	284.64	550.26	275.63	H	637.41	319.21	620.39	310.70			5
6	681.36	341.18	663.35	332.18	L	500.36	250.68	483.33	242.17			4
7	780.43	390.72	762.41	381.71	V	387.27	194.14	370.24	185.63			3
8	893.51	447.26	875.50	438.25	L	288.20	144.61	271.18	136.09			2
9					R	175.12	88.06	158.09	79.55			1

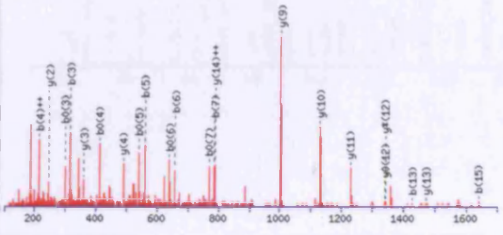

#	b	b++	b*	b+++	b0	b0++	Seq.	y	y++	y*	y+++	y0	y0++	#
1	102.05	51.53			84.04	42.53	T							16
2	215.14	108.07			197.13	99.07	I	1686.88	843.94	1669.85	835.43	1668.87	834.94	15
3	316.19	158.60			298.18	149.59	T	1573.80	787.40	1556.77	778.89	1555.78	778.40	14
4	429.27	215.14			411.26	206.13	L	1472.75	736.88	1455.72	728.36	1454.74	727.87	13
5	558.31	279.66			540.30	270.66	E	1359.66	680.34	1342.64	671.82	1341.65	671.33	12
6	657.38	329.19			639.37	320.19	V	1230.62	615.81	1213.59	607.30	1212.61	606.81	11
7	786.42	393.72			768.41	384.71	E	1131.56	566.28	1114.53	557.77	1113.54	557.27	10
8	883.48	442.24			865.47	433.24	P	1002.51	501.76	985.48	493.25	984.50	492.75	9
9	970.51	485.76			952.50	476.75	S	905.46	453.23	888.43	444.72	887.45	444.23	8
10	1085.54	543.27			1067.53	534.27	D	818.43	409.72	801.40	401.20	800.41	400.71	7
11	1186.58	593.80			1168.57	584.79	T	703.40	352.20	686.37	343.69	685.39	343.20	6
12	1299.67	650.34			1281.66	641.33	I	602.35	301.68	585.32	293.17	584.34	292.67	5
13	1428.71	714.86			1410.70	705.85	E	489.27	245.14	472.24	236.62	471.26	236.13	4
14	1542.75	771.88	1525.73	763.37	1524.74	762.88	N	360.22	180.62	343.20	172.10			3
15	1641.82	821.41	1624.80	812.90	1623.81	812.41	V	246.18	123.59	229.15	115.08			2
16							K	147.11	74.06	130.09	65.55			1

Spot No. 802 HSP68

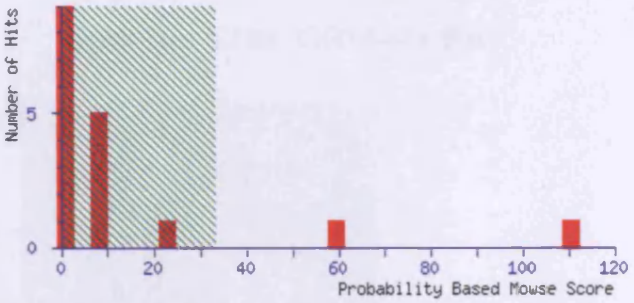

1. gi|7301096 **Mass:** 70043 **Score:** 110 **Queries matched:** 2
CG5436-PA [Drosophila melanogaster]

Query	Observed	Mr(expt)	Mr(calc)	Delta	Miss	Score	Expect	Rank	Peptide
☑ 4	585.33	1168.65	1168.66	-0.00	0	57	0.00023	1	DAGRIAGINVLR
☑ 12	941.98	1881.94	1881.96	-0.02	0	54	0.00032	1	DNNVLGTFDLTGVPPAPR

```
  1 MPAIGIDLGT TYSCVGVFQY GKVEIIANDQ GNRTTPSYVA FTDSERLIGD
 51 AAKNQVAMNP KNSVFDAKRL IGRRFDDSKI QEDIKHWPFK VINDNGKPKI
101 SVEFKGANKC FSPEEISSMV LTKMKETAEA YLGTTVKDAV ITVPAYFNDS
151 QRQATKDAGA IAGINVLRII NEPTAAALAY GLDKNLKGER NVLIFDLGGG
201 TFDVSILTID EGSLFEVRST AGDTHLGGED FDNRLVNHFA EEFKRKYKKD
251 LRSNPRALRR LRTAAERAKR TLSSSTEASL EIDALYEGHD FYSKVSRARF
301 EELCGDLFRN TLEPVEKALK DAKMDKSQIH DIVLVGGSTR IPKVQNLLQN
351 FFGGKTLNLS INPDEAVAYG AAIQAAILSG DKSSEIKDVL LVDVAPLSLG
401 IETAGGVMTK LIERNSRIPC KQSKTFTTYA DNQPAVTIQV FEGERALTKD
451 NNVLGTFDLT GVPPAPRGVP KIDVTFDLDA NGILNVTAKE QGTGNAKNIT
501 IKNDKGRLSQ ADIDRMLSEA EKYAEEDERH RQRIAARNQL ETYLFGVKEA
551 AENGGDRISA ADKSSIVERC SEAMKWLDSN TTAEKEEYEY KLKELEQFCS
601 PIMTKMHKGG GDGQQAPNFG QQAGGYKGPT VEEVD
```

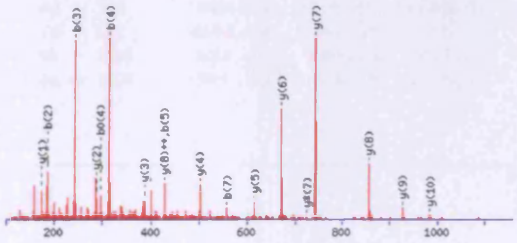

#	b	b++	b*	b+++	b0	b0++	Seq.	y	y++	y*	y+++	#
1	116.03	58.52			98.02	49.52	D					12
2	187.07	94.04			169.06	85.03	A	1054.64	527.82	1037.61	519.31	11
3	244.09	122.55			226.08	113.54	G	983.60	492.30	966.57	483.79	10
4	315.13	158.07			297.12	149.06	A	926.58	463.79	909.55	455.28	9
5	428.21	214.61			410.20	205.61	I	855.54	428.27	838.51	419.76	8
6	499.25	250.13			481.24	241.12	A	742.46	371.73	725.43	363.22	7
7	556.27	278.64			538.26	269.63	G	671.42	336.21	654.39	327.70	6
8	669.36	335.18			651.35	326.18	I	614.40	307.70	597.37	299.19	5
9	783.40	392.20	766.37	383.69	765.39	383.20	N	501.31	251.16	484.29	242.65	4
10	882.47	441.74	865.44	433.22	864.46	432.73	V	387.27	194.14	370.24	185.63	3

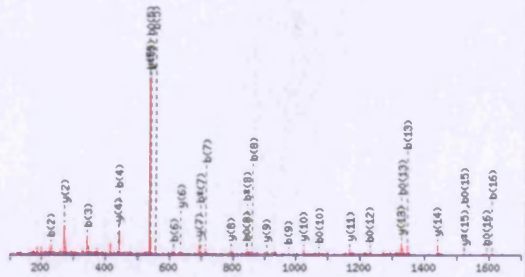

#	b	b++	b*	b+++	b0	b0++	Seq.	y	y++	y*	y+++	y0	y0++	#
1	116.03	58.52			98.02	49.52	D							18
2	230.08	115.54	213.05	107.03	212.07	106.54	N	1767.94	884.47	1750.91	875.96	1749.93	875.47	17
3	344.12	172.56	327.09	164.05	326.11	163.56	N	1653.90	827.45	1636.87	818.94	1635.89	818.45	16
4	443.19	222.10	426.16	213.58	425.18	213.09	V	1539.85	770.43	1522.83	761.92	1521.84	761.42	15
5	556.27	278.64	539.25	270.13	538.26	269.63	L	1440.78	720.90	1423.76	712.38	1422.77	711.89	14
6	613.29	307.15	596.27	298.64	595.28	298.15	G	1327.70	664.35	1310.67	655.84	1309.69	655.35	13
7	714.34	357.67	697.32	349.16	696.33	348.67	T	1270.68	635.84	1253.65	627.33	1252.67	626.84	12
8	861.41	431.21	844.38	422.70	843.40	422.20	F	1169.63	585.32	1152.60	576.81	1151.62	576.31	11
9	976.44	488.72	959.41	480.21	958.43	479.72	D	1022.56	511.79	1005.54	503.27	1004.55	502.78	10
10	1089.52	545.26	1072.49	536.75	1071.51	536.26	L	907.54	454.27	890.51	445.76	889.53	445.27	9
11	1190.57	595.79	1173.54	587.27	1172.56	586.78	T	794.45	397.73	777.43	389.22	776.44	388.72	8
12	1247.59	624.30	1230.56	615.79	1229.58	615.29	G	693.40	347.21	676.38	338.69			7
13	1346.66	673.83	1329.63	665.32	1328.65	664.83	V	636.38	318.70	619.36	310.18			6
14	1443.71	722.36	1426.68	713.85	1425.70	713.35	P	537.31	269.16	520.29	260.65			5
15	1540.76	770.89	1523.74	762.37	1522.75	761.88	P	440.26	220.63	423.24	212.12			4
16	1611.80	806.40	1594.77	797.89	1593.79	797.40	A	343.21	172.11	326.18	163.59			3
17	1708.85	854.93	1691.83	846.42	1690.84	845.93	P	272.17	136.59	255.15	128.08			2
18							R	175.12	88.06	158.09	79.55			1

Spot No. 1780 CG10424-PA

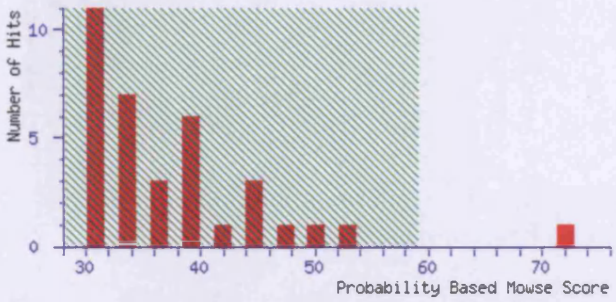

1. gi|7293823 **Mass:** 32532 **Score:** 72 **Expect:** 0.0028 **Queries matched:** 7
CG10424-PA [Drosophila melanogaster]

```
   1 MAAVSDIPVH LPKLLALFKT VVPKLVNNKH KGQYGRIGVI GGSLEYTGAP
  51 YFAAISSIRV GADLAHVFCH SNASAIIKSY SPDLIVHPVL DCVDAVERIA
 101 PWLERLHVVV IGPGLGREPG ILKTASNVLK LCMDTKKPVV IDADGLFLLN
 151 DNLNLICGQP NVILTPNVME FQRLFGEDDQ AARQKMSLLG AGVTVLEKGA
 201 NDKIYLPHCN EVHSMPSGGS GRRCGGQGDL LSGSLATFFS WSLQSGEPNP
 251 ALVAACASSY FVKKLNAAAF QKFGRSLLAS DMVNQIPSVF QTEFENSDPQ
 301
```

Start - End	Observed	Mr(expt)	Mr(calc)	Delta	Miss	Sequence
2 - 13	1288.70	1287.70	1287.72	-0.02	0	AAVSDIPVHLPK N-Acetyl (Protein)
14 - 19	704.40	703.40	703.46	-0.07	0	LLALFK
37 - 59	2342.21	2341.20	2341.23	-0.03	0	IGVIGGSLEYTGAPYFAAISSIR
60 - 78	2009.98	2008.98	2009.02	-0.04	0	VGADLAHVFCHSNASAIIK
79 - 98	2284.03	2283.02	2283.12	-0.10	0	SYSPDLIVHPVLDCVDAVER
99 - 105	884.49	883.48	883.49	-0.01	0	IAPWLER
106 - 117	1216.75	1215.75	1215.75	0.00	0	LHVVVIGPGLGR

Spot No. 1786 CG10160

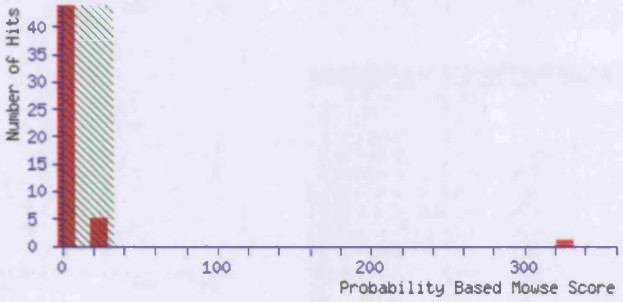

1. gi|7295348 **Mass:** 35800 **Score:** 326 **Queries matched:** 9
CG10160-PA [Drosophila melanogaster]

```
  1 MAAIKDSLLA QVAEVLPSSG HKVTIVGIGQ VGMASAFSIL AQNVSKEVCL
 51 IDVCADKLQG ELMDLQHGSN FLKNPQITAS TDFAASANSR LCIVTAGVRQ
101 KEGESRLSLV QRNTDILKNI IPKLVEYSPD TILLMVSNPV DIMTYVAWKL
151 SGLPKNRVIG SGTNLDSSRF RFLMSQRLGV APTSCHGWII GEHGDSSVPV
201 WSGVNIAGVR LRELNPILGT GEDPEKWNEL HKQVVDSAYE VIKLKGYTSW
251 AIGLSTASLA SAILRNTSSV AAVSTSVLGE HGIDKDVFLS LPCVLNANGV
301 TSVVKQILTP TEVEQLQKSA NIMSDVQAGL KF
```

	Query	Observed	Mr(expt)	Mr(calc)	Delta	Miss	Score	Expect	Rank	Peptide
☑	3	494.77	987.52	987.55	-0.04	0	50	0.0014	1	LCIVTAGVR
☑	16	603.29	1204.56	1204.60	-0.04	0	81	1e-006	1	VIGSGTNLDSSR
☑	20	617.30	1232.59	1232.63	-0.04	0	51	0.0011	1	QVVDSAYEVIK + Pyro-glu (N-term Q)
☑	23	625.82	1249.64	1249.66	-0.02	0	(42)	0.0071	1	QVVDSAYEVIK
☑	35	661.29	1320.57	1320.61	-0.04	0	33	0.054	1	EVCLIDVCADK
☑	44	755.39	1508.77	1508.81	-0.04	0	48	0.0016	1	QILTPTEVEQLQK + Pyro-glu (N-term Q)
☑	46	756.36	1510.71	1510.75	-0.04	0	40	0.0096	1	ELNPILGTGEDPEK
☑	48	763.90	1525.78	1525.84	-0.05	0	(23)	0.47	1	QILTPTEVEQLQK
☑	65	1066.54	2131.07	2131.13	-0.07	0	25	0.18	1	DVFLSLPCVLNANGVTSVVK

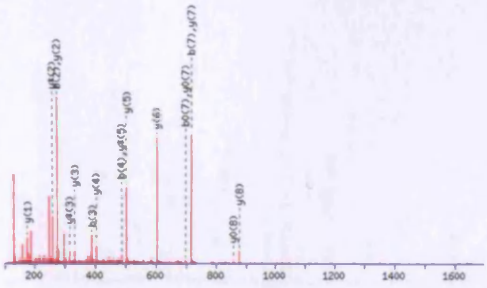

#	b	b++	b0	b0++	Seq.	y	y++	y*	y+++	y0	y0++	#
1	114.09	57.55			L							9
2	274.12	137.56			C	875.48	438.24	858.45	429.73	857.47	429.24	8
3	387.21	194.11			I	715.45	358.23	698.42	349.71	697.44	349.22	7
4	486.27	243.64			V	602.36	301.68	585.34	293.17	584.35	292.68	6
5	587.32	294.16	569.31	285.16	T	503.29	252.15	486.27	243.64	485.28	243.15	5
6	658.36	329.68	640.35	320.68	A	402.25	201.63	385.22	193.11			4
7	715.38	358.19	697.37	349.19	G	331.21	166.11	314.18	157.59			3
8	814.45	407.73	796.44	398.72	V	274.19	137.60	257.16	129.08			2
9					R	175.12	88.06	158.09	79.55			1

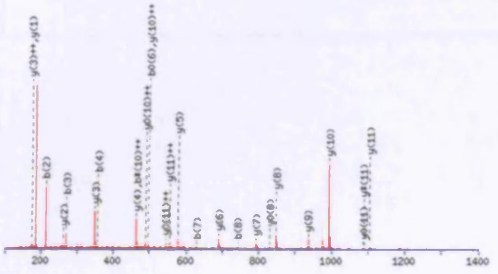

#	b	b++	b*	b+++	b0	b0++	Seq.	y	y++	y*	y+++	y0	y0++	#
1	100.08	50.54					V							12
2	213.16	107.08					I	1186.54	593.78	1169.52	545.26	1168.53	584.77	11
3	270.18	135.59					G	973.46	487.23	956.43	488.72	955.45	478.23	10
4	387.21	179.11			339.20	170.10	S	916.44	458.72	899.41	450.21	898.43	449.72	9
5	414.23	207.62			396.22	198.62	G	849.41	425.21	832.38	416.69	831.40	416.20	8
6	515.28	258.14			497.27	249.14	T	792.38	396.70	775.36	388.18	774.37	387.69	7
7	629.33	315.17	612.30	306.65	611.31	306.16	N	691.34	346.17	674.31	337.66	673.33	337.17	6
8	742.41	371.71	725.38	363.20	724.40	362.70	L	577.29	289.15	560.27	280.64	559.28	280.15	5
9	857.44	429.22	840.41	420.71	839.43	420.22	D	464.21	232.61	447.18	224.10	446.20	223.60	4
10	944.47	472.74	927.44	464.22	926.46	463.73	S	349.18	175.10	332.16	166.58	331.17	166.09	3
11	1031.50	516.25	1014.47	507.74	1013.49	507.25	S	262.15	131.58	245.12	123.07	244.14	122.57	2
12							R	175.12	88.06	158.09	79.55			1

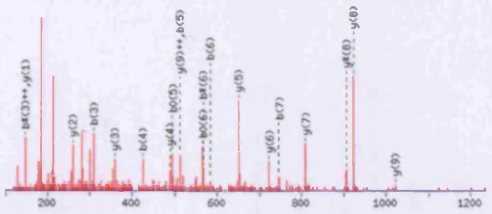

#	b	b++	b*	b*++	b0	b0++	Seq.	y	y++	y*	y*++	y0	y0++	#
1	112.04	56.52	95.01	48.01			Q							11
2	211.11	106.06	194.08	97.54			V	1122.60	561.81	1105.58	553.29	1104.59	552.80	10
3	310.18	155.59	293.15	147.08			V	1023.54	512.27	1006.51	503.76	1005.53	503.27	9
4	425.20	213.11	408.18	204.59	407.19	204.10	D	924.47	462.74	907.44	454.22	906.46	453.73	8
5	512.24	256.62	495.21	248.11	494.22	247.62	S	809.44	405.22	792.41	396.71	791.43	396.22	7
6	583.27	292.14	566.25	283.63	565.26	283.13	A	722.41	361.71	705.38	353.19	704.40	352.70	6
7	746.34	373.67	729.31	365.16	728.32	364.67	Y	651.37	326.19	634.34	317.68	633.36	317.18	5
8	875.38	438.19	858.35	429.68	857.37	429.19	E	488.31	244.66	471.28	236.14	470.30	235.65	4
9	974.45	487.73	957.42	479.21	956.44	478.72	V	359.27	180.14	342.24	171.62			3
10	1087.53	544.27	1070.50	535.76	1069.52	535.26	I	260.20	130.60	243.17	122.09			2
11							K	147.11	74.06	130.09	65.55			1

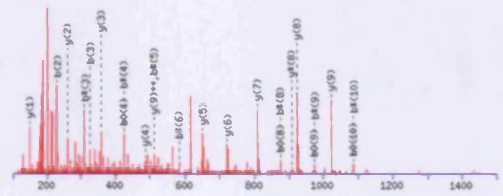

#	b	b++	b*	b*++	b0	b0++	Seq.	y	y++	y*	y*++	y0	y0++	#
1	129.07	65.04	112.04	56.52			Q							11
2	228.13	114.57	211.11	106.06			V	1122.60	561.81	1105.58	553.29	1104.59	552.80	10
3	327.20	164.10	310.18	155.59			V	1023.54	512.27	1006.51	503.76	1005.53	503.27	9
4	442.23	221.62	425.20	213.11	424.22	212.61	D	924.47	462.74	907.44	454.22	906.46	453.73	8
5	529.26	265.13	512.24	256.62	511.25	256.13	S	809.44	405.22	792.41	396.71	791.43	396.22	7
6	600.30	300.65	583.27	292.14	582.29	291.65	A	722.41	361.71	705.38	353.19	704.40	352.70	6
7	763.36	382.18	746.34	373.67	745.33	373.18	Y	651.37	326.19	634.34	317.68	633.36	317.18	5
8	892.40	446.71	875.38	438.19	874.39	437.70	E	488.31	244.66	471.28	236.14	470.30	235.65	4
9	991.47	496.24	974.45	487.73	973.46	487.23	V	359.27	180.14	342.24	171.62			3
10	1104.56	552.78	1087.53	544.27	1086.55	543.78	I	260.20	130.60	243.17	122.09			2
11							K	147.11	74.06	130.09	65.55			1

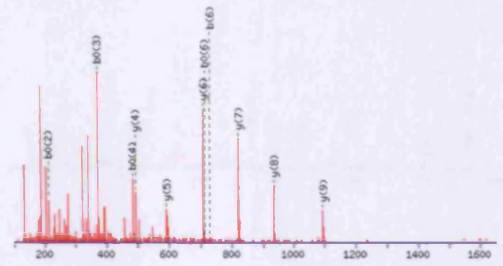

#	b	b++	b0	b0++	Seq.	y	y++	y*	y*++	y0	y0++	#
1	130.05	65.53	112.04	56.52	E							11
2	229.12	115.06	211.11	106.06	V	1192.57	596.79	1175.54	588.28	1174.56	587.78	10
3	389.15	195.08	371.14	186.07	C	1093.50	547.25	1076.48	538.74	1075.49	538.25	9
4	502.23	251.62	484.22	242.61	L	933.47	467.24	916.44	458.73	915.46	458.23	8
5	615.32	308.16	597.31	299.16	I	820.39	410.70	803.36	402.18	802.38	401.69	7
6	730.34	365.68	712.33	356.67	D	707.30	354.16	690.28	345.64	689.29	345.15	6
7	829.41	415.21	811.40	406.20	V	592.28	296.64	575.25	288.13	574.27	287.64	5
8	989.44	495.23	971.43	486.22	C	493.21	247.11	476.18	238.59	475.20	238.10	4
9	1060.48	530.74	1042.47	521.74	A	333.18	167.09	316.15	158.58	315.17	158.09	3
10	1175.51	588.26	1157.50	579.25	D	262.14	131.57	245.11	123.06	244.13	122.57	2
11					K	147.11	74.06	130.09	65.55			1

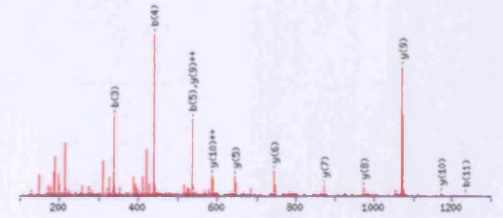

#	b	b++	b*	b*++	b0	b0++	Seq.	y	y++	y*	y*++	y0	y0++	#
1	112.04	56.52	95.01	48.01			Q							13
2	225.12	113.07	208.10	104.55			I	1398.78	699.90	1381.76	691.38	1380.77	690.89	12
3	338.21	169.61	321.18	161.09			L	1285.70	643.35	1268.67	634.84	1267.69	634.35	11
4	439.26	220.13	422.23	211.62	421.24	211.13	T	1172.62	586.81	1155.59	578.30	1154.61	577.81	10
5	536.31	268.66	519.28	260.14	518.30	259.65	P	1071.57	536.29	1054.54	527.77	1053.56	527.28	9
6	637.36	319.18	620.33	310.67	619.35	310.18	T	974.52	487.76	957.49	479.25	956.50	478.76	8
7	766.40	383.70	749.37	375.19	748.39	374.70	E	873.47	437.24	856.44	428.72	855.46	428.23	7
8	865.47	433.24	848.44	424.72	847.46	424.23	V	744.43	372.72	727.40	364.20	726.41	363.71	6
9	994.51	497.76	977.48	489.24	976.50	488.75	E	645.36	323.18	628.33	314.67	627.35	314.18	5
10	1122.57	561.79	1105.54	553.27	1104.56	552.78	Q	516.31	258.66	499.29	250.15			4
11	1235.65	618.33	1218.63	609.82	1217.64	609.32	L	388.26	194.63	371.23	186.12			3
12	1363.71	682.36	1346.68	673.85	1345.70	673.35	Q	275.17	138.09	258.14	129.58			2
13							K	147.11	74.06	130.09	65.55			1

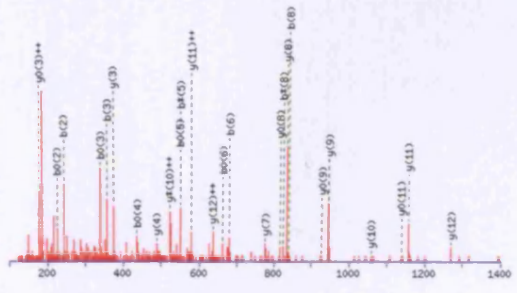

#	b	b++	b*	b*++	b0	b0++	Seq.	y	y++	y*	y*++	y0	y0++	#
1	130.05	65.53			112.04	56.52	E							14
2	243.13	122.07			225.12	113.07	L	1382.72	691.86	1365.69	683.35	1364.71	682.86	13
3	357.18	179.09	340.15	170.58	339.17	170.09	N	1269.63	635.32	1252.61	626.81	1251.62	626.31	12
4	454.23	227.62	437.20	219.11	436.22	218.61	P	1156.59	578.30	1138.56	569.78	1137.58	569.29	11
5	567.31	284.16	550.29	275.65	549.30	275.16	I	1059.54	529.77	1041.51	521.26	1040.53	520.77	10
6	680.40	340.70	663.37	332.19	662.39	331.70	L	945.45	473.23	928.43	464.72	927.44	464.22	9
7	737.42	369.21	720.39	360.70	719.41	360.21	G	832.37	416.69	815.34	408.17	814.36	407.68	8
8	838.47	419.74	821.44	411.22	820.46	410.73	T	775.35	388.18	758.32	379.66	757.34	379.17	7
9	895.49	448.25	878.46	439.73	877.48	439.24	G	674.30	337.65	657.27	329.14	656.29	328.65	6
10	1024.53	512.77	1007.50	504.26	1006.52	503.76	E	617.28	309.14	600.25	300.63	599.27	300.14	5
11	1139.56	570.28	1122.53	561.77	1121.55	561.28	D	488.24	244.62	471.21	236.11	470.22	235.62	4
12	1236.61	618.81	1219.58	610.30	1218.60	609.80	P	373.21	187.11	356.18	178.59	355.20	178.10	3
13	1365.65	683.33	1348.63	674.82	1347.64	674.32	E	276.16	138.58	259.13	130.07	258.14	129.58	2
14							K	147.11	74.06	130.09	65.55			1

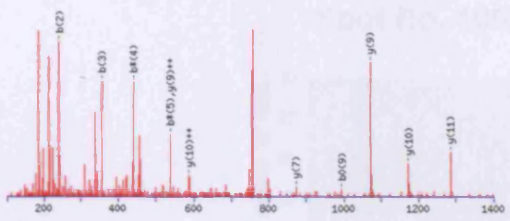

#	b	b++	b*	b*++	b0	b0++	Seq.	y	y++	y*	y*++	y0	y0++	#
1	129.07	65.04	112.04	56.52			Q							13
2	242.15	121.58	225.12	113.07			I	1398.78	699.90	1381.76	691.38	1380.77	690.89	12
3	355.23	178.12	338.21	169.61			L	1285.70	643.35	1268.67	634.84	1267.69	634.35	11
4	456.28	228.64	439.26	220.13	438.27	219.64	T	1172.62	586.81	1155.59	578.30	1154.61	577.81	10
5	553.33	277.17	536.31	268.66	535.32	268.17	P	1071.57	536.29	1054.54	527.77	1053.56	527.28	9
6	654.38	327.69	637.36	319.18	636.37	318.69	T	974.52	487.76	957.49	479.25	956.50	478.76	8
7	783.42	392.22	766.40	383.70	765.41	383.21	E	873.47	437.24	856.44	428.72	855.46	428.23	7
8	882.49	441.75	865.47	433.24	864.48	432.74	V	744.43	372.72	727.40	364.20	726.41	363.71	6
9	1011.54	506.27	994.51	497.76	993.53	497.27	E	645.36	323.18	628.33	314.67	627.35	314.18	5
10	1139.59	570.30	1122.57	561.79	1121.58	561.30	Q	516.31	258.66	499.29	250.15			4
11	1252.68	626.84	1235.65	618.33	1234.67	617.84	L	388.26	194.63	371.23	186.12			3
12	1380.74	690.87	1363.71	682.36	1362.73	681.87	Q	275.17	138.09	258.14	129.58			2
13							K	147.11	74.06	130.09	65.55			1

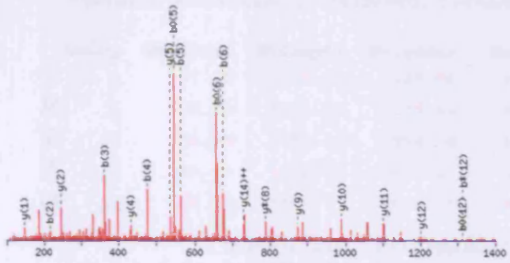

#	b	b++	b*	b*++	b0	b0++	Seq.	y	y++	y*	y*++	y0	y0++	#
1	116.09	58.52			98.02	49.52	D							20
2	215.18	108.05			197.09	99.05	V	2017.12	1009.06	2000.09	1000.55	1999.10	1000.06	19
3	362.17	181.59			344.16	172.58	F	1918.05	959.53	1901.02	951.01	1900.04	950.52	18
4	475.26	238.13			457.24	229.13	L	1770.98	885.99	1753.95	877.48	1752.97	876.99	17
5	562.29	281.65			544.28	272.64	S	1657.89	829.45	1640.87	820.94	1639.88	820.45	16
6	675.37	338.19			657.36	329.18	L	1570.86	785.93	1553.84	777.42	1552.85	776.93	15
7	772.42	386.72			754.41	377.71	F	1457.78	729.39	1440.75	720.88	1439.77	720.39	14
8	932.43	466.73			914.44	457.73	C	1360.73	680.87	1343.70	672.35	1342.71	671.86	13
9	1031.52	516.27			1013.51	507.26	V	1200.69	600.85	1183.67	592.34	1182.68	591.85	12
10	1144.61	572.81			1126.60	563.80	L	1101.63	551.32	1084.60	542.80	1083.62	542.31	11
11	1258.65	629.83	1241.62	621.32	1240.64	620.82	N	988.54	494.77	971.52	486.26	970.53	485.77	10
12	1329.69	665.35	1312.66	656.83	1311.68	656.34	A	874.50	437.75	857.47	429.24	856.49	428.75	9
13	1443.73	722.37	1426.70	713.86	1425.72	713.36	N	803.46	402.23	786.44	393.72	785.45	393.23	8
14	1500.75	750.88	1483.72	742.37	1482.74	741.87	G	689.42	345.21	672.39	336.70	671.41	336.21	7
15	1599.82	800.41	1582.79	791.90	1581.81	791.41	V	632.40	316.70	615.37	308.19	614.39	307.70	6
16	1700.87	850.94	1683.84	842.42	1682.86	841.93	T	533.33	267.17	516.30	258.66	515.32	258.16	5
17	1787.90	894.45	1770.87	885.94	1769.89	885.45	S	432.28	216.64	415.26	208.13	414.27	207.64	4
18	1886.97	943.99	1869.94	935.47	1868.96	934.98	V	345.25	173.13	328.22	164.62			3
19	1986.04	993.52	1969.01	985.01	1968.03	984.52	V	246.18	123.59	229.15	115.08			2
20							K	147.11	74.06	130.09	65.55			1

Spot No. 1902 Cysteine proteinase-1

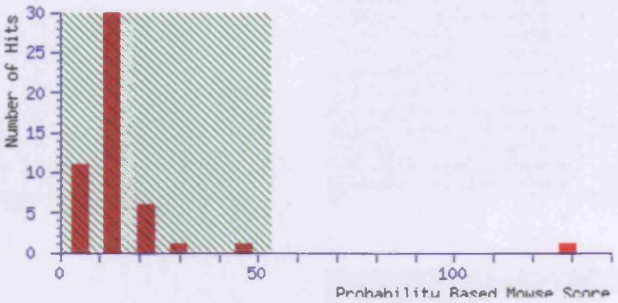

1. gi|24653514 Mass: 41974 Score: 129 Queries matched: 5
Cysteine proteinase-1 CG6692-PC, isoform C [Drosophila melanogaster]

	Query	Observed	Mr(expt)	Mr(calc)	Delta	Miss	Score	Expect	Rank	Peptide
☑	4	576.25	1150.48	1150.50	-0.02	0	44	0.44	1	K.NSWGTTWGDK.G
☑	6	603.78	1205.54	1205.56	-0.02	0	35	3.9	1	R.GFTDIPQGDEK.K
☑	15	798.35	1594.68	1594.73	-0.05	0	7	3.3e+003	1	K.ENQCGIASASSYPLV.-
☑	16	919.42	1836.83	1836.87	-0.04	1	20	1.8e+002	1	R.NKENQCGIASASSYPLV.-
☑	17	923.36	1844.70	1844.77	-0.07	0	23	68	1	K.SYPYEAIDDSCMFNK.G

```
  1 MNHLGVFETR FRPRTRHKSQ RAQLIPEQIT MRTAVLLPLL ALLAVAQAVS
 51 FADVVMEEWH TFKLEHRKNY QDETEERFRL KIFNENKHKI AKHNQRFAEG
101 KVSFKLAVNK YADLLHHEFR QLMNGFNYTL HKQLRAADES FKGVTFISPA
151 HVTLPKSVDW RTKGAVTAVK DQGHCGSCWA FSSTGALEGQ HFRKSGVLVS
201 LSEQNLVDCS TKYGNNGCNG GLMDNAFRYI KDNGGIDTEK SYPYEAIDDS
251 CMFNKGTVGA TDRGFTDIPQ GDEKKMAEAV ATVGPVSVAI DASHESFQFY
301 SEGVYNEPQC DAQNLDHGVL VVGFGTDESG EDYWLVKNSW GTTWGDKGFI
351 KMLRNKENQC GIASASSYPL V
```

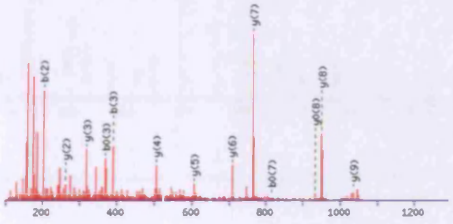

#	b	b++	b*	b+++	b0	b0++	Seq.	y	y++	y*	y+++	y0	y0++	#
1	115.05	58.03	98.02	49.52			N							10
2	202.08	101.54	185.06	93.03	184.07	92.54	S	1017.47	519.24	1020.44	510.72	1019.46	510.23	9
3	388.16	194.58	371.14	186.07	370.15	185.58	W	958.44	479.72	933.41	467.21	932.43	466.72	8
4	445.18	223.10	428.16	214.58	427.17	214.09	G	764.36	382.68	747.33	374.17	746.35	373.68	7
5	546.23	273.62	529.20	265.11	528.22	264.61	T	707.34	354.17	690.31	345.66	689.33	345.17	6
6	647.28	324.14	630.25	315.63	629.27	315.14	T	606.29	303.65	589.26	295.13	588.28	294.64	5
7	833.36	417.18	816.33	408.67	815.35	408.18	W	505.24	253.12	488.21	244.61	487.23	244.12	4
8	890.38	445.69	873.35	437.18	872.37	436.69	G	319.16	160.08	302.13	151.57	301.15	151.08	3
9	1005.41	503.21	988.38	494.69	987.40	494.20	D	262.14	131.57	245.11	123.06	244.13	122.57	2
10							K	147.11	74.06	130.09	65.55			1

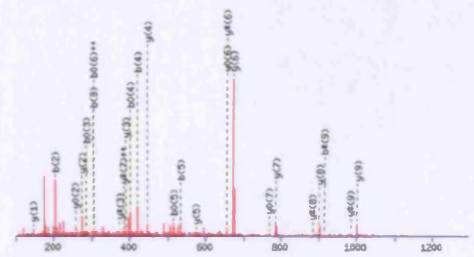

#	b	b++	b*	b+++	b0	b0++	Seq.	y	y++	y*	y+++	y0	y0++	#
1	58.03	29.52					G							11
2	205.10	103.05					F	1149.54	575.27	1132.52	566.76	1131.53	566.27	10
3	306.14	153.58			288.13	144.57	T	1002.47	501.74	985.45	493.23	984.46	492.74	9
4	421.17	211.09			403.16	202.08	D	901.43	451.22	884.40	442.70	883.42	442.21	8
5	534.26	267.63			516.25	258.63	I	786.40	393.70	769.37	385.19	768.39	384.70	7
6	631.31	316.16			613.30	307.16	P	673.32	337.16	656.29	328.65	655.30	328.16	6
7	759.37	380.19	742.34	371.67	741.36	371.18	Q	576.26	288.63	559.24	280.12	558.25	279.63	5
8	816.39	408.70	799.36	400.18	798.38	399.69	G	448.20	224.61	431.18	216.09	430.19	215.60	4
9	931.42	466.21	914.39	457.70	913.41	457.21	D	391.18	196.09	374.16	187.58	373.17	187.09	3
10	1060.46	530.73	1043.43	522.22	1042.45	521.73	E	276.16	138.58	259.13	130.07	258.14	129.58	2
11							K	147.11	74.06	130.09	65.55			1

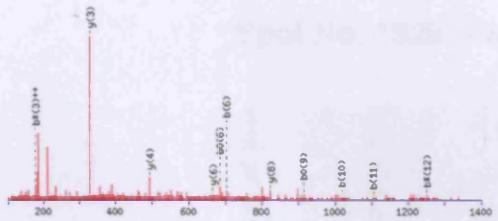

#	b	b++	b*	b+++	b0	b0++	Seq.	y	y++	y*	y+++	y0	y0++	#
1	130.05	65.53			112.04	56.52	E							15
2	244.09	122.55	227.07	114.04	226.08	113.54	N	1466.69	733.85	1449.67	725.34	1448.68	724.85	14
3	372.15	186.58	355.12	**178.07**	354.14	177.57	Q	1352.65	676.83	1335.62	668.32	1334.64	667.82	13
4	532.18	266.59	515.16	258.08	514.17	257.59	C	1224.59	612.80			1206.58	603.79	12
5	589.20	295.11	572.18	286.59	571.19	286.10	G	1064.56	532.78			1046.55	523.78	11
6	**702.29**	351.65	685.26	343.13	**684.28**	342.64	I	1007.54	504.27			989.53	495.27	10
7	773.32	387.17	756.30	378.65	755.31	378.16	A	894.46	447.73			876.45	438.73	9
8	860.36	430.68	843.33	422.17	842.35	421.68	S	**823.42**	412.21			805.41	403.21	8
9	931.39	466.20	914.37	457.69	**913.38**	457.20	A	736.39	368.70			718.38	359.69	7
10	**1018.43**	509.72	1001.40	501.20	1000.42	500.71	S	**665.35**	333.18			647.34	324.17	6
11	**1105.46**	553.23	1088.43	544.72	1087.45	544.23	S	578.32	289.66			560.31	280.66	5
12	1268.52	634.76	**1251.49**	626.23	1250.51	625.76	V	**491.25**	246.15					4
13	1365.57	683.29	1348.55	674.78	1347.56	674.29	P	**328.22**	164.62					3
14	1478.66	739.83	1461.63	731.32	1460.65	730.83	L	231.17	116.09					2
15							V	118.09	59.55					1

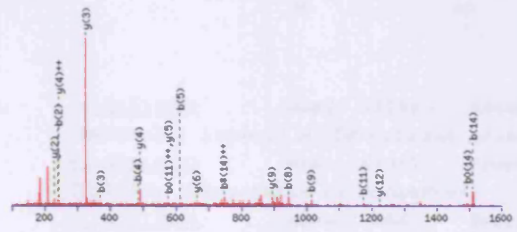

#	b	b++	b*	b+++	b0	b0++	Seq.	y	y++	y*	y+++	y0	y0++	#
1	115.05	58.03	98.02	49.52			N							17
2	**243.15**	122.08	226.12	113.56			K	1723.83	862.42	1706.81	853.91	1705.82	853.41	16
3	**372.19**	186.60	355.16	178.08	354.18	177.59	E	1595.74	798.37	1578.71	789.86	1577.73	789.37	15
4	**486.23**	243.62	469.20	235.11	468.22	234.61	N	1466.69	733.85	1449.67	725.34	1448.68	724.85	14
5	**614.29**	307.65	597.26	299.13	596.28	298.64	Q	1352.65	676.83	1335.62	668.32	1334.64	667.82	13
6	774.32	387.66	757.29	379.15	756.31	378.66	C	**1224.59**	612.80			1206.58	603.79	12
7	831.34	416.17	814.31	407.66	813.33	407.17	G	1064.56	532.78			1046.55	523.78	11
8	**944.43**	472.72	927.40	464.20	926.41	463.71	I	1007.54	504.27			989.53	495.27	10
9	**1015.46**	508.23	998.44	499.72	997.45	499.23	A	**894.46**	447.73			876.45	438.73	9
10	1102.49	551.75	1085.47	543.24	1084.48	542.75	S	823.42	412.21			805.41	403.21	8
11	**1173.53**	587.27	1156.51	578.76	1155.52	**578.26**	A	736.39	368.70			718.38	359.69	7
12	1260.56	630.79	1243.54	622.27	1242.55	621.78	S	**665.35**	333.18			647.34	324.17	6
13	1347.60	674.30	1330.57	665.79	1329.59	665.30	S	**578.32**	289.66			560.31	280.66	5
14	**1518.66**	759.83	1493.63	**747.32**	**1492.65**	746.83	V	**491.29**	**246.15**					4
15	1607.71	804.36	1590.69	795.85	1589.70	795.35	P	**328.22**	164.62					3
16	1720.80	860.90	1703.77	852.39	1702.79	851.90	L	**231.17**	116.09					2
17							V	118.09	59.55					1

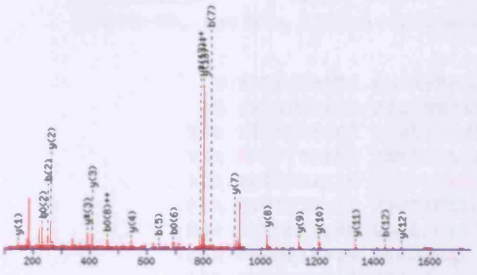

#	b	b++	b*	b+++	b0	b0++	Seq.	y	y++	y*	y+++	y0	y0++	#
1	88.04	44.52			70.03	35.52	S							15
2	**251.10**	126.05			**233.09**	117.05	V	1758.74	879.88	1741.72	871.36	1740.73	870.87	14
3	348.16	174.58			330.14	165.58	P	1595.68	**798.34**	1578.65	**789.83**	1577.67	789.34	13
4	511.22	256.11			493.21	247.11	V	**1498.63**	749.82	1481.60	741.30	1480.62	740.81	12
5	**640.26**	320.63			622.25	311.63	E	**1339.56**	**668.29**	1318.54	659.77	1317.55	659.28	11
6	711.30	356.15			**693.29**	347.15	A	**1296.52**	633.76	1189.49	595.25	1188.51	594.76	10
7	**824.38**	412.69			806.37	403.69	I	**1138.48**	568.25	1118.46	559.73	1117.47	559.24	9
8	939.41	470.21			921.40	**461.20**	D	**1022.48**	511.70	1005.37	503.19	1004.39	502.70	8
9	1054.44	527.72			1036.43	518.72	D	**907.37**	454.19	890.35	445.68	889.36	445.18	7
10	1141.47	571.24			1123.46	562.23	S	792.35	396.68	775.32	388.16	774.34	387.67	6
11	1301.50	651.25			1283.49	642.25	C	705.31	353.16	688.29	344.65			5
12	**1430.56**	719.78			1420.55	710.78	H	**546.28**	273.15	528.26	264.63			4
13	1583.63	793.32			1567.62	784.31	F	**408.22**	204.62	**391.20**	196.10			3
14	1699.67	850.34	1682.64	841.83	1681.66	841.33	N	**261.16**	131.08	244.13	122.57			2
15							K	**147.11**	74.06	130.09	65.55			1

Spot No. 1929 Fragile X-related protein 1

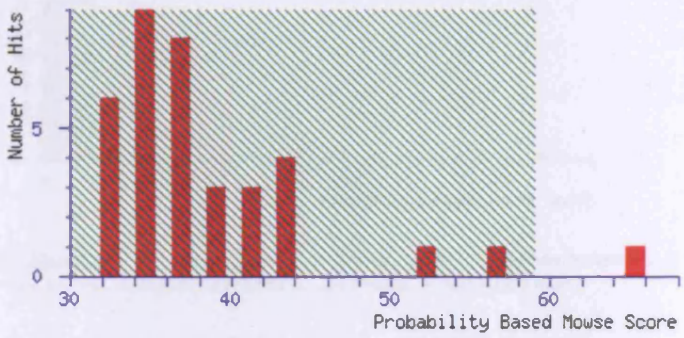

1. gi|23170873 **Mass:** 59899 **Score:** 65 **Expect:** 0.013 **Queries matched:** 13
CG6203-PB, isoform B [Drosophila melanogaster]
gi|40216002 **Mass:** 64241 **Score:** 61 **Expect:** 0.04 **Queries matched:** 13
GH22839p [Drosophila melanogaster]
gi|10717161 **Mass:** 75967 **Score:** 60 **Expect:** 0.048 **Queries matched:** 13
KH domain containing RNA-binding protein FMR1 [Drosophila melanogaster]
gi|23170870 **Mass:** 76001 **Score:** 60 **Expect:** 0.048 **Queries matched:** 13
CG6203-PD, isoform D [Drosophila melanogaster]

```
  1 MEDLLVEVRL DNGAYYKGQV TAVADDGIFV DVDGVPESMK YPFVNVRLPP
 51 EETVEVAAPI FEEGMEVEVF TRTNDRETCG WWVGIIKMRK AEIYAVAYIG
101 FETSYTEICE LGRLRAKNSN PPITAKTFYQ FTLPVPEELR EERQKDGIMK
151 EFQRTIDAGV CNYSRDLDAL IVISKFEHTQ KRASMLKDMM FRNLSQKVML
201 LKRTEEAARQ LETTKLMSRG NYVEEFRVRD DLMGLAIGSH GSNIQAARTV
251 DGVTNIELEE KSCTFKISGE TEESVQRARA MLEYAEEFFQ VPRELVGKVI
301 GKNGRIIQEI VDKSGVFRIK DQNIPRELAH VPFVFIGTVE SIANAKVLLE
351 YHLSHLKEVE QLRQEKMEID QQLRAIQESS MGSTQSFPVT RRSERGYSSD
401 IESVRSMRGG GGGQRGRVRG RGGGGPGGGN GLNQRYHNNR RDEDDYNSRG
451 DMQRDQQRGY NDRGGGDNTG SYRGGGGGAG GPGNNRRGGI NRRPPRNDQQ
501 NGRDYQHHNH TTEEVRETRE MSSVERDTN
```

Start - End	Observed	Mr(expt)	Mr(calc)	Delta	Miss	Sequence
141 - 154	1714.75	1713.74	1713.84	-0.10	2	EERQKDGIMKEFQR
183 - 192	1235.58	1234.57	1234.60	-0.03	1	RSMLKDMMFR
183 - 192	1251.64	1250.64	1250.59	0.05	1	RSMLKDMMFR Oxidation (M)
188 - 197	1291.65	1290.64	1290.61	0.03	1	DMMFRNLSQK Oxidation (M)
210 - 219	1206.56	1205.55	1205.64	-0.09	1	QLETTKLMSR
210 - 227	2201.01	2200.01	2200.09	-0.09	2	QLETTKLMSRGNYVEEFR
367 - 374	1032.55	1031.54	1031.51	0.04	0	MEIDQQLR
375 - 392	1997.94	1996.93	1996.96	-0.03	1	AIQESSMGSTQSFPVTRR Oxidation (M)
393 - 408	1874.87	1873.86	1873.86	0.00	2	SERGYSSDIESVRSMR Oxidation (M)
441 - 454	1762.72	1761.71	1761.74	-0.03	2	RDEDDYNSRGDMQR
455 - 463	1151.49	1150.48	1150.51	-0.03	1	DQQRGYNDR
459 - 486	2597.00	2595.99	2596.11	-0.12	2	GYNDRGGGDNTGSYRGGGGGAGGPGNNR
517 - 526	1223.61	1222.60	1222.56	0.04	1	ETREMSSVER

Spot No. 1930 1-cys peroxiredoxin 2540

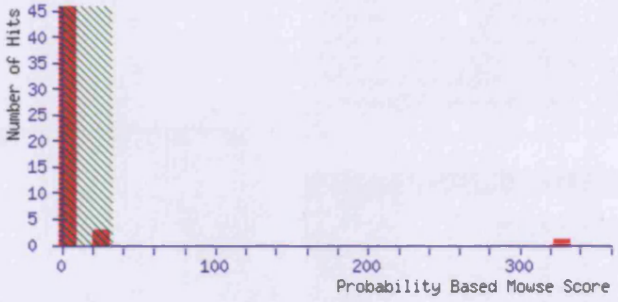

1. gi|12044363 Mass: 24926 Score: 327 Queries matched: 7
1-cys peroxiredoxin DPx-2540-1 [Drosophila melanogaster]

	Query	Observed	Mr(expt)	Mr(calc)	Delta	Miss	Score	Expect	Rank	Peptide
☑	11	570.30	1138.59	1138.61	-0.02	0	23	0.54	1	IAVMQPEFAK
☑	12	570.82	1139.62	1139.63	-0.02	0	55	0.00031	1	ALFIISPDMK
☑	13	581.29	1160.56	1160.60	-0.04	0	53	0.00062	1	TIDSLQLTDR
☑	23	612.79	1223.57	1223.60	-0.03	0	54	0.0004	1	VSMPSGVNYVR + Oxidation (M)
☑	37	671.35	1340.68	1340.71	-0.03	0	53	0.00054	1	VVATPANWTPGTK
☑	41	760.86	1519.70	1519.75	-0.06	0	18	1.3	1	LGQTVPNFEADTTK
☑	44	782.36	1562.71	1562.75	-0.04	0	71	7.3e-006	1	DLAVSLGMLDEEQK + Oxidation (M)

```
  1 MRLGQTVPNF EADTTKGPIK FHEWQGNSWV VLFSHPADFT PVCTTELGRI
 51 AVHQPEFAKR NTKCLAHSVD ALNSHVDWVN DIKSYCLDIP GDFPYPIIAD
101 PTRDLAVSLG MLDEEQKKDP EVGKTIRALF IISPDHKVRL SMFYPMSTGR
151 NVDEILRTID SLQLTDRLKV VATPANWTPG TKVMILPTVT DEEAHKLFPK
201 GFDKVSMPSG VNYVRTTENY
```

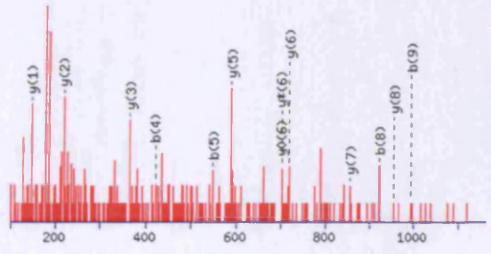

#	b	b++	b*	b+++	b0	b0++	Seq.	y	y++	y*	y+++	y0	y0++	#
1	114.09	57.55					I							10
2	185.13	93.07					A	1026.54	513.77	1009.51	505.26	1008.53	504.77	9
3	284.20	142.60					V	955.50	478.25	938.47	469.74	937.49	469.25	8
4	421.26	211.13					H	856.43	428.72	839.40	420.21	838.42	419.71	7
5	549.31	275.16	532.29	266.65			Q	719.37	360.19	702.35	351.68	701.36	351.18	6
6	646.37	323.69	629.34	315.17			P	591.31	296.16	574.29	287.65	573.30	287.16	5
7	775.41	388.21	758.38	379.70	757.40	379.20	E	494.26	247.63	477.23	239.12	476.25	238.63	4
8	922.48	461.74	905.45	453.23	904.47	452.74	F	365.22	183.11	348.19	174.60			3
9	993.52	497.26	976.49	488.75	975.50	488.26	A	218.15	109.58	201.12	101.07			2
10							K	147.11	74.06	130.09	65.55			1

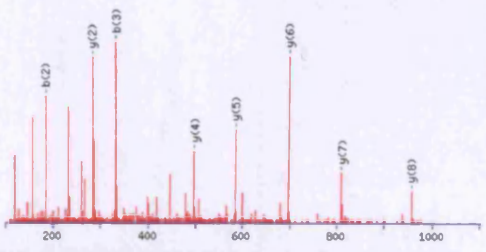

#	b	b++	b0	b0++	Seq.	y	y++	y*	y+++	y0	y0++	#
1	72.04	36.53			A							10
2	185.13	93.07			L	1069.60	535.31	1052.58	526.79	1051.59	526.30	9
3	332.20	166.60			F	956.52	478.76	939.49	470.25	938.51	469.76	8
4	445.28	223.14			I	809.45	405.23	792.43	396.72	791.44	396.22	7
5	558.36	279.69			I	696.37	348.69	679.34	340.17	678.36	339.68	6
6	645.40	323.20	627.39	314.20	S	583.28	292.15	566.26	283.63	565.27	283.14	5
7	742.45	371.73	724.44	362.72	P	496.25	248.63	479.22	240.12	478.24	239.62	4
8	857.48	429.24	839.47	420.24	D	399.20	200.10	382.17	191.59	381.19	191.10	3
9	994.54	497.77	976.53	488.77	H	284.17	142.59	267.15	134.08			2
10					K	147.11	74.06	130.09	65.55			1

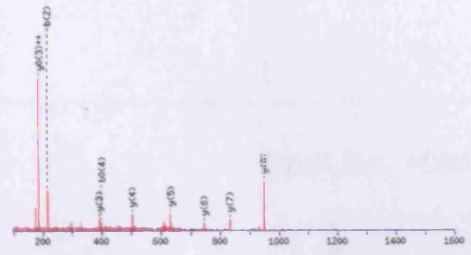

#	b	b++	b*	b***	b0	b0++	Seq.	y	y++	y*	y***	y0	y0++	#
1	102.05	51.53			84.04	42.53	T							10
2	216.14	108.07			197.13	99.07	I	1060.56	530.79	1043.54	522.27	1042.55	521.78	9
3	330.17	165.59			312.16	156.58	D	947.48	474.24	930.45	465.73	929.47	465.24	8
4	417.20	209.10			399.19	200.10	S	832.45	416.73	815.43	408.22	814.44	407.72	7
5	530.28	265.64			512.27	256.64	L	745.42	373.21	728.39	364.70	727.41	364.21	6
6	658.34	329.67	641.31	321.16	640.33	320.67	Q	632.34	316.67	615.31	308.16	614.33	307.67	5
7	771.42	386.22	754.40	377.70	753.41	377.21	L	584.28	292.64	487.25	244.13	486.27	243.64	4
8	872.47	436.74	855.45	428.23	854.46	427.73	T	391.19	196.10	374.17	187.59	373.18	187.18	3
9	987.50	494.25	970.47	485.74	969.49	485.25	D	290.15	145.58	273.12	137.06	272.14	136.57	2
10							R	175.12	88.06	158.09	79.55			1

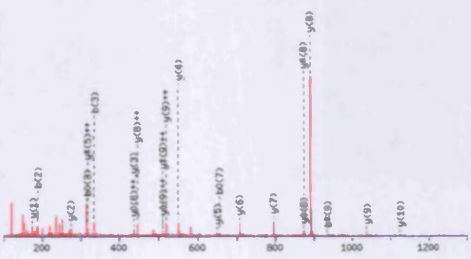

#	b	b++	b*	b***	b0	b0++	Seq.	y	y++	y*	y***	y0	y0++	#
1	100.08	50.54					V							11
2	187.11	94.06			169.10	85.05	S	1125.54	563.27	1108.51	554.76	1107.53	554.27	10
3	334.14	167.58			316.13	158.57	M	1038.50	519.76	1021.48	511.24	1020.49	510.75	9
4	431.20	216.10			413.19	207.10	P	891.47	446.24	874.44	437.72	873.46	437.23	8
5	518.23	259.62			500.22	250.61	S	794.42	397.71	777.39	389.20	776.40	388.71	7
6	575.25	288.13			557.24	279.12	G	707.38	354.20	690.36	345.68			6
7	674.32	337.66			656.31	328.66	V	650.36	325.68	633.34	317.17			5
8	788.36	394.68	771.33	386.17	770.35	385.68	N	551.29	276.15	534.27	267.64			4
9	951.42	476.22	934.40	467.70	933.41	467.21	Y	437.25	219.13	420.22	210.62			3
10	1050.49	525.75	1033.47	517.24	1032.48	516.74	V	274.19	137.60	257.16	129.08			2
11							R	175.12	88.06	158.09	79.55			1

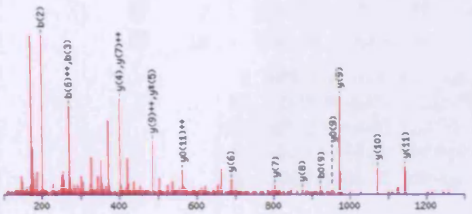

#	b	b++	b*	b***	b0	b0++	Seq.	y	y++	y*	y***	y0	y0++	#
1	100.08	50.54					V							13
2	199.14	100.08					V	1242.65	621.83	1225.62	613.31	1224.64	612.82	12
3	270.18	135.59					A	1143.58	572.29	1126.55	563.78	1125.57	563.29	11
4	371.23	186.12			353.22	177.11	T	1072.54	536.77	1055.52	528.26	1054.53	527.77	10
5	468.28	234.64			450.27	225.64	P	971.49	486.25	954.47	477.74	953.48	477.25	9
6	539.32	270.16			521.31	261.16	A	874.44	437.72	857.42	429.21	856.43	428.72	8
7	653.36	327.18	636.34	318.67	635.35	318.18	N	803.40	402.21	786.38	393.69	785.39	393.20	7
8	839.44	420.22	822.41	411.71	821.43	411.22	W	689.36	345.18	672.34	336.67	671.35	336.18	6
9	940.49	470.75	923.46	462.23	922.48	461.74	T	503.28	252.14	486.26	243.63	485.27	243.14	5
10	1037.54	519.27	1020.51	510.76	1019.53	510.27	P	402.23	201.62	385.21	193.11	384.22	192.62	4
11	1094.56	547.79	1077.54	539.27	1076.55	538.78	G	305.18	153.09	288.16	144.58	287.17	144.09	3
12	1195.61	598.31	1178.58	589.80	1177.60	589.30	T	248.16	124.58	231.13	116.07	230.15	115.58	2
13							K	147.11	74.06	130.09	65.55			1

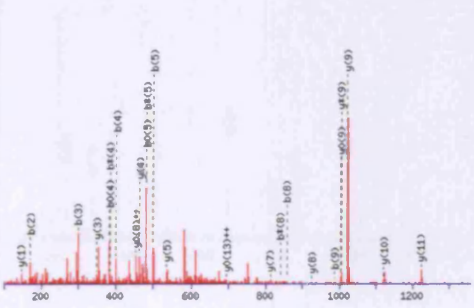

#	b	b++	b*	b***	b0	b0++	Seq.	y	y++	y*	y***	y0	y0++	#
1	114.09	57.55					L							14
2	171.11	86.06					G	1407.68	704.34	1390.65	695.83	1389.66	695.34	13
3	299.17	150.09	282.14	141.58			Q	1350.65	675.83	1333.63	667.32	1332.64	666.83	12
4	400.22	200.61	383.19	192.10	382.21	191.61	T	1222.59	611.80	1205.57	603.29	1204.58	602.80	11
5	499.29	250.15	482.26	241.63	481.28	241.14	V	1121.55	561.28	1104.52	552.76	1103.54	552.27	10
6	596.34	298.67	579.31	290.16	578.33	289.67	P	1022.48	511.74	1005.45	503.23	1004.47	502.74	9
7	710.38	355.70	693.36	347.18	692.37	346.69	N	925.43	463.22	908.40	454.70	907.42	454.21	8
8	857.46	429.23	840.43	420.72	839.44	420.22	F	811.38	406.20	794.36	397.68	793.37	397.19	7
9	986.49	493.75	969.47	485.24	968.48	484.75	E	664.31	332.66	647.29	324.15	646.30	323.66	6
10	1057.53	529.27	1040.50	520.76	1039.52	520.26	A	535.27	268.14	518.25	259.63	517.26	259.13	5
11	1172.56	586.78	1155.53	578.27	1154.55	577.78	D	464.24	232.62	447.21	224.11	446.22	223.62	4
12	1273.61	637.31	1256.58	628.79	1255.60	628.30	T	349.21	175.11	332.18	166.59	331.20	166.10	3
13	1374.65	687.83	1357.63	679.32	1356.64	678.83	T	248.16	124.58	231.13	116.07	230.15	115.58	2
14							K	147.11	74.06	130.09	65.55			1

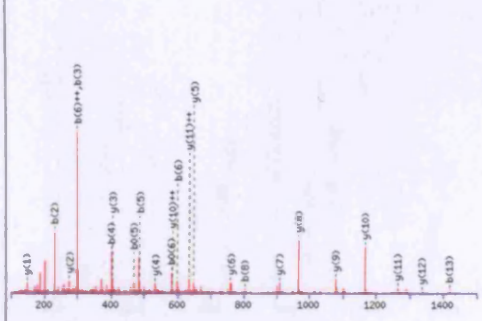

#	b	b++	b*	b***	b0	b0++	Seq.	y	y++	y*	y***	y0	y0++	#
1	116.03	58.52			98.02	49.52	D							14
2	229.12	115.06			211.11	106.06	L	1448.73	724.87	1431.70	716.36	1430.72	715.86	13
3	300.16	150.58			282.14	141.58	A	1335.68	668.33	1318.62	659.81	1317.64	659.32	12
4	399.22	200.12			381.21	191.11	V	1264.61	632.81	1247.58	624.29	1246.60	623.80	11
5	484.26	243.63			468.25	234.63	S	1165.54	583.27	1148.51	574.76	1147.53	574.27	10
6	599.34	300.17			581.33	291.17	L	1078.51	539.76	1061.48	531.24	1060.50	530.75	9
7	656.36	328.68			638.35	319.68	G	965.42	483.22	948.40	474.70	947.41	474.21	8
8	803.40	402.20			785.39	393.20	M	908.40	454.71	891.38	446.19	890.39	445.70	7
9	916.48	458.74			898.47	449.74	L	761.37	381.19	744.34	372.67	743.36	372.18	6
10	1031.51	516.26			1013.50	507.25	D	648.28	324.65	631.26	316.13	630.27	315.64	5
11	1160.55	580.78			1142.54	571.77	E	533.26	267.13	516.23	258.62	515.25	258.13	4
12	1289.59	645.30			1271.58	636.29	E	404.21	202.61	387.19	194.10	386.20	193.61	3
13	1417.65	709.33	1400.62	700.82	1399.64	700.32	Q	275.17	138.09	258.14	129.58			2
14							K	147.11	74.06	130.09	65.55			1

Spot No. 1984 Glutathione S transferase E9

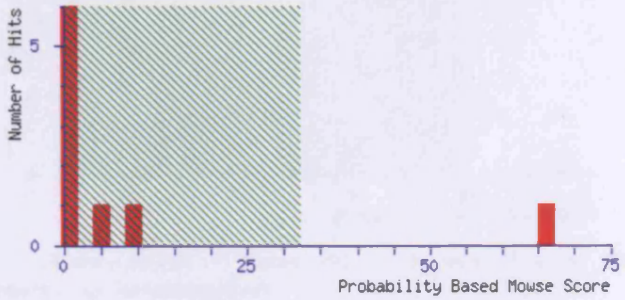

1. gi|7302612 **Mass:** 25094 **Score:** 66 **Queries matched:** 2
CG17534-PA [Drosophila melanogaster]

Query	Observed	Mr(expt)	Mr(calc)	Delta	Miss	Score	Expect	Rank	Peptide
5	539.81	1077.60	1077.62	-0.02	0	21	0.88	1	NIAIPLFYK
18	700.38	1398.76	1398.79	-0.03	0	45	0.0029	1	LVLYGVEASPPVR

```
  1 MGKLVLYGVE ASPPVRACKL TLDALGLQYE YRLVNLLAGE HKTKEFSLKN
 51 PQHTVPVLED DGKFIWESHA ICAYLVRRYA KSDDLYPKDY FKRALVDQRL
101 HFESGVLFQG CIRNIAIPLF YKNITEVPRS QIDAIYEAYD FLEAFIGNQA
151 YLCGPVITIA DYSVVSSVSS LVGLAAIDAK RYPKLNGWLD RMAAQPNYQS
201 LNGNGAQMLI DMFSSKITKI V
```

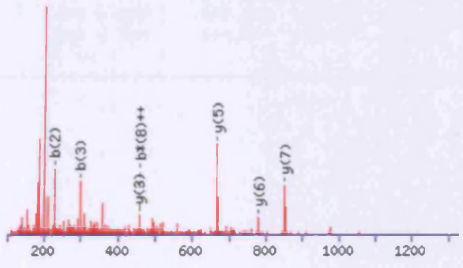

#	b	b++	b*	b*++	Seq.	y	y++	y*	y*++	#
1	115.05	58.03	98.02	49.52	N					9
2	228.13	114.57	211.11	106.06	I	964.59	482.80	947.56	474.28	8
3	299.17	150.09	282.14	141.58	A	851.50	426.25	834.48	417.74	7
4	412.26	206.63	395.23	198.12	I	780.47	390.74	763.44	382.22	6
5	509.31	255.16	492.28	246.64	P	667.38	334.19	650.35	325.68	5
6	622.39	311.70	605.37	303.19	L	570.33	285.67	553.30	277.15	4
7	769.46	385.23	752.43	376.72	F	457.24	229.13	440.22	220.61	3
8	932.52	466.77	915.50	458.25	Y	310.18	155.59	293.15	147.08	2
9					K	147.11	74.06	130.09	65.55	1

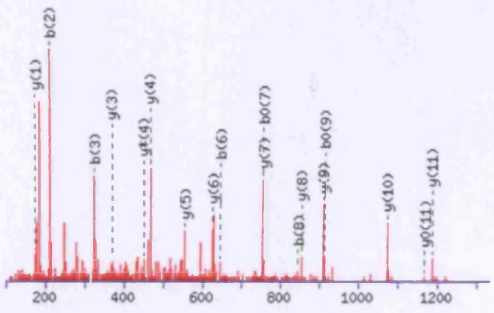

#	b	b++	b0	b0++	Seq.	y	y++	y*	y*++	y0	y0++	#
1	114.09	57.55			L							13
2	213.16	107.08			V	1286.71	643.86	1269.68	635.35	1268.70	634.85	12
3	326.24	163.63			L	1187.64	594.32	1170.62	585.81	1169.63	585.32	11
4	489.31	245.16			Y	1074.56	537.78	1057.53	529.27	1056.55	528.78	10
5	546.33	273.67			G	911.49	456.25	894.47	447.74	893.48	447.25	9
6	645.40	323.20			V	854.47	427.74	837.45	419.23	836.46	418.73	8
7	774.44	387.72	756.43	378.72	E	755.40	378.21	738.38	369.69	737.39	369.20	7
8	845.48	423.24	827.47	414.24	A	626.36	313.68	609.34	305.17	608.35	304.68	6
9	932.51	466.76	914.50	457.75	S	555.32	278.17	538.30	269.65	537.31	269.16	5
10	1029.56	515.28	1011.55	506.28	P	468.29	234.65	451.27	226.14			4
11	1126.61	563.81	1108.60	554.81	P	371.24	186.12	354.21	177.61			3
12	1225.68	613.34	1207.67	604.34	V	274.19	137.60	257.16	129.08			2
13					R	175.12	88.06	158.09	79.55			1

Spot No. 2011 Glutatione S transferase D5

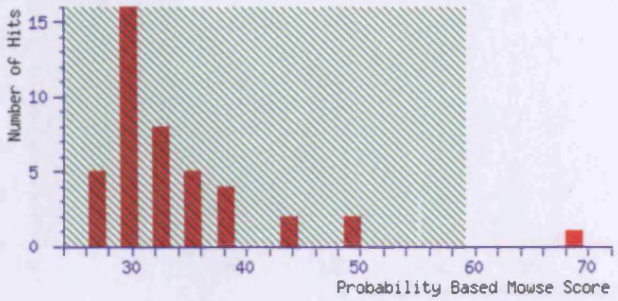

1. gi|45446464 **Mass:** 24755 **Score:** 69 **Expect:** 0.0061 **Queries matched:** 9
CG12242-PA [Drosophila melanogaster]

```
  1 MDFYYSPRGS GCRTVIMVAK ALGVKLNMKL LNTLEKDQLK PEFVKLNPQH
 51 TIPTLVDNGF SIWESRAIAV YLVEKYGKDD TLFPKDPKKQ ALVNQRLYFD
101 MGTLYDSFAK YYYPLFHTGK PGSDEDFKKI ESSFEYLNIF LEGQNYVAGD
151 HLTVADIAIL STVSTFEIFD FDLNKYPNVA RWYANAKKVT PGWEENWKGA
201 VELKGVFDAR QAAAKQ
```

Start - End	Observed	Mr(expt)	Mr(calc)	Delta	Miss	Sequence	
1 - 8	1120.48	1119.47	1119.47	0.00	0	MDFYYSPR	N-Acetyl (Protein)
1 - 8	1136.45	1135.44	1135.46	-0.03	0	MDFYYSPR	N-Acetyl (Protein); Oxidation (M)
67 - 75	1005.56	1004.55	1004.59	-0.04	0	AIAVYLVEK	
76 - 85	1183.58	1182.57	1182.59	-0.02	1	YGKDDTLFPK	
90 - 96	828.44	827.43	827.46	-0.03	0	QALVNQR	
97 - 110	1670.74	1669.73	1669.77	-0.04	0	LYFDMGTLYDSFAK	
97 - 110	1686.72	1685.71	1685.76	-0.06	0	LYFDMGTLYDSFAK	Oxidation (M)
182 - 187	752.33	751.33	751.37	-0.04	0	WYANAK	
205 - 210	664.28	663.27	663.33	-0.06	0	GVFDAR	

Spot No. 326 CG5706

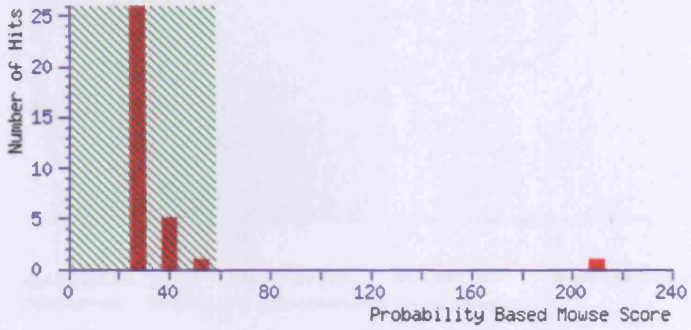

1. gi|21355211 **Mass:** 66477 **Score:** 210 **Expect:** 3.5e-017 **Queries matched:** 19
CG5706-PA [Drosophila melanogaster]

```
  1 MPTIGVKRDL LFEALGKTYT DDEFQDLCFA FGLELDEVTT EKQMLTKEQG
 51 DVAAAANASE EIIYRIDIPA NRYDLLCLEG LVTGLLVFQG KLKPPKFQFV
101 ELAKRQVLKI DPSTAQIRPY AVAAVLENVT FTQASYNSFI DLQDKLHQNI
151 CRKRTLVAIG THDLDTLQGP FSYEALAPDQ IKFKPLNQTK EMTGSELMDF
201 YSTHAQLKQY LPIIRESPVY PVIYDANRVV LSLPPIINGD NSKITLKTKN
251 VEIECTATDR TKAKVVLDTI VCLFSEHCAQ KFTVEPCDVV QPDGSVISYP
301 ELEVREERIS VKRANAYIGI DEPAEKLADM LTRMYLEAKV DGDSLVVKIP
351 PTRHDVIHAC DIYEDVAIAY GYNNIKKSLP AFMQIAKQFP LNKLTEQLRE
401 QVAQAGFTEA LTFTLCSRDD IGRKLNKNID ALPAVHIGNP KTLEFQVVRT
451 TLLPGLLKTL VANRKMPLPL KLFEISDVVV ADESTEVGAR NERRVCAVNC
501 NKTAGFEVVK GLLDRVMQLL SVPWKSASGT KGYYLQATED PSYFPGRCAN
551 VMYDGVVIGK IGVLHPTVLQ AFELTTPCSA VEFTIEPFV
```

Start - End	Observed	Mr(expt)	Mr(calc)	Delta	Miss	Sequence
9 - 17	1005.55	1004.54	1004.55	-0.01	0	DLLFEALGK
48 - 65	1906.92	1905.91	1905.91	0.01	0	EQGDVAAAANASEEIIYR
97 - 104	981.52	980.51	980.53	-0.02	0	FQFVELAK
110 - 127	1941.04	1940.04	1940.08	-0.05	0	IDPSTAQIRPYAVAAVLR
128 - 145	2090.97	2089.96	2090.00	-0.03	0	NVTFTQASYNSFIDLQDK
155 - 182	3013.53	3012.52	3012.54	-0.02	0	TLVAIGTHDLDTLQGPFSYEALAPDQIK
209 - 215	902.54	901.54	901.54	-0.00	0	QYLPIIR
216 - 228	1522.77	1521.76	1521.75	0.02	0	ESPVYPVIYDANR
229 - 243	1588.89	1587.88	1587.90	-0.02	0	VVLSLPPIINGDNSK
250 - 260	1325.63	1324.62	1324.61	0.01	0	NVEIECTATDR
282 - 305	2735.33	2734.32	2734.32	0.01	0	FTVEPCDVVQPDGSVISYPELEVR
378 - 387	1121.59	1120.58	1120.60	-0.02	0	SLPAFMQIAK Oxidation (M)
400 - 418	2129.05	2128.04	2128.03	0.02	0	EQVAQAGFTEALTFTLCSR
428 - 441	1458.80	1457.80	1457.80	-0.00	0	NIDALPAVHIGNPK
442 - 449	991.56	990.55	990.55	0.00	0	TLEFQVVR
465 - 471	842.51	841.50	841.51	-0.01	1	KMPLPLK Oxidation (M)
472 - 490	2036.01	2035.01	2035.01	-0.00	0	LFEISDVVVADESTEVGAR
503 - 515	1413.77	1412.76	1412.74	0.02	0	TAGFEVVKGLLDR
532 - 547	1863.86	1862.85	1862.85	0.00	0	GYYLQATEDPSYFPGR

Spot No. 362 CG4199

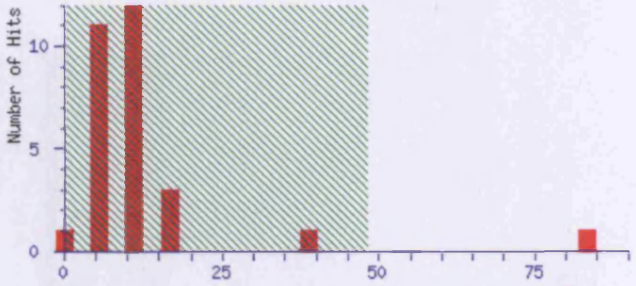

1. gi|7290254 Mass: 61481 Score: 83 Queries matched: 2
CG4199-PA, isoform A [Drosophila melanogaster]

Query	Observed	Mr(expt)	Mr(calc)	Delta	Miss	Score	Expect	Rank	Peptide
☑ 1	693.82	1385.63	1385.76	-0.13	0	43	0.19	1	LPCDLLILGTGSK
☑ 3	808.37	1614.72	1614.86	-0.14	0	40	0.34	1	DPIVAQFAELISQGK

```
  1 MSTEESSPDS EYTSAVPVDC RVTDLKENEM KQVDFDEDTR VLLVKQNDRL
 51 LAVGAKCTHY GAPLQTGALG LGRVRCPWHG ACFNLENGDI EDFPGLDSLP
101 CYRVEVGNEG QVMLRAKRSD LVNNKRLKNM VRRKPDDQRV FIVVGGGPSG
151 AVAVETIRQE GFTGRLIFVC REDYLPYDRV KISKAMNLEI EQLRFRDEEF
201 YKEYDIELWQ GVAAEKLDTA QKELHCSNGY VVKYDKIYLA TGCSAFRPPI
251 PGVNLENVRT VRELADTKAI LASITPESRV VCLGSSFIAL EAAAAGLVSKV
301 QSVTVVGREN VPLKAAPGAE IGQRVLQLFE DNKVVMRMES GIAEIVGNED
351 GKVSEVVLVD DTRLPCDLLI LGTGSKLNTQ FLAKSGVKVN RNGSVDVTDF
401 LESNVPDVYV GGDIANAHIH GLAHDRVNIG HYQLAQYHGR VAAINMCGGV
451 KKLEAVPFFF TLIFGKGIRY AGHGSYKDVI IDGSMEDFKF VAYFINEADT
501 VTAVASCGRD PIVAQFAELI SQGKCLGRGQ IEDPATREDW TKKLGQPLPQ
551 VR
```

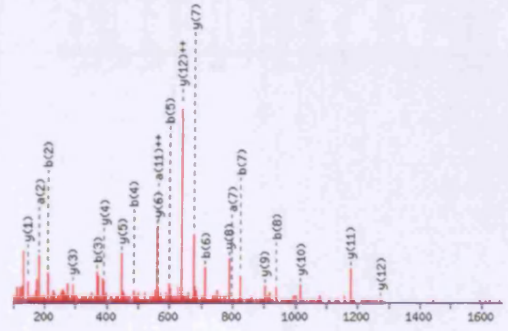

#	a	a**	b	b**	Seq.	y	y**	y*	y***	#
1	86.10	43.55	114.09	57.55	L					13
2	183.15	92.08	211.14	106.08	P	1273.68	637.34	1256.66	628.83	12
3	343.18	172.09	371.17	186.09	C	1176.63	588.82	1159.60	580.30	11
4	458.21	229.61	486.20	243.60	D	1016.60	508.80	999.57	500.29	10
5	571.29	286.15	599.29	300.15	L	901.57	451.29	884.55	442.78	9
6	684.37	342.69	712.37	356.69	L	788.49	394.75	771.46	386.23	8
7	797.46	399.23	825.45	413.23	I	675.40	338.21	658.38	329.69	7
8	910.54	455.78	938.54	469.77	L	562.32	281.66	545.29	273.15	6
9	967.56	484.29	995.56	498.28	G	449.24	225.12	432.21	216.61	5
10	1068.61	534.81	1096.61	548.81	T	392.21	196.61	375.19	188.10	4
11	1125.63	563.32	1153.63	577.32	G	291.17	146.09	274.14	137.57	3
12	1212.67	606.84	1240.66	620.83	S	234.14	117.58	217.12	109.06	2
13					K	147.11	74.06	130.09	65.55	1

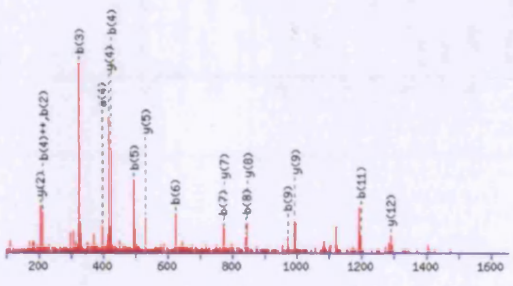

#	a	a**	a*	a***	b	b**	b*	b***	Seq.	y	y**	y*	y***	#
1	88.04	44.52			116.03	58.52			D					15
2	185.09	93.05			213.08	107.03			P	1500.84	750.92	1483.82	742.41	14
3	286.18	143.59			328.17	163.59			I	1403.79	702.40	1386.76	693.88	13
4	387.24	194.13			425.24	213.12			V	1290.71	645.86	1273.68	637.34	12
5	458.28	229.64			486.28	243.64			A	1191.64	596.32	1174.61	587.81	11
6	586.34	293.67	579.31	290.16	634.34	317.67	607.31	304.16	Q	1120.60	560.80	1103.57	552.29	10
7	743.41	372.21	726.38	363.69	771.40	386.21	754.38	377.69	F	992.54	496.77	975.51	488.26	9
8	814.45	407.73	797.42	399.21	842.44	421.72	825.41	413.21	A	845.47	423.24	828.45	414.73	8
9	943.49	472.25	926.46	463.73	971.48	486.25	954.46	477.73	E	774.44	387.72	757.41	379.21	7
10	1056.57	528.79	1039.55	520.28	1084.57	542.79	1067.54	534.27	L	645.39	323.20	628.37	314.69	6
11	1169.66	585.33	1152.63	576.82	1197.68	599.33	1180.62	590.82	I	532.31	266.66	515.28	258.14	5
12	1256.69	628.85	1239.66	620.33	1284.68	642.85	1267.66	634.33	S	419.22	210.12	402.20	201.60	4
13	1384.75	692.88	1367.72	684.36	1412.74	706.87	1395.72	698.36	Q	332.19	166.60	315.17	158.09	3
14	1441.77	721.39	1424.74	712.87	1469.76	735.39	1452.74	726.87	G	204.13	102.57	187.11	94.06	2
15									K	147.11	74.06	130.09	65.55	1

Spot No. 363 HSP60

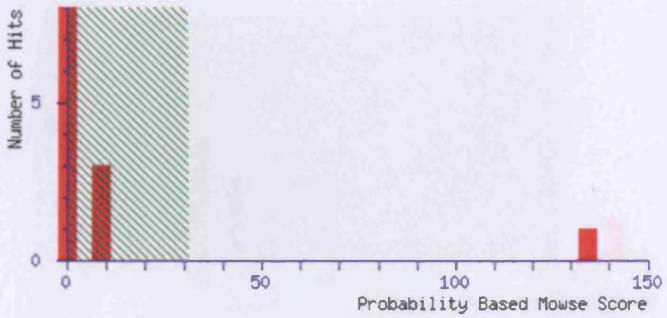

1. gi|7292599 **Mass:** 60885 **Score:** 134 **Queries matched:** 2
CG12101-PB, isoform B [Drosophila melanogaster]

Query	Observed	Mr(expt)	Mr(calc)	Delta	Miss	Score	Expect	Rank	Peptide
2	752.86	1503.70	1503.82	-0.12	0	77	1.9e-006	1	VEFQDALLLLSEK
4	955.46	1908.90	1909.06	-0.17	0	58	0.00013	1	ISSVQSIIPALELANAQR

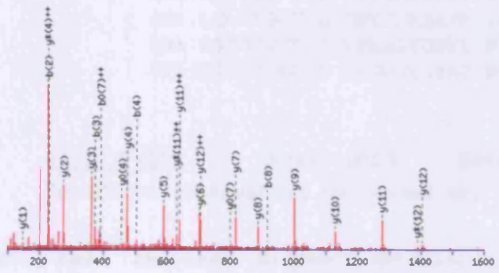

#	b	b++	b*	b*++	b0	b0++	Seq.	y	y++	y*	y*++	y0	y0++	#
1	100.08	50.54					V							13
2	229.12	115.06			211.11	106.06	E	1488.76	783.38	1388.73	694.87	1387.75	694.38	12
3	376.19	188.60			358.18	179.59	F	1276.71	638.86	1259.69	630.35	1258.70	629.86	11
4	504.25	252.63	487.22	244.11	486.23	243.62	Q	1129.66	565.33	1112.62	556.81	1111.64	556.32	10
5	619.27	310.14	602.25	301.63	601.26	301.13	D	1001.59	501.30	984.56	492.78	983.58	492.29	9
6	690.31	345.66	673.28	337.15	672.30	336.65	A	886.56	443.78	869.53	435.27	868.55	434.78	8
7	803.39	402.20	786.37	393.69	785.38	393.28	L	815.52	408.27	798.50	399.75	797.51	399.26	7
8	916.48	458.74	899.45	450.23	898.47	449.74	L	702.44	351.72	685.41	343.21	684.43	342.72	6
9	1029.56	515.28	1012.53	506.77	1011.55	506.28	L	589.36	295.18	572.33	286.67	571.34	286.18	5
10	1142.65	571.83	1125.62	563.31	1124.63	562.82	L	476.27	238.64	459.24	230.13	458.26	229.63	4
11	1229.68	615.34	1212.65	606.83	1211.67	606.34	S	363.19	182.10	346.16	173.58	345.18	173.09	3
12	1358.72	679.86	1341.69	671.35	1340.71	670.86	E	276.16	138.58	259.13	130.07	258.14	129.58	2
13							K	147.11	74.06	130.09	65.55			1

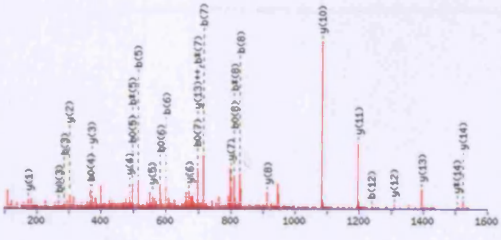

#	b	b++	b*	b*++	b0	b0++	Seq.	y	y++	y*	y*++	y0	y0++	#
1	114.09	57.55					I							18
2	201.12	101.07			183.11	92.06	S	1796.99	899.00	1779.96	890.48	1778.98	889.99	17
3	288.16	144.58			270.14	135.58	S	1709.95	855.48	1692.93	846.97	1691.94	846.48	16
4	387.22	194.12			369.21	185.11	V	1622.92	811.96	1605.90	803.45	1604.91	802.96	15
5	515.28	258.14	498.26	249.63	497.27	249.14	Q	1523.88	762.43	1506.85	753.92	1505.84	753.43	14
6	602.31	301.66	585.29	293.15	584.30	292.66	S	1395.80	698.40	1378.77	689.89	1377.78	689.40	13
7	715.40	358.20	698.37	349.69	697.39	349.20	I	1308.76	654.89	1291.74	646.37	1290.75	645.88	12
8	828.48	414.74	811.46	406.23	810.47	405.74	I	1195.68	598.34	1178.65	589.83	1177.67	589.34	11
9	925.54	463.27	908.51	454.76	907.52	454.27	P	1082.60	541.80	1065.57	533.29	1064.58	532.80	10
10	996.57	498.79	979.55	490.28	978.56	489.78	A	985.54	493.27	968.52	484.76	967.53	484.27	9
11	1109.66	555.33	1092.63	546.82	1091.65	546.33	L	914.51	457.76	897.48	449.24	896.49	448.75	8
12	1238.70	619.85	1221.67	611.34	1220.69	610.85	E	801.42	401.21	784.39	392.70	783.41	392.21	7
13	1351.78	676.40	1334.76	667.88	1333.77	667.39	L	672.38	336.69	655.35	328.18			6
14	1422.82	711.91	1405.79	703.40	1404.81	702.91	A	559.29	280.15	542.27	271.64			5
15	1536.86	768.94	1519.84	760.42	1518.85	759.93	N	488.26	244.63	471.23	236.12			4
16	1607.90	804.45	1590.87	795.94	1589.89	795.45	A	374.21	187.61	357.19	179.10			3
17	1735.96	868.48	1718.93	859.97	1717.95	859.48	Q	303.18	152.09	286.15	143.58			2
18							R	175.12	88.06	158.09	79.55			1

Spot No. 415 Misato

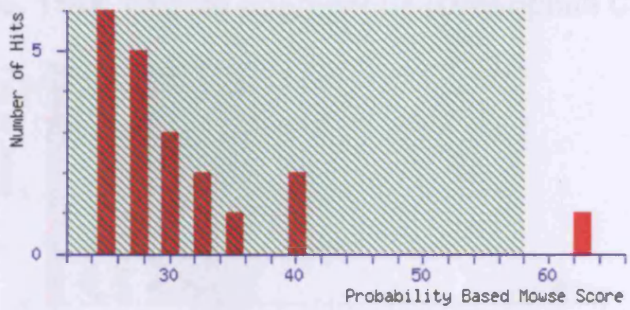


```
  1 MDYTREILTF QFGTYANYVG THFWNQQEAN FRYGDESEQV AEEQLPNNDI
 51 LYREGRNDLN RTTYTPRLLS VDLSGTLGHL PVTGELYGNF VQRDEELLPL
101 STGEELEQVR KRAEESGVCS PEQLEVQEQS KASISEYQRD LLKNAVVPEK
151 NYQLAATANS WVDFLYARYH PRTLNVLPGL IRDPTAQALG TYSAGTEMWQ
201 EVSFNEEFCD RIRLYVEECD GLQGFHVLFD IDDGFGGLAG KCLEHLNDEY
251 SRASFALPLH YPRITSYPQA DTRLSHSIRV VNNVLGYHQL SEQALMFTPL
301 STLETIWRNN NLKSRSLPGL QWETDNLYQT SALLAAFFDT ATLSYRLRQT
351 PESLLRFCEC VTPAGRKMTA AGLALPFGLR EGQDLIEFLD QSGDHALLTQ
401 LTPGCEPGTS YVVQSVTARG IPAERLKRPR ELAGDQLRMA AYSCDSISHM
451 LQLYYQCTYH GSVTNAAATP LPLKTQLPFP YEMFAAGISR DGYRLPEGAE
501 RETGSRVDSA PMLAAVQNST KLGEHLDNVH AQSHRVQLAK LQAYSNSGLE
551 RDEYDTALDQ LLEFRDLYAD SQYL
```

1. gi|17737379 **Mass:** 65256 **Score:** 63 **Expect:** 0.019 **Queries matched:** 6
CG1424-PA [Drosophila melanogaster]

Start - End	Observed	Mr(expt)	Mr(calc)	Delta	Miss	Sequence
94 - 110	1957.07	1956.06	1955.97	0.09	0	DEELLPLSTGEELEQVR
173 - 182	1095.70	1094.69	1094.68	0.01	0	TLNVLPGLIR
253 - 263	1271.70	1270.70	1270.68	0.01	0	ASFALPLHYPR
368 - 380	1333.71	1332.71	1332.72	-0.02	0	MTAAGLALPFGLR Oxidation (M)
475 - 490	1843.97	1842.97	1842.90	0.07	0	TQLPFPYEMFAAGISR Oxidation (M)
552 - 565	1727.88	1726.88	1726.80	0.07	0	DEYDTALDQLLEFR

Spot No. 1184 Capsid polypeptide (Drosophila C virus)

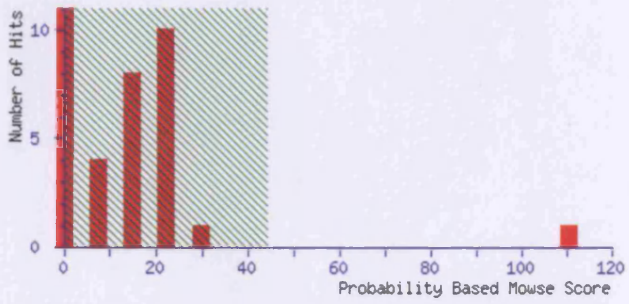

1. gi|2388674 **Mass:** 100435 **Score:** 111 **Queries matched:** 3
capsid polyprotein [Drosophila C virus]

Query	Observed	Mr(expt)	Mr(calc)	Delta	Miss	Score	Expect	Rank	Peptide
1	587.28	1172.54	1172.65	-0.11	0	69	0.00056	1	VSLVNSTLQGR
4	991.86	1981.71	1981.91	-0.19	0	29	0.66	1	LMLQYYPYAQYMQNR + 2 Oxidation (M)
2	1186.14	3555.40	3555.73	-0.33	0	13	56	1	EIVMFSSEGVTPSTTAVPDIVSLSTDYLSMTTR + Oxidation (M)

```
  1 ANFQTNNNNI ENEDRKITSE QKEIVMFSSE GVTPSTTAVP DIVSLSTDYL
 51 SMTTREDRIH TIKDFLSRPI IIQTGLWSSA TTAETQLYTA NFPEVFISNT
101 MYQEKLRGFV GLRATLVIKV QVNSQPFQQG RLMLQYYPYA QYMQNRVSLV
151 NSTLQGRSGC PRTDLDLSVG TEVEMRIPYV SPHVYYNLIT GQGSFGAIYL
201 VVYSQLRDQV TGTGSVEYTV WAHLEDVDVQ YPTGANIFTG SSPNFASLGQ
251 KMSDGKFTEK DLRDIWTSKA YNKQPDKIFA QVASEITQLK ESGTISSGIG
301 QVSEGLSTMS KIPILGNMFT KPAWISAQVS NIFKMLGFSK PTVQGLPCES
351 KLRGQVRMAN FDGADTSHKL ALSAQNEIET KSGLSGTSPD EMDLSHVLSI
401 PNFWDRFTWN TTDATSSILW DNYVTPMKIK PYSSTILDRF RCTHMGFVAN
451 THGYWCGSIV YTFKFVKTQF HSGRLRISFI PFYYNTTISA GVPDVSRTQK
501 VIVDLRTSTE VSFTIPYVSS RPWMYCIRPE ASWLGTDNAL MYNAVTGIVR
551 VEVLNQLVAA NNVFQSIDTI VEVSGGPDLT FAAPMAPSYV PYSGGFTLAD
601 DAAAKKQREE EYDNNIPQTI SNRGKREVED ARIVAQVMGE DLAIQRNDAQ
651 HGVHPMTIDT HKIDSNWSPE AHCIGEKIMS IRQLIKRFGM ALNSLNLISD
701 APNTLIAPFS VQHPTPVVAP AEPMSLFEYY YFIYGFWRGG MRFKLQAVRT
751 NSAETSVKTD TTWTVNLWNS VQDSFNSLIN VFSTTDYPIK STGALPAGTS
801 GFGNSMTYID PEVEGFMEFE IPYYNISHIS PATTYVRGTE SPITINSVLR
851 GHLPPQIVAV APQGTIATTD VVNAQFARAP SDDFSFMYLV GVPPLTNVAR
901 P
```

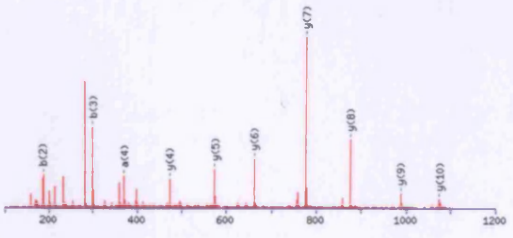

#	a	a**	a*	a***	b	b**	b*	b***	Seq.	y	y**	y*	y***	#
1	72.08	36.54			100.08	50.54			V					11
2	159.11	80.06			187.11	94.06			S	1074.59	537.80	1057.56	529.29	10
3	272.20	136.60			300.19	150.60			L	987.56	494.28	970.53	485.77	9
4	371.27	186.14			399.26	200.13			V	874.47	437.74	857.45	429.23	8
5	485.31	243.16	468.28	234.64	513.30	257.16	496.28	248.64	N	775.41	388.21	758.38	379.69	7
6	572.34	286.67	555.31	278.16	600.34	300.67	583.31	292.16	S	661.36	331.19	644.34	322.67	6
7	673.39	337.20	656.36	328.68	701.38	351.20	684.36	342.68	T	574.33	287.67	557.30	279.16	5
8	786.47	393.74	769.45	385.23	814.47	407.74	797.44	399.22	L	473.28	237.15	456.26	228.63	4
9	914.53	457.77	897.50	449.26	942.53	471.77	925.50	463.25	Q	360.20	180.60	343.17	172.09	3
10	971.55	486.28	954.53	477.77	999.55	500.28	982.52	491.76	G	232.14	116.57	215.11	108.06	2
11									R	175.12	88.06	158.09	79.55	1

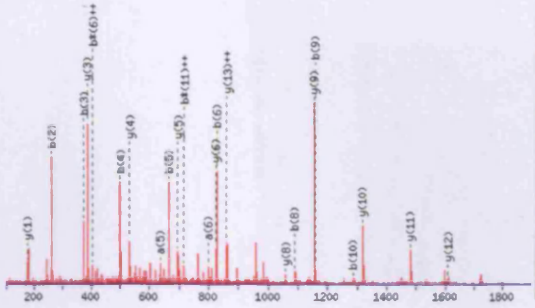

#	a	a++	a*	a+++	b	b++	b*	b+++	Seq.	y	y++	y*	y+++	#
1	86.10	43.55			114.09	57.55			L					15
2	233.13	117.07			**261.13**	131.07			M	1869.83	935.42	1852.80	926.91	14
3	346.22	173.61			**374.21**	187.61			L	1722.79	**861.90**	1705.77	853.39	13
4	474.27	237.64	457.25	229.13	**502.27**	251.64	485.24	243.13	Q	**1609.71**	805.36	1592.68	796.85	12
5	**637.34**	319.17	620.31	310.66	**665.33**	333.17	648.31	324.66	Y	**1481.66**	741.33	1464.63	732.82	11
6	**800.40**	400.70	783.37	392.19	**828.40**	414.70	811.37	**406.19**	Y	**1318.59**	659.80	1301.56	651.28	10
7	897.45	449.23	880.43	440.72	925.45	463.23	908.42	454.71	P	**1156.53**	578.27	1138.50	569.75	9
8	1060.52	530.76	1043.49	522.25	**1088.51**	544.76	1071.49	536.25	Y	**1058.47**	529.74	1041.45	521.23	8
9	1131.55	566.28	1114.53	557.77	**1159.55**	580.28	1142.52	571.76	A	895.41	448.21	878.38	439.69	7
10	1259.61	630.31	1242.59	621.80	**1287.61**	644.31	1270.58	635.79	Q	**824.37**	412.69	807.35	404.18	6
11	1422.68	711.84	1405.65	703.33	1450.67	725.84	1433.64	**717.33**	Y	**696.31**	348.66	679.29	340.15	5
12	1569.71	785.36	1552.69	776.85	1597.71	799.36	1580.68	790.84	M	**533.25**	267.13	516.22	258.62	4
13	1666.76	833.89	1649.74	825.37	1694.76	847.88	1677.73	839.37	P	**386.21**	193.61	369.19	185.10	3
14	1780.81	890.91	1763.78	882.39	1808.80	904.90	1791.78	896.39	N	289.16	145.08	272.14	136.57	2
15									R	**175.12**	88.06	158.09	79.55	1

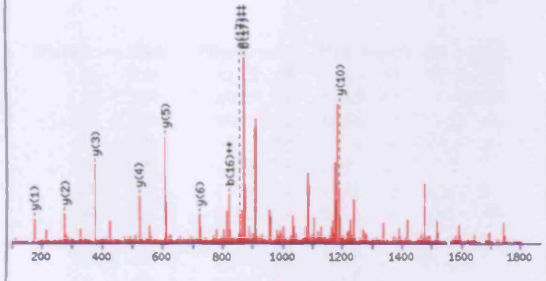

#	a	a++	b	b++	Seq.	y	y++	y*	y+++	#
1	102.05	51.53	130.05	65.53	E					33
2	215.14	108.07	243.13	122.07	I	3427.69	1714.35	3410.67	1705.84	32
3	314.21	157.61	342.20	171.60	V	3314.61	1657.81	3297.58	1649.30	31
4	451.27	226.14	479.26	240.13	H	3215.54	1608.27	3198.51	1599.76	30
5	598.33	299.67	626.33	313.67	F	3078.48	1539.74	3061.46	1531.23	29
6	685.37	343.19	713.36	357.18	S	2931.41	1466.21	2914.39	1457.70	28
7	772.40	386.70	800.39	400.70	S	2844.38	1422.69	2827.36	1414.18	27
8	901.44	451.22	929.44	465.22	E	2757.35	1379.18	2740.32	1370.67	26
9	958.46	479.74	986.46	493.73	G	2628.31	1314.66	2611.28	1306.14	25
10	1057.53	529.27	1085.53	543.27	V	2571.29	1286.15	2554.26	1277.63	24
11	1158.58	579.79	1186.57	593.79	T	2472.22	1236.61	2455.19	1228.10	23
12	1255.63	628.32	1283.63	642.32	P	2371.17	1186.09	2354.14	1177.58	22
13	1342.66	671.84	1370.66	685.83	S	2274.12	1137.56	2257.09	1129.05	21
14	1443.71	722.36	1471.71	736.36	T	2187.08	1094.05	2170.06	1085.53	20
15	1544.76	772.88	1572.75	786.88	T	2086.04	1043.52	2069.01	1035.01	19
16	1615.80	808.40	1643.79	**822.40**	A	1984.99	993.00	1967.96	984.49	18
17	1714.86	**857.94**	1742.86	**871.93**	V	1913.95	957.48	1896.93	948.97	17
18	1811.92	906.46	1839.91	920.46	P	1814.88	907.95	1797.86	899.43	16
19	1926.94	963.98	1954.94	977.97	D	1717.83	859.42	1700.80	850.91	15
20	2040.03	1020.52	2068.02	1034.52	I	1602.80	801.91	1585.78	793.39	14
21	2139.10	1070.05	2167.09	1084.05	V	1489.72	745.36	1472.69	736.85	13
22	2226.13	1113.57	2254.12	1127.57	S	1390.65	695.83	1373.63	687.32	12
23	2339.21	1170.11	2367.21	1184.11	L	1303.62	652.31	1286.59	643.80	11
24	2426.24	1213.63	2454.24	1227.62	S	**1190.54**	595.77	1173.51	587.26	10
25	2527.29	1264.15	2555.29	1278.15	T	1103.50	552.26	1086.48	543.74	9
26	2642.32	1321.66	2670.31	1335.66	D	1002.46	501.73	985.43	493.22	8
27	2805.38	1403.20	2833.38	1417.19	V	887.43	444.22	870.40	435.70	7
28	2918.47	1459.74	2946.46	1473.73	L	**724.37**	362.69	707.34	354.17	6
29	3005.50	1503.25	3033.49	1517.25	S	**611.28**	306.14	594.26	297.63	5
30	3152.53	1576.77	3180.53	1590.77	M	**524.25**	262.63	507.22	254.12	4
31	3253.58	1627.29	3281.58	1641.29	T	**377.21**	189.11	360.19	180.60	3
32	3354.63	1677.82	3382.62	1691.82	T	**276.17**	138.59	259.14	130.07	2
33					R	**175.12**	88.06	158.09	79.55	1

Spot No. 2273 Cofilin

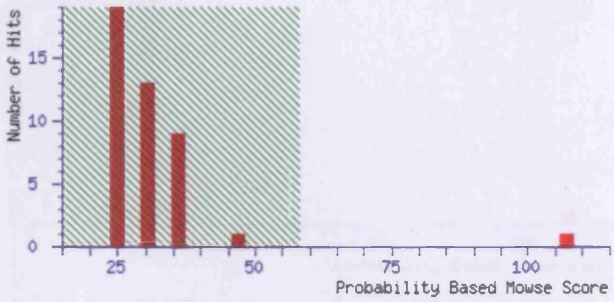

1. gi|17136986 **Mass:** 17428 **Score:** 107 **Expect:** 6.9e-007 **Queries matched:** 17
CG4254-PA [Drosophila melanogaster]

```
  1 MASGVTVSDV CKTTYEEIKK DKKHRYVIFY IRDEKQIDVE TVADRNAEYD
 51 QFLEDIQKCG PGECRYGLFD FEYMHQCQGT SESSKKQKLF LMSWCPDTAK
101 VKKKMLYSSS FDALKKSLVG VQKYIQATDL SEASREAVEE KLRATDRQ
```

Start - End	Observed	Mr(expt)	Mr(calc)	Delta	Miss	Sequence	
2 - 12	1122.59	1121.58	1121.54	0.04	0	ASGVTVSDVCK	
2 - 19	1987.02	1986.02	1985.96	0.05	1	ASGVTVSDVCKTTYEEIK	
13 - 20	1011.53	1010.53	1010.53	-0.00	1	TTYEEIKK	
26 - 32	973.55	972.54	972.54	-0.00	0	YVIFYIR	
36 - 45	1128.56	1127.56	1127.55	0.01	0	QIDVETVADR	Pyro-glu (N-term Q)
36 - 45	1145.58	1144.57	1144.57	-0.00	0	QIDVETVADR	
46 - 58	1612.75	1611.74	1611.74	-0.00	0	NAEYDQFLEDIQK	
59 - 65	835.33	834.33	834.31	0.02	0	CGPGECR	
66 - 85	2413.93	2412.93	2413.00	-0.07	0	YGLFDFEYMHQCQGTSESSK	
66 - 85	2429.98	2428.97	2428.99	-0.02	0	YGLFDFEYMHQCQGTSESSK	Oxidation (M)
87 - 100	1707.79	1706.79	1706.82	-0.03	1	QKLFLMSWCPDTAK	Pyro-glu (N-term Q)
89 - 100	1468.69	1467.68	1467.69	-0.01	0	LFLMSWCPDTAK	
89 - 100	1484.68	1483.67	1483.68	-0.01	0	LFLMSWCPDTAK	Oxidation (M)
105 - 115	1261.62	1260.61	1260.61	0.01	0	MLYSSSFDALK	
105 - 116	1405.71	1404.70	1404.70	0.00	1	MLYSSSFDALKK	Oxidation (M)
117 - 123	730.42	729.42	729.44	-0.02	0	SLVGVQK	
124 - 135	1353.67	1352.66	1352.66	0.01	0	YIQATDLSEASR	

Spot No.370 Albumin

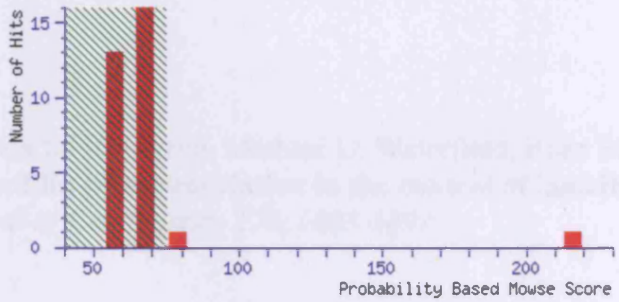

1. gi|30794280 **Mass:** 71274 **Score:** 216 **Expect:** 4.4e-016 **Queries matched:** 2
albumin [Bos taurus]

```
  1 MKWVTFISLL LLFSSAYSRG VFRRDTHKSE IAHRFKDLGE EHFKGLVLIA
 51 FSQYLQQCPF DEHVKLVNEL TEFAKTCVAD ESHAGCEKSL HTLFGDELCK
101 VASLRETYGD MADCCEKQEP ERNECFLSHK DDSPDLPKLK PDPNTLCDEF
151 KADEKKFWGK YLYEIARRHP YFYAPELLYY ANKYNGVFQE CCQAEDKGAC
201 LLPKIETMRE KVLTSSARQR LRCASIQKFG ERALKAWSVA RLSQKFPKAE
251 FVEVTKLVTD LTKVHKECCH GDLLECADDR ADLAKYICDN QDTISSKLKE
301 CCDKPLLEKS HCIAEVEKDA IPENLPPLTA DFAEDKDVCK NYQEAKDAFL
351 GSFLYEYSRR HPEYAVSVLL RLAKEYEATL EECCAKDDPH ACYSTVFDKL
401 KHLVDEPQNL IKQNCDQFEK LGEYGFQNAL IVRYTRKVPQ VSTPTLVEVS
451 RSLGKVGTRC CTKPESERMP CTEDYLSLIL NRLCVLHEKT PVSEKVTKCC
501 TESLVNRRPC FSALTPDETY VPKAFDEKLF TFHADICTLP DTEKQIKKQT
551 ALVELLKHKP KATEEQLKTV MENFVAFVDK CCAADDKEAC FAVEGPKLVV
601 STQTALA
```

tart - End	Observed	Mr(expt)	Mr(calc)	Delta	Miss	Sequence
66 - 75	1163.61	1162.61	1162.62	-0.02	0	LVNELTEFAK
89 - 100	1419.69	1418.68	1418.69	-0.01	0	SLHTLFGDELCK
161 - 167	927.49	926.48	926.49	-0.01	0	YLYEIAR
169 - 183	1888.94	1887.93	1887.92	0.01	0	HPYFYAPELLYYANK
184 - 197	1747.71	1746.71	1746.70	0.01	0	YNGVFQECCQAEDK
205 - 211	922.47	921.46	921.46	0.00	1	IETMREK Oxidation (M)
319 - 340	2458.26	2457.25	2457.17	0.08	1	DAIPENLPPLTADFAEDKDVCK
347 - 359	1567.77	1566.76	1566.74	0.03	0	DAFLGSFLYEYSR
360 - 371	1439.82	1438.82	1438.80	0.01	1	RHPEYAVSVLLR
361 - 371	1283.70	1282.69	1282.70	-0.01	0	HPEYAVSVLLR
387 - 399	1554.66	1553.66	1553.65	0.01	0	DDPHACYSTVFDK
402 - 412	1305.70	1304.69	1304.71	-0.02	0	HLVDEPQNLIK
421 - 433	1479.81	1478.80	1478.79	0.02	0	LGEYGFQNALIVR
437 - 451	1639.96	1638.95	1638.93	0.02	1	KVPQVSTPTLVEVSR
452 - 468	1964.97	1963.96	1963.96	0.01	2	SLGKVGTRCCTKPESER
469 - 482	1740.84	1739.83	1739.82	0.01	0	MPCTEDYLSLILNR Oxidation (M)
499 - 507	1138.47	1137.46	1137.49	-0.03	0	CCTESLVNR
508 - 523	1880.95	1879.94	1879.91	0.03	0	RPCFSALTPDETYVPK
529 - 544	1907.95	1906.94	1906.91	0.03	0	LFTFHADICTLPDTEK
549 - 557	1014.58	1013.57	1013.61	-0.04	0	QTALVELLK
569 - 580	1415.66	1414.66	1414.68	-0.02	0	TVMENFVAFVDK Oxidation (M)

PUBLICATIONS

Eleonora Jovceva, Martin R. Larsen, Michael D. Waterfield, Buzz Baum and John F. Timms "**Dynamic cofilin phosphorylation in the control of lamellipodial actin homeostasis**. *Journal of Cell Science 120, 1888-1897*

Dynamic cofilin phosphorylation in the control of lamellipodial actin homeostasis

Eleonora Jovceva[1], Martin R. Larsen[2], Michael D. Waterfield[1], Buzz Baum[1,*] and John F. Timms[1,3]

[1]Ludwig Institute for Cancer Research, UCL Branch, London, W1W 7BS, UK
[2]Department of Biochemistry and Molecular Biology, University of Southern Denmark, DK-5230 Odense, Denmark
[3]Translational Research Laboratory, Institute of Women's Health, University College London, London, WC1E 6DH, UK
*Author for correspondence (e-mail: b.baum@ucl.ac.uk)

Accepted 3 April 2007
Journal of Cell Science 120, 1888-1897 Published by The Company of Biologists 2007
doi:10.1242/jcs.004366

Summary

During animal cell chemotaxis, signalling at the plasma membrane induces actin polymerisation to drive forward cell movement. Since the cellular pool of actin is limited, efficient protrusion formation also requires the coordinated disassembly of pre-existing actin filaments. To search for proteins that can monitor filamentous and globular actin levels to maintain the balance of polymerisation and disassembly, we followed changes in the proteome induced by RNA interference (RNAi)-mediated alterations in actin signalling. This unbiased approach revealed an increase in the levels of an inactive, phosphorylated form of the actin-severing protein cofilin in cells unable to generate actin-based lamellipodia. Conversely, an increase in F-actin levels induced the dephosphorylation and activation of cofilin via activation of the Ssh phosphatase. Similarly, in the context of acute phosphoinositide 3-kinase (PI3K) signalling, dynamic changes in cofilin phosphorylation were found to depend on the Ssh phosphatase and on changes in lamellipodial F-actin. These results indicate that changes in the extent of cofilin phosphorylation are regulated by Ssh in response to changes in the levels and/or organisation of F-actin. Together with the recent finding that Ssh phosphatase activity is augmented by F-actin binding, these results identify Ssh-dependent regulation of phosphorylated cofilin levels as an important feedback control mechanism that maintains actin filament homeostasis during actin signalling.

Supplementary material available online at
http://jcs.biologists.org/cgi/content/full/120/11/1888/DC1

Key words: Actin Cytoskeleton, Proteomics, Cofilin, Phospho-regulation

Introduction

Animal cells respond to a variety of signalling events at the plasma membrane by remodelling their actin cytoskeleton (Ridley et al., 2003). This drives changes in cell shape and is important for a variety of morphogenetic events, including cell migration and axon pathfinding. In many of these systems, actin signalling is triggered by ligand-receptor binding at the outer leaflet of the plasma membrane. This induces the activation of intracellular phosphoinositide 3-kinase (PI3K), which leads to the local activation of Rho family GTPases (Katso et al., 2001; Vanhaesebroeck et al., 2001). Rho family GTPases serve as 'master regulators' of the actin cytoskeleton (Ridley et al., 2003). Once active and loaded with GTP, Cdc42 and Rac GTPases bind Arp2/3 activator complexes, WASp and SCAR, respectively (Ibarra et al., 2005; Vartiainen and Machesky, 2004), triggering the Arp2/3-dependent nucleation of actin filaments and the generation of local actin-dependent protrusions. Since the burst of actin polymerisation in response to signalling is limited by the availability of actin monomers, a robust protrusive response also requires the coincident disassembly of the existing actin network. This is catalysed by the conserved actin-binding protein cofilin (Bamburg, 1999; Carlier et al., 1997; Hotulainen et al., 2005; Nishita et al., 2005) For a robust chemotactic response, the turnover of newly formed actin-based protrusions must also be tightly regulated, so that a cell can follow dynamic changes in the direction of an extracellular gradient. Finally, it has been proposed that cofilin aids directional motility by severing actin filaments close to the cell front to create new barbed ends to promote new local actin polymerisation (Ghosh et al., 2004).

Although data from the literature suggest that Rho family GTPases help to achieve coordinated control of actin filament nucleation and disassembly (Arber et al., 1998; Yang et al., 1998), little is known about the molecular mechanisms that monitor changes in actin organisation to ensure that a protrusive response to signalling is robust and self-limiting. To identify cytoskeletal regulators that function in this way, we used 2D difference gel electrophoresis (2D-DIGE) together with RNA interference (RNAi) to search for protein isoforms that are sensitive to changes in actin filament organisation and to actin signalling in *Drosophila* S2R$^+$ cells. This identified Ssh-dependent changes in cofilin phosphorylation that mirror changes in actin filament levels. Taken together, our data suggest that the dynamic regulation of cofilin activity acts as a feedback control mechanism, which monitors the level of actin filaments and helps to restore the resting state of the cytoskeleton following acute signalling.

Results

Levels of phosphorylated cofilin change in response to changes in actin filament organisation and PI3K signalling

The ability of animal cells to control and coordinate cortical actin-filament-based protrusive activity, suggests the existence of cellular machinery that monitors and regulates actin filament levels. To explore this possibility, we took an unbiased approach, using 2D-DIGE to search for protein isoforms that are sensitive to RNAi-induced changes in actin cytoskeleton organisation. We chose *Drosophila* S2R$^+$ cells, an adherent isolate of the commonly used haemocyte-derived S2 cell line (Yanagawa et al., 1998), as a model system for this analysis. Triplicate cultures were treated with double-stranded RNA (dsRNA) to silence genes that affect lamellipodial formation (Kunda et al., 2003); 2D-DIGE was performed to identify corresponding changes in the S2R$^+$ proteome, taking advantage of the fact that cytoskeletal proteins are relatively abundant in S2R$^+$ extracts. Protein expression was first assayed in lysates from untreated control cells and from cells treated with dsRNAs targeting Cdc42, Rac1+Rac2 and Arp3 prepared on different days. These treatments all eliminate lamellipodial formation (Kunda et al., 2003). This analysis revealed a number of proteins whose expression differed between untreated control and one or more of the experimental conditions (>1.5-fold average up- or downregulation; $P<0.05$; $n=3$). Each of these protein spots was excised from the gels for mass spectrometry (MS)-based protein identification (supplementary material Table S1). In this way, a protein corresponding to *Drosophila* Twinstar – the homologue of the actin depolymerising and severing protein cofilin – was identified with high confidence. This cofilin isoform was expressed at elevated levels following loss of Cdc42, Rac and Arp3 expression (Fig. 1A, B and supplementary material Fig. S1).

Cdc42 and Rac have been implicated in the dynamic regulation of cofilin activity in several systems (Arber et al., 1998; Yang et al., 1998) and are thought to act as part of a PI3K signalling cascade (Benard et al., 1999; Hawkins et al., 1995; Kotani et al., 1995; Reif et al., 1996). These facts led us to use RNAi to explore whether PI3K signalling also influences the expression of this cofilin isoform in S2R$^+$ cells. To do this, we treated cells with dsRNAs targeting *Drosophila* PI3K or the phosphatidylinositol (3,4,5)-trisphosphate [PtdIns(3,4,5)P_3] phosphatase PTEN to perturb PtdIns(3,4,5)P_3 levels in opposing directions. In addition, we used RNAi to silence two crucial downstream targets of PI3K signalling, Akt and Ras. GFP dsRNA was included as an irrelevant control for the effects of RNAi. A quantitative analysis revealed a significant reduction in the level of this cofilin spot in PTEN dsRNA-treated cells (–1.57-fold; $P=0.005$) and a moderate upregulation in PI3K dsRNA-treated cells, as expected for a genuine target of PI3K signalling (Fig. 1 and supplementary material Table S1). The decrease in the level of this cofilin isoform observed in Akt RNAi cells fell below our confidence limit (Fig. 1B,C). As expected, GFP dsRNA treatment did

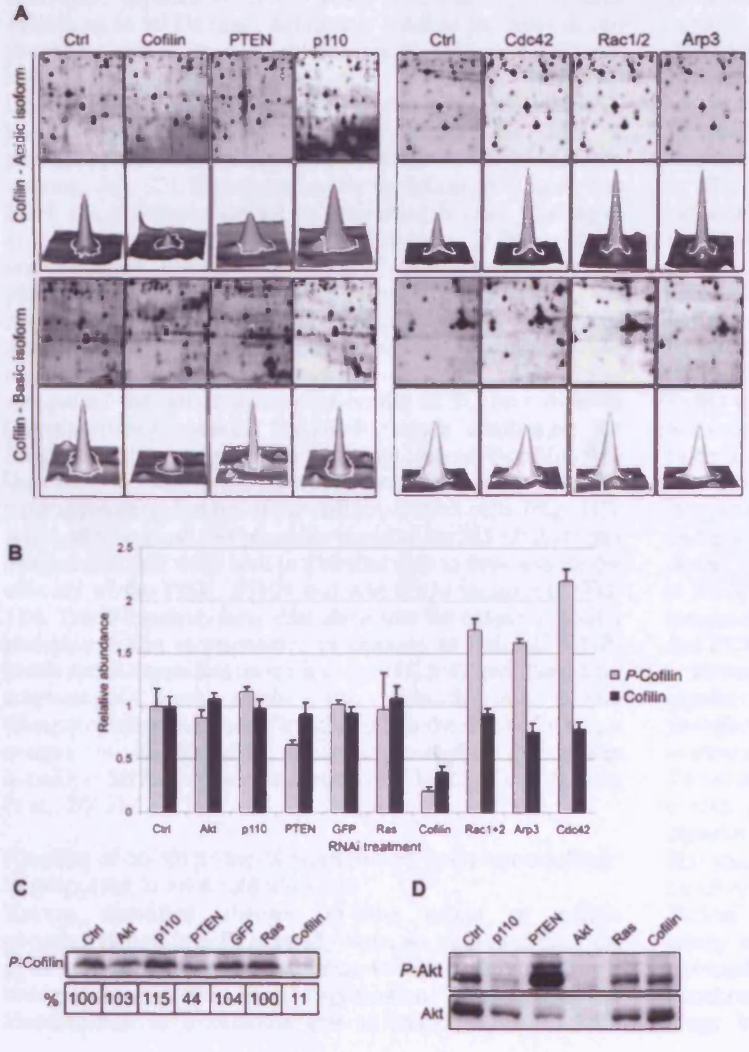

Fig. 1. *P*-cofilin levels change in response to alterations in actin filament organisation and PI3K signalling. (A) Representative 2D-DIGE gel images and 3D-fluorescence profiles of acidic and basic cofilin isoforms are shown for untreated (Ctrl) cells and cells treated with control dsRNA and dsRNA targeting cofilin, PTEN, PI3K p110 catalytic subunit (p110), Cdc42, Rac1 and Rac2 (Rac1/2), and Arp3. (B) The relative abundances of *P*-cofilin (acidic isoform) and cofilin (basic isoform) are shown for RNAi-treated cells from 2D-DIGE image analysis. Values represent the average of three measurements from biological replicates. Error bars represent the standard deviation. (C) Immunoblots show *P*-cofilin levels in untreated control and dsRNA-treated S2R$^+$ cell lysates confirming 2D-DIGE data. Relative abundance is shown below the blot as a percentage of the control, and is the average calculated from densitometry measurements of blots from three independent experiments. (D) Immunoblot of *P*-Akt and total Akt levels in control and dsRNA-treated S2R$^+$ cell lysates confirms the loss of PI3K, PTEN and Akt expression.

not affect cofilin expression. Nevertheless, one protein, identified as annexin B11, exhibited significant differences in its expression between dsRNA-treated cells and the untreated control. This suggests that dsRNA treatment or the engagement of the RNAi machinery itself can alter the expression of some proteins even in the absence of a target mRNA.

A second more basic isoform of cofilin was identified on these 2D gels by matrix-assisted laser desorption/ionization time-of-flight (MALDI-TOF)-based peptide mass fingerprinting (supplementary material Fig. S1A), and the identification of both isoforms was confirmed by the concomitant reduction of both the basic and acidic gel features in cofilin RNAi-treated cells (supplementary material Table S1 and Fig. 1C,D). Based on previous 2D studies (de Graauw et al., 2005; Hensbergen et al., 2005), we reasoned that the acidic isoform of cofilin may be phosphorylated. To test whether this was indeed the case, TiO_2 micro-columns were used to enrich for tryptic phosphopeptides from the acidic cofilin gel feature, which were then subjected to MALDI-TOF analysis. This identified a peptide with a mass corresponding to a phosphorylated form of the N-terminal tryptic peptide of cofilin (Ac-ASGVTVSDVCK+*P*; 1244.5 Da), with the equivalent peptides from the acidic and basic gel features exhibiting an 80 Da mass difference, equal to the mass of one phosphate group (supplementary material Fig. S1C). Nano-liquid chromatography-electrospray ionization collision-induced dissociation tandem mass spectrometry (LC-MS/MS)-based sequencing was used to identify the site of phosphorylation as being serine residue 3 (supplementary material Fig. S2). Significantly, this modification is known to block the activity of cofilin by preventing it from binding to and severing actin filaments (Bamburg, 1999). Since commercially available antibodies raised against cofilin phosphorylated at Ser3 (hereafter referred to as *P*-cofilin) did not recognise the *Drosophila* protein, a rabbit polyclonal antibody was raised against the *Drosophila* phospho-peptide sequence. The affinity-purified antibody specifically recognised the acidic isoform of cofilin in 2D immunoblots (supplementary material Fig. S1D), again confirming the identity of this protein. This antibody against *P*-cofilin was then used to validate the results of the proteomic analysis by immunoblotting lysates of the dsRNA-treated cells (Fig. 1C). Antibodies against Akt phosphorylated at Ser505 (*P*-Akt) and against total Akt were used in a similar way to demonstrate the efficacy of the PI3K, PTEN and Akt RNAi treatments (Fig. 1D). Taken together, these data show that the extent of cofilin phosphorylation is responsive to changes in PtdIns(3,4,5)P_3 levels and is dependent on the activity of Cdc42 and Rac. More surprisingly, these results also indicate that cofilin phosphorylation is affected by changes in the level of Arp3, a component of the actin nucleation complex that drives lamellipodial formation downstream of Cdc42 and Rac (Kunda et al., 2003).

Kinetics of cofilin phosphorylation and actin remodelling in response to an acute stimulus

Having identified changes in the extent of cofilin phosphorylation in cells at steady state, we next examined the dynamics of cofilin phosphorylation in cells undergoing acute changes in actin cytoskeletal organisation. This required the identification of a stimulus able to induce dynamic actin remodelling. In testing a number of growth factors in $S2R^+$ cells [10% foetal calf serum (FCS), 2-day-old conditioned medium, bovine insulin, human EGF, murine vascular endothelial growth factor (VEGF) and human platelet-derived growth factor (PDGF)], only insulin was found to activate signalling, as monitored by immunoblotting with specific antibodies against *P*-Akt, S6K phosphorylated at Thr398 (*P*-S6K) and ERK phosphorylated at Thr198 and Tyr200 (*PP*-ERK) (supplementary material Fig. S3A) and Lizcano et al. (Lizcano et al., 2003). Insulin also induced an increase in the level of lamellipodial F-actin in these cells within 5 minutes of treatment (Fig. 2A). Elevated levels of filamentous actin remained at the cell cortex for 30-40 minutes, before moving to the cell interior (perhaps as the result of retrograde flow in the absence of new polymerisation). Since actin polymerisation is known to generate the force for membrane protrusion, we used time-lapse microscopy to determine whether this burst of actin filament formation is translated into protrusive activity, imaging cells every 20 seconds before and after addition of insulin, starting 10 minutes before and finishing 30 minutes after addition. (Fig. 2B). As can be seen in the corresponding kymographs, insulin induced a significant increase in the rate of membrane ruffling. Insulin was also found to induce strong cortical F-actin staining in more rounded Kc167 cells, which do not possess lamellipodia (Fig. 2C). This suggests that the induction of actin polymerisation is the primary response, which in adherent $S2R^+$ cells is translated into the formation of F-actin-based protrusions.

The kinetics of this actin response was mirrored by changes in PI3K signalling, as measured using *P*-Akt. The insulin-induced change in Akt phosphorylation reached its maximum level within 2 minutes. High levels of *P*-Akt were then maintained for 10-20 minutes, before declining gradually to background levels (Fig. 2E). This kinetic profile was confirmed in fixed cells where, in response to insulin, *P*-Akt was first seen to rapidly accumulate at the plasma membrane, the site of PtdIns(3,4,5)P_3 generation (supplementary material Fig. S3B). *P*-Akt then became localised to the nucleus, before declining to barely detectable levels by 120 minutes. We confirmed this to be a generic response of fly cells by observing similar *P*-Akt dynamics in Kc167 cells following insulin stimulation (supplementary material Fig. S3C). We then used immunoblotting to follow cofilin phosphorylation dynamics during the course of this response. *P*-cofilin levels responded to PI3K signalling, but did not peak until ~30 minutes after insulin stimulation (Fig. 2D); long after the initial burst of actin and PI3K signalling.

Having established that insulin induces a robust PI3K signal together with a striking change in actin organisation and cofilin phosphorylation, we used the PI3K inhibitors LY294002 and wortmannin to test whether these events are causally linked. The addition of LY294002 (100 μM) or wortmannin (100 nM) to resting $S2R^+$ cells (Fig. 3A) and Kc167 cells (supplementary material Fig. S4A) led to a profound loss of cortical actin filaments. Moreover, both inhibitors blocked normal membrane ruffling in cells (Fig. 3B), suggesting a role for PtdIns(3,4,5)P_3 in the regulation of actin dynamics in cells at steady state. In addition, LY294002 and wortmannin induced a retraction of the cell edge, leaving a few relatively inactive membrane processes attached to the substrate. Similarly, both drugs blocked the ruffling response to insulin treatment

(supplementary material Fig. S4B). The ability of these compounds to block insulin-induced PI3K activity was confirmed by immunoblotting for *P*-Akt (Fig. 3C). We were then able to use LY294002 to show that insulin-stimulated cofilin phosphorylation is a consequence of PI3K signalling itself, because treatment with this compound led to a significant reduction in the ability of insulin to induce cofilin phosphorylation (Fig. 3D). Thus, PtdIns(3,4,5)P_3 is required

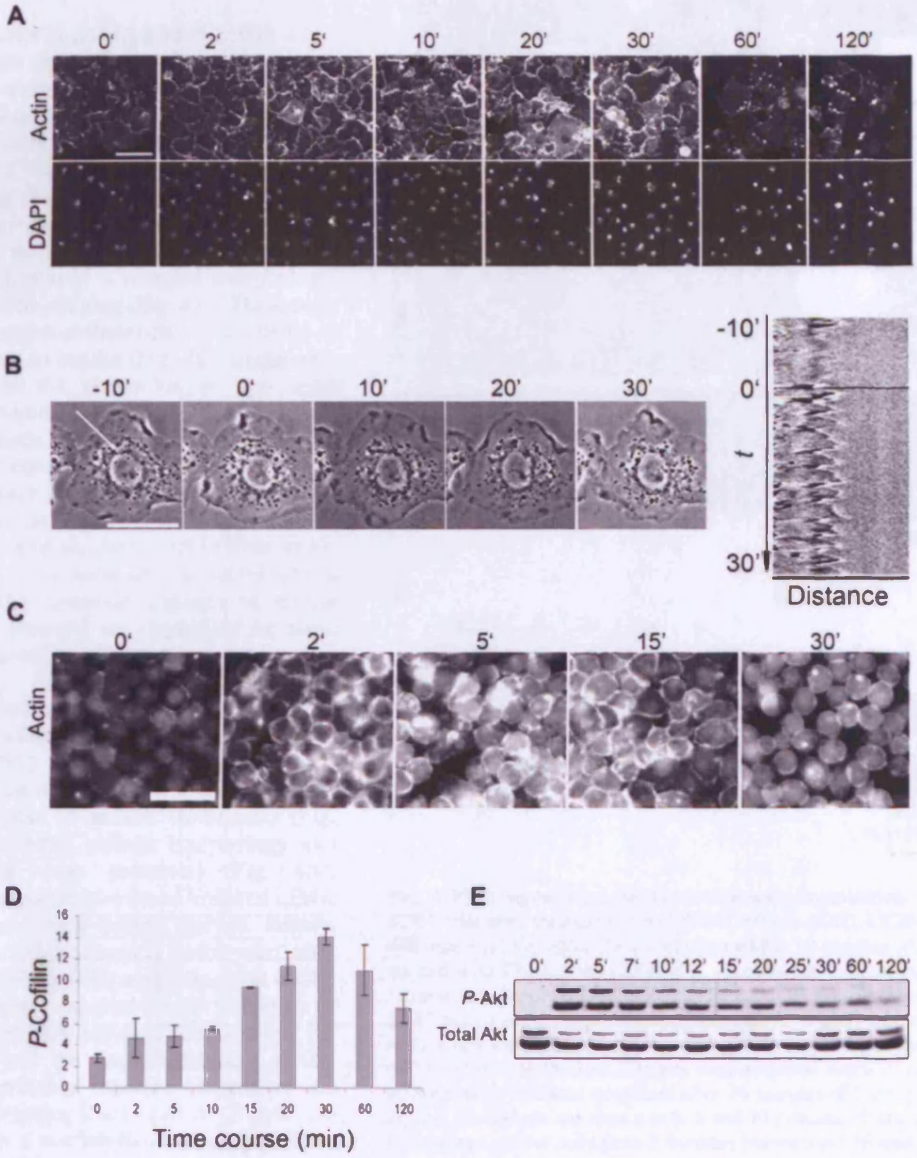

Fig. 2. The kinetics of actin remodelling and cofilin phosphorylation following an acute stimulus. (A) S2R$^+$ cells stained for F-actin (Rhodamine-phalloidin) and nuclei (DAPI) are shown at various times after insulin stimulation (10 μg/ml). Bar, 50 μm. (B) Images from a time-lapse movie of S2R$^+$ cells stimulated with insulin (10 μg/ml) for the times indicated. Cells were filmed in phase-contrast on a time-lapse microscope using a 100× oil-immersion lens; frames were acquired every 20 seconds, 10 minutes prior to insulin addition and for 30 minutes after addition. Images are representative of five independent experiments. Bar, 50 μm. Right panel shows a kymograph of the movie from which the presented images were taken, generated from pixel intensities along a line transecting the cell membrane (shown in first image). It shows increased protrusion dynamics after insulin stimulation. (C) F-actin immunostaining (Rhodamine-phalloidin) of serum-starved Kc167 cells stimulated with insulin (10 μg/ml) for the indicated times. Bar, 50 μm. (D) Cofilin is transiently phosphorylated in S2R$^+$ cells in response to insulin. S2R$^+$ cells were grown in serum-free medium overnight and stimulated with insulin at 10 μg/ml for the indicated times. Lysates were prepared and immunoblotted with antibody against *P*-cofilin. Blots were analysed by densitometry. Values represent the mean *P*-cofilin signal from two experiments after normalising with respect to β-actin levels. Error bars represent the standard deviation. (E) Time course of Akt activation in insulin stimulated S2R$^+$ cells. S2R$^+$ cells were maintained in Schneider's serum-free medium overnight, and then stimulated with bovine insulin (10 μg/ml) for the times indicated. Immunoblotting was used to assess levels of *P*-Akt and total Akt.

for the maintenance of an actin-rich cortex, the normal ruffling behaviour of resting cells, and for the insulin-induced stimulation of actin polymerisation and cofilin phosphorylation in S2R$^+$ cells.

Functional analysis of cofilin and *P*-cofilin during acute actin signalling

Using RNAi, we were then able to define roles for cofilin and phosphorylated cofilin (*P*-cofilin) in the response of S2R$^+$ cells to PI3K signalling. As before, insulin was used to stimulate PI3K-dependent membrane ruffling (Fig. 4). We first tested the role of cofilin in this process. Five days after the treatment of cells with cofilin dsRNA, the majority of cells (>90%) displayed a rounded morphology, with increased F-actin staining (Fig. 4A). These cells were unable to re-organise their actin cytoskeleton or to ruffle in response to insulin (Fig. 4B), implying a role for cofilin in the generation of new actin filaments, as previously described (Ghosh et al., 2004). Second, since the kinase and phosphatase responsible for the control of cofilin phosphorylation have been previously identified in both *Drosophila* and other systems, as LIMK (Arber et al., 1998; Yang et al., 1998) and slingshot (Ssh) (Niwa et al., 2002), respectively, we were able to use RNAi to assess whether the dynamic changes in cofilin phosphorylation observed are dependent on these proteins and important for the protrusive response to PI3K signalling. As expected, RNAi-induced silencing of Ssh led to an increase in basal cofilin phosphorylation, whereas silencing of LIMK led to a decrease (Fig. 5A). Ssh silencing also induced a significant reduction in the ability of cells to mount a protrusive response to insulin stimulation (Fig. 4B), even though gross cellular morphology and actin organisation were preserved (Fig. 4A). Conversely, cells expressing reduced levels of LIMK were found to have well-defined cortical lamella (Fig. 4A) and to ruffle intensely before and after insulin stimulation (Fig. 4B), suggesting that cofilin phosphorylation is not required for the formation of new protrusions. Finally, we used RNAi to test for the role of Rac and the Arp2/3 complex in this response. As previously reported (Kunda et al., 2003), dsRNAs targeting Rac1+2 or Arp3 gave rise to S2R$^+$ cells with a starfish-like phenotype. These cells proved unable to mount a morphological response to insulin treatment (Fig. 4A,B). Thus, the Rac-Arp2/3 pathway is required for the generation of new actin filament-based protrusions downstream of acute PI3K signalling, as is active cofilin.

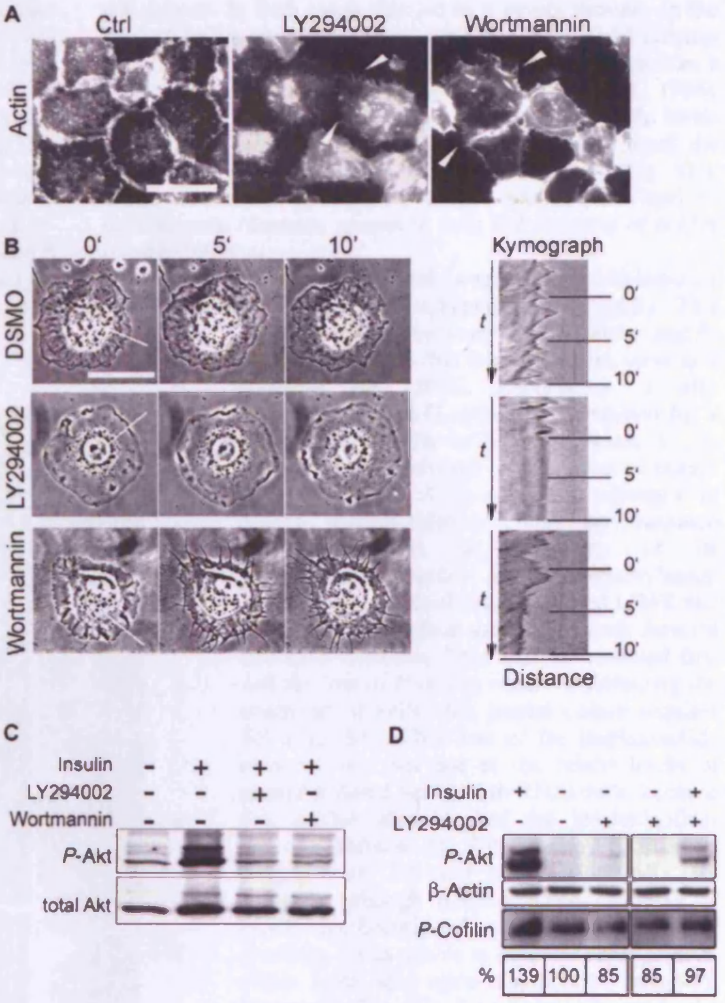

Fig. 3. PI3K-signalling controls cortical actin organisation. (A) Actin staining of S2R$^+$ cells after treatment with DMSO vehicle (Ctrl), LY294002 (100 μM) and wortmannin (100 nM). Cells were treated for 10 minutes and then fixed and stained with Rhodamine-phalloidin. Arrowheads indicate regions of cell retraction to leave protrusions. Bar, 50 μm. (B) Images of time-lapse movies of S2R$^+$ cells treated with DMSO, LY294002 (100 μM) and wortmannin (100 nM). Cells were filmed in phase-contrast on a time-lapse microscope using a 100× oil-immersion lens. Frames were acquired every 10 seconds for 30 minutes with inhibitor treatment after 10 minutes of filming (designated 0' in the figure). Snapshots are shown at 0, 5 and 10 minutes. The corresponding kymographs show cells from 3 minutes before until 10 minutes after insulin stimulation and were constructed from pixel intensities taken along the lines depicted in the images on the left. Bar, 50 μm. (C) Immunoblotting of *P*-Akt and total Akt in untreated S2R$^+$ cells and cells treated with insulin (for 10 minutes) with and without pre-treatment (for 10 minutes) with LY294002 (100 μM) or wortmannin (100 nM). (D) Immunoblotting of *P*-Akt, β-actin and *P*-cofilin in S2R$^+$ cells treated for 10 minutes with LY294002 (100 μM) and insulin (10 μg/ml), alone and in combination. Relative abundance is represented as a percentage of the control below the blot and is the average calculated from densitometry measurements of blots from three independent experiments.

Actin filaments control cofilin phosphorylation dynamics

The proteomic analysis showed that cells lacking lamellipodia (Rac1/2, Cdc42 or Arp3 RNAi cells) express relatively high levels of *P*-cofilin (Fig. 1). This suggested the possibility that the observed changes in cofilin phosphorylation are triggered as a response to the loss of lamellipodial actin. To test whether this correlation also holds during an acute response to PI3K signalling, we used Rac1 + Rac2 RNAi to block lamellipodial formation in cells stimulated

with insulin. This RNAi treatment eliminated dynamic changes *P*-cofilin, supporting the idea that changes in cofilin activity follow changes in the levels of actin filaments in this system (Fig. 5B). Similarly, Ssh RNAi cells, which have an impaired ruffling response, do not display the dynamic changes in cofilin phosphorylation in response to insulin/PI3K signalling (Fig. 5B). To examine the kinetics of this response more directly, we used actin inhibitors to induce acute changes in the relative levels of F-actin and G-actin, and tracked the resulting changes in *P*-cofilin levels. Both the G-actin-sequestering agent latrunculin B and the barbed-end capping toxin cytochalasin D eliminated the actin-rich cell cortex within minutes (Kiger et al., 2003) (data not shown). In both cases, this led to a steady increase in the level of cofilin phosphorylation over a period of 30-60 minutes (Fig. 5C). Conversely, the addition to cells of jasplakinolide, a drug that promotes actin filament formation (Bubb et al., 1994), induced the rapid loss of *P*-cofilin (to barely detectable levels within 10 minutes). Jasplakinolide was also able to block the accumulation of *P*-cofilin in insulin-treated cells (Fig. 5D). These data reveal a direct correlation between the level of cortical actin filaments present in cells and the level of cofilin phosphorylation.

RNAi-induced silencing of actin was also found to induce a robust increase in cofilin phosphorylation (Fig. 6D). This confirms the link between actin filaments and *P*-cofilin, and shows that free cofilin can serve as a substrate for LIMK. Importantly, it also demonstrates that G-actin is not required for a change in F-actin or G-actin levels to be translated into a change in the extent of cofilin phosphorylation. Actin-dependent changes in cofilin phosphorylation could be mediated through changes in the rate of its phosphorylation and/or its dephosphorylation. To explore both possibilities, we used LIMK and Ssh dsRNA to reduce the rate of both forward and back reactions. This analysis revealed first that the loss of *P*-cofilin observed following the treatment of cells with jasplakinolide requires Ssh (Fig. 6A). This loss of the jasplakinolide response was not due to the raised levels of phosphorylated Ser3 in Ssh RNAi cells, because Ssh dsRNA also blocked the jasplakinolide-induced decrease in *P*-cofilin levels in cells lacking both Ssh and LIMK (Fig. 6B). By contrast, although RNAi-induced silencing of LIMK significantly reduced the overall levels of *P*-cofilin, it was unable to suppress changes in *P*-cofilin levels seen upon treatment of cells with latrunculin (Fig. 6C). Significantly, however, the addition of Ssh dsRNA to LIMK RNAi cells overrode this latrunculin-induced increase in *P*-cofilin levels. These results suggest that the downregulation of Ssh phosphatase activity after latrunculin treatment plays an important role in the regulation of the *P*-cofilin response, as does its upregulation in the presence of jasplakinolide. Thus, Ssh is likely to be the key regulator of dynamic regulation of cofilin phosphorylation this system.

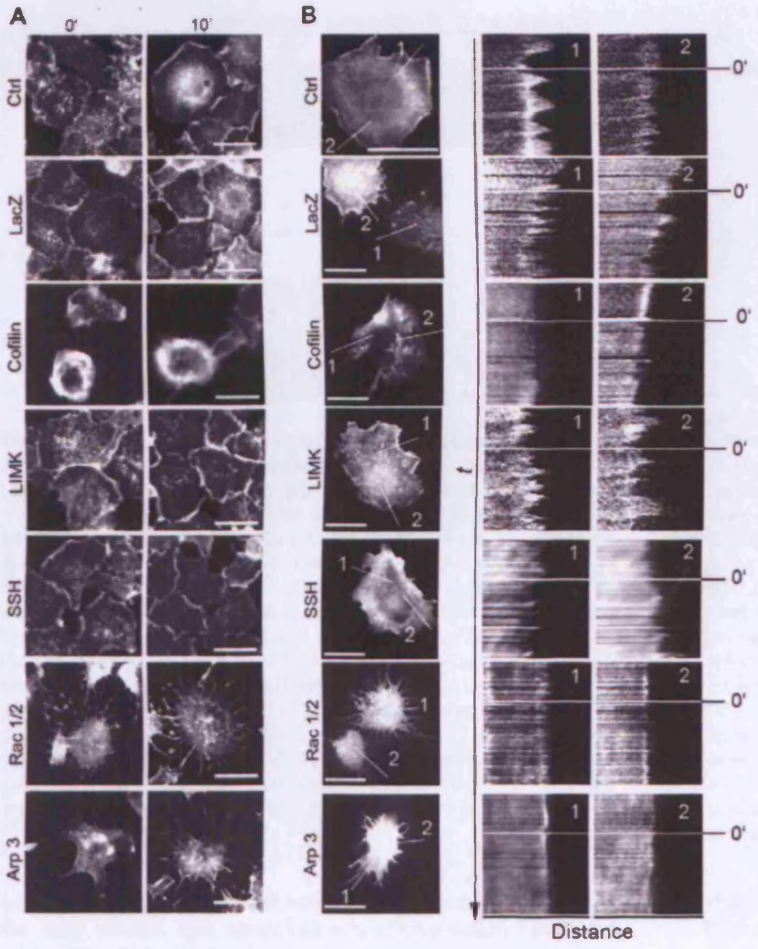

Fig. 4. Functional analysis of cofilin during acute actin signalling. (A) Actin staining in dsRNA-treated cells stimulated with insulin. S2R$^+$ cells were incubated with dsRNAs targeting LacZ, cofilin, LIMK, Ssh, Rac1and Rac2 (Rac1/2) and Arp3 for 5 days. On day 5, cells were treated with insulin for 10 minutes (10') or left untreated (0'). Cells were then fixed and stained for F-actin with Rhodamine-phalloidin. Bars, 50 μm. (B) Visualisation of actin dynamics in dsRNA-treated cells using GFP-labelled moesin. Snapshots of time-lapse movies just before the addition of insulin are shown on the left. Bars, 50 μm. The two lines used to generate the kymographs (right) are indicated on the cell images. Actin reorganisation was filmed for 3 minutes before and for 10 minutes after the addition of 10 μg/ml insulin, the point of insulin addition labelled as 0'. Images are representative of at least two independent experiments.

Discussion

In this study, we have used *Drosophila* cell lines as a model system to explore the molecular mechanisms governing the dynamic remodelling of the cortical actin cytoskeleton. First, we sought to identify mechanisms that enable cells to sense and respond to changes in actin filament levels. To do this, we took an unbiased approach, making use of the relative abundance of cytoskeletal regulators to combine proteome expression profiling with RNAi-dependent gene silencing to identify proteins that are responsive

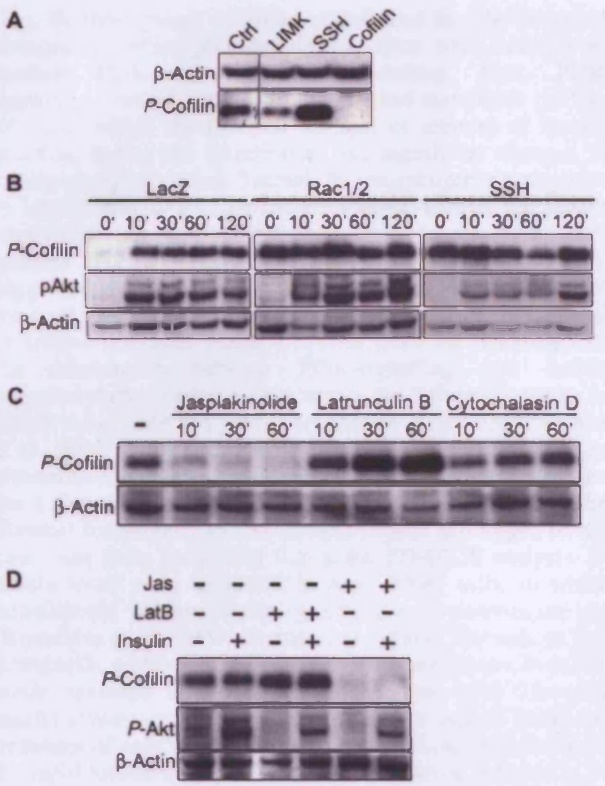

Fig. 5. PI3K-induced changes in cofilin phosphorylation are the result of actin cytoskeletal remodelling. (A) LIMK and Ssh are regulators of cofilin phosphorylation. S2R$^+$ cells were left untreated (Ctrl) or were treated with dsRNA for knockdown of expression of LIMK, Ssh and cofilin for 5 days. Cells were lysed and *P*-cofilin and β-actin levels assessed in the lysates by immunoblotting. (B) Immunoblotting of *P*-cofilin, *P*-Akt and β-actin in lysates of dsRNA-treated cells stimulated with insulin. S2R$^+$ cells were cultured in the presence of dsRNA targeting LacZ (control), Rac1+2 and Ssh and then treated with 10 μg/ml insulin for the indicated times prior to lysis and immunoblotting. (C) *P*-cofilin and β-actin levels were assessed in extracts from S2R$^+$ cells treated with jasplakinolide (1 μg/ml), latrunculin B (1 μg/ml) or cytochalasin D (2 μg/ml) for the times indicated. (D) *P*-cofilin, *P*-Akt and β-actin levels are shown for S2R$^+$ cells pre-treated for 10 minutes with latrunculin B (1 μg/ml) or jasplakinolide (1 μg/ml) followed by 20 minutes of insulin treatment (10 μg/ml) or vehicle alone.

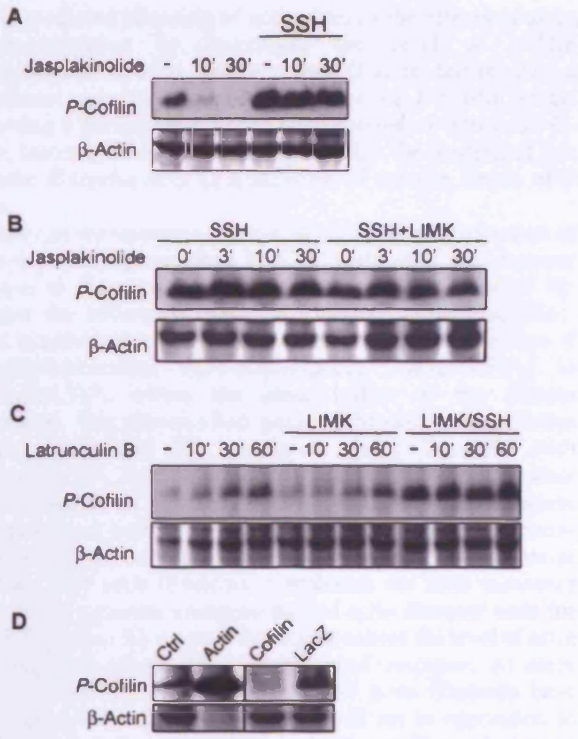

Fig. 6. Slingshot is the major regulator of actin-dependent cofilin phosphorylation. (A) Ssh RNAi blocks jasplakinolide-induced loss of cofilin phosphorylation. Control S2R$^+$ cells and cells treated with dsRNA targeting Ssh were treated with jasplakinolide (1 μg/ml) for the times indicated and *P*-cofilin and β-actin levels assessed in the lysates by immunoblotting. (B) LIMK RNAi does not reverse Ssh dsRNA blockade of jasplakinolide-induced loss of cofilin phosphorylation. Cells treated with dsRNA targeting Ssh (SSH) or Ssh and LIMK together (SSH/LIMK) were treated with jasplakinolide (1 μg/ml) for the indicated times, and *P*-cofilin and β-actin levels assessed in lysates by immunoblotting. (C) The effect of LIMK and Ssh on latrunculin B-induced cofilin-phosphorylation. Cells treated with control dsRNA and dsRNA targeting LIMK or LIMK and SSH together (LIMK/SSH) were treated with latrunculin B (1 μg/ml) for the indicated times, and *P*-cofilin and β-actin levels in lysates were determined by immunoblotting. (D) Loss of actin expression induces cofilin phosphorylation. *P*-cofilin and β-actin levels were determined by immunoblotting in lysates of control cells (untreated) and cells treated with dsRNAs targeting actin, cofilin and LacZ.

to changes in lamellipodial actin organisation. *P*-cofilin was the only protein spot identified whose expression correlated with actin filament levels. Significantly, phosphorylation of cofilin on the evolutionarily conserved Ser3 prevents the binding of cofilin to actin filaments, completely inhibiting its ability to promote filament disassembly (Bamburg, 1999). *P*-cofilin levels were also altered in opposing directions in response to changes in levels of PtdIns(3,4,5)P_3 induced following PI3K and PTEN RNAi, but were unaffected by RNAi-induced silencing of Ras and Akt. Thus, the level of cofilin phosphorylation is responsive to changes in actin organisation and is regulated by actin-signalling events downstream of PtdIns(3,4,5)P_3 (Firtel and Chung, 2000).

Having established a possible link between PI3K-actin signalling and cofilin phosphorylation, we were then able to use RNAi together with live cell imaging to look for a role for the active dephosphorylated form of cofilin in actin remodelling. The ability of cells to mount a ruffling response in this system was found to require cofilin and, to a lesser extent, its dedicated phosphatase Ssh, in agreement with previous reports (Ghosh et al., 2004; Nishita et al., 2004). Moreover, levels of *P*-cofilin were found to respond to PI3K signalling, as has been observed in other systems (Mouneimne et al., 2004; Nishita et al., 2004). In S2R$^+$ cells, *P*-cofilin levels peak 30 minutes after insulin stimulation before gradually returning to baseline levels. Although this dynamic response reveals a link between PI3K signalling and cofilin phosphorylation, as suggested by the analysis in steady state

(Fig. 4), three pieces of evidence indicated that the observed changes in cofilin phosphorylation status were unlikely to mediate PI3K-induced actin remodelling. First, PI3K signalling, cortical actin accumulation and membrane ruffling all occur within the first few seconds or minutes of insulin addition; before the detection of any significant changes in cofilin phosphorylation. Second, the morphogenetic response to insulin was unaffected by the loss of LIMK, the kinase responsible for cofilin phosphorylation in this and other systems (Fig. 4) (Arber et al., 1998; Yang et al., 1998), suggesting that an increase in cofilin phosphorylation is not required for cytoskeletal remodelling during the initial protrusive response. Third, it is clear from the literature that the relationship between PI3K-signalling and cofilin phosphorylation varies widely across the different systems in which it has been analysed (Mouneimne et al., 2004; Nishita et al., 2004; Song et al., 2006). These data led us to explore an alternative model in which changes in cofilin phosphorylation are a downstream effect of PI3K-induced changes in actin filament formation. The first indication that this might be the case came from the finding that in our 2D-DIGE analysis, *P*-cofilin levels were increased in Arp3 RNAi cells, in which lamellipodia and the underlying cortical actin network are lost (Biyasheva et al., 2004; Kunda et al., 2003). Second, in Rac RNAi cells, which are unable to generate protrusions, *P*-cofilin levels remained at a constant and elevated level following insulin stimulation – as expected by such a model. Third, the treatment of cells with latrunculin B or cytochalasin D caused the rapid loss of cortical F-actin, and a delayed increase in *P*-cofilin levels. Conversely, the actin toxin jasplakinolide induced ectopic actin filament formation and a relatively rapid and complete loss of the *P*-cofilin signal. Moreover, jasplakinolide also blocked the ability of insulin to induce cofilin phosphorylation in these cells. Taken together these data show that actin remodelling is required for dynamic changes in the level of cofilin Ser3 phosphorylation, and that acute changes in actin filaments levels are sufficient to alter the cofilin phosphorylation status.

It is noticeable that the increase in cofilin phosphorylation is observed in cells with a paucity of cortical actin filaments, where it will limit the rate of filament disassembly. Conversely, cofilin is dephosphorylated and activated in cells with excess actin filaments, therefore maintaining the monomeric actin pool. This suggests a role for the dynamic regulation of cofilin phosphorylation in the maintenance of actin filament homeostasis and implies the existence of a sensor that can measure dynamic changes in actin filament levels. Four recent studies have implicated Ssh in this role, by showing that Ssh is activated through binding to actin filaments (Nagata-Ohashi et al., 2004; Soosairajah et al., 2005; Tanaka et al., 2005; Yamamoto et al., 2006). Similarly, our data show that Ssh is likely to be the key regulator of *P*-cofilin levels in S2R$^+$ cells because it is required for dynamic changes in *P*-cofilin levels in response to insulin and because the kinetics of loss of cofilin phosphorylation following jasplakinolide treatment are more rapid than the effects of latrunculin B – as would be expected if the dynamics of *P*-cofilin were regulated by a constitutively active LIMK and a phosphatase whose activity is regulated by the level of actin filaments. Furthermore, Ssh RNAi suppresses both jasplakinolide- and latrunculin-induced changes in *P*-cofilin whereas, on its own, LIMK RNAi cannot. Because RNAi-mediated silencing of actin mimics the effects of actin depolymerisation by increasing the level of cofilin phosphorylation, it is unlikely that G-actin levels play a significant role in driving the change in *P*-cofilin levels following a perturbation of the ratio between F-actin and G-actin. Instead, we favour a model in which the binding of Ssh to actin filaments acts as a measure of relative levels of F actin.

How can we reconcile the role of cofilin in the formation of actin-dependent protrusions in S2R$^+$ cells with the observed changes in *P*-cofilin following an acute PI3K response? We suggest the following scenario: following insulin addition, PI3K is activated within 2 minutes, inducing the conversion of phosphatidylinositol (4,5)-bisphosphate [PtdIns(4,5)P_2] to PtdIns(3,4,5)P_3 within the inner leaflet of the plasma membrane. This activates Rac, possibly through the association of an unidentified PH domain-containing Rac-GEF with PtdIns(3,4,5)P_3, leading to the nucleation of Arp2/3-dependent actin filaments at the cell cortex with subsequent filament elongation and protrusion formation. In these cells, active non-phosphorylated cofilin at the cell front will depolymerise existing ADP-actin filaments to replenish the actin monomer pool and to generate uncapped barbed actin filament ends for new elongation. We propose that Ssh monitors the level of actin filaments throughout this morphological response. At early stages, before significant levels of new actin filaments have been formed, low-level Ssh activity will act in opposition to LIMK to maintain a limited pool of active cofilin sufficient to remodel the existing actin filament network. Later, as new actin filaments accumulate and the PI3K signal declines at between 30 and 60 minutes after insulin stimulation, Ssh activity will come to dominate through its association with actin filaments and, perhaps, through inhibition of LIMK (Soosairajah et al., 2005). This will reduce cofilin phosphorylation increasing the level of actin depolymerisation to restore the F-actin:G-actin equilibrium. This dynamic regulation, we suggest, helps the cell to generate the robust but self-limiting actin filament response to acute actin signalling. In the context of a graded extracellular signal in the developing embryo (Wood et al., 2006), a similar system could act over spatially distinct regions of the cell to facilitate chemotaxis by coordinating the polymerisation of actin filaments at the cell front, with their disassembly at the cell rear.

Materials and Methods

Cell culture methods

S2R$^+$ and Kc167 cells were maintained in Schneider's *Drosophila* medium (Invitrogen) supplemented with 10% (v/v) heat-inactivated foetal calf serum (FCS) (Helena Biosciences) and antibiotics (50 units/ml penicillin and 50 μg/ml streptomycin; both from Sigma) in T25 flasks (Falcon, BD Biosciences) at 24°C. For passage of S2R$^+$ cells, cells were removed from culture flasks using trypsin-EDTA (Invitrogen). To determine the effect of insulin on PI3K signalling including actin reorganisation, cells were grown in serum-free medium overnight and then treated with bovine insulin (10 μg/ml; Sigma) for different times. Other growth factors used in this study were human EGF at 200 ng/ml (R&D Systems), murine VEGF at 50 ng/ml and human PDGF-BB at 125 ng/ml (both from PeproTech Inc.). For inhibitor treatments, cells were treated with 100 nM wortmannin (Calbiochem), 10-100 μM LY294002 (Calbiochem), 1 μg/ml latrunculin B (Calbiochem), 1 μg/ml jasplakinolide (Invitrogen) or 2 μg/ml cytochalasin D (Sigma). All inhibitors were made up in DMSO, which served as a vehicle-alone control.

dsRNA production and RNAi

Primer sequences of ~21 bp (supplementary material Table S2) flanked with T7 sites, were chosen to PCR amplify ~500-1500 bp of exonic sequences of the genes to be silenced. PCR was carried out using HotStarTag DNA polymerase (Qiagen).

PCR amplification was confirmed by 1% agarose gel electrophoresis using the GeneRuler 1-kb marker to assess the size of PCR products. dsRNAs were generated from PCR products by in vitro transcription using the MEGAscript™ High Yield Transcription Kit (Ambion). Reactions were conducted at 37°C overnight and dsRNAs were purified using Multiscreen PCR_{96} purification plates (Millipore) attached to a vacuum pump. Purified dsRNAs were re-suspended in TE buffer (10 mM Tris-HCl pH 8.0, 1 mM EDTA) and annealed at 95°C for 15 minutes followed by slow cooling to room temperature (RT). The dsRNA concentration was estimated on 1% agarose gels using 500 ng of the GeneRuler 1-kb marker and dsRNAs were stored at −20°C until used. For dsRNA treatment, $S2R^+$ cells were typically suspended at 2×10^6 cells/ml in Schneider's serum-free medium and 300 μl of cells per well were plated into 6-well tissue culture plates (Falcon, BD Biosciences). dsRNA was added directly to the medium to a final concentration of 0.3 μM, followed by gentle agitation. Cells were incubated for 30 minutes at RT followed by addition of 1 ml of Schneider's medium supplemented with 10% FCS. For proteomic experiments, each dsRNA treatment was conducted in triplicate on separate days. To allow turnover of target proteins cells were incubated for 5 days prior to harvesting for analysis.

Sample preparation for 1D and 2D SDS-PAGE

Cells were washed gently with ice-cold PBS and lysed in NP40 lysis buffer (50 mM HEPES, 150 mM NaCl, 1% NP40, 1 mM EDTA) or 2D lysis buffer (8 M urea, 2 M thiourea, 4% CHAPS, 1 mM EDTA, 10 mM Tris-HCl pH 8.3), both supplemented with protease inhibitors (17 μg/ml aprotinin; 1 μg/ml pepstatin; 1 μg/ml leupeptin, 100 μg/ml AEBSF) and phosphatase inhibitors (2 mM sodium orthovanadate, 5 μg/ml BpVphen, 5 μM fenvalerate, 1 μM okadaic acid). For 1D SDS-PAGE, cells were lysed in NP40 lysis buffer and scraped off on ice. Cells lysed in 2D lysis buffer were homogenised by passage (six times) through a 25G needle. Insoluble material was removed by centrifugation (13,000 rpm for 10 minutes at 4°C). Protein concentrations were determined using Coomassie Protein Assay Reagent (Pierce) and a bovine serum albumin (BSA) standard curve with three replicate assays performed per sample. For 1D SDS-PAGE, lysates were denatured in Laemmli sample buffer [50 mM Tris-HCl pH 6.8, 10% (v/v) glycerol, 2% (w/v) SDS, 0.1% (w/v) Bromophenol Blue, 2% (v/v) β-mercaptoethanol] and heated at 100°C for 5 minutes. 1D SDS-PAGE was performed following standard procedures.

Fluorescence 2D-DIGE protein expression profiling

The N-hydroxy-succinimidyl (NHS) ester of Cy2 was purchased from GE Healthcare, whereas NHS-Cy3 and Cy5 were synthesized in-house following the protocol outlined in Chan et al. (Chan et al., 2005). 2D difference gel electrophoresis (2D-DIGE) was carried out in a dedicated clean-room essentially as described (Weeks et al., 2006). For this, 120 μg of protein extract from each triplicate sample was labelled with NHS-Cy3 or NHS-Cy5 at 4 pmol dye/μg protein on ice in the dark for 30 minutes. Equal amounts of protein extract from each experiment were pooled together and labelled with NHS-Cy2 to create an internal standard which was run on all gels against the Cy3- and Cy5-labelled samples to aid in spot matching and quantification (Gharbi et al., 2002). Labelling reactions were quenched with a 20-fold molar excess of free L-lysine to dye and differentially labelled samples mixed appropriately. Final volumes were adjusted to 450 μl with 2D lysis buffer with final concentrations of 65 mM DTT, 2% carrier Ampholine/ Pharmalytes (50:50 v/v) pH 3-10 and 0.05% Bromophenol Blue. For 2D SDS-PAGE, 24-cm, non-linear pH 3-10 IPG strips (GE Healthcare) were rehydrated with Cy-labelled samples overnight in the dark at RT prior to isoelectric focusing on a Multiphor II apparatus (GE Healthcare) for 80 kVh at 18°C. Strips were then incubated for 10 minutes in equilibration buffer (50 mM Tris-HCl pH 6.8, 6 M (w/v) urea, 30% (v/v) glycerol, 2% (w/v) SDS) containing 65 mM DTT, and then for 10 minutes in the same buffer containing 240 mM iodoacetamide. IPG strips were transferred onto 1.5-mm thick 24×20 cm 12% polyacrylamide gels cast between low-fluorescence glass plates and bonded to the inner surface of one plate with bind-silane (PlusOne, GE Healthcare). Strips were overlaid with 0.5% (w/v) low-melting point agarose in Tris-glycine-SDS electrophoresis buffer (Severn Biotech) with Bromophenol Blue. Gels were run at 2 W per gel at 8°C in an Ettan 12 apparatus (GE Healthcare) until the dye front had run off and were then scanned (between plates) on a Typhoon 9400 multicolour fluorescence imager using ImageQuant software (GE Healthcare). Images were imported into DeCyder™ image analysis software (GE Healthcare) for comparison of sample feature volumes with the corresponding internal standard feature volumes giving a standardised abundance for each matched gel feature. Standardised abundances were then averaged from the triplicates for each experimental condition and features found on all images were selected for MS-based identification if they displayed a $\geq$1.5-fold average change in abundance versus the untreated control with $P\leq0.05$ (Student's *t*-test). Proteins were then visualised by staining of gels with colloidal Coomassie Brilliant Blue and the gels were imaged and matched to the corresponding Cy-dye images using DeCyder software essentially as described (Chan et al., 2005). From this, a list of coordinates of spots of interest was generated for automated spot excision using an Ettan spot-picking robot (GE Healthcare).

Protein identification by mass spectrometry

In-gel tryptic digestion of excised gel pieces was performed as previously described (Weeks et al., 2006). For peptide mass fingerprinting, 0.5 μl of tryptic digest was mixed with 1 μl of matrix – saturated aqueous 2,5-dihydroxybenzoic acid (DHB) – and spotted onto a sample target and dried. Matrix-assisted laser desorption/ionization time-of-flight (MALDI-TOF) mass spectra were acquired using an externally calibrated Ultraflex mass spectrometer (Bruker Daltonics) in the reflector mode. After internal calibration using trypsin autolysis peaks, prominent peaks in the mass range m/z 500-5000 were used to generate a peptide mass fingerprint which was searched against the updated NCBI database using Mascot version 2.0.02 (Matrix Sciences). Identifications were accepted when a minimum of six peptide masses matched a particular protein (mass error of ±100 ppm, allowing one missed cleavage), sequence coverage was >25%, MOWSE scores were higher than a threshold value of P=0.05, the predicted protein mass agreed with the gel-based mass and *Drosophila* sequences were identified. Identifications were also made by peptide sequencing using nano-liquid chromatography-electrospray ionization collision-induced dissociation tandem mass spectrometry (LC-MS/MS). This was performed on an Ultimate HPLC (Dionex) with a PepMap C18 75 μm inner-diameter column (LC Packings) at a flow rate of 300 nl/minutes, coupled to a Quadrupole Time-Of-Flight 1 (QTOF1) mass spectrometer (Waters/Micromass, Manchester, UK). Spectra were processed using MassLynx software (Waters) and submitted to Mascot database search routines. Positive identifications were accepted when at least two peptide sequences matched an entry with MOWSE scores above the P=0.05 threshold value.

Phosphopeptide analysis using TiO_2 micro-columns and LC-MS/MS

Enrichment of phosphorylated peptides from peptides generated by in-gel digestion of selected protein spots was performed using TiO_2 essentially as described in (Larsen et al., 2005). Briefly, ~3-mm-long TiO_2 micro-columns were packed in GELoader tips with a small C8 3M Empore plug. The trypsin digests from the two cofilin protein spots were diluted into 5% TFA, 80% acetonitrile (with inclusion of 50 mg/ml phthalic acid) and loaded onto the TiO_2 micro-columns. The columns were washed with 5% TFA, 80% acetonitrile and bound phosphorylated peptides were eluted with 15 μl ammonia solution [10 μl ammonia (25% solution) in 490 μl water]. Eluates were acidified and analyzed by MALDI-TOF MS and LC-MS/MS. MALDI-TOF MS was performed on a Voyager STR mass spectrometer (PerSeptive Biosystems, Framingham, MA). All spectra were obtained in the positive reflector mode and DHB (20 g/l) in 50% acetonitrile, 1% phosphoric acid was used as the matrix. Data analysis was performed using MoverZ software (www.proteometrics.com) and peptide assignment was accomplished using GPMAW software (welcome.to/gpmaw). LC-MS/MS was performed on a Proxeon Biosystem Easy-nLC nanoflow system (Proxeon Biosystems, Odense, Denmark) coupled to a QTOF Ultima mass spectrometer (Waters/Micromass, Manchester, UK). Peptides were loaded onto a 75 μm inner-diameter fused silica pre-column (ReproSil–Pur, Germany) and eluted with a 1.5% gradient (buffer A: 0.5 % acetic acid; buffer B: 0.5% acetic acid in 80% acetonitrile) onto a 50 μm inner-diameter fused silica analytical column (ReproSil-Pur) and into the mass spectrometer. The mass spectrometer was operated in data-dependent acquisition mode and two of the most intense ions were selected for collision-induced dissociation per MS scan. The data were processed using MassLynx software and pkl files were searched using an in-house version of Mascot.

Immunoblotting and immunofluorescence staining

Extracts separated by 1D or 2D SDS-PAGE were blotted onto Immobilon P membrane (Millipore) and blocked with 5% (w/v) BSA in TBS-T [50 mM Tris pH 8.0, 150 mM NaCl, 0.1% (v/v) Tween-20]. Membranes were probed with antibodies against C-terminal *Drosophila* Akt, *P*-Akt (both from S. Leevers, CRUK), *P*-S6K (Cell Signalling Technology), *PP*-ERK (Sigma), β-actin (Sigma) or *P*-cofilin (against the peptide acetyl-ApSGVTVSDC, Eurogentec). Membranes were washed (three times 10 minutes) in TBS-T, incubated with the appropriate horseradish-peroxidase-conjugated secondary antibody (Amersham Pharmacia), washed again and developed using enhanced chemiluminescence (PerkinElmer, Inc.). For immunostaining, cells were washed with PBS and fixed with 4% (v/v) formaldehyde in PBS for 10 minutes. After washing with PBS, cells were permeabilised with 0.1% (v/v) Triton X-100 in PBS for 5 minutes, washed again and blocked with 5% (w/v) BSA in PBS for 1 hour. For *P*-Akt staining, cells were incubated with primary antibody (1:300 in PBS) overnight at 4°C, followed by incubation with secondary anti-rabbit antibody conjugated to Cy5 for 1 hour at RT. For actin, tubulin and DNA staining, the fixed and permeabilised cells were incubated for 1 hour at RT with Rhodamine-phalloidin (1:1000), FITC-conjugated anti-tubulin antibody (1:1000) and DAPI (1:2000) respectively, all diluted in PBS. Fluorescent images were acquired using a Nikon 2000E microscope with 20× and 40× objectives fitted with a cooled CCD camera (Cool Snap; Roper) and using MetaMorph software (Universal Imaging Inc.). Within each experiment, all images were acquired and processed in an identical fashion to enable comparison across the image series.

Time-lapse microscopy

Phase-contrast and fluorescence time-lapse movies were taken on a Nikon 2000E microscope with a 100× oil immersion lens at 20-second intervals. Actin dynamics were analysed in live dsRNA-treated cells by time-lapse fluorescence microscopy using GFP-moesin to visualise F-actin. For this, cells were treated for 4 days with dsRNAs and then plated onto uncoated glass dishes. Baculovirus harbouring DNA driving the expression of the actin-binding region of moesin fused to GFP from the actin5c promoter was then added to the cells and incubated overnight. Actin reorganisation in the cells was filmed from 3 minutes before until 10 minutes after addition of 10 μg/ml insulin. Kymographs were generated from time-lapse movie images using MetaMorph software. For this, five to ten 1-pixel-thick lines were drawn across the cell edges of one to three cells in the field and the pixel intensities along each line combined to generate the kymographs. Representative cells, lines and kymographs are shown for each experiment.

We are grateful to Anne Ridley for the critical reading of the manuscript, and to Tao Liu and Richard Foxon for technical support. E.J. was funded by a UCL University Overseas Research Scholarship and by the Ludwig Institute for Cancer Research.

References

Arber, S., Barbayannis, F. A., Hanser, H., Schneider, C., Stanyon, C. A., Bernard, O. and Caroni, P. (1998). Regulation of actin dynamics through phosphorylation of cofilin by LIM-kinase. *Nature* **393**, 805-809.

Bamburg, J. R. (1999). Proteins of the ADF/cofilin family: essential regulators of actin dynamics. *Annu. Rev. Cell. Dev. Biol.* **15**, 185-230.

Benard, V., Bohl, B. P. and Bokoch, G. M. (1999). Characterization of rac and cdc42 activation in chemoattractant-stimulated human neutrophils using a novel assay for active GTPases. *J. Biol. Chem.* **274**, 13198-13204.

Biyasheva, A., Svitkina, T., Kunda, P., Baum, B. and Borisy, G. (2004). Cascade pathway of filopodia formation downstream of SCAR. *J. Cell Sci.* **117**, 837-848.

Bubb, M. R., Senderowicz, A. M., Sausville, E. A., Duncan, K. L. and Korn, E. D. (1994). Jasplakinolide, a cytotoxic natural product, induces actin polymerization and competitively inhibits the binding of phalloidin to F-actin. *J. Biol. Chem.* **269**, 14869-14871.

Carlier, M. F., Laurent, V., Santolini, J., Melki, R., Didry, D., Xia, G. X., Hong, Y., Chua, N. H. and Pantaloni, D. (1997). Actin depolymerizing factor (ADF/cofilin) enhances the rate of filament turnover: implication in actin-based motility. *J. Cell Biol.* **136**, 1307-1322.

Chan, H. L., Gharbi, S., Gaffney, P. R., Cramer, R., Waterfield, M. D. and Timms, J. F. (2005). Proteomic analysis of redox- and ErbB2-dependent changes in mammary luminal epithelial cells using cysteine- and lysine-labelling two-dimensional difference gel electrophoresis. *Proteomics* **5**, 2908-2926.

de Graauw, M., Tijdens, I., Cramer, R., Corless, S., Timms, J. F. and van de Water, B. (2005). Heat shock protein 27 is the major differentially phosphorylated protein involved in renal epithelial cellular stress response and controls focal adhesion organization and apoptosis. *J. Biol. Chem.* **280**, 29885-29898.

Firtel, R. A. and Chung, C. Y. (2000). The molecular genetics of chemotaxis: sensing and responding to chemoattractant gradients. *Bioessays* **22**, 603-615.

Gharbi, S., Gaffney, P., Yang, A., Zvelebil, M. J., Cramer, R., Waterfield, M. D. and Timms, J. F. (2002). Evaluation of two-dimensional differential gel electrophoresis for proteomic expression analysis of a model breast cancer cell system. *Mol. Cell. Proteomics* **1**, 91-98.

Ghosh, M., Song, X., Mouneimne, G., Sidani, M., Lawrence, D. S. and Condeelis, J. S. (2004). Cofilin promotes actin polymerization and defines the direction of cell motility. *Science* **304**, 743-746.

Hawkins, P. T., Eguinoa, A., Qiu, R. G., Stokoe, D., Cooke, F. T., Walters, R., Wennstrom, S., Claesson-Welsh, L., Evans, T., Symons, M. et al. (1995). PDGF stimulates an increase in GTP-Rac via activation of phosphoinositide 3-kinase. *Curr. Biol.* **5**, 393-403.

Hensbergen, P., Alewijnse, A., Kempenaar, J., van der Schors, R. C., Balog, C. A., Deelder, A., Beumer, G., Ponec, M. and Tensen, C. P. (2005). Proteomic profiling identifies an UV-induced activation of cofilin-1 and destrin in human epidermis. *J. Invest. Dermatol.* **124**, 818-824.

Hotulainen, P., Paunola, E., Vartiainen, M. K. and Lappalainen, P. (2005). Actin-depolymerizing factor and cofilin-1 play overlapping roles in promoting rapid F-actin depolymerization in mammalian nonmuscle cells. *Mol. Biol. Cell* **16**, 649-664.

Ibarra, N., Pollitt, A. and Insall, R. H. (2005). Regulation of actin assembly by SCAR/WAVE proteins. *Biochem. Soc. Trans.* **33**, 1243-1246.

Katso, R., Okkenhaug, K., Ahmadi, K., White, S., Timms, J. and Waterfield, M. D. (2001). Cellular function of phosphoinositide 3-kinases: implications for development, homeostasis, and cancer. *Annu. Rev. Cell. Dev. Biol.* **17**, 615-675.

Kiger, A., Baum, B., Jones, S., Jones, M., Coulson, A., Echeverri, C. and Perrimon, N. (2003). A functional genomic analysis of cell morphology using RNA interference. *J. Biol.* **2**, 27.

Kotani, K., Hara, K., Kotani, K., Yonezawa, K. and Kasuga, M. (1995). Phosphoinositide 3-kinase as an upstream regulator of the small GTP-binding protein Rac in the insulin signaling of membrane ruffling. *Biochem. Biophys. Res. Commun.* **208**, 985-990.

Kunda, P., Craig, G., Dominguez, V. and Baum, B. (2003). Abi, Sra1, and Kette control the stability and localization of SCAR/WAVE to regulate the formation of actin-based protrusions. *Curr Biol* **13**, 1867-1875.

Larsen, M. R., Thingholm, T. E., Jensen, O. N., Roepstorff, P. and Jorgensen, T. J. (2005). Highly selective enrichment of phosphorylated peptides from peptide mixtures using titanium dioxide microcolumns. *Mol. Cell. Proteomics* **4**, 873-886.

Lizcano, J. M., Alrubaie, S., Kieloch, A., Deak, M., Leevers, S. J. and Alessi, D. R. (2003). Insulin-induced Drosophila S6 kinase activation requires phosphoinositide 3-kinase and protein kinase B. *Biochem. J.* **374**, 297-306.

Mouneimne, G., Soon, L., DesMarais, V., Sidani, M., Song, X., Yip, S. C., Ghosh, M., Eddy, R., Backer, J. M. and Condeelis, J. (2004). Phospholipase C and cofilin are required for carcinoma cell directionality in response to EGF stimulation. *J. Cell Biol.* **166**, 697-708.

Nagata-Ohashi, K., Ohta, Y., Goto, K., Chiba, S., Mori, R., Nishita, M., Ohashi, K., Kousaka, K., Iwamatsu, A., Niwa, R. et al. (2004). A pathway of neuregulin-induced activation of cofilin-phosphatase Slingshot and cofilin in lamellipodia. *J. Cell Biol.* **165**, 465-471.

Nishita, M., Wang, Y., Tomizawa, C., Suzuki, A., Niwa, R., Uemura, T. and Mizuno, K. (2004). Phosphoinositide 3-kinase-mediated activation of cofilin phosphatase Slingshot and its role for insulin-induced membrane protrusion. *J. Biol Chem.* **279**, 7193-7198.

Nishita, M., Tomizawa, C., Yamamoto, M., Horita, Y., Ohashi, K. and Mizuno, K. (2005). Spatial and temporal regulation of cofilin activity by LIM kinase and Slingshot is critical for directional cell migration. *J. Cell Biol.* **171**, 349-359.

Niwa, R., Nagata-Ohashi, K., Takeichi, M., Mizuno, K. and Uemura, T. (2002). Control of actin reorganization by Slingshot, a family of phosphatases that dephosphorylate ADF/cofilin. *Cell* **108**, 233-246.

Reif, K., Nobes, C. D., Thomas, G., Hall, A. and Cantrell, D. A. (1996). Phosphatidylinositol 3-kinase signals activate a selective subset of Rac/Rho-dependent effector pathways. *Curr. Biol.* **6**, 1445-1455.

Ridley, A. J., Schwartz, M. A., Burridge, K., Firtel, R. A., Ginsberg, M. H., Borisy, G., Parsons, J. T. and Horwitz, A. R. (2003). Cell migration: integrating signals from front to back. *Science* **302**, 1704-1709.

Song, X., Chen, X., Yamaguchi, H., Mouneimne, G., Condeelis, J. S. and Eddy, R. J. (2006). Initiation of cofilin activity in response to EGF is uncoupled from cofilin phosphorylation and dephosphorylation in carcinoma cells. *J. Cell Sci.* **119**, 2871-2881.

Soosairajah, J., Maiti, S., Wiggan, O., Sarmiere, P., Moussi, N., Sarcevic, B., Sampath, R., Bamburg, J. R. and Bernard, O. (2005). Interplay between components of a novel LIM kinase-slingshot phosphatase complex regulates cofilin. *EMBO J.* **24**, 473-486.

Tanaka, K., Okubo, Y. and Abe, H. (2005). Involvement of slingshot in the Rho-mediated dephosphorylation of ADF/cofilin during Xenopus cleavage. *Zoolog. Sci.* **22**, 971-984.

Vanhaesebroeck, B., Leevers, S. J., Ahmadi, K., Timms, J., Katso, R., Driscoll, P. C., Woscholski, R., Parker, P. J. and Waterfield, M. D. (2001). Synthesis and function of 3-phosphorylated inositol lipids. *Annu. Rev. Biochem.* **70**, 535-602.

Vartiainen, M. K. and Machesky, L. M. (2004). The WASP-Arp2/3 pathway: genetic insights. *Curr. Opin. Cell Biol.* **16**, 174-181.

Weeks, M. E., Sinclair, J., Butt, A., Chung, Y. L., Worthington, J. L., Wilkinson, C. R., Griffiths, J., Jones, N., Waterfield, M. D. and Timms, J. F. (2006). A parallel proteomic and metabolomic analysis of the hydrogen peroxide- and Sty1p-dependent stress response in Schizosaccharomyces pombe. *Proteomics* **6**, 2772-2796.

Wood, W., Faria, C. and Jacinto, A. (2006). Distinct mechanisms regulate hemocyte chemotaxis during development and wound healing in Drosophila melanogaster. *J. Cell Biol.* **173**, 405-416.

Yamamoto, M., Nagata-Ohashi, K., Ohta, Y., Ohashi, K. and Mizuno, K. (2006). Identification of multiple actin-binding sites in cofilin-phosphatase Slingshot-1L. *FEBS Lett.* **580**, 1789-1794.

Yanagawa, S., Lee, J. S. and Ishimoto, A. (1998). Identification and characterization of a novel line of Drosophila Schneider S2 cells that respond to wingless signaling. *J. Biol. Chem.* **273**, 32353-32359.

Yang, N., Higuchi, O., Ohashi, K., Nagata, K., Wada, A., Kangawa, K., Nishida, E. and Mizuno, K. (1998). Cofilin phosphorylation by LIM-kinase 1 and its role in Rac-mediated actin reorganization. *Nature* **393**, 809-812.